Advancing the Understanding of Xyloglucan Biosynthesis and Function in Plants through Diverse Genetic Engineering Approaches

Dissertation

Ronja Catharina Immelmann

August 2025

Advancing the Understanding of Xyloglucan Biosynthesis and Function in Plants through Diverse Genetic Engineering Approaches

Inaugural Dissertation

for the attainment of the doctoral degree
in the Faculty of Mathematics and Natural Sciences
at Heinrich Heine University Düsseldorf

Presented by
Ronja Catharina Immelmann
from Bielefeld

Düsseldorf, August 2025

From the Institute for Plant Cell Biology and Biotechnology
at Heinrich-Heine-University Düsseldorf

Published with the permission of the
Faculty of Mathematics and Natural Sciences at
Heinrich-Heine-University Düsseldorf

Rapporteurs:

1. Prof. Dr. Markus Pauly
2. Prof. Dr. Ilka Axmann

Date of oral examination: 17.12.2025

Für Ole.

Statutory Declaration

I hereby declare that this dissertation is the result of my own independent work and has been completed without unauthorized external assistance, in accordance with the “Rules on the principles for safeguarding good research practice at Heinrich Heine University Düsseldorf”. Furthermore, I declare that I have not submitted this dissertation to any other faculty or institution. I also confirm that I have not previously undergone any unsuccessful or successful doctoral examination procedures.

Ronja Catharina Immelmann Düsseldorf, 06.08.2025

Abstract

Plant cells are enclosed by a complex cell wall primarily composed of the polysaccharides cellulose, hemicellulose and pectin. Xyloglucan (XyG) is the predominant hemicellulose in the primary cell walls of dicot plants and is characterized by a glucan backbone substituted with xylosyl residues. These xylose residues are often further decorated with glycosyl and non-glycosyl residues, which vary in a species- and tissue-specific manner.

While several enzymes involved in XyG biosynthesis have been identified, others remain to be discovered, and the functions of many known enzymes require further characterization. In this thesis, previously uncharacterized XyG-related glycosyltransferases were identified and functionally analysed. Focus was placed on XyG:xylosyltransferases (XXTs) from *Hymenaea courbaril*, a species that produces highly xylosylated XyG. Three Hymenaea XXT homologs were identified and one of these induced hyperxylosylation in an *Arabidopsis thaliana* complementation approach. The resulting XyG structures were analysed using mass spectrometry, providing novel insights into the functional diversity within the XXT enzyme family.

Additionally, a xylosyltransferase from blueberry responsible for the synthesis of a unique xylosylated sidechain (“U” sidechain) was identified and characterized. Functional complementation in Arabidopsis followed by mass spectrometry, glycosidic linkage analysis and NMR spectroscopy of XyG oligosaccharides confirmed its role.

A synthetic biology approach was employed using *Pichia pastoris* to reconstitute XyG biosynthesis and determine the enzymatic components required to generate a plant-like xylosylated glucan polymer. Building on the prior successful synthesis of a glucan backbone in Pichia, efforts were focused on enhancing xylosylation by co-expressing additional XyG biosynthetic enzymes and modifying the nucleotide sugar biosynthesis pathways required for XyG synthesis.

Given the evolutionary interest in the origin of XyG biosynthesis, Pichia was also utilized to assess the functionality of putative XyG biosynthetic enzymes from various algal species. This analysis revealed that some charophycean green algae, which are evolutionarily close to land plants, possess functional XyG biosynthesis enzymes.

Although XyG deficiency in Arabidopsis results in only mild and tissue-specific phenotypes, it has been proposed that functional redundancy with other wall components may compensate for its absence. To test this hypothesis, Arabidopsis lines lacking multiple wall polymers were generated and analysed, providing insight into potential compensatory mechanisms among cell wall components.

Table of contents

List of abbreviations

β-GGM	β-galactoglucomannan
AcGGM	acetylated galactoglucomannan
AIR	Alcohol Insoluble Residue
At	*Arabidopsis thaliana*
ANOVA	analysis of variance
ApE	A Plasmid Editor
Ara	arabinose
att	attachment
AXY	altered xyloglucan
BEDS	Bicine-NaOH, Ethylene glycol, Dimethyl sulfoxide, Sorbitol
BLAST	Basic Local Alignment Search Tool
BMGY	buffered complex glycerol medium
BMMY	buffered complex methanol medium
CAZy	carbohydrate-active enzymes
Cc	*Coffea canephora*
CGA	Charophycean green algae
Ch	chapter
CSLA	CELLULOSE SYNTHASE-LIKE A
CSLC	CELLULOSE SYNTHASE-LIKE C
DMSO	dimethyl sulfoxide
DTT	dithiothreitol
D2O	deuterium oxide
E-CELBA	cellulase (endo-1,4-β-D-glucanase) (*Bacillus amyloliquefaciens*)
EDTA	ethylenediaminetetraacetic acid
EXT	extensin
Fuc	fucose
FUT1	fucosyltransferase1
Gal	galactose
GalA	galacturonic acid
GDP	guanidine diphosphate
GDV	Genome Database for Vaccinium
GFP	green fluorescence protein
Glc	glucose
GOI	gene of interest
GT	Glycosyltransferase
Hc	*Hymenaea courbaril*

HCl	hydrogen chloride
HPAEC-PAD	high-performance anion exchange chromatography coupled with pulsed amperometric detection
Hs	*Homo sapiens*
HSD	Honestly Significant Difference
HPAT	hydroxyproline *O*-arabinosyltransferases
Hyp	hydroxyprolin
irx	irregular xylem
Kfl	*Klebsormidium flaccidum*
Kn	*Klebsormidium nitens*
MAFFT	multiple alignment using fast Fourier transform
MALDI-TOF	matrix-assisted laser-desorption ionization time of flight
Man	mannose
Me	*Mesotaenium endlicherianum*
MS	mass spectrometry
MSA	multiple sequence alignment
NaCl	sodium chloride
NMR	nuclear magnetic resonance
OLIMP	oligosaccharide mass profiling
RFP	red fluorescence protein
Rha	rhamnose
RMSD	root mean square deviation
Rn	*Rattus norvegicus*
rpm	rounds per minute
PACE	polysaccharide analysis by carbohydrate electrophoresis
PCR	polymerase chain reaction
PCW	plant cell wall
S	supplemental
SDM	site directed mutagenesis
SDS	sodium dodecyl sulfate
Ser	serine
Sm	*Spirogloea muscicola*
SPE	solid phase extraction
TAIR	The Arabidopsis Information Resource
TBL	trichome birefringence-like
TFA	trifluoroacetic acid
Tm	*Tropaeolum majus*

UDP	uridine diphosphate
UGD	UDP-glucose dehydrogenase
UUAT1	UDP-Uronic Acid Transporter 1
UXS	UDP-glucuronic acid decarboxylase/ UDP-xylose synthase
UXT	UDP-Xyl transporter
Vc	*Vaccinium corymbosum*
WT	wildtype
XBT	xyloglucan β-xylosyltransferase
XDT	xyloglucan D-sidechain transferase
XEG	XyG endoglucanase
XEH	xyloglucan endohydrolases
XET	xyloglucan endotransglycosylase
XLT2	xyloglucan L-sidechain Galactosyltransferase Position 2
XST	xyloglucan S-sidechain transferase
XTH	xyloglucan endotransglucosylase/hydrolase
XUT	xyloglucan-specific galacturonosyltransferase
XXT	xyloglucan xylosyltransferase
XyBAT	xyloglucan backbone acetylation
Xyl	xylose
XyG	xyloglucan

List of figures

1. Introduction

1.1 Plant cell wall

Plant cells are surrounded by a primarily polysaccharide-based network, the plant cell wall (PCW). The PCW was first observed by Robert Hook who found honeycomb like structures in thin slices of cork with a microscope in 1665 (Hooke et al., 1665). In contrast to the extracellular matrix of animal cells the walls of neighbouring plant cells are more rigid, thicker and stronger (Alberts et al., 2022). The structural principal of the PCW is based on a polymer network providing tensile strength and compression resistance (Alberts et al., 2022).

PCWs consist of three main polysaccharides: cellulose, hemicelluloses and pectins (Delmer et al., 2024; Cosgrove, 2024). Furthermore, PCWs can further contain wall-associated proteins e.g. glycoproteins (Delmer et al., 2024), lignin (Emonet and Hay, 2022), and water (Thompson and Islam, 2021).

The main polysaccharide in most PCWs is cellulose. It is built up from numerous parallel unbranched β-(1,4)-linked glucan chains which form microfibrils (Keegstra, 2010; Cosgrove, 2024). These crystalline microfibrils are stabilized by directional hydrogen bonds (Wohlert et al., 2022). Cellulose is synthesized at the plasma membrane by cellulose synthase complexes (Purushotham et al., 2020; Wilson et al., 2021; Pedersen et al., 2023; Cosgrove, 2024).

Hemicelluloses are typically alkali-extractable and include xyloglucans (XyG), mannans, xylans and/or mixed-linkage glucans. Hemicellulosic polysaccharides have β-(1,4)-glycosyl linked backbones that can be substituted with additional sugars and/or acetyl groups. Most hemicelluloses are present in the cell walls of all terrestrial plants (Scheller and Ulvskov, 2010).

Pectic polysaccharides encompass a variety of different structures. Common to pectic polysaccharide is their α-D-(1,4)-linked galacturonic acid content. Pectic polysaccharides are classified into five domains: unbranched homogalacturonan, rhamnogalacturonan I, rhamnogalacturonan II, xylogalacturonan and apiogalacturonan (Mohnen, 2008; Caffall and Mohnen, 2009; Atmodjo et al., 2013; Zdunek et al., 2021; Shahin et al., 2023).

The binding properties of wall polysaccharides and the network they form has been the subject of ongoing research. The traditional “tethered network” concept of PCW architecture suggest that XyG tethers cellulose microfibrils in a pectin hydrated matrix (Hayashi, 1989; Fry, 1989; Carpita and Gibeaut, 1993; Cosgrove, 2005). New models suggest a coherent grid of cellulose microfibrils and conformally diverse XyG with weak tethering effects in a gel-like network of pectin resulting in mainly cellulose determining wall extensibility (Zhang et al., 2019; Zhang et al., 2021b; Cosgrove, 2024).

The PCW has diverse functions on the level from single cells to the whole plant during the plant lifecycle. As plants are growing organisms in changing environments PCWs have to supply mechanical strength and dynamic extensibility. The mechanical strength of PCWs provides a structural basis for the plant and enables plant cells to resist the plant internal turgor

pressure and mechanical stress (Tang et al., 2022; Ali et al., 2023; Jarvis, 2023; Cosgrove, 2024). Flexibility of the PWC is necessary to support growth, cell division, and tissue differentiation (Ezquer et al., 2020; Cosgrove, 2024). The PCW hosts pores and membranous channels (plasmodesmata) for molecular transport and intercellular communication (Knox and Benitez-Alfonso, 2014; Tameshige et al., 2015; Wolf, 2022). Furthermore, the PCW plays an important role in biotic and abiotic stress resistance as it is a structural barrier for environmental hazards (Wang et al., 2014; Zhao et al., 2019; Rui and Dinneny, 2020) and prevents invasion by plant pathogens (Houston et al., 2016; Wan et al., 2021; Kozieł et al., 2021). In plant storage tissues like seeds PCWs are used as repository of storage polysaccharides (Buckeridge et al., 2000; Buckeridge, 2010).

In addition to the plant itself, humans have utilised the PCW and resulting products: fibres for textiles, wood for construction, paper products, fuel for heating and transportation, and as medicine and food source (Burton and Fincher, 2014; Johnson et al., 2018; Koshani et al., 2025). In recent decades, increasing attention has been given to the PCW as a renewable energy resource, as it represents the largest source of renewable carbohydrates on Earth (Pauly and Keegstra, 2008; Burton and Fincher, 2014; Loqué et al., 2015). Furthermore, photosynthetic assimilation of atmospheric carbon dioxide by plants and sequestration into cell walls is a major carbon sink in the terrestrial ecosystem. It provides a huge potential to mitigate elevated levels of atmospheric carbon dioxide which drives global warming and climate change (Jansson et al., 2010; van de Wouwer et al., 2018; Pottier et al., 2023; Li et al., 2024).

1.2. Xyloglucan

XyG was found in the late 1950s as a seed storage “amyloid” in nasturtium (*Tropaeolum majus,* Tm*)*, tamarind (*Tamarindus indica*) and other plants (Kooiman, 1957, 1960). About a decade later XyG was also detected in suspension-cultured cells of sycamore (*Acer pseudoplatanus*) (Aspinall et al., 1969; Bauer et al., 1973). Today, it is known that XyG is the major primary-wall hemicellulose of spermatophytes excluding grasses, in which the XyG abundance is much lower. In secondary PCWs XyG is minor or absent (Scheller and Ulvskov, 2010).

1.2.1. Xyloglucan Structure and Diversity

Xyloglucan is - as the name implies - a xylosylated glucan. It has a β-(1,4)-glucan backbone with α-(1,6)-linked D-xylose (Xyl) residues in a regular pattern (Fig. 1.1). The xylosyl-residues can be further substituted with glycosyl and nonglycosyl residues resulting in unique XyG sidechains. The XyG structure depends on several factors including plant species, tissue and cell type and cell development stage (Lampugnani et al., 2013; Schultink et al., 2014; Liu et al., 2015; Zavyalov et al., 2019).

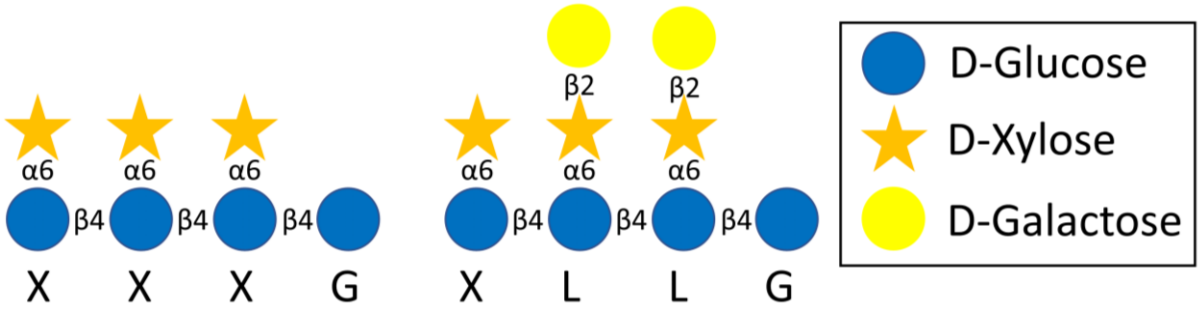

Figure 1.1: Example structure of the hemicellulose xyloglucan. Nomenclature by one-letter code. Blue dots: glucopyranose (Glc*p*), orange stars: xylopyranose (Xyl*p*), yellow dots: galactopyranose (Gal*p*).

In order to simplify the naming of the various XyG sidechain structures a nomenclature based on single letters was established (Fry et al., 1993; Tuomivaara et al., 2015): G represents the unsubstituted Glucose (Glc) of the backbone and X represents a Glc substituted with an α-D-xylopyranose.

The two dominant XyG xylosylation patterns are XXGG and XXXG in which two and three contiguous out of four backbone Glc are xylosylated, respectively (Vincken et al., 1997). The occurrence of the motifs are mainly species-specific, but in some cases also tissue specific (Pauly and Keegstra, 2016; Zavyalov et al., 2019).

Galactosylation at the *O*-2 of the xylosyl residue (L sidechain) is a ubiquitous structure in all plants (Pauly and Keegstra, 2016). In the XXXG-type XyG, the second and third xylosyl residue can be substituted with galactose, resulting in the XLXG, XXLG and/or XLLG motifs (Marry et al., 2003; Hsieh and Harris, 2009). Fucosylation at the *O*-2 of the galactosyl residue (F sidechain) of XXXG-type XyG is another common XyG structure (Brennan and Harris, 2011; Pauly and Keegstra, 2016; Zavyalov et al., 2019).

Less common XyG structures contain an additional xylosyl residue (U sidechain) (Ray et al., 2004; Hilz et al., 2007; Hotchkiss et al., 2015; Immelmann et al., 2023; Wilson et al., 2023), arabinopyranosyl-residues (D and E sidechain) (Peña et al., 2008; Hsieh and Harris, 2012; Zhu et al., 2018), arabinofuranose-residues (S sidechain) (Jia et al., 2005; Schultink et al., 2013; Wilson et al., 2023), or galacturonic acid (GalA) (Y sidechain) (Peña et al., 2008; Peña et al., 2012) at the *O*-2 of the xylosyl moiety.

Some XyG sidechains can be *O*-acetylated (denoted by the underlined corresponding sidechain letter) (York et al., 1988; Kiefer et al., 1989; Gille et al., 2011b). Acetylation seems to be limited to the unsubstituted glucosyl backbone residues (G) (York et al., 1988; Jia et al., 2005; Gille et al., 2011b; Liu et al., 2016; Zhong et al., 2020) the galactosyl-residue (L, F and J sidechains) (York et al., 1988; Kiefer et al., 1989; Gille et al., 2011b; Zhong et al., 2018) and arabinofuranosyl-residue (S sidechain) (Jia et al., 2005).

1.2.2. Xyloglucan Biosynthesis and Function

XyG is synthesized by Carbohydrate-Active Enzyme (CAZy; https://www.cazy.org/) glycosyltransferase (GT) families located in the Golgi apparatus membranes (Scheller and Ulvskov, 2010). GTs utilize nucleotide sugars and add a sugar residues to the emerging polysaccharide (Pauly and Keegstra, 2016; Julian and Zabotina, 2022). The nucleotide sugars for XyG biosynthesis are produced by sugar or nucleotide sugar conversion in the cytosol and inside the Golgi. Some are moved across the Golgi membrane by nucleotide sugar transporters (Seifert, 2004; Bar-Peled and O'Neill, 2011; Rautengarten et al., 2014; Pauly and Keegstra, 2016; Zhang et al., 2021a). After biosynthesis in the Golgi XyG is trafficked through the trans-Golgi network, sorted into secretory vesicles and secreted to the extracellular matrix via the plasma membrane (Pauly and Keegstra, 2016; Hoffmann et al., 2021; Hoffmann and McFarlane, 2024).

Based on the common occurrence of XyG in dicot plants (Scheller and Ulvskov, 2010) XyG is thought to be responsible for formation, maintenance, and functions of the primary cell wall structure (Zavyalov et al., 2019).

GT	Enzyme	Product	GT family	Source
CLSC	CSLC4/5/6/8/12	G_{n+1}	2	(Cocuron et al., 2007; Kim et al., 2020; Li et al., 2022)
XXT	XXT1/2	XXGG	34	(Zabotina et al., 2008; Cavalier et al., 2008; Zabotina et al., 2012; Wang et al., 2014; Culbertson et al., 2018)
	XXT3/4/5	XXXG *		(Culbertson et al., 2016; Zhang et al., 2023b)
GalT	XLT2	XLXG	47	(Jensen et al., 2012; Liu et al., 2015)
	MUR3	XXLG		(Madson et al., 2003; Lopes et al., 2010; Schultink et al., 2013; Liu et al., 2015)
XylT	XBT1	XUXG		(Immelmann et al., 2023; Wilson et al., 2023)
GalAT	XUT1	YXXG		(Peña et al., 2012)
Ara*f*T	XST1/2	XXSG		(Schultink et al., 2013)
Ara*p*T	XDT	XXDG		(Zhu et al., 2018)
FucT	FUT1	XLFG XXFG	37	(Rocha et al., 2016; Urbanowicz et al., 2017)

AceT	XyBAT	XXGG, XSGG	-	(Liu et al., 2016; Zhong et al., 2020)
	AXY4	XXFG, XLFG	-	(Gille et al., 2011b; Zhong et al., 2018)

Figure 1.2: Overview of the enzymes involved in XyG biosynthesis. Nomenclature of product by one-letter code; Gal = galactose, Xyl = xylose, GalA = galacturonic acid, Ara = arabinose, Fuc = fucose, Ace = acetyl; *f* = furanose, *p* = pyranose, T = Transferase, GT = Glycosyltransferase, CSLC = cellulose synthase-like C, XXT = XyG xylosyltransferase, XLT = Xyloglucan L-sidechain Galactosyltransferase Position 2, XBT = xyloglucan β-xylosyltransferase, XUT = XyG specific galacturonosyltransferase, XST = XyG S-sidechain transferase, XDT = xyloglucan D-sidechain transferase, FUT = XyG specific fucosyltransferase, XyBAT = XyG backbone 6-*O*-acetyltransferase, AXY = altered xyloglucan; * requires XXT1/XXT2 to add first two Xyl

The XyG glucan backbone is synthesised by proteins of the cellulose synthase-like C (CSLC) family (Cocuron et al., 2007), which belong to the CAZy GT family 2 (Fig. 1.2). CSLCs are integral membrane proteins with six transmembrane domains (Davis et al., 2010; Julian and Zabotina, 2022). Five CSLC enzymes have been identified so far in Arabidopsis: CSLC4, 5, 6, 8, and 12. The five CSLCs vary in expression in different plant tissues. CSLC4 is widely expressed in Arabidopsis and higher expressed than any of the other CSLCs (Kim et al., 2020). CLSCs are thought to utilize cytosolic uridine diphosphate (UDP)-Glc at the cytoplasmic catalytic domain of the enzyme and elongate the glucan backbone, while transporting it through the transmembrane helice canal of CSLC across the Golgi membrane (Pauly and Keegstra, 2016; Julian and Zabotina, 2022).

The xylosylation of the glucan backbone appears to be accomplished by xylosyltransferases (XXTs) (Faik et al., 2002) from CAZy GT family 34 (Fig. 1.2). In Arabidopsis XXT1 and 2 are responsible for the addition of the first and second xylosyl residues (XXGG motif) while XXT3, 4 and 5 add the xylosyl residue to the third glucose in the glucan chain (XXXG motif) (Zabotina et al., 2008; Cavalier et al., 2008; Zabotina et al., 2012; Zhang et al., 2023b). XXTs use UDP-Xyl as substrate in the Golgi lumen. UDP-Xyl is synthesized from UDP-Glc via UDP-GlcA, through the action of UDP-glucose dehydrogenase and UDP-glucuronic acid decarboxylase/UDP-xylose synthase, and transported into the Golgi by UDP-Xylose Transporters (Zhao et al., 2018; Zhang et al., 2021a).

Proper XyG xylosylation is essential for plant growth, as altering the glucan backbone of Arabidopsis through acetylation disrupts xylosylation patterns and impairs cell expansion (Zhong et al., 2020).

In contrast, XyG appears non-essential for overall wall architecture, as Arabidopsis mutants lacking XyG (*cslc456812*, *xxt1xxt2* and *xxt1xxt2xxt5*, from now on *xxt12* and *xxt125* respectively, numbers corresponding to the enzymes in Arabidopsis) show only mild, tissue-specific phenotypes (Cavalier et al., 2008; Zabotina et al., 2012; Kim et al., 2020). However,

XyG deficiency correlates with weaker seedlings and reduced turgor pressure, a key factor in cell growth and wall resistance (Ortega, 1985; Ali et al., 2023; Bou Daher et al., 2024).

Galactosylation of the xylosyl residues on the glucan backbone is performed by galactosyltransferases MUR3 and Xyloglucan L-sidechain Galactosyltransferase Position 2 (XLT2) of the CAZy GT family 47 (Fig. 1.2). MUR3 is responsible for the galactosylation of the third Xyl residue and XLT2 for the galactosylation the second Xyl residue as shown in Arabidopsis knockout lines and complementation in Arabidopsis (Madson et al., 2003; Jensen et al., 2012). MUR3 and XLT2 utilize UDP-Gal which is formed by interconversion of UDP-Glc and UDP-Gal in a reversible reaction by UDP-galactose/glucose 4-epimerase (Zhang et al., 2021a).

Further members of the GT47 family are the root specific XyG specific Galacturonosyltransferase1 (XUT1, previously GT16) identified in Arabidopsis (Peña et al., 2012; Jensen et al., 2012), arabinofuranosyltransferases XyG S-sidechain transferase1 (XST1 and XST2) identified in tomato (Schultink et al., 2013) and arabinopyranosyltransferase xyloglucan D-sidechain transferase (XDT) identified in the moss *Physcomitrella patens* (Zhu et al., 2018).

XyG sidechains are important for XyG function and plant growth as mutant lines with galactose-depleted XyG (Arabidopsis double mutant *mur3.1xlt2* (Jensen et al., 2012)) is dysfunctional and leads to severe dwarfism in Arabidopsis. XyG and pectin are not properly secreted and accumulate within intracellular aggregates instead which also causes defects in cellular trafficking (Kong et al., 2015; Xiang et al., 2023; Hoffmann and McFarlane, 2024). The defects can be rescued by complementation with various XyG GT47s resulting in further substituted XyG backbone and in normal plant growth. This suggests that XyG galactosylation can be replaced by other sugar substituents (Schultink et al., 2013; Liu et al., 2015; Zhu et al., 2018; Immelmann et al., 2023; Wilson et al., 2023).

Fucosylation of the galactosyl-residues is conducted by α-(1,2)-fucosyltransferase Fucosyltransferase1 (FUT1) of the GT family 37. FUT1 drives the fucosylation of Gal residues of the third position of the XLLG and XXLG motifs utilizing GDP-fucose (Perrin et al., 1999; Faik et al., 2000; Faik et al., 2002; Vanzin et al., 2002; Cicéron et al., 2016; Rocha et al., 2016). XyG with fucosyl-residues seem to have a regulatory function in plant cell expansion as antagonists to auxin (York et al., 1984; Paque et al., 2014).

O-acetylation of XyG galactose residues is mediated by altered xyloglucan4 (AXY4) and AXY4L which belong to the Trichome-Birefringence-Like (TBL) protein family (Gille et al., 2011b; Zhong et al., 2018; Pauly and Ramírez, 2018). Both enzymes were identified in studies of the Arabidopsis-altered xyloglucan (*axy*) lines with reduction in xyloglucan *O*-acetylation. Mass spectrometrical analysis of T-DNA mutant line *ayx4* resulted in a loss of acetyl groups on XyG from all tested tissues except seeds. *axy4l* showed the same results exclusively in

seeds. AXY4 and AXY4L act exclusively on XyG (Gille et al., 2011b). AXY9, another putative acetyltransferase, has been shown to be involved in the *O*-acetylation of multiple hemicelluloses (Schultink et al., 2015). XyG Gal acetylation is proposed to improve solubility properties. In XyG from tamarind seeds chemical acetylation of Gal residues furthermore improves thermal stability and reduces viscosity (Zhang et al., 2022).

Acetyltransferase XyBAT1 mediates the 6-*O*-acetylation of the glucan-backbone in species that produce the XXGG pattern of XyG (Liu et al., 2016; Zhong et al., 2020). XyBAT1 knockout mutants have a reduction in XyG acetylation and a modified xylosylation pattern (XXXG motif) (Liu et al., 2016). Acetylation of the glucan backbone therefore was suggested to compete with xylosylation and might be responsible for the lack of xylosylation on the third Glc in XXGG subunits (Liu et al., 2016; Zhong et al., 2020).

XyG displays a large variety of substituents that can be tissue and species specific (Pauly and Keegstra, 2016). It was suggested that cellphysiological roles of XyG are unlikely to be the driving force for the sidechain diversity (Wilson et al., 2023). Comparing the impact of XyG deficient mutants (*xxt12*, *xxt125* and *cslc456812*) (Cavalier et al., 2008; Zabotina et al., 2012; Kim et al., 2020) with the impact of altered XyG (XXXG missing sidechains) (Jensen et al., 2012) it became evident that an unsubstituted XyG rather than a lack of XyG negatively effects physiological roles in the plant cell wall. Therefore, presence of XyG sidechain is important but the composition of the sidechain seems to be flexible (Hoffmann and McFarlane, 2024). Overall, XyG sidechains are vital for the assembly, secretion, and mechanical function of plant cell walls, directly impacting plant morphology and adaptability (Schultink et al., 2013; Schultink et al., 2014; Kong et al., 2015; Hoffmann and McFarlane, 2024).

Some of the proposed functions of XyG are based on the ability of XyG to bind to cellulose: XyG binds cellulose via hydrogen bonds (Valent and Albersheim, 1974; Hayashi, 1989), but recent findings suggest that dispersion forces and hydrophobic effects potentially act in binding to cellulose in an aqueous environment (Wohlert et al., 2022). In the tethering network model of the PCW XyG and cellulose form a network, in which XyG binds to cellulose microfibrils in different lamellae (well-aligned cellulose microfibrils in distinct layers) and restrains wall enlargement (Hayashi, 1989; Fry, 1989; Carpita and Gibeaut, 1993; Cosgrove, 2005, 2024). However, this model has been under revision since research on XyG deficient Arabidopsis lines (*xxt12, xxt125* and *cslc456812*) revealed only mild phenotypes (Cavalier et al., 2008; Zabotina et al., 2012; Kim et al., 2020), and XyG digestion on cell walls *in vitro* had negligible biomechanical effects in the plant cell walls (Park and Cosgrove, 2012a, 2012b; Zhang et al., 2019). These results contradict the fact that XyG tethers cellulose microfibrils. Alternative models suggest that XyG may bind cellulose microfibrils in limited junctions (“biomechanical hotspots”) (Park and Cosgrove, 2012a; Cosgrove, 2022a, 2024). These junctions are proposed to be key sites of cell wall loosening. XyG may also indirectly influence cell wall mechanics by

binding to cellulose surfaces and modulation of the cellulose microfibril network assembly (Cosgrove, 2022b).

As plant cell walls have to be able to adapt to changing environmental conditions, cleavage and reconnections of XyG is important to keep up wall plasticity. Enzymes responsible belong to the XyG endotransglucosylase/hydrolase (XTH) family (Ishida and Yokoyama, 2022). The enzymes are divided into two groups according to their function: cleavage of XyG by xyloglucan endohydrolases (XEH) and transfer to another sugar polymer by xyloglucan endotransglycosylases (XET) (Xu et al., 2010; Stratilová et al., 2020; Ishida and Yokoyama, 2022). Both enzyme groups are supposed to regulate the cell wall plasticity along with non-catalytic expansins (Hrmova et al., 2022). XET enzymes are essential in the assembly of the cell wall network and in modifications during plant growth and development (Hrmova et al., 2022; Yuan et al., 2024). XTHs are not necessary for cell wall loosening in cell expansion but are crucial for responses to environmental cues (Ishida and Yokoyama, 2022) including aluminum toxicity (Zhu et al., 2012; Zhu et al., 2014; Wu et al., 2021), salinity (Han et al., 2013; Xuan et al., 2016), drought (Cho et al., 2006; Choi et al., 2011; Yuan et al., 2024) and freezing (Takahashi et al., 2021). Besides XyG XTHs recognise a wide range of polysaccharides (Ishida and Yokoyama, 2022).

Several glycosidases can degrade XyG by trimming sidechains: Xylosidase XYL1 which cleaves xylosyl residues from the non-reducing end of XyG (Sampedro et al., 2001; Sampedro et al., 2010; Shigeyama et al., 2016; Suzuki et al., 2025), galactosidase BGAL10 which has β-galactosidase activity against XyG (Sampedro et al., 2012) and fucosidase AXY8 which cleaves fucose residues (Günl et al., 2011).

In some plant species XyG functions as a seed storage polymer (tamarind (Kooiman, 1961), nasturtium (Hoth et al., 1986), diesel tree (*Copaifera langsdorffii*) (Buckeridge et al., 1992) and *Hymenaea courbaril* (Tiné et al., 2006)). In Hymenaea seeds the XyG-cellulose matrix is supposed to work as a water buffer under periods of stress following radicle emergence (Grandis et al., 2024).

XyG have also been shown to act a potent elicitor of plant immunity based on the fact that XyG-derived oligosaccharides activate disease resistance against pathogens and trigger defence reactions (Wan et al., 2021).

XyG is furthermore used in various sectors of industry: Food (food additive, food packaging (Perumal Thivya et al., 2023; Pontes et al., 2023)), cosmetic (Ning et al., 2025), textile and paper (Brumer, 2010), chemical (coating (Vilaseca et al., 2020)), and pharmaceutical (drug delivery system (Bhalekar et al., 2016), tissue engineering (Dutta et al., 2020), tissue regeneration, wound healing (Zacharski et al., 2015)) industries. The major source of commercial XyG are tamarind seeds (Zhang et al., 2022), which has the advantages of high availability and low production costs, non-toxicity, biocompatibility and stability in a wide range

of pH, temperature and ionic solutions (Kulkarni et al., 2017; Santos et al., 2019; Perumal Thivya et al., 2023). Tamarind seed XyG is a galactoxyloglucan (Buckeridge et al., 1992; Kulkarni et al., 2017; Perumal Thivya et al., 2023). The galactose sidechains are important for the solubility of tamarind XyG in water. Enzymatic removal of Gal sidechains results in a water insoluble polymer (Kochumalayil and Berglund, 2014; Kulkarni et al., 2017). Impacts of the presence of galactose sidechains or enzymatically de-galactosylated tamarind XyG on medical hydrogel formation (Zhang et al., 2017) and prebiotic activity (Zhou et al., 2024) provide two examples of sidechain importance in industrial applications of XyG.

1.3 Thesis objective

Throughout the last decades major progress elucidating XyG structure and biosynthesis have been obtained. Nevertheless, many unanswered questions regarding XyG structural diversity and biosynthesis, XyG evolution as well as XyG interaction with other components of the plant cell wall remain unanswered.

The aim of this thesis was to identify and characterize hitherto unknown XyG related glycosyltransferases to gain new insights into XyG biosynthesis and how polymer substitution relates to XyG function *in planta*. Of particular interest were an unknown xylosyltransferase responsible for the generation of the U sidechain in Ericales, and XXTs from *Hymenaea courbaril* potentially responsible for a higher degree of xylosylation of the glucan backbone (XXXXG, XXXXXG) compared to the common xylosylation motif in dicots (XXXG).

Furthermore, the reconstruction of XyG biosynthesis in the yeast *Pichia pastoris* using plant-derived XyG biosynthetic genes was a key focus of this thesis, aimed at identifying the enzymes required and sufficient for producing plant-like XyG structures. This synthetic biology approach of XyG production in Pichia builds on previous results of Jean-Christophe Cocuron (Cocuron et al., 2007), Dr. Alex Schultnik and Dr. Balakumaran Chandrasekar. Pichia was also used as an orthologous host to test the functionality of algae and Poales XyG biosynthetic enzymes.

Cell wall polymers form a complex network essential for proper plant growth and development. As the absence of XyG does not result in a major phenotype (Cavalier et al., 2008; Zabotina et al., 2012; Kim et al., 2020), it has been hypothesized that other wall components, such as the hemicellulose mannan or the glycoprotein extensin, may compensate for its function (Gille et al., 2009; Kim et al., 2020; Sowinski et al., 2022). To test this functional redundancy hypothesis, Arabidopsis lines deficient in the biosynthesis of multiple such polymers were generated and analysed.

2. Material and methods

2.1 Chemicals and laboratory equipment

Chemicals were purchased from Sigma-Aldrich/Merck (Darmstadt), Carl Roth (Karlsruhe) and ThermoFisher/Invitrogen (Schwerte). Laboratory glassware and other equipment were acquired from VWR (Darmstadt), Sarstedt (Nümbrecht), Sigma-Aldrich/Merck, BioRad (Feldkirchen), ThermoFisher/Invitrogen and Zymo Research (Freiburg). All materials were purchased from the central chemical storage of the Heinrich Heine University in Düsseldorf or directly from the respective company.

2.2 Software and online tools

Benchling (https://www.benchling.com) was used as a digital labbook to plan, record, and analyse experimental workflows and results. It was furthermore used to visualize plasmids and analyse sequences with alignment (MAFFT (multiple alignment using fast Fourier transform) or Clustal Omega) and translation tools.

A Plasmid Editor (ApE) (https://jorgensen.biology.utah.edu/wayned/ape/) (Davis and Jorgensen, 2022) was applied for visualizing and designing DNA sequences as well as *in silico* cloning projects.

Clustal Omega Multiple Sequence Alignment (MSA) by European Molecular Biology Laboratory - European Bioinformatics Institute (https://www.ebi.ac.uk/jdispatcher/msa/clustalo) (Madeira et al., 2022) or UniPRot (https://www.uniprot.org/align) (Sievers et al., 2011; Sievers and Higgins, 2018) was utilized to generate alignments between three or more sequences using seeded guide trees and hidden Markov model profile-profile techniques.

Ncbi's Basic Local Alignment Search Tool (BLAST) (https://blast.ncbi.nlm.nih.gov/Blast.cgi) was used to find regions of similarity between nucleotide or protein sequences and to compare them to sequence databases (Altschul et al., 1990; Camacho et al., 2009; Camacho et al., 2023).

Gene and protein sequences were obtained from The Arabidopsis Information Resource (tair) (http://www.arabidopsis.org) (Huala et al., 2001), UniProt (https://www.uniprot.org/), Rice Genome Annotation Project (https://rice.uga.edu/index.shtml) and Genome Database for Vaccinium (GDV) (https://www.vaccinium.org).

Phylogenetic trees were generated using the standard One Click Workflow (PhyML/OneClick) from https://ngphylogeny.fr/ (Dereeper et al., 2008; Lemoine et al., 2019). The amino acid sequences were uploaded in Fasta format. The Multiple alignment program used was MAFFT (Katoh and Standley, 2013). Alignment Curation was done by Block Mapping and Gathering with Entropy (Criscuolo and Gribaldo, 2010). The phylogeny software PhyML created the tree inference based on the maximum-likelihood (Guindon et al., 2010) and tree rendering was

done by Newick Display to display a phylogenetic tree as Scalable Vector Graphic. iTOL (https://itol.embl.de/) was used to manage, annotate and export phylogenetic trees.
Prediction of transmembrane helices in proteins was performed using DeepTMHMM - 1.0 (https://services.healthtech.dtu.dk/services/DeepTMHMM-1.0/) (Hallgren et al., 2022).
Heatmapper (www.heatmapper.ca/) was used to visualize expression data in the form of heat maps (Babicki et al., 2016).
ChimeraX1.9 is a molecular analysis and visualization software (www.cgl.ucsf.edu/chimerax/) (Goddard et al., 2018; Pettersen et al., 2021; Meng et al., 2023). AlphaFold was used to predict protein structures (Mirdita et al., 2022).
The image processing package Fiji/ImageJ (Schindelin et al., 2012) was downloaded from imagej.net/software/fiji/ and used for photo analysis (phenotype analysis of Arabidopsis).
One-way ANOVA (ANalysis Of VAriance) with post-hoc Tukey HSD (Honestly Significant Difference) by https://astatsa.com/ (Navendu Vasavada, 2016) a provider of online web statistical calculators for categorical data analysis was used as test calculator for comparing multiple treatments in statistical analysis, or ANOVA Calculator by Statistic Kingdom (www.statskingdom.com/180Anova1way.html).
Chromosome Maps were created with the Chromosome Map Tool (arabidopsis.org/jsp/ChromosomeMap/tool.jsp) by tair.
If digital tools were employed for translation, DeepL (www.deepl.com/de/translator) was used. Additionally, ChatGPT (OpenAI, 2025; chatgpt.com) served as a scientific writing and language support tool. The Consensus Search Engine (consensus.app) and Google AI were used to find relevant scientific literature.

2.3 Primers

Primers were designed for DNA amplification via polymerase chain reaction (PCR) (Chapter Ch. 2.9.5) and genotyping via sanger sequencing (Ch. 2.9.14) based on the respective DNA sequence.
In general primers were designed using the best practice rules of primer design: primer length of 18-24 bases, G/C content of 40-60%, end with a G/C pair, a melting temperature of 50-60 °C, melting temperature within 5 °C and no complementary regions in primer pair.
Primers were additionally designed according to their application in cloning projects: For restriction-based cloning, restriction sites were incorporated into the primer sequences. Therefore, the primer sequences contained a restriction site and additional base pairs required for complete digestion by the respective enzyme as stated by the manufacturer (ThermoFisher for FastDigest Enzymes). For Gateway cloning (Ch. 2.9.7.4) primers were designed containing attB1 and attB2 sites. For site directed mutagenesis cloning (Ch. 2.9.8) the GeneArt® Primer

and Construct Design Tool by ThermoFisher (https://www.thermofisher.com/order/oligoDesigner/) was used.
Genotyping primers were designed using the Primer3Web tool (https://primer3.ut.ee/) (Untergasser et al., 2012; Koressaar and Remm, 2007; Kõressaar et al., 2018).
Further tools used in primer design and analysis were Multiple Primer Analyzer (https://www.thermofisher.com/de/de/home/brands/thermo-scientific/molecular-biology/molecular-biology-learning-center/molecular-biology-resource-library/thermo-scientific-web-tools/multiple-primer-analyzer.html#/legacy=www.thermoscientificbio.com) by ThermoFisher and Tm Calculator (https://www.thermofisher.com/de/de/home/brands/thermo-scientific/molecular-biology/molecular-biology-learning-center/molecular-biology-resource-library/thermo-scientific-web-tools/tm-calculator.html) by ThermoFisher.
Degenerated primers were used to amplify DNA fragments with unknown precise nucleotide sequence of the target DNA. They contain a mixture of similar primer sequences that incorporate variations.
Primers were ordered from Sigma-Aldrich (Merck KGaA, Darmstadt, Germany) at a scale of 0,025 µmol and desalted.

2.4 Vectors

For complementation approaches in Arabidopsis the following vectors were used: For complementation with *Vc* GTs in Arabidopsis *mur3.1xlt2* pORE-E4 (Coutu et al., 2007) was used. For complementation with Hymenaea XXTs in Arabidopsis *xxt1xxt2* and *xxt1xxt2xxt5* pH2GW7 (Karimi et al., 2002) (ordered from VIB-UGent Center for Plant Systems Biology) and pGpGWB202 (Ishizaki et al., 2015) (pMpGWB202 was a gift from Takayuki Kohchi (Addgene plasmid #68593; http://n2t.net/addgene:68593 ; RRID:Addgene_68593)) were used.
For localization of *Vc* GTs in *Nicotiana benthamiana* pMDC83 (Curtis and Grossniklaus, 2003) and pVKH18En6:ST-RFP (Saint-Jore et al., 2002; Runions et al., 2006) were applied.
For work with *Pichia pastoris* the vectors pPICZ B (Invitrogen™, EasySelect™ Pichia Expression Kit, cat. no. K174001) and pPICZ eH (created from pPICZ B and BB3_eH14* from GoldenPICS Pichia Kit) were used as vectors for methanol-inducible intracellular expression of a protein at the AOX and 5'-*ENO1* genome integration region respectively.
pDONR207 was used as Gateway donor vector and pJET1.2 was used as positive selection cloning vector. Vector maps can be assessed in the appendix.

2.5 Enzymes

Restriction enzymes	All restriction Enzymes were purchased from ThermoFisher Scientific.

Xyloglucan-specific endo-beta-1,4-glucanase (XEG)	The XEG from *Aspergillus aculeatus* (Pauly et al., 1999) was used to solubilize XyG oligosaccharides from plant cell walls for further analysis.
Zymolyase	Zymolyase is a β-1,3 glucanase and β-1,3-glucan laminaripentao-hydrolase, hydrolyzes glucose polymers at the β-1,3-glucan linkages in yeast and fungal cell walls. Zymolyase, purchased from Roth (Zymolyase® 20T, cat. no. 9324.2, >20U/mg)
Pustulanase	thermostable β-1,6-endoglucanase, catalyses the cleavage of β-1,6 bonds in pustulan and other beta-glucans containing 1,6 linked glucose units, purchased from Prokazyme (CEL136, 3U/mg).
Cellulase (endo-1,4-β-D-glucanase) (Bacillus amyloliquefaciens) (E-CELBA)	E-CELBA was used for *endo*-hydrolysis of (1,4)-β-D-glucosidic linkages in cellulose, purchased from Megazyme (1,400 U/mL).
α-Amylase from *Bacillus sp*.	α-Amylase breaks down starch by hydrolysis of the α-(1,4) glucan linkages, purchased from Sigma-Aldrich (1500 U/mg, cat. no A6380).
Pullunanase (pullulan 6-alpha-glucanohydrolase) (*Bacillus licheniformis*) (E-PULBL)	Pullunanase for hydrolysis of (1,6)-α-D-glucosidic linkages (destarch), purchased from Megazyme (1000 U/ml)

Figure 2.1: Enzymes used in the scope of this thesis.

2.6 Bacteria and yeast strains

Escherichia coli was used for cloning and replication of plasmid DNA because of its relative simplicity and its rapid and inexpensive growth in the laboratory. *E. coli* has been studied for the last decades and can be considered the most extensively investigated prokaryotic model organism (Muhammad Kamran Taj et al., 2014). In general *E. coli* Top10F' were used for microbiology work like restriction cloning and plasmid retransformation. In other cloning projects like site directed mutagenesis (Ch. 2.9.8) or Gateway cloning (Ch. 2.9.7.4) *E. coli* One Shot ® MAX Efficiency® DH5α™ -T1 R Cells (cat. no. 12297016) from ThermoFisher Scientific were used. For retransformation of Gateway vectors, the *E. coli* strain DB3.1 was used, as this strain is resistant to the toxic effects of the *ccdB* gene.

For expression of genes of interest in *Pichia Pastoris* the strain X-33 from the Easy Select Pichia Expression Kit (Invitrogen) was used.

Agrobacterium tumefaciens strain GV3101 (pMP90) (Koncz and Schell, 1986) was used for plant transformations.

2.7 Plant strains and plant material

Arabidopsis thaliana was used as a dicot model plant. In the scope of this thesis Arabidopsis was used for complementation approaches similar to (Cavalier et al., 2008; Jensen et al., 2012; Schultink et al., 2013; Zhu et al., 2018) and for phenotypical analysis of TDNA lines (Gille et al., 2009; Goubet et al., 2009; Kim et al., 2020).

Arabidopsis ecotype Columbia (Col-0) was used as wild type. Arabidopsis double mutant *mur3.1 xlt2* (Jensen et al., 2012) was used as the background for the complementation approach of blueberry GTs. For the complementation approach with Hymenaea XXTs the double and triple mutants *xxt1xxt2* (Cavalier et al., 2008) and *xxt1xxt2xxt5* (Zabotina et al., 2012) were used, respectively. Further used Arabidopsis knock-out lines obtained from public sources (Nottingham Arabidopsis Stock Centre) were *cslc456812* (*cslc4-3* (SAIL_837B10), *cslc5-1* (SAIL_187G09), *cslc6-1* (SALK_088720-11), *cslc8* (WiscDsLox_497-02H), and *cslc12-2* (SAIL_168F02)) (Kim et al., 2020) and *xeg113* (*xeg113-2*, SALK_066991) (Alonso et al., 2003) as well as *csla2* and *csla9* (*csla2* (SALK_065083), *csla9* (SALK_071916)) (Goubet et al., 2009).

For determining subcellular localization of XyG biosynthetic enzymes Agrobacterium-mediated transient expression in *Nicotiana benthamiana* was used (Sparkes et al., 2006).

The Hymenaea leaf material used for experiments in the scope of this thesis was obtained from the Palmengarten Frankfurt from a 16-year-old tree (IPEN: XX-0-FRP-24326). After harvest, the leafs were immediately frozen and transported on dry ice. The plant material was obtained by Prof. Markus Pauly. The material was stored on -60 °C.

Blueberry plant material *V. corymbosum* bluecrop was obtained from Farm Vinnemann in Olfen, Germany.

2.8 Media, competent cells, stocks and growth conditions

2.8.1 Growth media

Media was prepared by sterilizing the various components (Fig. 2.2) by autoclaving or sterile filtering. For pouring of plates the agar containing medium was heated in a microwave until liquid, then cooled to ~60 °C. The appropriate volume of antibiotic from a stock solution was added to achieve the final antibiotic concentration. The medium was then mixed and ~20 mL was poured per plate. Plates were left to solidify and stored at 4 °C. Media for growth of *Pichia pastoris* was prepared according to the directions in the Easy Select Pichia Expression Kit manual (Invitrogen).

Media	Manufacturer	Contents
LB broth (Luria/Miller)	Roth (cat. no X968)	tryptone 10 g/l, yeast extract 5 g/l, sodium chloride 10 g/l, pH 7,0 ±0,2
LB agar (Luria/Miller)	Roth (cat. no X969)	tryptone 10 g/l, yeast extract 5 g/l, sodium chloride 10 g/l, agar-agar 15 g/l, pH 7,0 ±0,2
LB broth (Lennox) (low salt)	Roth (cat. no X964)	tryptone 10 g/l, yeast extract 5 g/l, sodium chloride 5 g/l, pH 7,0 ±0,2
LB agar (Lennox) low salt	-	Use LB broth (Lennox) (low salt) and add 3 g bacto agar (CAS no 9002-18-0) per 200 ml broth.
YPD (yeast extract peptone dextrose)	-	1% yeast extract (w/v), 2% peptone (w/v), 2% glucose monohydrate (w/v)
YPD agar	-	Use YPD and add 10 g bacto agar per 500 ml broth.
YPDS (yeast extract peptone dextrose sorbitol)	-	1% yeast extract (w/v), 2% peptone (w/v), 1 M sorbitol, 2% glucose monohydrate (w/vv)
YPDS agar	-	Use YPDS and add 10 g bacto agar per 500 ml broth.
BMMY (buffered complex methanol medium)	-	1% yeast extract (w/v), 2% peptone (w/v), 100 mM potassium phosphate pH 6.0*, 1.34% YNB**, 4 x 10^{-5}% biotin**, 0.5% methanol**
BMGY (buffered complex glycerol medium)	-	1% yeast extract (w/v), 2% peptone (w/v), 100 mM potassium phosphate pH 6.0*, 1.34% YNB**, 4 x 10^{-5}% biotin**, 1% glycerol**
Murashige and Skoog (MS) Media	Duchefa Biochemie	https://www.duchefa-biochemie.com/product/details/number/M0245

Figure 2.2: Growth media composition. LB was used for growth of *E. coli* and *A. tumefaciens*, YPD for growth of *P. pastoris* and MS for growth of *A. thaliana*. * stock solution autoclaved separately from other components. ** stock solution prepared by filter sterilization

Antibiotic	Concentration
Ampicillin	100 µg/ml (*E. coli*)
Gentamycin	25 µg/ml (*A. tumefaciens),* 100 µg/ml (*A. thaliana)*
Hygromycin B	100 µg/ml (*E. coli*), 200 µg/ml (*P. pastoris*), 25 µg/ml (*A. thaliana)*
Kanamycin	50 µg/ml (*E. coli, A. tumefaciens, A. thaliana*)
Rifampicin	50 µg/ml (*A. tumefaciens*)
Spectinomycin	50 µg/ml (*E. coli)*

Zeocin (cat. no. R25001)	25 µg/ml (*E. coli*), 100 µg/ml (*P. pastoris*)

Figure 2.3: Antibiotics used for selection. The antibiotics used for selection of transformants in the various systems listed with the concentrations used.

2.8.2 Competent cells

If available, the competent cells included in the kits were used (e.g. GeneArt™ Site-Directed Mutagenesis PLUS System by ThermoFisher). Otherwise, competent cells were prepared as follows:

2.8.2.1 Preparation of *E. coli* calcium competent cells

The desired *E. coli* strain was streaked out from frozen glycerol stock onto a LB plate without antibiotics and grown overnight at 37 °C. A single colony was selected to inoculate a 10 ml starter culture of LB broth without antibiotic and grown at 37 °C in shaker at 225 rpm overnight. 1 l of LB media was inoculated with the 10 ml starter culture and grown in 37 °C shaker at 225 rpm. At an OD_{600} of 0,35 to 0,4 the cells were put on ice and chilled for 20 to 30 minutes with occasional swirling. The 1 l culture was split into ice cold centrifuge bottles. The cells were harvested by centrifugation at 3000 g for 15 minutes at 4 °C. The supernatant was decanted and each pellet was gently resuspended in about 100 ml of ice cold 100 mM $MgCl_2$. Afterwards, all suspensions were combined into one centrifuge bottle. The cells were again harvested by centrifugation at 2000 g for 15 minutes at 4 °C. The supernatant was decanted and the pellet was resuspended in about 200 ml of ice cold 100mM $CaCl_2$. The suspension was chilled on ice for at least 20 minutes. The cells were harvested by centrifugation at 2000 g for 15 minutes at 4 °C. The supernatant was decanted and the pellet was resuspended in ~50 ml of ice cold 85 mM $CaCl_2$, 15 % glycerol (v/v). The suspension was transferred to an ice cold 50 ml conical tube. The cells were harvested by centrifugation at 1000 g for 15 minutes at 4 °C. The supernatant was decanted and the pellet was resuspended in 2 ml of ice cold 85 mM $CaCl_2$, 15 % glycerol. The suspension were aliquoted (50 µl) into sterile and ice cold 1,5 ml microfuge tubes and snap frozen with liquid nitrogen. The competent cells were stored in a -80 °C freezer.

2.8.2.2 Preparation of electrocompetent *P. pastoris* competent cells

The *Pichia pastoris* strain (5 ml) was grown in YPD in a 50 ml conical flask at 30 °C overnight. The next morning the overnight culture was diluted to an OD_{600} of 0,15 to 0,2 in 50 ml YPD in a 500 ml flask. The culture was grown to an OD_{600} of 0,8 to 1,0. The culture was split into 2 conical tubes and centrifuged at 500 g for 5 minutes at room temperature. The supernatant was decanted. The cell pellet was resuspended in 9 mL of ice-cold BEDS solution (10 mM Bicine-NaOH, pH 8,3, 3 % (v/v) Ethylene glycol, 5 % (v/v) Dimethyl sulfoxide, 1 M Sorbitol) supplemented with 1 ml 1,0 M dithiothreitol (DTT). The cells were incubated for 5 min at 100

rpm in the 30 °C shaking incubator. The cell suspension was centrifuged at 500 g for 5 min at room temperature and resuspend in 1 ml of BEDS solution. Aliquots of 40 µl were prepared in 1,5 ml tubes. The competent cells were directly used for transformation (Ch. 2.9.11) or slowly cooled down to -80 °C.

2.8.2.3 Preparation of *A. tumefaciens* competent cells

The *A. tumefaciens* strain GV3101 was streaked out from a frozen glycerol stock onto a LB plate and grown at 28 °C. A single colony was selected to inoculate a 3 ml starter culture of LB broth with antibiotics (Rifampicin and Gentamycin) and grown in a 50 ml falcon tube at 28 °C in shaker at 225 rpm overnight. The starter culture (1 ml) was used to inoculate 50 ml of LB in a 250 ml flask. The culture was grown to an OD_{600} of 0,5 to 1,0. The culture was chilled on ice for 5 to 10 minutes and centrifuged at 3000 rpm for 5 minutes on 4 °C. The supernatant was discarded and the cell pellet was washed in 10 ml of ice cold 1X TE buffer (10 mM TRIS-hydrochloride, pH 7,5, 1 mM Ethylenediaminetetraacetic acid (EDTA)). The cell suspension was centrifuged at 3000 rpm for 5 minutes at 4 °C. The supernatant was discarded and the cell pellet was resuspended in 2 ml ice cold 20 mM $CaCl_2$. The suspension was dispensed (100 µl) into chilled 1,5 ml tubes. The competent cells were stored in a -80 °C freezer.

2.8.3 Glycerol stocks

Glycerol stocks were prepared to store bacterial and yeast cultures for extended periods of time. Glycerol stocks of *E. coli* and *A. tumefaciens* cultures were prepared by mixing 812 µL of overnight liquid culture and 188 µL 80 % (v/v) glycerol in sterile Cryo Pure tubes (Sarstedt, 72.380) and kept at -80 °C for long term storage. Glycerol stocks for *P. pastoris* cultures were prepared by centrifuging 1 to 1,5 ml of overnight liquid culture at 500g. After decanting the supernatant, the cell pellet was resuspended in 812 µl of YPD medium. Glycerol (188 µl 80 % (v/v)) was added, the cells were carefully resuspended and the tubes were put on -80 °C.

2.8.4 Bacteria and yeast growth conditions

E. coli, *P. pastoris* and *A. tumefaciens* cells were grown on agar plates or in liquid medium containing the appropriate antibiotic to select cells. Liquid cultures were grown in a rotating shaker at 225 rpm, temperature was set to 37 °C for *E. coli*, 30 °C for *P. pastoris* and 28 °C for *A. tumefaciens*. *E. coli* and *Agrobacterium* were grown in or on LB media while Pichia was grown in or on YPD media. For expressing recombinant Pichia strains following the EasySelect™ Pichia Expression Kit the yeast was grown from 24 to 72 hours in BMGY (buffered complex glycerol medium) followed by 24 to 96 hours in BMMY (buffered complex methanol medium) (Fig. 2.2). To test glucan production Pichia strains were grown in BMGY for 72 h followed by 24 hours of growth in BMMY. To test for xylosylation Pichia strains were grown in BMGY for 72 h and 96 hours in BMMY. While growing in BMMY the media was either

renewed after 24 h by centrifugation of the culture and resuspension in fresh BMMY, or 0,5 % sterile MeOH were added.

2.8.5 Plants

2.8.5.1 Sterilization of *A. thaliana* seed surface with ethanol/triton X-100

For sterilization of the Arabidopsis seed surface, seeds were incubated with 1 ml 70 % ethanol containing 0,1 % Triton X-100 (v/v) for 7 minutes at room temperature and vortex-mixed frequently. The liquid was removed and the seeds were washed five times with sterile water for about one minute. Afterwards the seeds were ready for stratification (Ch. 2.8.5.3).

2.8.5.2 Sterilization of *A. thaliana* seed surface with chlorine gas

Because of the hazardous gas in this experiment, the procedure was performed in a desiccator jar in a fume hood. The seeds were placed in 1,5 ml tubes. The tubes were placed in a rack which was put in the desiccator. In a 250 ml glass beaker in the desiccator 100 ml bleach was mixed with 3 ml concentrated Hydrogen chloride (HCl). The desiccator was sealed with parafilm and left to incubate without moving for 2 to 4 hours. Afterwards, the desiccator was opened (still under the fume hood) and left to ventilate for 15 to 30 minutes. Afterwards the seeds were ready for stratification (Ch. 2.8.5.3).

2.8.5.3 Stratification of Arabidopsis seeds

Arabidopsis seeds were resuspended in 1 ml sterile water/0,1 % agarose or plated on ½ MS plates and stored in the fridge for 2 to 4 days.

2.8.5.4 Growth of *A. thaliana* on soil

The sterilized (Ch. 2.8.5.1 & 2) and stratified (Ch. 2.8.5.3) seeds were put on water-saturated soil and placed in the Celltherm growth chamber with 16 hours light, 8 hours dark at 20/19 °C (day/night) with 40/75 % (day/night) humidity or in a Phytotron 16 hours light, 8 hours dark at 21 °C with 70 % humidity (for phenotyping). Plant trays with freshly sowed or transferred Arabidopsis was covered with a lid for the first 3 to 7 days. The plants were watered as needed and fertilized with Miracle Gro All-Purpose Soluble Plant Food as recommended by the manufacturer.

2.8.5.5 Growth of *N. benthamiana* on soil

Seeds were put on water-saturated soil and placed in the Celltherm growth chamber with 12 hours light/12 hours dark at 20/19 °C (day/night) with 40/75 % (day/night) humidity. The plant tray was covered with a lid and the plants were transferred to bigger pots two weeks after germination. The plants were watered as needed.

2.8.5.6 Growth of *A. thaliana* on plates

½ MS plates were prepared by dissolving Murashige & Skoog medium in water. The pH was adjusted to 5,6 using 1 M KOH. Plant agar was added, and the solution was autoclaved. After autoclaving 2% (w/v) sucrose was added to the liquid solution. For selection plates an antibiotic was added at an appropriate temperature. The medium was poured on Petri dishes.
For selection of seedlings after transformation using Agrobacterium (Ch. 2.9.16) sterilized and stratified seeds were sown on MS plates and placed into a Percival plant growth chamber or a Celltherm growth chamber with 16 hours light and 8 hours dark for 10 to 14 days. Seedlings with resistance to the antibiotic were afterwards transferred to soil for further growth (Ch. 2.8.5.4).
For growth of etiolate Arabidopsis hypocotyls sterilized and stratified seeds sown on MS plates (without antibiotics) were exposed to light for 2 to 3 hours to stimulate growth. The plates got wrapped in 3 layers of aluminium foil and placed on 21 °C for 5 days. The etiolated hypocotyls were afterwards photographed and measured using Fiji/ImageJ or used for XyG analysis (Ch. 2.11).
To prevent contamination with fungi or bacteria the plates were sealed with 3M™ Micropore™ tape (VWR, cat. no. 115-8172).

2.8.5.7 Crossing of *A. thaliana*

Mature siliques, open flowers and buds that have already a white tip were removed from the inflorescence of the mother plant with fine scissors or forceps. The meristem with buds that were too small were also removed. Flower buds were opened by inserting the tip of one pair of forceps between petals and sepals. The petals, sepals, and anthers were removed. A mature flower from the father plant was taken with forceps and the petals, sepals and the pistil were removed. An anther with visible pollen shedding from the father plant was tapped on the stigma of the mother plant and covered with pollen grains.

2.9 Molecular biology techniques

2.9.1 Extraction of genomic DNA from plant material

Plant material was collected in 1,5 ml tubes. Small glass beads (3) were added, and the plant tissue was grinded in a Retsch Mill (MM 400) for 1 minute at 30 Hz. After a quick spin down 500 µl extraction buffer (100 mM Tris-HCl pH 8,0, 50 mM EDTA, 100 mM sodium chloride (NaCl), 0.35 % (w/v) sodium dodecyl sulphate (SDS)) was added, and the samples were vortexed. Ice-cold 5 M potassium acetate (130 µl) was added and the tubes were invert several times. After centrifugation at 15.000 g for 15 minutes 450 µl of the supernatant was transferred to a new tube. Ice-cold isopropanol (350 µl) was added and the samples were mixed by inverting. The samples were centrifuged at 16.000 g for 10 minutes to pellet the DNA. The

supernatant was discarded and the DNA pellet was washed with 500 µl 70 % EtOH. The samples were centrifuged at 16.000 g for 5 minutes and the supernatant was carefully removed using a pipette. The DNA pellet was dried and resuspended in 100 µl TE buffer. For optimal results the samples were stored in the fridge overnight.
In an alternative experimental setup, a 96 well plate was used to scale up the throughput. The first steps were performed as mentioned above. The 450 µl supernatant were then transferred to a 96 well plate and 350 µl of cold isopropanol was added. The plate was mixed by inverting. The well plate was centrifuged at 4000 rpm for 10 minutes to pellet the DNA. The supernatant was removed using a multichannel pipette. The samples were washed with 750 µl 70 % EtOH. The well plate was centrifuged again (4000 rpm, 10 min) and the EtOH was removed using a multichannel pipette. The leftover EtOH was dried by placing the well plate in an incubator for 10 minutes at 50 °C. The DNA pellet was resuspended in 100 µl TE buffer and the plate was placed on 50 °C for another 10 minutes. The well plate was carefully vortexed and stored in the fridge overnight. The next day the samples were transferred to a 96 PCR plate.

2.9.2 DNA extraction by anion exchange chromatography

DNA extraction chromatography for purification of high molecular weight DNA was performed using the NucleoBond HMW DNA kit by Macherey-Nagel (cat. no. 740160.20) according to the manufacturer's manual except for the following modifications: The lysis incubation was extended to 1 h and the samples were mixed by inverting every 15 min during this incubation. The extraction was performed on 1 g of plant material grinded to fine powder by Retsch Mill. Wide Orifice Pipette Tips and Eppendorf DNA LoBind 1,5 ml tubes (cat. no 022431021) were used to protect the DNA and maximise the extraction outcome.

2.9.3 DNA quantification

The DNA content of samples was measured using an Eppendorf BioSpectrometer (µCuvette® G1.0, standard dsDNA settings) and in some cases an Invitrogen Qubit 3 with dsDNA broad range measurement settings.

2.9.4 Concentration of DNA

DNA samples were concentrated using the Zymoclean Clean & Concentrator Kit (cat. no. D4003). The procedure was carried out according to the manufacturer's manual. To reduce the loss of DNA during the process the final elution and centrifugation were repeated.

2.9.5 Amplification of genes for cloning using PCR

Phusion™ High-Fidelity DNA-Polymerase (ThermoFisher, cat. no. F530S) was used for amplification of DNA sequences for plasmid construction. The manufacturer's recommendations were followed initially, with alteration of extension time and annealing temperature as recommended by the Tm Calculator by ThermoFisher (Ch. 2.2). To increase

the final copies of DNA a combination of a 2-step 3-step protocol (3-step: denaturation, annealing and extension, 2-step: combines the annealing and extension) in the manufacturer's manual was used. Furthermore, GC buffer (ThermoFisher, cat. no. F539L) and DMSO were used for GC-rich amplicons.

2.9.6 Gel electrophoresis and gel extraction

Gel electrophoresis was used for separation and analysis of DNA. The sizes of the separated DNA fragments were determined by comparison to the ready-to-use Gene Ruler 1kb DNA Ladder (Thermo Scientific™, cat. no. SM0313), GeneRuler 100 bp (Thermo Scientific™, cat. no. SM0241) or 1 Kb Plus DNA Ladder (Invitrogen™, cat. no. 10787018). DNA was detected by the fluorescent nucleic acid dye GelRed™ (2,5 µL per 50 mL gel). Samples without dye from previous experiments (samples not produced with Red Taq DNA Polymerase Mix (Ch. 2.9.12), green Phusion Buffer (Ch. 2.9.5) or FastDigest Green Buffer (supplied with the enzymes from ThermoFisher) were mixed with Gel Loading Dye (Purple (6X) by NEB, cat. no. B7024S). Usually 1 % agarose in 1 x TAE buffer was used for the electrophoresis, which was performed at 110 V for 35 min to 45 minutes or at 90 V for 60 minutes. For improved separation, the period was extended if necessary. The DNA bands were visualized using the BioRad ChemiDoc™ XRS+.
For extraction of DNA fragments that were separated by gel electrophoresis the Zymoclean Gel DNA Recovery Kit (cat. no. D4002) was used following the manufacturers manual. To increase the gain of DNA the final elution and centrifugation were repeated.

2.9.7 Cloning strategies

2.9.7.1 pJET cloning

The CloneJET™ PCR Cloning Kit with DH10B Competent Cells (Thermo Scientific™, cat. no K123120) was used for high efficiency cloning in positive selection cloning vector pJET1.2/blunt following the manufacturers manual.

2.9.7.2 Restriction/Ligation cloning

Plasmid (backbone) and a linear DNA fragment (insert) were digested creating sticky ends with appropriate FastDigest DNA restriction enzymes (Fig. 2.1) from ThermoFisher following the manufacturer's recommendations with the FastDigest Green Buffer (10X) supplied with the enzymes. The vectors were dephosphorylated using Thermo Scientific™ FastAP Thermosensitive Alkaline Phosphatase (Thermo Scientific™, cat. no. EF0654). The digested products were purified by gel electrophoresis and gel extraction (Ch. 2.9.6) or using the Zymo DNA Clean & Concentrator kit. The purified products were ligated using Thermo Scientific T4 DNA Ligase (NEB, cat. no. M0202S) following the sticky-end ligation protocol to ligate a DNA insert into vector DNA. A molar ratio of 1:3 DNA insert to vector backbone was used. Incubation

time and temperature verified, optimal results were achieved by overnight incubation at 4 °C. The ligation reaction was then used to transform competent *E. coli.*

2.9.7.3 Cloning of multimer constructs in *Pichia Pastoris* vectors

Vectors containing multiple expression cassettes were produced by cutting the expression cassette (AOX promotor pAOX1, gene of interest GOI and transcription terminator TT) from one vector and ligating it into a linearized vector containing the second expression cassette (Fig. 2.4). This process was repeated until all desired expression cassettes were inserted. Restriction enzymes FD BamHI and FD BglII were used based on the instructions in the manual of the Multi-Copy Pichia Expression Kit (Invitrogen™, cat. no. K175001).

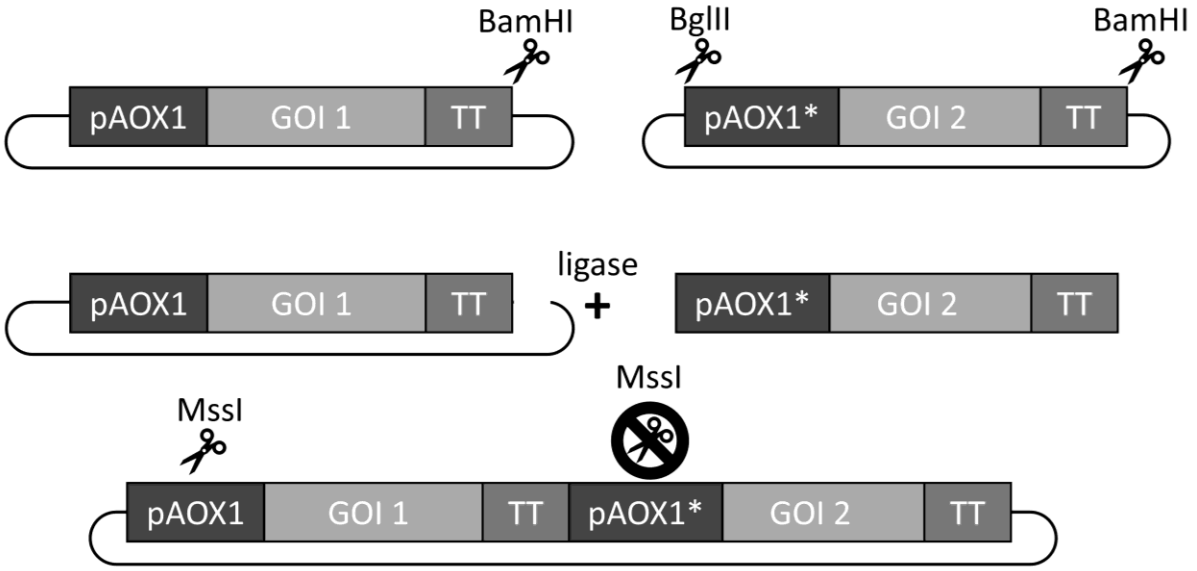

Figure 2.4: Cloning strategies of multimer constructs. Restriction enzyme cut sites are symbolised by scissors. One Pichia vector is linearized behind the expression cassette. The expression cassette including a modified pAOX1 of a second Pichia vector is cut out. The expression cassette is integrated into the linearized vector. The construct is linearized by MssI for transformation into Pichia.

2.9.7.4 Gateway cloning

Gateway cloning was used as an alternative cloning method to restriction cloning and is only compatible with Gateway vectors. It is based on the site-specific recombination properties of bacteriophage lambda (Landy, 1989). Lambda integration into the *E. coli* chromosome occurs via intermolecular DNA recombination between specific attachment (att) sites on the interacting DNA molecules. The genes of interest were amplified with primers containing attB1 and attB2 sites. The BP Reaction which facilitates the recombination of an attB substrate (attB-PCR product) with an attP substrate (donor vector pDONR207) to create an attL-containing entry clone was catalysed by Gateway™ BP Clonase™ II Enzyme mix (ThermoFisher, cat. no. 11789020) according to the manufacturers protocol. After verification of the pDONR + gene of interest via sequencing (Ch. 2.9.14) the LR Reaction was performed to facilitate recombination

of an attL substrate (entry clone) with an attR substrate (destination vector) which creates an attB-containing expression clone. This reaction is catalysed by Gateway™ LR Clonase™ II Enzyme mix (ThermoFisher, cat. no. 11791020). The resulting expression clone was also verified via sequencing (Ch. 2.9.14).

2.9.8 Site directed mutagenesis

Site directed mutagenesis (SDM) was performed to remove sites of restriction enzymes from genes of interest for restriction cloning (Ch. 2.9.7.2) and cloning of multimere constructs (Ch. 2.9.7.3). SDM was performed using the GeneArt™ Site-Directed Mutagenesis PLUS System (ThermoFisher, cat. no. A14604) following the manufacturer's protocol with primers designed with GeneArt® Primer and Construct Design Tool by ThermoFisher (https://www.thermofisher.com/order/oligoDesigner/) and a PCR setup adjusted to Phusion™ High-Fidelity DNA-Polymerase (ThermoFisher, cat. no. F530S).

2.9.9 Heat-shock transformation of E. coli

The following heat-shock transformation was used to transform TOP10'F and DB3.1 *E. coli*. Other *E. coli* strains (Ch. 2.6) were transformed as recommended by the manufacturer's manual.

For heat-shock transformation, 50 µl of TOP10F' (or other *E. coli* strains) competent cells were taken from a -80 °C freezer and placed on ice. After defrosting (about ten minutes) 5 µl of ligation reaction or 10 pg to 100 ng plasmid DNA (maximum 5 µl) were directly added to the competent cells and mixed by gently tapping. The cells were then incubated on ice for 30 minutes. The tubes with the cells were then incubated for exactly 30 seconds in a 42 °C water bath and afterwards placed on ice for 2 minutes. 500 µl of (low salt) LB medium was added to each tube which were then incubated horizontally for 60 minutes at 37 °C and 225 rpm. 200 µl (variable) of each transformation reaction was plated on (low salt) LB plates supplemented with appropriate antibiotics for selection. The plates were sealed with micropore tape and incubated overnight at 37 °C, in the dark.

2.9.10 Freeze and thaw Transformation of *A. tumefaciens*

Electrocompetent *A. tumefaciens* (strain GV3101) stocks were taken from a -80°C freezer and placed on ice for defrosting. Plasmid (1 µg) was added to 100 µl of bacterial suspension and gently mixed. The cells were then frozen in liquid N2 for 2 minutes and thawed up on 37 °C for 5 minutes. Afterwards 1 ml of LB medium was added, and the tubes were incubated for 2 hours at 28 °C shaking at 400 rpm. The tubes were centrifuged for 5 minutes at 6000 rpm and the resulting cell pellet was resuspended in 100 µl of LB medium after removing the supernatant. The suspension was plated on LB plates with the appropriate antibiotics and incubated for 2 days at 28 °C.

2.9.11 Transformation of *P. pastoris* by electroporation

The electrocompetent Pichia cells were mixed with 4 µl of MssI/PmeI linearized DNA and transferred to an ice-cold 0,2 cm gap electroporation cuvette. The cuvette with the cells was incubated on ice for 2 minutes. The samples were electroporated at a charging voltage of 1500 V (resistance 200 Ω; capacitance 25 µF). 1 ml of 1:1 (v/v) sorbitol and YPD medium were immediately added to the cuvette. Transfer the cuvette contents to a sterile culture tube and incubate in a 30 °C shaker for 1 h at 225 rpm. Either 100 µl were directly spread on YPD or YPDS plates containing the appropriate antibiotic, or the samples were centrifuged at 500 g for 5 minutes, the supernatant was removed and the pellet was resuspended in 100 µl YPD medium and the spread on a plate. The plates were incubated for multiple days at 30 °C.

2.9.12 Red Taq DNA Polymerase PCR

Red Taq DNA Polymerase (2X Master Mix 1,5 mM MgCl2, cat. no. 733-1320P) was used for colony, genotyping, and pJET cloning (Ch. 2.9.7.1) PCRs. For colony PCR a pipet tip of cell culture of transformed organism (*E. coli*, Pichia, Agrobacterium), and for genotyping experiments (Arabidopsis transformants, Arabidopsis T-DNA insertion lines, Pichia) and PCRs for pJET cloning (Hymenaea candidate genes) 1 to 2 µl gDNA (or plasmid) was used as template. Forward and reverse primers were added in a final concentration of 0,2 µM (0,1 - 1,0 µM). PCR-grade water was added until the 2x master mix was diluted to a final concentration of 1x. In some PCRs DMSO was added for enhanced PCR amplification and increased specificity and yield of the PCR reaction.
The cycling conditions were based on the manufactures protocol: 2 minutes at 95 °C initial denaturation, 25 to 35 cycles of 20 - 30 seconds denaturation at 95 °C, 20 - 40 seconds annealing 57°C (can be adjusted to 50 - 65 °C depending on the annealing temperature of the primers), one minute per 1000 bp of elongation at 72 °C, final elongation at 72 °C for 5 min.

2.9.14 DNA sequencing

Sanger sequencing and whole plasmid sequencing by Eurofins Genomics was used to determine the sequence of PCR products and plasmids. For sanger sequencing purified DNA (PCR products: 150-300 bp 5 ng, 300-1000 bp 25 ng, 1000-3000 bp 50ng; plasmid: 250-500 ng) was combined with 25 pmol of the appropriate primer in 10 µl total volume.
For whole plasmid sequencing 300 ng of plasmid in a volume of 10 µl were sent to Eurofins Genomics. Sequencing results were downloaded from Eurofins Genomics website and the obtained sequences were aligned to *in silico* generated DNA templates via the alignment tool feature of Benchling (Ch. 2.2).

2.9.15 DNA isolation of *P. pastoris*

DNA from *P. pastoris* was isolated using the *Quick*-DNA Fungal/Bacterial Miniprep Kit (Zymo Research, cat. no. D6005). Pichia liquid cultures were centrifuged at 500 g for 5 minutes at room temperature. The supernatant was removed and the pellet was resuspended in 200 µl water. After transferring the cell suspension in a ZR BashingBead™ Lysis Tube and adding 750 µl BashingBead™ Buffer, the cells were grinded using a Retsch mill at 30 Hz for 5 minutes. The miniprep was then continued following the manufacturer's instructions and finally eluted in 50 µl DNA elution buffer. To maximise the gain of DNA the final elution and centrifugation were eventually repeated.

2.9.13 Plasmid DNA extraction

Plasmid DNA was extracted from *E. coli* liquid cultures after overnight growth using the Zyppy Plasmid Miniprep Kit (Zymo Research, cat. no. D4019) following the manufacturer's manual. To maximise the yield of DNA the final elution and centrifugation were repeated.

2.9.16 Transformation of *A. thaliana* using Agrobacterium

This method was adapted from (Clough and Bent, 1998). The Agrobacterium strain carrying a suitable binary vector was used to inoculate 5 ml LB medium (with antibiotics that select for both the Ti and the T-DNA plasmids) and incubated at 28 °C with vigorous agitation. This culture was used to inoculate 200 ml of LB medium (with antibiotics that select for both the Ti and the T-DNA plasmids) and incubated again with vigorous agitation for an additional 24 hours at 28 ºC. The Agrobacterium cells were pelleted by centrifuging at 5000 rpm for 15 minutes at room temperature. The cell pellet was resuspended in 200 ml of infiltration medium (0,5xMS, 5 % Sucrose, 10 µl/l 6-benzylaminopurine solution (1 mg/ml in DMSO, cat. no. B3274), 0,02% Silwet L-77 (dimethylsiloxane-ethylene oxide block copolymer, 75% viscosity; abrc AB 111806)). The Agrobacterium suspension was incubated in the dark on room temperature for 3 hours. Afterwards the suspension was transferred to a convenient vessel for dipping plants that just started flowering. The inflorescence shoots were submerged in the suspension for about 30 seconds. After dipping, the plants were covered individually in transparent plastic bags and watered to retain humidity. After 24 hours the transparent covers were cut to enable a slow decrease in humidity. After another 24 hours the plastic covers were removed. Seeds were collected about two weeks after the transformation.

2.9.17 Transient expression in *Nicotiana benthamiana*

Transient expression of proteins for sub-cellular localization studies in *A. tumefaciens* was performed as described by Sparkes et al. (Sparkes et al., 2006).
Agrobacterium strains containing the desired transgene were grown in LB medium containing the appropriate antibiotics overnight shaking 200 rpm at 28 °C. The Agrobacterium cells were

collected by centrifugation at 4.000 g for 10 min and resuspended in infiltration buffer (10 mM 2-(N-morpholino) ethanesulfonic acid pH 5,6, 10 mM $MgCl_2$, 100 µM acetosyringone) to a final OD600 of 1. The infiltration suspension was incubated in the dark for 3 hours without shaking on room temperature. The abaxial surface of 4 to 6 weeks old *N. benthamiana* plants was infiltrated using a syringe (without needle) after removing the wax cuticle by gentle rubbing. The infiltrated leaf areas were imaged one to three days after infiltration.

2.9.18 Identification of Homologous Gene Sequences by PCR

This method is used to identify unknown members of a gene family or orthologous genes from different organisms without genomic information (Lang and Orgogozo, 2011). Sequences of the proteins from other species were aligned to search for conserved regions (tools see Ch. 2.2). Degenerate primers, a mixture of similar oligonucleotides, were designed based on the identified conserved regions and used to amplify a part of the gene of interest in the desired species. PCR products were cloned into pJET (Ch. 2.9.7.1) and sequenced. To then identify the less conserved regions at the 5' and 3' ends of the gene of interest DNA was cut using restriction enzymes creating sticky ends, ligated into circular DNA molecules and then used as a template for PCRs with (degenerate) primers directed outwards from the known DNA region. Nested PCRs, which involve two primer sets and two successive PCR reactions, were used to improve the sensitivity and specificity. The first set of primers was designed to anneal to sequences upstream from the second set of primers and were used in an initial PCR reaction. The PCR results with the unknown regions were sequenced and the known sequence was extended with the new sequence information (Nazir et al., 2019).

2.9.19 Extraction of RNA from plant tissue and Synthesis of cDNA from RNA

RNA was extracted from blueberry material using the Plant/Fungi Total RNA Purification kit from Norgen (Thorold, Canada, cat. no. 25800) following the manufacturer's protocol. cDNA was synthesized using iScript™ Reverse Transcription Supermix (cat. no. 1708840) following the manufacturer's protocol.

2.10 Microscopy

For imaging of transient expression in *N. benthamiana* the Olympus FV3000 Confocal Laserscanning (DFG-INST 1358/44-1 FUGB) of Center for Advanced Imaging (CAi) at Heinrich Heine University Düsseldorf was used with the help of Dr. Sebastian Hänsch. Etiolated hypocotyls were imaged using a Leica DM 2000 LED.

2.10.1 Propidium iodine staining

Etiolated hypocotyls were stained in a 10 µg/ml propidium iodide for 30 minutes. Afterwards the hypocotyls were carefully washed in water two times and imaged using a Leica DM 2000 LED (TXR (Excitation: 560/40, Emission: 630/76)).

2.11 Plant and hypocotyl phenotyping

Arabidopsis plants were phenotyped by measuring and comparing their stem height six to eight weeks of growth on soil. The plants were either measured with a ruler or photographed and afterwards measured with the image processing software Fiji (Ch. 2.2).

2.12 Analytical methods

2.12.1 Preparation of alcohol insoluble residue (AIR) from plant tissue

Cell wall isolation was essentially performed as shown in (Günl et al., 2010). To prepare AIR material three- to five-week-old Arabidopsis leaves, 2-week-old seedlings or etiolated Arabidopsis hypocotyls were collected. For some downstream experiments the plant material was also freeze dried (e.g. monosaccharide analysis). The plant material was grinded in a Retsch mill using glass or steel balls. A short centrifugation (and potential removal of the steel balls) was followed by an extraction with 70 % (v/v) aqueous ethanol and one (to three) washes with chloroform:methanol (1:1) and a wash with acetone. Afterwards the AIR material was dried in a desiccator using vacuum or in a heatblock (Dri-Block DB200/3) at 45 °C.

2.12.2 Preparation AIR from yeast

After growth of Pichia in BMGY/BMMY (Ch. 2.8.4) the cells were harvested by spinning for 2 min at 10000 g in screw cap tubes. Afterwards, 2 small scoops of glass beads (Sigma G8772) were added to each pellet. The tubes containing the cell pellet and glass beads were grinded at 30 Hz for 2:30 minutes at room temperature using a Retsch mill. The pellets were resuspended in 1 ml 70% ethanol by vortexing. After spinning for 2 minutes at 10000 g the supernatant was decanted and the pellet was resuspended in 1 ml of chloroform:methanol (1:1 v/v) by milling 1 min at 30 Hz. The tubes were spun again for 2 minutes at 10.000 g and the supernatant was removed. The cell pellet was resuspended in 1 ml of acetone by vortexing. Spinning and removing of supernatant was performed as described before. The pellet was again resuspended in 300 µl acetone by vortexing. Pichia AIR material in acetone (100 µl) was dried in glass tubes (threaded glass tubes, 100x13 mm, behr, cat. no. 6059727) and used for linkage analysis (Ch. 2.12.8).

2.12.3 Analysis of XEG-released oligosaccharides by OLIMP on plant material

Matrix-assisted laser-desorption ionization time of flight mass spectrometry (MALDI-TOF MS or XyG oligosaccharide mass profiling (OLIMP)) was performed on *A. thaliana* leave material (Günl et al., 2010; Jensen et al., 2012). Small steel balls (3) were added to the tube containing the leave. The tubes were milled for 1 min at 30 Hz in a Retsch mill. Afterwards the tubes were spun down and the plant pellet was resuspended in 1,5 ml 70 % ethanol. The steel balls were removed using a magnet. The samples were centrifuged at 20.000 g for 10 min and the supernatant was discarded. The pellet was resuspended the 1,5 ml chloroform:methanol (1:1, v/v). The tubes were sentrifuged again and the supernatant was discarded. The chloroform:methanol wash was repeated. The pellets were dried in a desiccator under vacuum for 30 minutes. The pellet was resuspended in 46 µl of 25 mM Ammonium formate buffer pH 4,5. 4 µl. Xyloglucan-specific endo-beta-1,4-glucanase (XEG, 0,05 U/µl) was added and the samples were incubated for a minimum of 1 hour at 37 °C in a shaker (600 rpm). After incubation the samples were spun down at 14.000 rpm for 5 min. The supernatant was used for spotting or further diluted before spotting. Matrix (1 µl, 10 mg/ml 2,5-Dihydroxybenzoic acid in 50 mM NaCl) was spotted onto a target plate (MTP 384 polished steel) and dried under vacuum. The XEG-digested supernatant (1 µl) was added onto the dried DHB and dried under vacuum. A MALDI-TOF mass spectrometer (Bruker Daltonik, Rapiflex; positive polarity; ion source 20.000 kV; smartbeam 3D laser) was used to obtain the mass profiles of released XyG oligosaccharides.

2.12.4 Solid phase extraction

Solid Phase Extraction (SPE) was used for rapid and selective sample preparation and purification of XyG oligosaccharides, prior to analysis by MALDI-TOF MS or injection onto High-performance anion-exchange chromatography (HPAEC) equipped with a pulsed amperometric detector (PAD). The dried down supernatant obtained from XEG digestion of plant material was resuspend in 2 ml MilliQ water. The Supelclean™ ENVI-Carb™ SPE Tubes (Supelco, cat. no. 1 ml: 57109-U, 3ml: 57088) were conditioned using two column volumes of 50 % acetonitrile. Afterwards the columns were equilibrated using two column volumes of MilliQ water. The sample was applied and washed once with one column volume. The samples were eluted using 1 or 2 ml 50 % Acetonitrile and dried under N_2 gas at 45 °C.

2.12.5 Analysis of oligosaccharides by OLIMP on yeast material

This protocol was developed by a previous lab member, Dr. Balakumaran Chandrasekar.
After Pichia growth and induction in BMGY (72h) and BMMY (96h) (Ch. 2.8.4) the 4 ml cultures were spun down and the supernatant was removed. Cell pellets of five 4 ml cultures were pooled in a 2 ml screw cap tube.

To prepare the ethanol insoluble fraction 1 ml of 70 % of ethanol and four small spoons of glass beads (glass beads, acid-washed, 425-600 µm) were added to the Pichia cells. The cells were grinded at 30 Hz for 2,5 minutes. The samples were centrifuged, and the supernatant was discarded.

For the alkali insoluble fraction 1,5 ml of 1M NaOH/10 mM NaBH4 were added to the Pichia cells and the cells were resuspended by grinding at 30 Hz for 2,5 minutes. The samples were incubated in a heatblock at 75 °C at 1400 rpm for one hour. To neutralize the reaction 160 µl of 50 % acetic acid were added to the samples and mixed by vortexing. The samples were centrifuged at maximum speed for 20 min at room temperature and the supernatant was discarded. The pellet was resuspended in 1 ml water by grinding with a Retsch mill. After centrifugation the supernatant was discarded and the water wash was repeated. The pellet was washed in 100 mM Potassium phosphate buffer by adding 1 ml of the buffer, resuspending the pellet, centrifugation and discarding the supernatant.

For Zymolyase (Fig. 2.1) digest the pellet was resuspended in 800 µl 100 mM Potassium phosphate buffer pH 6,5 and 200 µl of sodium azide (0,01 mg/ml) and 10 µl of Zymolyase (Zymolyase® 20T, cat. no. 9324.2, >20 U/mg) enzyme (2,5 U/ul) and incubated at 45 °C overnight. The next morning the samples were centrifuged and the supernatant was removed. The pellet was again resuspended in 800 µl of 100 mM Potassium phosphate buffer pH 6,5 and 200 µl of sodium azide (0,01 mg/ml) and 10 µl of Zymolyase enzyme and incubated for about 8 hours at 45 °C. The samples were centrifuged and the supernatant was removed.

For the Pustulanase digest the pellet was resuspended in 800 µl of 100 mM Potassium phosphate buffer pH 6,5 and 200 µl of sodium azide and 5 µl of Pustulanase (Prokazyme, cat. CEL136, 3 U/mg) enzyme (0,25 U/µl) and incubated at 60 °C overnight. The next morning the samples were centrifuged and the supernatant was removed. The pellet was again resuspended in 800 µl of 100 mM Potassium phosphate buffer pH 6,5 and 200 µl of sodium azide and 5 µl of Pustulanase and incubated for about 8 hours at 60 °C. The samples were centrifuged and the supernatant was removed.

The pellet was washed with 1 ml water and resuspended in 250 µl of water and 3 µl of E-CELBA enzyme (E-CELBA, megazyme, 1400 U/ml). The samples were incubated at 40 °C. After incubation the samples were centrifuged and the supernatant was transferred to a new tube. 1 µl of digest was spotted onto 1 µl of dried DHB matrix and shot in MALDI-TOF using the same conditions as in Ch. 2.12.3

2.12.6 Reduction of XEG released oligos

The supernatant of a XEG digest (Ch. 2.12.3) was dried down with a SpeedVac at 45 °C. Ammonium hydroxide (1 M) containing 10 mg/ml sodium borohydride (200 µl) were added and mixed by vortexing. After incubation on room temperature for 1 h the samples were neutralized

with 150 µL glacial acetic acid. Afterwards the samples were purified using SPE (Ch. 2.12.4) and further analysed using HPAEC PAD (Ch. 2.12.7) or HPLC-ELSD (Ch. 2.12.9).

2.12.7 Analysis of XEG-released oligosaccharides using HPAEC-PAD

Oligosaccharides of XEG digested Arabidopsis material were reduced (Ch. 2.12.6) and purified using SPE (Ch. 2.12.4). The XEG-released oligosaccharides were analysed and separated for further experiments by HPAEC PAD (IC Amperometric Detector, Metrohm, Dionex™ CarboPac™ PA200-IC-Column, sample loop volume 25 µl, injection volume 10 µl, flow rate 0,4 ml/min, linear gradient of 100 % 100 mM NaOH to 100 % 80 mM sodium acetate in 100 mM NaOH in 22 minutes, linear gradient from 100 % 80 mM sodium acetate in 100 mM NaOH to 100 % 100 mM NaOH in 4 minutes, flush with 100 % 100 mM NaOH for 6 min). For downstream experiments samples were neutralized with 0,5 M sulfuric acid, desalted using a Metrohm Suppressor Modul (MSM HC-A 6.2842.000) and collected. As standard a XyG oligosaccharide mixture (O-XGHON, by Megazyme) was used.

2.12.8 Glycosidic Linkage

All samples for linkage analysis were dried before the analysis. Stirring bars and all glassware for the steps prior to and during methylation were heat-dried (>1 h at 100 °C).
A small stirring bar was added to each sample tube and 200 µl dry DMSO (DMSO stored with silica gel) was added using a dry graduated glass pipette. The tubes were closed, vortexed and sonicated for 15 minutes. Afterwards the samples were stirred overnight at room temperature at 200 rpm.
For the next step sodium hydroxide (NaOH) in DMSO was prepared by the following steps: Dry methanol (200 µl, MeOH stored with silica gel) and 140 µl of 50 % NaOH were added to glass tubes and vortexed. Dry DMSO (5 ml) was added with a graduated glass pipette, vortexed and sonicated for 5 minutes. The tubes were centrifuged for 2 min at 2000 rpm and the DMSO supernatant was removed with a glass Pasteur pipette. The steps from adding 5 ml dry DMSO until removing the DMSO supernatant were repeated for a total of 4 times (or until solution was clear). Dry DMSO (2,8 ml) were added, the tubes were vortexed and sonicated again.
After overnight incubation 200 µL of prepared NaOH/DMSO (vortexed and sonicated one final time before use) was added to the samples with graduated glass pipette. The tubes were stirred for 15 minutes at room temperature (200 rpm). Methyl iodide (iodomethane, CH_3I, 100 µl) were added with a 100 µl glass syringe. Nitrogen atmosphere was added, the tubes were closed, vortexed and stirred for at least 2,5 hours at room temperature.
After this incubation the samples were sonicated for 5 min. Water (2 ml) was added to quench the reaction and the samples were vortexed. Afterwards a stream of nitrogen was flushed through the samples using a 230 mm Pasteur pipettes until the solution became a clear,

layerless solution. Dichloromethane (methylene chloride, CH_2Cl_2, 2ml) was added and the samples were vortexed. The samples were centrifuged for 2 min at 2000 rpm. Then ~1,5 mL of lower phase was transferred to new glass tubes with short glass Pasteur pipette. The organic solvent was dried under nitrogen gas in a heat block at 40 °C.

For hydrolysis 300 µl 2 M TFA were added to the samples which were then tightly capped, vortexed, and heated at 121 °C in a heat block. After 90 minutes the blocks were cooled on ice and the liquid was evaporated under nitrogen gas. 2-Propanol (300 µl) was added, the samples were vortexed and the isopropanol was evaporated.

For reduction 200 µl fresh 10 mg/ml sodium borodeuteride in 1 M ammonium hydroxide was added. The samples were vortexed and incubated for 60 min at room temperature. After this incubation the reaction was neutralized with 150 µl glacial acetic acid. methanol:acetic acid (300 µl 9:1 (v:v)) was added, the samples were vortexed and the solution was evaporated. methanol:acetic acid (300 µl 9:1 (v:v)) were added a second time, vortexing and evaporation were repeated. Afterwards the samples were washed with methanol by adding 300 µl MeOH, vortexing and evaporation three times.

For acetylation 50 µl acetic anhydride and 50 µl pyridine were added and the samples were vortexed. The samples were incubated for 20 min at 121 °C in a heat block. The blocks were cooled on ice and the solvent was evaporated. Afterwards 200 µl toluene were added, the tubes were vortexed and evaporate. This toluene wash was repeated.

For clean-up the samples were dissolved in 1,2 ml ethyl acetate and swirled. 5 ml water were added and the samples were vortexed again. After centrifugation for 2 min at 2000 rpm the organic phase was transferred to new glass tubes and evaporated.

The samples were dissolved in 300 µl acetone and gently vortexed. Each sample (100 µl) was transferred to GC vials with inserts and capped tightly. The sample (2 µl) were injected to the GC-MS system which consisted of an Agilent Technologies 7890B GC System, a 5977A MSD and Fused Silica Capillary Column (SP-2380, 30 m × 0,25 mm i.d. × 0,20 µm film thickness; Supelco, cat. no. 24110-U). The Oven temperature was hold on 80 °C for 3 min initially, followed by a gradient of +30 °C per minute to 170 °C (3 min) and a gradient of +4 °C per minute to 240 °C (17,5 min) and a hold of 15 min at 240 °C.

2.12.9 Separation of XyG oligosaccharides by reversed phase chromatography

XEG-released oligosaccharides were reduced (Ch. 2.12.6), purified by SPE (Ch. 2.12.4) and applied to High-performance liquid chromatography (HPLC) equipped with an evaporative Light Scattering Detector (ELSD) for analysis and separation. An HPLC system (Knaur, Azura P6.1 C and AS 6.1 L, avantor Vydac 238TP 5 µm column, cat. no. 238TP54) equipped with an evaporative light scattering detector (SEDEX-LC LT-ELSD, Sedere) was used. The samples (50 µl) were injected to the following gradient conditions: flow: 0,5 ml/min; linear gradient from 100 % 6 % MeOH to 98 % 6 % MeOH and 2 % 50 % MeOH in 40 min, linear gradient to 100

% 50 % MeOH in 10 min, linear gradient to 100 % 6% MeOH in 5 min, flushing with 100 % 6 % MeOH for 15 min. The oven temperature of the ELSD detector was 41 °C utilizing N2 pressure of 3,1 to 3,3 bar.

2.12.10 NMR

Reduced (Ch. 2.12.6), HPLC separated (Ch. 2.12.9) and freeze-dried oligosaccharides were dissolved in deuterium oxide (D_2O) (99,9%, Sigma-Aldrich, cat. no. 151882-100G), freeze-dried and again dissolved in 0,4 ml of D_2O (99,97%) containing 0,05% of 3-(trimethylsilyl)-propionic-*2,2,3,3-d*$_4$ acid, sodium salt (Sigma-Aldrich, cat. no. 450510-10X0.75ML). The ^{1}H NMR spectra were recorded on a Bruker Avance III 600 MHz NMR spectrometer at 298 K. All chemical shifts were referenced relative to 3-(trimethylsilyl) propionic-2,2,3,3-*d*$_4$ acid (0,00 ppm for ^{1}H). The NMR data processing and analysis were performed using MestreLab's MestReNova software. NMR spectra were recorded at the CeMSA@HHU and the analysis was performed by Prof. Markus Pauly.

2.12.11 Monosaccharide analysis

Monosaccharide analysis was performed on Arabidopsis leaf material and on XyG oligosaccharide samples after separation by HPAEC (Ch. 2.12.7).

For monosaccharide analysis on leaf material 4-week-old Arabidopsis leaves were collected, freeze dried and grinded in a Retsch Mill (30 Hz) using two steel balls. AIR prep was performed by washing with 1,5 ml 70 % Ethanol once, 1,5 ml chloroform:methanol (1:1) three times and 1,5 ml acetone once. The pellet was dried and resuspended in 1 ml 0,1 M Citrate- Buffer pH 5,0. After addition of a steel ball and resuspension by milling 500 µl digestion mixture (458 µl $_{dd}$H2O, 22 µl Pullulanase (Fig. 2.1), 10 µl 0,01 g/ml sodium azide, 10 µl α-Amylase (100 µg/ml) (Fig. 2.1)) was added to each sample. The samples were incubated vertically at 37 °C in shaking incubator at 220 rpm for 16 h. After overnight incubation the samples were heated for 10 min to 80 °C and afterwards cooled on ice. The steel ball was removed and the sample was centrifuged for 15 min at 12.000 rpm. The supernatant was discarded and the pellet washed in 1,5 ml water (15 min centrifugation 12.000 rpm, decanting supernatant) three times. The pellet was dried in a heatblock at 50 °C. The dry pellet was transferred to a new tube, two 3 mm glass balls were added and the pellet was resuspended in $_{dd}H_2O$ to a final concentration of 10 mg/ml by the Retsch Mill for 2,5 min to create a slurry. 100 µl of slurry were used in TFA hydrolysis.

The following steps were carried out on the samples and suitable sugar standards (dried): 100 µl 1 mg/ml ribose solution was added to dried samples and standards and dried again. 300 µl 2 M Trifluoroacetic acid (TFA) were added. The samples were mixed by vortexing and heated to 121 °C for 90 min. After cooling down and a short centrifugation the acid was evaporated under nitrogen flow in a heatblock at 40 °C. The samples were washed twice with 300 µl of 2-

Propanol and resuspended in 1000 µl water. After vertexing the samples were spun at 12.000 rpm for 10 min. The sample (300µl) was transferred to new tube and the centrifugation was repeated.

200 µl of sample were transferred to IC Vials. 10 µl sample were injected to IC Device (Knaur, Azura P6.1 L and AS 6.1 L, Dionex™ CarboPac™ PA20-IC-Column) and run under the following conditions: flow 0,4 ml/min, 100 % 2 mM NaOH for 23 min, linear gradient from 100 % 2 mM NaOH to 30 % 2 mM NaOH and 70 % 700 mM NaOH for 1 min, 30 % 2 mM NaOH and 70 % 700 mM NaOH for 6 min, linear gradient from 30 % 2 mM NaOH and 70 % 700 mM to 100 % 700 mM NaOH for 1 min, 100 % 700 mM NaOH for 3 min, linear gradient from 100 % 700 mM NaOH to 100 % 2 mM NaOH for 1 min, 100 % 2 mM NaOH for 9 min.

For XyG oligosaccharide monosaccharide analysis the samples were dried after separation via HPAEC PAD followed by TFA hydrolysis as described above and compositional analysis by HPAEC (Dionex™ CarboPac™ PA20-IC-Column, sample loop volume 10µl, injection volume 10 µl, 0,4 ml flow rate, 2mM NaOH for 23 min, linear gradient for 1 min to 30 % 2mM NAOH and 70 % 700mM NaOH, 30 % 2mM NAOH and 70 % 700mM NaOH for 5 minutes, linear gradient for 1 min to 100 % 700 mM NaOH, 100 % 700 mM NaOH for 3 min, linear gradient for 1 min to 2 mM NaOH, flush with 2 mM NaOH for 24 min).

3. Results

3.1 Identification and Characterization of XXTs from *Hymenaea courbaril*

3.1.1 Background

XyG xylosylation patterns can vary among plant species and cell types. The dominant patterns are the XXGG and XXXG type, in which two or three of four consecutive backbone glucosyl residues are xylosylated, respectively. (Vincken et al., 1997). The XXGG type is present in early land plants (mosses and liverworts, lycophytes and Polypodiales ferns (Peña et al., 2008; Hsieh and Harris, 2012)), in some commelinid monocotyledons (e.g. grasses (Poales)) (Gibeaut et al., 2005; Hsieh and Harris, 2009; Ishida et al., 2023; Hsiung et al., 2023) and plants from the Solanales order (Vincken et al., 1996; York et al., 1996; Jia et al., 2003; Jia et al., 2005; Hoffman et al., 2005). In some tissues in plants of the Poales and Solanales orders the XXXG-type XyG is also present, but only in specific tissues (root hairs/outer root epidermis, pollen tubes) (Lampugnani et al., 2013; Dardelle et al., 2015; Liu et al., 2015).The XXXG type is present in all higher-plant families (Brennan and Harris, 2011; Schultink et al., 2014; Pauly and Keegstra, 2016).

The XXGG type XyG can be extended by additional unsubstituted glucosyl-residues resulting in an $XXGG_n$ -type XyG, where only two out of the four or more backbone glucosyl residues (n typically ranging from one to three) are xylosylated (Hoffman et al., 2005; Gibeaut et al., 2005; Peña et al., 2008; Hsieh and Harris, 2012). Another XyG type with a higher degree of xylosylation is the XXXXG-type has been found the seeds of the tropical legume tree *Hymenaea courbaril* (Buckeridge et al., 1997; Tiné et al., 2006).

Xylosylation of the glucan backbone and the required XXTs have been extensively studied in the past years. In Arabidopsis five XXTs (AtXXT1-5) have been identified that group in the two clades: XXT1/2 and XXT3/4/5 (Zhang et al., 2023b). AtXXT1 and AtXXT2 seem to be partially redundant, even though expression and distribution in Arabidopsis tissues are different. At least one of the two XXTs must be present for the biosynthesis of XyG as *xxt12* double mutants lack detectable XyG (Cavalier et al., 2008; Zabotina et al., 2012). Single mutants (*xxt1*, *xxt2*) lead to a modest reduction of XyG content based on HPAEC-PAD analysis of XyG defining substructure disaccharide isoprimeverose released by Driselase. However, the *xxt2* single mutant has a stronger reduction in XyG content than the *xxt1* single mutant (Cavalier et al., 2008). The *xxt5* single mutant showed a 50% reduction in total XyG content and altered XyG patterns with fewer XXXG and more XXGG subunits in comparison to WT plants (Zabotina et al., 2008; Zabotina et al., 2012).

Recombinantly expressed AtXXTs were tested for their ability to xylosylate Glc residues, which resulted in tri- and tetra-xylosylated cellohexaose by XXT1 and XXT2. AtXXT4 was able to mono- and di-xylosylate cellohexaose and tri-xylosylate AtXXT1-catalyzed products. AtXXT5

was barely adding one Xyl onto cellohexaose and unable to further xylosylate AtXXT1-catalyzed products (Zhong et al., 2021). Determination of the xylosylation pattern of the tri- and tetra-xylosylated cellohexaose by negative ion electrospray ionization tandem mass spectrometry (ESI-MS/MS) revealed that AtXXT1/2 are capable of xylosylating three to four contiguous Glc residues leading to the hypothesis that the two enzymes are solely responsible for *in vivo* xylosylation of XyG (Zhong et al., 2021). However, the addition of three consecutive Xyl residues could be caused by motional freedom of truncated XXTs in solution (Culbertson et al., 2018; Julian and Zabotina, 2022).

XXTs are attached to the plant Golgi membrane via their transmembrane domain and continuously xylosylate an elongating glucan chain synthesized by CSLCs (Culbertson et al., 2018). Crystal structure and homology models show similar steric requirements for acceptor (glucan) interactions with AtXXT1 and AtXXT2, but different requirements for AtXXT5 (Culbertson et al., 2018). XXT1, XXT2 and XXT5 have identical positions for all residues in the active site except for an isoleucine/glycine residue at subsite 2 proximal to the 6-hydroxyl group of the second glucosyl from the reducing end of cellohexaose for XXT1/2 and XXT5, respectively (Culbertson et al., 2018). The glycine in XXT5 likely allows xylosylation of glucose N when the N + 2 glucosyl toward the reducing end has been xylosylated (Culbertson et al., 2018) (Fig. 3.1).

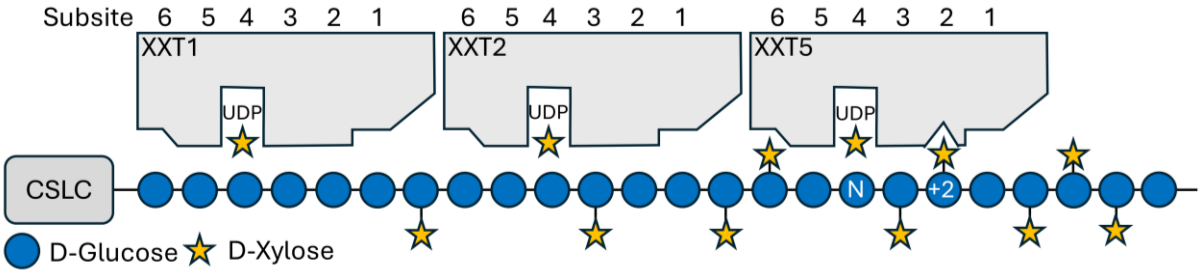

Figure 3.1: Model of xylosylation of the XXXG-type xyloglucan by XXTs. CSLC adds a glucosyl residue onto the nonreducing end of the growing glucan chain. Steric limitation prevent subsite 2 from accommodating a xylosyl adduct in XXT1 and XXT2, while XXT5 allows xylosylation of glucose N when the N + 2 glucosyl toward the reducing end has been xylosylated. Figure modified from (Culbertson et al., 2018)

According to this hypothesis, Arabidopsis XXT1 and XXT2 are responsible for synthesizing XXGG motifs by adding Xyl to the first two consecutive Glc. This was supported by OLIMP analysis of the *xxt3xxt4xxt5* triple mutant, which detected XyG with only XXGG and XLGG units (Zhang et al., 2023b). XXT5 (or XXT3 and XXT4) finish xylosylation by adding the third Xyl, producing the XXXG pattern (Culbertson et al., 2018; Zhang et al., 2023b).

In plants with XXGG XyG core pattern (Poales, Solanales) acetyltransferase (XyBAT) enzymes seem to compete with XXTs for substitutions at *O*-6 of the glucan backbone and thus disrupt the regular XXXG xylosylation pattern (Liu et al., 2016; Zhong et al., 2020). However, those plants do have homologs to AtXXT3/4/5 based on phylogenetic analysis (e.g. rice (Wang

et al., 2014; Mansoori et al., 2015; Zhong et al., 2021) and tomato (Mansoori et al., 2015)). *XyBAT1* knockout in grass Brachypodium led to detection of oligosaccharide with mass signals similar to XXXG by OLIMP (Liu et al., 2016). Furthermore the XXXG pattern was detected in specific tissues in plants with predominantly XXGG XyG pattern (Liu et al., 2015). This suggests that XXGG XyG type plants have XXT3/4/5s that can be involved in the XyG biosynthesis similar to XXT3/4/5s in Arabidopsis in the absence of competing acetylation or in a tissue specific manner.

Tomatoes are members of the Solanaceae family, which have mainly the XXGG type XyG and XXXG type XyG only in specific tissues (Vincken et al., 1996; York et al., 1996; Jia et al., 2003; Jia et al., 2005; Hoffman et al., 2005). Mansoori et al. expressed tomato XXTs in the Arabidopsis mutants *xxt12* and *xxt125.* This resulted in production of an XXXG type XyG (Mansoori et al., 2015). Dicot species like Arabidopsis lack *O*-acetylation of the glucan backbone, which results in the presence of the XXXG-type XyG pattern rather than the XXGG-type pattern typically observed in tomato (Mansoori et al., 2015). *O*-acetyl-substituents thus prevent xylosylation explaining the presence of the XXGG motif in tomato and grasses, which harbour XyBAT enzymes (Liu et al., 2016; Zhong et al., 2020). Arabidopsis harbours XyBAT homologs that exhibited *O*-acetyltransferase activity toward cellohexaose. This indicates that Arabidopsis might have XXGG-type XyG in some specialized cell types (Zhong et al., 2020).

Complete xylosylation (XXXX) has not been observed for reasons unknown.

Hyperxylosylated XXXXG and XXXXXG units have been found in addition to the XXXG in the seeds of the tropical legume tree *Hymenaea courbaril* by HPAEC-PAD analysis of *endo*-β-glucanase hydrolysed seed XyG (Buckeridge et al., 1997; Tiné et al., 2006; Vinueza et al., 2013). These XyG oligosaccharides and several galactosylated versions including XLXXG, XXLXG and XXXLG are specific to the seeds of Hymenaea and are therefore thought to function as storage polymers. This XyG is never fucosylated (Tiné et al., 2006) just like other seed storage XyG (Buckeridge et al., 1992; Desveaux et al., 1998; Buckeridge, 2010). Hymenaea XyGs oligosaccharides isolated at various stages of seed development show that at early developmental states XyG is mainly composed of XXXG and thus likely represents primary wall XyG before deposition of storage XXXXG-type XyG at later stages (Tiné et al., 2006).

The arrangements of XXXG and XXXXG units in XyG polymers are not arranged randomly (Tiné et al., 2006; Buckeridge, 2010). Both types of units exist in the same polymer. This was revealed by electrospray ionization mass spectrometry since the dimer XXXG-XXXXG/XXXXG-XXXG and a series formed by the addition of one to four galactosyl residues were detected (Tiné et al., 2006). This indicates that XXXG and XXXXG are synthesized by the same synthase-glycosyltransferase complex (Tiné et al., 2006). The detection of XXXG-XXXXG/XXXXG-XXXG series of oligosaccharides by MS and their molar ratio indicates that

the Hymenaea XyG synthase complex might harbour additional xylosyl transferases, which lead to the specific patterns of xylose decoration on Hymenaea XyG (Tiné et al., 2006; Buckeridge, 2010). There might be two kinds of XyG synthase complexes: One for fucosylated XyG in the primary wall of growing cells and another one for the unfucosylated storage XyG (Tiné et al., 2006).

It was hypothesized that an undescribed XXT might be responsible for the longer xylosylated XyG oligosaccharides in Hymenaea (Tiné et al., 2006). To test this hypothesis, candidate genes were identified and cloned from the Hymenaea genome to elucidate the necessity, identity and potential structural characteristics of the proposed unique xylosyltransferase(s).

3.1.2 Results

Hymenaea courbaril is a tree species native to a region from southern Brazil to central Mexico (Lacerda et al., 2008). In Germany Hymenaea trees can be found in green houses of some botanical gardens. Unfortunately, genomic sequence information of *Hymenaea courbaril* is not available. Hence, DNA was extracted from frozen Hymenaea leaves obtained from the botanical garden in Frankfurt (Ch 2.9.2). Homologous XXT candidate genes from Hymenaea were cloned by PCR with degenerate primers (Ch. 2.9.18, SFig. 6.14). This method is used to identify unknown members of a gene family or orthologous genes from different organisms with limited or no genomic information (Lang and Orgogozo, 2011).

Based on the sequence information of already identified XXTs from Arabidopsis (Faik et al., 2002; Cavalier and Keegstra, 2006; Cavalier et al., 2008; Zabotina et al., 2008; Zabotina et al., 2012), nasturtium (Jensen et al., 2012; Mansoori et al., 2015), and rice (*Oryza sativa*) (Wang et al., 2014) conserved regions found in all XXTs (Zhang et al., 2023b) were used to design degenerate primers to amplify XXT candidates from Hymenaea DNA. It was also taken into account that XXTs are divided into two clades, XXT1/2 and XXT3/4/5 (Zhang et al., 2023b), and primers for XXTs from both clades were designed (SFig. 6.14). Hymenaea DNA was extracted from leaf material (Ch. 2.9.2) and a PCR was performed using the degenerate primers (Ch. 2.9.18, Fig. 3.3). The PCR products were subcloned a pJET vector (Ch. 2.9.7.1, SFig. 6.16) and sequenced (Ch. 2.9.14). Using this procedure parts of three different *HcXXT* candidate genes designated *HcXXTA*, *HcXXTB* and *HcXXTC* were identified.

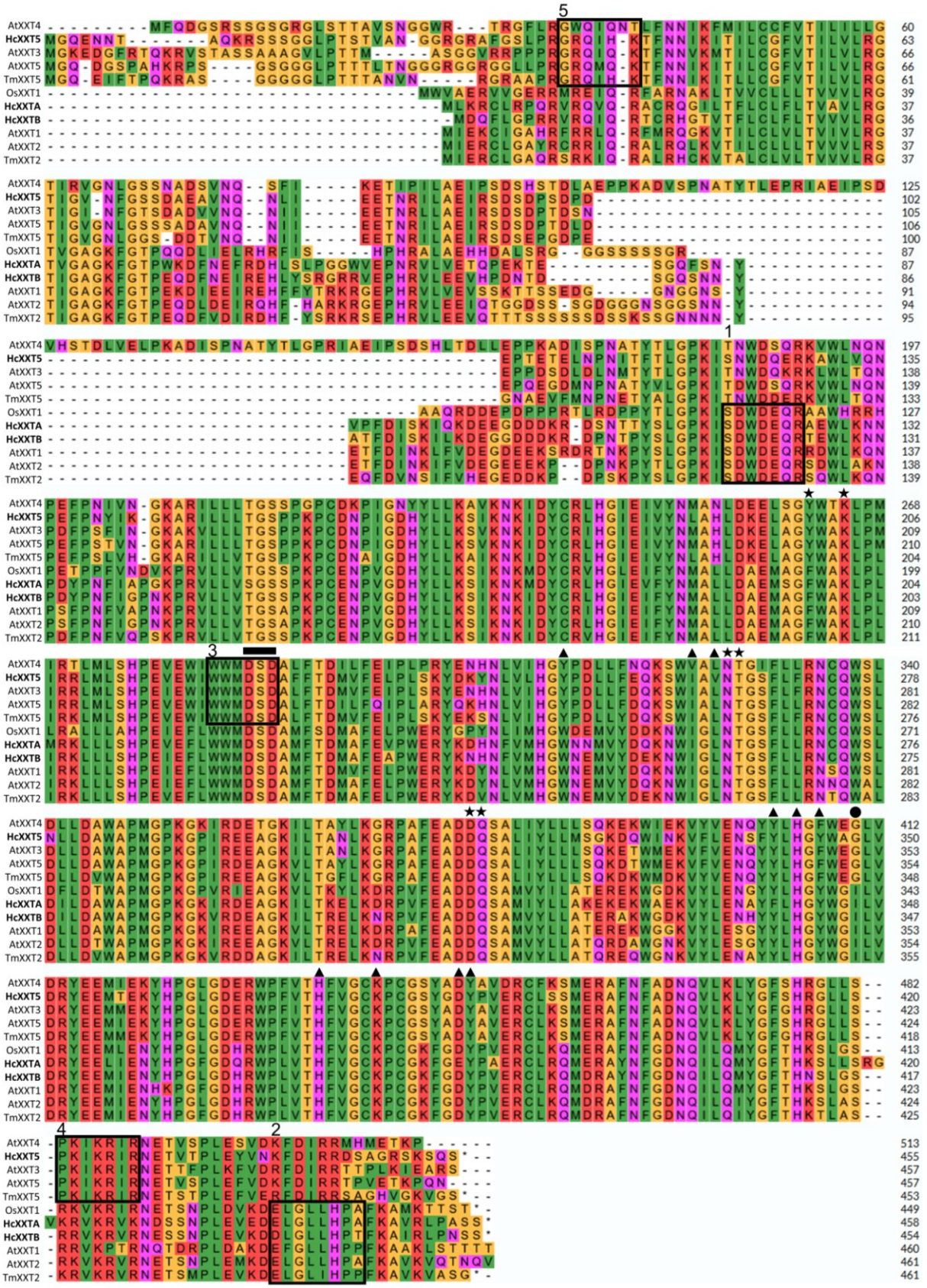

Figure 3.2: Protein sequence alignment of Arabidopsis, nasturtium, rice and Hymenaea XXTs. Clustal Omega alignment of known XXTs and Hymenaea XXT candidates (bold), black boxes indicate conserved regions across XXT1/2 (boxes 1 & 2) or XXT3/4/5 (boxes 3 - 5) clades that were used to design primers to identify the unknown Hymenaea XXTs, the black circle indicates the isoleucine (I) in XXT1/2 and glycine (G) in XXT3/4/5, black bar

indicates DXD motif that coordinates metal cofactors, black stars indicate amino acids that were suggested to form the pocket for UDP-Xyl, black triangles indicate amino acids that were suggested to form the acceptor binding site (Culbertson et al., 2018); Hymenaea (Hc), Arabidopsis (At), rice (Os) and nasturtium (Tm)

The next challenge was to determine the sequence of the less conserved 5' and 3' ends of the *HcXXTs*. The Hymenaea DNA was cut using restriction enzymes (BspI, EcoRI, NdeI, PflI) creating sticky ends, ligated into circular DNA molecules, and then used as a template for PCRs with primers (SFig. 6.14) directed outwards from the already amplified DNA region of the *XXTs* (Ch. 2.9.18, Fig. 3.3). Nested PCRs, which involve two primer sets and two successive PCR reactions, were used to improve sensitivity and specificity. The first set of primers was designed to anneal to sequences upstream from the second set of primers and were used in an initial PCR reaction. The PCR results with the unknown regions were sequenced (Ch. 2.9.14) and the known sequence was extended with the new sequence information. The full sequence of Hymenaea *XXTA* and *XXTB* candidates was identified using a single nested PCR setup (Fig. 3.3).

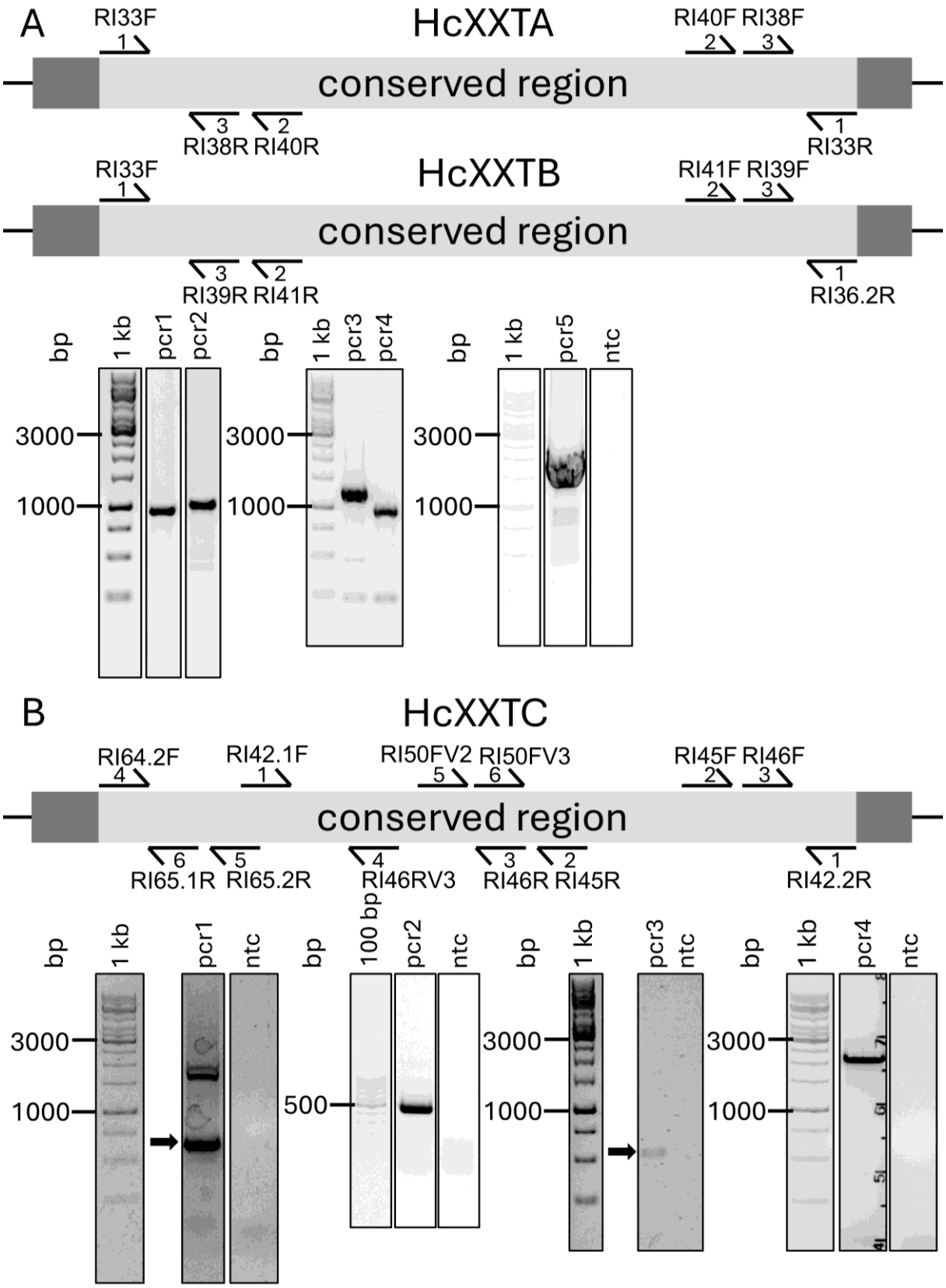

Figure 3.3: Scheme of Hymenaea *XXT* candidates with primer binding sites. Hymenaea *XXT* candidates were identified by a combination of PCRs using degenerated primers based on conserved *XXT* regions and nested PCRs with primers facing outwards of the known sequence. **A) PCRs to amplify Hymenaea *XXTA/B* candidates.** The order of the primers is indicated by numbers in the scheme. **PCR1 & 2**: Primers used here were designed based on conserved regions of known *XXT1/2* from Arabidopsis, nasturtium and rice (Fig. 3.2, box 1 and 2). PCR1:

RI33F&R, expected size 0,97 kbp, this will later be part of *HcXXTA*; PCR2: RI33F & RI36.2R, expected size 0,97 kbp, this will later be part of *HcXXTB*; **PCR3-5**: A nested PCR are two PCRs in which the first PCR uses digested Hymenaea DNA as template and the second PCR uses the product of the first PCR as template. All Primers bind in the already known sequence of parts of the Hymenaea *XXT* candidates. Both primer pairs bind towards the 3' and 5' end of the known sequences. The primers of the second PCR bind closest to the 3' and 5' end of the known sequences. The expected sizes are unknown. PCR3 & 4: to amplify parts of *HcXXTA*, first PCR was performed with RI40F&R on PflI (PCR3) and BspI (PCR4) digested Hymenaea DNA, second PCR was performed with RI38F&R on product of first PCR; PCR5: to amplify parts of HcXXTB, first PCR was performed with RI41F&R on NdeI digested Hymenaea DNA, second PCR was performed with RI39F&R on product of first PCR; **B) PCRs to amplify Hymenaea *XXTC*.** The order of the primers is indicated by numbers in the scheme. **PCR1:** Primers used here were designed based on conserved regions of known *XXT3/4/5* from Arabidopsis, nasturtium and rice (Fig. 3.2, box 3 and 4). PCR1: RI42.1F & RI42.2R, expected size 0,61 kbp, this will later be part of *HcXXTC*; **PCR2**: nested PCR, the expected size is unknown, first PCR was performed with RI45F&R on BspI digested Hymenaea DNA, second PCR was performed with RI46F&R on product of first PCR, **PCR3:** Primer RI64.2F was again designed based on conserved regions of known *XXT3/4/5* from Arabidopsis, nasturtium and rice (Fig. 3.2, box 5). PCR was performed with RI64.2F & RI46RV3 on Hymenaea DNA (undigested), expected size: 0,5 kbp; **PCR4:** nested PCR, the expected size is unknown. First PCR was performed with RI50FV2 & RI65.2R on EcoRI digested Hymenaea DNA, second PCR was performed with RI50FV3 & RI65.1R on product of first PCR; bp = base pairs, no template control = ntc

For the Hymenaea *XXTC* candidate, the sequence was first extended using the above-described nested PCR approach (Fig. 3.3), but the 5`-end of the sequence could not be identified. Additional degenerated primers were designed based on the starting region of known *XXTs* from the XXT3/4/5 clade similar as in the experimental setup to identify the conserved middle part of Hymenaea *XXTs*. One of these primers (RI64.2F) was used in combination with a primer binding in the known sequence and resulted in new information on the 5`-end sequence of the third Hymenaea *XXT* candidate (Fig. 3.3). Then the nested PCR procedure was repeated with primers closer to the 5' end of the by now known sequence and the full sequence was identified (Fig. 3.3).

A total of three *HcXXTs* (HcXXTA, B and C) sequences were identified. A phylogenetic tree of the newly identified sequences with the already described XXT sequences was generated (Ch. 2.2, ngphylogeny.fr) based on the amino acid sequences of the XXTs (Fig. 3.4). HcXXTA and HcXXTB candidates group together with known XXT1s and XXT2s in the XXT1/2 clade, while the HcXXTC candidate groups with known XXT3/4/5s. The two HcXXTs in the XXT1/2 clade are more similar to each other than with any other XXT.

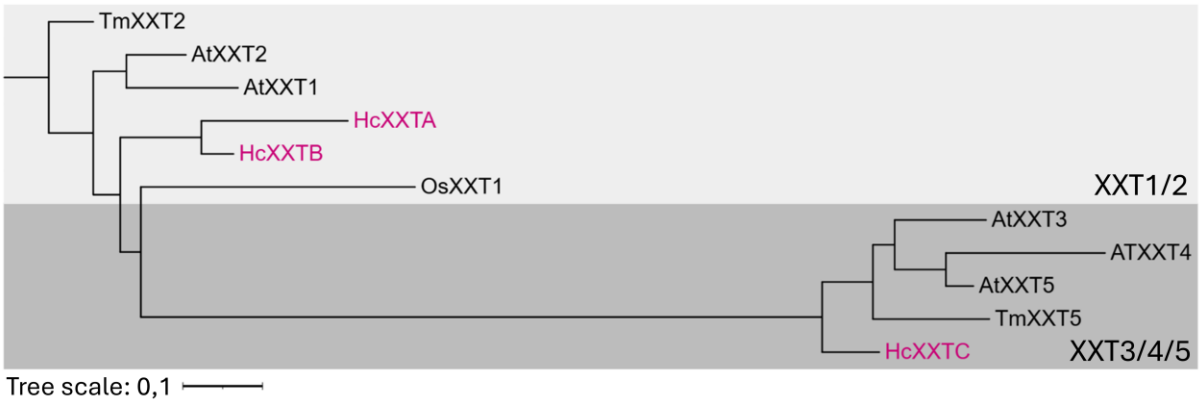

Figure 3.4: Phylogeny of Hymenaea XXTs and already characterized XXTs. Phylogenetic tree based on amino acid sequences of Hymenaea (Hc), Arabidopsis (At), rice (Os) and nasturtium (Tm) XXTs, the scale bar indicates the number of substitutions per site, branch lengths are directly related to the amount of genetic change between shown genes, pink font: Hymenaea proteins; gene information for Arabidopsis and rice can be found in UniProt database; XXT1/2 and XXT3/4/5 clades are indicated in different shades of grey

Based on percentage similarity of the amino acid sequences and the root mean square deviation (RMSD), which is computed between aligned pairs of the backbone C-alpha atoms in superposed structures, HcXXTA is most similar to HcXXTB, HcXXTB to TmXXT2, and HcXXTC to TmXXT5 (SFig. 6.22).

The amino acid sequence was compared in more detail (Fig. 3.2), which revealed that all three HcXXT candidates contain a DxD motif (Asp-x-Asp, in XXTs DSD, Asp-Ser-Asp), which coordinates metal cofactors of GTs (Culbertson et al., 2018). HcXXTA/B have an isoleucine residue also found in XXT1/2s in the essential amino acid region (Zhang et al., 2023b). This residue has been proposed to contribute to the functional differences between the two XXT clades (Culbertson et al., 2018). HcXXTC has a conserved glycine residue as found in XXT3/4/5s. Interestingly, in HcXXTC this glycine residue is preceded by an alanine residue (A), while in all other known XXT3/4/5 it is preceded by a glutamic acid (E). However, the secondary structure of the essential amino acid region (Zhang et al., 2023b) of all HcXXTs and AtXXT1, AtXXT2 and AtXXT5 do not differ noticeably (SFig. 6.23).

The donor substrate binding site based on crystal structures of AtXXT1 (Culbertson et al., 2018) was compared to the HcXXTs (Fig. 3.2): K206, N268, T269, D318 and Q319 (numbers based on AtXXT1) are conserved in all XXTs. F203 is conserved in the XXT1/2 clade but is represented by a Y in the XXT3/4/5 clade. Similar results apply for the acceptor substrate binding sites (Fig. 3.2): W254 is conserved in the XXT1/2 clade, while Y in the XXT3/4/5 clade. Y348 is conserved in the XXT1/2 clade and is present in HcXXTC, but all other XXT3/4/5 clade members contain an F at this position. I265, L267, N268, Y344, H346, H377, K382, D389, and Y390 are conserved across all compared XXTs including the Hymenaea XXT candidates with sometimes a single substitution in one of the amino acids. However, only in HcXXTA Y344 and D389 are an F and E, respectively. Taken together, this could indicate a change in the acceptor binding site and a potentially changed function for HcXXTA.

The impact of the three HcXXT candidates on XyG structure was assessed by a functional complementation approach in the Arabidopsis double *xxt12* (Cavalier et al., 2008) and triple knock-out mutant *xxt125* (Zabotina et al., 2012), both of which lack detectable XyG. For this purpose, the three *HcXXT* candidate genes were amplified from Hymenaea DNA (Ch. 2.9.5) and cloned into binary Gateway vectors with 35S promotors driving constitutive expression (Ch. 2.9.7.4, gene sequences SFig. 6.1, *HcXXTA/B* in pH2GW7, *HcXXTC* in pMpGWB202, SFig. 6.7 and 6.8, SFig. 6.17 and 6.18). Vectors were chosen based on antibiotic selection marker for potential cotransformation. The sequence verified plasmids (Ch. 2.9.14) with the HcXXT candidate genes were individually transformed into *Agrobacterium tumefaciens* (Ch. 2.9.10). The transformation was verified via colony PCR (Ch. 2.9.12, SFig. 6.19) and the confirmed strains were used to transform *xxt12* and *xxt125* with each of the three *HcXXTs* (Ch. 2.9.16). Resistant plants on selection media (Ch. 2.8.5.6, Fig. 2.3, Hygromycin for plants with pH2GW7, Gentamicin for plants with pMpGWB202) were transferred to soil and genotyped for background and insertion (Ch. 2.9.12, SFig. 6.20 and 6.21). Confirmed T1 plants were selfed and the seeds were again sown on plates with a selective antibiotic (Ch. 2.8.5.6, Fig. 2.3). Plants from plates with 75% resistant plants were transferred to soil (Ch. 2.8.5.4) and selfed as a 75% antibiotic resistance as this indicates that the T1 plant is heterozygous for the insert. Confirmed T2 plants (by PCR Ch. 2.9.12, Fig. 3.5) were selfed and the seeds were again sown on plates with a selective antibiotic (Ch. 2.8.5.6, Fig. 2.3). Plants from plates with 100% resistant plants were transferred to soil (Ch. 2.8.5.4) and selfed as a 100% resistance indicates that the T2 plant is homozygous for the insert.

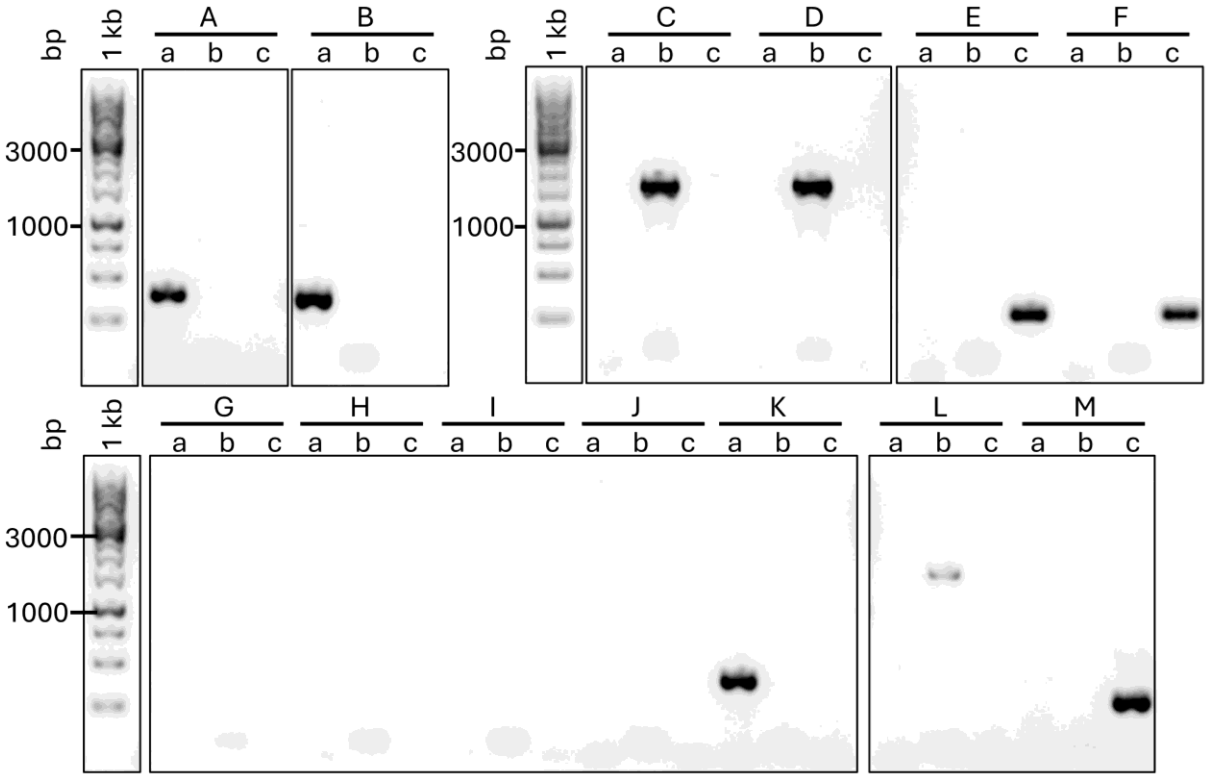

Figure 3.5: PCR to confirm T2 Arabidopsis transformants. Arabidopsis *xxt12* and *xxt125* transformed with pH2GW7 + *HcXXTA/B* or pMpGWB202 + *HcXXTC* were verified via PCR using gDNA as template; a: RI71F & RI72R2, bind exclusively in *HcXXTA*, expected size 0,4 kbp; b: RI71F & RI73R1, bind exclusively in *HcXXTB*, expected size 1,5 kbp; c: RI71F & RI74R2, bind exclusively in *HcXXTC*, expected size 0,3 kbp; **A)** pH2GW7 + *HcXXTA* in *xxt12;* **B)** pH2GW7 + *HcXXTA* in *xxt125;* **C)** pH2GW7 + *HcXXTB* in *xxt12*; **D)** pH2GW7 + *HcXXTB* in *xxt125*; **E)** pMpGWB202 + *HcXXTC* in *xxt12;* **F)** pMpGWB202 + *HcXXTC* in *xxt125*; **G)** no template controls; **H)** *xxt12*; **I)** *xxt125*; **J)** Arabidopsis WT; **K)** T1 pH2GW7 + *HcXXTA* in *xxt12*; **L)** T1 pH2GW7 + *HcXXTB* in *xxt12*; **M)** T1 pMpGWB202 + *HcXXTC* in *xxt12;* bp = base pairs

The XyG structure of the confirmed homozygous insert lines was assessed by OLIMP (Ch. 2.12.3). Seedling material of the various complemented Arabidopsis lines was collected after 2 weeks of growth on selective plates (Ch. 2.8.5.6, Fig. 2.3). AIR material was prepared and digested by a xyloglucan-specific endo-beta-1,4-glucanase (XEG) from *Aspergillus aculeatus* (Pauly et al., 1999) which specifically hydrolyses the XyG glucan backbone at unsubstituted glucosyl residues (Ch. 2.5). The released XEG oligosaccharides were analysed by OLIMP (Fig. 3.6). The OLIMP profile of the untransformed Arabidopsis *xxt12* double and *xxt125* triple mutant lacked detectable XyG oligosaccharides as previously shown (Cavalier et al., 2008; Zabotina et al., 2012).

In the double mutant background two out of three HcXXT candidates result in detectable XyG oligosaccharides when expressed: *HcXXTA* expressed in *xxt12* results in mass signals with *m/z* 1085 (XXXG), *m/z* 1247 (XLXG/XXLG), *m/z* 1289 (XLXG/XXLG), *m/z* 1393 (XXFG), and *m/z* 1435 (XXFG). Furthermore, mass signals to novel oligosaccharides appeared with *m/z* 1379, *m/z* 1541 and *m/z* 1835 which are consistent with oligosaccharides build of 5 hexoses and 4 pentoses, 6 hexoses and 4 pentoses, and 7 hexoses and 5 pentoses, which could correspond to hyperxylosylated XyG oligosaccharides being detected in Hymenaea seeds (Buckeridge et al., 1997; Tiné et al., 2006; Vinueza et al., 2013).

Expression of *HcXXTB* in *xxt12* leads to mass signals with *m/z* 1085 (XXXG), *m/z* 1247(XLXG/XXLG), *m/z* 1289 (XLXG/XXLG), *m/z* 1393 (XXFG), and *m/z* 1435 (XXFG), but no unusual XyG oligosaccharides. No mass signals of XyG oligosaccharides were detected in *xxt12* expressing *HcXXTC*.

In the triple mutant background only the expression of *HcXXTB* results in detection of oligosaccharide mass signals with *m/z* 1085 (XXXG), *m/z* 1247(XLXG/XXLG), *m/z* 1289 (XLXG/XXLG), *m/z* 1393 (XXFG) and *m/z* 1435 (XXFG). *xxt125* expressing HcXXTA and HcXXTC did not result in XyG oligosaccharides detected by OLIMP

In some samples, multiple mass signals relating to masses of oligosaccharides entirely made of hexoses with a varying degree of polymerization were found (*m/z* 1175 and *m/z* 1337) in addition to the typical Arabidopsis XyG oligosaccharide ion signals. This indicates the presence of a polysaccharide made of hexoses. Further detected signals (e.g. *m/z* 1001, *m/z* 1079, *m/z* 1100, *m/z* 1612) could not be assigned to oligosaccharides.

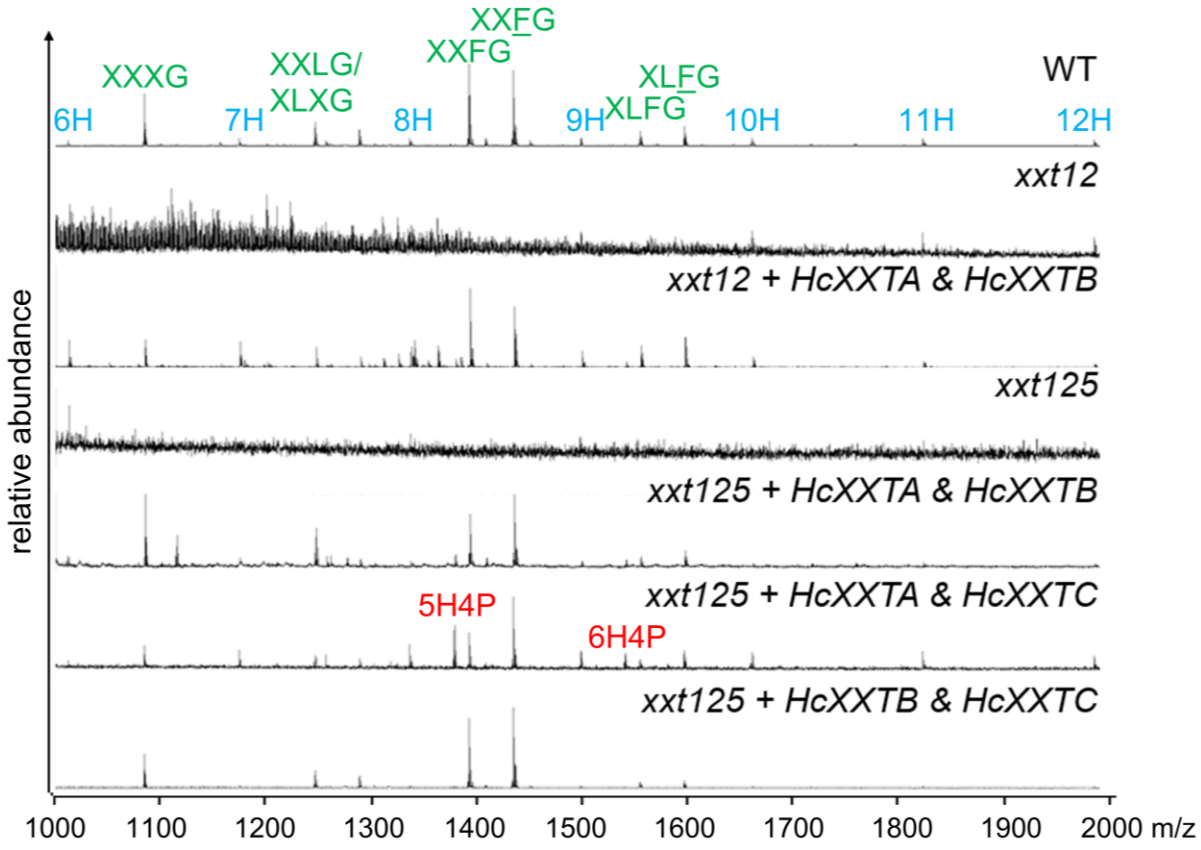

Figure 3.6: XyG oligosaccharide mass profiling of Hymenaea XXT complemented Arabidopsis lines. XyG oligosaccharide profiles derived from seedlings of Arabidopsis wildtype (WT), untransformed *xxt12* double and *xxt125* triple mutant and transgenic lines expressing *HcXXTs* in *xxt12* and *xxt125 gene*tic background; mass signals are labelled with suggested oligosaccharide structures indicated by the one-letter code or number of hexoses (H) and pentoses (P), green labels: Arabidopsis typical XyG motifs, red label: novel oligosaccharides, blue label: hexose ladder

Due to the functional diversity among XXTs in terms of which glucosyl residues they xylosylate within the backbone and the proposed formation of multienzyme complexes among XyG biosynthetic glycosyltransferases (Chou et al., 2012; Chou et al., 2015; Culbertson et al., 2018; Zabotina et al., 2021) multiple *HcXXTs* were expressed in the Arabidopsis *xxt12* and *xxt125* mutants to assess their functional roles. For this purpose, heterozygous T1 plants expressing each one of the *HcXXTs* were crossed (Ch. 2.8.5.7) resulting in the next generation in *xxt12* expressing *HcXXTA* and *HcXXTB*, *xxt125* expressing *HcXXTA* and *HcXXTB*, or *HcXXTA* and *HcXXTC*, or *HcXXTB* and *HcXXTC*. The F1 generation of these crossings was genotyped (Ch. 2.9.12, Fig. 3.7). The T1 plants were heterozygous for the Hymenaea *XXTs*.

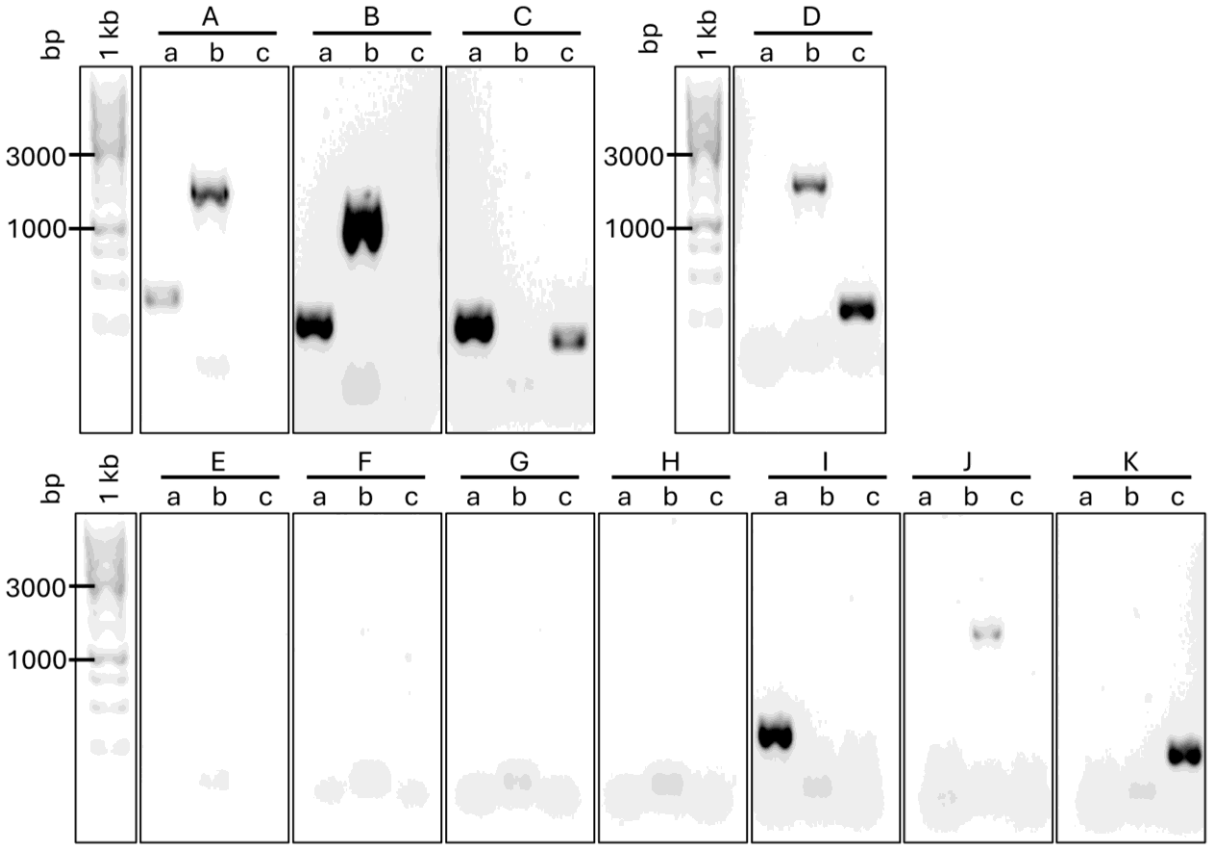

Figure 3.7: PCR to confirm crossed Arabidopsis transformants. Arabidopsis *xxt12* expressing *HcXXTA* and *HcXXTB*, *xxt125* expressing *HcXXTA* and *HcXXTB*, or *HcXXTA* and *HcXXTC*, or *HcXXTB* and *HcXXTC* were verified via PCR using gDNA as template; a: RI71F & RI72R2, bind exclusively in *HcXXTA*, expected size 0,4 kbp; b: RI71F & RI73R1, bind exclusively in *HcXXTB*, expected size 1,5 kbp; c: RI71F & RI74R2, bind exclusively in *HcXXTC*, expected size 0,3 kbp; **A)** *HcXXTA* & *HcXXTB* in *xxt12;* **B)** *HcXXTA* & *HcXXTB* in *xxt125;* **C)** *HcXXTA* & *HcXXTC* in *xxt125;* **D)** *HcXXTB* & *HcXXTC* in *xxt125*; **E)** no template controls; **F)** Arabidopsis WT; **G)** *xxt12*; **H)** *xxt125*; **I)** T1 pH2GW7 + *HcXXTA* in *xxt12*; **J)** T1 pH2GW7 + *HcXXTB* in *xxt12*; **K)** pMpGWB202 + *HcXXTC* in *xxt12;* bp = base pairs

Plants expressing two *HcXXTs* were analysed for their XyG structure by OLIMP (Ch. 2.12.3, Fig 3.8). Arabidopsis *xxt12 and xxt125* expressing *HcXXTA* and *HcXXTB* resulted in mass signals at *m/z* 1085 (XXXG), *m/z* 1247 (XLXG/XXLG), *m/z* 1289 (XLXG/XXLG), *m/z* 1393 (XXFG), *m/z* 1435 (XXFG), *m/z* 1555 (XLFG) and *m/z* 1597 (XLFG). Minor mass signals at *m/z* 1379 and *m/z* 1541 suggest the presence of oligosaccharides build of 5 hexoses and 4 pentoses, and 6 hexoses and 4 pentoses, respectively.

Samples of Arabidopsis *xxt125* expressing *HcXXTA* and *HcXXTC* show mass signals at *m/z* 1085 (XXXG), *m/z* 1247 (XLXG/XXLG), *m/z* 1289 (XLXG/XXLG), *m/z* 1379 (5 hexoses and 4 pentoses), *m/z* 1393 (XXFG), *m/z* 1435 (XXFG), *m/z* 1541 (6 hexoses and 4 pentoses), *m/z* 1555 (XLFG) and *m/z* 1597 (XLFG).

The OLIMP profile of *xxt125* expressing *HcXXTB* and *HcXXTC* displays mass signals at *m/z* 1085 (XXXG), *m/z* 1247 (XLXG/XXLG), *m/z* 1289 (XLXG/XXLG), *m/z* 1393 (XXFG), *m/z* 1435 (XXFG), *m/z* 1555 (XLFG) and *m/z* 1597 (XLFG), but no hyperxylosylated oligos.

In almost all samples, multiple mass signals relating to masses of oligosaccharides entirely made of hexoses with a varying degree of polymerization were detected again (*m/z* 1013, *m/z* 1175, *m/z* 1337, *m/z* 1499, *m/z* 1661, *m/z* 1823 and *m/z* 1985).

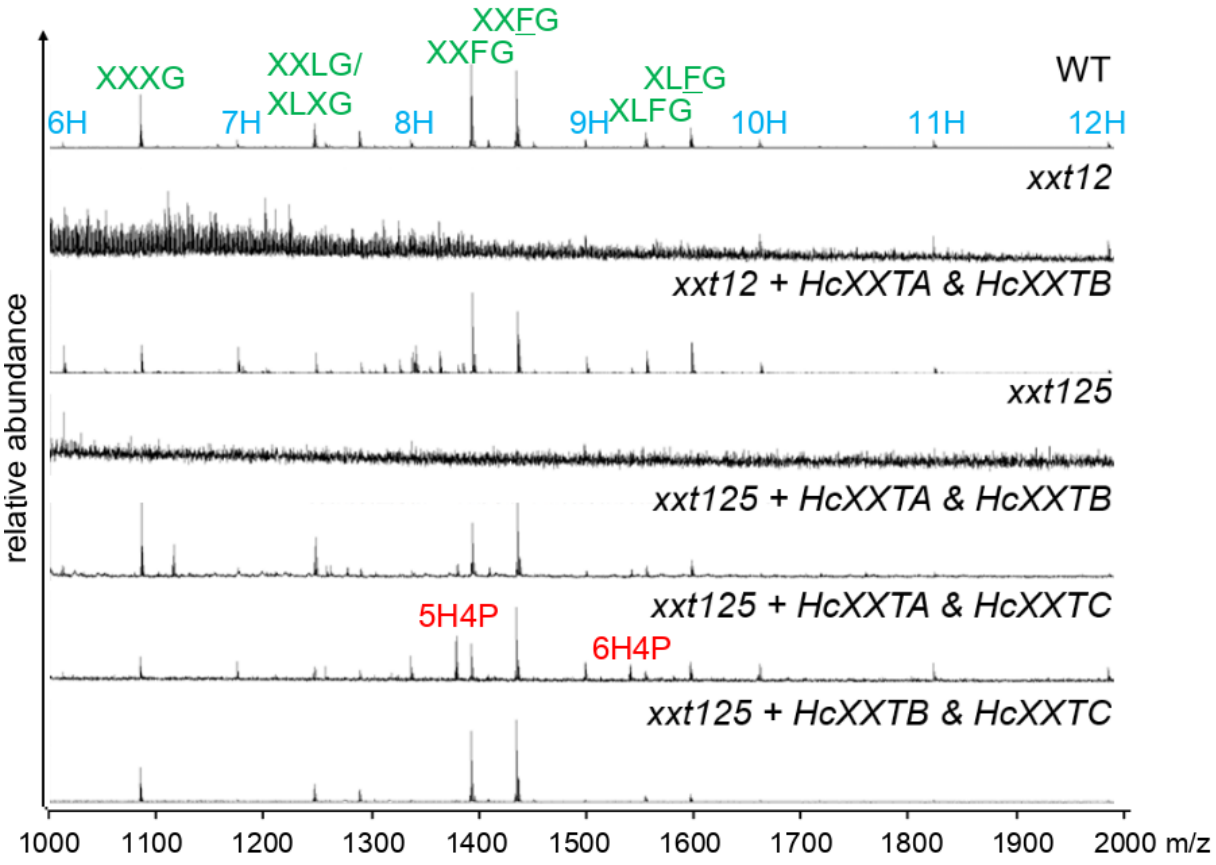

Figure 3.8: XyG oligosaccharide mass profiling of HcXXT complemented Arabidopsis crosses. XyG oligosaccharide profiles derived from leaf material of Arabidopsis wildtype (WT), untransformed *xxt12* double and *xxt125* triple mutant, and transgenic lines expressing two *HcXXTs (xxt12 + HcXXTA* & *HcXXTB*, *xxt125 + HcXXTA* & *HcXXTB, xxt125 + HcXXTA* & *HcXXTC*, *xxt125 + HcXXTA* & *HcXXTC*), mass signals are labelled with suggested oligosaccharide structures indicated by the one-letter code or number of hexoses (H) and pentoses (P), green labels: Arabidopsis typical XyG motifs, red label: novel oligosaccharides, blue label: hexose ladder

The Arabidopsis double and triple mutant *xxt12* and *xxt125* lacking XyG exhibit somewhat reduced growth resulting in a smaller size at maturity (Cavalier et al., 2008; Zabotina et al., 2012) (Fig 3.9). The reduced growth phenotype (stem hight of six-week-old plants) of *xxt12* compared to the Arabidopsis wildtype was confirmed (Xiao et al., 2016; Yu et al., 2022). The only difference in growth phenotype was detected in *xxt125* expressing *HcXXTC* since those plants had significantly reduced growth.

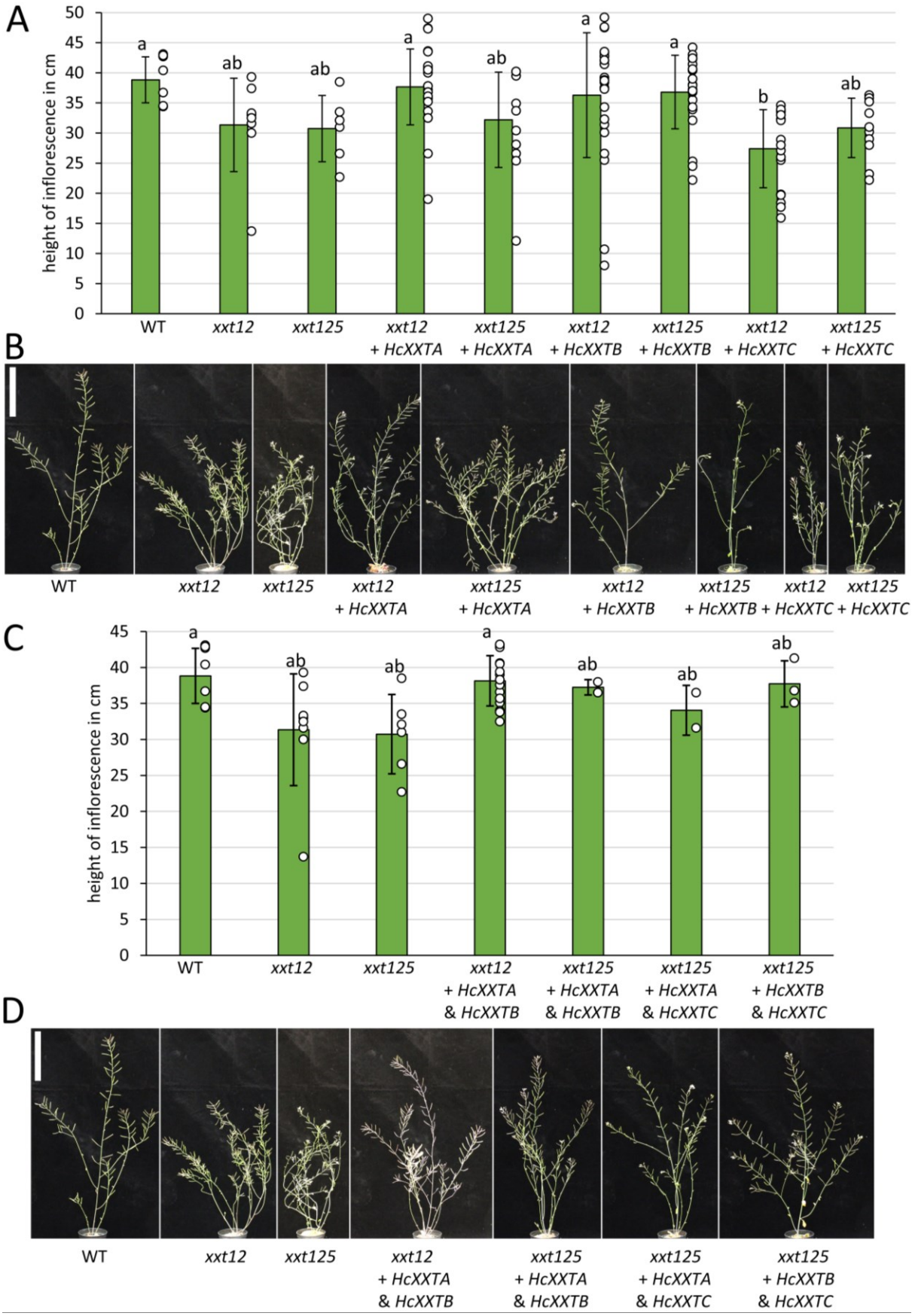

Figure: 3.9: Plant height of complemented *xxt12* and *xxt125* plants expressing Hymenaea XXTs. A) Height of inflorescence stems of 6-week-old Arabidopsis plants expressing one Hymenaea XXT, WT n = 9; *xxt12* n = 8, *xxt125* n = 6, *xxt12* + *HcXXTA* n = 26, *xxt125* + *HcXXTA* n = 14, *xxt12* + *HcXXTB* n = 24 , *xxt125* + *HcXXTB* n =

22, *xxt12* + *HcXXTC* n = 18, *xxt125* + *HcXXTC* n = 11; results of ANOVA analysis and subsequent Tukey's test are indicated ($P < 0,05$), error bars indicate standard deviation; **B)** Representative pictures from the genotypes shown in A), scale bar: 10 cm, **C)** Height of inflorescence stems of 6-week-old Arabidopsis plants expressing two Hymenaea XXTs; WT n = 9; *xxt12* n = 8, *xxt125* n = 6, xxt12 + *HcXXTA* and *HcXXTB* n = 15, xxt125 + *HcXXTA* and *HcXXTB* n = 2, *xxt125* + *HcXXTA* and *HcXXTC* n = 2, *xxt12t5* + *HcXXTB* and *HcXXTC* n = 2) results of ANOVA analysis and subsequent Tukey's test are indicated ($P < 0,05$); error bars indicate standard deviation **D)** Representative pictures from the genotypes shown in C), scale bar: 10 cm

3.1.3 Discussion

Is it possible that the unusual xylosylation pattern found in the seed storage XyG of Hymenaea seeds is caused by specific hitherto undescribed xylosyltransferases? This hypothesis was tested here by identifying and characterizing Hymenaea XXTs. XXT1 and XXT2 from Arabidopsis are suggested to have a steric constrain in their 3D-structure which prevents accommodation of an xylosyl adduct on specific positions of the growing glucan chain (Fig. 3.1): XXT1 and 2 cannot transfer a xylosyl residue to the glucosyl residue N when glucosyl residue N + 2 has a xylosyl adduct (Culbertson et al., 2018). XXT5 on the other hand can accommodate a partially xylosylated glucan chain in its acceptor binding cleft. This most likely also applies to XXT3 and XXT4 (Culbertson et al., 2018; Zhang et al., 2023b). Since the Hymenaea XyG motifs of interest are highly xylosylated at least one of the XXTs involved in the synthesis must accommodate a partially xylosylated glucan chain as acceptor, i.e. it could belong to the XXT3/4/5 clade or a novel XXT clade.

Through a functional complementation approach, Hymenaea candidate XXTs were cloned and expressed in Arabidopsi*s xxt12* double and *xxt125* triple mutant. Complementation of the *xxt12* double mutant with HcXXTA, one of two HcXXT candidates grouping in the XXT1/2 clade, resulted in a restoration of the complete XyG structure found in the Arabidopsis wildtype including galactosylation and fucosylation. *HcXXTA* is thus a functional equivalent to AtXXT1 and/or 2. In addition, unusual oligosaccharides were found consistent with hyperxylosylation found in Hymenaea (Tiné et al., 2006) (Fig. 3.6). The Hymenaea specific mass signals at *m/z* 1379, *m/z* 1541, and *m/z* 1835 match the masses of XyG oligosaccharides XXXXG, XXXXG (one of the Xs also containing an additional galactosyl-unit resulting in the sidechain "L") and XXXXXG (one of the X sidechains is galactosylated) respectively. Mass signals *m/z* 1541 would also fit to oligosaccharide XXXXGG. The presence of a consecutive GG was however not detected in Hymenaea (Tiné et al., 2006). The precise structure of the XyG motifs has to be further analysed by glycosidic linkage analysis and NMR.
xxt12 expressing *HcXXTA* likely produces an XXXG, XXXXG and XXXXXG-type XyG which proves that the hyperxylosylation is caused by an XXT. The hyperxylosylated XyG motifs account for about 40 % of the detected XyG oligosaccharides. While the XXXG type can be galactosylated, fucosylated and *O*-acetylated, XXXXG and XXXXXG types are only

hexosylated (likely galactosylated) not fucosylated or acetylated based on missing mass signals of these substituents.
Complementation of the *xxt125* triple mutant expressing *HcXXTA* did not result in restoration of any XyG structure, based on the lack of detectable XyG oligosaccharide in the OLIMP profile (Fig. 3.6). These plants can thus still be considered XyG deficient. This is different from XXTs from the XXT1/2 clade analysed so far since XXT2 from Arabidopsis and nasturtium were able to fully restore the complete XyG structure found in the Arabidopsis wildtype in a complementation approach in the triple mutant *xxt125* (Mansoori et al., 2015).

Complementation of the Arabidopsis *xxt12* double and *xxt125* triple mutant with HcXXTB, the other HcXXT candidate grouping in the XXT1/2 clade, resulted in a restoration of the XyG structure similar to that found in the wildtype Arabidopsis without hyperxylosylated XyG oligosaccharides. The fact that HcXXTB is able to restore an Arabidopsis wildtype-like XyG even without the presence of an XXT5 in the triple mutant indicates that AtXXT5 does not impact the function of HcXXTB. Similar results were shown in a complementation approach expressing AtXXT2 and TmXXT2 in *xxt125* analysed by OLIMP which both restored the XyG structure of the Arabidopsis wildtype (Mansoori et al., 2015). However, AtXXT3 and AtXXT4 are still present in the triple mutant, even though they have a comparatively low expression compared to AtXXT5 (tair data). AtXXT3, AtXXT4, and AtXXT5 are redundant and essential to adding xylosyl residues to the third glucose in the glucan backbone to fully synthesize XyG (Zhang et al., 2023b). The wildtype XyG structure in the HcXXTB expressing *xxt125* indicates that HcXXTB and AtXXT3 and/or AtXXT4 are able to synthesize wildtype like XyG together.

Expression of *HcXXTC*, which phylogenetically groups in the XXT3/4/5 clade, did not result in any detectable XyG oligosaccharides in neither the *xxt12* double nor the *xxt125* triple mutant. This result suggests that HcXXTC alone is not sufficient for XyG production in Arabidopsis. This is probably due to the fact that the partially xylosylated acceptor substrate (XXGG) is missing in the absence of XXT1/XXT2 as proposed in the work of (Zhang et al., 2023b).

To further elucidate the function of the HcXXTs and their effect Arabidopsis lines expressing two *HcXXTs* were created and analysed by XyG OLIMP (Fig. 3.8). Complementation of the *xxt12* double mutant and *xxt125* triple mutant expressing *HcXXTA* and *HcXXTB* both of which showed xylosyltransferase activity in the single *HcXXT* complemented lines, resulted in a restoration of the XyG structure similar to Arabidopsis wildtype with additional oligosaccharides representing Hymenaea XyG. However, the Hymenaea specific oligosaccharides (*m/z* 1379 and *m/z* 1541) were minor (<5 %) compared to the Arabidopsis typical XyG oligosaccharides. Hence HcXXTA, which does not produce XyG in the triple mutant background, becomes functional in *xxt125* when *HcXXTB* is co-expressed also resulting in the Hymenaea typical XyG

oligosaccharides. *HcXXTA* did not restore the lack of XyG in the triple mutant but does so when co-expressed together with *HcXXTB* or *HcXXTC*.
The oligosaccharides specific for Hymenaea are only detected in the lines that express *HcXXTA*. HcXXTA does not recover XyG in combination with AtXXT3 or AtXXT4, which are still expressed in the triple mutant, but in combination with AtXXT5, HcXXTB or HcXXTC. Therefore, it is possible that HcXXTA can form an enzyme complex with AtXXT5, HcXXTB and/or HcXXTC which is not only required for xylosyltransferase activity but also for hyperxylosylation.

Based on reverse genetics and structural studies AtXXT1 and AtXXT2 specifically add the xylosyl residue to the first two glucose residues, synthesizing the XXGG unit of XyG while AtXXT3, AtXXT4 and AtXXT5 use the product of AtXXT1 and AtXXT2, and specifically add the third xylosyl residues in the XXXG unit (Culbertson et al., 2018; Zhang et al., 2023b). The different function of the XXT1/2 and XX3/4/5 clade was explained by differences in the binding pocket which would restrict the binding of an acceptor glucan molecule with the xylosyl residues attached in AtXXT1 and AtXXT2, and would allow accommodation of the xylosylated glucan as an acceptor in AtXXT3, AtXXT4 and AtXXT5 (Culbertson et al., 2018).
HcXXTA, which belongs to the XXT1/2 clade based on sequence homology, does not match to this XyG synthesis scheme since it hyperxylosylates the glucan backbone (in the presence of AtXXT5 or HcXXTB or HcXXTC). This indicates that HcXXTA is able to accommodate a partially xylosylated acceptor and is no typical XXT1/2.
If one compares the essential amino acid sequence forming the proposed pocket structure (Zhang et al., 2023b) (Fig. 3.2) of HcXXTA with known XXTs from the XXT1/2 and XXT3/4/5 clade, which differs in an isoleucine (XXT1/2) substitution with glycine (XXT3/4/5), it becomes clear that HcXXTA indeed belongs in the XXT1/2 clade as it has an isoleucine in this particular position. Apparently, the glycine residue is not required to accommodate proper XXXG -type xylosylation or hyperxylosylation, and thus contradicts the steric rule proposed by Culbertson et al., 2018 and Zhang et al., 2023.
However, HcXXTA differs in two amino acids that Culbertson et al. identified as relevant for the acceptor binding site (Fig. 3.10): In HcXXTA Y344 and D389 (numbers based on AtXXT1) are represented by the amino acids F and E, respectively.

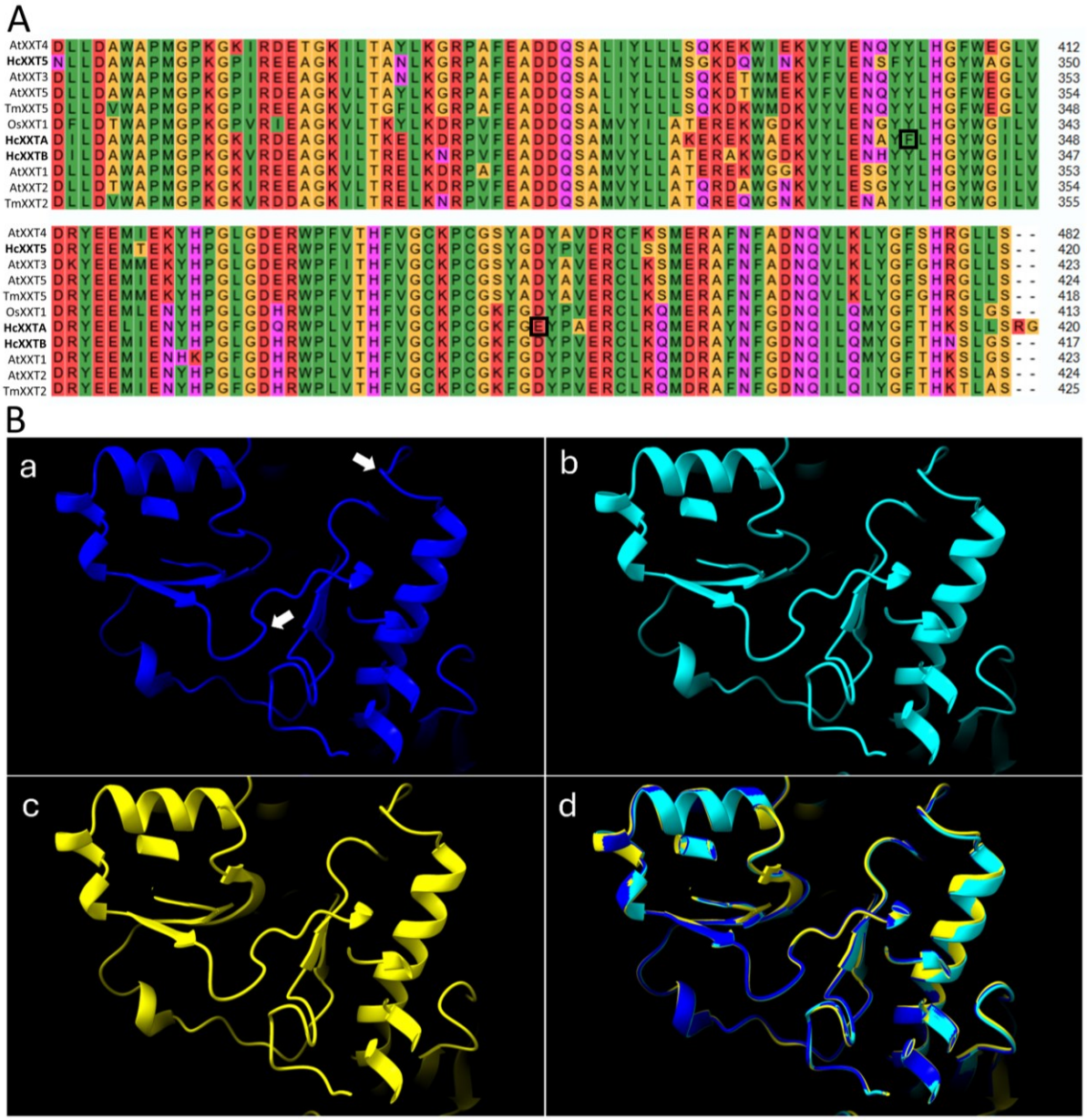

Figure 3.10: Structural comparison of XXTs. A) Partial protein sequence alignment of Arabidopsis (At), nasturtium (Tm), rice (Os) and Hymenaea (Hc) XXTs: Clustal Omega alignment of known XXTs and Hymenaea XXT candidates (bold), black boxes indicate Y344F and D389E substitutions; **B)** The secondary structure of XXTs was predicted by AlphaFold and visualized using ChimeraX. a: AtXXT1, arrows indicate Y344 and D389 that are substituted in HcXXTA to F and E, respectively. b: AtXXT2; c: HcXXTA; d: HcXXTA (yellow) in comparison with AtXXT1 (dark blue), AtXXT2 (light blue)

Culbertson et al. suggested that the sidechains of Y344 and two other amino acids in XXT1 would overlap with xylosyl extension at subsite 2 (Fig. 3.10). The xylose transfer to glucose unit N would block subsequent binding necessary for xylose transfer to glucose unit N + 2 (Culbertson et al., 2018). Could a change from tyrosine (Y) to phenylalanine (F) influence this hypothesis? Both amino acids are hydrophobic and have an aromatic sidechain. The structural difference between phenylalanine and tyrosine lies in a hydroxyl group attached to the phenyl ring in tyrosine. Phenylalanine has a phenyl ring with a hydrogen at the same position where

tyrosine has the hydroxyl group. The hydroxyl group of Y344 is proposed to interact with the cellohexaose (Culbertson et al., 2018). If Y344 is a phenylalanine in HcXXTA the hydroxyl group is not present and the acceptor substrate binding site likely changes. The change in the sidechain structure might allow a xylosyl extension at subsite 2. This could enable HcXXTA to hyperxylosylate already xylosylated glucans.

The other change in amino acids is a D389E substitution from AtXXT1 to HcXXTA. Both amino acids are acidic but differ in the length of their sidechains. The D389 of AtXXT1 hydrogen bonds to the glucan acceptor (Culbertson et al., 2018). The change to glutamic acid in the same position in HcXXTA might therefore also change the interaction with the acceptor substrate, which might enable the hyperxylosylation.

To test whether these specific amino-acid residues indeed allow HcXXTA to produce hyperxylosylated XyG oligosaccharides one should specifically introduce the amino acid changes into AtXXT1/2 and test its activity, e.g. through a complementation approach in *xxt12* and *xxt125*. Further analysis of the ligand-protein interaction (e.g. LigPlot+ like with AtXXT1 in Culbertson et al 2018) would also be helpful to understand the differences in the acceptor substrate binding site of known XXTs to HcXXTA.

3.2 Xyloglucan Production in Heterologous Host *Pichia pastoris*

3.2.1 Background

One approach to understand plant cell wall biosynthetic enzymes and their interactions is synthetic biology, which can be used to analyse individual GTs and/or entire biosynthetic machineries for the production of plant wall polysaccharides (Pauly et al., 2019). Heterologous expression of plant cell wall biosynthetic genes in orthologous systems such as unicellular yeasts can be used to characterize the *in vivo* function of the corresponding protein by detecting the product of the reaction (Pauly et al., 2019; Voiniciuc et al., 2019; Robert et al., 2021). Compared to the analysis in plants unicellular systems provide faster genetic engineering and therefore higher-throughput, and reduced glycan complexity (Pauly et al., 2019).

There are several possible systems that differ in terms of handling, costs, growth, ability of post-translational modifications and available tools (Pauly et al., 2019). Bacteria (e.g. *E. coli*) are a fast, cheap and simple choice. However, prokaryotes lack an endomembrane system and most post-translational modifications present in eukaryotes (Pouresmaeil and Azizi-Dargahlou, 2023).

Eukaryotic fungi offer endogenous nucleotide sugars and the associated transporters necessary for Golgi GT activity (Pauly et al., 2019). *Saccharomyces cerevisiae* for example harbours cytosolic GDP-mannose and UDP-glucose and the corresponding nucleotide sugar transporters for transport into the ER and Golgi apparatus (Orellana et al., 2016). Fungi feature endogenous post-translational modifications, while still providing low cost, easy genetic manipulation and handling (Popova et al., 2023).

Another possibility are immortal animal cell lines (such as Chinese ovary hamster or human embryonic kidney 293 cells), but these are more expensive and difficult to handle compared to the already mentioned systems (Pauly et al., 2019; Mukherjee et al., 2023).

The methylotrophic yeast *Pichia pastoris* was shown to be a favourable host organism for the functional expression and characterization of biosynthetic enzymes of the wall polymers (Petersen et al., 2009; Gille et al., 2011a; Voiniciuc et al., 2019). Pichia makes an ideal host because of its convenient cultivation (high cell density, growth speed, costs) and genetic manipulability (Obst et al., 2017; Pauly et al., 2019; Popova et al., 2023). Pichia belongs to the yeasts with mannose/glucose type cell walls based on monosaccharide analysis (Schweigkofler, 2002). Glycosidic linkage analysis of isolated extracellular matrices from Pichia cell walls revealed that they consist largely of β-1,3- and β-1,6-linked glucans. The presence of branched glucans and a significant proportion of 4-linked glucose was attributed to storage glycogen rather than to the actual wall material. This means that production of glucan containing polymers like XyG might be more difficult to detect in Pichia (Pauly et al.,

2019) since 4-Glc could derive from the Pichia native storage glycogen or a potentially produced XyG backbone like polysaccharide.

Plant mannan and glucomannan polymers have already been successfully synthesized in Pichia by expression of GTs from the cellulose synthase-like A (CSLA) family. Pichia likely has endogenous proteins capable of producing and supplying activated GDP-Man and GDP-Glc sugar donors to the glucomannan biosynthesis enzyme (Voiniciuc et al., 2019). XyG has not yet been heterologously synthesised in Pichia or in any other orthologous host since Pichia does not produce the required nucleotide sugars (UDP-Xyl, UDP-Gal, UDP-GlcA and UDP-Ara) for the biosynthesis of XyG (Cocuron et al., 2007; Pauly and Keegstra, 2016). UDP-Glc was however shown to be present in Pichia (Schultink, 2013). Pichia synthesizes small β-(1,4) glucan oligosaccharides if transformed with the XyG: glucansynthase *AtCSLC4*, and long oligomers of β-(1,4) glucan, if transformed with *AtCSLC4* and *AtXXT1* (Cocuron et al., 2007).

For the reproduction of the biosynthetic machineries of XyG (or a xylosylated glucan polymer) the synthesis pathway in plants can be used as a template: CLSCs are proposed to utilize cytosolic UDP-Glc and produce the glucan backbone while transporting the polymer into the Golgi lumen (Pauly and Keegstra, 2016; Julian and Zabotina, 2022). XXTs xylosylate the glucan backbone and use UDP-Xyl as substrate in the Golgi lumen. UDP-Xyl is produced from conversion of UDP-Glc to UDP-GlcA by a cytosolic UDP-glucose dehydrogenase (UGD). UDP-GlcA is then converted to UDP-Xyl by a UDP-glucuronic acid decarboxylase (UXS) and transported into the Golgi lumen by an UDP-Xyl transporter (UXT) (Zhao et al., 2018; Zhang et al., 2021a).

Former members of the Pauly Laboratory (Dr. Alexander Schultink and Dr. Balakumaran Chandrasekar) created a Pichia strain containing several XyG biosynthetic genes from *Tropaeolum majus*. Nasturtium has XyG rich seeds (Hoth et al., 1986) and is therefore a good organism for identifying the XyG GTs. Alexander Schultink performed an RNA-Seq analysis of developing nasturtium seeds, which identified genes involved in the XyG biosynthesis (*TmCSLC4*, *TmXXT2*, *TmMUR3* and *TmXLT2*) (Jensen et al., 2012). Codon-optimized *TmCSLC4* and *TmXXT2* were transformed into Pichia and glycosidic linkage analysis revealed that this strain was able to produce a glucan polysaccharide (Schultink, 2013). Furthermore, both proteins were present in the Golgi. For the synthesis pathway of UDP-Xyl TmUGD and TmUXS genes were identified in the nasturtium transcriptome and codon optimized versions were expressed in Pichia. Pichia expressing TmUGD and TmUXS accumulated UDP-Glc and UDP-xylose as shown by a nucleotide sugar analysis (Schultink, 2013). Afterwards, TmCSLC4, TmXXT2, TmUGD and TmUXS were coexpressed in a Pichia strain but glycosidic linkage analysis revealed a lack of xylosylated XyG (Schultink, 2013). Based on the genes used UDP-Xyl might be produced in the cytosol and is not transferred into the Golgi to the site of XXT2. Therefore, several nucleotide sugar transporter genes (mammalian UDP-Xyl

transporter SLC35B4 (Ashikov et al., 2005), UDP-GlcA transporter SLC35D1 (Kobayashi et al., 2006), and four putative nucleotide transporters with unknown specificity identified from the nasturtium transcriptional analysis) were cloned and expressed in a Pichia strain already expressing TmCSLC4, TmXXT2, TmUGD and TmUXS (Schultink, 2013). But none of these strains containing five genes did resulted in xylosylated XyG based on glycosidic linkage analysis. The five gene strain expressing SLC35D1 resulted in decreased 4-linked Glc abundance and a decrease in the relative amount of UDP-GlcA and UDP-Xyl compared to the strain with the TmCSLC4, TmXXT2, TmUGD and TmUXS alone (Schultink, 2013).

Construct (each gene had its own expression cassette) and growth protocol (growth in BMGY for 72 h, growth in BMMY for 96 h, 0,5 % of sterile methanol were added every 24 h) improvement on the five gene strain expressing TmCSLC4, TmXXT2, TmUGD, TmUXS and human (*Homo sapiens*, Hs) SLC35D1 (UDP-GlcA transport) by Dr. Balakumaran Chandrasekar resulted in the generation of a polymer containing t-Xyl and 4,6-Glc indicating a xylosylated glucan polymer (e.g. Fig. 3.15). This Pichia strain is hereafter referred to as the "five gene strain". In a digest of Pichia cell material with a β-1,3 glucanase, β-1,6 endoglucanase and β-D-1,4 endoglucanase (Ch. 2.5, Ch. 2.12.5) analysed by MALDI-TOF MS the five gene strain resulted in mass signals with *m/z* values corresponding to oligomers containing hexose and pentoses while the WT only results in oligomers containing only hexoses (e.g. Fig. 3.21). This result suggests that an oligosaccharide containing hexose (e.g. Glc) and pentose (e.g. Xyl) was produced in the five gene Pichia strain. However, the xylosylation rate is very low (less than 4%) compared to typical dicot XyG xylosylation level of 75% (XXXG motif).

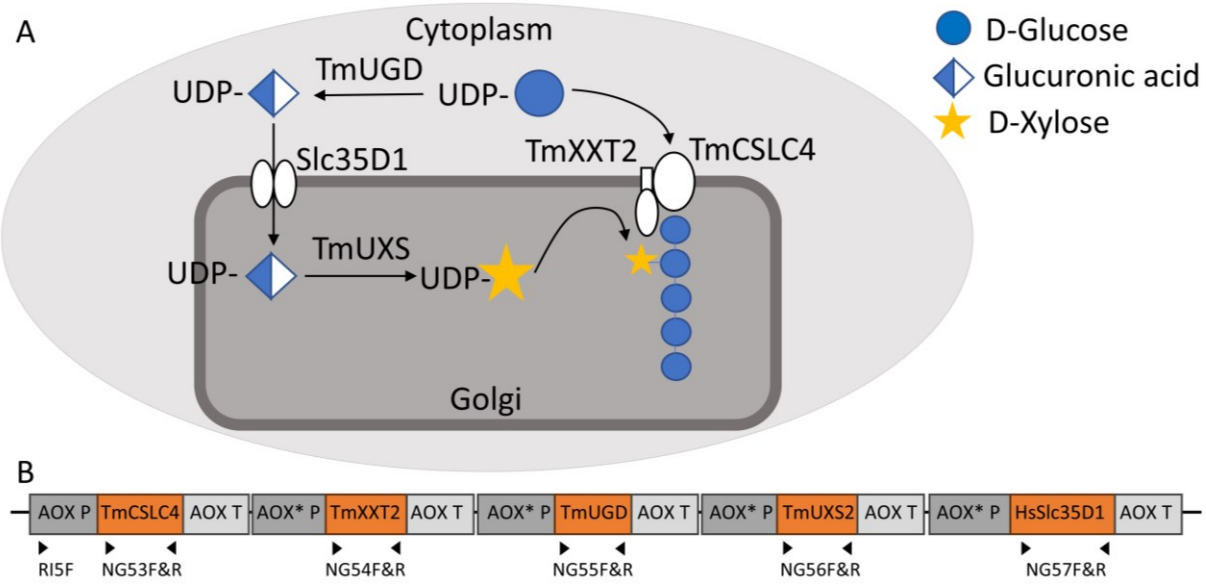

Figure 3.11: Strategy of producing XyG in *Pichia Pastoris*: Five gene strain. A) Mechanism of nucleotide sugar conversion and transport, model by Dr. Balakumaran Chandrasekar; **B)** Linear map of plasmid pPICZ + TmCSLC4, TmXXT2, TmUGD, TmUXS & HsSLC35D1 used to create five gene Pichia strain (P = promoter, T = Terminator,

AOX* = modified AOX promoter (without PmeI restriction site), NG_F&R = primers designed by Niklas Gawenda, F = forward, R = reverse)

In a model by Dr. Balakumaran Chandrasekar (Fig. 3.11) the synthetic XyG biosynthetic machinery in the five gene strain differs in one point from the postulated pathway in plants: UDP-Glc is transformed to UDP-GlcA by TmUGD in the cytosol. The human Slc35D1 transports the UDP-GlcA across the Golgi membrane into the lumen, where it is converted to UDP-Xyl by TmUXS. The transmembrane protein complex of TmCSLC4 and TmXXT2 synthesize the glucan backbone from UDP-Glc and the xylosylation from the UDP-Xyl. In contrast to what is known in plants, UDP-Xyl is not produced in the cytosol and transported into the Golgi lumen, but rather the UDP-GlcA is transported into the Golgi lumen and converted into UDP-Xyl there.

3.2.2 Results

In this thesis, different approaches for enhancing the level of XyG backbone xylosylation were tested in Pichia.

Based on data from complementation approaches of several Arabidopsis *xxt* knockout lines expressing AtXXTs analysed by OLIMP, an XXT1/2 and an XXT3/4/5 (phylogeny in Fig. 3.12). need to be present to produce a dicot like XyG (XXXG) since XXT1/2 add xylosyl residue specifically at the first and second glucose in the glucan chain while XXT3/4/5 add xylosyl residue specifically at the third glucose in the glucan chain (Zabotina et al., 2012; Zhang et al., 2023b). Expression of an XXT5 in the Pichia five gene strain was therefore the first focus to improve the xylosylation level.

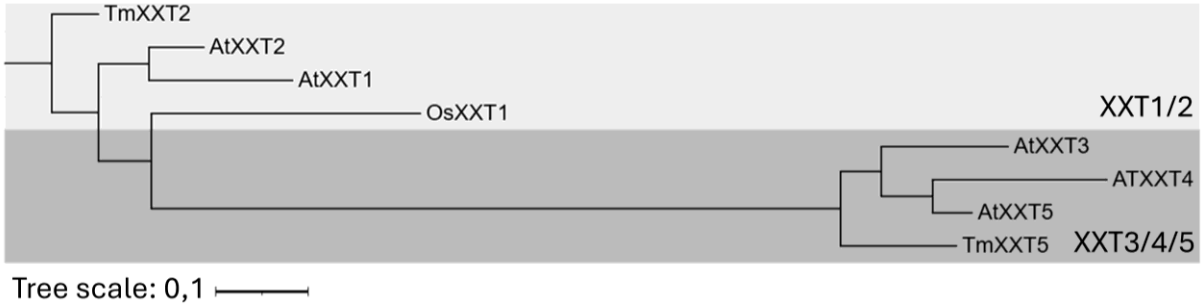

Figure 3.12: Phylogeny of XXTs from Arabidopsis, rice and nasturtium. Phylogenetic tree based on amino acid sequences of Arabidopsis (At), rice (Os) and nasturtium (Tm) XXTs, the scale bar indicates the number of substitutions per site, branch lengths are directly related to the amount of genetic change between shown genes, XXT1/2 and XXT3/4/5 clades are indicated in different shades of grey

To enhance xylosylation, TmXXT5 under the methanol inducible AOX1 promotor was added to the genetic repertoire of the five gene strain (Fig. 3.13).

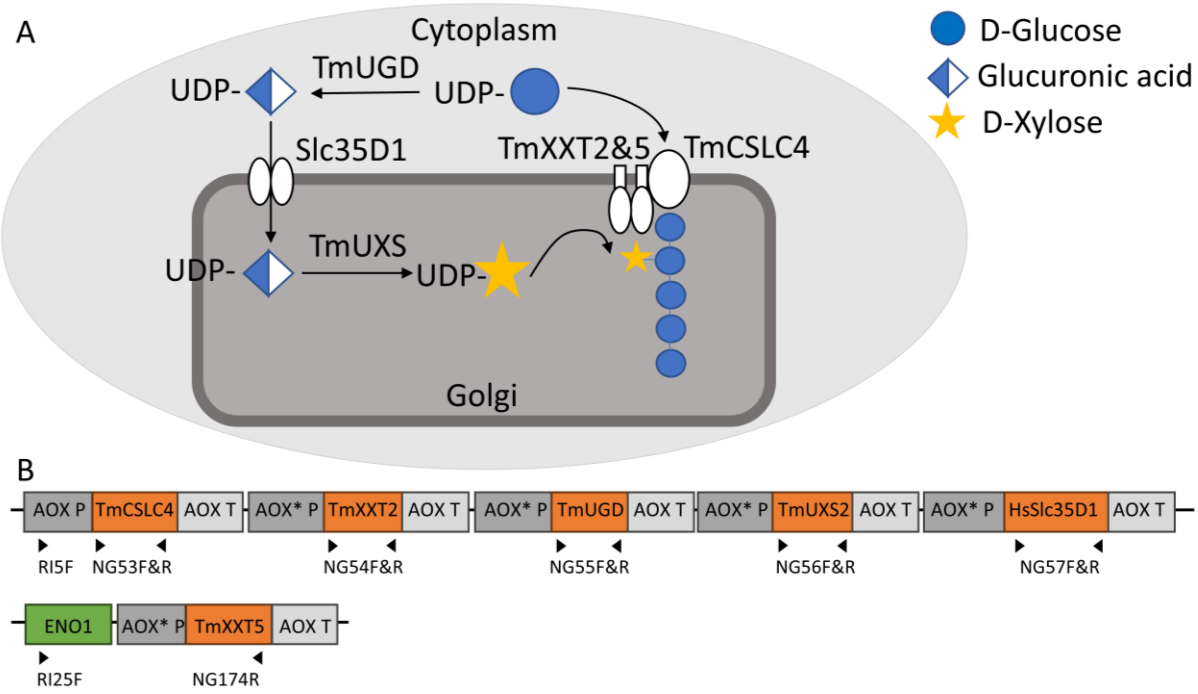

Figure 3.13: Strategy of producing XyG in *Pichia Pastoris*: Five gene strain + TmXXT5. A) Mechanism of nucleotide sugar conversion and transport of Pichia strain expressing TmCSLC4, TmXXT2, TmUGD, TmUXS, SLC35D1 and TmXXT5; **B)** Linear map of plasmid pPICZ + TmCSLC4, TmXXT2, TmUGD, TmUXS & SLC35D1 and plasmid pPICZ eH + TmXXT5 used to create five gene Pichia strain + TmXXT5 (P = promoter, T = Terminator, AOX* = modified AOX promoter, NG_F&R = primers designed by Niklas Gawenda (SFig. 6.12), F= forward, R = reverse)

For this purpose, *TmXXT5* was cloned in pPICZ eH (gene sequence SFig. 6.1, plasmid map SFig. 6.4, cloning by Niklas Gawenda) and transformed in the Pichia five gene strain (Ch. 2.9.11). The expression cassette will localize to the ENO1 integration locus and not to the AOX1 locus as with other pPICZ vectors. The new Pichia strain was selected by growth on selective plates (Zeocin, Hygromycin, Ch. 2.8.1) and confirmed via colony PCR on gDNA (Ch. 2.9.12, Fig. 3.14).

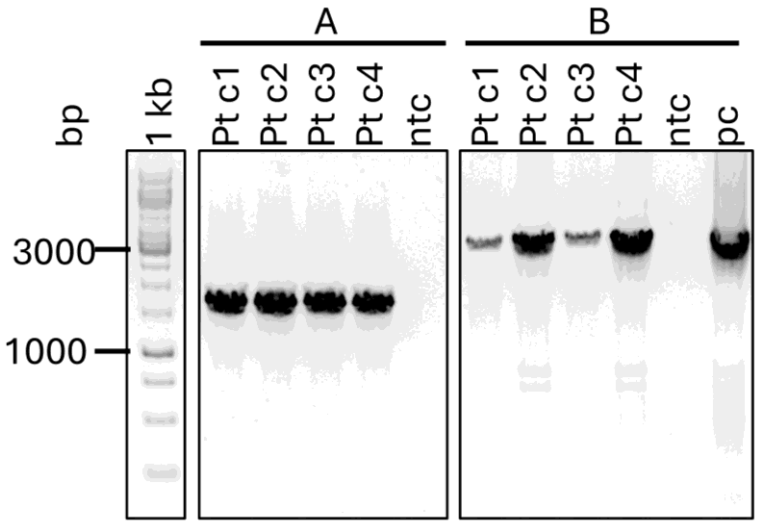

Figure 3.14: Genotyping PCR: To confirm Pichia transformants, (Pt) colonies (c1-c4) transformed with the linearized plasmid pPICZ eH + *TmXXT5* and a pPICZ B + *TmCSLC4*, *TmXXT2*, *TmUGD*, *TmUXS* and *HsSLC35D1* (five gene strain) background were verified via PCR using gDNA as template; **A)** confirms part of pPICZ B + five genes, RI5F & NG54R (bind in AOX promotor and *TmXXT2*, Fig. 3.13), expected size: 1,6 kbp; **B)** confirms pPICZ eH + *TmXXT5*, RI25F & NG174R (bind in AOX promotor and *TmXXT5*, Fig. 3.13), expected size: 2,9 kbp; bp = base pairs, no template control = ntc, plasmid control = pc

The new Pichia strain was grown in BMGY/BMMY medium (Ch. 2.8.4) under the same conditions that lead to detection of xylosylation in the five gene strain developed by Dr. Balakumaran Chandrasekar and analysed using glycosidic linkage analysis (Ch. 2.12.8, Fig. 3.15).

Selected glycosidic linkages of X-33 wildtype (from here on called WT), of the five gene strain (TmCSLC4, TmXXT2, TmUGD, TmUXS and HsSLC35D1) and of the five gene strain plus TmXXT5 indicate that the five gene strain produces polymers with significantly more 4-Glc and 4,6-Glc linkages compared to WT (Fig. 3.15 and SFig. 6.26). The 4- and 4,6-Glc linkages in the WT likely are derived from the storage glycogen (Pauly et al., 2019). Both XyG biosynthesis genes expressing strains produce polymers with a higher abundance of 4-Glc linkages and contain t-Xyl linkages. Even though t-Xyl and more 4-Glc and 4,6-Glc were detected in the new Pichia strain (TmCSLC4, TmXXT2, TmUGD, TmUXS, HsSLC35D1 and TmXXT5) compared to the WT, the abundance of these linkages did not increase compared to the five gene strain indicating that the degree of xylosylation of the produced polymer did not increase when TmXXT5 is co-expressed.

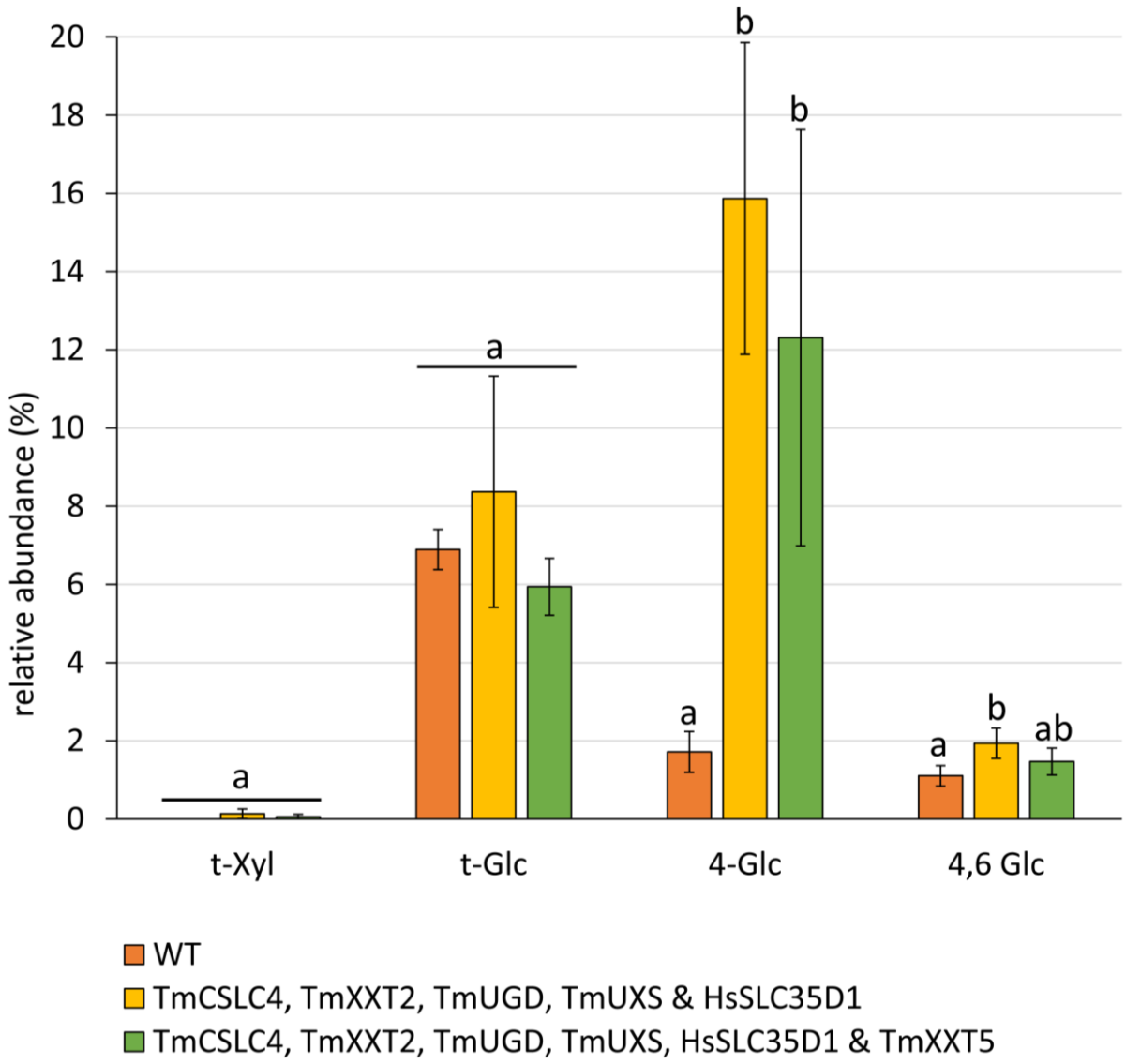

Figure 3.15: Glycosidic linkage analysis of Pichia strains expressing XyG biosynthesis genes - adding TmXXT5 to the five gene strain. Selected linkages of Pichia AIR material of WT and strains expressing XyG biosynthesis genes (TmCSLC4, TmXXT2, TmUGD, TmUXS and HsSLC35D1; TmCSLC4, TmXXT2, TmUGD, TmUXS, HsSLC35D1 and TmXXT5); WT n = 3, TmCSLC4, TmXXT2, TmUGD, TmUXS & HsSLC35D1 n = 3, TmCSLC4, TmXXT2, TmUGD, TmUXS, HsSLC35D1 & TXXT5 n = 4; results of ANOVA analysis and subsequent Tukey's test are indicated ($P < 0,05$); error bars indicate standard deviation

It was also tested whether TmXXT5 could replace TmXXT2 to produce glucan, if co-expressed with TmCSLC4 (Schultink, 2013). A Pichia strain expressing TmCSLC4 (created by Dr. Balakumaran Chandrasekar) was transformed (Ch. 2.9.11) with TmXXT5 in pPICZ eH (plasmid created by Niklas Gawenda). The new Pichia strain was selected by growth on selective plates (Zeocin, Hygromycin, Ch. 2.8.1) and confirmed by PCR (Ch. 2.9.12, Fig. 3.16).

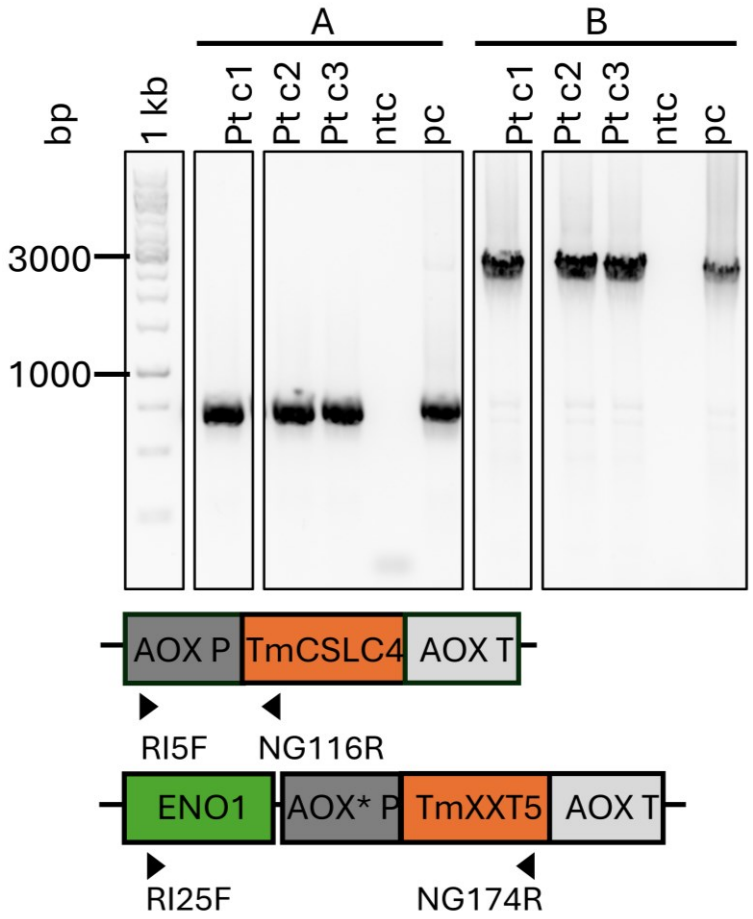

Figure 3.16: Genotyping PCR. To confirm Pichia transformants (Pt), colonies (c1-c3) transformed with the linearized plasmid pPICZ eH + *TmXXT5* and a pPICZ B + *TmCSLC4* background were verified via PCR using gDNA as template; **A)** Confirms pPICZ B + *TmCSLC4*, RI5F & NG116R (bind in AOX promotor and *TmCSLC4*), expected size: 0,8 kbp; **B)** Confirms pPICZ eH + *TmXXT5*, RI25F & NG174R (bind in AOX promotor and *TmXXT5*, Fig. 3.13), expected size: 2,9kb; bp = base pairs, no template control = ntc, plasmid control = pc; **linear maps** of plasmid pPICZ + *TmCSLC4* and plasmid pPICZ eH + *TmXXT5*, P = promoter, T = Terminator, AOX* = modified AOX promoter, NG_F&R = primers designed by Niklas Gawenda, F = forward, R = reverse)

The wildtype strain and strains expressing TmCSLC4 alone, TmCSLC4 and TmXXT2, and CSLC4 and TmXXT5 were grown in BMGY/BMMY medium (Ch. 2.8.4). The Pichia strain expressing TmCSLC4 alone did not result in polymers with significantly higher amounts of 4-Glc compared to the WT (Fig. 3.17 and SFig. 6.27). The Pichia strain expressing TmCSLC4 and TmXXT2 shows a significant increase in the abundance of 4-Glc indicating production of a glucan polymer compared to the WT. However, the TmCSLC4 and TmXXT5 expressing strain did not result in significantly higher 4-Glc values compared to the WT indicating that TmXXT5 does not functionally replace TmXXT2. 4,6-Glc was only detected in the strain expressing TmCSLC4 and TmXXT2. The 4,6-Glc likely derives from storage glycogen (Pauly et al., 2019).

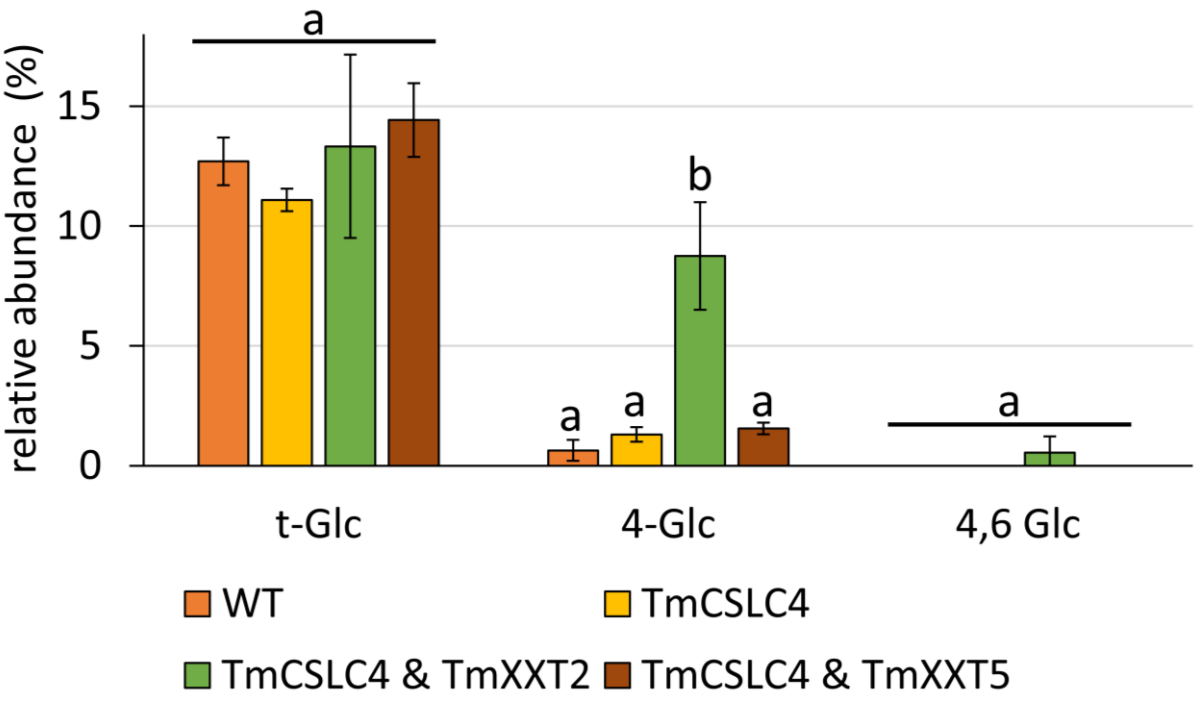

Figure 3.17: Glycosidic linkage analysis of Pichia strains expressing TmCSLC4 and TmXXTs. Selected linkages of Pichia AIR material of WT and strains expressing XyG biosynthesis genes (TmCSLC4; TmCSLC4 and TmXXT2; TmCSLC4 and TmXXT5); n = 4 for all strains; results of ANOVA analysis and subsequent Tukey's test are indicated ($P < 0,05$); error bars indicate standard deviation

Research on SLC35D1 revealed that this nucleotide sugar transporter is localized in the endoplasmic reticulum and Golgi (Hiraoka et al., 2007; Muraoka et al., 2001) and appears to function as a general UDP-sugar transporter *in vitro* as it transports UDP-Gal, UDP-Glc, UDP-GalA, UDP-GlcA, UDP-Ara*p*, UDP-Ara*f* and UDP-Xyl (Rautengarten et al., 2019). Furthermore, it has been proposed that SLC35D1 transports Golgi synthesised UDP-Xyl into the ER (Rautengarten et al., 2019). Even though the five gene strain expressing SLC35D1 produces a xylosylated glucan like polymer, alternative approaches impacting UDP-Xyl production and availability might enhance the degree of xylosylation.

Two alternative strategies were pursued here to enhance UDP-Xyl availability in the Golgi of Pichia: One strategy involves the replacement of the human SLC35D1 with a plant originating, more specific UDP-GlcA transporter localizing to the Golgi. In an Arabidopsis mutant screen for altered pectinaceous seed mucilage the Golgi-localized UDP-GlcA and UDP-GalA transporter UDP-Uronic Acid Transporter 1 (UUAT1) was identified and shown to have *in vitro* transport activity in *Saccharomyces cerevisiae* (Saez-Aguayo et al., 2017). AtUUAT1 was hence selected to be added to the five gene strain as an additional transporter (Fig. 3.18 A)., and to replace the human SLC35D1 in a novel five gene strain (Fig. 3.18 C).

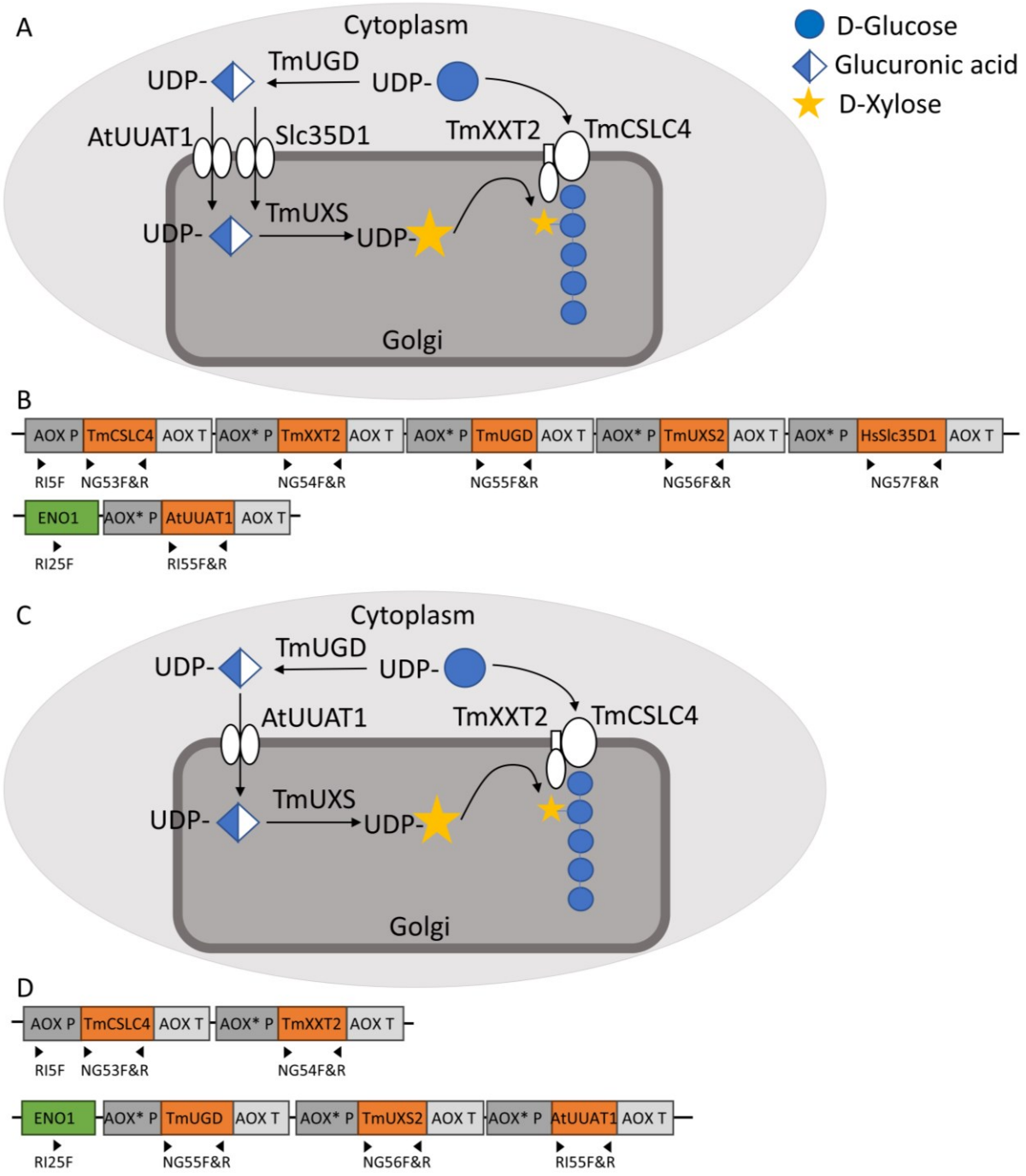

Figure 3.18: Strategy of producing XyG in *Pichia Pastoris*: Introducing a UDP-GlcA transporter. A) Mechanism of nucleotide sugar conversion and transport in six gene strain expressing AtUUAT1; **B)** Linear map of plasmid pPICZ + TmCSLC4, TmXXT2, TmUGD, TmUXS & SLC35D1 and plasmid pPICZ eH + AtUUAT1 used to create five gene Pichia strain + AtUUAT1; **C)** Mechanism of nucleotide sugar conversion and transport in novel five gene strain expressing AtUUAT1; **D)** linear map of plasmid pPICZ + TmCSLC4 + TmXXT2 and pPICZ eH + TmUGD, TmUXS & AtUUAT1 used to create a novel five gene Pichia strain expressing AtUUAT1; (P = promoter, T = Terminator, AOX* = modified AOX promoter, NG_F&R = primers designed by Niklas Gawenda, F = forward, R = reverse)

Another strategy entailed the use of plant originating, cytosolic UDP-xylose synthase and UDP-Xyl transporter instead of the human SLC35D1 UDP-GlcA transporter, which also transports non-specific nucleotides (Rautengarten et al., 2019), and the Golgi lumen localized UXS (Fig. 3.19). UXS catalyses the decarboxylation of UDP-GlcA to UDP-Xyl. In Arabidopsis six UXS have been identified, three membrane-anchored proteins in the Golgi (UXS1, UXS2, and UXS4) and three soluble proteins localized in the cytoplasm (UXS3, UXS5, and UXS6*;* (Harper and Bar-Peled, 2002; Kuang et al., 2016)). AtUXS3, AtUXS5 and AtUXS6 seem to play a prominent role in the supply of UDP-xylose for the biosynthesis of XyG as simultaneous down-regulation/mutations of these genes led to a reduction in the amount of XyG in the primary walls as detected by XyG specific monoclonal antibodies (Zhong et al., 2017). Since *AtUXS3* has the overall highest expression of the three genes (expression data by TAIR, www.arabidopsis.org) and has been shown to convert cytosolic UDP-GlcA to UDP-Xyl when expressed in *Saccharomyces cerevisiae* (Oka and Jigami, 2006) it was selected to replace the Golgi localized TmUXS.

In Arabidopsis the cytosolic UDP-Xyl is transported into the Golgi lumen by three members of the UXT family (UXT1, UXT2, UXT3). All three UXTs localized to Golgi, while UXT1 also localized to the endoplasmic reticulum suggesting a distinct functional role (Ebert et al., 2015). UXT2 and UXT3 are conserved in all plants, while UXT1 is less important in lower plants but conserved in angiosperms (Zhao et al., 2018). As AtUXT3 has a ubiquitous expression and the required localization it was selected for expression in Pichia in addition to AtUXS3.

The first approach was to add the cytosolic AtUXS3 to the original five gene strain (Fig. 3.19 A). A second approch was to add AtUXS3 and AtUXT3 instead of TmUXS and HsSLC35D1 while keeping TmCSLC4, TmXXT2 and TmUGD in a Pichia strain and thereby returning to the plant UDP-Xyl synthesis way with a cytosolic UXS (Fig. 3.19 C).

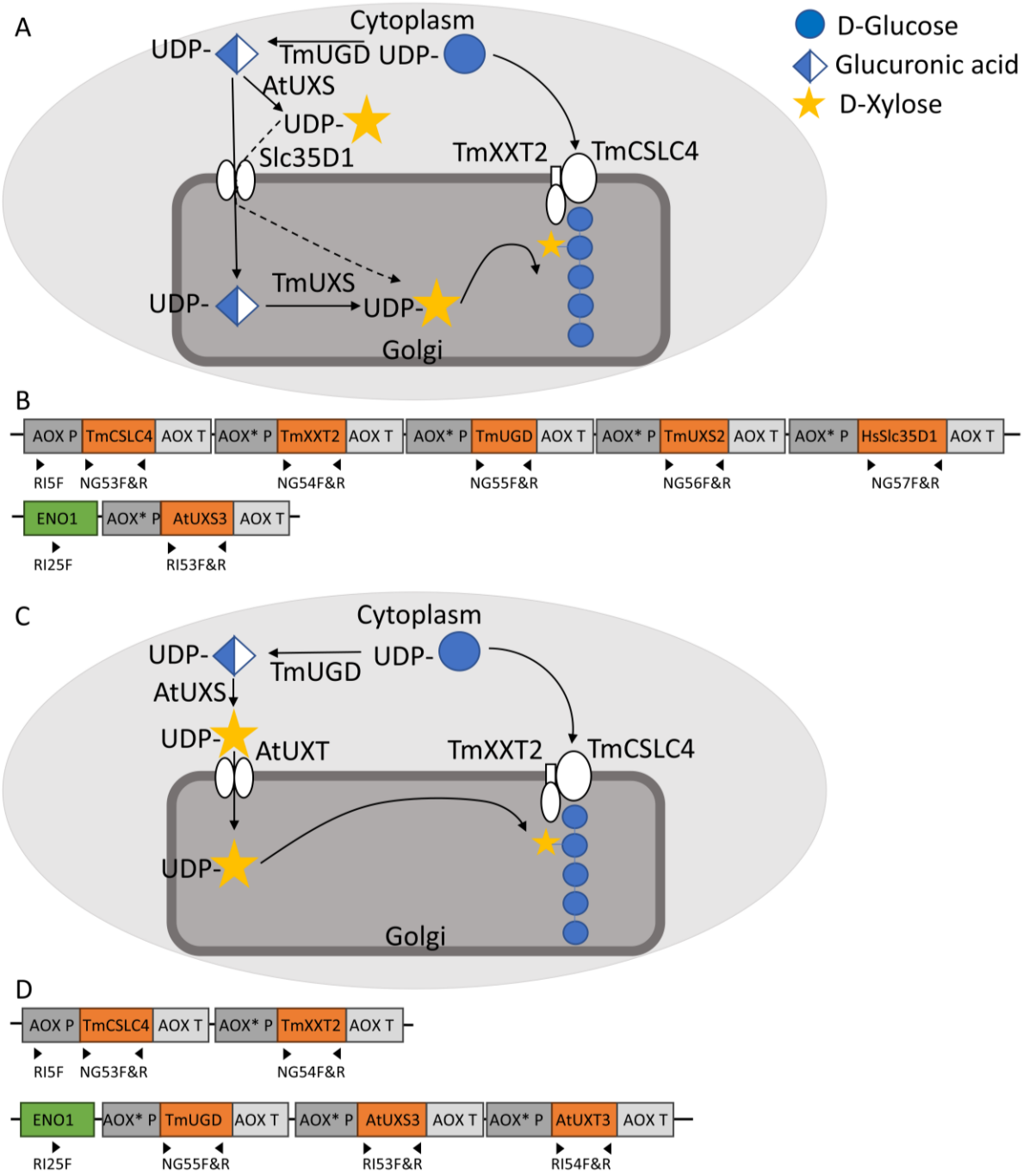

Figure 3.19: Strategy of producing XyG in *Pichia Pastoris*: Introducing a cytosolic UXS. A) Mechanism of nucleotide sugar conversion and transport in six gene strain expressing AtUXS3; **B)** Linear map of plasmid pPICZ + TmCSLC4, TmXXT2, TmUGD, TmUXS & SLC35D1 and plasmid pPICZ eH + AtUXS3 used to create five gene Pichia strain + AtUXS3; **C)** Mechanism of nucleotide sugar conversion and transport in novel five gene strain expressing AtUXS3 & AtUXT3; **D)** linear map of plasmid pPICZ + TmCSLC4 + TmXXT2 and pPICZ eH + TmUGD, AtUXS3 & AtUXT3 used to create a novel five gene Pichia strain expressing AtUXS3 & AtUXT3; (P = promoter, T = Terminator, AOX* = modified AOX promoter, NG_F&R = primers designed by Niklas Gawenda, F = forward, R = reverse)

All genes of interest were cloned into pPICZ eH (SFig. 6.4, cloning by Niklas Gawenda). In a first screen, the Pichia five gene strain (TmCSLC4, TmXXT2, TmUGD, TmUXS, SLC35D1) was transformed (Ch. 2.9.11) with *AtUXS3* or *AtUUAT1*, respectively (gene sequences SFig.

6.1), resulting in a Pichia strain expressing six XyG biosynthetic genes. The Pichia strains were selected by growth on selective plates (Zeocin, Hygromycin, Ch. 2.8.1) and confirmed via PCR (Ch. 2.9.12, Fig. 3.20)**.**

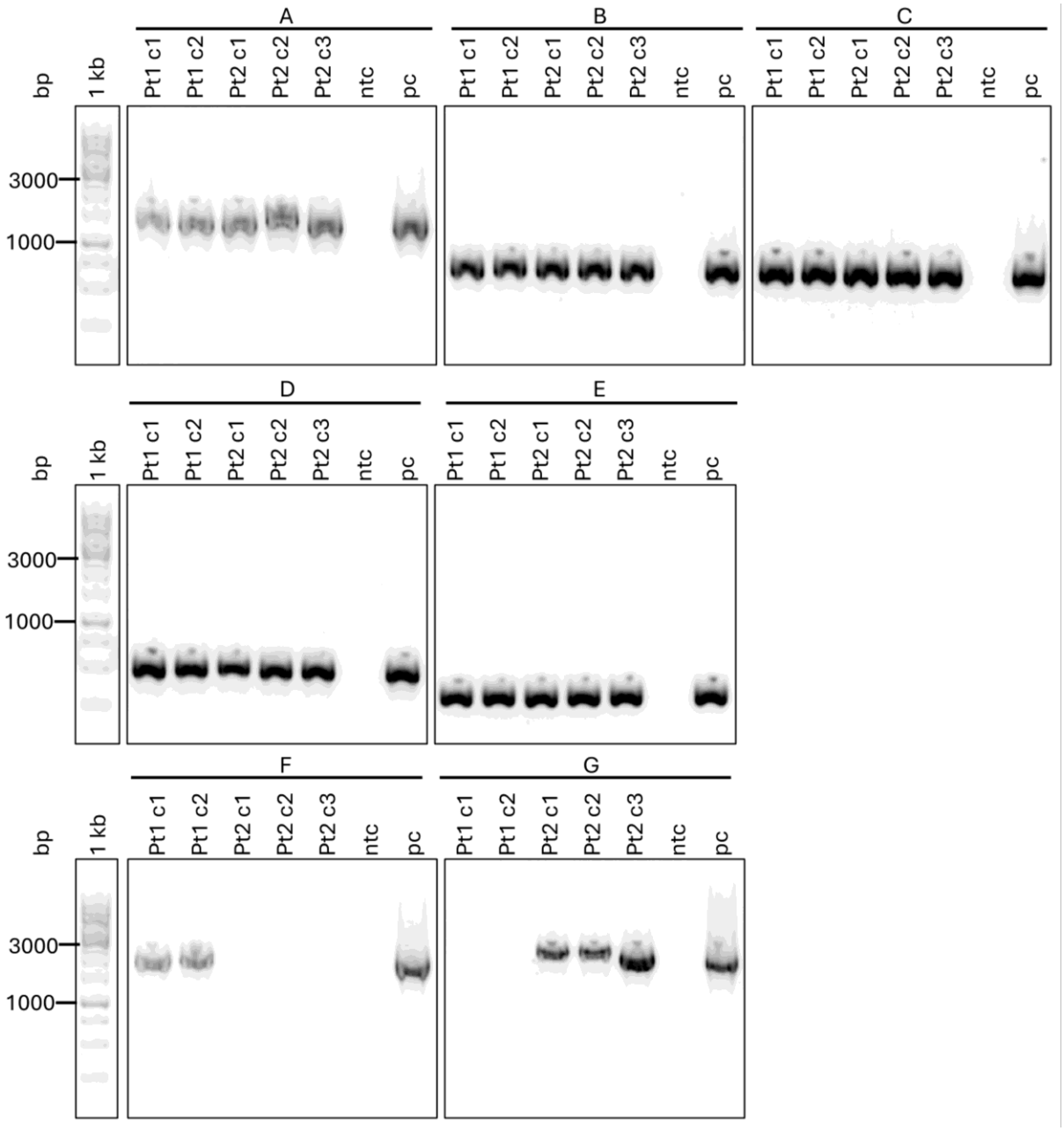

Figure 3.20: Genotyping PCR. To confirm Pichia transformants (Pt), colonies (c1-c2, c1-3)) transformed with the linearized plasmids (Pt1: pPICZ eH + *AtUXS3*, Pt2: : pPICZ eH + *AtUXS3*) and a pPICZ B + *TmCSLC4*, *TmXXT2*, *TmUGD*, *TmUXS* and *HsSLC35D1* (five gene strain) background were verified via PCR using gDNA as template; **A)** confirms part of pPICZ B + five genes, NG53F&R (bind in *TmCSLC4*, Fig 3.18/3.19), expected size: 1,56 kbp, **B)** confirms part of pPICZ B + five genes, NG54F&R (bind in *TmXXT2*, Fig 3.18/3.19), expected size: 0,8 kbp; **C)** confirms part of pPICZ B + five genes, NG55F&R (bind in *TmUGD*, Fig 3.18/3.19), expected size: 0,83 kbp, **D)** confirms part of pPICZ B + five genes, NG56F&R (bind in *TmUXS*, Fig 3.18/3.19), expected size: 0,68 kbp, **E)** confirms part of pPICZ B + five genes, NG57F&R (bind in *HsSLC35D1*, Fig 3.18/3.19), expected size: 0,44 kbp, **F)** confirms pPICZ eH + *AtUXS3*, RI25F & RI53R (bind in AOX promotor and *AtUXS3*, Fig 3.19), expected size: 2,33

kbp, **G)** confirms pPICZ eH + *AtUUAT1* RI25F & RI55R (bind in AOX promotor and *AtUUAT1*, Fig 3.18), expected size: 2,39 kbp, bp = base pairs, no template control = ntc, plasmid control = pc

Both six gene strains were grown in BMGY/BMMY medium under the same xylosylation producing conditions (Ch. 2.8.4) as in the five gene strain and the resulting fungal walls were analysed using glycosidic linkage analysis (Ch. 2.12.8, Fig. 3.21 A, SFig. 6.28) and OLIMP (Ch. 2.12.5, Fig. 3.21 B). In the linkage analysis all three strains (TmCSLC4, TmXXT2, TmUGD, TmUXS & HsSLC35D1; TmCSLC4, TmXXT2, TmUGD, TmUXS, HsSLC35D1 & AtUXS3; TmCSLC4, TmXXT2, TmUGD, TmUXS, HsSLC35D1 & AtUUAT1) expressing plant XyG biosynthetic genes produced t-Xyl, but at the same level. While both novel potential XyG producing strains had more 4-Glc linkages than the five gene strain, the difference is non-significant. Compared to the five gene strain even less or about the same 4,6-Glc linkages were detected. t-Glc was significantly reduced in the novel Pichia strain expressing AtUXS.
Since the AtUXS3 and AtUUAT1 expressing strains did not result in a higher level of t-Xyl and 4,6-Glc linkages it is unlikely that the respective addition of these genes to the five gene strain resulted in a higher xylosylation of the CSLC and XXT produced glucan polysaccharide.
OLIMP analysis of these Pichia strains treated with Zymolyase and Pustulanase to remove β1,3- and β1,6-linked glucans, digested with an endo-1,4-β-D-glucanase (CELBA) to release XyG oligosaccharides (Ch. 2.5, Ch. 2.12.5) resulted in occurrence of mass signals with *m/z* 851, *m/z* 1013, *m/z* 1175, *m/z* 1337, *m/z* 1499 and *m/z* 1661 in all samples. These mass signals relate to masses of oligosaccharides made entirely of hexoses with a varying degree of polymerization (dp, hexose ladder). In the strains containing plant XyG biosynthetic genes (five and novel six gene strains) also mass signals at *m/z* 821, *m/z* 983, *m/z* 1115, *m/z* 1145 *m/z* 1277 and *m/z* 1439 were observed. These mass signals relate to masses of oligosaccharides made from four hexoses and one pentose, five hexoses and one pentose, five hexoses and two pentoses, six hexoses and one pentose, six hexoses and two pentoses, and seven hexoses and two pentoses, respectively, suggesting the presence of xylosylated glycan oligos. The mass signal *m/z* 953 representing an oligosaccharide consisting of four hexoses and two pentoses was found in all tested Pichia strains. The common *m/z* 1085 (XXXG) usually observed in plant XyG was not detected in the Pichia samples.
Comparing the relative abundance of mass signals (Günl et al., 2011; Günl and Pauly, 2011) reveals that oligosaccharides of the hexose ladder make up about 70%, while oligosaccharides from hexoses and one or more pentoses make up about 30 % of all detected oligosaccharides in all strains in the shown range (Fig. 3.21 B). Introduction of AtUUAT1 or AtUXS3 to the 5 gene strain did not improve abundance of pentosylated (most likely xylosylated) mass signals.

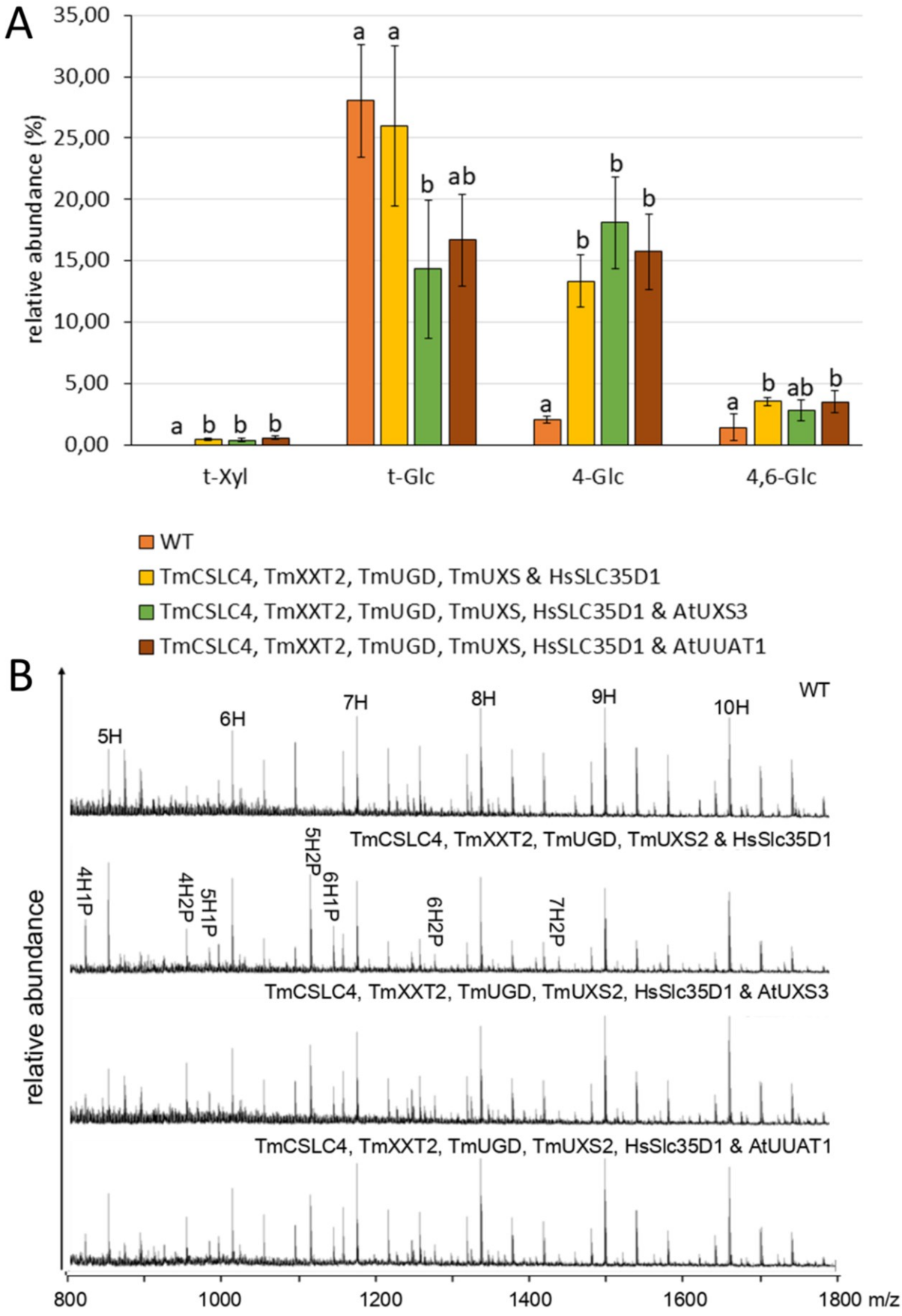

Figure 3.21: Glycosidic linkage analysis and XyG oligosaccharide mass profiling of *Pichia pastoris* strains expressing XyG biosynthesis genes - adding AtUXS3 and AtUUAT1 to the five gene strain. A) Selected

linkages of Pichia AIR material of WT and strains expressing XyG biosynthesis genes (TmCSLC4, TmXXT2, TmUGD, TmUXS and HsSLC35D1; TmCSLC4, TmXXT2, TmUGD, TmUXS, HsSLC35D1 and AtUXS3; TmCSLC4, TmXXT2, TmUGD, TmUXS, HsSLC35D1 and AtUUAT1); n = 4 for all strains; results of ANOVA analysis and subsequent Tukey's test are indicated ($P < 0,05$); error bars indicate standard deviation; **B)** MALDI-TOF MS analysis on CELBA released oligosaccharides from cell wall material from these Pichia strains, mass signals are labelled with suggested oligosaccharide structures indicated by number of hexoses (H) and pentoses (P)

For the second strategy a Pichia strain with TmCSLC4 and TmXXT2 (by Dr. Balakumaran Chandrasekar) was transformed (Ch. 2.9.11) with pPICZ eH containing *TmUGD*, *TmUXS* and *AtUUAT1* or *TmUGD*, *AtUXS3* and *AtUXT3* (for the UDP-Xyl synthesis pathway) (Fig. 3.18 and 3.19). The two constructs with the UDP-Xyl synthesis pathway were created using the multimer construct approach (Ch. 2.9.7.3). Unwanted restriction sites were removed using site directed mutagenesis (Ch. 2.9.8). First, the plasmid pPICZ eH + *TmUGD* and pPICZ eH + *TmUXS2* were created by amplifying (Ch. 2.9.5) both genes from the five gene plasmid and cloning them into pPICZ eH by restriction/ligation cloning (Ch. 2.9.7.2, confirmation via colony PCR Ch. 2.9.12, SFig. 6.24 A & B). Plasmids pPICZ eH + *AtUUAT1*, pPICZ eH + *AtUXS3* and pPICZ eH + *AtUXT3* were created by Niklas Gawenda. Afterwards, the plasmids pPICZ eH + *TmUGD* & *TmUXS* and pPICZ eH + *TmUGD* & *AtUXS3* were created (Ch. 2.9.7.3, confirmation via colony PCR Ch. 2.9.12, SFig. 6.24 C & D). Finally, pPICZ eH with *TmUGD*, *TmUXS* and *AtUUAT1* or *TmUGD*, *AtUXS3* and *AtUXT3* were created (Ch. 2.9.7.3, confirmation via colony PCR Ch. 2.9.12, SFig. 6.24 E & F). The Pichia strain with TmCSLC4 and TmXXT2 was individually transformed with pPICZ eH with *TmUGD*, *TmUXS* and *AtUUAT1*, or *TmUGD*, *AtUXS3* and *AtUXT3* (Ch. 2.9.9). The Pichia strains were selected by growth on selective plates (Zeocin, Hygromycin, Ch. 2.8.1) and confirmed via colony PCR (Fig. 3.22).

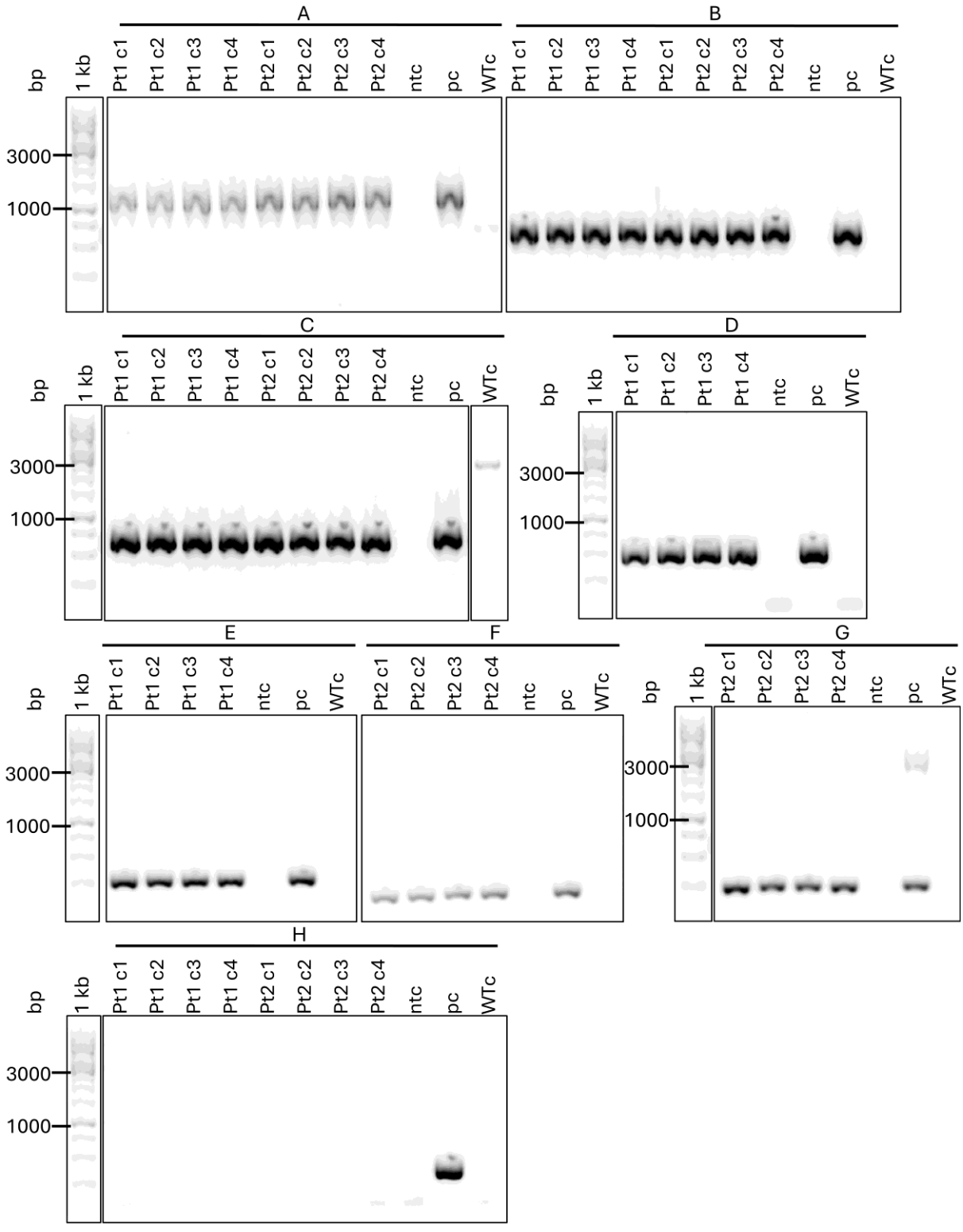

Figure 3.22: Genotyping PCR. To confirm Pichia transformants (Pt), colonies (c1-c4) transformed with the linearized plasmids (Pt1: pPICZ eH + *TmUGD* + *TmUXS2* + *AtUUAT1*, Pt2: : pPICZ eH + *TmUGD* + *AtUXS3* + *AtUXT3*) and a pPICZ B + *TmCSLC4* and *TmXXT2* background were verified via PCR using gDNA as template; **A)** confirms part of pPICZ B + *TmCSLC4* and *TmXXT2* background, NG53F&R (bind in *TmCSLC4*, Fig 3.18/3.19), expected size: 1,56 kbp, **B)** confirms part of pPICZ B + *TmCSLC4* and *TmXXT2* background, NG54F&R (bind in *TmXXT2*, Fig 3.18/3.19), expected size: 0,8 kbp; **C)** confirms part of both pPICZ eH + *TmUGD* , NG55F&R (bind in *TmUGD*, Fig 3.18/3.19), expected size: 0,83 kbp, **D)** confirms part of Pt1: pPICZ eH + *TmUGD* + *TmUXS2* + *AtUUAT1*, NG56F&R (bind in *TmUXS*, Fig 3.18/3.19), expected size: 0,68 kbp, **E)** confirms part of Pt1: pPICZ eH

+ *TmUGD* + *TmUXS2* + *AtUUAT1*, RI55F&R (bind in *AtUUAT1*, Fig 3.18), expected size: 0,3 kbp, **F)** confirms part of Pt2: pPICZ eH + *TmUGD* + *AtUXS3* + *AtUXT3*, RI54F&R (bind in *AtUXT3* , Fig 3.19), expected size: 0,28 kbp, **G)** confirms part of Pt2: pPICZ eH + *TmUGD* + *AtUXS3* + *AtUXT3*, RI53F&R (bind in *AtUXS3*, Fig 3.19), expected size: 0,23 kbp, **H)** confirms absence of *HsSLC35D1*, NG57F&R (bind in *HsSLC35D1*, Fig 3.18/3.19), expected size: 0,44 kbp; bp = base pairs, no template control = ntc, plasmid control = pc, Wtc = wildtype control (template is X33 gDNA)

These novel five gene strains were also analysed by glycosidic linkage (Ch. 2.12.8, Fig. 3.23 A, SFig. 6.29) and OLIMP analysis (Ch. 2.12.5, Fig. 3.23 B). The glycosidic linkage analysis of all three Pichia strains demonstrated the occurrence of t-Xyl, but all in the same range. Significantly more 4-Glc linkages were detected in all four strains expressing plant XyG biosynthetic genes compared to the WT. The novel five gene strains produce even more 4-Glc then the TmCSLC4 & TmXXT2 and the five gene strain suggesting that longer glucan chains may be produced by those strains.

OLIMP analysis (Fig. 3.23 B) resulted in mass signals at *m/z* 851, *m/z* 1013, *m/z* 1175, *m/z* 1337, *m/z* 1499 and *m/z* 1661 corresponding to a hexose ladder in all samples. In all samples with a UDP-Xyl synthesis pathway additional mass signals at *m/z* 821, *m/z* 953, *m/z* 983, *m/z* 1115, *m/z* 1145 *m/z* 1277 and *m/z* 1439 were detected, which relate to masses of oligosaccharides consisting of four hexoses and one pentose, four hexoses and two pentoses, five hexoses and one pentose, five hexoses and two pentoses, six hexoses and one pentose, six hexoses and two pentoses and seven hexoses and two pentoses, respectively. In the Pichia samples the *m/z* 1085 (XXXG) from plant XyG was again not detected.

Comparing the relative abundance of mass signals (Günl et al., 2011; Günl and Pauly, 2011) reveals that oligosaccharides of the hexose ladder and oligosaccharides from hexoses and one or more pentoses both make up about 50 % of all detected oligosaccharides in the five gene strain in the shown range (Fig. 3.23 B) while oligosaccharides from hexoses and one or more pentoses make up about 33% in the strain expressing TmCSLC4, TmXXT2, TmUGD, TmUXS, AtUXS3 & AtUXT3, and about 23% in the strain expressing TmCSLC4, TmXXT2, TmUGD, TmUXS & AtUUAT1. Introduction of an alternative UDP-GlcA transporter or the return to the plant UDP-Xyl biosynthesis pathway with a cytosolic UXS and a UXT did not improve abundance of pentosylated (most likely xylosylated) mass signals.

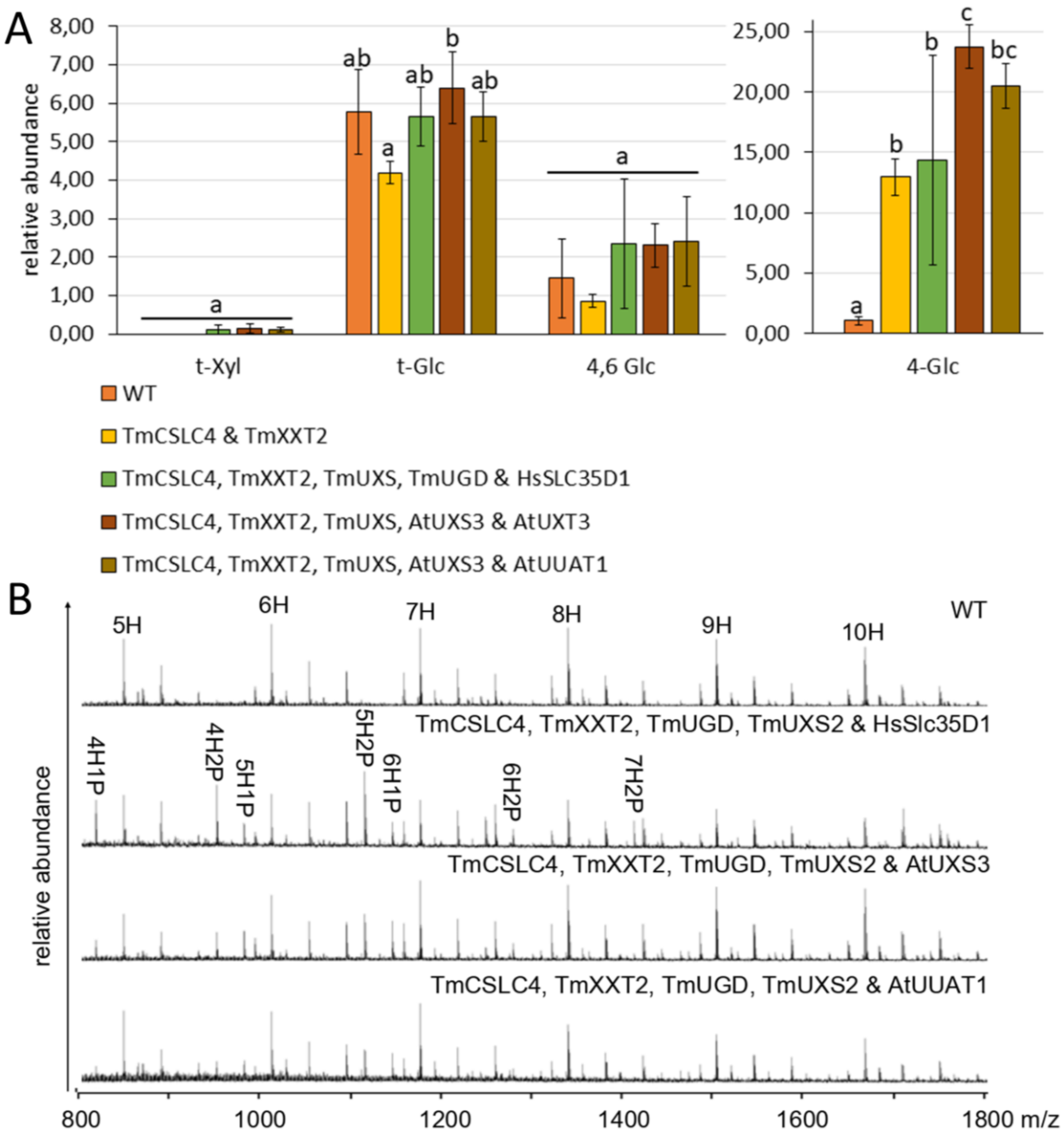

Figure 3.23: Glycosidic linkage analysis and XyG oligosaccharide mass profiling of *Pichia pastoris* strains expressing XyG biosynthesis genes - UDP-Xyl synthesis pathway with plant genes. A) Selected linkages of Pichia AIR material of WT and strains expressing XyG biosynthesis genes (TmCSLC4, TmXXT2; TmCSLC4, TmXXT2, TmUGD, TmUXS and HsSLC35D1; TmCSLC4, TmXXT2, TmUGD, AtUXT3 and AtUXS3; TmCSLC4, TmXXT2, TmUGD, TmUXS and AtUUAT1); n = 4 for all strains; results of ANOVA analysis and subsequent Tukey's test are indicated ($P < 0,05$); error bars indicate standard deviation; **B)** MALDI-TOF MS analysis on CELBA released oligosaccharides from cell wall material from these Pichia strains; mass signals are labelled with suggested oligosaccharide structures indicated by number of hexoses (H) and pentoses (P)

Another approach to producing XyG in Pichia is to introduce XyG biosynthetic enzymes from plant species other than *Tropaeolum majus* and Arabidopsis. Monocots typically produce XyG with a repeating XXGG motif, two consecutive xylosylated glucose residues followed by two unmodified glucose units, often *O*-acetylated (Vincken et al., 1997; Pauly and Keegstra, 2016). This structural variation is significant because it reflects species differences in XyG

architecture. Reconstructing monocot-type XyG in a heterologous system like Pichia may thus broaden our understanding of XyG biosynthesis and effects.

The first step would be to test whether rice CSLCs are able to produce a glucan polysaccharide in Pichia. The structures (exons and introns) of CSLC4 genes are different between monocots and eudicots. Furthermore, the distribution across the CSLC subfamilies is different (Kim et al., 2020).

So far, only dicot protein combinations of CSLC and XXT (here *Tropaeolum majus*) showed evidence of successful heterologous production of such a polysaccharide. Rice (*Oryza sativa,* Os) is a model monocot as it is an important crop with a small genome size (compared to other Poales) and easy applicable and efficient transformation (Ray et al., 2022). In rice nine CSLC candidates have been identified by BLAST searches using the Arabidopsis cellulose synthase and cellulose synthase-like proteins as queries (Hazen et al., 2002). More recent publications found six rice CSLCs (OsCSLC1, 2, 3, 7, 9 and 10) in a phylogenetic analysis of the same protein families (Li et al., 2022). Using CSLC amino acid sequences from Arabidopsis (from tair), rice (from UniProt) and TmCSLC4 a phylogenetic tree was created (Ch. 2.2, ngphylogeny.fr, Fig. 3.24 A). TmCSLC4 shares the highest similarity in amino acid sequence with OsCSLC3 and OsCSLC2.

Analysis of the rice proteins of the XXT GT34 family revealed that a total of five rice XXT candidates group together with AtXXTs in a phylogenetic analysis (OsXXT1, OsGT2, OsGT3, OsGT4 and OsGT5) (Wang et al., 2014; Zhong et al., 2021). OsXXT1 shares high sequence and structural similarity with AtXXT1 and AtXXT2. Complementing the Arabidopsis double mutant *xxt12* with OsXXT1 lead to repair of the root hair defect, slow growth and XyG synthesis (Wang et al., 2014). In mammalian cells OsXXT1 was shown to produce up to tetra-xylosylated cellohexaose with three and four consecutive xylosylated Glc residues (Zhong et al., 2021). A phylogenetic tree was created using amino acid sequences from Arabidopsis (from tair), rice (from UniProt and the Rice Genome Annotation Project) and TmXXT2 (Ch. 2.2, ngphylogeny.fr, Fig. 3.24 B). The phylogeny shows that OsXXT1 is the only rice XXT grouping in the XXT1/2 subclade. Two more rice GTs (OsGT2 and OsGT3) group in the XXT3/4/5 clade. Another two GTs are more distantly related to the XXTs and do not group in the XXT1/2 or XXT3/4/5 clade.

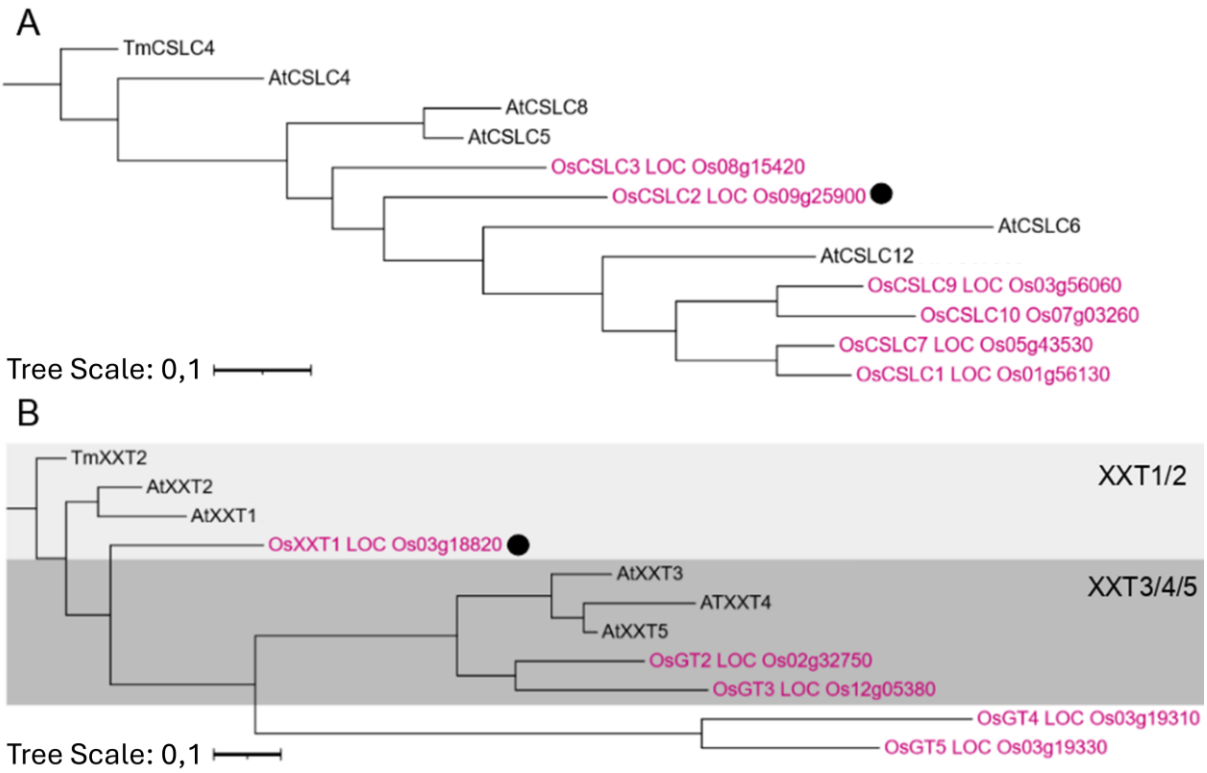

Figure 3.24: Phylogeny of CSLCs and XXTs from Arabidopsis, rice and nasturtium. The scale bar indicates the number of substitutions per site, branch lengths are directly related to the amount of genetic change between shown genes; rice gene names use a system that includes a locus identifier (LOC_Os), chromosome number, gene type and a unique number; **A)** Phylogenetic tree based on amino acid sequences of Arabidopsis (At), rice (Os) and nasturtium (Tm) CSLCs, pink font: rice proteins, dot represent rice CSLC expressed in Pichia **B)** Phylogenetic tree based on amino acid sequences of At, Os and Tm XXTs, pink font: rice proteins, XXT1/2 and XXT3/4/5 clades are indicated in different shades of grey, dot represent rice XXT expressed in Pichia

Based on the close similarity to TmCSLC4 and TmXXT2 OsCSLC2 (LOC_Os09g25900) and OsXXT1 (LOC_Os03g18820) were selected to be tested in Pichia. Two multimer constructs expressing OsCSLC2 + TmXXT2 and OsCSLC2 + OsXXT1 in a pPICZ vector were created using the method mentioned in Ch. 2.9.7.3 (single gene constructs were created by Niklas Gawenda, both rice genes were synthesized from GeneArt gene synthesis, confirmation of constructs via colony PCR Ch. 2.9.12, SFig. 6.25, gene sequences SFig. 6.1). The confirmed plasmids were transformed (Ch. 2.9.11) into Pichia. The new Pichia strains were selected by growth on selective plates (Zeocin, Ch. 2.8.1) and confirmed by PCR (Ch. 2.9.12, Fig. 3.25).

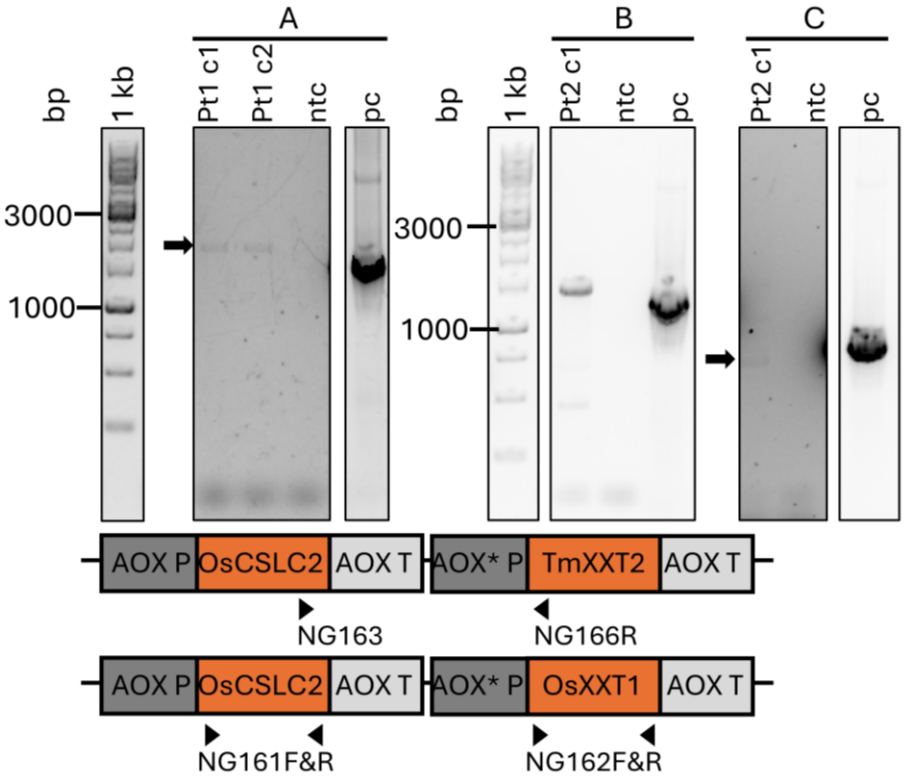

Figure 3.25: Genotyping PCR. To confirm Pichia transformants (Pt), colonies (c1, c2; c1) transformed with the linearized plasmid Pt1: pPICZ + *OsCSLC2* + *TmXXT2* and Pt2: pPICZ + *OsCSLC2* + *OsXXT1* were verified via PCR using gDNA as template; **A)** confirms part of pPICZ + *OsCSLC4* + *TmXXT2*, NG163F & NG166R (bind in *OsCSLC4* and *TmXXT2*), expected size: 1,7 kbp; **B)** confirms part of pPICZ + *OsCSLC4* + *OsXXT1*, NG161F&R (bind in *OsCSLC2*), expected size: 1,4 kbp; **C)** confirms part of pPICZ + *OsCSLC2* + *OsXXT1*, NG162F&R (bind in *OsXXT1*), expected size 0,9 kbp; bp = base pairs, no template control = ntc, plasmid control = pc; **linear maps** of plasmids pPICZ + *OsCSLC2* + *TmXXT2* and pPICZ + *OsCSLC2* + *OsXXT1*, P = promoter, T = Terminator, AOX* = modified AOX promoter, NG_F&R = primers designed by Niklas Gawenda, F = forward, R = reverse)

Liquid cultures were grown in BMGY (72h) and BMMY (24h) (Ch. 2.8.4) under the same conditions that led to the increased 4-Glc detection in the Pichia strain expressing TmCSLC4 and TmXXT2. Linkage analysis was performed on AIR material (Ch. 2.12.2, Ch. 2.12.8). The analysis resulted in a statistically higher 4-Glc and 4,6-Glc content in the strain with TmCSLC4 and TmXXT2 compared to the WT (Fig. 3.26, SFig. 6.30) confirming previous results of Dr. Alex Schultink. The Pichia strains with rice genes however did not result in significant changes in XyG relevant linkages compared to the Pichia wildtype. Xylosylation was not detected as the Pichia strains investigated here do not produce UDP-Xyl.

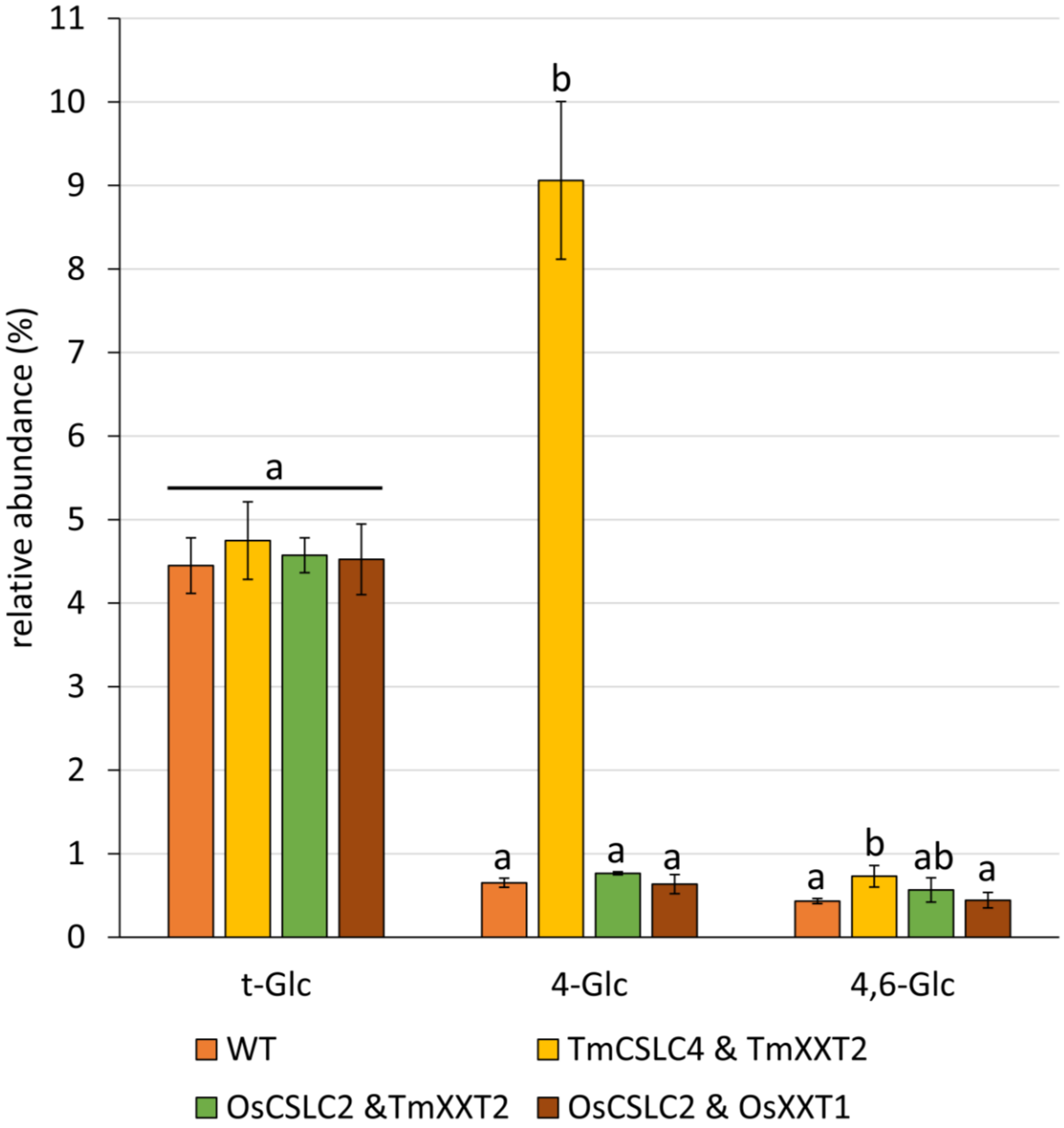

Figure 3.26: Glycosidic linkage analysis of Pichia strains expressing *Oryza sativa* CSLC and XXT. Selected linkages of Pichia AIR material of WT and strains expressing different combinations of nasturtium and rice CSLCs and XXTs; n = 4 for all strains; results of ANOVA analysis and subsequent Tukey's test are indicated ($P < 0,05$); error bars indicate standard deviation

3.2.3 Discussion

Pichia pastoris has been shown to function as a platform for heterologous synthesis of hemicellulosic polymers on the level from oligosaccharide to polysaccharide (Cocuron et al., 2007; Voiniciuc et al., 2019). Plant GTs can be stably integrated in the Pichia genome (Voiniciuc et al., 2019) and expressed when desired using the AOX promoter, which is considered a strong and easily controllable promoter (Dharmarathna et al., 2023). The wide availability of vectors for Pichia allows several genes of interest to be integrated at different locations in the genome (here AOX1 and ENO locus). Given that Pichia has relevant amounts

of some sugar compounds on its own, it cannot be considered as a blank screening background for testing GTs (Pauly et al., 2019). A further challenge in the heterologous production of complex plant cell wall polysaccharides like XyG is that Pichia does not possess all the necessary nucleotide sugars (Cocuron et al., 2007; Pauly and Keegstra, 2016) and that corresponding synthesis pathways needs to be introduced genetically to Pichia.

The aim to produce a xylosylated glucan and thus a XyG-like polysaccharide in Pichia was based on the preliminary work by Dr. Alex Schultink and Dr. Balakumaran Chandrasekar, who developed a Pichia strain expressing five genes (*TmCSLC4*, *TmXXT2*, *TmUGD*, *TmUXS* and *HsSLC35D1*) thereby producing a xylosylated glucan based on detection of t-Xyl, 4, Glc and 4,6-Glc in glycosidic linkage analysis and the OLIMP profile showing mass signals for oligosaccharides containing hexoses and pentoses (e.g. Fig. 3.21). In most dicot plants 75% of the XyG glucose units are substituted with a xylosyl residue (XXXG motif) (Culbertson et al., 2016). The Pichia five gene strain produced oligosaccharides with four to seven hexoses and one or two pentoses in the OLIMP analysis, which would mean a xylosylation rate of the glucan backbone of up to 50% (mass signal *m/z* 953, four hexoses and two pentoses). However, results of glycosidic linkage analysis indicate, that the overall production of a xylosylated glucan is less than 4% of the overall produced oligosaccharides (ratio of t-Xyl to difference of 4-Glc in transformed strain to WT).

Expression of both CSLC4 and XXT2 is required in Pichia for the production of a glucan chain, as the expression of only CSLC did not result in the production of a glucan chain (Fig. 3.17). This confirms previous result as CSLC need an XXT to produce long β-(1-4) glucans (Cocuron et al., 2007). XXT2 appears to have a non-catalytic role in the production of the glucan chain by e.g. forming a protein complex with CSLC.

The additional expression of TmXXT5 in the Pichia five gene strain resulted in the production of a xylosylated 4-linked glucan as revealed by glycosidic linkage analysis (Fig. 3.15). However, the xylosylation level did not improve as the levels of t-Xyl and 4,6-Glc did not exceed the ones from the five gene strain. The values even decreased, suggesting that TmXXT5 might hinder or slow down the XyG metabolism in this Pichia strain. In an enzymatic activity in vitro XXT5 shows significantly slower activity rate than XXT1 and XXT2 (Culbertson et al., 2016). Combination assays with XXT2 and XXT5 did not increase xylosylation compared to XXT2 and XXT5 single-enzyme reactions, which indicates that the protein-protein interaction with XXT2 does not increase the activity of XXT5 (Culbertson et al., 2016). XXT2 and XXT5 form a heterocomplex (Chou et al., 2012; Lund et al., 2015), and both XXTs use a different acceptor based on biochemical, bioinformatic and morphological data, resulting in xylosylation at different residues of the emerging glucan chain (Culbertson et al., 2018; Zhang et al., 2023b). It is possible that the activity rate of XXT5 also affects that of XXT2. However, it remains

unclear whether TmXXT5 influences the activity of TmXXT2 in the XyG biosynthesis enzyme complex.

Protein-protein interactions analysed by bimolecular fluorescence complementation showed the highest fluorescence index for the CSLC4-XXT5 pair. Therefore, XXT5 occupies the closest position to CSLC4 in comparison with the XXT1 and XXT2 (Chou et al., 2012). Lund et al. stated that there is a protein-protein interaction with high confidence between CSLC4 and XXT5 while no protein-protein interaction was indicated for CSLC4 with XXT2 (Lund et al., 2015). Could TmXXT5 in a Pichia strain functionally replace TmXXT2 if a TmCSLC4 is present? A TmCSLC4 and TmXXT5 expressing Pichia strain did not produce a glucan polysaccharide (Fig. 3.17) as 4-Glc levels remained stable for this Pichia strain compared to the WT. The 4-Glc detected in the WT is likely derived from storage glycogen (Pauly et al., 2019). Therefore, TmXXT5 does not functionally replace XXT2.

The two Pichia strains modulating UDP-Xyl biosynthesis and Golgi transport expressing 6 biosynthetic genes (TmCSLC4, TmXXT2, TmUGD, TmUXS, HsSLC35D1 and AtUUAT1 or ATUXS3) produce a xylosylated glucan (Fig. 3.21 A). The ratio of t-Glc to 4-Glc and the higher 4-Glc levels indicate the production of longer glucan chains. However, the xylosylation level did not improve by adding a more specific Glc-A transporter or a cytosolic UXS to the original five gene strain.
The novel five gene Pichia strains without the unspecific human SLC35D1 transporter express TmCSLC4 and TmXXT2, and TmUGD, TmUXS and AtUUAT1 or TmUGD, AtUXS3 and AtUXT3 as a UDP-Xyl synthesis pathway. Xylosylation did not improve, as t-Xyl and 4,6-Glc levels correspond to those of the original five gene strain (Fig. 3.23 A).
The OLIMP profiles of digested material from WT, original five and both six gene Pichia strains (five gene strain + AtUUAT1 or AtUXS3), as well as the novel five gene strains without the human nucleotide sugar transporter show a hexose ladder (Fig. 3.21 B and 3.23 B). Even though the digest with Zymolyase (β-1,3 glucanase) and Pustulanase (β-1,6-endoglucanase) and the following washing steps removed some of the native β1,3- and β1,6-linked glucans (Pauly et al., 2019), the native 4-linked glucans from storage glycogen (Pauly et al., 2019) are not removed and show up in the OLIMP profile after the CELBA (β-1,4-endoglucanase) digest. The mass signals in the OLIMP profile that do not appear in the WT are therefore of particular interest. Multiple mass signals with a mass-to-charge ratio that correspond to oligosaccharides consisting of hexoses and pentoses were detected in the three strains expressing XyG biosynthetic enzymes: *m/z* 821 - four hexoses and one pentose, *m/z* 983 - five hexoses and one pentose, *m/z* 1115 - five hexoses and two pentoses, *m/z* 1145 - six hexoses and one pentose, *m/z* 1277 - six hexoses and one pentose and *m/z* 1439 seven hexoses and two pentoses. Those are likely to represent xylosylated glucan oligosaccharides. However, further

experiments such as glycosidic linkage analysis on specific potentially xylosylated oligosaccharides would be necessary to be able to verify their structure unambiguously.
It should be noted that the OLIMP profiles do not differ between the five and six gene strains and therefore do not indicate an improvement in xylosylation in the newly created strains. However, the relative abundance of the mass signals for potentially xylosylated oligosaccharides differ. Dicot typical XyG oligosaccharide *m/z* 1085 representing XXXG was not detected indicating that the implemented xylosylation pathway in Pichia is not producing a plant like XyG.

It is interesting to note that in all Pichia strains expressing XyG glucan backbone, xylosylation and UDP-Xyl synthesis pathway genes, the proportion of t-Xyl remains relatively constant even though different synthesis routes are being tested.
Explanation of the non-improvement of the xylosylation level could be feedback inhibition of UGD and UXS by UDP-Xyl (Oka and Jigami, 2006; Zhao et al., 2018). In the Pichia strain expressing cytosolic UXS UDP-Xyl might inhibit UGD and the cytosolic AtUXS, while in the Pichia strain expressing UUAT1 the UDP-Xyl might inhibit the luminal TmUXS.
Furthermore, AtUXT1 might be a better choice as UDP-Xyl transporter than AtUXT3, since *AtUXT1* has the highest expression of the three *UXTs* and Arabidopsis *UXT3* mutants lack an obvious phenotype while *UXT1* mutants showed a significant decrease in cell wall-derived Xyl (Ebert et al., 2015). UXT1 might thus play a more important role providing UDP-Xyl for cell wall biosynthesis in the Golgi.
Another explanation for low xylosylation levels could be a slow synthesis rate in Pichia cultures, as the same protocol was used for all experiments investigating xylosylation. Prolonged induction with methanol was not tested. However, the induction over 96 h is already relatively long. Even though 96 hours are still in the recommended time frame of the EasySelect™ Pichia Expression Kit, optimal incubation time might be different. Another factor can be the methanol concentration. The optimal induction time for Pichia depends on the methanol concentration and the expressed proteins (Santoso et al., 2012; Naseem et al., 2021).
In summary, the constant outcome of the different Pichia strains could indicate that a component, a coenzyme, or a hitherto unknown parameter is missing for successful higher xylosylation. As enzymes involved in XyG biosynthesis are organized in multiprotein complexes (Chou et al., 2012; Chou et al., 2015; Julian and Zabotina, 2022) one or more enzymes might be missing to form an enzyme complex capable of higher level xylosylation. Potential enzyme candidates for improvement of the xylosylation include MUR3, XLT2 and FUT1 as they form heterocomplexes with CSLC4 (Chou et al., 2012; Chou et al., 2015). Due to high homology arabinosyltransferases and galacturonosyltransferases could also be part of XyG biosynthesis multienzyme complexes (Julian and Zabotina, 2022) and could be introduced to Pichia for improved xylosylation levels.

Many GTs are stimulated by the presence of divalent cations (Cavalier and Keegstra, 2006). AtXXT1 and AtXXT2 activities required Mn^{2+} (Cavalier and Keegstra, 2006). Mn^{2+} is present in yeast cells (Reddi et al., 2009) and should be supplied during cultivation by yeast extract in the growth media (BMGY and BMMY Ch. 2.8.4). However, too much or too little manganese can stress the cell (Reddi et al., 2009). One could test if different manganese concentrations in the growth media would influence the xylosylation rate in Pichia.
Furthermore, activity of GTs can depend on salt concentrations, pH, and temperature (Culbertson et al., 2016). XXT2 shows decreasing activity with increased sodium chloride concentration or with increased incubation temperature (37 °C), and a peak activity in pH 7,5 to 9. XXT5 showed highest activity between pH 7 and 8 (Culbertson et al., 2016). The temperature of incubation used here (30 °C) seems close enough to the optimal temperature for XXT activity stated by Culbertson et al. (22 - 28 °C).
The intracellular pH of yeast cells can vary depending on growth phase, nutrient availability and other environmental factors (Imai and Ohno, 1995; Orij et al., 2011). Optimal pH for GT activity and the intracellular pH of Pichia might not match here. One could try to influence the intracellular pH by changing the pH of the growth media to a higher pH.
Another aspect is that growth conditions of Pichia are mostly tested and optimized regarding protein secretion. To test cell wall enzymes in Pichia the cell density might be a more important factor. Protein levels are highest at 30 °C while highest viable cell density was detected at 25 °C (Joseph et al., 2022). One could therefore try incubating the cultures at 25°C which fits the activity optimum of XXT2 (Culbertson et al., 2016).

The Hymenaea XXTA (see Ch. 3.1) that produces a hyperxylosylated XyG could be introduced to Pichia and coexpressed with a CSLC4, an XXT2 and/or XXT5, and enzymes for the biosynthesis of UDP-Xyl. Since HcXXTA produces XXXXG and XXXXXG in a complementation approach in Arabidopsis it might also improve xylosylation in Pichia.

To further analyse the original five gene strain (TmCSLC4, TmXXT2, TmUGD, TmUXS and HsSLC35D1) the subcellular localization of HsSLC35D1 should be determined to confirm the concurring localization with the XyG biosynthesis site at the Golgi in Pichia since it localizes to the ER in mammalian cells (Rautengarten et al., 2019). The protein could be expressed with a fluorescence tag and analysed by microscopy.
Furthermore, nucleotide sugar analysis of microsomal extracts of transgenic Pichia strains expressing XyG Biosynthetic genes could be performed to analyse the presence of UDP-Xyl in the Golgi. Detection of UDP-Xyl in those microsomal extracts would indicate a sufficient supply of UDP-Xyl for the XyG biosynthesis, but could also indicate, that the UDP-Xyl is not used for the XyG biosynthesis and therefore builds up in the Golgi lumen. Absence or low amounts of UDP-Xyl could indicate a bottleneck in the UDP-Xyl supply (e.g. an issue with the

nucleotide sugar transporters) which would then hinder a successful XyG synthesis. On the other hand, absence or lower amounts of UDP-Xyl could also indicate that all or most of the available UDP-Xyl in the Golgi is successfully used by an XXT to synthesise XyG and would therefore not be detected by a nucleotide sugar analysis.

The glycosidic linkage analysis of Pichia strains expressing a rice CSLC2 and TmXXT2 or rice CSLC2 and XXT1 did not result in the production of a 4-linked glucan (Fig. 3.26). This might be related to the selection of the rice genes expressed, as OsCSLC3 based on gene sequence similarity it is the closest homolog to TmCSLC4. Although the phylogenetic similarity between OsCSLC3 and OsCSLC2 is high, OsCSLC3 may be more likely to take over the role of TmCSLC4 than OsCSLC2. OsXXT1 on the other hand seems to be the right choice based on phylogeny and the fact that OsXXT1 was shown to efficiently xylosylate cellohexaose in vitro and to produce up to four consecutive xylosylated Glc residues (Zhong et al., 2021).
Another potential explanation could be non-functional protein-protein interaction of OsCSLC2 with the two XXTs. TmXXT2 was previously shown to have a non-catalytic role in the production of the glucan chain by e.g. forming a protein complex with TmCSLC4. If OsCSLC2 is unable to form such a protein complex with TmXXT2 or OsXXT2, this could cause the inability to produce a glucan polysaccharide.
The phylogeny shows a high degree of similarity between TmXXT and OsXXT but it must still be noted that nasturtium is a dicot while rice is a monocot in which XyG has a different core structure (XXGG) (Scheller and Ulvskov, 2010). However, coexpression of OsCSLC and OsXXT, both from rice, also did not result in glucan production, and therefore XXTs used here do not seem to be the origin of the lack of glucan synthesis. A next step could be to test OsCSLC3 in combination with other XXT para- or orthologs to test whether it would take over dicot CSLC4 function since it is closer related to CSLC4 then OsCSLC2.

3.3 Characterization of Charophycean Green Algae Xyloglucan Biosynthesis Enzymes

3.3.1 Background

XyG is common in all higher land plants (Scheller and Ulvskov, 2010) and have also been found in early land plants (mosses, liverworts, hornworts, ferns, lycophytes) (Peña et al., 2008; Hsieh and Harris, 2012), but initially seemed to be absent in the walls of the charophytes Chara, Coleochaete and Klebsormidium using conventional biochemical methods (Popper and Fry, 2003). Hence, the question arises at what evolutionary point in time XyG first appeared and when the underlying biosynthetic mechanism evolved.

Ancestors of Charophycean green algae (CGA or basal streptophytes, Fig. 3.27) are considered the origin of land plants as they developed the ability to survive and conquer drier habitats (Niklas and Kutschera, 2010; Delwiche and Cooper, 2015; Bowman, 2022).

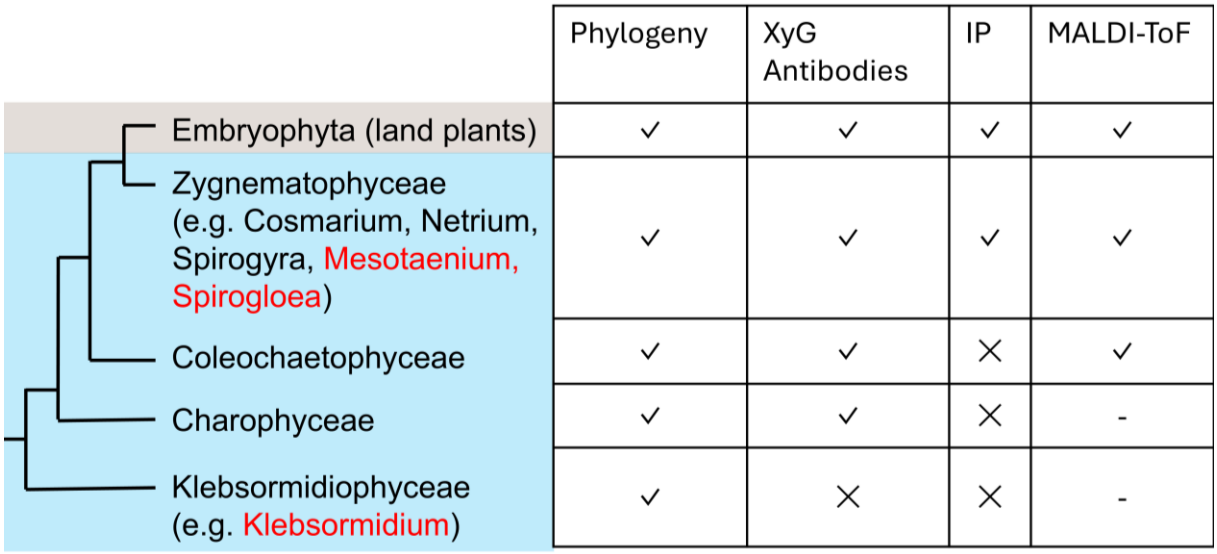

Figure 3.27: Cladogram of Streptophyta and detection of XyG. Embryophytes (grey) are nested within a grade of charophycean algae (blue). Cladogram designed based on (Del Bem and Vincentz, 2010; Del-Bem, 2018; Mikkelsen et al., 2021; Bowman, 2022). Presence of XyG based on different analysis methods. ✓ = detected, ✕ = not detected, - = not tested; Phylogeny: phylogenetic analyses of enzymes involved in XyG synthesis (Del Bem and Vincentz, 2010; Del-Bem, 2018; Mikkelsen et al., 2021), XyG antibodies: detection using XyG-specific monoclonal antibodies (Ikegaya et al., 2008; Sørensen et al., 2011; Mikkelsen et al., 2021), IP: isoprimeverose detection (S. C. Fry, 2000; Mikkelsen et al., 2021), OLIMP: detection of mass signals matching known XyG oligosaccharides (Mikkelsen et al., 2021); species in red: analysed in this thesis

A XyG like polysaccharide was shown to be present in Spirogyra by immunocytochemical analysis against XyG, and hydrolysis followed by gas chromatography (Ikegaya et al., 2008). In *Chara corallina, Coleochaete nitellarum, Cosmarium turpini* and *Netrium digitus* XyG epitopes were detected by XyG-specific antibodies (Domozych et al., 2009; Domozych et al., 2010; Sørensen et al., 2011), while in Spirogyra sp. XyG typical linkages were detected

(Sørensen et al., 2011). However, a glycosidic linkage cannot necessarily be assigned to specific polysaccharide because of the lack of knowledge about CGA cell wall structure (Sørensen et al., 2011). The use of XyG specific antibodies also harbours limitations since they have different specificities and sensitivities (Mikkelsen et al., 2021). Recent work underpins the presence of XyG in CGAs using XyG-specific monoclonal antibodies, Driselase digestion releasing isoprimeverose, and xyloglucanase digestion followed by OLIMP (Mikkelsen et al., 2021). However, detection of XyG oligosaccharides following enzymatic digestion with Driselase or xyloglucanases can be hindered by the limited accessibility of XyG within the cell wall matrix and by structural constraints imposed by XyG sidechains that prevent effective enzyme-substrate interaction (Popper and Fry, 2005; Matsuzawa et al., 2019).

Comparative genomic analysis of XyG biosynthetic enzymes delivered indication of the presence of XyG biosynthetic enzymes in various CGAs (Del Bem and Vincentz, 2010; Del-Bem, 2018; Mikkelsen et al., 2014). Phylogenetic analysis of GT2 family (includes CSLCs) and GT34 family (includes XXTs) of Mesotaenium, Spirogloea and Spirogyra (Mikkelsen et al., 2021) indicate that late divergent CGA may have the biosynthetic machinery for production of XyG such as CSLCs, XXTs and GTs for further sidechain extension (GT37 and 47 families).

Taken together, there is now considerable evidence that XyG and its biosynthetic machinery most likely evolved prior to the transition of plants to land and potentially originated in CGA (Del-Bem, 2018; Han et al., 2019; Mikkelsen et al., 2021). However, putative XyG biosynthetic enzymes from CGA have not yet been functionally characterized. Here, biosynthetic XyG enzymes from three CGA species will be characterized: Zygnematophyceae (here *Mesotaenium endlicherianum* and *Spirogloea muscicola*) and Klebsomidophyceae (here *Klebsormidium nitens*). While Zygnematophyceae are situated as the closest living relatives to land plants, Klebsomidiophyceae are classes of earlier evolved CGA (Mikkelsen et al., 2021).

3.3.2 Results

To elucidate whether XyG biosynthetic enzymes from CGA species are able to produce XyG, collaborators Luiz-Eduardo Del-Bem (Bioinformatics & Evolutionary Genomics, University of São Paulo) and Sang-Jin Kim (Plant Research Laboratory, Michigan State University) identified potential CSLC gene candidates to characterize.

Here, the amino acid sequences of the CGA Klebsormidium Mesotaenium and Spirogloea CSLCs, Arabidopsis CSLCs and a nasturtium CSLC were used to create a phylogenetic tree (Ch. 2.2, ngphylogeny.fr, Fig. 3.28, gene sequences SFig. 6.1). The phylogenetic tree shows that Spirogloea and Mesotaenium gene candidates are closely related to land plant CSLCs while Klebsormidium CSLC candidates are more distinct.

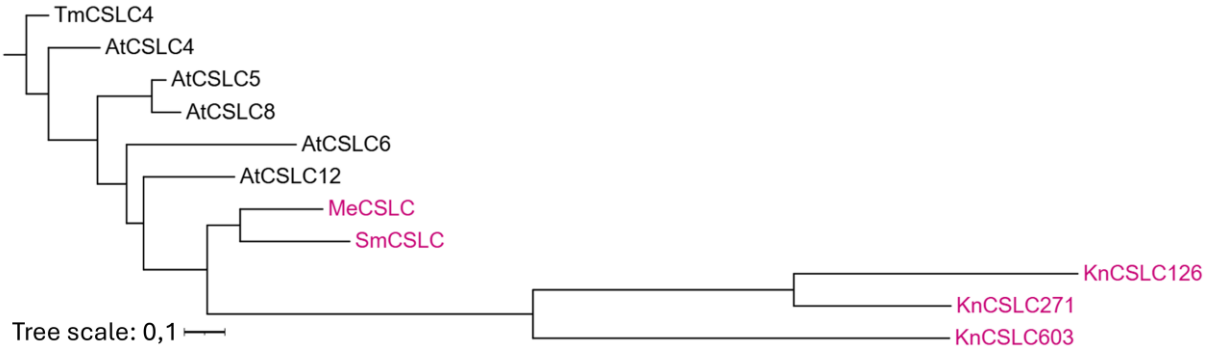

Figure 3.28: Phylogeny of algae CSLCs and characterized CSLCs. Phylogenetic tree based on amino acid sequences of algae, Arabidopsis (At) and nasturtium (Tm) CSLCs, the scale bar indicates the number of substitutions per site, branch lengths are directly related to the amount of genetic change between shown genes, pink font: algae proteins, *Klebsormidium nitens* (Kn, taxonomically reclassified from *Klebsormidium flaccidum Kfl*, kfl00126_0150_v1.1 = KnCSLC126, kfl00271_0180_v1.1 = KnCSLC271, kfl00603_0080_v1.1 =KnCSLC603), *Mesotaenium endlicherianum* (*Me,* ME000209S02952 = MeCSLC) and *Spirogloea muscicola* (*Sm*, SM000017S02811 = SmCSLC); gene information for Arabidopsis can be found in UniProt database

The partial protein sequence alignment (Fig. 3.29) of characterized (Arabidopsis and nasturtium) and algae CSLCs (from Klebsormidium, of Mesotaenium and Spirogloea) show no difference in the key domains (Kim et al., 2020) DD, DAD and DMD thought to define the nucleotide sugar binding domain and the catalytic site of GT2 family enzymes (A. Richmond and R. Somerville, 2001; Morgan et al., 2013; Kim et al., 2020). Only in the domain QQxRW are slight variations. The predicted topology based on the amino acid sequence (SFig. 6.35) shows differences in the number of transmembrane domains for two of the Klebsormidium CSLC candidates, since they have 5 and 8 predicted transmembrane domains (KnCSLC126 and KnCSLC603, respectively) while the other analysed CSLCs (Arabidopsis, nasturtium, other CGA) have 6 transmembrane domains as demonstrated for Arabidopsis in earlier research (Davis et al., 2010; Julian and Zabotina, 2022).

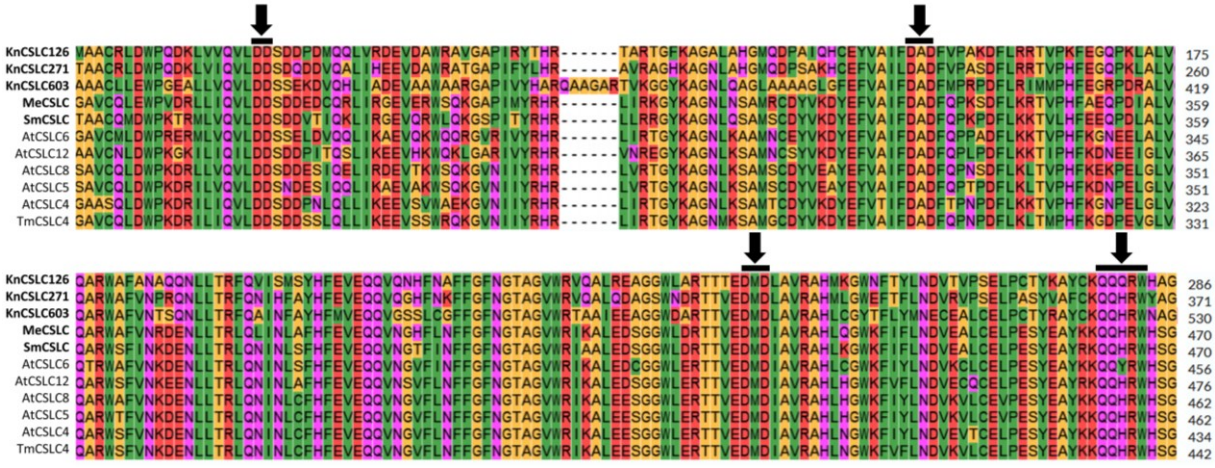

Figure: 3.29: Partial protein sequence alignment of Arabidopsis, nasturtium and CGA CSLCs. Clustal Omega alignment of known CSLCs and algae CSLC candidates (bold); black arrows show key domains: DD, DAD, DMD, QQxRW

The collaborators performed a complementation approach similar to Kim et al., 2020. The Arabidopsis *cslc456812* quintuple mutant (Kim et al., 2020) was transformed with CSLC genes from CGAs using a pGWB515 gateway binary vector for N-terminal fusion with 3xHA (CaMV35S promoter) and a pGWB542 gateway binary vector for N-terminal fusion with eYFP (CaMV35S promoter). The collaborators labelled XyG in 6-day old roots of the resulting Arabidopsis complementation lines with the LM15 antibody to detect XyG in the root. In the WT Col0 strong LM15 labelling at both root and root hair were detected, while the empty vector complemented line showed no labelling. Complemented Arabidopsis lines with Mesotaenium and Spirogloea CSLC resulted in strong LM15 labelling in root hair walls, but only weak LM15 labelling was found in the roots of the Klebsormidium CSLC complemented line. Root hair length was restored in Spirogloea complemented line and partially restored in Mesotaenium complemented lines. Klebsormidium complemented lines had the same root phenotype as the empty vector control Arabidopsis CSLC quintuple mutant. These results indicate that the algae species Mesotaenium and Spirogloea might contain parts of the XyG biosynthesis machinery or more specifically functional CSLCs.

To further validate the data of the collaborator's Arabidopsis complementation approach the occurrence and structure of XyG in the roots of the complemented Arabidopsis lines was investigated here. For this purpose, root AIR material of Arabidopsis *csla456812* complemented with algae CSLCs was XEG digested and analysed by OLIMP (Ch. 2.12.3, Fig. 3.30). Arabidopsis WT contains mass signals at *m/z* 1085, 1393, 1435 and 1555, which are consistent with the XyG oligo structures XXXG, XXFG, XXFG and XLFG, respectively, representing a typical XyG structure found in Arabidopsis (Lerouxel et al., 2002). In the Arabidopsis *cslc* quintuple mutant (*cslc456812*) XyG is lacking (Kim et al., 2020), and hence also in the empty vector control (pGWB542) no XyG mass signals were detected. The quintuple mutant lines complemented with SmCSLC and MeCSLC had mass signals at *m/z* 1085, 1393 and 1435 representing XXXG, XXFG and XXFG. This result also suggests functional CSLC activity for the two algal CSLC candidates. In the Klebsormidium CSLC complemented no XyG typical mass signals were observed.

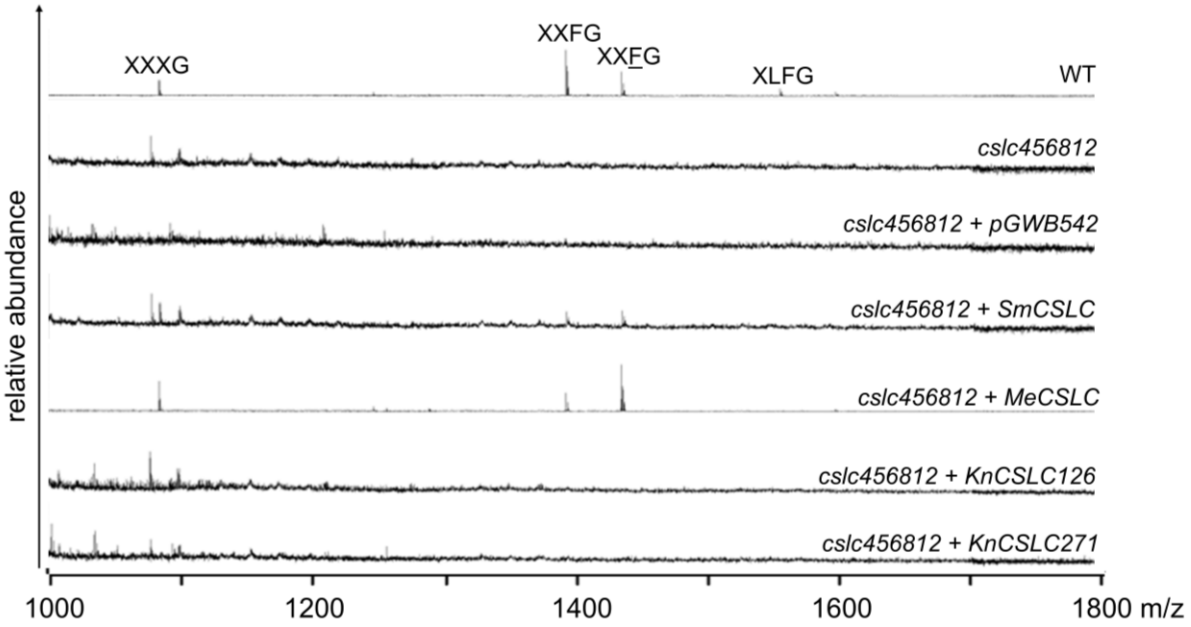

Figure 3.30: XyG oligosaccharide mass profiling of XEG digested Arabidopsis root AIR of CGA CSLC complemented lines. OLIMP was performed on AIR material prepared from Arabidopsis roots send by the collaborators. Assignment of oligosaccharide structures by XyG one-letter code. *cslc456812*: Arabidopsis quintuple mutant, pGWB542: empty vector control, *Klebsormidium nitens* (Kn), *Mesotaenium endlicherianum* (Me), *Spirogloea muscicola* (Sm)

In addition, the algae *CSLC* genes were transformed into the heterologous host *Pichia pastoris* to ascertain their activity. For this purpose, Pichia strains expressing an algae *CSLC* and *TmXXT2* were produced using vectors pPICZ B (SFig. 6.2, or pPICZ Gateway. SFig. 6.3) and pPICZ eH (SFig. 6.4) under the control of the AOX promotor (Ch. 2.4). *CSLC* was coexpressed with an *XXT* because both proteins are required to produce long oligomers of β-(1,4) glucan (Cocuron et al., 2007). *TmXXT2* was utilized because its expression successfully led to the production of a 4-linked glucan in in Pichia when combined with *TmCSLC4* (Ch. 3.2.2). The constructs were created using restriction/ligation (Ch. 2.9.7.2, SFig. 6.32. A) or Gateway cloning (Ch. 2.9.7.4, SFig. 6.32 B) based on plasmids supplied by the collaborators. The Pichia strains with pPICZ eH with *TmXXT2* (construct by Niklas Gawenda, confirmed by colony PCR Ch. 2.9.12, SFig. 6.31) and pPICZ B with one CGA *CSLC* respectively (constructs with *KnCSLC126*, *MeCSLC* and *SmCSLC* by Niklas Gawenda) were transformed by electroporation (Ch. 2.9.11). The transformants were selected by growth on selective plates (Zeocin, Hygromycin, Ch. 2.8.1) and confirmed by colony PCR on gDNA (Ch. 2.9.12, Fig. 3.31).

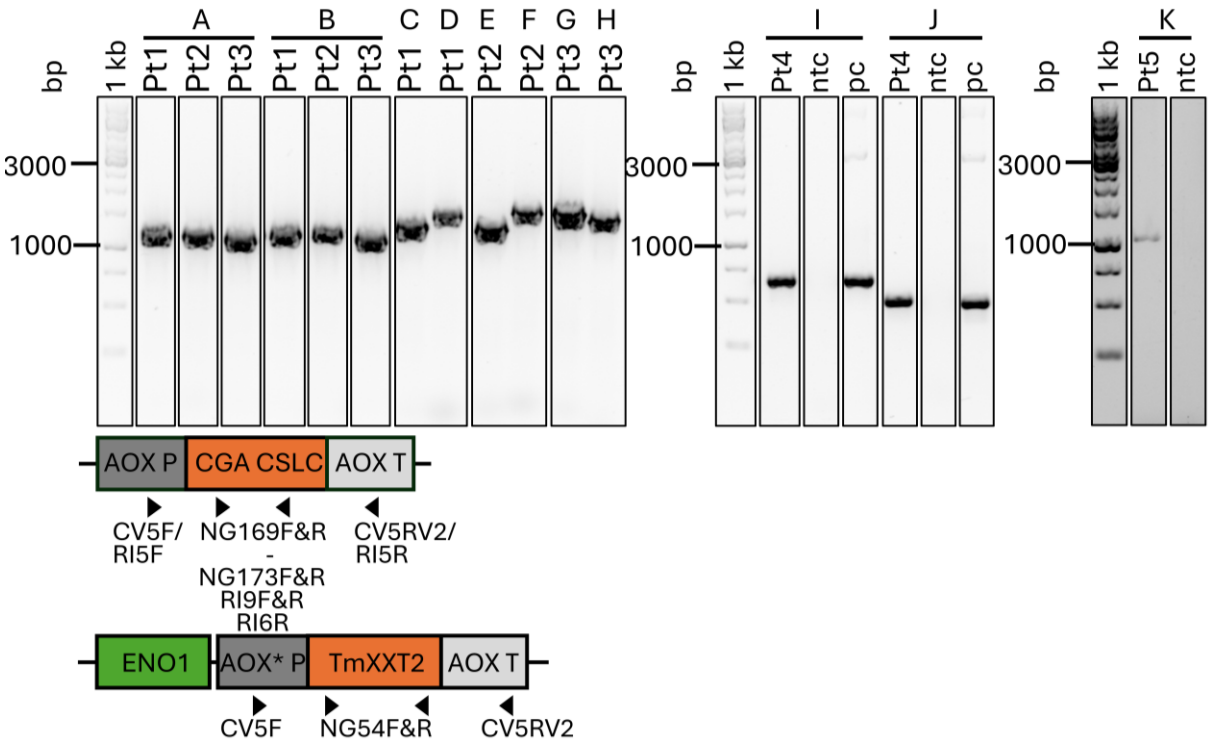

Figure 3.31: Genotyping PCR. To confirm Pichia transformants (Pt), colonies transformed with the linearized plasmids (Pt1: pPICZ B + *KnCSLC126*, Pt2: pPICZ B + *MeCSLC*, Pt3: pPICZ B + *SmCSLC*, Pt4: pPICZ B + *KnCSLC271*, Pt5: pPICZ Gateway + *KnCSLC603*) and a pPICZ eH + *TmXXT2* background were verified via PCR using gDNA as template; **A)** CV5F and NG54R (bind in AOX promoter and *TmXXT2*), expected size: 1,2 kbp; **B)** NG54F and CV5RV2 (bind in *TmXXT2* and AOX terminator), expected size 1,25 kbp; **C)** CV5F and NG169R (bind in AOX promoter and *KnCSLC126*), expected size: 1,35 kbp; **D)** NG169F and CV5RV2 (bind in *KnCSLC126* and AOX terminator), expected size 1,5 kbp; **E)** CV5F and NG172R (bind in AOX promoter and *MeCSLC*), expected size: 1,4 kbp; **F)** NG172F and CV5RV2 (bind in *MeCSLC* and AOX terminator), expected size 1,65 kbp; **G)** CV5F and NG173R (bind in AOX promoter and *SmCSLC*), expected size: 1,7 kbp; **H)** NG173F and CV5RV2 (bind in *SmCSLC* and AOX terminator), expected size 1,6 kbp; **I)** RI5F and RI9R (bind in AOX promoter and *KnCSLC271*), expected size: 0,68 kbp; **J)** RI9F and RI5R (bind in *KnCSLC271* and AOX terminator), expected size 0,68 kbp; **K)** RI5F and RI6R (bind in AOX promoter and *KnCSLC603*), expected size: 1 kbp; bp = base pairs, no template control = ntc, plasmid control = pc; **linear maps** of plasmid pPICZB/pPICZ Gateway + CGA *CSLC* and pPICZ eH + *TmXXT2*, P = promoter, T = Terminator, AOX* = modified AOX promoter, NG_F&R = primers designed by Niklas Gawenda, CV_F&R = primers designed by Catalin Voiniciuc, F = forward, R = reverse)

Confirmed strains were grown in BMGY (72h) and BMMY (24h) (Ch. 2.8.4). Afterwards AIR was extracted from the collected pellet (Ch. 2.12.2) and glycosidic linkage was performed (Ch. 2.12.8).

Results of the linkage analysis show that all three strains harbouring a Klebsormidium *CLSLC* gene did not result in any difference of the abundance of 4-linked glucose (Fig. 3.32, full dataset SFig. 6.38). In contrast, the strain with the Mesotaenium *CLSLC* gene has a threefold increase of 4-Glc compared to Pichia WT, while the strain with the Spirogloea *CLSLC* gene also displays an increase in 4-Glc linkages, indicating the enhanced production of a glucan polysaccharide.

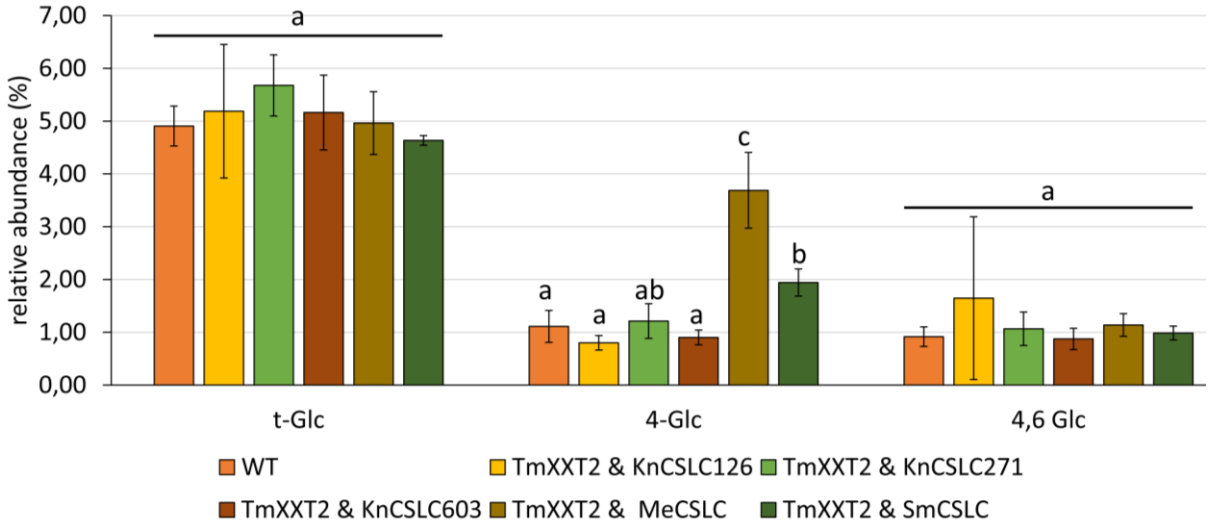

Figure 3.32: Glycosidic linkage analysis of *Pichia pastoris* strains expressing a CGA CSLC and TmXXT2. Selected linkages of Pichia AIR material of WT and strains containing an algae CSLC each; n= 4 for all strains; results of ANOVA analysis and subsequent Tukey's test are indicated ($P < 0,05$); error bars indicate standard deviation

Control lines testing if MeCSLC and SmCSLC would produce a glucan polysaccharide without an XXT gene were produced by transforming the Pichia wildtype with pPICZ B + *MeCSLC* or *SmCSLC* (Ch. 2.9.11, confirmation via colony PCR 2.9.12, Fig. 3.33).

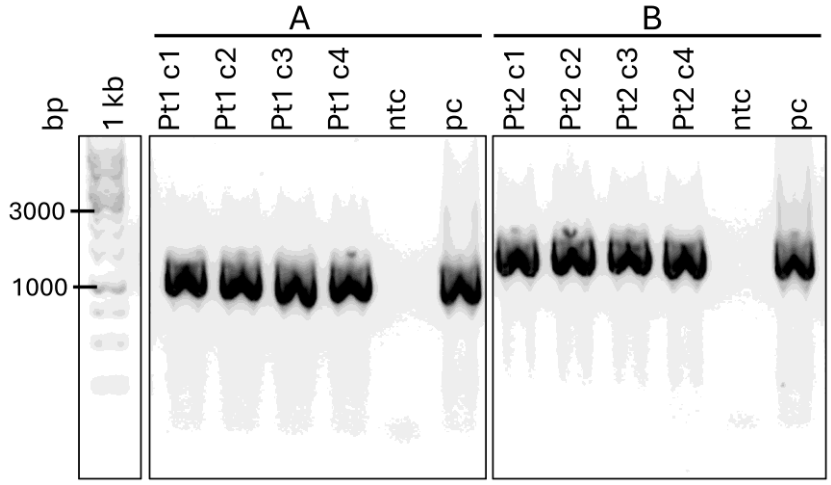

Figure 3.33: Genotyping PCR. To confirm Pichia transformants (Pt) colonies (c1-c4) transformed with the linearized plasmids (Pt1: pPICZ B + *MeCSLC*, Pt2: pPICZ Gateway + *SmCSLC*) were verified via PCR using gDNA as template; A) CV5F & NG172R (bind in AOX promoter and *MeCSLC*, Fig. 6.31), expected size: 1,4 kbp; B) CV5F & NG173R (bind in AOX promoter and *SmCSLC*, Fig. 6.31), expected size: 1,7 kbp; bp = base pairs, no template control = ntc, plasmid control = pc

Both lines did result in differences glycosidic linkages compared to the WT (Fig. 3.34 and SFig. 6.39). The strain containing the Mesotaenium gene resulted in significantly more 4-Glc linkages compared with the Pichia WT. However, the increase in 4-Glc is not as high as in the strain expressing TmXXT2 and MeCSLC (Fig. 3.32). The difference is most likely based on 4-

Glc derived from storage glycogen and not from a XyG backbone like glucan chain. In this particular linkage analysis no 4,6-Glc was detected for any of the Pichia strains. Even though the cultivation process is tried to keep as similar as possible between the different Pichia strains, small differences resulting in changed growth rates cannot be excluded. This can therefore result in differences in the linkage analysis since Pichia can increase or decrease accumulation of storage carbohydrates based on environmental conditions (Rebnegger et al., 2016).

The different outcomes of the linkage analysis with only CSLC or CSLC and XXT expressed in Pichia indicate that presence of a XXT is required for activity of the respective CSLC.

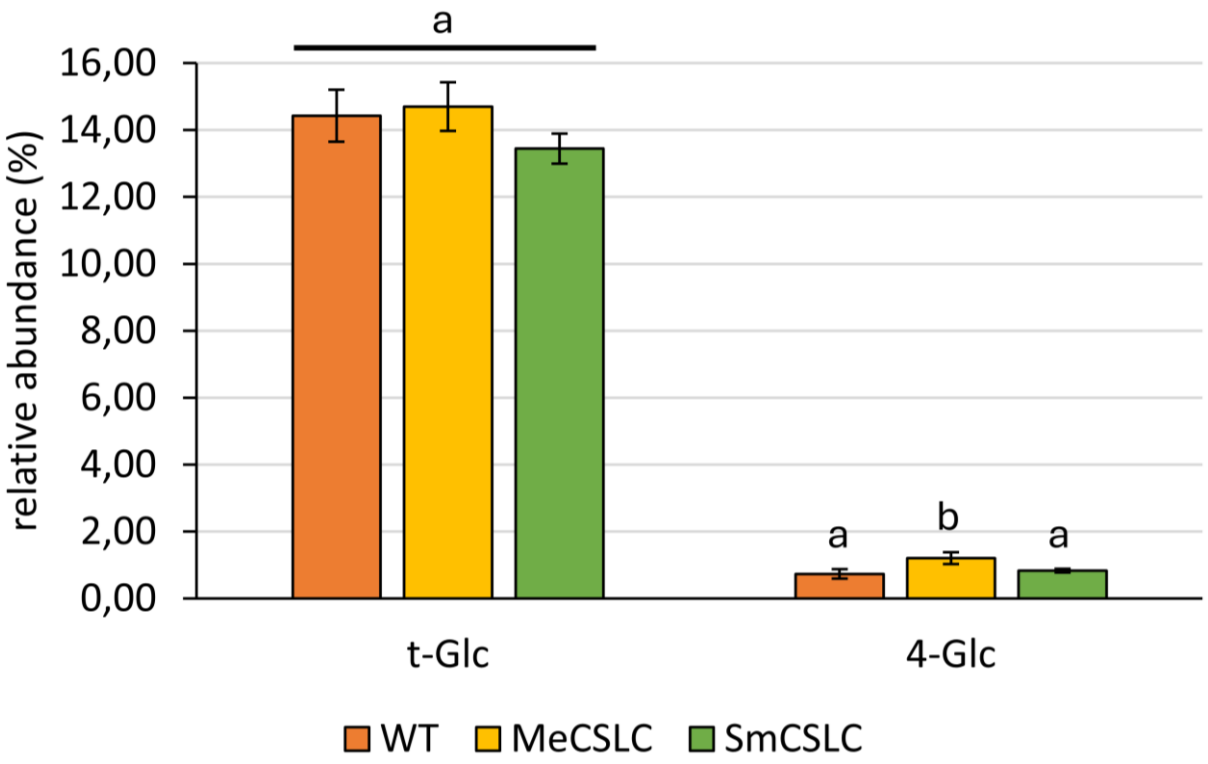

Figure 3.34: Glycosidic linkage analysis of *Pichia pastoris* strains expressing a CGA CSLC. Selected linkages of Pichia AIR material of WT and strains containing an algae CSLC each; n= 4 for all strains; results of ANOVA analysis and subsequent Tukey's test are indicated ($P < 0,01$); error bars indicate standard deviation

To test potential algae XXT candidate genes the collaborators performed a phylogenetic analysis of the genome of the three algae species and selected potential XXT candidates (among them *SmXXT*, *MeXXT* and *KnXXT*). The candidates were selected based on the smallest genetic distance to known Arabidopsis genes (i.e. *AtXXT1/2*). Close charophyte orthologs from Zygnematophyceae species (Spirogloea and Mesotaenium) were chosen for further investigation. From the deep-divergent Klebsormidiophyceae (Klebsormidium) lineage the genes are more divergent and gene candidates most similar in terms of primary amino acid sequence to Arabidopsis XXT1 and XXT2 were selected.

Here, a phylogenetic tree was created with the amino acid sequence of CGA and land plant XXTs (Ch. 2.2, ngphylogeny.fr, Fig. 3.35). XXTs split up in a clade of XXT1/2 and XXT3/4/5 related to their divergent proposed functions (Zhang et al., 2023b). The selected algae XXTs are not located in the two clades but seem to be closer related to the XXT3/4/5 clade. Again, Spirogloea and Mesotaenium candidates are relatively closely related to land plant XXTs while the Klebsormidium XXT is more distant.

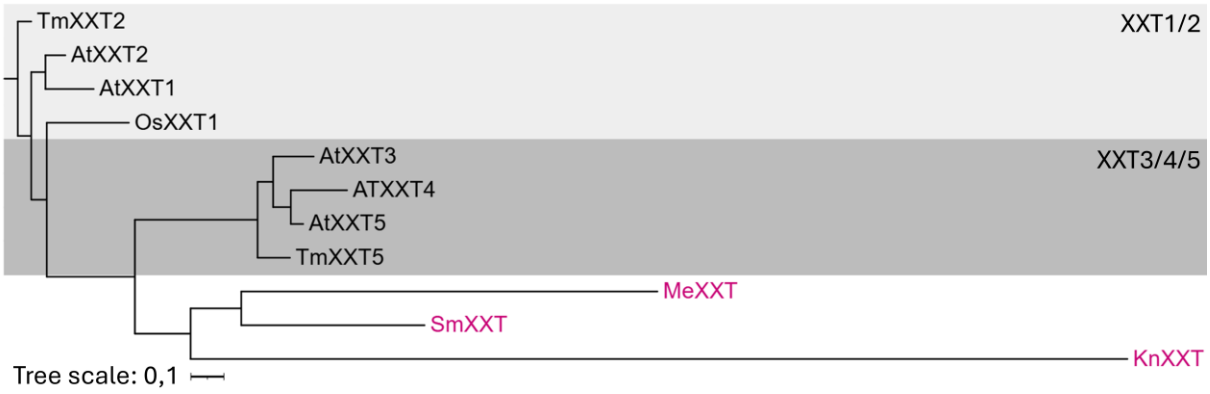

Figure 3.35: Phylogeny of algae XXTs and characterized XXTs. Phylogenetic tree based on amino acid sequences of algae, Arabidopsis (At), rice (Os) and nasturtium (Tm) XXTs, the scale bar indicates the number of substitutions per site, branch lengths are directly related to the amount of genetic change between shown genes, pink font: algae proteins, *Klebsormidium nitens* (Kn, taxonomically reclassified from *Klebsormidium flaccidum* Kfl, kfl00101_0170_v1.1 = KnXXT), *Mesotaenium endlicherianum* (Me, ME000051S08080 = MeXXT) and *Spirogloea muscicola* (Sm, SM000081S22676 = SmXXT); gene information for Arabidopsis and rice can be found in UniProt database; XXT1/2 and XXT3/4/5 clades are indicated in different shades of grey.

The DxD (Asp-x-Asp) motif, which is supposed to coordinate metal cofactors of GTs (Culbertson et al., 2018), is present in all compared XXTs (highlighted in amino acid sequence SFig. 6.37). The essential amino acid structure (Zhang et al., 2023b) (Fig. 3.36) reveals that Klebsormidium and Mesotaenium XXTs differ quite drastically from the known XXTs in their essential amino acid sequence (Zhang et al., 2023b) as they neither have a isoleucine nor a glycine in their acceptor molecule pocket structure like XXT1/2 and XXT3/4/5, respectively. The Spirogloea XXT candidate seems to be closest to known XXTs based on the amino acid structure, it has an isoleucine in the XXT1/2 typical position in the pocket structure. These differences can also be seen in the secondary structure (SFig. 6.36) of the essential amino acids (Zhang et al., 2023b). While KnXXT and MeXXT differ from the structure of AtXXT1, AtXXT2 and AtXXT5, the secondary structure of SmXXT is very similar to that of the Arabidopsis XXTs.

The analysis of the predicted topology based on amino acid sequence of the Mesotaenium XXT candidate further reveals that it is a globular protein without a transmembrane domain (SFig. 6.37). XXTs normally have a transmembrane domain and localize to the Golgi

membrane (Chou et al., 2012). Klebsormidium and Spirogloea XXT both have a predicted transmembrane domain.

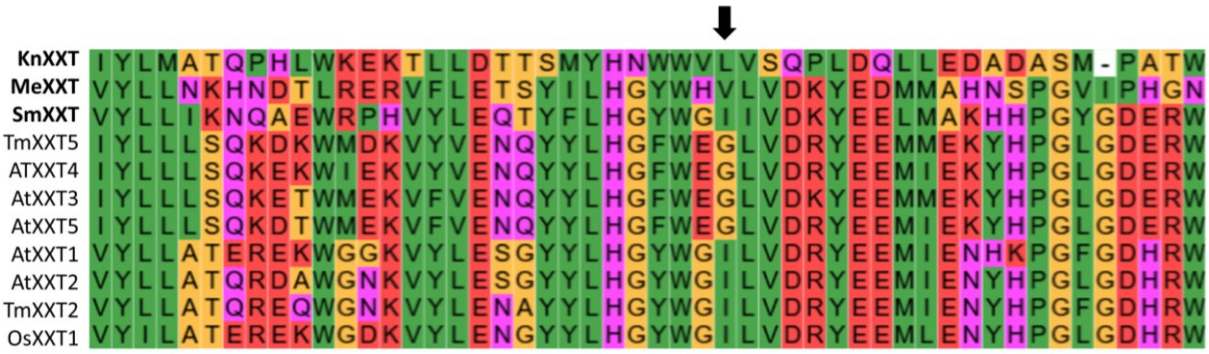

Figure 3.36: Patrial protein sequence alignment of Arabidopsis, nasturtium, rice and CGA XXTs. Clustal Omega alignment of known XXTs and algae CSLC candidates (bold); black arrow shows the isoleucine (I) in XXT1/2; glycine (G) in XXT3/4/5.

The *XXT* candidates (gene sequences in SFig. 6.1) were cloned in the pPICZ eH vector (SFig. 6.4) by restriction/ligation cloning (Ch. 2.9.7.2) based on pUC-GW-Kan plasmids containing the algae *XXT* candidate genes supplied by the collaborators. The construct was confirmed via colony PCR (Ch. 2.9.12, SFig. 6.33) and sequencing (Ch. 2.9.14). The Pichia wildtype was first transformed (Ch. 2.9.11) with pPICZ eH containing an algal *XXT* and confirmed via colony PCR (Ch. 2.9.12, SFig. 6.34). These strains were further transformed Ch. 2.9.11) with pPICZ B (pPICZ Gateway) containing an algal *CSLC*. Pichia strains expressing an algae *CSLC* and the corresponding algal *XXT* of the same species were selected by growth on selective plates (Zeocin, Hygromycin, Ch. 2.8.1) and confirmed by PCR (Fig. 3.37).

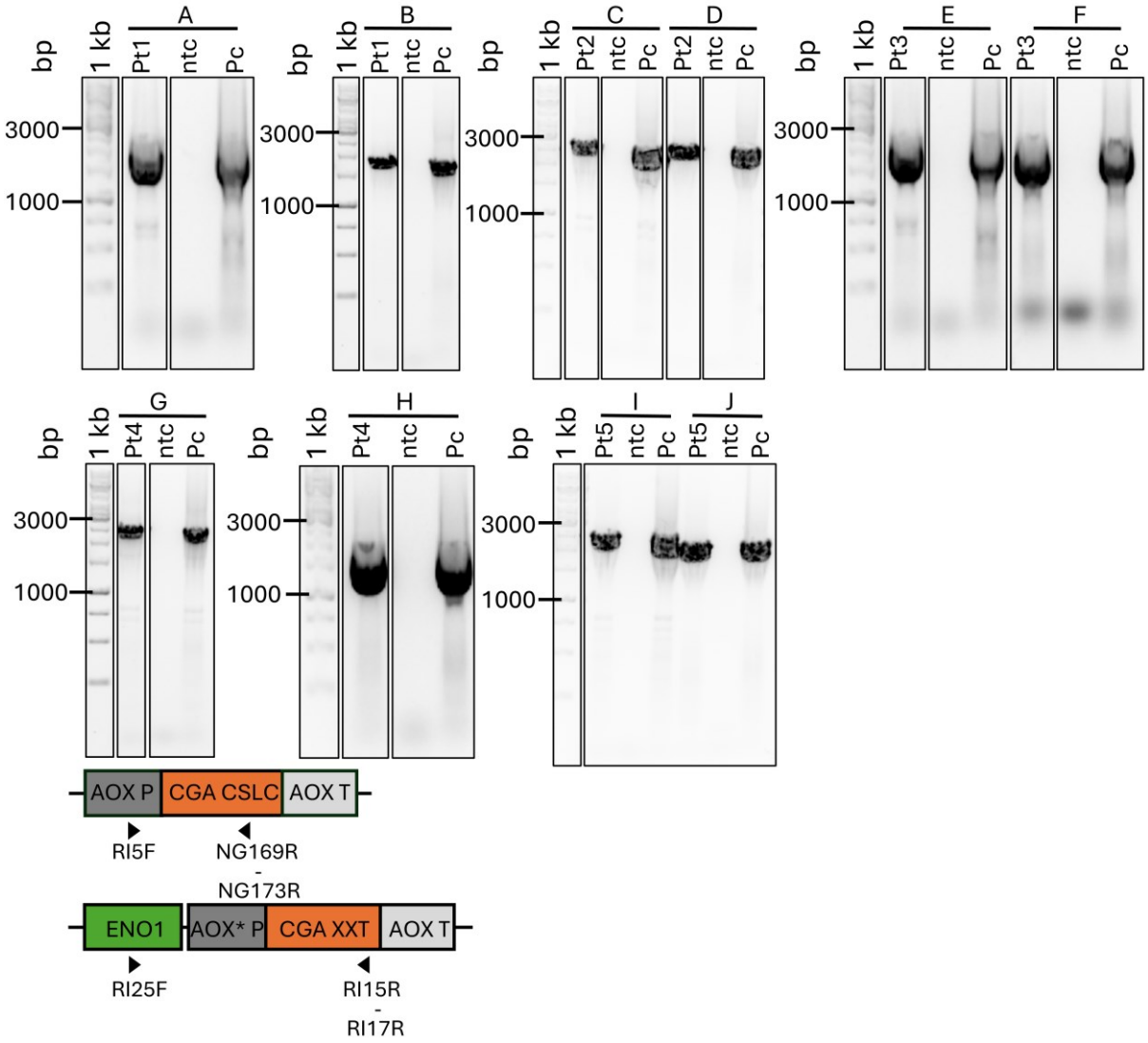

Figure 3.37: Genotyping PCR. To confirm Pichia transformants (Pt) colonies transformed with the linearized plasmids (Pt1: pPICZ B + *KnCSLC126*, Pt2: pPICZ B + *KnCSLC271*, Pt3: pPICZ Gateway + *KnCSLC603*, Pt4: pPICZ B + *MeCSLC*, Pt5: pPICZ Gateway + *SmCSLC*) and a Pt1-3: pPICZ eH + *KnXXT*, Pt4: pPICZ eH + *MeXXT*, Pt5: pPICZ eH + *SmXXT* background were verified via PCR using gDNA as template; **A)** RI25F & RI15R (bind in in ENO1 and *KnXXT*), expected size 2,3 kbp; **B)** RI5F & NG169R (bind in AOX promotor and *KnCSLC126*), expected size 2,2 kbp; **C)** RI25F & RIPhD15R (bind in in ENO1 and *KnXXT*), expected size 2,3 kbp **D)** RI5F & NG170R (bind in AOX promotor and *KnCSLC271*), expected size 2,3 kbp; **E)** RI25F & RIPhD15R (bind in in ENO1 and *KnXXT*), expected size 2,3 kbp; **F)** RI5F & NG171R (bind in AOX promotor and *KnCSLC603*), expected size 2,0 kbp; **G)** RI25F & RI16R (bind in in ENO1 and *MeXXT*), expected size: 2,4 kbp; **H)** RI5F & NG172R (bind in AOX promotor and *MeCSLC*), expected size: 1,8kb; **I)** RI25F & RI17R (bind in in ENO1 and *SmXXT*), expected size: 2,4 kbp; **J)** RI5F & NG173R (bind in AOX promotor and *SmCSLC*), expected size: 2,1 kbp; bp = base pairs, no template control = ntc, plasmid control = pc; **linear maps** of plasmid pPICZB + CGA *CSLC* and pPICZ eH + CGA *XXT*, P = promoter, T = Terminator, AOX* = modified AOX promoter, NG_F&R = primers designed by Niklas Gawenda, F = forward, R = reverse)

Pichia strains expressing an algal CSLC and algal XXT were grown in BMGY and BMMY as described (Ch. 2.8.4). Afterwards glycosidic linkage analysis was performed on AIR material of the cell pellet collected after growth (Ch. 2.12.8, Fig. 3.38 and SFig. 6.40). The strain

expressing a Mesotaenium XXT and CSLC contains more 4-Glc linkages indicating the potential production of a glucan polysaccharide. The Pichia strain expressing a Spirogloea XXT and CSLC has significantly more 4,6-Glc linkages compared to the WT indicating the increase of a substituted glucan chain.

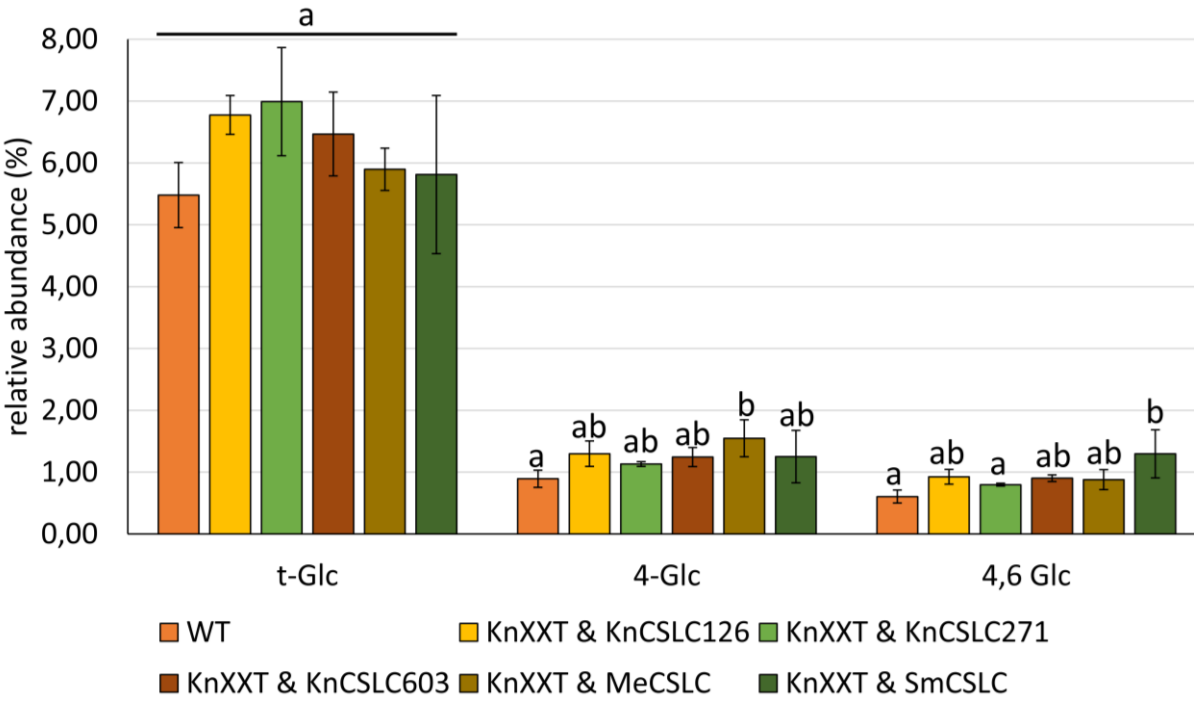

Figure 3.38: Glycosidic linkage analysis of *Pichia pastoris* strains expressing a CGA CSLC and XXT. Selected linkages of Pichia AIR material of WT and strains expressing an algae CSLC and an algae XXT; WT n= 4, KnXXT & Kn126CSLC n = 2, KnXXT & Kn271CSLC n = 3, KnXXT & Kn603CSLC n = 4, KnXXT & MeCSLC n = 4, KnXXT & SmCSLC n = 2; results of ANOVA analysis and subsequent Tukey's test are indicated ($P < 0,05$); error bars indicate standard deviation

3.3.3 Discussion

The effect of the selected CGA enzymes on XyG biosynthesis was assessed by individual heterologous expression in the Arabidopsis quintuple mutant *cslc456812*, whose walls lack detectable XyG (Kim et al., 2020). The OLIMP profile of the untransformed Arabidopsis quintuple mutant and the line transformed with the empty vector show no mass signals that represent XyG oligosaccharides (Fig. 3.30). The OLIMP profile of the XEG digested root AIR material from Arabidopsis quintuple mutant transformed with the empty vector demonstrates that the vector backbone has no influence on the synthesis of XyG. A similar OLIMP profile was observed when *Klebsormidium nitens* CSLCs were expressed in Arabidopsis. It can be concluded that these genes are not involved in XyG synthesis or the proteins are nonfunctional due to absence, instability or mislocalization. Compared to the other algal CSLCs tested, those of Klebsormidium are phylogenetically most distant from the CSLCs previously identified and characterised in land plants (Fig. 3.28).

In contrast, expression of Mesotaenium and Spirogloea CSLC candidate genes in Arabidopsis *cslc456812* restored the synthesis of XyG including the additions of substituents (Fig. 3.30). This indicates that the Mesotaenium and Spirogloea CSLC enzymes represent functional XyG: glucan synthases.
The protein sequence (Fig. 3.29) provides only limited explanation for the different results of the CGA species since already characterized and the here analysed CSLCs have mostly similar key domains (A. Richmond and R. Somerville, 2001; Morgan et al., 2013; Kim et al., 2020). However, differences in the number of transmembrane domains (SFig. 6.35) for two of the Klebsormidium CSLC candidates (KnCSLC126 and KnCSLC603) could indicate a different protein structure and a thereby changed functionality.

To further investigate the catalytic activity of the algal CSLC candidates they were expressed in *Pichia pastoris* together with TmXXT2 and the yeast's wall analysed by glycosidic linkage analysis (Fig. 3.32, SFig. 6.38). Pichia strains expressing Klebsormidium CSLCs and TmXXT2 did not result in the production of a glucan polysaccharide based on 4-Glc values. Analysis of Mesotaenium and Spirogloea CSLC and TmXXT2 expressing Pichia strains on the other hand did result in higher 4-Glc values, which could indicate the biosynthesis of a XyG backbone like polysaccharide. This suggests, that Klebsormidium CSLC do not participate in conjunction with a TmXXT2 in XyG biosynthesis, while Mesotaenium and Spirogloea CSLCs exhibit a glucan synthase function in the presence of TmXXT2.

The data obtained from the Arabidopsis complementation approach and yeast reconstruction approach are confirmative - neither Klebsormidium CSLC complemented Arabidopsis lines produce XyG nor Klebsormidium CSLC expressing Pichia strains produce a glucan polysaccharide similar to a XyG backbone. However, Mesotaenium and Spirogloea complemented Arabidopsis lines produce XyG and linkage analysis also suggests that a glucan polysaccharide is synthesised, which would suggest that the selected CSLC candidate of these two species exhibit XyG:glucan synthase activity.

To test whether the mentioned algae species also contain functional XXTs and if expression of algae CSLC and XXT from the same species could influence the glucan polysaccharide production, Pichia strains with CSLC and XXT from the same algae species were assessed (Fig 3.38, SFig. 6.40). Pichia strains expressing CSLCs and XXT of Klebsormidium and Spirogloea did not result in the production of a glucan polysaccharide based on the unchanged wall 4-Glc values similar to the WT. Hence, Klebsormidium and Spirogloea CSLC in combination with an XXT of the same species has no glucan synthesis function. A strain expressing Mesotaenium CSLCs and XXT did result in a 4-Glc value compared to the WT, but not as high as in the Pichia strain expressing Mesotaenium CSLC and TmXXT2 (Fig. 3.32). Whether Mesotaenium CSLC is maintaining a glucan synthesis function in combination with

spezies' own XXT remains open and will need to be further assessed by longer induction followed by linkage analysis.

The essential amino acid structure (Zhang et al., 2023b) shows that Klebsormidium and Mesotaenium XXTs differ from the known XXTs while the Spirogloea XXT candidate seems to be closest to known XXTs (Fig. 3.35). A topology analysis of the Mesotaenium XXT further revealed that is has no a transmembrane domain like the other algal or beforehand characterized XXTs (Chou et al., 2012). However, it could be a peripheral protein attached to a Golgi membrane tethered protein. This should be further investigated by analysing the subcellular localization of the Mesotaenium XXT using a fluorescence tag. Regardless, the Mesotaenium XXT could have a non-catalytic role in the production of the glucan chain by e.g. forming a protein complex with CSLC. Since the combination of algal CSLC and algal XXT of both Spirogloea and Klebsormidium does not lead to the synthesis of a glucan polymer (Fig. 3.38), its catalytic activity could not be demonstrated. This might be explained by the phylogeny of the protein candidates as the algal XXT candidates seem to be closest related to the XXT3/4/5 clade. In Pichia so far CSLC activity was only shown when coexpressed with members of the XXT1/2 clade. However, also the Mesotaenium XXT is closest related to the XXT3/4/5 clade and seems to play role in the production of the glucan chain.

While Klebsormidium might have the genetic machinery for synthesis of XyG (Mikkelsen et al., 2014; Del-Bem, 2018) the presence of XyG by XyG-specific antibodies was negative (Mikkelsen et al., 2021). As shown here, putative Klebsormidium CSLC orthologs do not complement the XyG in Arabidopsis quintuple mutant *cslc456812*, nor do they produce a XyG backbone-like polysaccharide when co-expressed with TmXXT or a species-specific XXT in Pichia. This is consistent with the notion that Klebsormidium might not be able to produce XyG or at least the structure known from higher plants.
Zygnematophyceae harbour not only the genetic machinery for the synthesis of XyG (Mikkelsen et al., 2014; Del-Bem, 2018), but were also shown to contain a XyG-like polysaccharide in the cell wall by methylation analysis using GCMS (Ikegaya et al., 2008), labelling with XyG-specific antibodies, and xyloglucanase digest OLIMP (Mikkelsen et al., 2021). As shown here CSLC candidates of two Zygnematophyceae species (*Mesotaenium endlicherianum* and *Spirogloea muscicola*) were able to complement XyG in quintuple mutant *cslc456812* and to generate a XyG backbone-like glucan polysaccharide in the heterologous host Pichia when CSLC was co-expressed with TmXXT2.
However, only the Mesotaenium CSLC synthesised a glucan polysaccharide when co-expressed with a species-specific XXT in Pichia. These results demonstrate that a XyG biosynthetic pathway is present in the Zygnematophyceae genome but is also able to produce

functional XyG biosynthetic enzymes. Mesotaenium and Spirogloea CSLCs can act in synergy with a land plant XXT.
In summary, this suggests that the structure of higher plant XyG and its biosynthesis machinery indeed originated in CGA and evolved prior to the transition of plants to land.

Sequencing of further genomes of different CGA species and their analysis with regard to XyG GTs could also help to identify the origin of XyG. Further experiments such as the coexpression of algae CSLC with XXTs from the same species that are closer related to the XXT1/2 clade then the XXTs tested here could help to understand the complex topic of development of XyG and its biosynthesis machinery in plant terrestrialization. As XyG enzymes form multienzyme complexes (Chou et al., 2012; Chou et al., 2015; Culbertson et al., 2018; Zabotina et al., 2021) it might also be of interest, if GT37 and GT47 members could improve the glucan production when coexpressed with CSLC (and XXT) as orthologs of GT37 and GT47 have been identified in algae (Mikkelsen et al., 2021).

3.4 Identification and Characterization of a Xyloglucan Xylosyltransferase from *Vaccinium corymbosum*

The content of this chapter was published under the title “Identification of a xyloglucan beta-xylopyranosyltransferase from *Vaccinium corymbosum*” in Plant Direct (2023 Jul 25; 7(7)). Permission to reuse this published material in this thesis was granted by Dr. Jonathan Ingram, Supervising Editor at Plant Direct, on May 28, 2025 (SFig. 6.44).

3.4.1 Background

Many of the various XyG sidechains are synthesised by members of the glycosyltransferase family 47 (Fig. 3.39): For example, in Arabidopsis the XyG backbone is galactosylated by GT47 members MUR3 and XLT2 (Madson et al., 2003; Jensen et al., 2012).

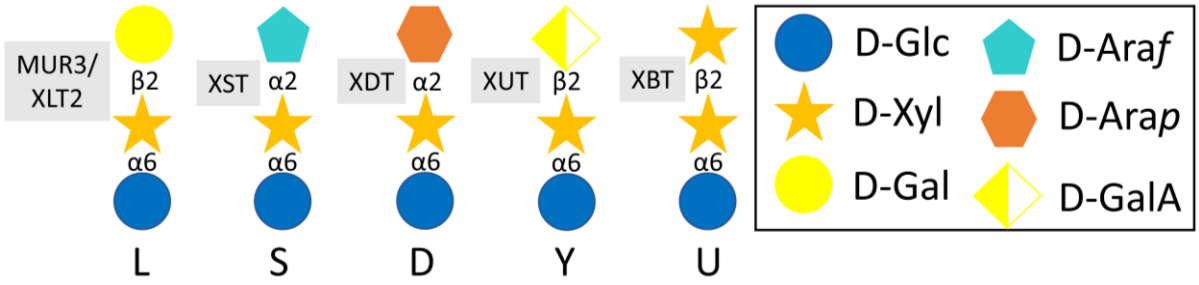

Figure 3.39: Xyloglucan sidechains synthesized by GT47s. The XyG one-letter code nomenclature is indicated below the structure. MUR3 and XLT2: galactosyltransferases; XST: arabinofuranosyltransferase; XDT: arabinopyranosyltransferase: XUT: galacturonosyltransferase, XBT: β-xylosyltransferase, Glc = Glucose, Xyl = xylose, Gal = Galactose, Ara*f* = arabinofuranose, Ara*p* = arabinopyranose, GalA = galacturonic acid

AtMUR3 was initially discovered by screening chemically mutagenized Arabidopsis plants targeting abnormal cell wall monosaccharide composition (Reiter et al., 1997). Fractionation of the wall material revealed that *mur3* affects polysaccharides extracted by alkali. It leads to a reduction in galactose and fucose in the respective fractions. Further analysis of the *mur3* mutant line and *mur3* transformed with a wildtype AtMUR3 by HPAEC and MALDI-TOF MS resulted in detection of XXXG and XLXG for *mur3* and all wildtype oligosaccharides in the complemented plants. It was therefore suggested that AtMUR3 is a site-specific XyG galactosyltransferase, which specifically adds a galactose to the third xylose residue in the XXXG core leading to XXLG (Madson et al., 2003). Analysis of putative MUR3 of *Eucalyptus grandis* in *mur3* by complementation followed by cell wall analysis by OLIMP led to restoration of the XyG structure similar to that found in the Arabidopsis wildtype and therefore to the identification of an AtMUR3 homolog (Lopes et al., 2010). Jensen et al. identified the nasturtium galactosyltransferase TmXLT2. Nasturtium XyG GTs were identified by comparing Arabidopsis GTs in a nasturtium seed RNA-Seq database and computing expression data by regression analysis. The most highly abundant GT was found to be highly similar to an uncharacterized Arabidopsis gene in GT family 47 (Jensen et al., 2012). Analysis of the

corresponding Arabidopsis *xlt2* insertional mutant line by HPAEC-PAD and OLIMP detected XXLG and XXFG but not XLXG and XLFG. *xlt2* plants complemented with XLT2 regained the oligosaccharides containing galactose at the second position (Jensen et al., 2012). A double mutant *mur3.1xlt2* (*mur3.1* contains a MUR3 point mutation, from here on termed *mur3 xlt2*) consists primarily of XXXG oligosaccharides and results in a dwarfed growth phenotype (Jensen et al., 2012). Two putative MUR3 and one putative XLT2 were identified in tomato and rice by screening the genome of the respective plants for homologs of AtMUR3 and AtXLT2 and transforming candidate genes in the double mutant *mur3 xlt2* (Schultink et al., 2013; Liu et al., 2015). Another XLT2 ortholog from the moss *Physcomitrella patens* differs from other XLT2s in the sense that PpXLT2 also exhibits MUR3 activity (Zhu et al., 2018). That led to the hypothesis that regioselectivity of this GT has evolved later than the GT activity itself as it is conserved across land plants (Zhu et al., 2018).

Furthermore, GT47s arabinofuranosyltransferase XyG S-sidechain transferase XST of tomato (Schultink et al., 2013) and arabinopyranosyltransferase XyG D-sidechain transferase XDT of moss *Physcomitrella patens* (Zhu et al., 2018) were identified using similar complementation approaches. A root hair XyG specific galacturonosyltransferase XUT was identified based on phylogeny and proteome data followed by analysis of corresponding T-DNA insertion lines and complementation of *xut1* with AtXUT1 (Peña et al., 2012).

XyG substitution beyond the core XXXG motif is required for proper XyG transport to the cell wall and plant growth (Hoffmann and McFarlane, 2024). For example, *mur3* mutants with reduced Gal and no Fuc sidechains show a dwarfed phenotype with cabbage-like rosettes (Kong et al., 2015). Galactose-deficient XyG seems to be dysfunctional (Xu et al., 2017) and lead to intracellular aggregations that contain multiple organelles and disrupted cellular trafficking (Hoffmann and McFarlane, 2024). However, complementation of *mur3 xlt2* with different GT47s indicates that the presence and not the type of sugar moiety of XyG sidechains is essential for XyG functionality (Jensen et al., 2012; Schultink et al., 2013; Liu et al., 2015; Zhu et al., 2018; Hoffmann and McFarlane, 2024). XyG substitution with these sidechains was proposed to be important for polymer solubility during secretion to the cell wall (Hoffmann and McFarlane, 2024).

The XyG structure β-D-Xyl*p*-(1,2)-α-D-Xyl*p*-(1,6)-β-D-Glc*p* (U sidechain) present in the Argan tree (Ray et al., 2004) and bilberries (Hilz et al., 2007) is likely also synthesized by a hitherto unknown member of the GT47 family based on similarity in the acceptor substrate. Here, the responsible XyG:Beta-xylosylTransferase (XBT) was identified in blueberry. The work described below has been published in “Identification of a xyloglucan beta-xylopyranosyltransferase from Vaccinium corymbosum” (Immelmann et al., 2023).

3.4.2 Results

The XyG U sidechain has been previously found in bilberry fruit material (Hilz et al., 2007). However, because of genomic sequence information availability another member of the Ericaceae, blueberry, was selected as a potential source for the identification of the enzyme responsible for transferring the xylosyl-moiety to XyG. Various tissues of a blueberry plant (fruit, leaf, stem, root) were collected and subjected to OLIMP analysis of XEG released XyG oligosaccharides (Ch. 2.12.3) to check for the presence of the U sidechain (Fig. 3.40). The analysis revealed numerous mass signals in fruit, leaf, and stem material, which are consistent with oligosaccharides that contain one or two additional pentoses on the regular XyG motifs (e.g. found in Arabidopsis). Those ion signals are *m/z* 1217 (XXXG + pentose), *m/z* 1349 (XXXG + 2 pentoses), *m/z* 1379 (XXLG + pentose), *m/z* 1421 (XXLG + pentose), *m/z* 1567 (XXFG + pentose) and *m/z* 1625 (XLLG + pentose). Blueberry roots did not show any of these additional pentose mass signal.

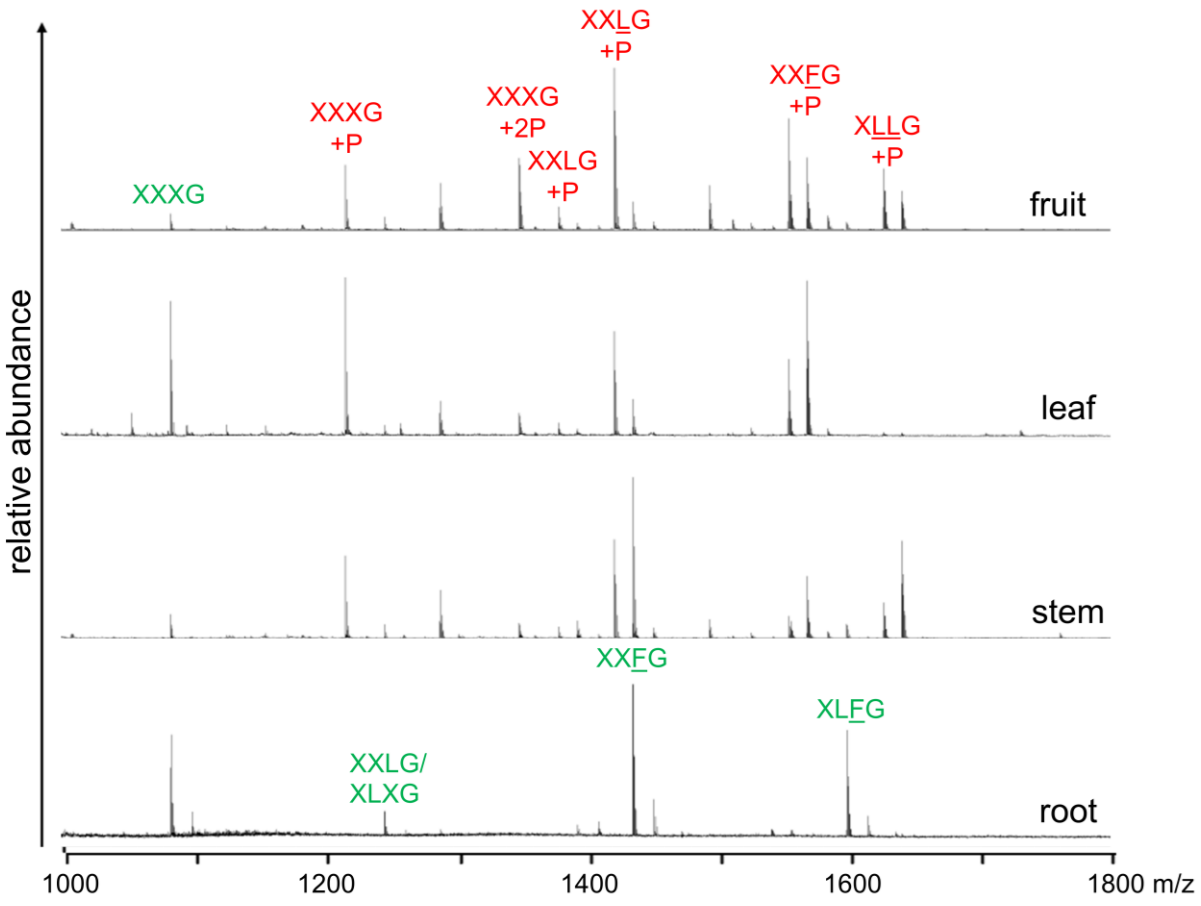

Figure 3.40: XyG oligosaccharide mass profiling of different blueberry tissues. OLIMP of XEG digested AIR material from blueberry fruit, leaf, stem and root material. Suggested XyG oligosaccharide structures of selected ion signals are labelled according to the one-letter code and number of pentoses (P), green labels: Arabidopsis typical XyG motifs, red label: novel oligosaccharides

The xylosyl-moiety in the U sidechain replaces the galactosyl-moiety in the L-sidechain. Hence, a putative xylosyltransferase is exposed to the same acceptor substrate (X-sidechain) and forms the same glycosidic linkage β-(1,2) as the galactosyltransferases MUR3 or XLT2. Therefore, it was hypothesized that such a xylosyltransferase would also belong to the GT47 family. Therefore, one of the Arabidopsis GT47 (AtXLT2) amino acid sequence was used as the probe in the BLAST tool of the Genome Database for Vaccinium (https://www.vaccinium.org/) V. corymbosum cv. Draper v1.0 genome peptides database to identify related GT candidates. A total of 59 protein sequences were identified in the blueberry genome (E-Value < E-39). Blasting AtMUR3 results in the same 59 protein sequences with different E-Values.

The amino acid sequences of these protein candidates and those of known GT47 members were used to create a phylogenetic tree (Ch. 2.2, ngphylogeny.fr, SFig. 6.42). Many of the blueberry protein candidates occur in clusters of four, probably due to the fact that blueberry is tetraploid (Krebs and Hancock, 1989; Colle et al., 2019) with four allele variants of the same gene. Some blueberry candidates are phylogenetically closely related to functionally characterized galactosyltransferases XLT2 (AtXLT2, TmXLT2, and OsXLT2) or MUR3 (OsMUR3, SlMUR3, EgMUR3, AtMUR3, and TmMUR3). In between these two clades are blueberry homologs of uncharacterized Arabidopsis GT47s (GT11-15, 17, 19, 20) and galacturonosyltransferase AtXUT. A large cluster consisting of only blueberry GT47 sequences most likely harbours an unidentified Xyloglucan:Beta-xylosylTransferase XBT. The closest related GT to this cluster is the tomato arabinofuranosyltransferase SlXST1, which transfers an arabinopentosyl-moiety.

In addition to the phylogenetic relationship to characterized GTs, the tissue expression level of the genes was considered when selecting gene candidates for functional testing since the U-sidechain does not appear in root tissues. The expression levels of blueberry genes have been determined in different plant tissues (Colle et al., 2019). To visualize the expression data a heatmap was created using the data from all 59 in blueberry identified GT47 homologs using Heatmapper Expression tool (Ch. 2.2, heatmapper.ca, SFig. 6.43). In the heatmap the expression data of eleven blueberry tissues including fruit, leaf, shoot and root is shown.

In summary, one putative VcMUR3, two VcXLT2s (1 and 2), and four putative VcXBTs (1 to 4) present in the unique blueberry GT47 clade were selected for functional testing based on highest expression in fruit tissue.

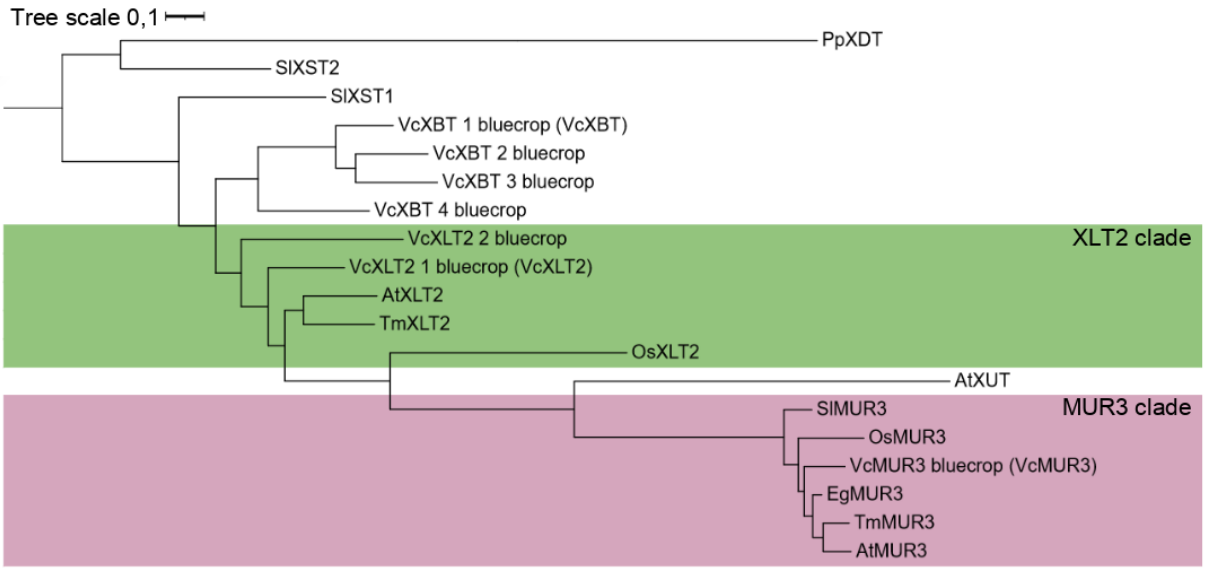

Figure 3.41: Phylogeny of XyG-related GT47 proteins. Phylogenetic tree of protein sequences of blueberry bluecrop cultivar and functionally described GT47 XyG glycosyltransferases from various species. XLT2 and MUR3 clades are indicated in green and purple, respectively. Naming of blueberry proteins based on clustering in clades and on function (in parentheses). The scale bar indicates the number of substitutions per site; branch lengths are directly related to the amount of genetic change between shown genes. At, *Arabidopsis thaliana*; Os, *Oryza sativa* (rice); Tm, *Tropaeolum majus* (nasturtium); Sl, *Solanum lycopersicum* (tomato); Eg, *Eucalyptus grandis* (Eucalyptus); Pp, *Physcomitrella patens*

The selected blueberry GT47 genes were amplified from genomic DNA or cDNA of blueberry fruits of *V. corymbosum* bluecrop cultivar (Fig. 3.42 A). Primers (SFig. 6.11) were designed based on the gene sequences from the GDV database. The final GT47 candidates differ from the GDV results as the database uses the genome of the blueberry Draper cultivar and the genomic DNA and cDNA for cloning was extracted/synthesized from the bluecrop cultivar (Ch. 2.9.1, Ch. 2.9.19, phylogeny of bluecrop GT47 candidates in Fig. 3.41). The amino acid sequences of the seven cloned bluecrop GT47 genes were added in the phylogenetic tree with the 59 protein candidates from the GDV database and other functionally characterized GT47s (Ch. 2.2; SFig. 6.42 for extended phylogenetic tree). The blueberry GT47 candidates were named based on their clustering in phylogenetic clades and function.

The functional characterization of the selected blueberry GT47 enzymes was performed by complementation in Arabidopsis *mur3 xlt2*, which lacks XyG substitution beyond the core XXXG structure (Jensen et al., 2012).

Two of seven genes (*VcXLT2*, *VcXBT_3*, gene sequences in SFig. 6.1) were cloned into the binary plant vector pORE-E4 (Ch. 2.9.7.2, plasmid map SFig. 6.9, verification by colony PCR Ch. 2.9.12, Fig. 3.42 B). The sequencing verified plasmids (Ch. 2.9.14) with the blueberry GT47 candidate genes were individually transformed into *Agrobacterium tumefaciens* (Ch. 2.9.10). The transformation was verified via colony PCR (Ch. 2.9.12, Fig. 3.42 C) and the confirmed strains were used to transform *mur3 xlt2*. Resistant plants on selection media (Kanamycin, Ch. 2.8.5.6) were transferred to soil and genotyped for the insertion (Fig. 3.42 D

and E). Confirmed T1 plants were selfed and the seeds were again sown on plates with a selective antibiotic (Kanamycin, Ch. 2.8.5.6). Plants from plates with 75% resistant plants were transferred to soil and selfed as a 75% antibiotic resistance indicates that the T1 plant is heterozygous for the insert. T2 plants were selfed and the seeds were again sown on plates with a selective antibiotic (Kanamycin, Ch. 2.8.5.6). Plants from plates with 100% resistant plants were transferred to soil and selfed as a 100% antibiotic resistance indicates that the T2 plant is homozygous for the insert.

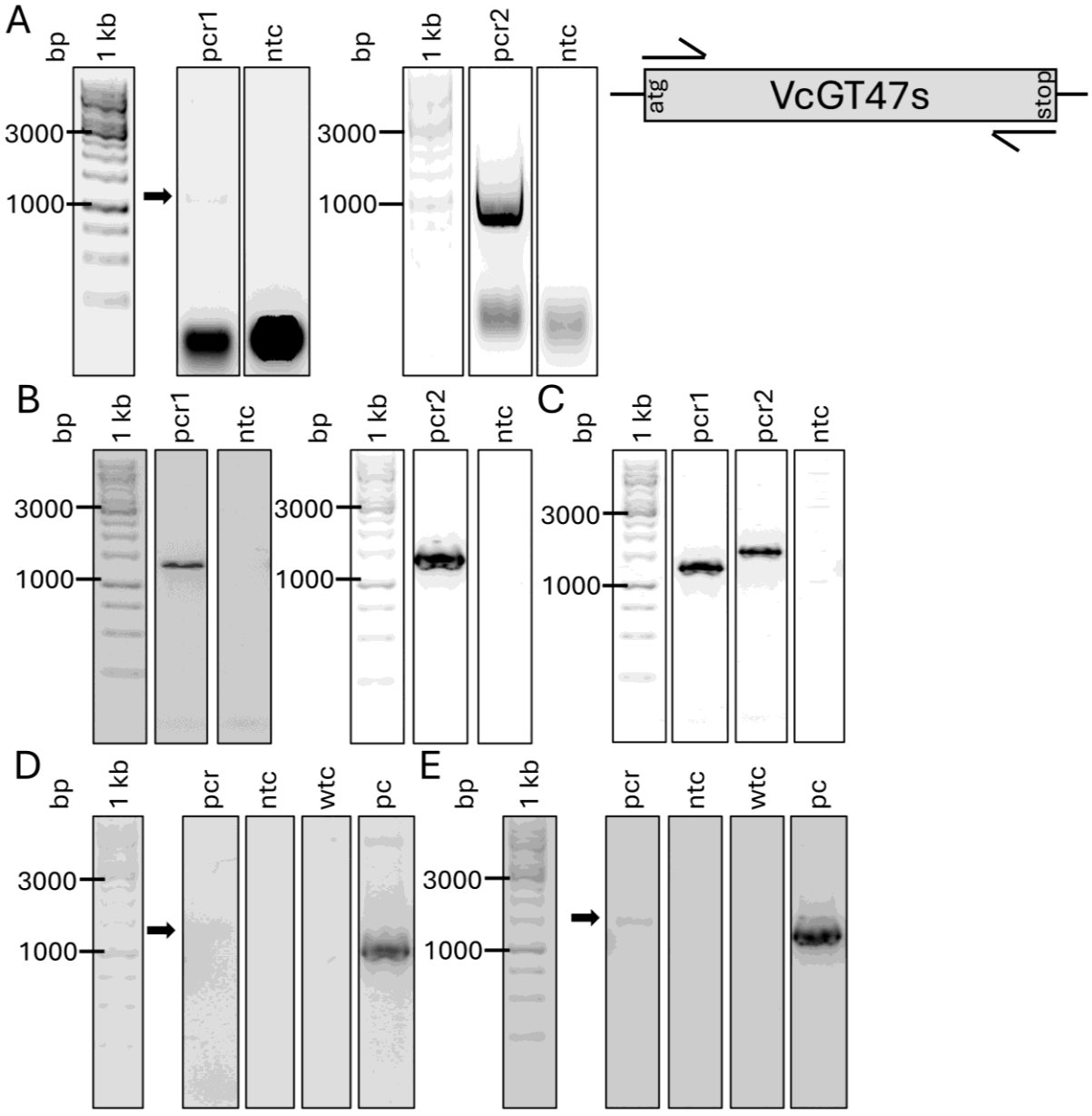

Figure 3.42: PCR to amplify, clone and confirm blueberry GT47s. A) Amplification of *VcXBT3* and *VcXLT2*, pcr1: to amplify *VcXBT3* from blueberry cDNA using primers XBT3_1F&R, expected size 1,2 kbp; pcr2: to amplify *VcXLT2* from blueberry gDNA using primers XLT2L_1F&R, expected size 1,5 kbp; **B)** Colony PCR of pORE-E4 + *VcXBT3* or *VcXLT2* to confirm *E. coli* transformants. *E. coli* transformed with plasmids were verified via PCR using cell material as template with primers NG106F & PUCR2; pcr1: pORE-E4 + *VcXBT3*, expected size 1,2 kbp; pcr2: pORE-E4 + *VcXLT2*, expected size 1,5 kbp; **C)** Colony PCR of pORE-E4 + *VcXBT3* or *VcXLT2* to confirm

Agrobacterium transformants. Agrobacterium transformed with plasmids were verified via PCR using cell material as template with primers NG106F & PUCR2; pcr1: pORE-E4 + *VcXBT3*, expected size 1,2 kbp; pcr2: pORE-E4 + *VcXLT2*, expected size 1,5 kbp; **D)** Genotyping PCR to confirm Arabidopsis transformants (T1). Arabidopsis *mur3 xlt2* transformed with *VcXBT3* were verified via PCR using gDNA as template with primers NG106F & inXBT3R, expected size 1,2 kbp; **E)** Genotyping PCR to confirm Arabidopsis transformants (T1). Arabidopsis *mur3 xlt2* transformed with *VcXLT2* were verified via PCR using gDNA as template with primers NG106F & inXLT2R, expected size 1,5 kbp; bp = base pairs, no template control = ntc, wtc = wildtype control, pc = plasmid control

Niklas Gawenda cloned an additional five genes (*VcMUR3*, *VcXLT2_2*, *VcXBT_1*, *VcXBT2*, *VcXBT4*) into the binary plant vector pORE-E4, transformed them into *Agrobacterium tumefaciens* and then into the Arabidopsis mutant *mur3 xlt2*, creating stable transgenic lines homozygous for those blueberry GT47 candidate genes.

The XyG structure of the various complemented Arabidopsis lines was analysed by OLIMP of XEG digested AIR material of leaves (Ch. 2.12.3, Fig. 3.43). The untransformed *mur3 xlt2* primarily showed the mass signal at *m/z* 1085 representing XXXG (Jensen et al., 2012). Expression of one of the putative VcXBT (VcXBT_1) resulted in a new XyG oligosaccharide with *m/z* 1217 representing XXXG with an additional pentose, which might represent the xylosylated XyG backbone. Expression of VcXLT2_1 resulted in another new mass signals of *m/z* 1247, representing a hexosylated (likely galactosylated) XyG oligosaccharide. The expression of VcMUR3 resulted in several new mass signals at *m/z* 1247 and *m/z* 1289 representing likely a galactosylated XyG and an acetylated galactosylated XyG oligosaccharide, as well as *m/z* 1393 and 1435, which likely represent the fucosylated form of galactosylated XyG (XXFG) and its acetylated form (XXFG), thus indicating VcMUR3 being a functional MUR3 homolog.

Four complemented lines (Fig. 3.43: VcXBT_3, data not shown: VcXBT_2, VcXBT_4, VcXLT2_2) resulted in a similar OLIMP profile as *mur3 xlt2* only showing one mass signal at *m/z* 1085. Hence, the added blueberry genes did not affect the XyG structure.

For the purposes of simplicity, from here on VcXLT2_1 will only be referred to as VcXLT2 and VcXBT_1 as VcXBT.

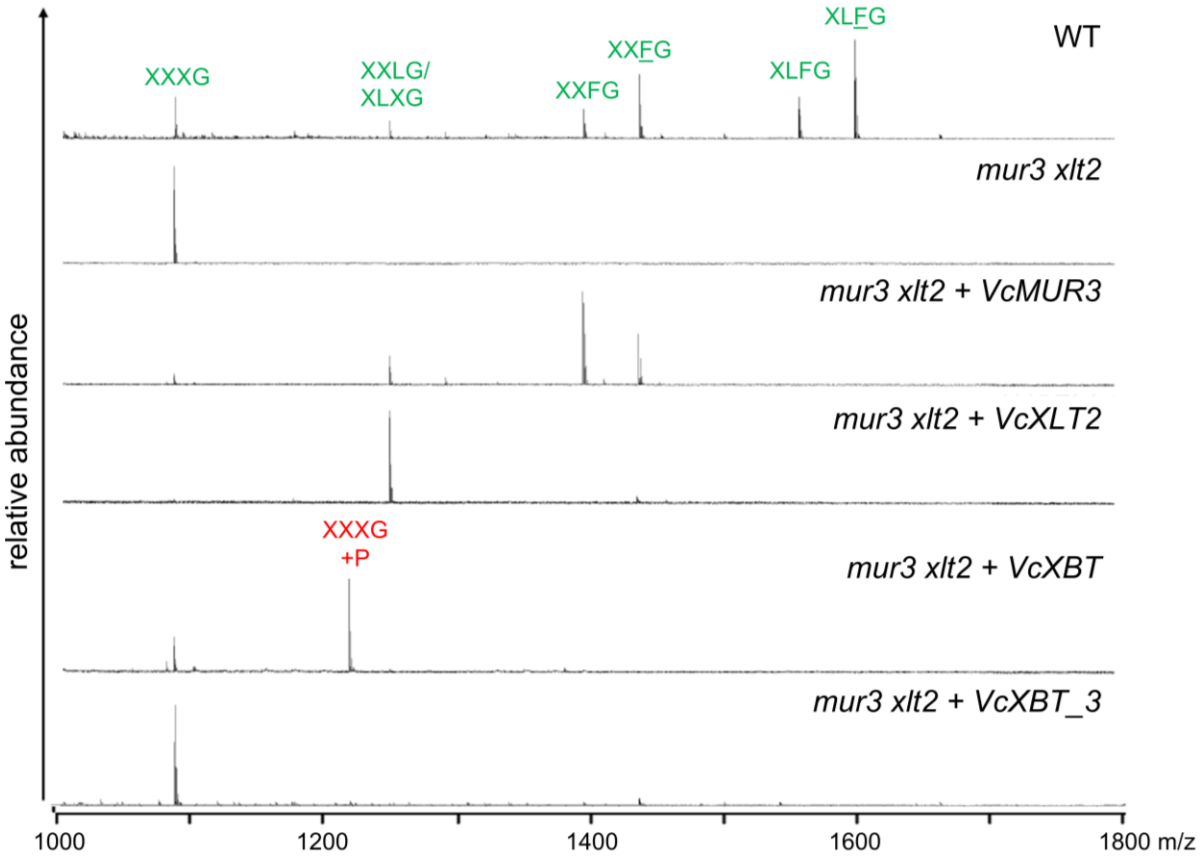

Figure 3.43: XyG oligosaccharide mass profiling of blueberry GT47 complemented Arabidopsis lines. XyG oligosaccharide profiles derived from leaf tissue of Arabidopsis WT Col-0, untransformed *mur3 xlt2* double mutant and transgenic lines expressing *VcMUR3, VcXLT2, VcXBT* and *VcXBT_3* in the *mur3 xlt2* genetic background; suggested oligosaccharide structures of selected ions are indicated by the one-letter code and number of pentoses (P), green labels: Arabidopsis typical XyG motifs, red label: novel oligosaccharide

To further investigate the nature of the substitution brought about by the enzymes VcMUR3 and VcXLT2 the XEG digested XyG oligosaccharides derived from the Arabidopsis leaf AIR material were subjected to high-performance anion-exchange chromatography with pulsed amperometric detection (HPAEC-PAD) (Ch. 2.12.7, Fig. 3.44). A standard XyG oligosaccharide mixture (XXXG, XXLG, XLXG and XLLG) was used to determine the elution profile of the samples. In addition, XyG oligosaccharides from the Arabidopsis WT and the untransformed *mur3 xlt2* double mutant were included for comparison. The profile of the *mur3 xlt2* sample results only in one peak with the same retention time and mass signal as XXXG in the standard and the WT. The *VcMUR3* complemented sample contains the XXXG peak and peaks that can be assigned to XXLG and its fucosylated form XXFG by retention time and mass spectrometry. The elution profile of the *VcXLT2* complemented line contains peaks for XXXG and XLXG based on retention time and mass spectrometry. The WT and both *VcMUR3* and *VcXLT2* complemented samples have additional peaks eluting after minute 23, which cannot be assigned to any known XyG oligosaccharide by retention time or mass

spectrometry. The results of the chromatography and mass spectrometry of *VcMUR3* and *VcXLT2* indicate that the enzymes are functional MUR3 and XLT2 homologs, respectively.

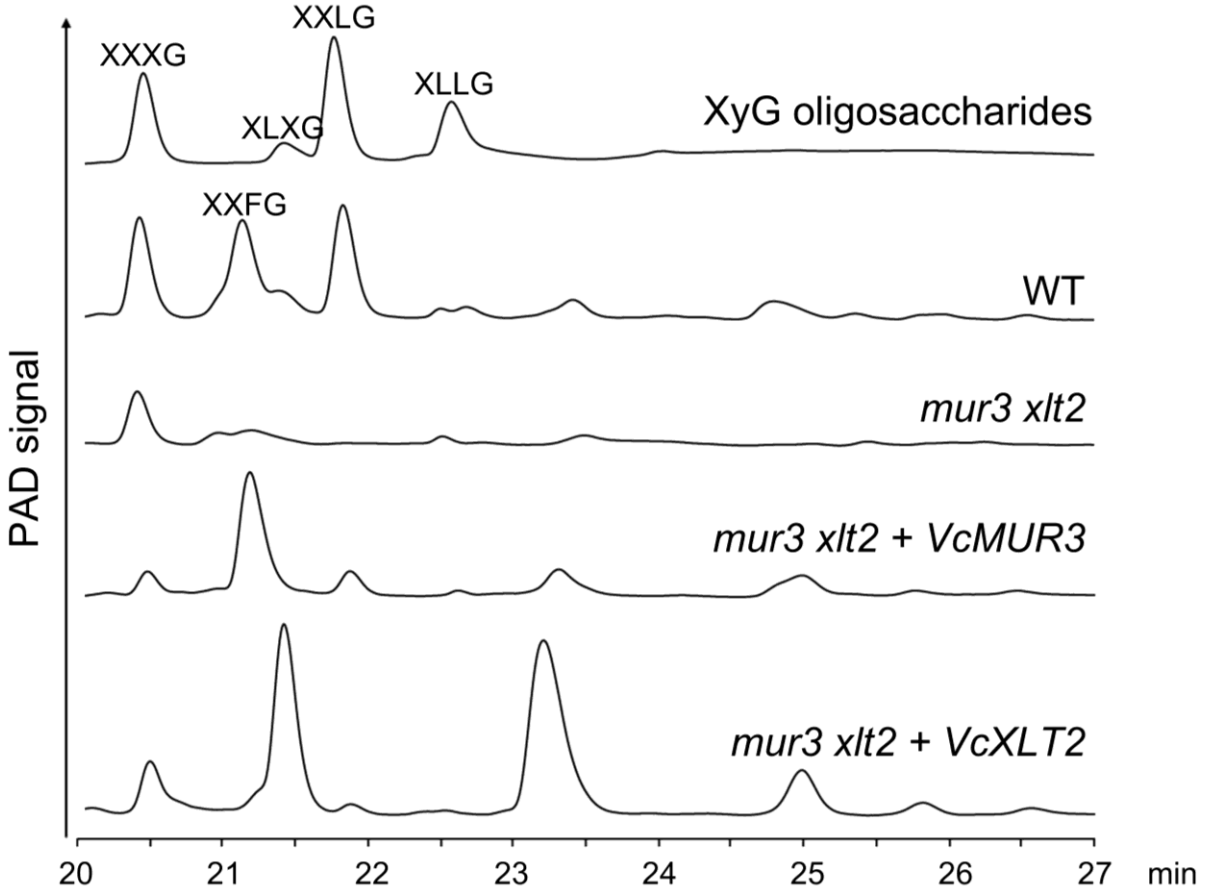

Figure 3.44: XyG oligosaccharide separation by HPAEC-PAD. Standard XyG oligosaccharides, XyG oligosaccharides derived from leaf tissue of Arabidopsis WT, *mur3 xlt2*, and transgenic lines expressing *VcMUR3* and *VcXLT2* in *mur3 xlt2* genetic background. Peaks were assigned according to Schultink et al. (2013) as well as based on mass spectrometry.

Since expression of VcXBT resulted in a new XyG oligosaccharide, which might represent a XyG with a U-sidechain, the XyG oligosaccharide mixture obtained from *VcXBT* expressed in *mur3 xlt2* was subjected to HPAEC (Ch. 2.12.7, Fig. 3.45 A) and the peaks were analysed by mass spectrometry (Fig. 3.45 B) to further elucidate the nature of the detected oligosaccharide(s). The first and second peak contained an oligosaccharide with a mass of *m/z* 1085. Since the second peak has a different retention time than XXXG but the same mass signal this oligosaccharide is likely a structural isomer such as XXGG + 1 pentose. The third peak contained at least two oligosaccharides with *m/z* 1085 and *m/z* 1217 which likely represent another XXGG + 1 pentose, and one with *m/z* 1217 representing XXXG + 1 pentose, respectively. One peak can contain oligosaccharide with different masses as the elution behaviour in HPAEC is not only based on mass but also monosaccharide composition, glycosidic linkages, charge and isomeric form (Patil and Rohrer, 2021). The fourth peak (f4) contained only oligosaccharide(s) with *m/z* 1217. The HPAEC fractions (f1-4) were pooled to

enhance the yield of the oligosaccharides and subjected to a monosaccharide compositional analysis (Ch. 2.12.11, Fig. 3.45 C). The dominant monosaccharides present were glucose and xylose with only minor traces of fucose, arabinose, and galactose. This data indicates that the oligosaccharide produced by *mur3 xlt2* expressing *VcXBT* is a xylosylated glucan.

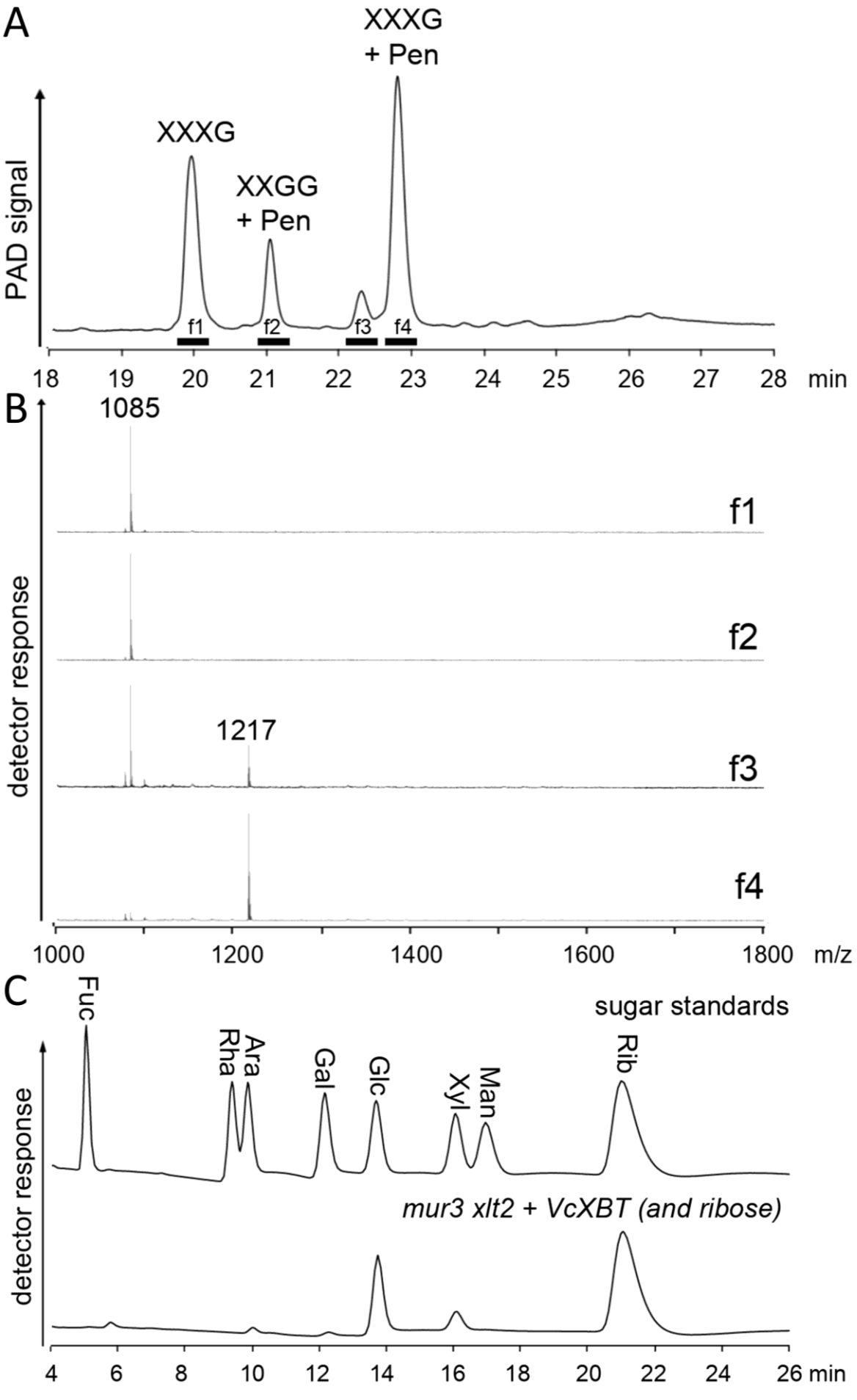
A
XXXG
+ Pen
XXXG
XXGG
+ Pen
PAD signal
f1
f2
f3
f4
18
19
20
21
22
23
24
25
26
27
28
min
B
1085
f1
f2
1217
f3
f4
detector response
1000
1200
1400
1600
1800
m/z
C
Fuc
sugar standards
Rha
Ara
Gal
Glc
Xyl
Man
Rib
mur3 xlt2 + VcXBT (and ribose)
detector response
4
6
8
10
12
14
16
18
20
22
24
26 min

Figure 3.45: Analysis of *mur3 xlt2* + *VcXBT* released oligosaccharides. A) Separation by HPAEC-PAD, XyG oligosaccharides derived from etiolated hypocotyls, **B)** Oligosaccharide mass profiling (OLIMP) of collected peak fractions (f) f1 to f4 indicated by lines in A), **C)** Monosaccharide composition analysis of pooled XyG oligosaccharides (f1-4) from A).

To further elucidate the structure of the novel oligosaccharide in the walls of *mur3 xlt2* expressing *VcXBT* the XEG derived XyG oligosaccharide mixture was subjected to reversed phase chromatography on an HPLC system using an evaporative light scattering detector (Ch. 2.12.9; Fig. 3.46 A). The peaks were collected and analysed by mass spectrometry. While the first two peaks contained carbohydrate(s) with a mass signal of *m/z* 1085, the third peak contained carbohydrate(s) with a *m/z* of 1217 (Fig. 3.46 B). The detection of two peaks containing carbohydrate(s) with a mass signal of *m/z* 1085 is consistent with the HPAEC and implies the presence of XXXG and structural isomer such as XXGG + 1 pentose. The third peak contained carbohydrate(s) with a *m/z* of 1217 which is likely the xylosylated XyG backbone (one U sidechain).

The collected fraction of the third peak was also subjected to ^{1}H NMR (Ch. 2.12.10) by Prof. Markus Pauly at CeMSA, Heinrich-Heine Universität. Numerous anomeric signals were observed (Fig. 3.46 C) in the chemical shift region of previously characterized XyG oligosaccharides (York et al., 1993; Tuomivaara et al., 2015). There are several H-1 signals belonging to α-sugars in the region of δ 4,94-5,18 ($\int_{1,2}$ 3,2-3,6 Hz) and β-sugars (δ 4,50-4,66 [$\int_{1,2}$ 7,8 Hz]). H-1 signal of substituted α-Xyl*p* (*δ* 5,155 [$\int_{1,2}$ 3,6 Hz]) has an integral ratio of 1:2 to the unsubstituted, terminal α-Xyl*p* (δ 4,961-δ 4,949 [$\int_{1,2}$ 3,2-3,6 Hz]). The H-1 signal δ 4,578 ($\int_{1,2}$ 7,8 Hz) was assigned to β-Xyl*p* based on published data concerning this sugar (Ray et al., 2004; Hilz et al., 2007). The other signals can be attributed to β-Glc*p* units of the oligosaccharide backbone (δ 4,646 [$\int_{1,2}$ 7,9 Hz]; δ 4.551 [$\int_{1,2}$ 7,8 Hz]; δ 4,546 [$\int_{1,2}$ 7,2 Hz]). The NMR-data provides thus evidence for the presence of a terminal β-linked xylopyranose as an additional substituent to the xylosylated glucan backbone.

In addition, a glycosidic linkage analysis (Ch. 2.12.8) was performed on the NMR sample (Fig. 3.47): The sugar moieties T-Man*p*/T-Glc*p,* 4-Glc*p*, 6-Glc*p*, and 4,6-Glc*p,* T-Xyl*p* and 2-Xyl*p*, were detected. Neither T-Ara*f* nor T-Ara*p* were detected. Particularly the presence of the 2-Xyl*p* residue is indicative of a further substituted XyG consistent with the U-sidechain.

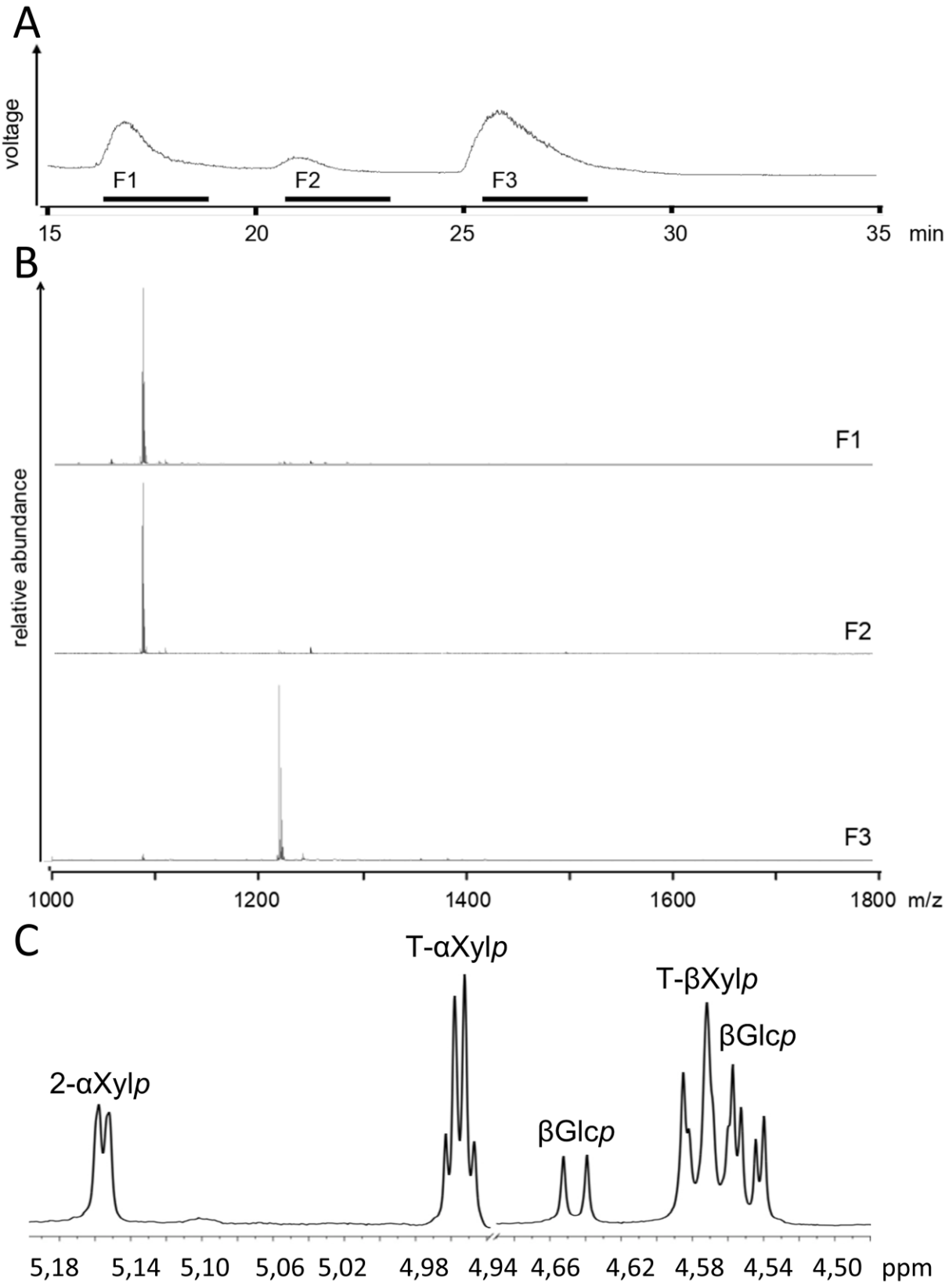

Figure 3.46: Analysis of *mur3 xlt2* + *VcXBT* released oligosaccharides. A) Reversed phase chromatography of XEG released XyG oligosaccharides of seedling tissue, fractions (F1-3) were collected for further analysis; **B)** Oligosaccharide mass profiling (OLIMP) of fractions indicated in A); **C)** Anomeric region of the ^{1}H NMR spectrum of the XyG oligosaccharide fraction F3*;* NMR performed by Prof. Markus Pauly, residues corresponding to each

group of anomeric proton resonances are indicated at the top of the figure, spectral region δ 4.67-4.92 containing the HDO signal has been deleted for clarity, Xyl*p*, xylopyranose; Glc*p*, glucopyranose

Sugar moiety	Abundance (%)
T-Ara*p*	Not detected
T-Ara*f*	Not detected
T-Xyl*p*	9,5
T-Man*p*/T-Glc*p*	1,5
2-Xyl*p*	9,4
6-Glc*p*	13,8
4-Glc*p*	4,0
4,6-Glc*p*	32,4

Figure 3.47: Glycosidic linkage analysis. XyG oligosaccharide fraction F3 in Fig. 3.46 with *m/z* 1217 from seedling material walls of *mur3 xlt2* + *VcXBT*; T-Ara*p*: terminal arabinopyranose, T-Ara*f:* terminal arabinofuranose, T-Xyl*p*: terminal xylopyranose, T-Man*p*: terminal mannopyranose, T-Glc*p*: terminal glucopyranose, 2-Xyl*p*: 2-linked xylopyranose, 6-Glc*p*: 6-linked glucopyranose, 4-Glc*p*: 4-linked glucopyranose, 4,6-Glc*p*: 4,6-linked glucopyranose

The novel XyG oligosaccharide produced by *VcXBT* expression in *mur3 xlt2* is a xylosylated glucan containing a β-xylopyranosyl residue as a terminal substitution on a xylosylated sidechain, consistent with the U-type sidechain (Fig. 3.48).

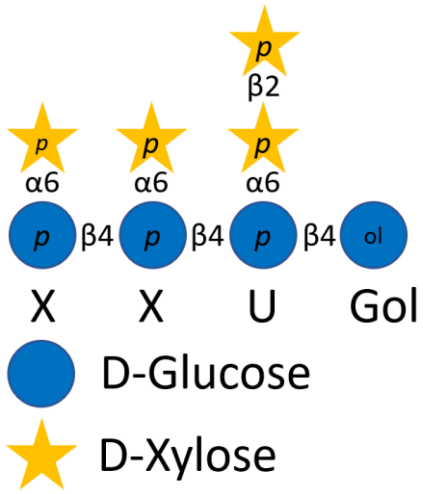

Figure 3.48: Proposed structure of XXUG oligosaccharide. Based on NMR and linkage analysis of XXUG. Nomenclature by one-letter code. Blue dots: D-Glucose (Glc*p*), orange stars: D-Xylose (Xyl*p*).

XyG biosynthesis occurs in the Golgi apparatus (Scheller and Ulvskov, 2010; Pauly and Keegstra, 2016; Julian and Zabotina, 2022) and all known XyG biosynthetic enzymes have been shown to be localized there (Chevalier et al., 2010; Jensen et al., 2012; Zhang et al., 2023b). Transient expression in tobacco (Ch. 2.9.17) was used to determine and confirm the predicted subcellular localization of *VcXBT*. C-terminal green fluorescence protein (GFP)-tagged *VcXBT* in pMDC83 (Curtis and Grossniklaus, 2003) (restriction/ligation cloning Ch.

2.9.7.2, confirmed by colony PCR Ch. 2.9.12, SFig. 6.41, plasmid map SFig. 6.10) and a vector with a Golgi-marker (rat (*Rattus norvegicus*, Rn) sialyltransferase (St) fused to red fluorescence protein (RFP), pVKH18En6:ST-RFP) (Saint-Jore et al., 2002; Runions et al., 2006) were expressed in tobacco leaves. A punctate pattern becomes visible when VcXBT:GFP is expressed (Ch. 2.10, Fig. 3.49). Co-expression of the RFP-tagged Golgi marker leads to an overlap of the two-colour signals demonstrating the localization of VcXBT to the Golgi apparatus.

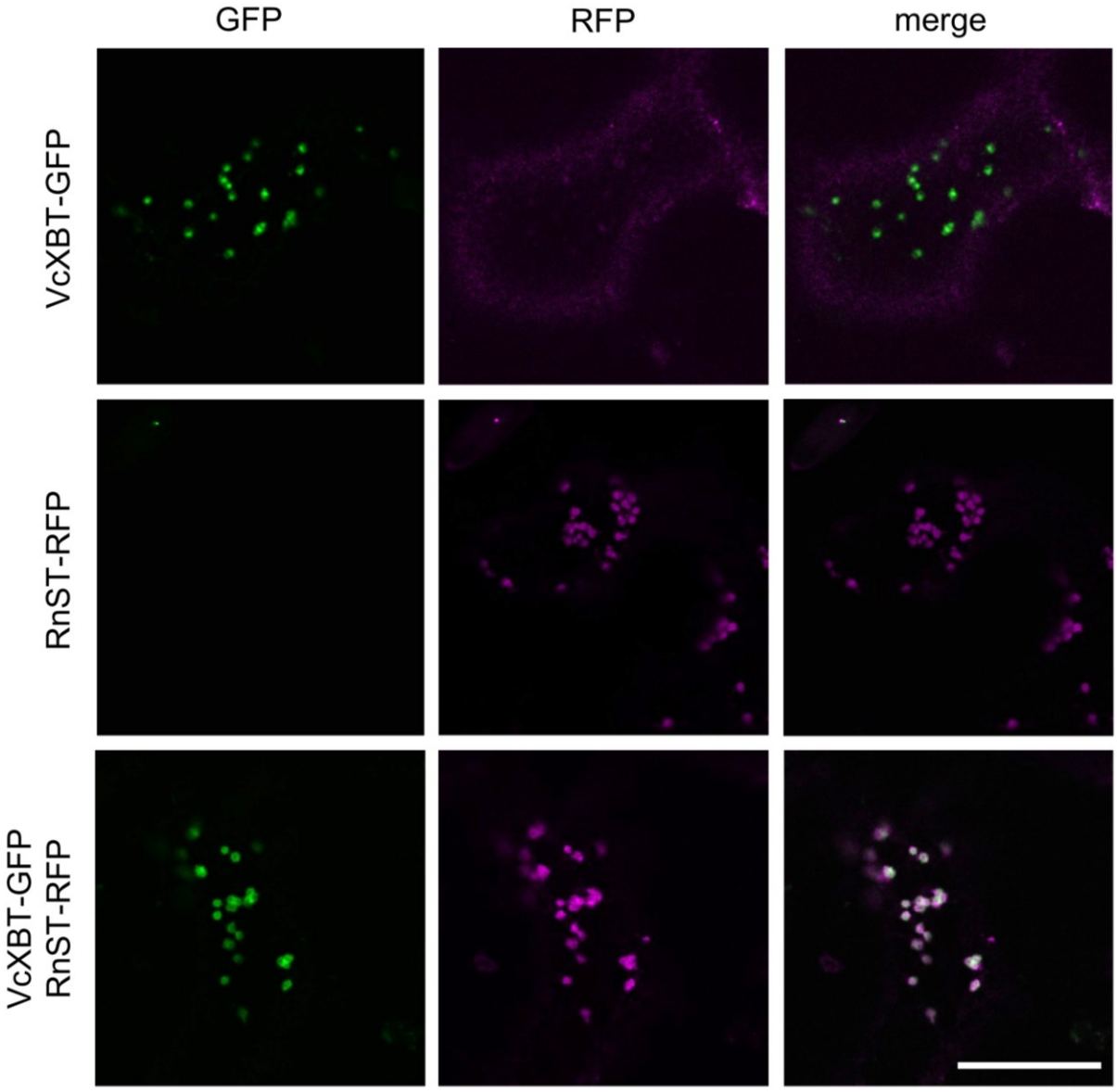

Figure 3.49: Subcellular localization of VcXBT. Visualized in *Nicotiana benthamiana* epidermal cells by confocal laser scanning microscopy (by Dr. Sebastian Hänsch); GFP signal from the VcXBT-GFP protein in green, RFP signal from the Golgi marker RnST-RFP in magenta, white bar = 20 µm

Complementation approaches expressing a number of GT47s in the Arabidopsis *mur3 xlt2* mutant affected vegetative growth of the plants (Jensen et al., 2012; Schultink et al., 2013; Liu et al., 2015; Zhu et al., 2018) as the *mur3 xlt2* double mutant has a dwarfed phenotype

compared to WT plants (Jensen et al., 2012; Schultink et al., 2013; Liu et al., 2015; Zhu et al., 2018).

When blueberry GT47s are expressed in *mur3 xlt2* the plant height was restored in most transgenic lines to nearly WT-levels (Fig. 3.50). One VcMUR3 expressing line was not able to restore the WT phenotype, nevertheless the plant height is still taller than *mur3 xlt2* plants. For VcXLT2 expressed in *mur3 xlt2* both individual transformants were able to restore growth to nearly WT heights. Two out of three transformants with VcXBT expressed in the *mur3 xlt2* resulted in plants with nearly WT heights. The third transformant was not able to restore the WT phenotype, nevertheless the plant height is still taller than *mur3 xlt2* plants.

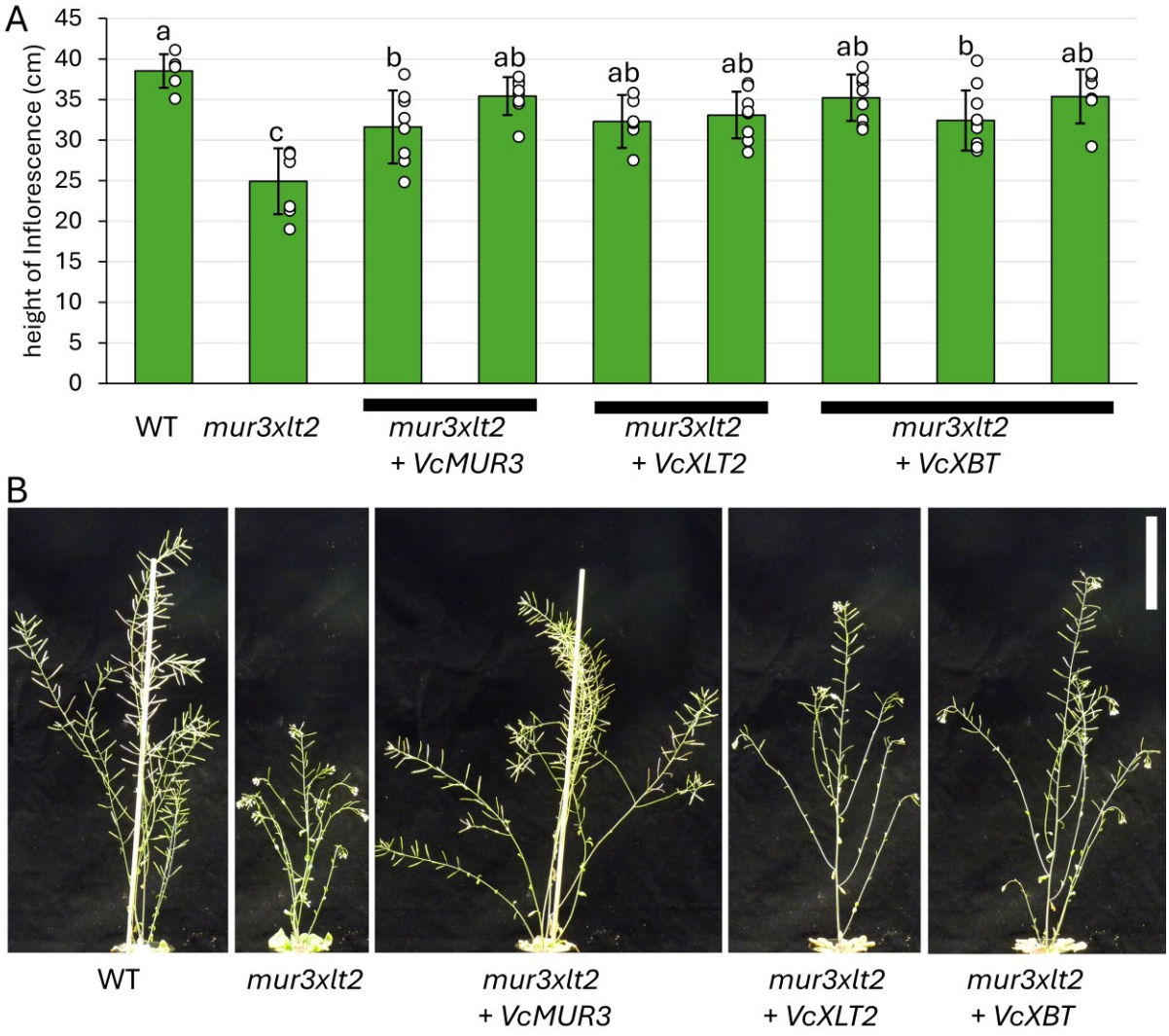

Figure 3.50: Plant height of complemented mur3 xlt2 plants expressing blueberry GT47s. A) Height of inflorescence stems of 8-week-old Arabidopsis plants (WT n = 6; *mur3 xlt2* n = 7; *mur3 xlt2* + *VcMUR3* n = 16 (8, 8); *mur3 xlt2* + *VcXLT2* n = 15 (6, 9); *mur3 xlt2* + *VcXBT* n = 25 (9, 10, 6)); results of ANOVA analysis and subsequent Tukey's test are indicated ($P < 0{,}05$); error bars indicate standard deviation; **B)** Representative pictures from the genotypes shown in A), scale bar: 10 cm

3.4.3 Discussion

Based on the presence of additional pentoses on the regular XyG oligosaccharides in the OLIMP profile of various blueberry tissues (Fig. 3.40) the β-D-Xyl*p*-(1,2)-α-D-Xyl*p*-(1,6)-β-D-Glc*p* (U sidechain) identified in Argan tree (Ray et al., 2004) and bilberries (Hilz et al., 2007) is likely to be present also in blueberry (*Vaccinium corymbosum*). However, the detected pentose moieties cannot be unambiguously identified in the OLIMP analysis as only information on mass is gathered and other pentoses have been shown to be present in XyG previously (Schultink et al., 2013; Pauly and Keegstra, 2016; Zhu et al., 2018).

In a functional complementation approach testing seven potential blueberry GT47 candidates in the Arabidopsis double mutant *mur3 xlt2* resulted in three of them impacting the structure of XyG (Fig. 3.43). Four blueberry GT47 candidates did not modify the XyG structure when expressed in the Arabidopsis *mur3 xlt2* mutant. These proteins might have a different substrate specificity in that they modify other polymers than XyG (xylan, mannan or pectin) (Zhang et al., 2023a). The lack of activity could also be caused by absence, instability and/or mislocalization of the respective proteins.
Complementation of *mur3 xlt2* with *VcXLT2* resulted in a XyG that contained an oligosaccharide of *m/z* 1247 likely representing a galactosylated XXXG, while complementation with *VcMUR3* resulted in an XXXG type XyG that can be galactosylated (*m/z* 1247 and 1289), fucosylated (*m/z* 1393 and 1435) and *O*-acetylated (*m/z* 1289 and 1435). Further analysis of the XyG oligosaccharides by HPAEC-PAD (Fig. 3.44) resulted in detection of XLXG and no fucosylated XyG oligosaccharides for *mur3 xlt2* expressing *VcXLT2*, and XXLG and its fucosylated form XXFG for *mur3 xlt2* expressing *VcMUR3*. Taken together, this provides evidence that both VcXLT2 and VcMUR3 have galactosyltransferase activity and are distinct functional homologs to XLT2 and MUR3, respectively.

Expression of *VcXBT* in the Arabidopsis *mur3 xlt2* mutant resulted in the occurrence of a novel XyG oligosaccharide with *m/z* 1217 representing XXXG with an additional pentose in the OLIMP profile (Fig. 3.43). Interestingly, no fucosylation and *O*-acetylation as in VcMUR3 complemented plants were detected. This might be due to Arabidopsis fucosyltransferase (Vanzin et al., 2002) and *O*-acetyltransferases AtAXY4/AtAXY4L (Gille and Pauly, 2012) not recognizing the further pentosylated XXXG motif as an acceptor substrate.
Analysis of the XyG oligosaccharides by HPAEC-PAD followed by MALDI-TOF MS on fractions resulted in confirmation of XXXG (Fig. 3.45 A and B) and three additional peaks containing unusual pentosylated XyG oligosaccharides potentially representing a structural isomer to XXXG such as XXGG + 1 pentose (*m/z* 1085 and retention time different than XXXG), another XXGG with one additional pentose and one representing XXXG with one additional pentose (two oligosaccharides, *m/z* 1085 and 1217), and another XXXG with one

additional pentose (*m/z* 1217). XyG motifs present could be XUGG and UXGG for the oligosaccharides with m/z 1085 and XXUG, XUXG or UXXG for the oligosaccharides with *m/z* 1217. Monosaccharide compositional analysis of the pooled fractions indicated the near exclusive presence of glucose and xylose (Fig. 3.45 C).

Reversed phase chromatography on enzymatically derived XyG oligosaccharides from *mur3 xlt2* expressing VcXBT followed by OLIMP of a collected fraction from one peak (Fig. 3.46 A and B) detected an oligosaccharide with *m/z* 1217 indicating XXXG with one additional pentose. ^{1}H NMR (Fig. 3.46 C) revealed that the fraction contains a mixture of XyG oligosaccharides which are likely isomers of XyG alditols with a single xylosyl substituent on different position of the xylosyl residues on the XXXG oligosaccharide. The ratio of substituted α-Xyl*p* to unsubstituted, terminal α-Xyl*p* also supports this fact. β-Xyl*p* and β-Glc*p* units of the oligosaccharide backbone were also detected. The fraction was subjected to glycosidic linkage analysis. 4-Glc*p*, 6-Glc*p* and 4,6-Glc*p*, T-Xyl*p* and 2-Xyl*p* were detected (Fig. 3.47) representing a partially xylosylated glucan backbone. 2-Xyl*p* demonstrates that the xylosyl sidechain had an additional substituent on its *O*-2 position.

In summary, the analysed XyG oligosaccharide fraction contains a XyG oligosaccharide with the β-Xyl*p*-(1,2)-α-Xyl*p*-(1,6)-β-D-Glc*p* (U-) sidechain (Fig. 3.48). Based on the NMR analysis a mixture of two isomers (e.g. XUXG and XXUG) is present in the fraction. Therefore, the analysed VcXBT is a GT47 family member and XyG:β-xylopyranosyltransferase.

The subcellular localization of VcXBT was determined by transient expression of a VcXBT::GFP fusion construct in *Nicotiana benthamiana* leaves alongside an RFP-tagged Golgi marker (rat sialyltransferase) (Fig. 3.49). The colocalization demonstrates that VcXBT is present in the Golgi apparatus, which is consistent with the localization of XyG biosynthesis and localization of XyG biosynthetic enzymes (Jensen et al., 2012; Pauly and Keegstra, 2016).

Arabidopsis *mur3 xlt2* mutants without Gal and Fuc sidechains show a dwarfed phenotype (Jensen et al., 2012). Galactose-deficient XyG seems to be dysfunctional (Xu et al., 2017) and leads to intracellular polymer and vesicular aggregations (Hoffmann and McFarlane, 2024). However, *mur3 xlt2* plants expressing functional blueberry GT47s rescue the dwarfed phenotype of the double mutant in most of the transgenic lines (Fig. 3.50) similar to what has been observed when expressing *AtXLT2* (Jensen et al., 2012), *SlMUR3* (Schultink et al., 2013), *OsMUR3* (Liu et al., 2015) and *PpXLT2* (Zhu et al., 2018) in the same mutant line.

Since *VcXLT2* and *VcMUR3* expressing *mur3 xlt2 Arabidopsis* lines have a recovered XyG structure with galactosylated XyG oligosaccharide, most likely no intracellular aggregation happens, and the phenotype is rescued. Apparently, also other sugar substituents of the core XXXG motif (such as the U-sidechain created here) can prevent aggregation and recover the normal *Arabidopsis* phenotype, since *mur3 xlt2* expressing *VcXBT* is also growing normally.

Recently, Wilson et al. identified a XyG β-xylosyltransferase XBT in coffee (*Coffea canephora*, Cc) based on putative donor-sugar-binding residues. Phylogenetic analysis of characterized GT47 members and potential asterid GT47 protein sequences was performed, and three subclades were identified. The AlphaFold-predicted structure of AtXLT2 was used to identify likely substrate-binding residues. The potential binding pocket for the substrate was identified and found to be conserved in multiple MUR3s and XLT2s. Family members with unusual substitutions in these regions could potentially harbour novel activities. For characterization of CcXBT the complementation in Arabidopsis *mur3 xlt2* has also been utilized and resulted in a full rescue of the stunted phenotype of *mur3 xlt2* (Wilson et al., 2023).

3.5 Functional Redundancy of the Hemicellulose Xyloglucan

3.5.1 Background

Xyloglucan makes up to 25% of the amount of polysaccharides in dicot primary cell walls and is therefore the most abundant hemicellulose in dicots (Scheller and Ulvskov, 2010). However, loss of XyG surprisingly has no effect on the viability of plants: Knockout plant mutants have only subtle, tissue specific phenotypes compared to the wildtype (Cavalier et al., 2008; Park and Cosgrove, 2012b; Kim et al., 2020) and treatment of plant cell walls with xyloglucanase *in vivo* resulted in negligible biomechanical effects (Park and Cosgrove, 2012a, 2012b; Zhang et al., 2019). These results undermine the traditional tethered network model of plant cell walls in which XyG tethers cellulose microfibrils and both polysaccharides form a load-bearing network (Hayashi, 1989; Fry, 1989; Cosgrove, 2024). Solid-state NMR of Arabidopsis wild type and an XyG lacking mutant indicate that XyG−cellulose contacts are more limited than previously thought and that pectins are in close proximity to cellulose and XyG (Pérez García et al., 2011).

Enzyme digestions utilizing bifunctional endoglucanases that hydrolyse XyG and disordered cellulose, and the combination of XyG-specific endoglucanase with a cellulose-specific endoglucanase, which interestingly showed no equivalent biomechanical effect, still implicate a mechanical role for XyG but only in regions of limited enzyme accessibility. These “biomechanical hotspots” were hypothesized to be tight XyG-mediated junctions between cellulose microfibrils (Cosgrove, 2018, 2022a). Recent models of the plant cell wall network envision that XyG bind to one, two or more cellulose microfibrils in different (extended or coiled) potentially even tether-like configuration, but these tethers are mechanically weak (Cosgrove, 2024).

One way of how plants may compensate the loss of the most abundant hemicellulose is through compensation mechanisms. One theory state that in XyG lacking mutants the loss of XyG is compensated for by an increase of other wall components: Sowinsky et al. showed a specific increase in the relative abundance of homogalacturonan and glucomannan in XyG deficient plants (Sowinski et al., 2022). The relative increase of other wall components might be caused by an increase in production or a decrease of turnover of the compensating cell wall component to maintain higher levels of this component in the wall (Bou Daher et al., 2024). However, a relative increase of other cell wall polysaccharides occurs naturally if one polysaccharide is lost, therefore interpretation of these results is difficult. Comparative RNA-seq analyses on a XyG deficient mutant and wild type did not show significant changes in the levels of expression for genes responsible for the synthesis of homogalacturonan, rhamnogalacturonan I and II, cellulose and/or xylogalacturonan (Kim et al., 2020).

Another theory states that some wall component might be able to substitute for XyG without an increase in its level because of functional redundancy among wall components (Kim et al.,

2020). This hypothesis is based of solid-state NMR studies of the cell walls of Arabidopsis wild type and an XyG lacking mutant since the plant cell wall network (cellulose, pectin and XyG) can continue to function in the absence of XyG (Pérez García et al., 2011).

Glucomannans were proposed to functionally substitute XyG since their relative abundance is increased in XyG deficient plants (Sowinski et al., 2022) and they have structural and biosynthetic similarities to XyG (Yu et al., 2022; Grieß-Osowski and Voiniciuc, 2023). Linkages of backbone and sidechains of XyG and glucomannan are analogous and synthesized by glycosyltransferases from the same CAZy families (Yu et al., 2022; Grieß-Osowski and Voiniciuc, 2023). In Arabidopsis nine CSLAs have been identified (Liepman et al., 2007) - four CSLAs influence β-mannan content or structure: CSLA2 (At5g22740), CSLA3 (At1g23480), CSLA7 (At2g35650) and CSLA9 (At5g03760) (Liepman et al., 2005; Liepman et al., 2007; Goubet et al., 2009; Voiniciuc et al., 2019).

The CSLAs differ in terms of which glucomannan structure is synthesised: AtCSLA2 synthesises a glucomannan with a repeating Glc-β-1,4-Man disaccharide backbone that can be substituted with galactosyl residues (β-galactoglucomannan, β-GGM, Fig. 3.51) (Yu et al., 2022). AtCSLA9 produces a random patterned glucomannan with few or no galactose residues and acetylated mannose residues (acetylated galactoglucomannan, AcGGM, Fig. 3.51) (Yu et al., 2022). The glucomannan structures were identified by enzymatic digestions followed by polysaccharide analysis by carbohydrate electrophoresis (PACE) or MALDI-TOF MS, high-energy collision-induced dissociation tandem mass spectrometry on the main peaks detected with PACE, and NMR (Yu et al., 2022). Plants lacking β-galactoglucomannan like *csla2* mutants showed marginal reductions in height (Yu et al., 2022).

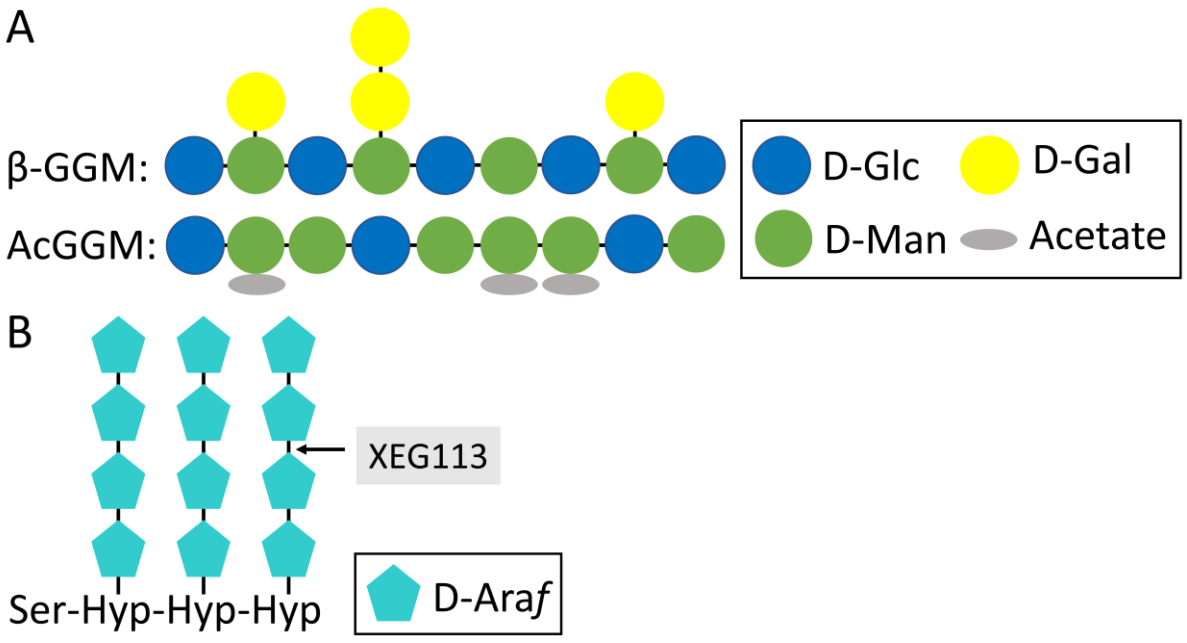

Figure 3.51: Galactoglucomannan structure and glycosylation patterns on an extensin repeat. A) β-galactoglucomannan (β-GGM) backbone is synthesized by CSLA2. It has a strictly repeating pattern of glucose and

mannose units, and galactose sidechains. The acetylated galactoglucomannan (AcGGM) backbone is synthesized by CSLA9. It is composed of a random order of Man and Glc units. AcGGM mannose residues are often acetylated. AcGGM has few or no galactose sidechains in Arabidopsis. Glc = Glucose, Man = Mannose, Gal = Galactose, based on (Yu et al., 2022; Ishida et al., 2023) **B)** Extensin hydroxyproline residues are glycosylated with arabinoses. Ara residues are added by glycosyl-transferases. The third Ara is linked by XEG113. Ara*f* = arabinofuranose, Ser = Serine, Hyp = Hydroxyprolin. Based on (Marzol et al., 2018; Moussu and Ingram, 2023)

csla2xxt1xxt2, a mutant lacking XyG and β-galactoglucomannan showed a slightly altered rosette appearance and shorter stems at six to eight week old plants than the only XyG deficient line *xxt1xxt2* (Yu et al., 2022) indicating that a loss/alteration of two cell wall components lead to more severe phenotypes but still no breakdown of the wall network since the plant is viable. Yu et al. also hypothesised that an additional loss of other hemicelluloses might reveal more severe impacts on wall function.

XyG and the glycoprotein network made of extensins (EXT) are hypothesized to have similar, but redundant functions since enzymatic degradation of XyG *in vivo* caused greater hypocotyl elongation in a mutant with defects in EXT glycosylation (Gille et al., 2009; Kim et al., 2020).

EXTs are hydroxyproline-rich glycoproteins which are defined by a conserved repetitive amino-acid motif (Serine-Proline$_{3\text{-}5}$) (Marzol et al., 2018). EXTs are integrated in the plant cell wall network and are proposed to have key responsibilities in modulation and regulation of the network. They are thought to influence plant growth and development, and pathogen defence (Marzol et al., 2018; Castilleux et al., 2021; Moussu and Ingram, 2023), which would be similar to some XyG functions. However, many Arabidopsis EXT mutants have inconspicuous phenotypes, probably due to high genetic redundancy in multiple genes encoding EXTs (Marzol et al., 2018; Doll et al., 2022; Moussu and Ingram, 2023). For example, the Arabidopsis gene XYLOGLUCANASE 113 (XEG113), whose T-DNA mutant *xeg113* was identified through an XEG liquid culture screen, was found to cause under-arabinosylation of extensins, leading to more elongated hypocotyls and increased growth in the plant phenotype (Gille et al., 2009). XEG113 plays a role in posttranslational modifications of the proline-rich EXT motif: Proline residues are hydroxylated to hydroxyproline. Hydroxyproline residues are then sequentially glycosylated with 4-5 arabinoses (Ara) (Fig. 3.51). XEG113 acts as an arabinosyltransferase and is responsible for adding the third arabinose residues (Moussu and Ingram, 2023). Other EXT arabinosylation mutants like loss-of-function of Hydroxyproline *O*-arabinosyltransferases (HPAT1, HPAT2, HPAT3)**,** which add the first arabinose to hydroxyproline residues, revealed no severe phenotypes (Ogawa-Ohnishi et al., 2013; MacAlister et al., 2016). *hpat1 hpat2* double mutant has longer hypocotyls than the wild type (Ogawa-Ohnishi et al., 2013). Common across all EXT arabinosyltransferase and proline hydroxylation Arabidopsis mutant lines is the reduced root hair growth (Gille et al., 2009; Velasquez et al., 2011; Ogawa-Ohnishi et al., 2013; Velasquez et al., 2015).

3.5.2 Results

To test the hypothesis of functional redundancy of multiple wall components an Arabidopsis mutant was generated that lacks/alters three wall components: XyG (mutant *cslc456812*), mannan (mutant *csla29*) and EXT (mutant *xeg113*). For this purpose, Niklas Gawenda generated an Arabidopsis mutant lacking XyG (mutant *cslc456812*) and altered EXT arabinosylation (mutant *xeg113*). The XyG deficient quintuple mutant *cslc456812* (*cslc4-3* (SAIL_837B10), *cslc5-1* (SAIL_187G09), *cslc6-1* (SALK_088720-11), *cslc8* (WiscDsLox_497-02H), and *cslc12-2* (SAIL_168F02)) (Kim et al., 2020) was crossed with *xeg113* (*xeg113-2 (*SALK_066991) (Alonso et al., 2003; Gille et al., 2009). The uniformly heterozygous offspring were crossed again with the *cslc456812* quintuple mutant, and progeny plants that were heterozygous for *xeg113* and homozygous for as many *cslc* alleles as possible were selected. In the next generation a mutant homozygous for *xeg113* and all *cslcs* was identified (*cslc456812xeg113*, termed sextuple mutant, confirmation by PCR Ch. 2.9.12, SFig. 6.45).
Here, the mannan deficient mutant a *csla2 csla9* double mutant was utilized. A PACE analysis of *csla2 csla9* double mutant did not release any oligosaccharides in an *endo*-mannanase digest (Yu et al., 2022) and a monosaccharide composition analysis of the same mutant line indicated no detection of mannose (Goubet et al., 2009) suggesting the loss of glucomannan. Therefore, *csla2* and *csla9* mutant plants were selected to create a double mutant and afterwards an octuple mutant by crossing with the sextuple mutant.
In theory, Arabidopsis genes display a Mendelian segregation pattern when lines are crossed. However, non-Mendelian segregation can occur after crossing multiple T-DNA lines (Curtis et al., 2009; O'Malley et al., 2015) even if the insertions are on different chromosomes (Raabe et al., 2024). To exclude non-Mendelian segregation caused by close chromosomal location of the various genes in the creation of the octuple mutant the loci of the genes were mapped using TAIR Chromosome Map Tool (Ch. 2.2; Fig. 3.52). The mapping shows that the genes are distributed on four of the five Arabidopsis chromosomes. AtCSLC8 and AtXEG113 are linked the closest (~4500 kbp) but sufficiently far for segregation.

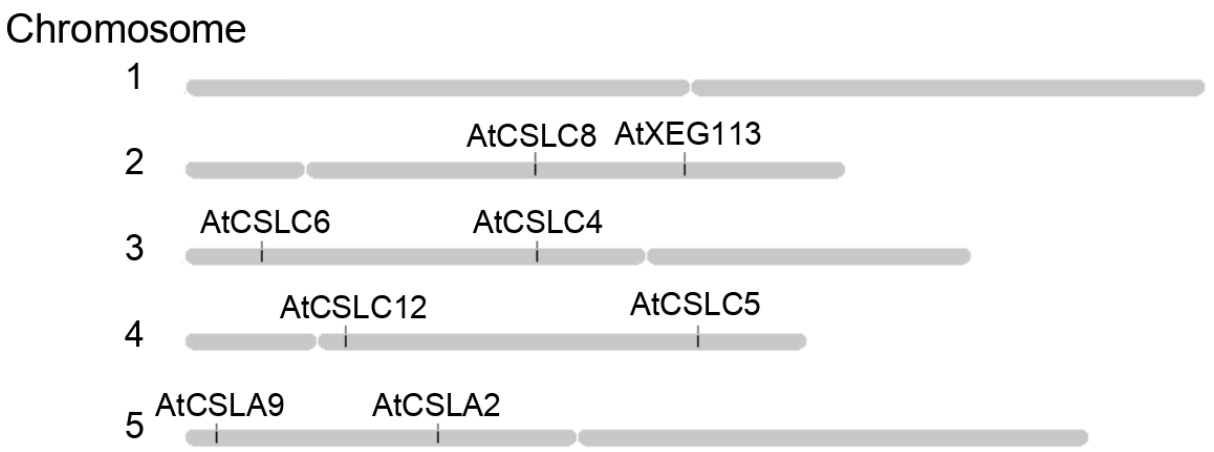

Figure 3.52: Map of the Arabidopsis genome with octuple mutant gene loci. Arabidopsis chromosomes with all eight gene loci of genes used to create the octuple mutant. Map was produced with TAIR Chromosome Map Tool

csla2 and *csla9* were crossed (*csla2* (SALK_065083), *csla9* (SALK_071916)) (Goubet et al., 2009), the heterozygous offspring were selfed and a homozygous mutant for *csla2* and *csla9* was identified (Fig. 3.53). All genotyping was performed via PCR (Ch. 2.9.12) with the corresponding primers for Arabidopsis T-DNA insertional mutant lines (primers SFig. 6.15).

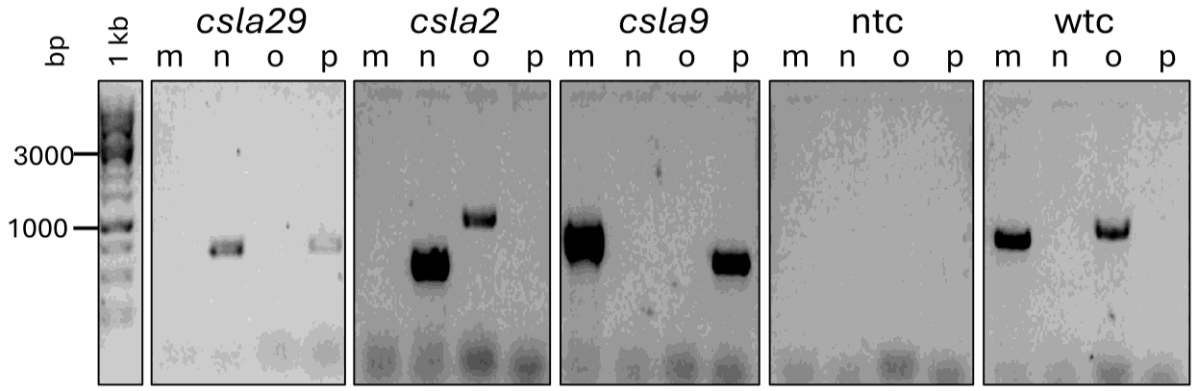

Figure 3.53: Genotyping PCR of double mutant *csla29* and controls. PCR products amplifying a genomic fragment spanning the T-DNA insertion and a fragment from the T-DNA border to a genomic position to confirm presence or absence of T-DNA insertion; m: SALK_065083-LP & RP, *CSLA2* WT specific; n: SALK_065083-RP & LBb1.3, *csla2* T-DNA insertion; o: SALK_071916-LP & RP, *CSLA9* WT specific; p: SALK_071916-RP + LBb1.3, *csla9* T-DNA insertion; ntc = no template control, wtc = wildtype controls, plant with no T-DNA insertion; bp = base pairs

To create the octuple mutant *cslc456812xeg113csla29* the sextuple mutant was crossed to the *csla* double mutant. The heterozygous offsprings were crossed with the sextuple mutant again. The F1 generation of this crossing was screened by PCR (Ch. 2.9.12) for plants heterozygous for both *csla* genes and homozygous mutant for as many of the sextuple mutant genes as possible. The selected plants were selfed, and the subsequent generations were screened by PCR (Ch. 2.9.12) for individuals that were homozygous for as many of the eight genes as possible. This was repeated until a *cslc456812xeg113csla29* octuple mutant line was identified (termed octuple mutant, Fig. 3.54).

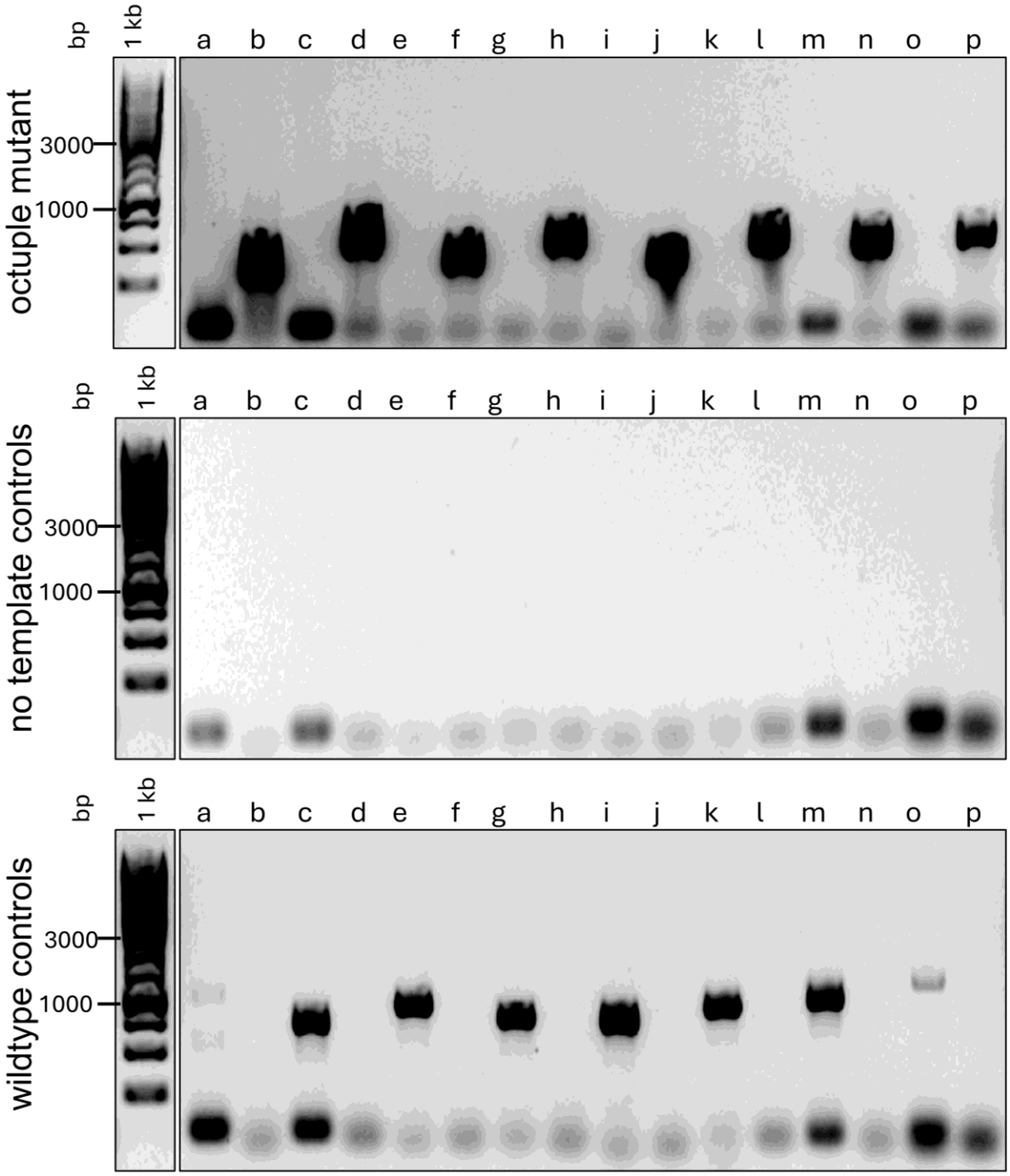

Figure 3.54: Genotyping PCR of octuple mutant *xeg113cslc456812csla29* and controls. PCR products amplifying a genomic fragment spanning the T-DNA insertion and a fragment from the T-DNA border to a genomic position to confirm presence or absence of T-DNA insertion; a: SALK_06691-LP & RP, *XEG113* WT specific; b: SALK_06691-RP & LBb1.3, *xeg113* T-DNA insertion; c: SAIL_837B10-LP & RP, *CSLC4* WT specific; d: SAIL_837B10-RP & LB-3, *cslc4* T-DNA insertion; e: SAIL_187G09-LP & RP, *CSLC5* WT specific; f: SAIL_187G09-RP & LB-3, *cslc5* T-DNA insertion; g: SALK_088270-LP & RP, *CSLC6* WT specific; h: SALK_088270-RP & LBb1.3, *cslc6* T-DNA insertion; i: WiscDsLox_497-02H-LP & RP, *CSLC8* WT specific; j: WiscDsLox_497-02H-RP & P745, *cslc8* T-DNA insertion; k: SAIL_168F02-LP & RP, *CSLC12* WT specific; l: SAIL_168F02-RP & LB-3, *cslc12* T-DNA insertion; m: SALK_065083-LP & RP, *CSLA2* WT specific; n: SALK_065083-RP & LBb1.3, *csla2* T-DNA insertion; o: SALK_071916-LP & RP, *CSLA9* WT specific; p: SALK_071916-RP + LBb1.3, *csla9* T-DNA insertion; wildtype controls, plant with no T-DNA insertion; bp = base pairs

As a *cslc456812xeg113csla29* octuple mutant was identified and viable, the combination of altered/lack of cell wall components is apparently non-lethal.

The phenotype and the cell wall of various mutants was analysed in detail. The hypocotyls of etiolated seedlings grow almost exclusively by expanding cells without cell division (Gendreau et al., 1997; Martín and Duque, 2022). Measuring hypocotyl length and investigating hypocotyl cellular morphology are common methods to analyse Arabidopsis T-DNA insertion lines with altered cell wall structures (Alonso et al., 2003; Gille et al., 2009; Kim et al., 2020; Yu et al., 2022). Etiolated hypocotyls of the octuple mutant and controls (WT Col0, *xeg113*, *clsa29*, *cslc456812*) were grown in the dark for five days (Ch. 2.8.5.6) and measured afterwards (Ch. 2.11). Compared to WT all lines show a significant difference in the hypocotyl length: While *xeg113*, *csla29* and *cslc456812* are significantly longer compared to the WT, the octuple mutant is significantly shorter and measures less than half of the length of the wild type hypocotyls (Fig. 3.55 A). While WT, *xeg113*, *csla29* and *cslc456812* display relatively straight growth with a light curvature at the base of the *cslc456812* hypocotyls, the octuple mutant hypocotyls show a severely shortened and twisted growth (Fig. 3.55 B).

The etiolated hypocotyls were stained using propidium iodine (Ch. 2.10.1) and imaged using a microscope to visualize plant cell walls (Rounds et al., 2011). The microscopy images (Fig. 3.56) show that the cells in etiolated hypocotyls are elongated and almost rectangular in an organised cell structure in WT, *xeg113*, *csla29* and *cslc456812* samples. In contrast, the octuple mutant has less elongated bulging cells and some epidermal cells are detached from other cells and display aberrant cell shapes. The epidermal cells in *xeg113* look like the wildtype while *csla29* and *cslc456812* epidermal cells seem slightly bulged.

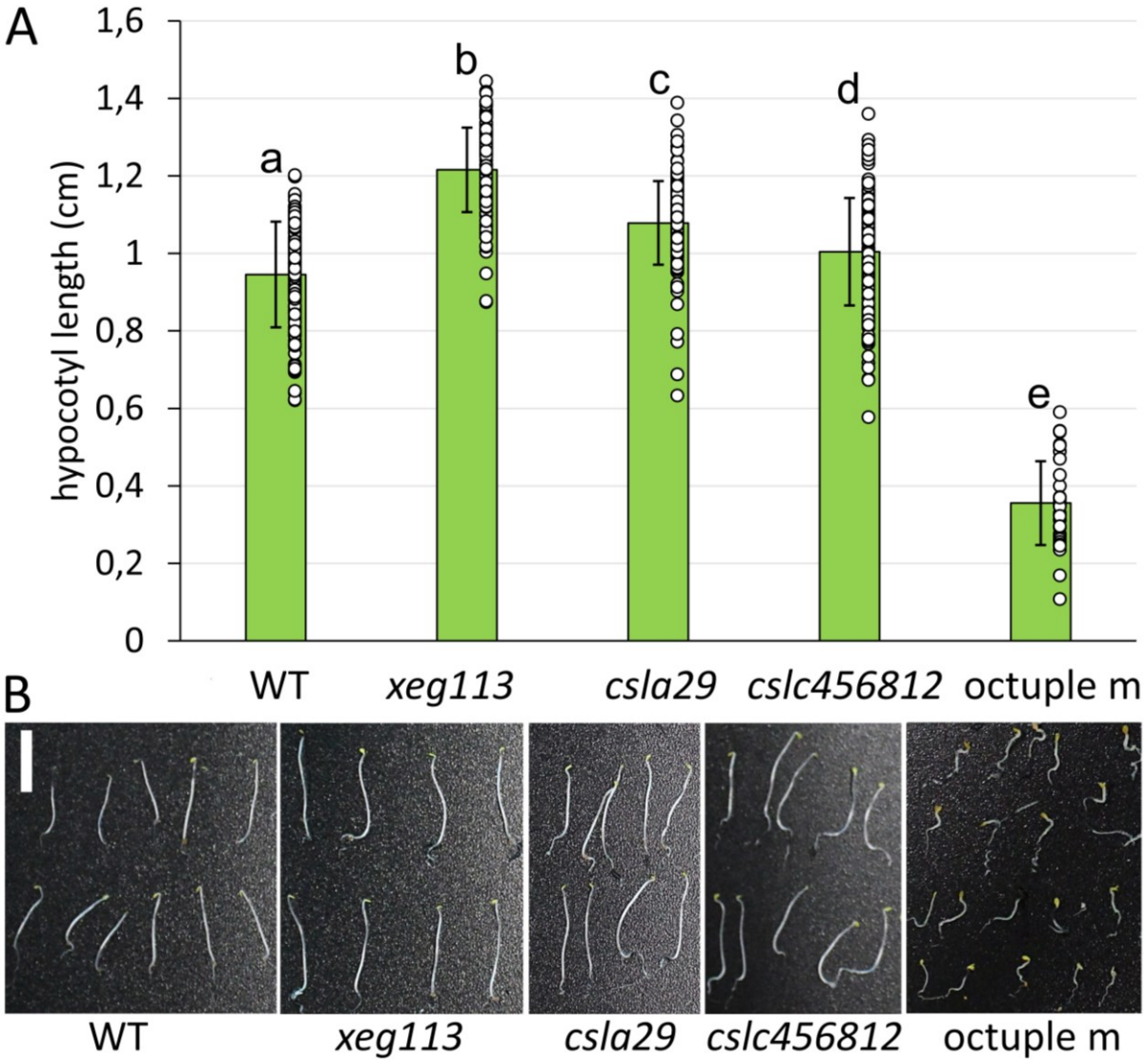

Figure 3.55: Phenotyping of etiolated hypocotyls of the octuple mutants and controls. A) Length of five-day-old hypocotyls (Col0 n = 164, *xeg113* n= 150, *csla29* n = 151, *cslc456812* n = 150, octuple mutant n = 38), results of ANOVA analysis and subsequent Tukey's test are indicated ($P < 0,01$), **B)** Representative pictures from the genotypes shown in A), five-day-old hypocotyls grown on MS medium with sucrose, scale bar: 1 cm

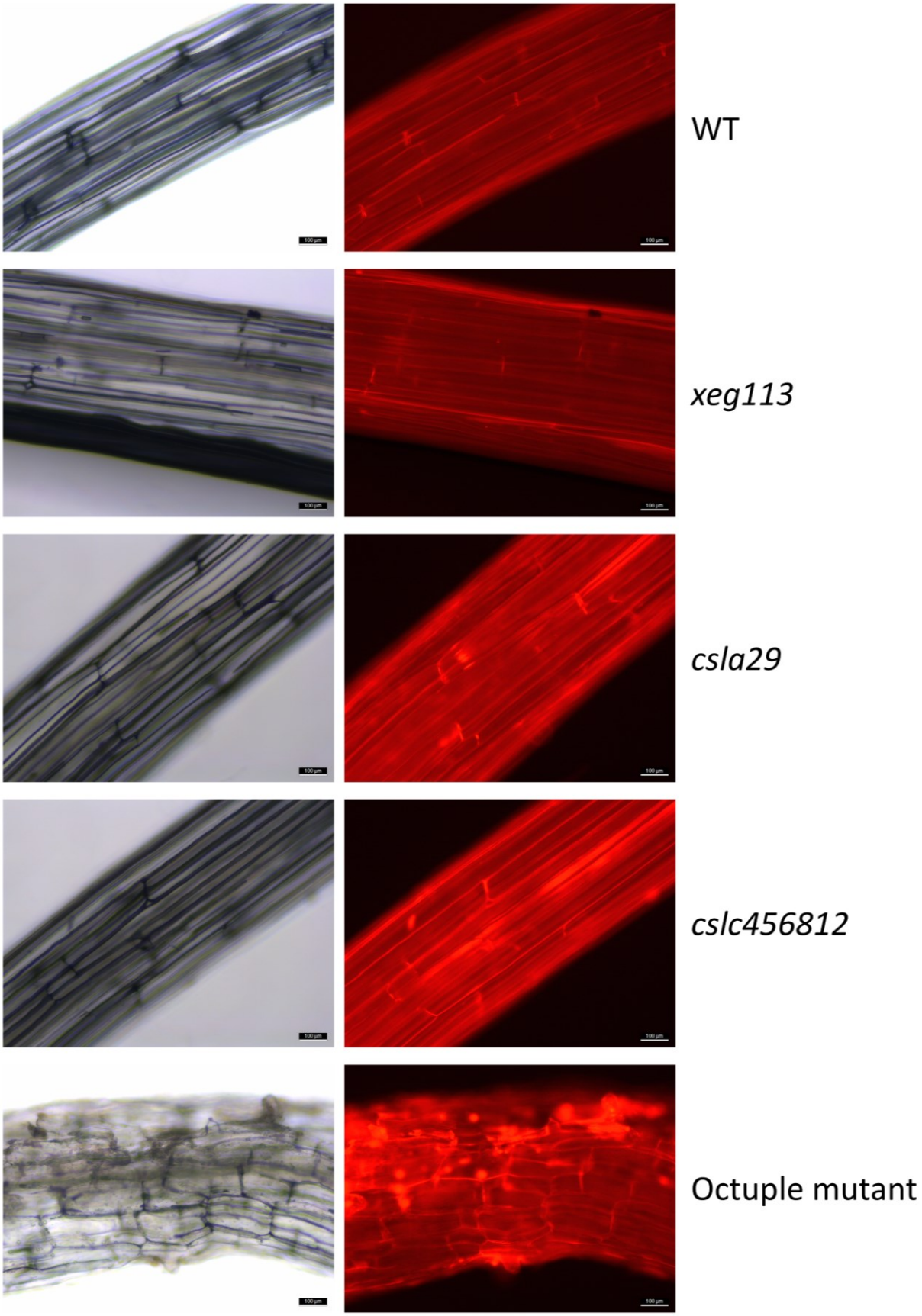

Figure 3.56: Imaging of etiolated hypocotyls of the octuple mutants and controls. Brightfield (left) and laser (right, Excitation: 560nm, Emission: 630) microscopy of five-day-old hypocotyls stained with propidium iodine, scale bar: 100 µm

The growth phenotypes of the different lines were further investigated after 6 weeks of growth (Ch. 2.11, Fig. 3.57). Wildtype and *xeg113* and *cslc456812* plants had similar inflorescence height, while *csla29* shows a significantly reduced stem height. The octuple mutant has a severely shorter inflorescence compared to the other genotypes.

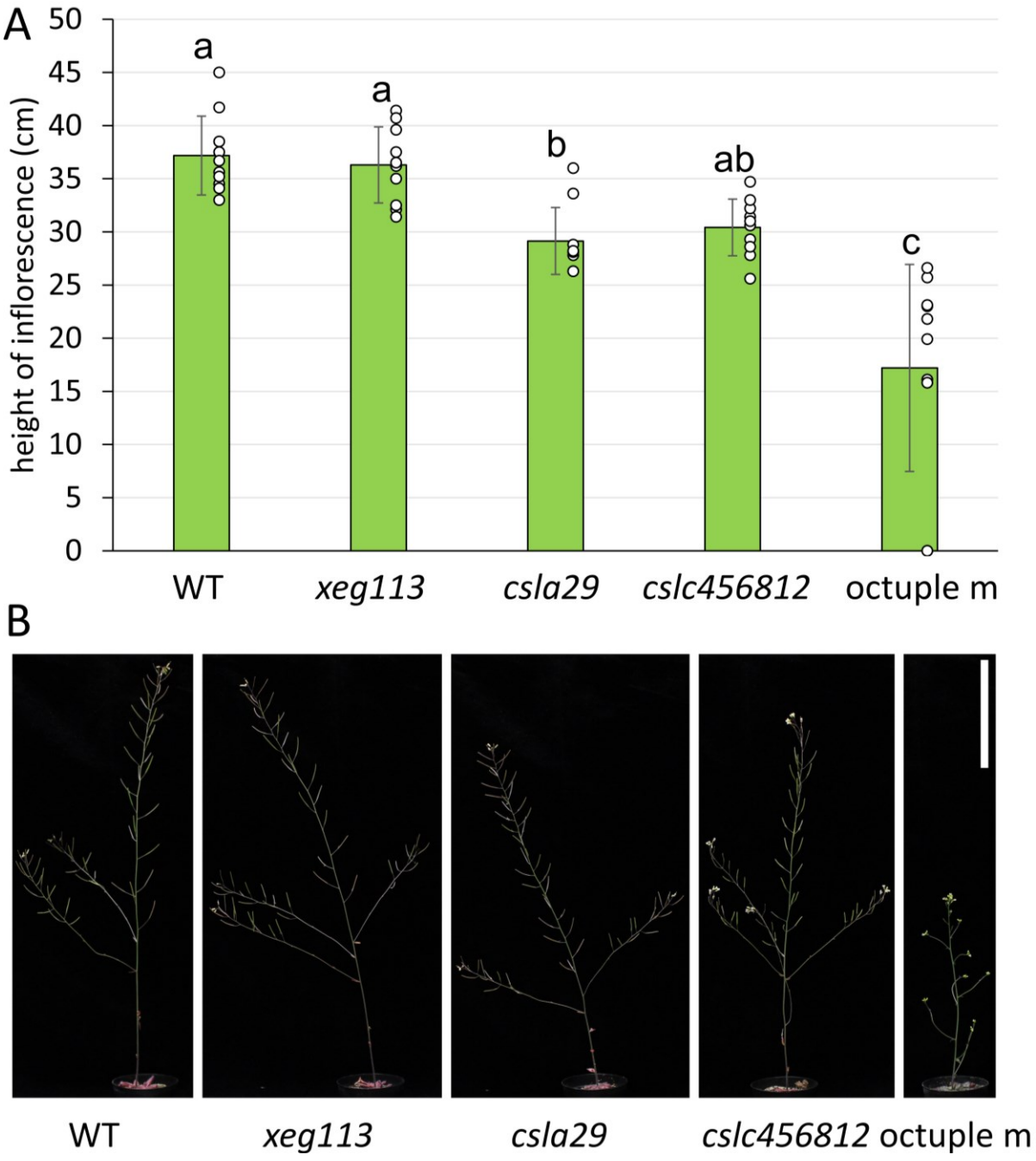

Figure 3.57: Phenotyping of octuple mutants and controls. A) Length of inflorescence after 6 weeks (n = 10 for all lines), results of ANOVA analysis and subsequent Tukey's test are indicated ($P < 0{,}05$); error bars indicate standard deviation; **B)** Representative pictures from the genotypes shown in A), six-week-old plants, scale bar: 10 cm

Analyses of the monosaccharide composition of the matrix polymers released by weak acid hydrolysis (Ch. 2.12.11) of 5-day-old etiolated seedlings and of leaf material of 4-week-old

plants was performed (absolute Fig. 3.58 and relative SFig. 6.46). XyG is represented by glucose, xylose, galactose and fucose (Pauly and Keegstra, 2016), while glucomannan is represented by glucose, mannose and galactose (Yu et al., 2022). EXT arabinosylation is represented by the presence of arabinose (Gille et al., 2009). In etiolated wildtype Arabidopsis hypocotyls the major sugars are galactose and galacturonic acid. Other sugars are present in considerably smaller quantities. A comparison of the different Arabidopsis lines shows significantly less fucose and xylose in *cslc456812* and in the octuple mutant, less mannose and glucuronic acid in *csla29* and the octuple mutant compared to the WT, which is consistent with some of the monosaccharides present in XyG and glucomannan, respectively. In leaf material glucose (in three out of five lines) and galacturonic acid are the major sugars whereby fucose and glucuronic acid form the minor components. *cslc456812* and the octuple mutant have significantly less fucose, which is probably due to the loss of fucosylated XyG sidechains, and more arabinose than WT. *csla29* and the octuple mutant have significantly less glucose and mannose then the wildtype, which is consistent with the building blocks of the backbone of glucomannan (Yu et al., 2022). The double mutant *csla29* shows significantly more galactose and glucuronic acid compared to the WT. *xeg113* is similar to WT Arabidopsis for all monosaccharides in both analyses.

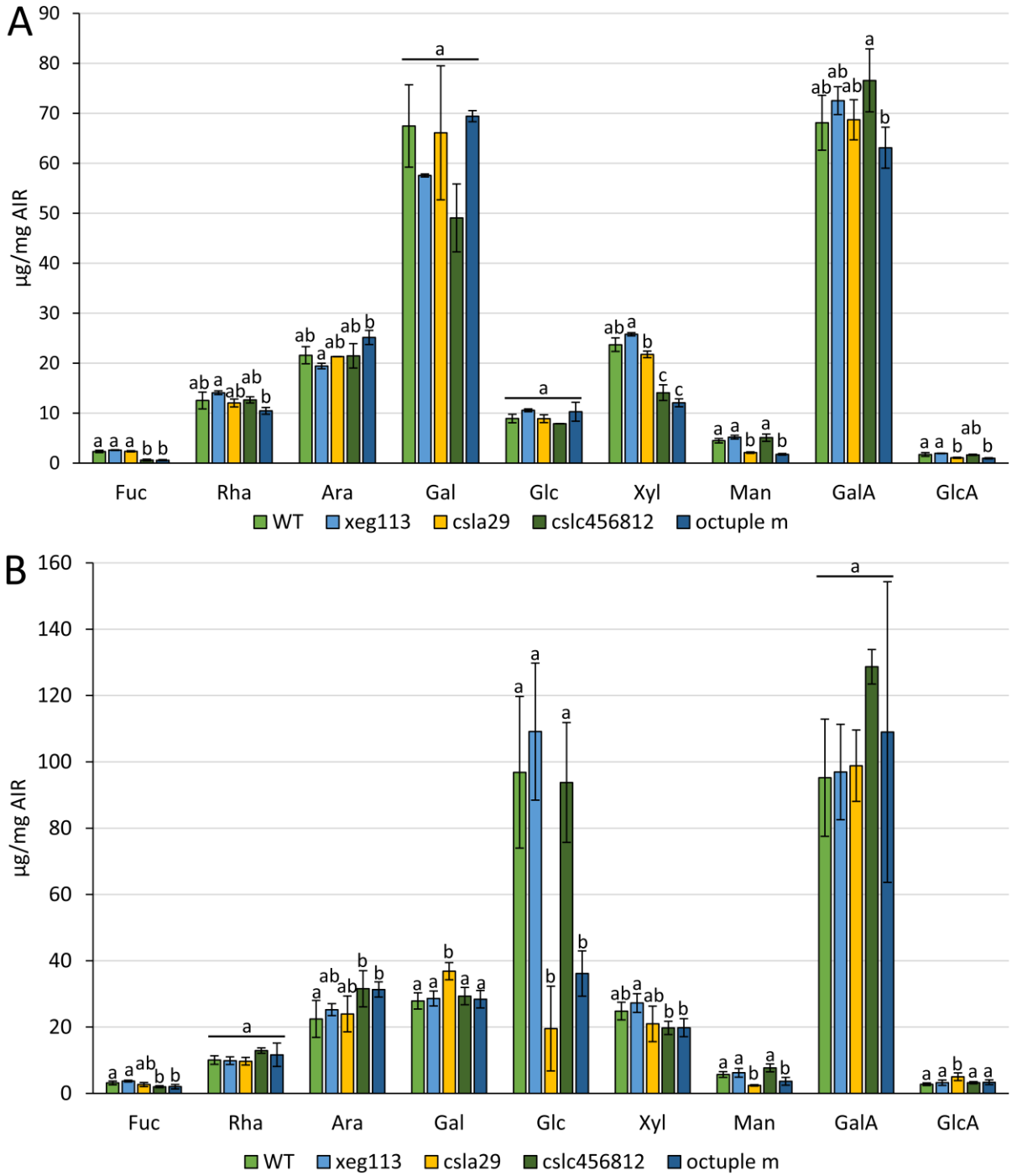

Figure 3.58: Monosaccharide composition of Arabidopsis etiolated hypocotyls and leaf material of octuple mutant and controls (absolute). A) Monosaccharide composition of total AIR (µg/mg) of 5 days-old etiolated seedlings, results of ANOVA analysis and subsequent Tukey's test are indicated ($P < 0,05$); error bars indicate standard deviation; WT n = 4, *xeg113* n=2, *csla29* n =3, *cslc456812* n= 3, octuple mutant n = 3; **B)** Monosaccharide composition of total AIR (µg/mg) of 4 weeks old leaf material, results of ANOVA analysis and subsequent Tukey's test are indicated ($P < 0,05$), WT n = 6, *xeg113* n=6, *csla29* n =3, *cslc456812* n= 5, octuple mutant n = 5; Fuc = fucose, Rha = rhamnose, Ara = arabinose, Gal = galactose, Glc = glucose, Xyl = xylose, Man = mannose, GalAc = galacturonic acid, GlcA = glucuronic acid

3.5.3 Discussion

Even though XyG is the most abundant hemicellulose in dicot plants (Scheller and Ulvskov, 2010), XyG loss leads only to subtle or tissue specific phenotypes (Cavalier et al., 2008; Park and Cosgrove, 2012b; Kim et al., 2020). XyG deficient plants (here *cslc456812*) have longer dark grown hypocotyls compared to the Arabidopsis wildtype (Fig. 3.55) with elongated almost rectangular cells in an organised cell structure (Fig. 3.56). For Bou Daher et al. *cslc456812* mutant hypocotyls displayed slightly reduced elongation over time. Other XyG deficient lines (*xxt12* and *xxt125*) also had a reduced final length (Sowinski et al., 2022; Yu et al., 2022). The XyG deficient hypocotyls here show an opposite trend as they are longer than the wildtype hypocotyls. This discrepancy might be due to differences in growth media (here 2% sucrose, 1% sucrose in Sowinski et al., Yu et al., and Bou Daher et al., without sucrose in Sowinski et al.). The overall appearance (Fig. 3.55 B) of the etiolated hypocotyls of wildtype Arabidopsis and *cslc456812* are very similar. The curvature at the base of the hypocotyls for XyG deficient lines has been observed before (Xiao et al., 2016; Sowinski et al., 2022). The cell length in etiolated hypocotyls appeared wildtype-like here (Fig. 3.56) but showed a reduction of cell length in an *xxt12* (Xiao et al., 2016). This might be due to imaging quality or magnification settings of the microscope here. Epidermal cells in *cslc456812* seem slightly altered compared to the ones of wildtype hypocotyls. Aberrant swelling and bulging of the epidermal cells were also detected in *xxt12* and *xxt125* (Sowinski et al., 2022).

After 6 weeks of growth the *cslc456812* plants here were slightly shorter than the wildtype plants with a straight stem (Fig. 3.57). This does not mirror previous results concerning XyG deficient *cslc456812* (Kim et al., 2020) and *xxt* mutants (Xiao et al., 2016; Yu et al., 2022) since plants were significantly shorter there and had bent stems. While six-week-old plants were measured here and by Kim et al., Xiao et al. measured five-week-old plants and Yu et al. analysed six- to eight-week-old plants. Since the growth conditions here and used by Xiao et al., Yu et al. and Kim et al. were similar (16-h light/8-h dark cycle, 22 °C) with 1 °C difference in temperature by Yu et al (21 °C) the difference in the growth phenotype was likely not introduced by the general growth conditions. Maybe the individual handling (fertilizer, watering) has introduced the difference.

Monosaccharide analysis of hypocotyl and leaf material revealed reduced Xyl and Fuc in hypocotyls and reduced Fuc and increased Ara in leave material (Fig. 3.58 and SFig. 6.46). The lower Xyl and Fuc are consistent with the previous analysis of *cslc456812* (Kim et al., 2020) and another XyG deficient mutant (*xxt12*) (Cavalier et al., 2008; Zabotina et al., 2012) both performed on 7-day-old etiolated hypocotyls. As Xyl and Fuc are major components of XyG (Pauly and Keegstra, 2016) the decrease in these sugar moieties is reasonable. The increase in Ara has also already been shown in *cslc456812* (Kim et al., 2020) and in an experimental setup growing Arabidopsis wildtype in the presence of XyG hydrolysing XEG

(Gille et al., 2009), and might be caused by an increase in arabinose-rich polymers such as certain types of pectin or arabinoxylans.

Etiolated hypocotyls of glucomannan deficient *cslc29* (Yu et al., 2022) are significantly longer compared to the Arabidopsis wildtype (Fig. 3.55). In *csla2* no significant difference was observed compared to the WT concerning hypocotyl length (Yu et al., 2022). However, completely glucomannan deficient hypocotyls, based on the lack of detected glucomannan oligosaccharides in a mannanase digest of the double mutant (Yu et al., 2022), were not analysed for their length. Cell length seems to be similar as in the wildtype Arabidopsis hypocotyls but the epidermal cells in *csla29* is slightly bulged compared to the WT (Fig. 3.56). Six-week-old *csla29* were shorter than the WT (Fig. 3.57), which is similar to observation of the *csla2* single mutant line (Yu et al., 2022). Glucomannan deficient samples contained less Man and GlcA in hypocotyls and less Man and Glc but more Gal and GluAc in leaf material (Fig. 3.58 and SFig. 6.46). The lower Man and Glc content was to be expected in a mutant lacking two glucomannans and is consistent with previously analysed *csla* mutants (Goubet et al., 2009).

xeg113 displays significantly longer hypocotyls compared to Arabidopsis wildtype (Fig. 3.55), which matches the previously published data for *xeg113* from Gille et al., 2009. While *xeg113* had the same height of the inflorescence stem as wildtype plants at 6 weeks old here (Fig. 3.57), *xeg113* has previously been shown to display earlier inflorescence bolting compared with WT at 7 weeks old (Gille et al., 2009). The monosaccharide analysis (Fig. 3.58 and SFig. 6.46) of *xeg113* resulted in a similar composition as the Arabidopsis wildtype in hypocotyl and leaf material. Gille et al. detected a significant decrease of Ara in hypocotyls in a similar experimental setup. This trend is also detected here, however it is nonsignificant. As XEG113 represents an EXT:arabinosyltransferase (Gille et al., 2009; Velasquez et al., 2011), the decrease of Ara was to be expected.

The crossing of several Arabidopsis t-DNA insertion lines led to the identification of a line combining *cslc456812, xeg113* and *csla29* (Fig. 3.54). The octuple mutant, which lacks hemicelluloses XyG and glucomannan, and has an altered glycoprotein EXT structure is still viable. However, the phenotype and chemotype of etiolated hypocotyls and of the grown plant are quite different from Arabidopsis wildtype and lines only lacking one of the altered cell wall components. The hypocotyls of the octuple mutant have severely shorter hypocotyls (Fig. 3.55). The triple mutant *csla2xxt1xxt2* which lacks β-galactoglucomannan and XyG has shorter hypocotyls than the Arabidopsis WT caused by reduced cell expansion (Yu et al., 2022). This result might indicate a trend towards shorter hypocotyls in lines with more severely changed cell walls that progresses in the octuple mutant. The overall appearance (Fig. 3.55 B) of the etiolated hypocotyls of the octuple mutant are severely shortened and twisted. A similar but

less sever phenotype was observed in *csla2xxt1xxt2* (Yu et al., 2022). The epidermal cells of the octuple mutant are bulging and the diameter of the octuple mutant seems broader than the reference plants (Fig. 3.56). The swelling of epidermal cells like in *csla29*, *cslc456812* and the octuple mutant has previously been observed in plant lines without XyG-specific fucosyl- and galactosyl-transferases FUT1/MUR2 and MUR3, and was supposed to be caused by loss of tensile strength (Peña et al., 2004).

The detached epidermal cells observed in the octuple mutant might be the result from impaired cell adhesion. Given the substantial alterations in cell wall composition, the structural integrity of the wall may be insufficient to withstand the internal turgor pressure. A similar hypothesis was proposed by Daher et al. for the XyG-deficient *csla456812* mutant. However, in mutants lacking only XyG, such as the quintuple mutant, feedback mechanism between cell wall composition and mechanical properties appear to reduce turgor pressure, maintaining a functional balance (Bou Daher et al., 2024). In contrast, the simultaneous disruption of multiple wall components in the octuple mutant may disrupt this balance, creating a mismatch between turgor pressure and wall strength. This imbalance could lead to mechanical failure at the epidermis, manifesting as the observed phenotype.

The growth phenotype of six-week-old octuple mutant plants is severely stunted (Fig. 3.57). If one compares hypocotyls with fully grown plants, it is noticeable how different the severity of the effects on phenotypes is. Growth-derived stress dominates in hypocotyls (Verger et al., 2018). While the stem apex grows relatively slowly, hypocotyls grow fast and primarily in one direction, through anisotropic cell expansion (Gendreau et al., 1997).

As all altered or missing cell wall components in the octuple mutant are suggested to have an impact on cell elongation (Gille et al., 2009; Yu et al., 2022) the changed appearance of the cells in the octuple mutant is of no surprise. Even though the change or absence of one cell wall polysaccharide has minor effects, potentially caused by complementation or redundancy of the different polysaccharides (Gille et al., 2009; Kim et al., 2020), the octuple mutant is not able to keep up a normal cell elongation in plant development. This means that one or two plant cell wall polysaccharides that may functionally compensate for the loss of another cell wall component or have functional redundancy may be missing in the octuple mutant.

The octuple mutant combines some of the above-mentioned decreases and increases of monosaccharides (Fig. 3.58 and SFig. 6.46): It has less Fuc, Xyl, Man and GlcA in hypocotyl material and less Fuc, Glc and Man but higher Ara in leaf material. Lower Xyl and Fuc values can probably be attributed to the XyG deficiency. Lower Man and Glc is linked to loss of glucomannans. The decrease in GlcA in hypocotyls is similar as in the *cslc29* mutant and the increase in Ara in leaf material is similar to the *cslc456812* line.

Yu et al., 2022 hypothesized that the changed cell elongation in galactoglucomannan and XyG deficient plants might be caused by altered cellulose microfibril arrangements. Changes in

cellulose organization and content were also observed in the XyG deficient plants (Xiao et al., 2016; Bou Daher et al., 2024). Based on physical simulations and tensile testing of epidermal cell walls it was hypothesized that cellulose itself may form network that meets the requirements for strength and expandability of the primary cell wall (Zhang et al., 2021b; Cosgrove, 2024). It is therefore highly likely that there is also a change in the cellulose organization in the octuple mutant, but this will need to be assessed in future studies.

Turgor pressure influences the mechanical properties of plant cells (Bou Daher et al., 2024). This must be considered when properties of the wall are analysed since feedback mechanism linking cell wall polysaccharide levels and internal cellular pressure exist (Bou Daher et al., 2024).

XyG, glucomannan, and arabinosylated EXTs display evidence of functional redundancy, as mutants lacking only one polymer show only mild, tissue-specific phenotypes. The normal or only slightly altered cell shapes observed in etiolated hypocotyls suggest that these components can compensate for one another during cell elongation (Fig. 3.56). Similarly, near wildtype growth in mature plants lacking XyG or arabinosylated EXT (Fig. 3.57) support the idea of compensatory mechanisms within the cell wall matrix. This suggests that other cell wall components may compensate for their loss. Examples of other polymers include cellulose, the hemicellulose xylan, and pectic polysaccharides. However, mutant lines with impaired cellulose synthesis exhibit severe growth and developmental defects due to compromised cell wall structure and function. Arabidopsis mutations in the cellulose synthase genes (CesA1 and CesA3) are lethal (Persson et al., 2007). Even partial loss of function in these genes leads to a significant reduction in cellulose production and results in a range of cellulose-deficient phenotypes, including dwarfism and swollen cells (Endler and Persson, 2011; McFarlane et al., 2014). Mutants that disrupt xylan biosynthesis (irregular xylem (irx) *irx7, irx8, irx9, irx10, irx14* and *parvus*) show severe reductions in xylan content, leading to notable phenotypes in cell walls, including deformed or collapsed xylem vessels, reduced wall thickening and stunted growth (Hao and Mohnen, 2014). Hence, cellulose and xylans appear to have little or no functional redundancy as components of the plant cell wall, as mutants lacking them have severe or even lethal phenotypes.

Pectic polysaccharides, which form a group of polysaccharides rich in galacturonic acid, might be responsible for remaining functional redundancies. This hypothesis is based of solid-state NMR studies of the cell walls of Arabidopsis wild type and an XyG lacking mutant since the plant cell wall network (cellulose, pectin and XyG) can continue to function in the absence of XyG (Pérez García et al., 2011).The abundance GalA is increased in both hypocotyl and leaf material of the octuple mutant (Fig. 3.58 and SFig. 6.46). This is consistent with data of XyG deficient plant lines from Sowinsky et al.

The increased Ara indicates an increase in Ara containing wall polymers such as arabinogalactan proteins. Analysis of pectic and hemicellulosic polysaccharides in XyG deficient *xxt* mutants by Sowinski et al., 2022 detected no increase of pectic RG-I and arabinan, but a slight increase in arabinoxylan based on a combination of monosaccharide and linkage analyses. So potentially also xylans could have a functional redundancy with one or more cell wall components missing or altered in the octuple mutant. Transcriptomic data also indicated that a gene encoding arabinogalactan-protein was upregulated in XyG deficient mutants (Sowinski et al., 2022).

In summary, XyG, glucomannan, and arabinosylated EXTs likely exhibit functional redundancy or may be compensated by other wall components such as pectins and arabinoxylans. The severe phenotype of the octuple mutant highlights how disrupting multiple polysaccharides overwhelms compensatory mechanisms, resulting in impaired cell elongation and development.

Future experiments: Analysing only monosaccharide composition of the various mutant lines is not sufficient to describe potential compensation effects of different wall components as different composition can result from structural changes of multiple wall polymers. A precise analysis of the frequency of the individual cell wall components is required. The combination of monosaccharide and linkage analyses (Sowinski et al., 2022) could be a promising approach. In addition, enzymatic digestion followed by mass spectrometry, as demonstrated by Sowinski et al., can be used to analyse the presence and relative abundance of oligosaccharides, including XyG-, xylan-, and pectic polymer derived fragments (Brown et al., 2007; Ralet et al., 2009; Sowinski et al., 2022).

Furthermore, comparative RNA-seq studies specifically of genes involved in polymer biosynthesis, such as Kim et al. 2020, may offer valuable insights into expression differences between the mutant lines. However, this approach has limitations, including potential biases in library preparation and challenges in quantifying lowly expressed transcripts (Hirsch et al., 2015; Rao et al., 2018).

Computational modelling approaches such as coarse-grained molecular dynamics can provide valuable insights into the mechanical roles of plant cell wall components (Zhang et al., 2021b; Zhang et al., 2025). While the current models have advanced our understanding of polysaccharide interactions among cellulose microfibrils, hemicellulose, and pectin, they do not yet fully capture the structural diversity and functional variability of hemicelluloses and pectins (Zhang et al., 2021b; Zhang et al., 2025). Enhancing these models to better reflect the heterogeneity of hemicelluloses could help uncover how different types contribute to cell wall mechanics, and whether functional redundancy or compensatory mechanisms exist among them.

4. Conclusion and Outlook

This work advances the understanding of XyG biosynthesis and its structural diversity in plant cell walls. Novel glycosyltransferases involved in XyG biosynthesis were identified and characterized, including various XyG xylosyltransferases from Hy*menaea courbaril* and blueberry. However, to fully understand XyG biosynthesis and the broader landscape of polysaccharide production in the plant, further research on glycosyltransferases is essential. This includes elucidating the structural features determining their activity and the prediction of acceptor and donor specificity through structural modelling.

Reconstitution of XyG biosynthesis in *Pichia pastoris* demonstrated that a minimal set of dicot-derived enzymes is sufficient to generate a glucan backbone. However, achieving plant-like XyG with appropriate levels of xylosylation in this heterologous system remained challenging. This approach also provided evidence for the evolutionary origins of XyG biosynthesis within the plant lineage. However, the availability of associated components and cultivation conditions may limit the XyG biosynthesis in heterologous hosts and requires further investigation. Overcoming these metabolic constraints could substantially improve the recombinant production of complex plant polysaccharides, unlocking significant potential for diverse biotechnological applications.

To investigate functional redundancy within the cell wall matrix, Arabidopsis lines deficient in the biosynthesis of one or multiple matrix polymers were generated and analysed. Comparison of various mutant lines support the notion that other cell wall polymers can indeed functionally compensate for the absence of XyG, highlighting the dynamic nature of matrix polysaccharides in maintaining cell wall integrity during development. Future research should aim to investigate molecular mechanisms underlying this functional redundancy, including the regulatory networks that control compensatory responses and the physical interactions between matrix components. Mechanical modelling and systems-level transcriptomic analyses may help to clarify how different polysaccharides contribute to wall structure and function.

5. Literature

A. Richmond, T., and R. Somerville, C. (2001). Integrative approaches to determining Csl function. Plant Mol Biol **47** (1/2): 131–143.

Alberts, B., Heald, R., Johnson, A., Morgan, D., Raff, M., Roberts, K., Walter, P., Wilson, J.H., and Hunt, T. (2022). Molecular biology of the cell (New York, NY, London: W. W. Norton & Company).

Ali, O., Cheddadi, I., Landrein, B., and Long, Y. (2023). Revisiting the relationship between turgor pressure and plant cell growth. New Phytologist **238** (1): 62–69.

Alonso, J.M., Stepanova, A.N., Leisse, T.J., Kim, C.J., Chen, H., Shinn, P., Stevenson, D.K., Zimmerman, J., Barajas, P., Cheuk, R., Gadrinab, C., Heller, C., Jeske, A., Koesema, E., Meyers, C.C., Parker, H., Prednis, L., Ansari, Y., Choy, N., Deen, H., Geralt, M., Hazari, N., Hom, E., Karnes, M., Mulholland, C., Ndubaku, R., Schmidt, I., Guzman, P., Aguilar-Henonin, L., Schmid, M., Weigel, D., Carter, D.E., Marchand, T., Risseeuw, E., Brogden, D., Zeko, A., Crosby, W.L., Berry, C.C., and Ecker, J.R. (2003). Genome-wide insertional mutagenesis of Arabidopsis thaliana. Science (New York, N.Y.) **301** (5633): 653–657.

Altschul, S.F., Gish, W., Miller, W., Myers, E.W., and Lipman, D.J. (1990). Basic local alignment search tool. Journal of molecular biology **215** (3): 403–410.

Ashikov, A., Routier, F., Fuhlrott, J., Helmus, Y., Wild, M., Gerardy-Schahn, R., and Bakker, H. (2005). The human solute carrier gene SLC35B4 encodes a bifunctional nucleotide sugar transporter with specificity for UDP-xylose and UDP-N-acetylglucosamine. Journal of Biological Chemistry **280** (29): 27230–27235.

Aspinall, G.O., Molloy, J.A., and Craig, J.W. (1969). Extracellular polysaccharides from suspension-cultured sycamore cells. Canadian journal of biochemistry **47** (11): 1063–1070.

Atmodjo, M.A., Hao, Z., and Mohnen, D. (2013). Evolving views of pectin biosynthesis. Annual review of plant biology **64** (Volume 64, 2013): 747–779.

Babicki, S., Arndt, D., Marcu, A., Liang, Y., Grant, J.R., Maciejewski, A., and Wishart, D.S. (2016). Heatmapper: web-enabled heat mapping for all. Nucleic Acids Res **44** (W1): W147-53.

Bar-Peled, M., and O'Neill, M.A. (2011). Plant nucleotide sugar formation, interconversion, and salvage by sugar recycling. Annual review of plant biology **62** (Volume 62, 2011): 127–155.

Bauer, W.D., Talmadge, K.W., Keegstra, K., and Albersheim, P. (1973). The Structure of Plant Cell Walls: II. The Hemicellulose of the Walls of Suspension-cultured Sycamore Cells. Plant Physiol **51** (1): 174–187.

Bhalekar, M.R., Bargaje, R.V., Upadhaya, P.G., Madgulkar, A.R., and Kshirsagar, S.J. (2016). Formulation of mucoadhesive gastric retentive drug delivery using thiolated xyloglucan. Carbohydrate Polymers **136**: 537–542.

Bou Daher, F., Serra, L., Carter, R., Jönsson, H., Robinson, S., Meyerowitz, E.M., and Gray, W.M. (2024). Xyloglucan deficiency leads to a reduction in turgor pressure and changes in cell wall properties, affecting early seedling establishment. Current biology CB **34** (10): 2094-2106.e6.

Bowman, J.L. (2022). The origin of a land flora. Nat. Plants **8** (12): 1352–1369.

Brennan, M., and Harris, P.J. (2011). Distribution of fucosylated xyloglucans among the walls of different cell types in monocotyledons determined by immunofluorescence microscopy. Molecular Plant **4** (1): 144–156.

Brown, D.M., Goubet, F., Wong, V.W., Goodacre, R., Stephens, E., Dupree, P., and Turner, S.R. (2007). Comparison of five xylan synthesis mutants reveals new insight into the mechanisms of xylan synthesis. The Plant journal for cell and molecular biology **52** (6): 1154–1168.

Brumer, H. (2010). Enzymatic functionalization of cellulosic fibres for textile and other applications Xyloglucan as a molecular anchor (Elsevier).

Buckeridge, M.S. (2010). Seed cell wall storage polysaccharides: models to understand cell wall biosynthesis and degradation. Plant Physiol **154** (3): 1017–1023.

Buckeridge, M.S., Crombie, H.J., Mendes, C.J., Reid, J.S., Gidley, M.J., and Vieira, C.C. (1997). A new family of oligosaccharides from the xyloglucan of Hymenaea courbaril L. (Leguminosae) cotyledons. Carbohydrate Research **303** (2): 233–237.

Buckeridge, M.S., Pessoa dos Santos, H., and Tiné, M.A.S. (2000). Mobilisation of storage cell wall polysaccharides in seeds. Plant Physiology and Biochemistry **38** (1-2): 141–156.

Buckeridge, M.S., Rocha, D.C., Reid, J.S.G., and Dietrich, S.M.C. (1992). Xyloglucan structure and post-germinative metabolism in seeds of Copaifera langsdorfii from savanna and forest populations. Physiologia Plantarum **86** (1): 145–151.

Burton, R.A., and Fincher, G.B. (2014). Plant cell wall engineering: applications in biofuel production and improved human health. Current Opinion in Biotechnology **26**: 79–84.

Caffall, K.H., and Mohnen, D. (2009). The structure, function, and biosynthesis of plant cell wall pectic polysaccharides. Carbohydrate Research **344** (14): 1879–1900.

Camacho, C., Boratyn, G.M., Joukov, V., Vera Alvarez, R., and Madden, T.L. (2023). ElasticBLAST: accelerating sequence search via cloud computing. BMC bioinformatics **24** (1): 117.

Camacho, C., Coulouris, G., Avagyan, V., Ma, N., Papadopoulos, J., Bealer, K., and Madden, T.L. (2009). BLAST+: architecture and applications. BMC bioinformatics **10**: 421.

Carpita, N.C., and Gibeaut, D.M. (1993). Structural models of primary cell walls in flowering plants: consistency of molecular structure with the physical properties of the walls during growth. The Plant journal for cell and molecular biology **3** (1): 1–30.

Castilleux, R., Plancot, B., Vicré, M., Nguema-Ona, E., and Driouich, A. (2021). Extensin, an underestimated key component of cell wall defence? Ann Bot **127** (6): 709–713.

Cavalier, D.M., and Keegstra, K. (2006). Two xyloglucan xylosyltransferases catalyze the addition of multiple xylosyl residues to cellohexaose. Journal of Biological Chemistry **281** (45): 34197–34207.

Cavalier, D.M., Lerouxel, O., Neumetzler, L., Yamauchi, K., Reinecke, A., Freshour, G., Zabotina, O.A., Hahn, M.G., Burgert, I., Pauly, M., Raikhel, N.V., and Keegstra, K. (2008). Disrupting two Arabidopsis thaliana xylosyltransferase genes results in plants deficient in xyloglucan, a major primary cell wall component. Plant Cell **20** (6): 1519–1537.

Chevalier, L., Bernard, S., Ramdani, Y., Lamour, R., Bardor, M., Lerouge, P., Follet-Gueye, M.-L., and Driouich, A. (2010). Subcompartment localization of the side chain xyloglucan-synthesizing enzymes within Golgi stacks of tobacco suspension-cultured cells. The Plant Journal **64** (6): 977–989.

Cho, S.K., Kim, J.E., Park, J.-A., Eom, T.J., and Kim, W.T. (2006). Constitutive expression of abiotic stress-inducible hot pepper CaXTH3, which encodes a xyloglucan endotransglucosylase/hydrolase homolog, improves drought and salt tolerance in transgenic Arabidopsis plants. FEBS Letters **580** (13): 3136–3144.

Choi, J.Y., Seo, Y.S., Kim, S.J., Kim, W.T., and Shin, J.S. (2011). Constitutive expression of CaXTH3, a hot pepper xyloglucan endotransglucosylase/hydrolase, enhanced tolerance to salt and drought stresses without phenotypic defects in tomato plants (Solanum lycopersicum cv. Dotaerang). Plant Cell Reports **30** (5): 867–877.

Chou, Y.-H., Pogorelko, G., Young, Z.T., and Zabotina, O.A. (2015). Protein-protein interactions among xyloglucan-synthesizing enzymes and formation of Golgi-localized multiprotein complexes. Plant & cell physiology **56** (2): 255–267.

Chou, Y.-H., Pogorelko, G., and Zabotina, O.A. (2012). Xyloglucan xylosyltransferases XXT1, XXT2, and XXT5 and the glucan synthase CSLC4 form Golgi-localized multiprotein complexes. Plant Physiol **159** (4): 1355–1366.

Cicéron, F., Rocha, J., Kousar, S., Hansen, S.F., Chazalet, V., Gillon, E., Breton, C., and Lerouxel, O. (2016). Expression, purification and biochemical characterization of AtFUT1, a xyloglucan-specific fucosyltransferase from Arabidopsis thaliana. Biochimie **128-129**: 183–192.

Clough, S.J., and Bent, A.F. (1998). Floral dip: a simplified method for Agrobacterium-mediated transformation of Arabidopsis thaliana. The Plant journal for cell and molecular biology **16** (6): 735–743.

Cocuron, J.-C., Lerouxel, O., Drakakaki, G., Alonso, A.P., Liepman, A.H., Keegstra, K., Raikhel, N., and Wilkerson, C.G. (2007). A gene from the cellulose synthase-like C family encodes a beta-1,4 glucan synthase. Proceedings of the National Academy of Sciences of the United States of America **104** (20): 8550–8555.

Colle, M., Leisner, C.P., Wai, C.M., Ou, S., Bird, K.A., Wang, J., Wisecaver, J.H., Yocca, A.E., Alger, E.I., Tang, H., Xiong, Z., Callow, P., Ben-Zvi, G., Brodt, A., Baruch, K., Swale, T., Shiue, L., Song, G., Childs, K.L., Schilmiller, A., Vorsa, N., Buell, C.R., VanBuren, R., Jiang, N., and Edger, P.P. (2019). Haplotype-phased genome and evolution of phytonutrient pathways of tetraploid blueberry. GigaScience **8** (3).

Cosgrove, D.J. (2005). Growth of the plant cell wall. Nat Rev Mol Cell Biol **6** (11): 850–861.

Cosgrove, D.J. (2018). Diffuse Growth of Plant Cell Walls. Plant Physiol **176** (1): 16–27.

Cosgrove, D.J. (2022a). Building an extensible cell wall. Plant Physiol **189** (3): 1246–1277.

Cosgrove, D.J. (2022b). Plant Cell Growth and Cell Wall Enlargement. Pennsylvania State Univ., University Park, PA (United States) **2** (11).

Cosgrove, D.J. (2024). Structure and growth of plant cell walls. Nat Rev Mol Cell Biol **25** (5): 340–358.

Coutu, C., Brandle, J., Brown, D., Brown, K., Miki, B., Simmonds, J., and Hegedus, D.D. (2007). pORE: a modular binary vector series suited for both monocot and dicot plant transformation. Transgenic Res **16** (6): 771–781.

Criscuolo, A., and Gribaldo, S. (2010). BMGE (Block Mapping and Gathering with Entropy): a new software for selection of phylogenetic informative regions from multiple sequence alignments. BMC Evol Biol **10** (1): 210.

Culbertson, A.T., Chou, Y.-H., Smith, A.L., Young, Z.T., Tietze, A.A., Cottaz, S., Fauré, R., and Zabotina, O.A. (2016). Enzymatic Activity of Xyloglucan Xylosyltransferase 5. Plant Physiol **171** (3): 1893–1904.

Culbertson, A.T., Ehrlich, J.J., Choe, J.-Y., Honzatko, R.B., and Zabotina, O.A. (2018). Structure of xyloglucan xylosyltransferase 1 reveals simple steric rules that define biological patterns of xyloglucan polymers. Proceedings of the National Academy of Sciences of the United States of America **115** (23): 6064–6069.

Curtis, M.D., and Grossniklaus, U. (2003). A gateway cloning vector set for high-throughput functional analysis of genes in planta. Plant Physiol **133** (2): 462–469.

Curtis, M.J., Belcram, K., Bollmann, S.R., Tominey, C.M., Hoffman, P.D., Mercier, R., and Hays, J.B. (2009). Reciprocal chromosome translocation associated with TDNA-insertion mutation in Arabidopsis: genetic and cytological analyses of consequences for gametophyte development and for construction of doubly mutant lines. Planta **229** (4): 731–745.

Dardelle, F., Le Mauff, F., Lehner, A., Loutelier-Bourhis, C., Bardor, M., Rihouey, C., Causse, M., Lerouge, P., Driouich, A., and Mollet, J.-C. (2015). Pollen tube cell walls of wild and domesticated tomatoes contain arabinosylated and fucosylated xyloglucan. Ann Bot **115** (1): 55–66.

Davis, J., Brandizzi, F., Liepman, A.H., and Keegstra, K. (2010). Arabidopsis mannan synthase CSLA9 and glucan synthase CSLC4 have opposite orientations in the Golgi membrane. The Plant Journal **64** (6): 1028–1037.

Davis, M.W., and Jorgensen, E.M. (2022). ApE, A Plasmid Editor: A Freely Available DNA Manipulation and Visualization Program. Front. Bioinform. **2**: 818619.

Del Bem, L.E.V., and Vincentz, M.G.A. (2010). Evolution of xyloglucan-related genes in green plants. BMC Evol Biol **10** (1): 341.

Del-Bem, L.-E. (2018). Xyloglucan evolution and the terrestrialization of green plants. New Phytologist **219** (4): 1150–1153.

Delmer, D., Dixon, R.A., Keegstra, K., and Mohnen, D. (2024). The plant cell wall-dynamic, strong, and adaptable-is a natural shapeshifter. Plant Cell **36** (5): 1257–1311.

Delwiche, C.F., and Cooper, E.D. (2015). The Evolutionary Origin of a Terrestrial Flora. Current biology CB **25** (19): R899-910.

Dereeper, A., Guignon, V., Blanc, G., Audic, S., Buffet, S., Chevenet, F., Dufayard, J.-F., Guindon, S., Lefort, V., Lescot, M., Claverie, J.-M., and Gascuel, O. (2008). Phylogeny.fr: robust phylogenetic analysis for the non-specialist. Nucleic Acids Res **36** (Web Server issue): W465-9.

Desveaux, D., Faik, A., and Maclachlan, G. (1998). Fucosyltransferase and the biosynthesis of storage and structural xyloglucan in developing nasturtium fruits. Plant Physiol **118** (3): 885–894.

Dharmarathna, C.S., Kumar, S., Gunawardena, Yasanthi Illika Nilmini Silva, Dassanayake, R.S., and Hettiarachchi, C. (2023). AOX1 promoter-driven expression of yeast-enhanced green fluorescent protein in Pichia pastoris. The Microbe **1**: 100012.

Doll, N.M., Berenguer, E., Truskina, J., and Ingram, G. (2022). AtEXT3 is not essential for early embryogenesis or plant viability in Arabidopsis. New Phytologist **236** (5): 1629–1633.

Domozych, D.S., Sørensen, I., Pettolino, F.A., Bacic, A., and Willats, W.G.T. (2010). The Cell Wall Polymers of the Charophycean Green Alga Chara corallina Immunobinding and Biochemical Screening. International Journal of Plant Sciences **171** (4): 345–361.

Domozych, D.S., Sørensen, I., and Willats, W.G.T. (2009). The distribution of cell wall polymers during antheridium development and spermatogenesis in the Charophycean green alga, Chara corallina. Ann Bot **104** (6): 1045–1056.

Dutta, P., Giri, S., and Giri, T.K. (2020). Xyloglucan as green renewable biopolymer used in drug delivery and tissue engineering. International Journal of Biological Macromolecules **160**: 55–68.

Ebert, B., Rautengarten, C., Guo, X., Xiong, G., Stonebloom, S., Smith-Moritz, A.M., Herter, T., Chan, L.J.G., Adams, P.D., Petzold, C.J., Pauly, M., Willats, W.G.T., Heazlewood, J.L., and Scheller, H.V. (2015). Identification and Characterization of a Golgi-Localized UDP-Xylose Transporter Family from Arabidopsis. Plant Cell **27** (4): 1218–1227.

Emonet, A., and Hay, A. (2022). Development and diversity of lignin patterns. Plant Physiol **190** (1): 31–43.

Endler, A., and Persson, S. (2011). Cellulose synthases and synthesis in Arabidopsis. Molecular Plant **4** (2): 199–211.

Ezquer, I., Salameh, I., Colombo, L., and Kalaitzis, P. (2020). Plant Cell Walls Tackling Climate Change: Insights into Plant Cell Wall Remodeling, Its Regulation, and Biotechnological Strategies to Improve Crop Adaptations and Photosynthesis in Response to Global Warming. Plants (Basel, Switzerland) **9** (2): 1–27.

Faik, A., Bar-Peled, M., DeRocher, A.E., Zeng, W., Perrin, R.M., Wilkerson, C., Raikhel, N.V., and Keegstra, K. (2000). Biochemical characterization and molecular cloning of an alpha-1,2-fucosyltransferase that catalyzes the last step of cell wall xyloglucan biosynthesis in pea. Journal of Biological Chemistry **275** (20): 15082–15089.

Faik, A., Price, N.J., Raikhel, N.V., and Keegstra, K. (2002). An Arabidopsis gene encoding an alpha-xylosyltransferase involved in xyloglucan biosynthesis. Proceedings of the National Academy of Sciences of the United States of America **99** (11): 7797–7802.

Fry, S.C. (1989). Cellulases, hemicelluloses and auxin-stimulated growth: a possible relationship. Physiologia Plantarum **75** (4): 532–536.

Fry, S.C., York, W.S., Albersheim, P., Darvill, A., Hayashi, T., Joseleau, J.-P., Kato, Y., Lorences, E.P., Maclachlan, G.A., McNeil, M., Mort, A.J., Grant Reid, J.S., Seitz, H.U., Selvendran, R.R., Voragen, A.G.J., and White, A.R. (1993). An unambiguous nomenclature for xyloglucan-derived oligosaccharides. Physiologia Plantarum **89** (1): 1–3.

Gendreau, E., Traas, J., Desnos, T., Grandjean, O., Caboche, M., and Hofte, H. (1997). Cellular Basis of Hypocotyl Growth in Arabidopsis thaliana. Plant Physiol **114** (1): 295–305.

Gibeaut, D.M., Pauly, M., Bacic, A., and Fincher, G.B. (2005). Changes in cell wall polysaccharides in developing barley (Hordeum vulgare) coleoptiles. Planta **221** (5): 729–738.

Gille, S., Cheng, K., Skinner, M.E., Liepman, A.H., Wilkerson, C.G., and Pauly, M. (2011a). Deep sequencing of voodoo lily (Amorphophallus konjac): an approach to identify relevant

genes involved in the synthesis of the hemicellulose glucomannan. Planta **234** (3): 515–526.

Gille, S., Hänsel, U., Ziemann, M., and Pauly, M. (2009). Identification of plant cell wall mutants by means of a forward chemical genetic approach using hydrolases. Proceedings of the National Academy of Sciences of the United States of America **106** (34): 14699–14704.

Gille, S., and Pauly, M. (2012). O-acetylation of plant cell wall polysaccharides. Frontiers in plant science **3**: 12.

Gille, S., Souza, A., Xiong, G., Benz, M., Cheng, K., Schultink, A., Reca, I.-B., and Pauly, M. (2011b). O-acetylation of Arabidopsis hemicellulose xyloglucan requires AXY4 or AXY4L, proteins with a TBL and DUF231 domain. Plant Cell **23** (11): 4041–4053.

Goddard, T.D., Huang, C.C., Meng, E.C., Pettersen, E.F., Couch, G.S., Morris, J.H., and Ferrin, T.E. (2018). UCSF ChimeraX: Meeting modern challenges in visualization and analysis. Protein Science **27** (1): 14–25.

Goubet, F., Barton, C.J., Mortimer, J.C., Yu, X., Zhang, Z., Miles, G.P., Richens, J., Liepman, A.H., Seffen, K., and Dupree, P. (2009). Cell wall glucomannan in Arabidopsis is synthesised by CSLA glycosyltransferases, and influences the progression of embryogenesis. The Plant Journal **60** (3): 527–538.

Grandis, A., Santos, H.P., Tonini, P.P., Salles, I.S., Peres, A.S.C., Carpita, N.C., and Buckeridge, M.S. (2024). Role of cell wall polysaccharides in water distribution during seed imbibition of Hymenaea courbaril L. Plant Biology.

Grieß-Osowski, A., and Voiniciuc, C. (2023). Branched mannan and xyloglucan as a dynamic duo in plant cell walls. Cell surface (Amsterdam, Netherlands) **9**: 100098.

Guindon, S., Dufayard, J.-F., Lefort, V., Anisimova, M., Hordijk, W., and Gascuel, O. (2010). New algorithms and methods to estimate maximum-likelihood phylogenies: assessing the performance of PhyML 3.0. Syst Biol **59** (3): 307–321.

Günl, M., Gille, S., and Pauly, M. (2010). OLIgo mass profiling (OLIMP) of extracellular polysaccharides. Journal of visualized experiments JoVE (40).

Günl, M., Neumetzler, L., Kraemer, F., Souza, A. de, Schultink, A., Pena, M., York, W.S., and Pauly, M. (2011). AXY8 encodes an α-fucosidase, underscoring the importance of apoplastic metabolism on the fine structure of Arabidopsis cell wall polysaccharides. Plant Cell **23** (11): 4025–4040.

Günl, M., and Pauly, M. (2011). AXY3 encodes a α-xylosidase that impacts the structure and accessibility of the hemicellulose xyloglucan in Arabidopsis plant cell walls. Planta **233** (4): 707–719.

Hallgren, J., Tsirigos, K.D., Pedersen, M.D., Almagro Armenteros, J.J., Marcatili, P., Nielsen, H., Krogh, A., and Winther, O. (2022). DeepTMHMM predicts alpha and beta transmembrane proteins using deep neural networks. bioRxiv: 2022.04.08.487609.

Han, W., Fan, X., Teng, L., Kaczurowski, M.J.S., Zhang, X., Xu, D., Yin, Y., and Ye, N. (2019). Identification, classification, and evolution of putative xylosyltransferases from algae. Protoplasma **256** (4): 1119–1132.

Han, Y., Wang, W., Sun, J., Ding, M., Zhao, R., Deng, S., Wang, F., Hu, Y., Wang, Y., Lu, Y., Du, L., Hu, Z., Diekmann, H., Shen, X., Polle, A., and Chen, S. (2013). Populus euphratica XTH overexpression enhances salinity tolerance by the development of leaf succulence in transgenic tobacco plants. J Exp Bot **64** (14): 4225–4238.

Hao, Z., and Mohnen, D. (2014). A review of xylan and lignin biosynthesis: foundation for studying Arabidopsis irregular xylem mutants with pleiotropic phenotypes. Critical reviews in biochemistry and molecular biology **49** (3): 212–241.

Harper, A.D., and Bar-Peled, M. (2002). Biosynthesis of UDP-xylose. Cloning and characterization of a novel Arabidopsis gene family, UXS, encoding soluble and putative membrane-bound UDP-glucuronic acid decarboxylase isoforms. Plant Physiol **130** (4): 2188–2198.

Hayashi, T. (1989). Xyloglucans in the Primary Cell Wall. Annu. Rev. Plant. Physiol. Plant. Mol. Biol. **40** (1): 139–168.

Hazen, S.P., Scott-Craig, J.S., and Walton, J.D. (2002). Cellulose synthase-like genes of rice. Plant Physiol **128** (2): 336–340.

Hilz, H., Jong, L.E., Kabel, M.A., Verhoef, R., Schols, H.A., and Voragen, A.G.J. (2007). Bilberry xyloglucan--novel building blocks containing beta-xylose within a complex structure. Carbohydrate Research **342** (2): 170–181.

Hiraoka, S., Furuichi, T., Nishimura, G., Shibata, S., Yanagishita, M., Rimoin, D.L., Superti-Furga, A., Nikkels, P.G., Ogawa, M., Katsuyama, K., Toyoda, H., Kinoshita-Toyoda, A., Ishida, N., Isono, K., Sanai, Y., Cohn, D.H., Koseki, H., and Ikegawa, S. (2007). Nucleotide-sugar transporter SLC35D1 is critical to chondroitin sulfate synthesis in cartilage and skeletal development in mouse and human. Nat Med **13** (11): 1363–1367.

Hirsch, C.D., Springer, N.M., and Hirsch, C.N. (2015). Genomic limitations to RNA sequencing expression profiling. The Plant Journal **84** (3): 491–503.

Hoffman, M., Jia, Z., Peña, M.J., Cash, M., Harper, A., Blackburn, A.R., Darvill, A., and York, W.S. (2005). Structural analysis of xyloglucans in the primary cell walls of plants in the subclass Asteridae. Carbohydrate Research **340** (11): 1826–1840.

Hoffmann, N., King, S., Samuels, A.L., and McFarlane, H.E. (2021). Subcellular coordination of plant cell wall synthesis. Developmental Cell **56** (7): 933–948.

Hoffmann, N., and McFarlane, H.E. (2024). Xyloglucan side chains enable polysaccharide secretion to the plant cell wall. Developmental Cell.

Hooke, R., Allestry, J., and Martyn, J. (1665). Micrographia, or, Some physiological descriptions of minute bodies made by magnifying glasses :with observations and inquiries thereupon (London: Printed by Jo. Martyn and Ja. Allestry, printers to the Royal Society).

Hotchkiss, A., A. Nuñez, G. Strahan, H. Chau, Andre K. White, J. Marais, K. Hom, M. S. Vakkalanka, R. Di, K. Yam, and C. Khoo (2015). Cranberry Xyloglucan Structure and Inhibition of Escherichia coli Adhesion to Epithelial Cells. Journal of Agricultural and Food Chemistry.

Hoth, A., Blaschek, W., and Franz, G. (1986). Xyloglucan (amyloid) formation in the cotyledons of Tropaeolum majus L. seeds. Plant Cell Reports **5** (1): 9–12.

Houston, K., Tucker, M.R., Chowdhury, J., Shirley, N., and Little, A. (2016). The Plant Cell Wall: A Complex and Dynamic Structure As Revealed by the Responses of Genes under Stress Conditions. Frontiers in plant science **7**: 984.

Hrmova, M., Stratilová, B., and Stratilová, E. (2022). Broad Specific Xyloglucan:Xyloglucosyl Transferases Are Formidable Players in the Re-Modelling of Plant Cell Wall Structures. International Journal of Molecular Sciences **23** (3).

Hsieh, Y.S.Y., and Harris, P.J. (2009). Xyloglucans of monocotyledons have diverse structures. Molecular Plant **2** (5): 943–965.

Hsieh, Y.S.Y., and Harris, P.J. (2012). Structures of xyloglucans in primary cell walls of gymnosperms, monilophytes (ferns sensu lato) and lycophytes. Phytochemistry **79**: 87–101.

Hsiung, S.-Y., Li, J., Imre, B., Kao, M.-R., Liao, H.-C., Wang, D., Chen, C.-H., Liang, P.-H., Harris, P.J., and Hsieh, Y.S.Y. (2023). Structures of the xyloglucans in the monocotyledon family Araceae (aroids). Planta **257** (2): 39.

Huala, E., Dickerman, A.W., Garcia-Hernandez, M., Weems, D., Reiser, L., LaFond, F., Hanley, D., Kiphart, D., Zhuang, M., Huang, W., Mueller, L.A., Bhattacharyya, D., Bhaya, D., Sobral, B.W., Beavis, W., Meinke, D.W., Town, C.D., Somerville, C., and Rhee, S.Y. (2001). The Arabidopsis Information Resource (TAIR): a comprehensive database and web-based information retrieval, analysis, and visualization system for a model plant. Nucleic Acids Res **29** (1): 102–105.

Ikegaya, H., Hayashi, T., Kaku, T., Iwata, K., Sonobe, S., and Shimmen, T. (2008). Presence of xyloglucan-like polysaccharide in Spirogyra and possible involvement in cell–cell attachment. Phycological Research **56** (3): 216–222.

Imai, T., and Ohno, T. (1995). Measurement of yeast intracellular pH by image processing and the change it undergoes during growth phase. Journal of biotechnology **38** (2): 165–172.

Immelmann, R., Gawenda, N., Ramírez, V., and Pauly, M. (2023). Identification of a xyloglucan beta-xylopyranosyltransferase from Vaccinium corymbosum. Plant Direct **7** (7): e514.

Ishida, K., Ohba, Y., Yoshimi, Y., Wilson, L.F.L., Echevarría-Poza, A., Yu, L., Iwai, H., and Dupree, P. (2023). Differing structures of galactoglucomannan in eudicots and non-eudicot angiosperms. PLOS ONE **18** (12): e0289581.

Ishida, K., and Yokoyama, R. (2022). Reconsidering the function of the xyloglucan endotransglucosylase/hydrolase family. J Plant Res **135** (2): 145–156.

Ishizaki, K., Nishihama, R., Ueda, M., Inoue, K., Ishida, S., Nishimura, Y., Shikanai, T., and Kohchi, T. (2015). Development of Gateway Binary Vector Series with Four Different Selection Markers for the Liverwort Marchantia polymorpha. PLOS ONE **10** (9): e0138876.

Jansson, C., Wullschleger, S.D., Kalluri, U.C., and Tuskan, G.A. (2010). Phytosequestration: Carbon Biosequestration by Plants and the Prospects of Genetic Engineering. BioScience **60** (9): 685–696.

Jarvis, M.C. (2023). Forces on and in the cell walls of living plants. Plant Physiol **194** (1): 8–14.

Jensen, J.K., Schultink, A., Keegstra, K., Wilkerson, C.G., and Pauly, M. (2012). RNA-Seq analysis of developing nasturtium seeds (Tropaeolum majus): identification and characterization of an additional galactosyltransferase involved in xyloglucan biosynthesis. Molecular Plant **5** (5): 984–992.

Jia, Z., Cash, M., Darvill, A.G., and York, W.S. (2005). NMR characterization of endogenously O-acetylated oligosaccharides isolated from tomato (Lycopersicon esculentum) xyloglucan. Carbohydrate Research **340** (11): 1818–1825.

Jia, Z., Qin, Q., Darvill, A.G., and York, W.S. (2003). Structure of the xyloglucan produced by suspension-cultured tomato cells. Carbohydrate Research **338** (11): 1197–1208.

Johnson, K.L., Gidley, M.J., Bacic, A., and Doblin, M.S. (2018). Cell wall biomechanics: a tractable challenge in manipulating plant cell walls 'fit for purpose'! Current Opinion in Biotechnology **49**: 163–171.

Joseph, J.A., Akkermans, S., and van Impe, J.F.M. (2022). Effects of Temperature and pH on Recombinant Thaumatin II Production by Pichia pastoris. Foods (Basel, Switzerland) **11** (10).

Julian, J.D., and Zabotina, O.A. (2022). Xyloglucan Biosynthesis: From Genes to Proteins and Their Functions. Frontiers in plant science **13**: 920494.

Karimi, M., Inzé, D., and Depicker, A. (2002). GATEWAY vectors for Agrobacterium-mediated plant transformation. Trends in Plant Science **7** (5): 193–195.

Katoh, K., and Standley, D.M. (2013). MAFFT multiple sequence alignment software version 7: improvements in performance and usability. Mol Biol Evol **30** (4): 772–780.

Keegstra, K. (2010). Plant cell walls. Plant Physiol **154** (2): 483–486.

Kiefer, L.L., York, W.S., Darvill, A.G., and Albersheim, P. (1989). Xyloglucan isolated from suspension-cultured sycamore cell walls is O-acetylated. Phytochemistry **28** (8): 2105–2107.

Kim, S.-J., Chandrasekar, B., Rea, A.C., Danhof, L., Zemelis-Durfee, S., Thrower, N., Shepard, Z.S., Pauly, M., Brandizzi, F., and Keegstra, K. (2020). The synthesis of xyloglucan, an abundant plant cell wall polysaccharide, requires CSLC function. Proceedings of the National Academy of Sciences of the United States of America **117** (33): 20316–20324.

Knox, J.P., and Benitez-Alfonso, Y. (2014). Roles and regulation of plant cell walls surrounding plasmodesmata. Current Opinion in Plant Biology **22**: 93–100.

Kobayashi, T., Sleeman, J.E., Coughtrie, M.W.H., and Burchell, B. (2006). Molecular and functional characterization of microsomal UDP-glucuronic acid uptake by members of the nucleotide sugar transporter (NST) family. The Biochemical journal **400** (2): 281–289.

Kochumalayil, J.J., and Berglund, L.A. (2014). Water-soluble hemicelluloses for high humidity applications – enzymatic modification of xyloglucan for mechanical and oxygen barrier properties. Green Chem **16** (4): 1904–1910.

Koncz, C., and Schell, J. (1986). The promoter of TL-DNA gene 5 controls the tissue-specific expression of chimaeric genes carried by a novel type of Agrobacterium binary vector. Molec Gen Genet **204** (3): 383–396.

Kong, Y., Peña, M.J., Renna, L., Avci, U., Pattathil, S., Tuomivaara, S.T., Li, X., Reiter, W.-D., Brandizzi, F., Hahn, M.G., Darvill, A.G., York, W.S., and O'Neill, M.A. (2015). Galactose-depleted xyloglucan is dysfunctional and leads to dwarfism in Arabidopsis. Plant Physiol **167** (4): 1296–1306.

Kooiman, P. (1957). Amyloids of Plant Seeds. Nature **179** (4550): 107–109.

Kooiman, P. (1960). On the Occurrence of Amyloids in Plant Seeds. Acta botanica neerlandica **9** (2): 208–219.

Kooiman, P. (1961). The constitution of Tamarindus -amyloid. Recl. Trav. Chim. Pays-Bas **80** (8): 849–865.

Koressaar, T., and Remm, M. (2007). Enhancements and modifications of primer design program Primer3. Bioinformatics (Oxford, England) **23** (10): 1289–1291.

Kõressaar, T., Lepamets, M., Kaplinski, L., Raime, K., Andreson, R., and Remm, M. (2018). Primer3_masker: integrating masking of template sequence with primer design software. Bioinformatics (Oxford, England) **34** (11): 1937–1938.

Koshani, R., Pitcher, M.L., Yu, J., Mahajan, C.L., Kim, S.H., and Sheikhi, A. (2025). Plant Cell Wall-Like Soft Materials: Micro- and Nanoengineering, Properties, and Applications. Nano-Micro Lett. **17** (1): 103.

Kozieł, E., Otulak-Kozieł, K., and Bujarski, J.J. (2021). Plant Cell Wall as a Key Player During Resistant and Susceptible Plant-Virus Interactions. Frontiers in microbiology **12**: 656809.

Krebs, S.L., and Hancock, J.F. (1989). Tetrasomic inheritance of isoenzyme markers in the highbush blueberry, Vaccinium corymbosum L. Heredity **63** (1): 11–18.

Kuang, B., Zhao, X., Zhou, C., Zeng, W., Ren, J., Ebert, B., Beahan, C.T., Deng, X., Zeng, Q., Zhou, G., Doblin, M.S., Heazlewood, J.L., Bacic, A., Chen, X., and Wu, A.-M. (2016). Role of UDP-Glucuronic Acid Decarboxylase in Xylan Biosynthesis in Arabidopsis. Molecular Plant **9** (8): 1119–1131.

Kulkarni, A.D., Joshi, A.A., Patil, C.L., Amale, P.D., Patel, H.M., Surana, S.J., Belgamwar, V.S., Chaudhari, K.S., and Pardeshi, C.V. (2017). Xyloglucan: A functional biomacromolecule for drug delivery applications. International Journal of Biological Macromolecules **104** (Pt A): 799–812.

Lacerda, A.E.B., Kanashiro, M., and Sebbenn, A.M. (2008). Effects of Reduced Impact Logging on genetic diversity and spatial genetic structure of a Hymenaea courbaril population in the Brazilian Amazon Forest. Forest Ecology and Management **255** (3-4): 1034–1043.

Lampugnani, E.R., Moller, I.E., Cassin, A., Jones, D.F., Koh, P.L., Ratnayake, S., Beahan, C.T., Wilson, S.M., Bacic, A., and Newbigin, E. (2013). In vitro grown pollen tubes of Nicotiana alata actively synthesise a fucosylated xyloglucan. PLOS ONE **8** (10): e77140.

Landy, A. (1989). Dynamic, structural, and regulatory aspects of lambda site-specific recombination. Annual review of biochemistry **58**: 913–949.

Lang, M., and Orgogozo, V. (2011). Identification of homologous gene sequences by PCR with degenerate primers. Molecular Methods for Evolutionary Genetics **772**: 245–256.

Lemoine, F., Correia, D., Lefort, V., Doppelt-Azeroual, O., Mareuil, F., Cohen-Boulakia, S., and Gascuel, O. (2019). NGPhylogeny.fr: new generation phylogenetic services for non-specialists. Nucleic Acids Res **47** (W1): W260-W265.

Lerouxel, O., Choo, T.S., Séveno, M., Usadel, B., Faye, L., Lerouge, P., and Pauly, M. (2002). Rapid structural phenotyping of plant cell wall mutants by enzymatic oligosaccharide fingerprinting. Plant Physiol **130** (4): 1754–1763.

Li, Q., Zhao, Q., Yao, X., Zhang, B., and Lu, L. (2022). Genome-Wide Characterization of the Cellulose Synthase Gene Superfamily in Tea Plants (Camellia sinensis). Phyton **91** (10): 2163–2189.

Li, W., Lin, Y.-C.J., Chen, Y.-L., Zhou, C., Li, S., Ridder, N. de, Oliveira, D.M., Zhang, L., Zhang, B., Wang, J.P., Xu, C., Fu, X., Luo, K., Wu, A.-M., Demura, T., Lu, M.-Z., Zhou, Y., Li, L., Umezawa, T., Boerjan, W., and Chiang, V.L. (2024). Woody plant cell walls: Fundamentals and utilization. Molecular Plant **17** (1): 112–140.

Liepman, A.H., Nairn, C.J., Willats, W.G.T., Sørensen, I., Roberts, A.W., and Keegstra, K. (2007). Functional genomic analysis supports conservation of function among cellulose synthase-like a gene family members and suggests diverse roles of mannans in plants. Plant Physiol **143** (4): 1881–1893.

Liepman, A.H., Wilkerson, C.G., and Keegstra, K. (2005). Expression of cellulose synthase-like (Csl) genes in insect cells reveals that CslA family members encode mannan synthases. Proceedings of the National Academy of Sciences of the United States of America **102** (6): 2221–2226.

Liu, L., Hsia, M.M., Dama, M., Vogel, J., and Pauly, M. (2016). A Xyloglucan Backbone 6-O-Acetyltransferase from Brachypodium distachyon Modulates Xyloglucan Xylosylation. Molecular Plant **9** (4): 615–617.

Liu, L., Paulitz, J., and Pauly, M. (2015). The presence of fucogalactoxyloglucan and its synthesis in rice indicates conserved functional importance in plants. Plant Physiol **168** (2): 549–560.

Lopes, F.J.F., Pauly, M., Brommonshenkel, S.H., Lau, E.Y., Diola, V., Passos, J.L., and Loureiro, M.E. (2010). The EgMUR3 xyloglucan galactosyltransferase from Eucalyptus grandis complements the mur3 cell wall phenotype in Arabidopsis thaliana. Tree Genetics & Genomes **6** (5): 745–756.

Loqué, D., Scheller, H.V., and Pauly, M. (2015). Engineering of plant cell walls for enhanced biofuel production. Current Opinion in Plant Biology **25**: 151–161.

Lund, C.H., Bromley, J.R., Stenbæk, A., Rasmussen, R.E., Scheller, H.V., and Sakuragi, Y. (2015). A reversible Renilla luciferase protein complementation assay for rapid identification of protein-protein interactions reveals the existence of an interaction network involved in xyloglucan biosynthesis in the plant Golgi apparatus. J Exp Bot **66** (1): 85–97.

MacAlister, C.A., Ortiz-Ramírez, C., Becker, J.D., Feijó, J.A., and Lippman, Z.B. (2016). Hydroxyproline O-arabinosyltransferase mutants oppositely alter tip growth in Arabidopsis thaliana and Physcomitrella patens. The Plant Journal **85** (2): 193–208.

Madeira, F., Pearce, M., Tivey, A.R.N., Basutkar, P., Lee, J., Edbali, O., Madhusoodanan, N., Kolesnikov, A., and Lopez, R. (2022). Search and sequence analysis tools services from EMBL-EBI in 2022. Nucleic Acids Res **50** (W1): W276-W279.

Madson, M., Dunand, C., Li, X., Verma, R., Vanzin, G.F., Caplan, J., Shoue, D.A., Carpita, N.C., and Reiter, W.-D. (2003). The MUR3 gene of Arabidopsis encodes a xyloglucan galactosyltransferase that is evolutionarily related to animal exostosins. Plant Cell **15** (7): 1662–1670.

Mansoori, N., Schultink, A., Schubert, J., and Pauly, M. (2015). Expression of heterologous xyloglucan xylosyltransferases in Arabidopsis to investigate their role in determining xyloglucan xylosylation substitution patterns. Planta **241** (5): 1145–1158.

Marry, M., Cavalier, D.M., Schnurr, J.K., Netland, J., Yang, Z., Pezeshk, V., York, W.S., Pauly, M., and White, A.R. (2003). Structural characterization of chemically and enzymatically derived standard oligosaccharides isolated from partially purified tamarind xyloglucan. Carbohydrate Polymers **51** (3): 347–356.

Martín, G., and Duque, P. (2022). Etiolated Hypocotyls: A New System to Study the Impact of Abiotic Stress on Cell Expansion. Methods in molecular biology (Clifton, N.J.) **2494**: 195–205.

Marzol, E., Borassi, C., Bringas, M., Sede, A., Rodríguez Garcia, D.R., Capece, L., and Estevez, J.M. (2018). Filling the Gaps to Solve the Extensin Puzzle. Molecular Plant **11** (5): 645–658.

Matsuzawa, T., Watanabe, M., Kameda, T., Kameyama, A., and Yaoi, K. (2019). Cooperation between β-galactosidase and an isoprimeverose-producing oligoxyloglucan hydrolase is key for xyloglucan degradation in Aspergillus oryzae. The FEBS Journal **286** (16): 3182–3193.

McFarlane, H.E., Döring, A., and Persson, S. (2014). The cell biology of cellulose synthesis. Annual review of plant biology **65**: 69–94.

Meng, E.C., Goddard, T.D., Pettersen, E.F., Couch, G.S., Pearson, Z.J., Morris, J.H., and Ferrin, T.E. (2023). UCSF ChimeraX: Tools for structure building and analysis. Protein Science **32** (11): e4792.

Mikkelsen, M.D., Harholt, J., Ulvskov, P., Johansen, I.E., Fangel, J.U., Doblin, M.S., Bacic, A., and Willats, W.G.T. (2014). Evidence for land plant cell wall biosynthetic mechanisms in charophyte green algae. Ann Bot **114** (6): 1217–1236.

Mikkelsen, M.D., Harholt, J., Westereng, B., Domozych, D., Fry, S.C., Johansen, I.E., Fangel, J.U., Łężyk, M., Feng, T., Nancke, L., Mikkelsen, J.D., Willats, W.G.T., and Ulvskov, P. (2021). Ancient origin of fucosylated xyloglucan in charophycean green algae. Communications Biology **4** (1): 754.

Mirdita, M., Schütze, K., Moriwaki, Y., Heo, L., Ovchinnikov, S., and Steinegger, M. (2022). ColabFold: making protein folding accessible to all. Nat Methods **19** (6): 679–682.

Mohnen, D. (2008). Pectin structure and biosynthesis. Current Opinion in Plant Biology **11** (3): 266–277.

Morgan, J.L.W., Strumillo, J., and Zimmer, J. (2013). Crystallographic snapshot of cellulose synthesis and membrane translocation. Nature **493** (7431): 181–186.

Moussu, S., and Ingram, G. (2023). The EXTENSIN enigma. Cell surface (Amsterdam, Netherlands) **9**: 100094.

Muhammad Kamran Taj, Zohra Samreen, Ji Xiu Ling, Imran Taj, and Wei Yunlin (2014). ESCHERICHIA COLI AS A MODEL ORGANISM.

Mukherjee, S., Malik, P., and Mukherjee, T.K. (2023). Mammalian Cells, Tissues and Organ Culture: Applications. In Practical Approach to Mammalian Cell and Organ Culture (Springer, Singapore), pp. 1–78.

Muraoka, M., Kawakita, M., and Ishida, N. (2001). Molecular characterization of human UDP-glucuronic acid/UDP-N-acetylgalactosamine transporter, a novel nucleotide sugar transporter with dual substrate specificity. FEBS Letters **495** (1-2): 87–93.

Naseem, M.U., Tajti, G., Gaspar, A., Szanto, T.G., Borrego, J., and Panyi, G. (2021). Optimization of Pichia pastoris Expression System for High-Level Production of Margatoxin. Frontiers in pharmacology **12**: 733610.

Nazir, R., Rehman, S., Nisa, M., and Baba, U.a. (2019). Chapter 7 - Exploring bacterial diversity: from cell to sequence. In Freshwater microbiology: Perspectives of bacterial dynamics in lake ecosystems, S.A. Bandh, S. Shafi, and N. Shameem, eds (London, San Diego, CA, Cambridge, MA, Oxford: Elsevier Academic Press), pp. 263–306.

Niklas, K.J., and Kutschera, U. (2010). The evolution of the land plant life cycle. New Phytologist **185** (1): 27–41.

Ning, R., Feng, C., Zhang, F., Zong, S., and Jiang, J. (2025). Synthesis and Characterization of Superhigh Moisturizing Carboxymethyl Tamarind Xyloglucan and Its Potential Application in Cosmetics. Biomacromolecules **26** (3): 1647–1658.

Obst, U., Lu, T.K., and Sieber, V. (2017). A Modular Toolkit for Generating Pichia pastoris Secretion Libraries. ACS Synthetic Biology **6** (6): 1016–1025.

Ogawa-Ohnishi, M., Matsushita, W., and Matsubayashi, Y. (2013). Identification of three hydroxyproline O-arabinosyltransferases in Arabidopsis thaliana. Nat Chem Biol **9** (11): 726–730.

Oka, T., and Jigami, Y. (2006). Reconstruction of de novo pathway for synthesis of UDP-glucuronic acid and UDP-xylose from intrinsic UDP-glucose in Saccharomyces cerevisiae. The FEBS Journal **273** (12): 2645–2657.

O'Malley, R.C., Barragan, C.C., and Ecker, J.R. (2015). A user's guide to the Arabidopsis T-DNA insertion mutant collections. Methods in molecular biology (Clifton, N.J.) **1284**: 323–342.

Orellana, A., Moraga, C., Araya, M., and Moreno, A. (2016). Overview of Nucleotide Sugar Transporter Gene Family Functions Across Multiple Species. Journal of molecular biology **428** (16): 3150–3165.

Orij, R., Brul, S., and Smits, G.J. (2011). Intracellular pH is a tightly controlled signal in yeast. Biochimica et biophysica acta **1810** (10): 933–944.

Ortega, J.K. (1985). Augmented growth equation for cell wall expansion. Plant Physiol **79** (1): 318–320.

Paque, S., Mouille, G., Grandont, L., Alabadí, D., Gaertner, C., Goyallon, A., Muller, P., Primard-Brisset, C., Sormani, R., Blázquez, M.A., and Perrot-Rechenmann, C. (2014). AUXIN BINDING PROTEIN1 links cell wall remodeling, auxin signaling, and cell expansion in arabidopsis. Plant Cell **26** (1): 280–295.

Park, Y.B., and Cosgrove, D.J. (2012a). A revised architecture of primary cell walls based on biomechanical changes induced by substrate-specific endoglucanases. Plant Physiol **158** (4): 1933–1943.

Park, Y.B., and Cosgrove, D.J. (2012b). Changes in cell wall biomechanical properties in the xyloglucan-deficient xxt1/xxt2 mutant of Arabidopsis. Plant Physiol **158** (1): 465–475.

Patil, S., and Rohrer, J. (2021). An improved method for galactosyl oligosaccharide characterization. Journal of chromatography. B, Analytical technologies in the biomedical and life sciences **1184**: 122967.

Pauly, M., Andersen, L.N., Kauppinen, S., Kofod, L.V., York, W.S., Albersheim, P., and Darvill, A. (1999). A xyloglucan-specific endo-beta-1,4-glucanase from Aspergillus aculeatus: expression cloning in yeast, purification and characterization of the recombinant enzyme. Glycobiology **9** (1): 93–100.

Pauly, M., Gawenda, N., Wagner, C., Fischbach, P., Ramírez, V., Axmann, I.M., and Voiniciuc, C. (2019). The Suitability of Orthogonal Hosts to Study Plant Cell Wall Biosynthesis. Plants (Basel, Switzerland) **8** (11): 516.

Pauly, M., and Keegstra, K. (2008). Cell-wall carbohydrates and their modification as a resource for biofuels. The Plant Journal **54** (4): 559–568.

Pauly, M., and Keegstra, K. (2016). Biosynthesis of the Plant Cell Wall Matrix Polysaccharide Xyloglucan. Annual review of plant biology **67** (Volume 67, 2016): 235–259.

Pauly, M., and Ramírez, V. (2018). New Insights Into Wall Polysaccharide O-Acetylation. Frontiers in plant science **9**: 1210.

Pedersen, G.B., Blaschek, L., Frandsen, K.E.H., Noack, L.C., and Persson, S. (2023). Cellulose synthesis in land plants. Molecular Plant **16** (1): 206–231.

Peña, M.J., Darvill, A.G., Eberhard, S., York, W.S., and O'Neill, M.A. (2008). Moss and liverwort xyloglucans contain galacturonic acid and are structurally distinct from the xyloglucans synthesized by hornworts and vascular plants. Glycobiology **18** (11): 891–904.

Peña, M.J., Kong, Y., York, W.S., and O'Neill, M.A. (2012). A galacturonic acid-containing xyloglucan is involved in Arabidopsis root hair tip growth. Plant Cell **24** (11): 4511–4524.

Peña, M.J., Ryden, P., Madson, M., Smith, A.C., and Carpita, N.C. (2004). The galactose residues of xyloglucan are essential to maintain mechanical strength of the primary cell walls in Arabidopsis during growth. Plant Physiol **134** (1): 443–451.

Pérez García, M., Zhang, Y., Hayes, J., Salazar, A., Zabotina, O.A., and Hong, M. (2011). Structure and interactions of plant cell-wall polysaccharides by two- and three-dimensional magic-angle-spinning solid-state NMR. Biochemistry **50** (6): 989–1000.

Perrin, R.M., Derocher, A.E., Bar-Peled, M., Zeng, W., Norambuena, L., Orellana, A., Raikhel, N.V., and Keegstra, K. (1999). Xyloglucan Fucosyltransferase, an Enzyme Involved in Plant Cell Wall Biosynthesis. American Association for the Advancement of Science, June 99. https://www.science.org/doi/full/10.1126/science.284.5422.1976. Accessed 19 August 2024.

Persson, S., Paredez, A., Carroll, A., Palsdottir, H., Doblin, M., Poindexter, P., Khitrov, N., Auer, M., and Somerville, C.R. (2007). Genetic evidence for three unique components in primary cell-wall cellulose synthase complexes in Arabidopsis. Proceedings of the National Academy of Sciences of the United States of America **104** (39): 15566–15571.

Perumal Thivya, Nalla Bhanu Prakash Reddy, and Sinija Vadakkepulppara Ramachandran Nair (2023). Extraction of xyloglucan from tamarind industrial waste by different methods and their potential application in the food sector. International Journal of Food Science & Technology **58** (4): 2014–2020.

Petersen, B.L., Egelund, J., Damager, I., Faber, K., Jensen, J.K., Yang, Z., Bennett, E.P., Scheller, H.V., and Ulvskov, P. (2009). Assay and heterologous expression in Pichia pastoris of plant cell wall type-II membrane anchored glycosyltransferases. Glycoconjugate Journal **26** (9): 1235–1246.

Pettersen, E.F., Goddard, T.D., Huang, C.C., Meng, E.C., Couch, G.S., Croll, T.I., Morris, J.H., and Ferrin, T.E. (2021). UCSF ChimeraX: Structure visualization for researchers, educators, and developers. Protein Science **30** (1): 70–82.

Pontes, C.M., Sampaio, L.M.F., Lima, Antonia Carlota de Souza, Gallão, M.I., Miranda, M.R.A., Eça, K.S., Karbowiak, T., and Oliveira, L.d.S. (2023). Effect of xyloglucan-based coating enriched with cashew apple coproduct extract on quality and antioxidant metabolism of guava during ripening postharvest. Food Chemistry Advances **2**: 100226.

Popova, L.G., Khramov, D.E., Nedelyaeva, O.I., and Volkov, V.S. (2023). Yeast Heterologous Expression Systems for the Study of Plant Membrane Proteins. International Journal of Molecular Sciences **24** (13).

Popper, Z.A., and Fry, S.C. (2003). Primary cell wall composition of bryophytes and charophytes. Ann Bot **91** (1): 1–12.

Popper, Z.A., and Fry, S.C. (2005). Widespread Occurrence of a Covalent Linkage Between Xyloglucan and Acidic Polysaccharides in Suspension-cultured Angiosperm Cells. Ann Bot **96** (1): 91–99.

Pottier, D., Roitsch, T., and Persson, S. (2023). Cell wall regulation by carbon allocation and sugar signaling. The Cell Surface **9**: 100096.

Pouresmaeil, M., and Azizi-Dargahlou, S. (2023). Factors involved in heterologous expression of proteins in E. coli host. Archives of Microbiology **205** (5): 212.

Purushotham, P., Ho, R., and Zimmer, J. (2020). Architecture of a catalytically active homotrimeric plant cellulose synthase complex. Science (New York, N.Y.) **369** (6507): 1089–1094.

Raabe, K., Sun, L., Schindfessel, C., Honys, D., and Geelen, D. (2024). A word of caution: T-DNA-associated mutagenesis in plant reproduction research. J Exp Bot **75** (11): 3248–3258.

Ralet, M.-C., Lerouge, P., and Quéméner, B. (2009). Mass spectrometry for pectin structure analysis. Carbohydrate Research **344** (14): 1798–1807.

Rao, M.S., van Vleet, T.R., Ciurlionis, R., Buck, W.R., Mittelstadt, S.W., Blomme, E.A.G., and Liguori, M.J. (2018). Comparison of RNA-Seq and Microarray Gene Expression Platforms for the Toxicogenomic Evaluation of Liver From Short-Term Rat Toxicity Studies. Frontiers in genetics **9**: 636.

Rautengarten, C., Ebert, B., Moreno, I., Temple, H., Herter, T., Link, B., Doñas-Cofré, D., Moreno, A., Saéz-Aguayo, S., Blanco, F., Mortimer, J.C., Schultink, A., Reiter, W.-D., Dupree, P., Pauly, M., Heazlewood, J.L., Scheller, H.V., and Orellana, A. (2014). The Golgi localized bifunctional UDP-rhamnose/UDP-galactose transporter family of Arabidopsis. Proceedings of the National Academy of Sciences of the United States of America **111** (31): 11563–11568.

Rautengarten, C., Quarrell, O.W., Stals, K., Caswell, R.C., Franco, E., Baple, E., Burgess, N., Jokhi, R., Heazlewood, J.L., Offiah, A.C., Ebert, B., and Ellard, S. (2019). A hypomorphic allele of SLC35D1 results in Schneckenbecken-like dysplasia. Human Molecular Genetics **28** (21): 3543–3551.

Ray, B., Loutelier-Bourhis, C., Lange, C., Condamine, E., Driouich, A., and Lerouge, P. (2004). Structural investigation of hemicellulosic polysaccharides from Argania spinosa: characterisation of a novel xyloglucan motif. Carbohydrate Research **339** (2): 201–208.

Ray, S., Satya, P., Sharma, L., Roy, S., Bera, A., Santra, S., and Ghosh, S. (2022). Model Plants in Genomics. In Plant Genomics for Sustainable Agriculture, R.L. Singh, S. Mondal, A. Parihar, and P.K. Singh, eds (Singapore: Springer Nature Singapore; Imprint Springer), pp. 241–264.

Rebnegger, C., Vos, T., Graf, A.B., Valli, M., Pronk, J.T., Daran-Lapujade, P., and Mattanovich, D. (2016). Pichia pastoris Exhibits High Viability and a Low Maintenance Energy Requirement at Near-Zero Specific Growth Rates. Applied and Environmental Microbiology **82** (15): 4570–4583.

Reddi, A.R., Jensen, L.T., and Culotta, V.C. (2009). Manganese homeostasis in Saccharomyces cerevisiae. Chemical reviews **109** (10): 4722–4732.

Reiter, W.D., Chapple, C., and Somerville, C.R. (1997). Mutants of Arabidopsis thaliana with altered cell wall polysaccharide composition. The Plant journal for cell and molecular biology **12** (2): 335–345.

Robert, M., Waldhauer, J., Stritt, F., Yang, B., Pauly, M., and Voiniciuc, C. (2021). Modular biosynthesis of plant hemicellulose and its impact on yeast cells. Biotechnol Biofuels **14** (1): 140.

Rocha, J., Cicéron, F., Sanctis, D., Lelimousin, M., Chazalet, V., Lerouxel, O., and Breton, C. (2016). Structure of Arabidopsis thaliana FUT1 Reveals a Variant of the GT-B Class Fold and Provides Insight into Xyloglucan Fucosylation. Plant Cell **28** (10): 2352–2364.

Rounds, C.M., Lubeck, E., Hepler, P.K., and Winship, L.J. (2011). Propidium iodide competes with Ca(2+) to label pectin in pollen tubes and Arabidopsis root hairs. Plant Physiol **157** (1): 175–187.

Rui, Y., and Dinneny, J.R. (2020). A wall with integrity: surveillance and maintenance of the plant cell wall under stress. New Phytologist **225** (4): 1428–1439.

Runions, J., Brach, T., Kühner, S., and Hawes, C. (2006). Photoactivation of GFP reveals protein dynamics within the endoplasmic reticulum membrane. J Exp Bot **57** (1): 43–50.

S. C. Fry (2000). The Growing Plant Cell Wall: Chemical And Metabolic Analysis.

Saez-Aguayo, S., Rautengarten, C., Temple, H., Sanhueza, D., Ejsmentewicz, T., Sandoval-Ibañez, O., Doñas, D., Parra-Rojas, J.P., Ebert, B., Lehner, A., Mollet, J.-C., Dupree, P., Scheller, H.V., Heazlewood, J.L., Reyes, F.C., and Orellana, A. (2017). UUAT1 Is a Golgi-Localized UDP-Uronic Acid Transporter That Modulates the Polysaccharide Composition of Arabidopsis Seed Mucilage. Plant Cell **29** (1): 129–143.

Saint-Jore, C.M., Evins, J., Batoko, H., Brandizzi, F., Moore, I., and Hawes, C. (2002). Redistribution of membrane proteins between the Golgi apparatus and endoplasmic reticulum in plants is reversible and not dependent on cytoskeletal networks. The Plant journal for cell and molecular biology **29** (5): 661–678.

Sampedro, J., Gianzo, C., Iglesias, N., Guitián, E., Revilla, G., and Zarra, I. (2012). AtBGAL10 is the main xyloglucan β-galactosidase in Arabidopsis, and its absence results in unusual xyloglucan subunits and growth defects. Plant Physiol **158** (3): 1146–1157.

Sampedro, J., Pardo, B., Gianzo, C., Guitián, E., Revilla, G., and Zarra, I. (2010). Lack of α-xylosidase activity in Arabidopsis alters xyloglucan composition and results in growth defects. Plant Physiol **154** (3): 1105–1115.

Sampedro, J., Sieiro, C., Revilla, G., González-Villa, T., and Zarra, I. (2001). Cloning and expression pattern of a gene encoding an alpha-xylosidase active against xyloglucan oligosaccharides from Arabidopsis. Plant Physiol **126** (2): 910–920.

Santos, N.L., Braga, R.C., Bastos, M.S.R., Cunha, P.L.R., Mendes, F.R.S., Galvão, A.M.M.T., Bezerra, G.S., and Passos, A.A.C. (2019). Preparation and characterization of

Xyloglucan films extracted from Tamarindus indica seeds for packaging cut-up 'Sunrise Solo' papaya. International Journal of Biological Macromolecules **132**: 1163–1175.

Santoso, A., Herawati, N., and Rubiana, Y. (2012). EFFECT OF METHANOL INDUCTION AND INCUBATION TIME ON EXPRESSION OF HUMAN ERYTHROPOIETIN IN METHYLOTROPIC YEAST Pichia pastoris. MST **16** (1).

Scheller, H.V., and Ulvskov, P. (2010). Hemicelluloses. Annual review of plant biology **61** (Volume 61, 2010): 263–289.

Schindelin, J., Arganda-Carreras, I., Frise, E., Kaynig, V., Longair, M., Pietzsch, T., Preibisch, S., Rueden, C., Saalfeld, S., Schmid, B., Tinevez, J.-Y., White, D.J., Hartenstein, V., Eliceiri, K., Tomancak, P., and Cardona, A. (2012). Fiji: an open-source platform for biological-image analysis. Nat Methods **9** (7): 676–682.

Schultink, A., Cheng, K., Park, Y.B., Cosgrove, D.J., and Pauly, M. (2013). The identification of two arabinosyltransferases from tomato reveals functional equivalency of xyloglucan side chain substituents. Plant Physiol **163** (1): 86–94.

Schultink, A., Liu, L., Zhu, L., and Pauly, M. (2014). Structural Diversity and Function of Xyloglucan Sidechain Substituents. Plants (Basel, Switzerland) **3** (4): 526–542.

Schultink, A., Naylor, D., Dama, M., and Pauly, M. (2015). The role of the plant-specific ALTERED XYLOGLUCAN9 protein in Arabidopsis cell wall polysaccharide O-acetylation. Plant Physiol **167** (4): 1271–1283.

Schultink, A.C. (2013). Identification and characterization of genes involved in the biosynthesis of the plant cell wall polysaccharide xyloglucan.

Schweigkofler, W. (2002). Analysis of phylogenetic relationships among Ascomycota with yeast phases using ribosomal DNA sequences and cell wall sugars. Organisms Diversity & Evolution **2** (1): 1–17.

Seifert, G.J. (2004). Nucleotide sugar interconversions and cell wall biosynthesis: how to bring the inside to the outside. Current Opinion in Plant Biology **7** (3): 277–284.

Shahin, L., Zhang, L., Mohnen, D., and Urbanowicz, B.R. (2023). Insights into pectin O-acetylation in the plant cell wall: structure, synthesis, and modification. Cell surface (Amsterdam, Netherlands) **9**: 100099.

Shigeyama, T., Watanabe, A., Tokuchi, K., Toh, S., Sakurai, N., Shibuya, N., and Kawakami, N. (2016). α-Xylosidase plays essential roles in xyloglucan remodelling, maintenance of cell wall integrity, and seed germination in Arabidopsis thaliana. J Exp Bot **67** (19): 5615–5629.

Sievers, F., and Higgins, D.G. (2018). Clustal Omega for making accurate alignments of many protein sequences. Protein Science **27** (1): 135–145.

Sievers, F., Wilm, A., Dineen, D., Gibson, T.J., Karplus, K., Li, W., Lopez, R., McWilliam, H., Remmert, M., Söding, J., Thompson, J.D., and Higgins, D.G. (2011). Fast, scalable

generation of high-quality protein multiple sequence alignments using Clustal Omega. Molecular systems biology **7**: 539.

Sørensen, I., Pettolino, F.A., Bacic, A., Ralph, J., Lu, F., O'Neill, M.A., Fei, Z., Rose, J.K.C., Domozych, D.S., and Willats, W.G.T. (2011). The charophycean green algae provide insights into the early origins of plant cell walls. The Plant Journal **68** (2): 201–211.

Sowinski, E.E., Westman, B.M., Redmond, C.R., Kong, Y., Olek, A.T., Olek, J., McCann, M.C., and Carpita, N.C. (2022). Lack of xyloglucan in the cell walls of the Arabidopsis xxt1/xxt2 mutant results in specific increases in homogalacturonan and glucomannan. The Plant Journal **110** (1): 212–227.

Sparkes, I.A., Runions, J., Kearns, A., and Hawes, C. (2006). Rapid, transient expression of fluorescent fusion proteins in tobacco plants and generation of stably transformed plants. Nat Protoc **1** (4): 2019–2025.

Stratilová, B., Kozmon, S., Stratilová, E., and Hrmova, M. (2020). Plant Xyloglucan Xyloglucosyl Transferases and the Cell Wall Structure: Subtle but Significant. Molecules **25** (23): 5619.

Suzuki, H., Savane, P., Marion-Poll, L., Sechet, J., Frey, A., Berger, A., Belcram, K., Borrega, N., Seo, M., Voxeur, A., Mouille, G., and Marion-Poll, A. (2025). Analysis of xyloglucan metabolism mutants highlights the prominent role of xylose cleavage in seed dormancy. The Plant Journal **122** (1): e70063.

Takahashi, D., Johnson, K.L., Hao, P., Tuong, T., Erban, A., Sampathkumar, A., Bacic, A., Livingston, D.P., Kopka, J., Kuroha, T., Yokoyama, R., Nishitani, K., Zuther, E., and Hincha, D.K. (2021). Cell wall modification by the xyloglucan endotransglucosylase/hydrolase XTH19 influences freezing tolerance after cold and sub-zero acclimation. Plant, cell & environment **44** (3): 915–930.

Tameshige, T., Hirakawa, Y., Torii, K.U., and Uchida, N. (2015). Cell walls as a stage for intercellular communication regulating shoot meristem development. Frontiers in plant science **6**: 324.

Tang, Y., Wang, M., Cao, L., Dang, Z., Ruan, N., Wang, Y., Huang, Y., Wu, J., Zhang, M., Xu, Z., Chen, W., Li, F., and Xu, Q. (2022). OsUGE3-mediated cell wall polysaccharides accumulation improves biomass production, mechanical strength, and salt tolerance. Plant, cell & environment **45** (8): 2492–2507.

Thompson, D.S., and Islam, A. (2021). Plant Cell Wall Hydration and Plant Physiology: An Exploration of the Consequences of Direct Effects of Water Deficit on the Plant Cell Wall. Plants (Basel, Switzerland) **10** (7): 1263.

Tiné, M.A.S., Silva, C.O., Lima, D.U., Carpita, N.C., and Buckeridge, M.S. (2006). Fine structure of a mixed-oligomer storage xyloglucan from seeds of Hymenaea courbaril. Carbohydrate Polymers **66** (4): 444–454.

Tuomivaara, S.T., Yaoi, K., O'Neill, M.A., and York, W.S. (2015). Generation and structural validation of a library of diverse xyloglucan-derived oligosaccharides, including an update on xyloglucan nomenclature. Carbohydrate Research **402**: 56–66.

Untergasser, A., Cutcutache, I., Koressaar, T., Ye, J., Faircloth, B.C., Remm, M., and Rozen, S.G. (2012). Primer3--new capabilities and interfaces. Nucleic Acids Res **40** (15): e115.

Urbanowicz, B.R., Bharadwaj, V.S., Alahuhta, M., Peña, M.J., Lunin, V.V., Bomble, Y.J., Wang, S., Yang, J.-Y., Tuomivaara, S.T., Himmel, M.E., Moremen, K.W., York, W.S., and Crowley, M.F. (2017). Structural, mutagenic and in silico studies of xyloglucan fucosylation in Arabidopsis thaliana suggest a water-mediated mechanism. The Plant Journal **91** (6): 931–949.

Valent, B.S., and Albersheim, P. (1974). The structure of plant cell walls: v. On the binding of xyloglucan to cellulose fibers. Plant Physiol **54** (1): 105–108.

van de Wouwer, D., Boerjan, W., and Vanholme, B. (2018). Plant cell wall sugars: sweeteners for a bio-based economy. Physiologia Plantarum **164** (1): 27–44.

Vanzin, G.F., Madson, M., Carpita, N.C., Raikhel, N.V., Keegstra, K., and Reiter, W.-D. (2002). The mur2 mutant of Arabidopsis thaliana lacks fucosylated xyloglucan because of a lesion in fucosyltransferase AtFUT1. Proceedings of the National Academy of Sciences of the United States of America **99** (5): 3340–3345.

Velasquez, S.M., Ricardi, M.M., Dorosz, J.G., Fernandez, P.V., Nadra, A.D., Pol-Fachin, L., Egelund, J., Gille, S., Harholt, J., Ciancia, M., Verli, H., Pauly, M., Bacic, A., Olsen, C.E., Ulvskov, P., Petersen, B.L., Somerville, C., Iusem, N.D., and Estevez, J.M. (2011). O-glycosylated cell wall proteins are essential in root hair growth. Science (New York, N.Y.) **332** (6036): 1401–1403.

Velasquez, S.M., Ricardi, M.M., Poulsen, C.P., Oikawa, A., Dilokpimol, A., Halim, A., Mangano, S., Denita Juarez, S.P., Marzol, E., Salgado Salter, J.D., Dorosz, J.G., Borassi, C., Möller, S.R., Buono, R., Ohsawa, Y., Matsuoka, K., Otegui, M.S., Scheller, H.V., Geshi, N., Petersen, B.L., Iusem, N.D., and Estevez, J.M. (2015). Complex regulation of prolyl-4-hydroxylases impacts root hair expansion. Molecular Plant **8** (5): 734–746.

Verger, S., Long, Y., Boudaoud, A., and Hamant, O. (2018). A tension-adhesion feedback loop in plant epidermis. eLife Sciences Publications, Ltd, April 18. https://elifesciences.org/articles/34460. Accessed 19 January 2025.

Vilaseca, F., Serra, A., and Kochumalayil, J.J. (2020). Xyloglucan coating for enhanced strength and toughness in wood fibre networks. Carbohydrate Polymers **229**: 115540.

Vincken, J.P., Wijsman, A.J., Beldman, G., Niessen, W.M., and Voragen, A.G. (1996). Potato xyloglucan is built from XXGG-type subunits. Carbohydrate Research **288**: 219–232.

Vincken, J.P., York, W.S., Beldman, G., and Voragen, A.G. (1997). Two general branching patterns of xyloglucan, XXXG and XXGG. Plant Physiol **114** (1): 9–13.

Vinueza, N.R., Gallardo, V.A., Klimek, J.F., Carpita, N.C., and Kenttämaa, H.I. (2013). Analysis of xyloglucans by ambient chloride attachment ionization tandem mass spectrometry. Carbohydrate Polymers **98** (1): 1203–1213.

Voiniciuc, C., Dama, M., Gawenda, N., Stritt, F., and Pauly, M. (2019). Mechanistic insights from plant heteromannan synthesis in yeast. Proceedings of the National Academy of Sciences of the United States of America **116** (2): 522–527.

Wan, J., He, M., Hou, Q., Zou, L., Yang, Y., Wei, Y., and Chen, X. (2021). Cell wall associated immunity in plants. Stress Biology **1** (1): 3.

Wang, C., Li, S., Ng, S., Zhang, B., Zhou, Y., Whelan, J., Wu, P., and Shou, H. (2014). Mutation in xyloglucan 6-xylosytransferase results in abnormal root hair development in Oryza sativa. J Exp Bot **65** (15): 4149–4157.

Wilson, L.F.L., Neun, S., Yu, L., Tryfona, T., Stott, K., Hollfelder, F., and Dupree, P. (2023). The biosynthesis, degradation, and function of cell wall β-xylosylated xyloglucan mirrors that of arabinoxyloglucan. New Phytologist **240** (6): 2353–2371.

Wilson, T.H., Kumar, M., and Turner, S.R. (2021). The molecular basis of plant cellulose synthase complex organisation and assembly. Biochem Soc Trans **49** (1): 379–391.

Wohlert, M., Benselfelt, T., Wågberg, L., Furó, I., Berglund, L.A., and Wohlert, J. (2022). Cellulose and the role of hydrogen bonds: not in charge of everything. Cellulose **29** (1): 1–23.

Wolf, S. (2022). Cell Wall Signaling in Plant Development and Defense. Annual review of plant biology **73**: 323–353.

Wu, Z., Cui, C., Xing, A., Xu, X., Sun, Y., Tian, Z., Li, X., Zhu, J., Wang, G., and Wang, Y. (2021). Identification and response analysis of xyloglucan endotransglycosylase/hydrolases (XTH) family to fluoride and aluminum treatment in Camellia sinensis. BMC genomics **22** (1): 761.

Xiang, M., Yuan, S., Zhang, Q., Liu, X., Li, Q., Leng, Z., Sha, J., Anderson, C.T., and Xiao, C. (2023). Galactosylation of xyloglucan is essential for the stabilization of the actin cytoskeleton and endomembrane system through the proper assembly of cell walls. J Exp Bot **74** (17): 5104–5123.

Xiao, C., Zhang, T., Zheng, Y., Cosgrove, D.J., and Anderson, C.T. (2016). Xyloglucan Deficiency Disrupts Microtubule Stability and Cellulose Biosynthesis in Arabidopsis, Altering Cell Growth and Morphogenesis. Plant Physiol **170** (1): 234–249.

Xu, Q., Ye, X., Li, L.-Y., Cheng, Z.-M., and Guo, H. (2010). Structural basis for the action of xyloglucan endotransglycosylases/hydrolases: insights from homology modeling. Interdisciplinary sciences, computational life sciences **2** (2): 133–139.

Xu, Z., Wang, M., Shi, D., Zhou, G., Niu, T., Hahn, M.G., O'Neill, M.A., and Kong, Y. (2017). DGE-seq analysis of MUR3-related Arabidopsis mutants provides insight into how dysfunctional xyloglucan affects cell elongation. Plant science an international journal of experimental plant biology **258**: 156–169.

Xuan, Y., Zhou, Z.S., Li, H.B., and Yang, Z.M. (2016). Identification of a group of XTHs genes responding to heavy metal mercury, salinity and drought stresses in Medicago truncatula. Ecotoxicology and environmental safety **132**: 153–163.

York, W.S., Darvill, A.G., and Albersheim, P. (1984). Inhibition of 2,4-dichlorophenoxyacetic Acid-stimulated elongation of pea stem segments by a xyloglucan oligosaccharide. Plant Physiol **75** (2): 295–297.

York, W.S., Harvey, L.K., Guillen, R., Albersheim, P., and Darvill, A.G. (1993). Structural analysis of tamarind seed xyloglucan oligosaccharides using beta-galactosidase digestion and spectroscopic methods. Carbohydrate Research **248**: 285–301.

York, W.S., Kumar Kolli, V.S., Orlando, R., Albersheim, P., and Darvill, A.G. (1996). The structures of arabinoxyloglucans produced by solanaceous plants. Carbohydrate Research **285**: 99–128.

York, W.S., Oates, J.E., van Halbeek, H., Darvill, A.G., Albersheim, P., Tiller, P.R., and Dell, A. (1988). Location of the O-acetyl substituents on a nonasaccharide repeating unit of sycamore extracellular xyloglucan. Carbohydrate Research **173** (1): 113–132.

Yu, L., Yoshimi, Y., Cresswell, R., Wightman, R., Lyczakowski, J.J., Wilson, L.F.L., Ishida, K., Stott, K., Yu, X., Charalambous, S., Wurman-Rodrich, J., Terrett, O.M., Brown, S.P., Dupree, R., Temple, H., Krogh, Kristian B. R. M., and Dupree, P. (2022). Eudicot primary cell wall glucomannan is related in synthesis, structure, and function to xyloglucan. Plant Cell **34** (11): 4600–4622.

Yuan, W., Yao, F., Liu, Y., Xiao, H., Sun, S., Jiang, C., An, Y., Chen, N., Huang, L., Lu, M., and Zhang, J. (2024). Identification of the xyloglucan endotransglycosylase/hydrolase genes and the role of PagXTH12 in drought resistance in poplar. Forestry Research **4**: e039.

Zabotina, O.A., Avci, U., Cavalier, D., Pattathil, S., Chou, Y.-H., Eberhard, S., Danhof, L., Keegstra, K., and Hahn, M.G. (2012). Mutations in multiple XXT genes of Arabidopsis reveal the complexity of xyloglucan biosynthesis. Plant Physiol **159** (4): 1367–1384.

Zabotina, O.A., van de Ven, W.T.G., Freshour, G., Drakakaki, G., Cavalier, D., Mouille, G., Hahn, M.G., Keegstra, K., and Raikhel, N.V. (2008). Arabidopsis XXT5 gene encodes a

putative alpha-1,6-xylosyltransferase that is involved in xyloglucan biosynthesis. The Plant Journal **56** (1): 101–115.

Zabotina, O.A., Zhang, N., and Weerts, R. (2021). Polysaccharide Biosynthesis: Glycosyltransferases and Their Complexes. Frontiers in plant science **12**: 625307.

Zacharski, D.M., Brandt, S., Esch, S., König, S., Mormann, M., Ulrich-Merzenich, G., and Hensel, A. (2015). Xyloglucan from Tropaeolum majus Seeds Induces Cellular Differentiation of Human Keratinocytes by Inhibition of EGFR Phosphorylation and Decreased Activity of Transcription Factor CREB. Biomacromolecules **16** (7): 2157–2167.

Zavyalov, A.V., Rykov, S.V., Lunina, N.A., Sushkova, V.I., Yarotsky, S.V., and Berezina, O.V. (2019). Plant Polysaccharide Xyloglucan and Enzymes That Hydrolyze It (Review). Russ J Bioorg Chem **45** (7): 845–859.

Zdunek, A., Pieczywek, P.M., and Cybulska, J. (2021). The primary, secondary, and structures of higher levels of pectin polysaccharides. Comprehensive Reviews in Food Science and Food Safety **20** (1): 1101–1117.

Zhang, E., Li, J., Zhou, Y., Che, P., Ren, B., Qin, Z., Ma, L., Cui, J., Sun, H., and Yao, F. (2017). Biodegradable and injectable thermoreversible xyloglucan based hydrogel for prevention of postoperative adhesion. Acta biomaterialia **55**: 420–433.

Zhang, H., Zhao, T., Wu, Y., Xie, F., Xiong, Z., Song, Z., Ai, L., and Wang, G. (2022). Acetylation modification improved the physicochemical properties of xyloglucan from tamarind seeds. International Journal of Biological Macromolecules **223** (Pt A): 193–201.

Zhang, L., Prabhakar, P.K., Bharadwaj, V.S., Bomble, Y.J., Peña, M.J., and Urbanowicz, B.R. (2023a). Glycosyltransferase family 47 (GT47) proteins in plants and animals. Essays Biochem **67** (3): 639–652.

Zhang, N., Julian, J.D., Yap, C.E., Swaminathan, S., and Zabotina, O.A. (2023b). The Arabidopsis xylosyltransferases, XXT3, XXT4, and XXT5, are essential to complete the fully xylosylated glucan backbone XXXG-type structure of xyloglucans. New Phytologist **238** (5): 1986–1999.

Zhang, T., Tang, H., Vavylonis, D., and Cosgrove, D.J. (2019). Disentangling loosening from softening: insights into primary cell wall structure. The Plant Journal **100** (6): 1101–1117.

Zhang, W., Qin, W., Li, H., and Wu, A.-M. (2021a). Biosynthesis and Transport of Nucleotide Sugars for Plant Hemicellulose. Frontiers in plant science **12**: 723128.

Zhang, Y., Yu, J., and Cosgrove, D.J. (2025). Mechanical Roles of Polysaccharide Assembly and Interactions in Plant Cell Walls. Biomacromolecules.

Zhang, Y., Yu, J., Wang, X., Durachko, D.M., Zhang, S., and Cosgrove, D.J. (2021b). Molecular insights into the complex mechanics of plant epidermal cell walls. Science (New York, N.Y.) **372** (6543): 706–711.

Zhao, C., Zayed, O., Zeng, F., Liu, C., Zhang, L., Zhu, P., Hsu, C.-C., Tuncil, Y.E., Tao, W.A., Carpita, N.C., and Zhu, J.-K. (2019). Arabinose biosynthesis is critical for salt stress tolerance in Arabidopsis. New Phytologist **224** (1): 274–290.

Zhao, X., Liu, N., Shang, N., Zeng, W., Ebert, B., Rautengarten, C., Zeng, Q.-Y., Li, H., Chen, X., Beahan, C., Bacic, A., Heazlewood, J.L., and Wu, A.-M. (2018). Three UDP-xylose transporters participate in xylan biosynthesis by conveying cytosolic UDP-xylose into the Golgi lumen in Arabidopsis. J Exp Bot **69** (5): 1125–1134.

Zhong, R., Cui, D., Phillips, D.R., Richardson, E.A., and Ye, Z.-H. (2020). A Group of O-Acetyltransferases Catalyze Xyloglucan Backbone Acetylation and Can Alter Xyloglucan Xylosylation Pattern and Plant Growth When Expressed in Arabidopsis. Plant & cell physiology **61** (6): 1064–1079.

Zhong, R., Cui, D., and Ye, Z.-H. (2018). Xyloglucan O-acetyltransferases from Arabidopsis thaliana and Populus trichocarpa catalyze acetylation of fucosylated galactose residues on xyloglucan side chains. Planta **248** (5): 1159–1171.

Zhong, R., Phillips, D.R., and Ye, Z.-H. (2021). A Single Xyloglucan Xylosyltransferase Is Sufficient for Generation of the XXXG Xylosylation Pattern of Xyloglucan. Plant & cell physiology **62** (10): 1589–1602.

Zhong, R., Teng, Q., Haghighat, M., Yuan, Y., Furey, S.T., Dasher, R.L., and Ye, Z.-H. (2017). Cytosol-Localized UDP-Xylose Synthases Provide the Major Source of UDP-Xylose for the Biosynthesis of Xylan and Xyloglucan. Plant & cell physiology **58** (1): 156–174.

Zhou, Y., Tang, S., Lv, Y., Zhang, D., Huang, X., Chen, Y., Lai, C., and Yong, Q. (2024). The prebiotic impacts of galactose side-chain of tamarind xyloglucan oligosaccharides on gut microbiota. Heliyon **10** (18): e37864.

Zhu, L., Dama, M., and Pauly, M. (2018). Identification of an arabinopyranosyltransferase from Physcomitrella patens involved in the synthesis of the hemicellulose xyloglucan. Plant Direct **2** (3): e00046.

Zhu, X.F., Shi, Y.Z., Lei, G.J., Fry, S.C., Zhang, B.C., Zhou, Y.H., Braam, J., Jiang, T., Xu, X.Y., Mao, C.Z., Pan, Y.J., Yang, J.L., Wu, P., and Zheng, S.J. (2012). XTH31, encoding an in vitro XEH/XET-active enzyme, regulates aluminum sensitivity by modulating in vivo XET action, cell wall xyloglucan content, and aluminum binding capacity in Arabidopsis. Plant Cell **24** (11): 4731–4747.

Zhu, X.F., Wan, J.X., Sun, Y., Shi, Y.Z., Braam, J., Li, G.X., and Zheng, S.J. (2014). Xyloglucan Endotransglucosylase-Hydrolase17 Interacts with Xyloglucan Endotransglucosylase-Hydrolase31 to Confer Xyloglucan Endotransglucosylase Action and Affect Aluminum Sensitivity in Arabidopsis. Plant Physiol **165** (4): 1566–1574.

6. Supplemental material

HcXXTA	ATGTTGAAACGGTGTCTCCGTCCCCAGCGTGTCCGTCAGGTCCAGAGGGC GTGTCGCCAAGGCATCCTCACCTTCCTCTGCCTCTTTCTCACCGTCGCGGT CCTCCGTGGTACCGTCGGGGCCGGGAAGTTCGGGACTCCTTGGAAGGACT TCAATGAGTTCCGCGACCATCTCTCCTTGCCGGGGGGCTGGGTGGAGCCA AATCGCGTACTCGTGGAAACTCAACCCGAGAAAACCGAATCGGGCCAGTTC AGCAACTACGTCCCCTTCGATATCTCGAAGATACAAAAAGACGAAGAAGGCG ATGACGACAAGCGCGACTCCAACACAACGTACAGTCTCGGTCCCAAGATTT CCGATTGGGACGAACAGCGTGCTGAGTGGCTGAAGAACAACCCGGATTAC CCGAATTTTATCGCACCCGGTAAACCCCGGGTTCTTCTGGTTTCCGGGTCTT CACCTAAACCATGCGAGAACCCGGTTGGTGATCATTATCTATTGAAATCGATT AAGAACAAAATGGATTACTGCAGGCTTCATGGGATTGAGGTTTTCTATAACAT GGCTCTGCTCGATGCTGAAATGTCTGGATTTTGGGCGAAACTACCATTAATG CGAAAGCTGTTATTGTCACATCCTGAAGTTGAATTTCTATGGTGGATGGACA GTGACGCAATGTTCACCGACATGGCTTTCGAGGTTCCATGGGAGCGCTATA AAGATCACAACTTTGTGATGCACGGATGGAACAACATGGTCTACGATCAAAA GAACTGGATTGGATTAAACACGGGAAGTTTTCTGCTGAGAAATTGCCAATGG TCGCTGGATATCCTCGATGCGTGGGCTCCAATGGGTCCAAAAGGGAAAATC AGAGACGAAGCCGGAAAAATCCTCACCAAAGAGCTCAAAGACCGGCCAGT TTTCGAAGCTGATGATCAATCGGCAATGATTTATCTGTTGGCAAAGGAAAAG GAGAAGTGGGCTGAGAAAGTTTACTTAGAAAATGCTTACTTTCTTCATGGTTA CTGGGGGATTCTGGTGGATAGATATGAAGAACTGATCGAAAACTACCATCCT GGCTTTGGTGACCAGAGATGGCCTCTTGTGACTCACTTTGTGGGTTGCAAA CCTTGTGGGAAGTTTGGTGAGTACCCAGCTGAAAGGTGCTTGAGGCAGATG GAGAGAGCTTATAATTTTGGGGATAATCAGATTCTGCAGATGTATGGGTTTAC CCATAAGTCACTGCTGAGCCGCGGAGTGAAGAGAGTGAAGAGAGTGAAGA ATGATAGCAGCAATCCACTTGAAGTGGAGGATGAACTTGGTTTGCTTCATCC TGCTTTCAAAGCTGTCAGGTTGCCAGCTTCTTCTTGA
HcXXTB	ATGGATCAGTTTCTCGGCCCGCGCCGCGTCCGCCAGATCCAAAGGACGTG CCGCCACGGCACCGTCACCTTCCTCTGCCTCTTCCTCACCGTCGTCGTCCT ACGCGGTACCATCGGGGCCGGCAAATTTGGAACCCCCGAGCAAGACTTCA ACGAGATCCGTGAGCACCTCTACTCCCGAGGGCGGCGCGTGGAGCCCCAC CGCGTTCTGGAAGAAGTTCACCCCGATAACACTGATTCGGGTCAATCCAAC AACTACGCCACCTTTGATATCTCCAAGATACTCAAGGACGAAGGAGGCGATG ACGACAAGCGCGATCCGAACACGCCGTACAGTCTCGGGCCGAAGATTTCG GATTGGGACGAACAACGAACTGAGTGGTTGAAAAACAATCCAGACTACCCG AATTTCATCGGACCCAATAAGCCTCGGGTCCTCCTGGTTACCGGGTCATCG CCGAAACCGTGTGAGAATCCAGTTGGAGATCATTATCTGTTGAAGTCAATTA AGAACAAAATCGATTACTGCAGATTACATGGGATCGAGATTTTCTACAACATG GCTCTACTCGATGCGGAAATGGCTGGGTTTTGGGCGAAACTGCCATTGATT CGGAAGCTGCTCTTATCGCATCCTGAAATCGAGTTTCTATGGTGGATGGACA GTGACGCGATGTTCACAGACATGGCATTTGAAGCCCCATGGGAAAGGTACA AAAATCACAACTTTGTGATGCACGGATGGAACGAAATGGTGTATGATGAGAA GAACTGGATTGGGTTAAACACGGGGAGTTTTCTGCTCAGAAATTGTCAATGG TCGCTGGATATTCTCGATGCTTGGGCTCCAATGGGTCCGAAAGGGAAAGTC AGGGACGAAGCTGGGAAAATCCTTACCAGAGAACTCAAAAACCGACCCGTA TTTGAAGCCGATGATCAATCTGCAATGGTTTATTTGCTAGCAACAGAAAGGG CAAAATGGGGTGATAAAGTTTACCTTGAAAACCATTACTATTTGCATGGATATT GGGGAATTTTAGTTGATAGGTATGAAGAAATGATTGAGAATTACCATCCTGGC CTTGGTGATCACAGATGGCCACTTGTGACTCACTTCGTGGGTTGTAAACCTT GTGGGAAATTTGGGGATTACCCAGTTGAGAGGTGTTTGAAGCAAATGGATA GAGCTTACAACTTTGGGGATAACCAGATTTTGCAGATGTATGGTTTCACTCAT AACAGTCTTGGTAGTCGCAGGGTTAAGAGAGTGAGGAATGAGAGCAGCAAT CCGCTAGAAGTGAAGGATGATCTTGGTTTGCTTCATCCTACTTTCAAAGCTAT CAGATTACCAAATTCTTCTTGA

HcXXTC	ATGGGACAGGAGAATAACACAGCTCAGAAGAGAAGTAGCAGCGGTGGGTT GCCCACTTCCACTGTCGCTAATGGTGGCAGGGGCCGTGCATTTGGTAGCTT ACCTCGTGGCCGGCAGATCCACAAGACCTTCAACAACATCAAAATCACCAT CCTCTGTGGCTTCGTAACCATCCTGGTTCTTCGCGGCACCATTGGCGTTAAT TTCGGAAGCTCAGACGCCGAGGCCGTGAACCAAAACCTCATCGAAGAGAC GAACCGAATCCTCGCTGAGATCAGATCCGATAGTGATCCTTCCGATCCAGAT GAGCCCACTGAGACTGAGCTAAATCCGAATATCACCTTCACTCTGGGGCCG AAGATCAGCAATTGGGACCAGGAGCGCAAGGCCTGGCTGGTTCAGAATCCT GAGTTTCCGAATTATATTAAAGGTAAAGCTCGAATTTTGCTCCTTACTGGATC ACCTCCGAAACCTTGTGACAATCCAATTGGGGATCATTATTTATTGAAGTCGA TTAAGAATAAGATTGATTACTGTAGACTGCATGGGATTGAAATTGTGTATAATT TGGCTCATCTGGATAAGGAACTTGCTGGGTATTGGGCGAAATTGCCTATGAT TAGGAGATTGATGTTGTCACATCCGGAGGTGGAGTGGATTTGGTGGATGGA TAGTGATGCTTTCTTTACTGATATGGTGTTTGAGCTTCCCTTATCCAAGTATGA TAAGTATAATTTGGTTCTTCACGGGTACCCTGATCTATTATTTGAGCAAAAGTC ATGGATTGCAGTGAATACAGGGAGCTTTCTGTTCAGGAATTGCCAATGGTCA TTGAATTTGCTTGATGCTTGGGCTCCAATGGGTCCAAAGGGCCCCATTCGA GAAGAGGCAGGGAAGATTTTGACTGCAAATCTGAAGGGCAGACCGGCATTT GAGGCAGATGATCAATCTGCCCTGATATATTTATTGATGTCTGGGAAGGATCA ATGGATAAATAAGGTGTTTCTTGAGAATTCATTCTATTTGCATGGTTATTGGGC TGGTTTGGTTGATCGGTATGAAGAGATGACTGAGAAGTATCATCCGGGATTA GGTGACGAGAGGTGGCCGTTTGTGACACATTTTGTGGGTTGCAAGCCTTGT GGAAGCTATGGAGATTATCCAGTTGAGAGGTGCCTCAGTAGCATGGAGAGG GCTTTCAATTTTGCAGATAACCAGGTGCTGAAACTGTATGGCTTCAGTCATC GCGGTTTATTGAGCCCCAAGATCAAGAGAATCAGAAATGAGACAGTTACTCC TTTGGAGTATGTAAACAAGTTTGATATACGAAGAGATTCTGCAGGTCGCAGTA AATCACAAAGCTAG
TmCSLC4	ATGGCCCCTAACTCCGTTGTTGTTACTATAGAAAATCCCACCAGTATTTCCGT GAAAGAGATGATGAAAAAGAGTGACTCAGAAAGTCTGTTTCCAGACAAACA GAAAAAGTCAGTATCTTCTAAACAGTTTACTTGGTTCCTGCTATTGAAAGCCC ACAAGGCTTTAACGTGCTTGTCATGGCTGGCCATGGCTTCAAAGTCTTTATG TTCATCTGTCAAAAAGAGAGTGTCCTCCAGTGACATCTCCGAAGAGGAAGA GGAGCATCCAAAGAGTCGTGGGAAATTGTATCGATTCATCAAAGTGTTTTTG TCTATTTCTGTGTTAGCACTTATTGTCGAGATTATCGCCTATTACATGAAATGG AATTTGGGTTCAATGATACAACCATGGGGAATACAAGGCTTTCTGCACTGGT CCTATATGGCTTGGTTGTCTTTCAGACTTGATTACATTGCACCATTGGTTGGC CTGCTATCTCAGTTCTGTATTGTGTTATTCATGATTCAATCATTGGATCGTTTG ATTTTGTGTATTGGATGCTTTTGGATTAAGTACAAAAACTTGAAGCCAAAGAT AGATGAGAATGCATACGATATCGAAGATAACAGTTCCTTCCCTATGGTTTTAG TCCAAATTCCTATGTGCAATGAGCGAGAAGTCTACGAACAGTCTATCGGAGC TGTCTGTCAATTAGATTGGCCAAAAGATAGAATCCTTATCCAAGTTTTGGATG ACTCAGATGATTCCTCTTTACAGTTATTGATCAAGGAGGAAGTTTCCTCATGG CGTCAAAAAGGCGTAAACATCATCTATCGTCATAGATTGATTAGGACAGGGTA TAAGGCAGGGAATATGAAATCTGCAATGGGATGTGATTACGTTAAAGACTATG AGTTCGTGGCTATCTTTGATGCAGACTTCCAACCTAATCCCGACTTTTTGAAA CTGACTATGCCACATTTCAAAGGTGACCCCGAAGTTGGTCTAGTTCAAGCTA GATGGTCCTTTGTCAACAAAGATGAGAACTTGCTTACAAGGTTGCAAAACAT CAATCTTTGTTTTCACTTTGAAGTCGAGCAACAGGTTAACGGTGTTTTCCTTA ACTTTTTCGGTTTCAATGGAACCGCCGGTGTTTGGAGAATCAAGGCTCTTGA GGAATCCGGAGGCTGGCTAGAGAGAACAACTGTCGAGGACATGGATATTGC AGTTAGAGCCCACTTGAATGGGTGGAAGTTTGTCTTTTTGAATGACGTAAAG GTTCTATGCGAACTGCCAGAATCTTATGAAGCATACAAAAAGCAACAACATAG ATGGCATAGTGGTCCAATGCAGTTGTTTCGTCTTTGTCTGCCATCTGTGCTAT CTTCCAAGATATCCGCTTGGAAAAAGGCTAACCTGATCTTTTTGTTTTTCCTT TTGAGGAAATTGATTTTGCCCTTTTACTCTTTCACTCTTTTCTGCATCATCCTA CCTTTGACAATGTTCATACCAGAAACTGAATTACCTCTTTGGGTGATATGTTA

	CATTCCCATATTCATGTCATTCCTTAACATTCTGCCTAGTCCAAAATCCTTTCC TTTTCTGGTGCCTTATCTATTGTTCGAAAACACCATGAGTGTCACTAAGTTTA ACGCCATGATTTCCGGTTTGTTTCAGTTGGGTTCAGCTTATGAGTGGGTTGT AACGAAAAAGACCGGTAGATCATCTGAATCTGACTTACTTGCCCTGGCTGAA AAGGAAGAGAAGATATTGAGAAGGAATTCAGAATCAGGACTGGAAATGCTGT CAAAGCTTAAGGAACAGGAGGAGATTGCACCTCTGAAAAAGGTAACCAAGA AGAAGAAAAACAAGATTTTCCGAAAGGAATTAGCTCTTGCCTTTTTGCTACTT ACGGCTGCTGGTAGATCTCTACTTTCTGCTCAGGGTGTCCACTTCTACTTTT TGCTGTTCCAAGGATTAAGTTTTCTAGTCGTAGGATTAGACCTAATTGGAGAA CAAATGTCTTAA
TmXXT2	ATGATTGAACGATGCCTTGGCGCTCAGCGATCTAGAAAGATCCAGCGTGCTT TGAGACATTGCAAAGTTACGGCACTGTGTCTTGTCTTAACTGTGGTTGTTCT GCGTGGTACTATAGGTGCAGGGAAGTTTGGTACTCCAGAGCAAGATTTTGTA GATATTCGAGATCATTTCTACAGTAGGAAGAGAAGTGAACCACATAGAGTATT GGAAGAGGTGCAAACTACAACCTCCAGTTCCTCATCTTCTGACTCTTCAAAA TCATCAGGGAACAATAACAACTACGAGCAATTTGATGTCAATTCCATATTCGT ACATGAAGGCGAAGATGATAAGCCTGACCCTTCAAAGCCTTACAGTTTGGG ACCAAAGATTTCCGATTGGGACGAGCAGAGGTCACAATGGCTTAAACAAAAT CCAGATTTTCCAAACTTTGTCCAGCCTTCTAAACCCAGAGTTCTGTTAGTCA CCGGTTCATCCCCTAAGCCTTGCGAGAATCCAGTGGGAGATCATTACCTTTT GAAATCCATCAAAAACAAGATTGACTATTGTCGTGTGCATGGGATCGAGATTT TCTACAATATGGCACTACTGGATGCTGAAATGGCCGGATTCTGGGCAAAGTT GCCACTTATTCGAAAACTATTGTTATCTCACCCTGAAGTTGAGTTTTTGTGGT GGATGGATTCTGACGCTATGTTTACAGACATGGCTTTTGAACTACCTTGGGA AAGGTACAAGGATGTTAATCTGGTCATGCACGGTTGGAACGAAATGGTGTAT GACGAGAAAAACTGGATTGGATTGAATACTGGAAGTTTCCTTTTGAGAAACA CTCAATGGGCATTAGACTTGTTAGATGTTTGGGCTCCAATGGGACCCAAAGG AAAGGTTAGGGACGATGCTGGCAAGATTCTAACCAGAGAATTGAAAAACAG GCCAGTCTTTGAGGCCGATGATCAATCTGCTATGGTCTATTTGTTGGCTACC CAACGTGAGCAATGGGGTAACAAAGTTTACTTGGAGAATGCCTACTATCTAC ACGGTTATTGGGGTATCTTAGTAGACAGATATGAAGAGATGATTGAAAACTAC CACCCTGGCTTTGGAGATCACAGATGGCCCTTGGTTACTCACTTCGTGGGA TGTAAACCCTGTGGAAAGTTCGGTGACTATCCCGTCGAAAGATGTCTTAGAC AGATGGACAGAGCCTTCAATTTCGGAGACAATCAGATTTTGCAAATCTATGG TTTTACGCATAAGACATTAGCTTCCAAAAGAGTTAAGCGTGTTAGAAACGAAA CATCTATGCCATTGGAGGTTAAAGACGAACTGGGTCTGATACACCCACCTTT CAAGGCCGTAAAGGTTGCTAGTGGTTAA
TmUGD	ATGGTAAAGATTTGTTGTATAGGTGCCGGTTACGTTGGAGGGCCTACTATGG CCGTTATTGCATTGAAATGTCCTAACATTGAAGTCGCAGTGGTGGACATCTC TGTCCCAAGGATTAACGCCTGGAATTCAGAACAACTGCCAATCTACGAGCCA GGTTTAGATGATGTGGTCAAGGAATGCAGAGGTAGAAACCTGTTTTTCTCCA CCGACGTTGAGAAACATGTGTCAGAGGCTGATATTGTCTTTGTTTCTGTAAA CACACCTACAAAGACACAAGGACTTGGTGCTGGAAAAGCTGCAGATCTGAC CTATTGGGAATCCGCAGCTCGAATGATTGCAGATGTCAGTAAGTCCTCCAAA ATCGTGGTGGAAAAGTCTACTGTCCCTGTGAAAACTGCCGAAGCTATCGAG AAAATCTTAACACACAATAGTAAAGGTATCAGTTTCCAGATCCTATCTAACCCA GAGTTTTTGGCCGAGGGGACAGCTATAGAGGATTTGTTTGGTCCAGATAGG GTTCTAATTGGGGGTAGAGAGACTCCAGAAGGAGCTAAGGCAATCAAGGCT CTAAAGGATGTGTACGCACATTGGGTTCCAGAGGACAGAATCATTTGCACGA ACTTATGGTCCGCCGAGCTTTCTAAGCTGGCCGCAAATGCCTTTCTGGCCC AGAGAATCTCTTCTGTGAACGCTATGTCTGCATTATGCGAAGCTACTGGTGC AAATGTGTCCGAGGTTTCTCATGCTATTGGTAAGGACACTCGTATCGGAGCT AAGTTTTTGAACGCCTCAGTTGGATTCGGCGGTTCATGTTTTCAGAAAGACA TCCTGAATCTGGTCTACATTTGTGAATGCAATGGCTTGCCTGAGGTTGCTAA CTATTGGAAGCAAGTAATCAAAGTTAATGACTACCAAAAGTTTAGATTCGTGA ATAGGGTAGTTAGTTCAATGTTTAACACGGTTTCCGCCAAAAAGGTTGCCATA

	TTGGGATTTGCATTCAAAAAGGACACTGGAGACACAAGAGAAACCCCTGCA ATTGACGTTTGTAACGGATTACTAGCTGACAAAGCTCAGCTTTCTATCTACGA CCCTCAGGTCACGGAAGATCAGATTAGGAGAGATCTAGCTATGAAAAAGTTT GATTGGGATCACCCCGCTCACCTTCAACCTATGTCTCCCACCGACACTAAG CAGCAAGTTACTGTTGTTTCAGGTGCTTACGAAGCTACGAAAGATGCACATG GCATTTGCTTTCTGACTGAATGGGACGAGTTCAAAACATTGGACTTTCAAAA GATATACGACAATATGCAAAAGCCAGCTTTCGTATTTGACGGCAGAAACATTG TTGATCTTGAAAAGCTGAGACAAATTGGTTTCATAGTTTACTCTATTGGAAAA CCATTGGACAGTTGGTTGAAAGATATGCCAGCCGTCGCTTAA
TmUXS	ATGGCTTCCGAATTGATATACAGAGGCCATGAGACTGATCAACCTGTTTCCG ATTGGTATTCTCCCAAGAGGATCAAGCCTTGTTTTGCTGTTACACAATCAATT AGATATCTGTTAAGAGAGCAAAGATTGATATTCGTTATAGTCGGTATGGTGCT GGCTACTTTGGTATTTGCCTTTTTCCCACACTCCTCTAGATCCACGAATCTTC CAGACTATGTTGATCCTATTAGTGGTTCTGATTCCTATTACCCTATACAAACTC AGAAAAAGACTAATCTGGAATATCTGAACAGGGTGGGATTCGGCTCTGCAG GGGGCAAAGTGCCATTAGGATTGAAACGAAAGGGGTTGCGTATTGTCGTCA CGGGTGGGGCTGGTTTTGTTGGATCTCATCTTGTTGACCGTTTGATTGCCA GAGGTGATTCTGTAATCGTAGTAGACAACTTTTTCACAGGTAACAAGGAAAA CGTAATGCATCACTTTGGTAATCCTAACTTTGAATTGATAAGACACGATGTAG TGGAACCACTATTGCTTGAAGTAGATCAAATCTACCACCTTGCATGTCCAGC TTCTCCTGTTCACTACAAATTCAATCCTGTTAAGACCATTAAGACCAATGTCG TGGGAACCTTAAACATGTTAGGATTGGCCAAACGTGTTGGTGCCAGATTCCT GCTAACCAGTACTTCAGAAGTTTATGGTGACCCATTGCAACACCCACAGGTT GAGACTTATTGGGGAAATGTTAATCCCATTGGTGTTCGTAGTTGCTACGATGA AGGCAAAAGGACAGCTGAAACCTTAACAATGGATTATCACCGAGGGGCTGG AGTGGAGGTTAGAATTGCCAGGATCTTCAATACTTATGGCCCCAGAATGTGT ATTGATGATGGCCGAGTTGTTTCTAACTTTGTAGCTCAGGCATTACGTAAGGA GCCAATGACCGTCTATGGTGATGGTAAGCAAACTAGAAGTTTCCAATTCGTAT CAGATTTGGTTGAAGGATTGATGCGACTTATGGAAGGTGAACATGTCGGGC CTTTCAACTTGGGTAATCCCGGAGAATTCACCATGCTTGAACTAGCTAAAGT CGTGCAGGAAACTATAGACTCAAATGCTAAGATCGAATTTCGTCCTAACACA GAGGATGATCCACATAAGCGTAAGCCAGATATCACCAGAGCCAAAGATCTAC TTGGCTGGGAGCCCAAAGTCTCACTGCAAAAAGGTCTGCCTCTTATGGTTG CCGACTTCAGACATAGGATTTTCGGTGACCATAAGGAGGGATCAACCACTAC GACCACTACAACTACTACAACCACGAAAAACTCATCATAA
HsSLC35D1	ATGGCGGAAGTTCATAGACGTCAGCATGCTCGGGTTAAAGGAGAAGCCCCC GCGAAATCCTCCACACTCCGAGATGAGGAGGAGCTGGGGATGGCGTCGGC CGAAACGCTGACCGTGTTTCTGAAGCTGCTGGCCGCCGGCTTTTACGGCG TGAGCTCCTTCCTGATCGTGGTGGTGAATAAGAGCGTGCTCACCAATTACA GATTTCCCTCCTCACTATGTGTTGGACTTGGCCAGATGGTGGCCACAGTGG CAGTTCTCTGGGTGGGAAAGGCGCTCAGAGTAGTCAAGTTTCCTGACCTTG ACAGAAATGTACCTCGAAAGACGTTTCCACTACCTCTACTATATTTTGGGAAC CAAATCACGGGACTGTTCAGCACAAAGAAACTGAACTTGCCAATGTTTACAG TTCTGAGAAGGTTCTCCATCCTGTTTACAATGTTTGCTGAAGGAGTTTTACTC AAGAAGACTTTTTCTTGGGGTATTAAAATGACTGTATTTGCAATGATTATTGGA GCCTTTGTAGCTGCCAGCTCTGACTTGGCATTTGATCTGGAAGGATATGCTT TTATTCTGATAAACGATGTCCTAACAGCAGCAAATGGTGCATACGTAAAACAA AAATTAGATTCAAAAGAGCTGGGAAAATATGGACTGCTCTATTACAATGCACT GTTCATGATTCTGCCCACCCTGGCCATTGCGTATTTCACAGGAGATGCACAA AAGGCTGTGGAGTTTGAAGGCTGGGCTGACACCCTCTTTCTTCTGCAGTTC ACCCTCTCCTGTGTGATGGGGTTTATCTTAATGTACGCCACAGTACTCTGCA CGCAGTATAATTCTGCTCTTACAACTACAATAGTTGGCTGTATTAAGAATATAT TAATAACTTATATTGGAATGGTCTTTGGTGGAGATTATATTTTCACGTGGACAA ACTTCATTGGTTTAAATATCAGCATTGCTGGGAGCCTGGTATATTCCTATATCA

	CTTTCACTGAAGAGCAGCTGAGCAAACAGTCAGAGGCTAATAACAAGCTGG ACATTAAGGGGAAAGGAGCAGTGTAA
TmXXT5	ATGGGTCAGGAGATTTTCACGCCTCAAAAGCGAGCTTCCGGTGGCGGAGG CGGTCTACCGACGACCACCGCAAATGTTAATCGAGGTCGAGCGGCGCCAC GTGGGAGGCAGATCCATAAGACATTTAACAACATTAAGATTACGCTTCTCTGC GGTTTCGTTACCATCCTCGTCCTCCGTGGGACAATCGGCGTCGGTAATCTC GGTGGATCTGATGACACCGTCAACCAGAATATAATCGAGGAGACTAATCGGA TCCTTGCGGAGATTAGATCCGATTCCGAACCCGGTGATCCCGAAGGAAACG CTGAAGTTTTTATGAACCCTAACGAGACCTACGCACTTGGTCCGAAGATAAC GAATTGGGATGACGAAAGGAAGGTATGGCTTACTCAAAACCCTGAATTTCCT AGTCTTGTTCATGGTAAAGCTAGGATTCTCCTTGTAACTGGATCGCCTCCAA AACCCTGTGATAACGCGATTGGGGATCATTACTTGTTGAAAGCGATTAAGAA CAAGATTGATTACTGTAGACTTCATGGGATAGAGATAGTGTATAATTTGGCTC ATTTGGATAAAGAACTTGCTGGATACTGGGCAAAACTTCCATTGATTAGGAA GTTAATGTTATCTCATCCTGAAGTAGAGTGGATTTGGTGGATGGATAGTGATG CTTTATTTACAGACATGGTTTTCGAAATCCCCTTATCTAAATACGAAAAGTCGA ACCTAGTCATTCATGGGTATCCAGATTTGTTGTATGATCAGAAATCATGGATT GCTTTGAACACAGGAAGTTTTCTGTTCCGGAATTGTCAGTGGTCGTTGGATT TGTTGGACGTTTGGGCACCTATGGGGCCTAAAGGTCCTATCCGAGAGGAGG CTGGAAAAGTTCTAACtGGGTTTTTGAAAGGCCGACCAGCTTTCGAAGCCGA CGATCAATCCGCTTTGATTTACTTGCTTCTTTCTCAGAAAGATAAATGGATGG ACAAGGTGTACGTAGAGAATCAGTACTATTTGCACGGtTTCTGGGAAGGATT GGTCGATAGGTACGAGGAAATGATGGAGAAGTATCATCCTGGATTAGGTGAC GAAAGGTGGCCTTTCGTTACCCATTTCGTCGGCTGCAAACCTTGCGGGAGC TACGCGGATTACGCGGTCGAGCGATGCTTGAAGAGCATGGAAAGAGCTTTC AATTTCGCAGATAATCAAGTTCTTAAACTGTATGGATTCGGGCATAGAGGGTT GTTGAGTCCCAAGATTAAGAGGATCAGGAATGAGACGAGTACACCTTTGGA GTTTGTAGAAAGGTTTGATATTCGCAGATCAGCTGGACACGTTGGAAAAGTT GGATCATAG
AtUXS3 At5g59290	ATGACATTTAATGCGTACTCAGGATTGAGATCTCTCTCTCAAGCAATGGCAG CTACAAGTGAGAAACAGAACACCACAAAGCCTCCTCCTTCTCCTTCTCCTCT CCGCAATTCCAAGTTTTGTCAGCCCAATATGAGGATCTTGATCTCTGGAGGA GCTGGCTTCATTGGTTCTCACTTGGTTGATAAGCTTATGGAAAATGAGAAGA ATGAGGTGGTTGTTGCTGATAACTATTTCACTGGCTCAAAAGAAAACCTCAA GAAGTGGATCGGTCACCCCAGGTTTGAACTTATTCGTCACGATGTTACCGA GCCTTTGTTGATCGAGGTTGATCGGATTTACCATCTTGCTTGTCCTGCCTCT CCTATCTTCTACAAATACAACCCTGTTAAGACAATCAAGACCAATGTGATTGG TACACTCAACATGCTCGGTCTTGCCAAGCGTGTTGGAGCAAGAATTTTACTA ACCTCAACCTCTGAAGTGTATGGAGATCCTCTCATCCACCCTCAACCAGAGA GCTACTGGGGAAATGTCAACCCTATTGGGGTTCGGAGTTGCTATGACGAAG GCAAGCGGGTAGCCGAAACCTTGATGTTTGACTACCACAGACAACATGGCA TTGAAATCCGCATTGCTAGAATCTTCAACACATATGGTCCTCGAATGAACATC GATGATGGGCGTGTTGTGAGCAACTTCATTGCTCAAGCACTCCGGGGTGAG GCATTGACAGTTCAGAAACCGGGGACACAGACCCGCAGTTTCTGTTATGTC TCCGACATGGTGGATGGACTTATCCGTCTTATGGAAGGCAATGATACTGGCC CTATCAACATCGGTAACCCAGGTGAGTTCACAATGGTGGAACTGGCTGAGA CGGTTAAGGAGCTTATTAACCCAAGCATAGAGATAAAGATGGTGGAGAACAC ACCAGATGATCCAAGACAGAGGAAACCAGACATTAGTAAAGCCAAAGAAGT GTTGGGTTGGGAGCCAAAGGTGAAGCTCAGAGAAGGACTTCCTCTCATGG AAGAAGATTTCCGACTAAGGCTTAACGTCCCAAGAAACTAA
AtUXT3 At1g06890	ATGAGCGAGGGCCAGAAGTTCCAGTTGGGAACAATCGGCGCTTTGAGTTTG TCCGTTGTGTCATCTGTCTCGATTGTGATCTGTAACAAAGCGCTTATTAGCAC CCTTGGCTTCACATTCGCGACTACTTTGACAAGTTGGCATCTTTTGGTCACA TTTTGTTCCCTTCATGTGGCATTATGGATGAAGATGTTCGAACACAAGCCTTT TGATCCACGAGCTGTGATGGGATTTGGCATATTGAATGGGATATCCATAGGA

	CTATTGAACCTCAGCCTGGGCTTTAATTCTGTCGGTTTTTACCAGATGACTAA ACTAGCTATCATCCCCTGCACTGTTCTCTTGGAGACCCTCTTCTTCAGGAAA AAGTTCAGTCGAAAAATCCAGTTTTCATTAACCATCCTTCTCCTTGGTGTTGG AATTGCAACCGTCACAGATCTTCAACTTAATATGCTGGGTTCTGTCTTGTCGC TGCTGGCTGTTGTCACAACTTGTGTTGCTCAAATTATGACAAATACCATCCAG AAGAAGTTCAAAGTTTCATCCACGCAGCTTCTGTATCAGTCTTGCCCATATCA AGCAATCACTCTTTTCGTCACTGGGCCATTTTTAGATGGGCTCCTAACCAAT CAGAACGTGTTTGCTTTCAAGTACACTTCTCAAGTAGTGTTCTTCATCGTCCT GTCTTGCCTCATATCAGTCTCTGTAAACTTCAGCACATTTCTTGTCATTGGAA AAACATCTCCTGTCACATATCAGGTTCTAGGACATCTCAAAACATGCCTGGTT CTAGCATTTGGCTATGTGTTGCTGCGAGACCCATTCGACTGGCGCAACATTC TCGGTATTCTAGTGGCTGTGATTGGAATGGTTGTTTATTCCTATTACTGCTCG ATTGAGACTCAGCAGAAGGCAAGTGAAACCTCAACTCAGTTGCCTCAGATG AAAGAGAGCGAGAAGGATCCGCTAATAGCAGCTGAAAATGGAAGCGGAGTG TTATCAGATGGCGGCGGGGGAGTGCAGCAAAAGACGGTGGCTCCTGTATG GAACTCAAATAAAGATTTTCAAGCCTAA
AtUUAT1 At5G04160	ATGTCGTCGTCTGCGAAGAAACAAACCCTGTTCATATCGACATTAATCATCTC ATGGTACTCTTCAAACATCGGTGTTCTTCTCCTCAACAAGTTCCTTCTCTCGA ATTACGGATTCAAATTCCCGATTTTTCTCACAATGTGTCACATGTCCGCTTGC GCTATCCTTAGCTACATCTCCATTGTTTTCCTCAAGCTTGTTCCTCTCCAACA TCTCAAATCTCGTTCTCAATTCCTTAAGGTTGCTACTCTCAGCATCGTCTTTT GTGCTTCCGTCGTCGGTGGTAACATCTCCCTTCGTTACCTTCCTGTCTCTTT CAATCAAGCCGTCGGTGCTACGACGCCGTTTTTCACGGCTCTGTTTGCTTAT CTTATGACCTTTAAGAGAGAAGCTTGGGTTACTTATGGTGCTCTCGTCCCTG TCGTCGCCGGTGTCGTCATCGCCAGTGGGGGTGAGCCAGGATTTCACTGG TTTGGGTTCATAATGTGCATTAGTGCTACTGCGGCAAGAGCCTTTAAATCTGT TCTTCAAGGCATCTTACTTTCTTCAGAGGGGGAAAAATTGAACTCAATGAATT TGATGTTGTATATGTCTCCCATAGCTGTCATTGCTCTTCTTCCCGTTACGCTAT TTATGGAACCAGACGTGATCAGTGTGACCTTGACGCTTGCAAAACAACATCA GTACATGTGGATACTTCTTCTGGTTAACTCTGTCATGGCTTATTCAGCCAATC TGTTGAATTTTCTGGTTACCAAACACACAAGCGCCCTCACCCTCCAGGTTCT TGGAAATGCTAAAGGAGCAGTTGCAGTGGTGATTTCTATCTTGATCTTTCAAA ACCCGGTTACGGTTATGGGAATTGGCGGGTACTCCATAACCGTCCTTGGGG TGGTTGCTTATGGAGAGACAAAACGCAGATTTAGATGA
OsCSLC2 LOC_Os09g25900.1	ATGGCGCCGCCGGGGGTGGGGGTGGGTGTGGCGTACCTGTGGGGGAAG GGGAGGGGTGGGCGGAAGGGGACGCCGGTGGTGGTGACCATGGAGAGT CCCAACTACTCGGTGGTGGAGGTCGACGGGCCCGACGCGGAGGCGGAGC TGCGCACCGCCGCGGTGGCCATGGACAAGGGCGGCGGGCGTGGCAGGA GCAGGAGCAGGACCGCCAGGCAGCTCACCTGGGTGCTGCTCCTCCGCGC GCGCCGCGCCGCCGGCCGCCTCGCCTCCTTCGCCGCCGCCGCGGCGAG GCGCTTCCGGCGCTCCCCCGCTGACGCCGCCGACGAGCTCGGCCGCGGC CGGGGACGGCTGATGTACGGGTTCATCAGGGGGTTCCTGGCGCTCTCCCT GCTCGCCCTCGCCGTGGAGCTCGCCGCCTACTGGAACGGGTGGCGCCTC CGGCGGCCGGAGCTGCATGTGCCGGAGGCGGTGGAGATCGAGGGGTGG GCGCACTCGGCGTACATCTCGTGGATGTCATTCCGAGCCGACTACATCAGG AGGCCAATCGAGTTCTTGTCGAAAGCTTGCATCCTCCTCTTCGTCATCCAAT CCATGGACCGTCTCGTCCTTTGCTTGGGTTGCTTCTGGATCAAGCTGAGGA AGATCAAGCCGAGGATTGAAGGGGACCCGTTCAGGGAAGGATCAGGGTAT CAGCACCCCATGGTGCTCGTCCAGATTCCTATGTGCAATGAAAAGGAGGTC TATGAGCAGTCGATTTCGGCGGCTTGCCAGCTAGATTGGCCCAGGGAGAAG TTTCTGATTCAGGTGCTCGACGATTCCAGCGACGAGAGCATTCAGCTGCTG ATCAAGGCAGAAGTTTCCAAGTGGAGCCATCAGGGTGTGAACATTGTGTAT CGGCATCGGGTGCTGAGGACCGGTTATAAAGCTGGGAACCTCAAGTCTGCA ATGAGCTGTGACTATGTCAAAGATTATGAATTTGTCGCCATTTTCGACGCGGA CTTCCAGCCAACACCAGATTTTCTCAAGAAAACGATACCACATTTTGAGGGG AATCCTGAGCTTGGATTGGTTCAAGCACGATGGAGCTTTGTGAACAAGGAT

	GAGAACCTCTTGACCCGTCTTCAGAATATCAACCTGTGCTTCCACTTTGAAG TAGAGCAACAGGTCAATGGAGTCTTCTTGAACTTCTTTGGTTTCAATGGAAC TGCTGGAGTTTGGAGGATCCAAGCTCTAGAAGAATCCGGGGGGTTGGCTTGA GAGGACGACGGTGGAGGATATGGATATTGCTGTTCGAGCACACCTGAATGG ATGGAAATTTATCTTCCTCAATGATGTAAAGGTCCTGTGTGAACTCCCAGAAT CCTATGAAGCATATAGGAAACAGCAACACCGGTGGCATTCTGGTCCAATGCA CCTTTTCCGGCTGTGCCTTCCGGACATACTTACTGCCAAGATCTCATCATGG AAGAAGGCGAACTTAATACTATTATTCTTTCTTTTGAGGAAATTGATTCTTCCG TTCTATTCATTCACATTGTTTTGTGTCATTCTTCCGCTGACCATGTTTGTTCCT GAGGCTGAGCTGCCTGTTTGGGTCATCTGTTATGTGCCAGTTTGCATGTCCT TCCTGAACATTCTGCCATCACCAAGATCATTTCCTTTCATTGTGCCATACCTC CTTTTCGAGAACACCATGTCAGTGACAAAATTCAACGCAATGGTGTCTGGAC TGTTTAAACTTGGAAGCTCCTACGAATGGATTGTCACAAAGAAGTCTGGTCG ATCATCAGAATCAGATCTTTCAACAGCAGCGGAGAGGGATACAAAGGATCTT ACCCTTCCTCGGCTGCAGAAGCAAATATCTGAAAGTGAATTGATTGAGCTCA AAATGCAGAAAGAACGCCAAGAAAAGGCGCCGCTTGGTGCAAAAAAGGCTA ACAAAGTCTACAAGAAGGAGCTTGCTCTCTCTCTTCTCCTCCTCACCGCCG CAACTCGGAGCCTCTTGTCTGCTCAAGGAATTCACTTCTATTTCCTTCTCTTT CAGGGGGTATCATTCCTTTTTGTTGGCCTCGATCTAATTGGAGAACAGATAG ACTGA
OsXXT1 LOC_Os03g18820.1	ATGTGGGTTGCCGAGAGAGTTGTCGGAGAAAGAAGAATGAGAGAGATCCA GAGATTCGCCAGAAACGCCAAGTTGACCGTTGTCTGTTTGTTGTTGACCGT CGTCGTCTTGAGAGGTACTGTTGGTGCTGGTAAGTTCGGTACTCCACAGCA AGACTTGATCGAGCTGAGACACAGATTCATCTCTCACCCACATAGAGCTTTG GCTGAACACCACGATGCTTTGTCTAGAGGTGGTGGATCTTCTTCATCTTCCG GTAGAGCTGCTCAAAGAGATGACGAACCAGATCCACCTCCAAGAACCTTGA GAGATCCTCCATACACTCTGGGTCCAAAGATTTCTGACTGGGACGAACAAA GAGCTGCTTGGCATAGAAGGCATCCAGAAACTCCACCATTCGTCAACGACG TTAAGCCAAGAGTTTTGCTGGTTACCGGATCTTCCCCAAAGCCATGTGAAAA CCCAGTTGGTGACCACTACTTGCTGAAGTCCATCAAGAACAAGATGGACTA CTGCAGAGTGCACGGTCTGGAAATCTTCTACAACATGGCCTTGTTGGACGC TGAGATGGCTGGTTTTTGGGCTAAGTTGCCTTTGTTGAGAGCCTTGTTGTTG GCTCACCCAGAGATTGAATTCTTGTGGTGGATGGACTCCGACGCTATGTTCT CCGATATGGCTTTTGAACTGCCATGGGAGAGATACGGTCCATACAACTTGAT TATGCACGGTTGGGACGAGATGGTCTACGATGACAAGAACTGGATCGGTCT GAACACCGGTTCTTTCTTGTTGCGTAACTGTCAGTGGTCCTTGGACTTCTTG GATACTTGGGCTCCAATGGGTCCTAAGGGTCCAGTTAGAATTGAGGCCGGT AAGGTCTTGACCAAGTACCTGAAGGACAGACCAGTTTTCGAGGCTGATGAC CAATCCGCCATGGTTTACATTTTGGCTACTGAGAGGGAAAAGTGGGGTGAC AAGGTTTACTTGGAGAACGGTTACTACCTGCACGGTTACTGGGGTATCTTGG TTGACAGATACGAAGAGATGTTGGAGAACTACCATCCAGGTTTGGGTGATCA CAGATGGCCATTGGTTACTCACTTCGTTGGTTGTAAGCCATGCGGAAAGTTC GGTGACTACCCAGTTGAGAGATGCCTGAAGCAAATGGAAAGGGCCTTCAAC TTCGGTGACAACCAGATTCTGCAGATGTACGGTTTCACCCACAAGTCCTTG GGTTCCAGAAAGGTCAAGAGAATCAGAAACGAGACTTCTAACCCACTGGAC GTCAAGGACGAATTGGGTTTGTTGCACCCAGCTTTCAAGGCTATGAAGACTA CCTCCACTTAA
KnCSLC126 kfl00126_0150_v1.1	ATGTTCGCCTTTATTGTCCAGAGCATCGACAAGCTGCTGCTGATAACGGGGT ACTTTTACATCAGTTGGAAGCAGCCAACTAAGGAGGGGGACTCAGGCTCCC TAGCAGTCGGAGATTGTGGGGGCAATGAAGAGAAGCCTGCATTCGAGCCG GTTGTGCTGGTGCAGATCCCGATGCGCAATGAAAGGGAGTGTTACAAGCGG GGTATCATGGCGGCATGCCGGCTGGATTGGCCTCAGGATAAACTGGTGGTA CAGGTTTTGGATGATTCCGACGACCCAGACATGCAGCAGCTTGTCCGTGAC GAGGTCGATGCTTGGCGCGCGGTGGGGGCTCCCATCAGATATACGCACCG CACGGCGCGGACGGGGTTCAAAGCTGGTGCCCTGGCGCACGGAATGCAG GACCCTGCGATCCAGCACTGCGAGTACGTTGCCATCTTTGACGCCGATTTC

	GTGCCGGCCAAGGATTTCCTCCGGAGGACGGTGCCAAAGTTTGAGGGGCA GCCAAAGCTGGCCCTTGTGCAGGCCCGGTGGGCGTTTGCCAATGCGCAGC AGAACTTGCTGACGCGATTCCAGGTCATCAGCATGTCGTACCACTTCGAAG TGGAGCAACAGGTGCAGAACCACTTCAACGCGTTCTTTGGCTTCAACGGGA CGGCGGGCGTGTGGCGAGTTCAGGCGCTGCGAGAAGCAGGGGGGTGGCT CGCGAGAACGACCACTGAGGATATGGATCTAGCGGTGCGTGCCCACATGAA AGGCTGGAATTTCACGTACCTGAATGACGTCACGGTGCCCTCGGAGCTGCC CTGCACGTACAAGGCCTACTGCAAGCAGCAGCAAAGGTGGCACGCAGGCC CCGCGCGCCTGTTCATGCTGACGTGGCACCGCTCGCTGACGTGTCCCACG CTGAGCGCGTACCAGAAGTTCAACCTGCTGGTCTGCTTCTTCTGGTTCCGC CGCTTCGTGCTTCCGGTCACCGGATTCCTGCTCTACTGCATCATAATGCCGC TCGCCGTGTTACTGCCCGAGGCATCGCTGCCGCTCTGGTTCCTTGCTTATAT GCAGACACAGGCGATCCTGCACTGGCTGCCGCACCGCGGGAGCTGGTGC CTCTTGTTCCCCTACTACGCCTTCGAGAACGTCATGTACCGTGTCAAAGCGC AGGCCATTTTCAGCGGCCTCTTCAACCTACGCAGCGCCCACGTGTGGGTC GTCACTGCCAAGACTGGAATCGACGCCAAGACCGAAAACATCCAATCGGGG GGGTCAAAATGCGTGGGAAAAGAGGGGGGGGTGGCCAACGACGCGGAGC CGGTGAGCCCCGTTTCGGAGGGCTCGTCGGATGACGCGTTCGTGGCGCA CGCTAGCATGGATCCGCTCATAGCGTATGATCTGCCAGAACTAAGGGTGGG GCTAAAAGTGAGGACGGCGCACGGGCGCGGTGAGGAGACGAGCGGCCAT TGCACGGGGCTCGACTCCTCCGCAAAACGACGGGACTTCGGCCACGTGTC AAGCCCGATGAAGCGGGGCTTGTGGAGCCCGTCTGCCGGGCGGAGACTC TCTTTGCTGACGCCGACGGAAGAGAGGGCGGAGAGGGACCCGTCGCTGC TGACGTCATTCGAGGCCGGGGCCGCGTGGCGCCTGGAGCGGACGCTGTAT AGGCTGCCGTCGCTGCGGGAGGTGTGGGAGAAGGTGACGTGGGCCAACG TCAGGGGATTCATGGCAGTGCGAACGTTACACGTGCCAGAACTAGGATGGG CCGCGTTTGTGTTTGGCGCCATGACGTATGGTATAAGCGCCGGACGGTATG GGCTCTCCGTCTACTTGGGCATGCAAGGCTTGGGATACCTGATCGCGGGGC TTGACTTGATGGGCTACTAA
KnCSLC 271 kfl00271_0180_v1.1	ATGGGGCAAAGGAAGACTGACGCTGGGTTGCAACAGGAAGAGGGAACCCC CAAGAAGAGAGCACACCTCGTGAACTTTAGGAAAGTTCAGAGCATAGGGTT GCAAGTGGGATTCTTTGTGTTGCTGTGTTGGGCCCTGTCGCGCCTTGTGTA CGGCGGTACTCTTGATGCTGGCACGGCATCGAGAGGTTGGAAGGAGTTCC GAACGAGATGGGTGCTGCCGCTGATGCAGCCAGTGCTCAACTTCCTGGTG GGGGCGTTCCTGCTCCAGAGTGTTGACAAGGTGTTGCTGGTAGCGGCCGG TGTGTACCTCGGGTTGCGGCGGTCCGGGAAGGCGGGTGCCCCTTCTGTG GCAGCTGCCACCACTCAGGACGAGGGGACGGTGGTGGGCATGCCAGCGT ATGAGCCGGCTGTGGTGGTGCAAATCCCCATGTGCAACGAGCGGGAGTGC TACCGTCAGAGTATCACCGCGGCGTGCAGGCTGGACTGGCCCCAAGACAA GCTTGTGATACAGGTGTTGGACGACTCCGACCAGGACGACGTGCAGGCGC TCATTCACGAGGAGGTAGACGCCTGGCGCGCAACGGGCGCCCCCATCTTC TACCTGCACCGCGCGGTGCGGGCGGGGCACAAGGCGGGCAATCTGGCAC ACGGCATGCAGGACCCCTCCGCCAAGCACTGCGAGTTTGTGGCCATCCTG GATGCCGACTTTGTGCCAGCCAGCGACTTCCTCCGGAGGACAGTTCCGCA CTTTGAGGGACAGCCGAAGCTGGCGCTAGTGCAGGCACGGTGGGCGTTTG TGAACCCGCGGCAGAACCTGCTGACGCGCTTCCAGAACATCCACTTCGCG TATCACTTCGAGGTGGAGCAGCAGGTGCAGGGCCACTTCAACAAGTTCTTT GGCTTCAACGGCACCGCCGGCGTCTGGCGGGTGCAGGCGCTGCAGGACG CGGGCAGCTGGAACGACAGGACCACAGTGGAGGACATGGACCTGGCAGT GCGCGCCCACATGCTCGGCTGGGAGTTCACGTTCCTGAACGACGTGCGGG TGCCGTCGGAGCTACCCGCCAGCTACGTGGCCTTCTGCAAGCAGCAGCAC CGCTGGTATGCAGGCCCCATGCGGCTGTGCCTGCTGACGGCCGGCTCCAC GCTGGCGTCCCGCACGCTGACGGCGTGGCACAAGTTCAACCTGCTGGCGT GCTTCTTCGGCCTGCGCCGCCTGGTGCTCCCCCTCGCGGCGTACCCCCTC TTCTGCCTGCTGCTCCCCGCCACCGTGCTCGTCCCCGAGGCCACCGTGCC CGCCGCCGTCGTCTACGCCATGCCCCTCCTCCTCGCCTTCCTGCACTGGCT

	CCCGCACCCCGGGTCGTGGCCGCTGCTGCTGCCGTTCCTGGTGTTTGAGA ACGTGCTGTACCGCATCAAGTTCCAGGCCATCGTGAGCGGCGTGCTCGGC TTCAAGGGCGCCTCCGACTGGGTGGTCACCGCCAAGACGGGCGCCGTGC AGGAGGCCGACGAATTCGACGACGATCTGGACGGCGGCCTGGAGGACGT GCCGGAGGGTATCGAAGTCGAAGACGGCGCGCTCGGGGAGGCGCGCGAC GGGGACTCGGTCAGCCCGTGCTCGGCCAAGTCGGTGGACGCGTTTGTGG TGCACGCGGGCAGCGAGAGCAGCGACCAGCTGGCGGCGTACGACCTGCC GCCGCTCGCCGCGGGGCTGACCGTCAGGACCGGGCGGGAGCCGAGCGT GATGGGGGGCAAGAAGGGGGCGTTCCGGAGCGCAAGCCTGCCCCCCCAG ATGAAACGGCAACTGTCGGGCGCTGCTGAGCGCGCTCTGCTGAGTCCGAG CGCGAGCAGGAGACGGCCGGGGGGCACCCCGCGGAAGGGCGACGCGGC GTCGCTGCTGACACCCCGCGGCCGCGAGGTGGCGCTGAAGCGGCTGGAG CGGACGCTCTCGCGGCTGCCGTCCATGCAGCAGGTGCGGCAGAGGGTGA CGTGGGCCAGCTGCAAAAGGTTCTGGGCGGCGAGAAAGGTGCAGGGGCC GGAGATGGGGATGGCCGCTTATATGCTGGGCGCAGCGGCGTATGGCGTGG CTGTGGGCGACACGAGGTATACGCTCTTCCTCGTGGTGCAGGGAACGGGG TTCCTGGTGGCAGGCCTGGACCTGCTGGGCTGCTGA
KnCSLC 603 kfl00603_0080_v1.1	ATGCCCGCCCGTTGTCGGCCAAGCATGCCGCCTTCCTCCCTCTGCTGCGG CTGCGGTCTGTCCTGCTCTCCACCAAGGGCCTGGCACCGCTTGCAAAAGT TCCCCCTCAGCCGTGCACGCCAGGAGGCTGGAGGCCCTTCCCTGCGCCC GGCTGTCTCTTTCTGCTTTCTTGGCCTGCCTGGAGGCGCGGTGCCTCTTGC CGCCACGTTTCGCTGCCTCTTCCTGCCTCCTGCTGGCCCCTCCGCCATTGT CGTCTTGCTGAGTTCGCTGTCCCTTTCTTCATCCCACTTCGCTCCTGCTGTT CCTCACCGTCCGCCTGCTGCCATGGGGCGGCCCTCGGAGGGATCCCCTGC TGCTGCGGCCCCCCGCTCCCACCGCCAGCAGCAGCGCAAGGGCAATAAG CAGCCGCCCGCCCTCCCTACGCGCGCCCCCTTTCTGCGGCGCGGCTGGC GGGTGCCATGGCGCAGTGCGATGGTGACGCTGCTGGCGGGCGGCGCCGC GGTGGGCGTGAGCCTGGTGGCGTGGAGCGTGCTGTACGTCAGCGGCGCC GCGCTTGCGGCCGCGGTGGCCGGGGAGAGCCACCCGGGCACGCCGCTG GAAGGGTGGCGCTACGCGCGCGCCAAGCTGCTGGAGGGCCTGCCCCTGC TGCCCGCCGCATGGACGCGCCTGCGCCGCCGTCGCATCGCGCCCGCCCT GCAGGCTGCCGCGGACGCGGGCGTCGCCATCTTCCTGGTGCAGGCGCTG GACAAGCTGCTGCAGTGCGGCATGGCGGCCGCCATCTTCTGGAGCGCCGC CGGCCGAGCCACCCGCGCCGACCACGCCGCCCAGCAGCAGCAGCAGCAG CAGGCCCGCGCCCGTCCCACTCCGCGCGTCCTGGTGCAGGTGCCGATGT GCAACGAGCGCGAGGTGTACGCGCAGAGCATCGCGGCGGCGTGCCTGCT GGAGTGGCCGGGCGAGGCGCTGCTGGTGCAGGTGCTGGACGACAGCAGC GAGAAGGACGTGCAGCACCTCATCGCCGACGAGGTCGCCGCCTGGGCCG CGCGCGGCGCGCCCATCGTCTACCACGCCAGGCAAGCTGCCGGGGCAAG AACGGTGAAGGGCGGCTACAAGGCGGGCAATCTGCAGGCGGGCCTGGCC GCGGCAGCGGGGCTGGGCTTCGAGTTCGTGGCCATCTTCGACGCGGACTT TATGCCGCGCCCTGATTTCCTGCGCATCATGATGCCACACTTCGAAGGCAG GCCTGACCGCGCGCTCGTGCAGGCGCGGTGGGCTTTCGTGAACACGAGC CAGAACCTGCTGACACGCTTTCAGGCCATCAACTTCGCGTACCACTTCATG GTCGAGCAGCAGGTCGGCTCCAGCCTCTGCGGCTTCTTCGGCTTCAACGG CACCGCGGGCGTCTGGCGCACGGCCGCCATCGAGGAAGCAGGTGGCTGG GACGCGCGCACGACCGTGGAGGACATGGACCTGGCGGTGCGCGCGCACC TGTGCGGGTACACGTTCCTGTACATGAACGAGTGCGAGGCGCTGTGCGAG CTGCCGTGCACGTACCGCGCCTACTGCAAGCAGCAGCACCGCTGGAACGC AGGAAGGGCACGGCTCCGTCTCTTCAAAACCTACCAAGCACAAGTCTCAGC GCCTTCGACCTCCCTCATCAGACTGTTTCTCCTTTCGGCGGCATGCATGTTC CGCATCGCAACGATGGGCGCCGCCCACGTGTCGGAGCCTCTCGGCGCGG TTGCTGAGCTGCTGGCGTGTGTGCGGTGCGCAGGCCCGGTGGTGCTCTTC TTCTTGTGCCTGCCCGCCATTCTGCGTAGCCGCGCGCTGGGCGTGGCGCG CAAGGCGTACGTGGTGGCCGTCTTCTTCGTGCTGCGCAAGCTCATCCTGCC CACGCTCGCCTTCCTGCTCTTCTGTTTGCTGCTGCCGACGACGATCTTCAT

	CCCCGAGATCTCCGTCCCGGTGTGGGCCGTCTTCTACCTGCCCACCGTGC TCTCCCTCCTCCACACCGCGCCCTACCCCCGGGCGTGGCCGTACCTGTTT CCGTTCCTGCTCTTCGAGAACGTCATGACGCGCACCAAGTGCGGCGCCAT CTGGGACGGGCTGGTGGGTGTGCGCAGCGCCAAGGAGTGGGTGGTGACC AAGAAGACGGGTGCCCGCGCCGCCGCTCCGCCTGCCGCGGCCGCGTCTG CTGCTGCGTTCCACCTGGTGAGCGGCGACGCGGTGTCCCCGAGCGCGCG CGCGCTGGCGGGCGCGGGGCTGCTGCAGTCGCTGGAGGACGTGCTGGA GGCGGGGCTGTTCCCCGGGGACCCCACCGACGACGGCGCGGACCTGGTC AGCACGGCCAGCCCCACCGCGCGCCAGGTCGCGCACCTCATGACCGGCC GCGCCCCGCTCCCCGCGCCAGGCGGCGCCACCGGCGAACCTGGCAAGG CGGTCACAGACGGCGCGCCAGCTGATGTCGCGGTGCGGGGGGGCCCGTC GCGGCAGCTGAGCTGGGCGGACCTGGCGCTGGGGGCGTACCTGGTGGTG GCGGCGGGCTGGTCCGTGCTGGTGCTGGACGGGCGGCACGCCTTCTTCC TCGCCTTCCAGGGAGGCGCCTTCCTCGCGGCGGGGCTGGACCTCGTGGG GGACCCCTCCTGA
MeCSLC ME000209S02952	ATGGCTCCAAACATCAGGTTTACCGAATGGTGGGCCAGCCGGGATTATCCTA CGAGGCCCATCATAGTGAAGATGGAGAAAAACGCTTGGTCACTTCCAGAGT TGAAGGAGTCTGAGCCGTTGATGAAGGCTGAGGCGCCACCCGCGCCTGCA GTGGAGATGGTCAAGAGCCAGAGTGCAAAGCAATTCACCTGGCTCATGCTG CTGCAAGCCCATAAGGCTGCTGGGTGCCTTGCTTGGGTGGGACTGGGTGT TGCCGAGCTTGTGAAGCATGTGAGGAAAAGGTTATTGACAAAGGAGGCCAT TGAAGAAGGTGTGGGAAGCTCAGAGGAGAAGCCCCGTGGAAGGTTGCTAC AAGTCTTGAGGACCCTCCTGCTCATTTCCCTGGTGATGCTGGTCTTGGAAG CGTTCACGCATTTGAAGGGCTGGCAGTTCCAGAGCCCTGCCATGTCCATGC CCACAAGGGTCAACGTCCAGAACTTCCTCCACTGGGTCTACCTGGGCTGG GTACATTACAGGAGAGCGTACGTGGCGCCGGTCCTGCAATGGCTGGCCAA CTCGTGCACGCTGCTGTTCCTGGTCCAGTCCGTGGACCGCATCGTACTGTG CGCCGGCGCCGCCTACATCAAGCTGCGCGGCATCAAGCCTGTGCCCAAGG TGGACGTGTTTAGCGAGCAGGACCCCGAATCGCCGTACGAGTACCCCATG GTGCTGGTGCAAATCCCCATGTGCAACGAGAAAGAGTGTTACGAGCAATCC ATCGGCGCAGTGTGCCAGCTGGAGTGGCCGGTGGACCGCCTGCTCATCCA GGTGCTCGACGACTCTGATGACGAGGACTGCCAGCGGCTGATCCGGGGAG AGGTGGAGCGCTGGTCGCAGAAGGGTGCCCCCATCATGTACAGGCATCGC CTCATCAGGAAGGGCTACAAGGCAGGCAACTTGAACAGCGCCATGAGGTG CGACTACGTGAAGGACTACGAGTTTGTGGCCATCTTCGACGCCGACTTCCA GCCCAAGTCGGACTTCCTCAAGCGCACCGTCCCCCACTTTGCGGAGCAAC CGGACATTGCCCTGGTTCAGGCGCGGTGGGCGTTTGTGAACCGCGACGAG AACCTGCTGACGCGGTTGCAGCTCATCAACCTGGCGTTCCACTTCGAGGTG GAGCAGCAGGTCAACGGCCACTTCCTCAACTTCTTTGGCTTCAACGGCACG GCGGGCGTGTGGCGCATCAAGGCGCTGGAGGACTCGGGCGGCTGGCTGG ACCGCACCACCGTGGAGGACATGGACATTGCCGTGCGCGCGCACCTGCAG GGCTGGAAGTTCATCTTCCTCAACGACGTCGAGGCGCTGTGCGAGCTGCC GGAGTCGTACGAGGCGTACAAGAAGCAGCAGCACAGGTGGCACTCGGGC CCCATGCAGCTCTTCCGCCTCTGCCTGCCCTCCATCATCAAGGCCAAGATAT CCCTGTGGAAGAAGTTCAACATGGTGTTCCTCTTCTTCCTGCTGCGCAAGAT GGTGCTGCCCTTCTACTCCTTCACGCTGTTCTGCATCATCCTGCCGTGCAC CATGTTTGTGCCCGAGGCCAGCCTGCCCCTGTGGGTGGTGGCCTACGTCC CGGCCATCATGTCCATCCTCAACATCATCCCCGCCCCCAAGTCCTTCCCCTT CATCGTGCCGTACCTCCTGTTCGAGAACACCATGTCCGTCACCAAGTTCAA CGCCATGGTGGCGGGGCTGTTCCAGCTGGGAAGCGCGTACGAGTGGGTG GTGACAAAGAAGACGGGGCGCGCCTCCGAGGCCGATCTGCTGGCCATGGT CCACCCGGACCCTGCTGCTGAGACACTGCCGGCTCTGCACGCGCGCAGC GTGAGCGAGTCGGGCATCGACGCGCTTGCAGACAAGATGGTGACTGAACT GGTGGTGGCCCCCACCACGCCCGTGGCAACCACGCCCCCCCCTGCCAAG CCTGCTCCCAAGCAGAAGAAGATTCAGAAGATGTACCGGAAGGAGCTCTCG CTGGCGCTGCTGCTGCTGGTGGCGGCGTCGCGCAGCTTGCTGACGGAGC

	ACGGGATGCACTTCTACTTCCTCGCCTTTCAGGGTCTCACGTTCCTCGTGG TGGGCCTCGACCTCATTGGCGAGCACCAGCAGCTATAA
SmCSLC SM000017S02811	ATGCCGCCCAACCTGGACTTCCAGGACTGGTGCGCCGCCGCCGCCGCCA CCAAGGAGGCCCTGCCGCCGCGCCCGATCATGGTCAAGGTGGACAAGGC CGCCTACGCCATGCCCGAGCTCGACACCAGCCTGATCCCGGCGCTCCCGG AGATCGGCGAGCGCAAGCGCAACGCCAAGCAGCTCACGTGGGTGCTGCT GCTCAAGGCGCACAAGGCGGCGGGCTGCATCGCCTGGCTGGGGGTTGGC CTGGTCACCTTCTTGACCGCCGTCCGGCACCGCCTCCTGACCAAGCAGGG GCTCGGCAAGACGGTCGGCGGGGGCGACTCGAAGCCGAGGAGCCGGCTC CTCCGGGTCCTCCGCATCTTCCTCCTCGTCGTGCTCGGCTTCTTCGTCTTC GAGGCCGTCGCGCACGCGTTCGGCTGGCAGCACCACGTGCCGCAGTTCC ACCGCCTCTCCACTGTCGGCTTCTACAACCTCCTCCACTGGTCCTACCTGT CGTGGGTCTCCTTCAGGAAGAAGTACATCGCGCCTCCACTCCAGTTCTTCG CCAACACCTGCACCTACTTATTCATTTTCCAGTCCATCGATCGCGTGGTACT GAGCCTGGGCTGCTTCTGGATCAGACTGAGGGGCCTTAGGCCACAGCCCA AGGTGGAGCTCGAGGAGGCCGGCGCCGATCTGGAGAGAGCAGTGGATCA CTACCCCATGGTGCTCATCCAGGTGCCCATGTGCAATGAGAGGGAGTGCTA CGAGCAGGCCATCACGGCAGCGTGCCAGATGGACTGGCCCAAGACTCGCA TGCTCGTCCAGGTGTTGGACGACTCTGACGATGTGACGATCCAGAAGCTGA TCAGAGGGGAGGTTCAGAGGTGGTTGCAGAAGGGATCGCCGATCACATATA GGCACAGACTGCTACGGCGCGGATACAAGGCCGGCAACTTGCAGAGCGCC ATGAGCTGCGATTATGTGAAGGACTATGAGTTCGTGGCCATTTTTGACGCTG ATTTCCAGCCAAAGCCAGACTTTCTGAAGAAGACCGTACTCCACTTCGAGG AGCAACCTGACCTTGCCTTAGTACAAGCCCGGTGGTCCTTCATAAACAAGG ATGAGAACTTGCTGACGCGCCTTCAGAATATCAATCTCAGCTTTCACTTTGA GGTCGAGCAGCAGGTCAACGGCACCTTCATCAATTTCTTTGGCTTCAATGG CACTGCTGGTGTATGGAGGATTGCAGCGCTGGAAGATTCTGGAGGGTGGC TAGACCGCACGACTGTAGAGGACATGGATATTGCAGTTCGCGCACATCTGA AGGGCTGGAAATTCATCTTCCTCAATGACGTCGAGGCCCTCTGTGAGCTGC CGGAGTCTTATGAAGCATATCGCAAGCAGCAGCACCGCTGGCATTCGGGGC CAATGCAGCTGTTCCGCCTTTGCCTCCCTGACATCATCACGGCCAAGGTTG CCCTCTGGAAGAAGTTCAACATGATATTCCTGTTCTTCCTCCTCAGAAAAAT GATACTGCCCTTCTACTCGTTCACTCTGTTCTGCATCATCCTGCCGCTGACC ATGTTTGTTCCCGAGGCCAGCCTTCCGCTGTGGGTGGTGTGCTACATTCCA GGAGCAATGTCAATCCTGAACGTCATTCCGTCTCCCAGGTCCTTCCCATTCT TGGTCCCGTACTTATTGTTCGAGAACACGATGTCAGTGACCAAGTTCCAGG CCATGATTTCTGGCCTCTTCCAGCTCAATTCAGCATCTGAGTGGGTAGTAAC CAAGAAGACTGGGCGTTCGTCCGAGGCAGACCTCCTCGCTGCCGTGCGCG AGGTCAAGGCTGAAAACGGACCTCCTTTACCATCCCACGCACGGGCAGCG TCAGAGACTTGCTTGGACAGTCTGAAGGAGCAGCAATCGGCATTGCAAGTC GCTGCTGAGAGTCCAAAACTCAAGCTCAAGCCAAAACGGACTGTGCAGAG GATGTACAGAAAGGAGCTCGCCCTTGCACTTCTCCTCCTCGTGGCAGCTGC AAGGAGCCTGATGTCTGAGCGGGGGATGCATTTCTACTTTCTCCTTTTCCAG GGTTTGGCCTTCCTTGTGGTTGGCCTTGACCTCATAGGAGAGCCGCAGAAG CCGGACTCCTTCTTCGCCCTCCTGGCTGGCCACGCCATGGGTAAATGA
KnXXT kfl00101_0170_v1.1	ATGGCATTCAAGCCAACACTCTTCACAAAGGAAAAGAAGATGCAGCGGCCG TTCTTCCACTTCTGTATGTTTCTGGTTATATGCGTGGGGGCAATCACGCTTG CTAACTACAGGCGATCAAAGCTCCCGGCCTTGATCGGTGCAAAGCTTCCTC CCGCGATTGGAACCGTCGATCAGGGAGGCACTGACAACGCTGCAGATGGC GTGAGGCTGATGCTGGTGACCGGGACGGACGGACGGCCGTGCAGCAGCG CTCGGGGCGCGGAGATTCTAATCCGATCGCTCAAGAACAAGGTGGACTATG CAAGGCTGCACGACATTCCACTGTACTACGCCATGGAGACGTTTGACGACG CGTACGATATTTACTGGGTCAAGCTGCCGCTGCTCAAGAAACTGATGCACAC CCACCCCACTATCGAGTGGTTCATGTGGGTGGACTGCGACGCCATCTTTAC GGACATGACGCGGGGGATCCCTCTGGACGAGTACACTGACTACAACCTGG TGCTGTCGGGGAACGCCACAGCCGTATTTGAGGAGCCCGACTGGCTGGGC

	CTGAACACGGGCGCCTTTTTGATTCGTAATTGTCAGTGGTCGGTGGATCTG CTGGACGCCACCATGGCGCTCGGGAACAGGTACACCACGCGGCGGGACA CCGGGCTGCTGCTCAACAAGGTGCTCCGAGGCAGGGCGGAAGCGAGCCA CGGCAAAGAGTGGCCCGCCGACGATCAGACGACCCTTATCTACCTGATGGC CACCCAGCCACATCTCTGGAAGGAGAAGACTTTACTAGACACAACAAGCAT GTACCACAACTGGTGGGTTTTAGTCTCTCAGCCGCTAGACCAGCTGCTCGA GGATGCCGACGCAAGCATGCCAGCCACGTGGCGGCCGTTCATCTCCCACT TCACGGGGTGCAAGTTCTGCCACGTGCAGCACGCTGACGAGGGGCAAAAG GAGGCGTGCATGGACACCTTTGACCGGCTGTACCGCTTCGCGGACAACCA GGTGCTGGAGAGGTTCCAGCTCAGGCATAAGAGCGTGGACACCGAGGAAA TACAGGAGATCTAG
MeXXT ME000051S08080	ATGGAGATAAGGAAAGCTCGGCACCCCAGAGAAAGATATGGCACTATTAAAG CAACAACTTTCAATATTACATCAGAAGACGGGTGCAAAAAGATTGACTGGGA CAAGCAGCGCGAGGCCTACAAGGCCAGGCACCCCGGGTGCAACGTGTCG CGCACCACCGAGCAGCCGTCCATCATGATGCTCACGGGCTCCTCGCCCAA GGTGTGCGAGACCAGCATGGGGGACCGTCTGCTGCTGCAGGCGCTCAAG AACAAGATCGACTACTGCCGCCCGCGCGGCATCGAGATCTTCTACAACATG GCATCCTTCGATGCGGAGCTCACCAACTTCTGGGCCAAGCTGCCGGTGCT GCGCATGGCCATGTTAAAGCACCCGCATGTGGAGTGGTTCTGGTGGGTCG ACGCGGACGTGTACTTCACAGATATGCTGTTTGATATGCCCATGGCCTCTTA CGAGAAGTATGAAATGGTGGTACCAGGTTACTACGATCATGTCTACAAACAC AAGGACTGGGTGGGCCTCAACACGGGCGTCTTTCTCACACGCAACAATCA GTGGACGCTTGATCTGTTAGACATGTGGGCCGTCTTCGGTCCAGTCGGGAA AGTGAGAGATGAAGCTGGCTTGTTCTTTGAGAGGGAGCTTCCGGGCCGGC CCCCTTTTGAAGCGGACGACCAGAGTGCGCTGGTGTACCTCCTGAACAAG CACAACGACACGCTCAGAGAGCGCGTGTTTCTGGAGACGTCGTACATCTTG CACGGCTACTGGCACGTCCTCGTTGACAAGTATGAGGATATGATGGCCCAC AACAGTCCAGGTGTCATTCCCCACGGCAACGACAAGTGTCCCTTTACCACG CACTTCGTTGGGTGCAAGCCATGTGGCAACTATGGAGAAGATAGGCAACGC TGCTTCAGGCAGATGATCAGGGCATTCAATTTTGCCGACAACCAGATCATAA GGCGCATCGGTCTGCAGCACGTGAACCTGGCAAGCTGGCAGGTTAAGCCC CTTCCAGCTGTCAGAGAAGAAGCAGTTAAAAAAACCAAGACCGCGTGGACA TTGAAAGAGGAAGGGCTGGGACCTGGTCAGGCTGGGCTACCTCCTTGCTAT CACCAGAGGGAGGATGAAGTGGCAGCACGGAGGACACAGCTGCACCAGG ACCGTGTGATGTTTAGGGGCCACACACCCAGTAACAACTTTGTGCTGGTGG GCGGATACCGCACTGGTCCCCGCAGCTTCACAGCCATAGGCCTCGCCAGG CTGGCTTGGCGCAGCCAGCGCAAGGTAGAGAGGTGCACCTGGACGAGCTT GGATGGGGACCAGGAAGATGGCACTATGGAAAGTGAGCTCTCCCTGTTCCT CTGCCTCCCTCTTTGA
SmXXT SM000081S22676	ATGCGCGGCAGCGGCGGCGGCATGTGGCCGCCGACGGCCGGGGGCTGG GGCCGGCAGCTGGCGCGGGCGGCCAACAACGTCAAGATCACGCTCGTCT GCAGCCTCGTCACCTTCCTCGTCCTCCGCGGCACCCTCGGCGCCGGGCG CTTCGGCACGCCATCCCACGACGCCCAGCGCCTCGTCGGCGCCGCCTCG CTTCGCCCCCACCGCCGCGCCCTCAAGTGGCACGTCCTCGGCAGCGACAA GCCCCCGGAGGCCGAGGAGGAGTTCCTGTACGACCCCAGGCGGCCGTAC AGCCTGGGGCCCAAGATCAGCGACTGGAATGAGCGGCGGGAGATGGCGAT TGCGCACAAGCCGGGGTGCAACGTCTCCGCCTCTGGGCGGCCGCGCATG ATGCTCGTCACGGGTTCGCAGCCGAAGGAATGCGAGAACCCGTTGGGAGA CCACCTTCTCCTCATGGCTTTCAAGAACAAGATGGACTACTGCCGGCTGCA CGACGTCGAGGTGTTCTACAACATGGCGCACCTGGACCGCGTGATGTCGG GCTTCTGGGCGAAGCTGCCGTTGCTGCGGCACCTCATGCTGTCCCACCCA GAGATCGAGTGGTTCTGGTGGATGGACTCTGACGCGATGTTCACGGACATG GTCTTTGAGCTGCCTATGGAGAAGTACGAGCCGTATGACATGGTGCTGCAC GGGTGGGAGCGCGATGTTTACGAGCTTGAGCGCTGGGTGGGCCTCAACAC TGGCAGCTTCCTCATCCGTAACAATCAGTGGATCCTGGACATGCTGGACGTA TGGGCACAGATGGGCCCCAAGGGGCGGGTCCGCACGGAGGCTGGCAAGC

	TCCTCACAGCTGCCCTAAAGGATCGGCCAGCTTTCGAGGCAGACGATCAGT CGGCGCTGGTATATCTGCTCATCAAGAATCAGGCTGAGTGGCGGCCGCATG TATACTTGGAGCAGACATACTTCCTGCACGGTTACTGGGGAATCATTGTGGA CAAGTATGAGGAGCTGATGGCGAAGCACCACCCAGGGTATGGTGACGAGC GGTGGCCATTTGTGACACACTTTGTGGGGTGCAAGCCCTGCAGCCTTGCC GACAACTATGACGCAGAGCGCTGCGTTGTGCAGATGAATAGGGCGTTCAAT TTTGCCGACAACCAAGTGCTGCAACACTATGGCTACAGCCACAAGCATTTGA ACACAACTGCGATTGAGGCGGTCAACACTACGGCCCTGGAAGCTAGCAGG CACCCAGAGCAAGAGGATCCCACCTGA
VcXBT	ATGTTCCATCGAATTTTCGGCCACCCGTCGGCCGACCACGAAACCCCAAAA AAGCAGCCAAAATCTCCAGACCTCAAATCCACAGTAAAATCATTCCTATCCCA CCCAATCCATCGGTCAATACTCTTCGTCGTTATCCTCTTCCAAGTATTCCTCC TTTTATACTTTACTCGTACCCCTAATCTCTCTCTTTCATCCCAATCTCCTCCTC AACCTCCGCTTGAATCTGTACAACCTCCGCCTGAATTCCAACCCTCAGAATG CGATTCCCGTCGAATTTACGTCTACGACCTCCCCCCAATGTTCAATTACGAC CTCCGGAACAATTGCCACCGGTTAGACCCATGGCACGACAAATGCGACAAG TATTTGAACGACGGGTTGGGGCCGGCGGCGAAGGAGCTGGCCGGAATCGT GCCGGAGAGTATTCTCCCGGCCTGGTACTGGACCGATCATTATTGGGGGGA GGTGGTGTACCACAACCGGATGTTGAATTACAAGTGCCGAACCCTAGAGCC CGAATCCGCTACGGCGTTCTACATACCCTTTTACGCTGGGCTCGCGGTGGG CCAGTACTTGTTCGGCAATCACTCGACGAGCGAGCGCGATTGGCATTGCGA CAGGATGGTTGAGTGGGTCCAGCAGCAGAAGTGGTGGAAGAGATCCAACG GCTCCGATCACTTCATCATGCTTGGACGGTTGACGTGGGCTTTCCGACGGT TGAAACAGGATCCCGGTTGGGGGTCCTTCTTAATCCACAGGCCGGAGATGA AGAACGTCGTCCGCTTAGCCGTTGAGAGAAACGTGTGGGACCCGATGGAA ATCGCCGTGCCTTACCCCACCATATTCCACCCCAGGTCGCAATCGGATATCA CCGAGTGGCAGAGATTCGTACGCAGCCGGCGAAGGAACCACCTCTTCGCC TTGGTTGGCGGCGCACGCGCCTCGATCAAGAACGATTTCCGAGGGGTTCT GCAGAACCAGTGCCTCAGCGCGTCGGGCGCGTGCAGGCACGTGGACTGC AACCGTGAGAACTGCCTGGACGGTACGACTGCCATCATGGCGGCGTTTCTC GATTCCGATTTCTGTTTCCAGCCTAGAGGGGACGGGTTCACGCGGCGGTC GGTCTTTGACTGCATGCTGGCCGGTTCGATCCCGGTTTTCTTCTGGAGGAA GACGGCTTACTTGCAGTACGAGCGGTTCGTGCCGGACGAACCGGAGAGTT ACTCGGTTTTTATAGACCACAATGACGTGCGAAACGGGACGGATATAAGGAG AGTGTTGGAAGGATACCGGAAAGAAGAAGTGGAAAGAATGAGAGAGAAAGT TATAGAAAATATACCGAATTTTTTGTATGCGGAATCGAATCAAGGGTTGAAGG ATGGAAGAGATGCCTTTGATATCGCCATTGATGGGGTATTGAGCAAAATGCA AGGATCACATGGAGAAGGGGAGGATAGAGAATTCGATTGA
VcMUR3	ATGGATAAGGGGGGTACTAAGAATCAATGGTCCTGGATTAGTAGGTTAGCGG CTATATCGGTTTTTTTCTGGTTATTGTTATTGTACTTCCATTTTGTTTTTCTAGG AGGTAACACAGTTGATGATCTGTCATCACTAAGGGATCACATTTCAGCTAGTT CTGAGTCGATCGATAGCCGCCCTAGCGATTCCCAATCAAAGCCTGTTACTCG ACCTAGCATTGCCCAGCCAGACCCTAGTAGTTGGCGTATCCATGATCAATCC ACTCCTTTGAGTCAGCATAACAATGCCCAACCAATGCCTGCGAGTCAGCCG CTGACCAATACCCAGCCGAAAACAGAGAACTTTGAGTTCATGAAGGCATTAA GAACCATAGAGAATAAGAGTGATCCTTGTGGTGGGAGATACATATATGTCCAT GACCTTCCTCCTAGATTTAATGAAGATATGCTCAAGGAGTGTAGGAGTCTGA GTGTTTGGACTAACATGTGTAAGTTCACTATTAATGGTGGGCTTGGGCCCCC GCTCGAAAACGTTGAAGGGGTGTTCTCAGATACCGGATGGTATGCGACGAA TCAATTTATGGTCGATTTGATTTTCACTAACCGAATGAAGCAGTATGAGTGCT TGACGCGTGATTCTTCTCTTGCCGCTGCTATCTTTGTACCATTTTATGCGGGT TTTGATGCTTCGCGGTATCTTTGGGGGTACAATACGTCTATGAGGGATGCTG CTTCTCTTGCTTTGGTAGATTGGCTGATGAAGAAGCCGGAGTGGAGAGTTAT GGGAGGAAAAGATCATTTTCTTGTTGCTGGAAGGATTACTTGGGACATGAGA AGGTTAAGCGATGAAGATTCAGATTGGGGTAACAAGCTTCTACTTTTACCAG CTGCAAAGAATATGTCCATGCTTGTGGTAGAATCAAGCCCATGGAATGCGAA

	TGATTTCGGCATTCCATACCCCACTTACTTTCATCCGGCAAAGGATGCCGAT GTGTTCATTTGGCAGGACAGAATGATGAAACTGGAGCGAAAATGGCTCTTCT CTTTTGCCGGGGCCCCACGTCCTGGTAACCCTAAGTCCATTCGGGGGCAAA TCATCAACGAGTGCAAGAAATCCAACAATTGCAAGCTGCTGGAGTGCGATTT GGGGGATAGCAAGTGTCATTCTCCAAGCAGCATAATGAAGATGTTCCAGAG CTCCCTATTCTGCTTACAACCTCAAGGTGATTCATACACAAGGAGATCTGCG TTTGATTCGATATTGGCGGGTTGCATACCTGTCTTCTTCCACCCTGGTTCAG CTTACACGCAATACACTTGGCATCTTCCTAAAAATTATTCAAAGTACTCCGTC TTTATTCCAGAGGATGATATTCGGAAGAGGAATATAACAATCGAGCAACGGCT GAGTCAAATTTCTCCTGAGGAGGTGAAGATAATGAGGGAGGAGGTTATAAGT CTCATCCCCAGGCTTATTTATGCAGATCCCCGCTCTAAATTGGAGACCCTGA AAGATGCCTTTGATGTAGCTGTGCAGGCTGTTATTAACAAAGTTACTAAGATG AGGAGAGACATCATTGATGGTCGCACAGATGATGATTTCATTGAGGAGCTCA GTTGGAAATATGCTTTGTTAGATGAAGGGCAATATGTGGGTGCTCACGAATG GGATCCTTTTTTCTCAAAACCGAAAGGTGGCAATGTGGAGACCGAGGATAC ATCTGCAGAAGCAGCAAAGAATTCTTGGAAGAGTGAGCAAAGAGGACATTC ATGA
VcXLT2	ATGATTACCGTTATCGATAAAGCATCGTCGGAAGCACTCCAGCCCCTCAAGA AACCCAAAACCCCAGACTCAGACCGCAGAAACTGGTACAATTCCAAAAACC ACCCTCGCACATGGCTCATACTCTCCGTCTTCTTCGGCCAAATTTTCCTCCT CCTCATTGCTCGCTCACTCCCCACTTCCGTCTACCACCGCCGCCGTCACTT CCCCGCTCCCTCCACCCCTGCCGTCGCCGTTGTCGACCCCCAATGTACAG CCACAGTCTTCGTGTACGACCTACCACCTGTTTTCAATTCCGAATTATTACAA AAATGCAGTGAATTGGACCCCTGGGGGTCAAGATGCGAGGCCTTTTCAAAC GATGGGTTTGGCCGGAAAGCCACTGGGCTCAAGGGAATTGTGCCGGAGAA TTTGGCCCACGCGTGGTACTGGACGGACCAGTTCGCGTCCGAAATTATCTA CCACAACCGGATTTTAAATTACAAGTGCAGAACCCTCGAGCCGGAATCCGC CACGGCGTTCTACATCCCGTTCTACGCTGGACTCGCGGTGGGGAAGTACTT GTGGAAGAATTACACCGCGGAGGACCGCGATCGCCACTGCCATATGATGCT GAAGTGGGTCCAGGCCCAGCCGTACTGGTACAGATCCAACGGCTCGGATC ACTTCATCACGATGGGTCGAATTTCATGGGATTTCCGTCGCTCCAAGGACGA AGACTGGGGTTCCAGCTGTATATACTCGCCCGGTATGCGAAACGTCACGCG CCTGTTGATAGAGAGAAACCCATGGGACTACTTCGACGTCGGTGTGCCCTA CCCCACCGGATTCCACCCGTCGACGGCGTCCGATGTAGTGGCGTGGCAGG AGTTCGTCAGGACACGTAGGCGTTCGAGGCTGTACTGCTTCGCTGGTGCG ACACGTGTGTCCATCAAGAACGATTTCCGTGGCGTTTTATTGAGCCAGTGTT ACAGCGATTCTCAATCCGGGTCGTGTCGGGTCGTGGACTGTGGCGGGTCG AAGTGCTTAAACGGGTCGTCGGCGATTCTCGAGACGTTTCTTGACTCGGAC TTCTGTTTACAGCCCAGAGGGGACAGCTTCACGCGGCGGTCTGTTTTCGAT TGCATGGTGGCCGGTTCGATCCCGGTTTTCTTCTGGAAGCGGACGGCTTAC TATCAGTACGACTGGTTCTTGCCGGGTGAACCGGGGAGTTACTCTGTTTTTA TCGACCGGAATGCGGTGACGAATGGGACGTCGATCAGAGGTGAGCTTGAG AAAATTAGCAGGGAGGAGGTGAGGAGGATGAGAGAGAAAGTGATTGAATAT ATACCCAATCTTGTGTATGCGAAGCCTAGTGAGGGTTTGGTGGGGATTAAGG ATGCGTTCGATGTTGCCATTGATGGGGTGTTGAGGAGGATCAAGGAGCAAC AGGGTGAGTATAGCTTACAAGTGGAAAATTCGAGAAAAGGGTCATCGTAA

VcXBT_3	ATGTTCAACTACGACATGCAGAAAAACTGCGACGAATTAGACCCGAGGCAC AACAAATGCGAAAAATATTTGAACGACGGTCTGGGCCCGGCGGCGAAAGAG TTCGCCGGAATCCTACCGGAGAGTATTATCCCGGCGTTGTACTGGACTGATC TTTTTTGGGGGGAGGTGTTGTTCCACAACCGGATGCTGAATTACAAGTGCC GAACGCTAGAGCCCGAATCTGCTACGGCGTTCTACATACCTTTTCACGTTGG GCTGGCGGTGAGGAAATACTTGTGGGGCAATCACACTGCGAGAGAACGCG ATTGGCATGCCGTGATGTTGATTAAGTGGCTCCAGAACCAGAAATGGTGGAA CAGATCCAACGGCTCTGATCATTTCATTATGTTTGGACGGATGACATGGGATT TCCGACGACTGACAGACTCCGACGCCGATTGGGGAACGAGCTTCATCTATA TGCCGGAGATGAAGAACGTCATCCGTTTATCCGTCGAGCGAAGTATTTGGG ACAGCCTAGAAATCGCTGTACCCTACCCCACCGTATTCCACCCCAGGTCAG AATCAGATATCATGGTTTGGCAGAAATTCGTCCGGACACGCCGCCGGAACC ACCTCTTTAGCTTTGTCGGCGGCGGTCGCCGATCGATCAAGAATGATTTCC GAGACCTTTTAAAGGAACGGTGCCTAAACGAGCCAACGGCGTGCCGCCAC GTGGACTGTGCATGGGAGAACTGCCGCGACGGGAAGACGGCCGTCATGTC GGCTTTTCTTGACTCGGATTTCTGTCTGCAGCCAAGGGGCGACGCGTTCAC GAGGCGGTCGGTTTTTGACTGCATGTTGGCCGGGTCAATACCGGTTTTTTT CTGGAGAAGGACGGCTTACTTGCAGTACGAGTTTTTCCTGCCGGGTGAACC GGAGACGTACTCGGTTTTTATACACCGAGATGACGTGCGTAACGGAACGGA TATAAGGAAAGTTTTGGAAGGGTATGGGAGAGAGGAAGTGGAAATGATGAG AGAGAAAGTAACAGATTATATACCGAGATTTGTGTATGCGAAACCGAGTCAG GGGTTGGAGAAAACCCGAGATGCTTTTGATATTGCCATTGATGGGATATTGA GCAAATACAAGGAATCAAGGATCACATGCAGAGGGGCAGGATTGGGAATTT CAGTGAAATATAAATGGCAAAATGTACATCTTTAA

Figure 6.1: Gene sequences used in the scope of this thesis.

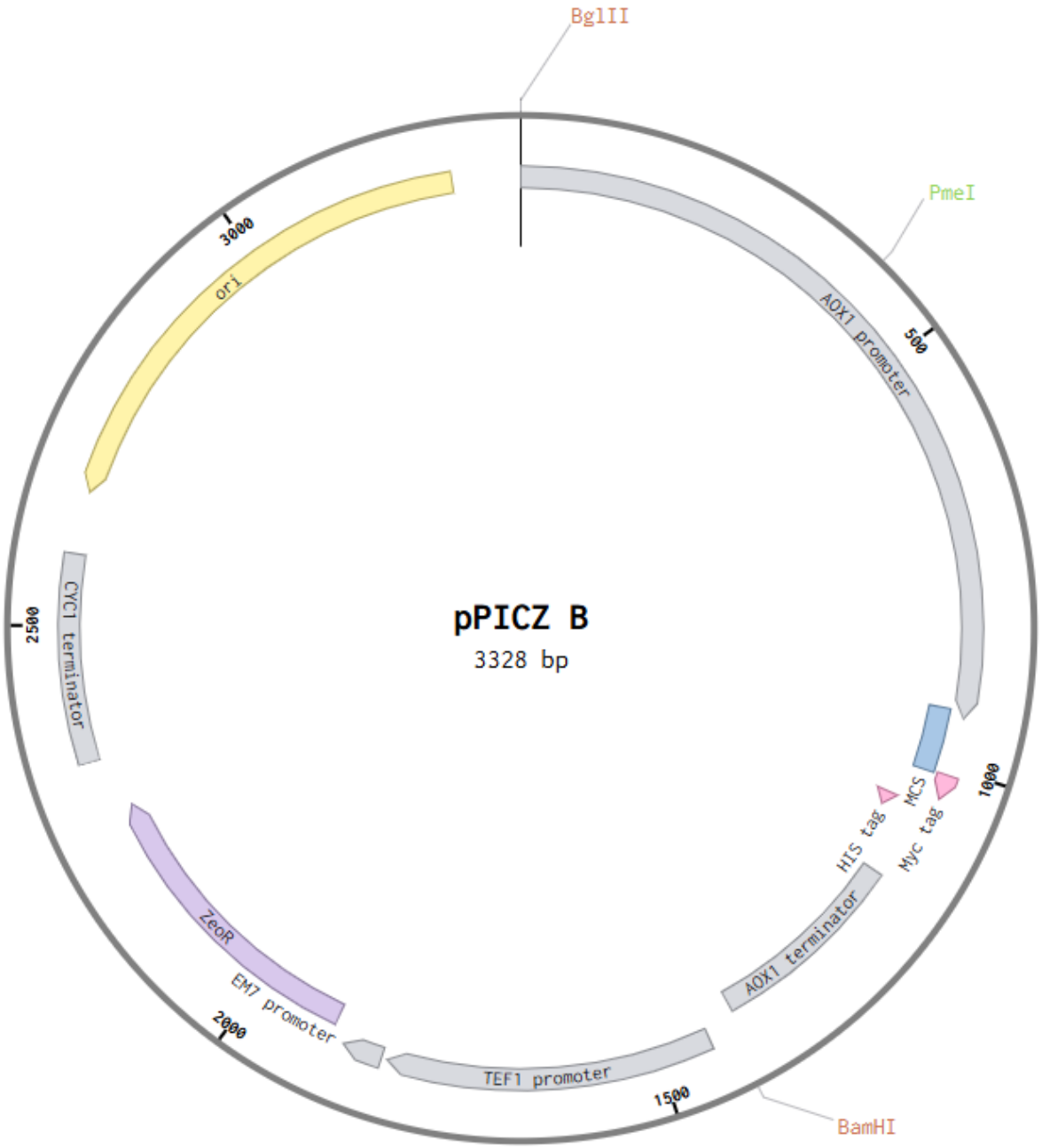

Figure 6.2: Vector map for plasmid pPICZB. This vector was used for expression of XyG biosynthesis related genes in *Pichia pastoris*. The AOX1 promoter allows methanol-inducible, high-level expression in Pichia. It targets plasmid integration to the AOX1 locus. The vector was linearized with PmeI prior to transformation.

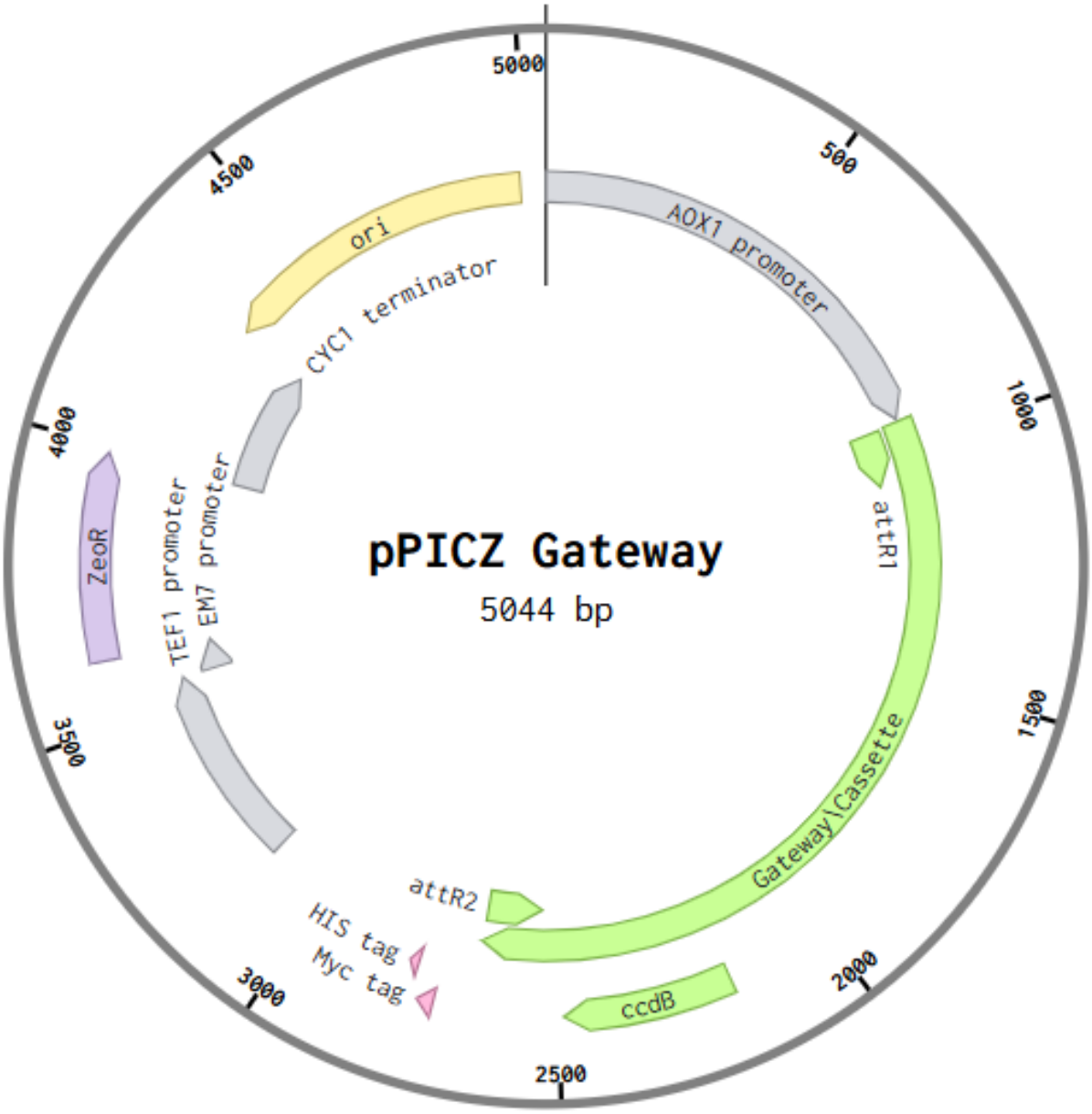

Figure 6.3: Vector map for plasmid pPICZ Gateway. This gateway cloning compatible vector was used for expression of XyG biosynthesis related genes in *Pichia pastoris*. The AOX1 promoter allows methanol-inducible, high-level expression in Pichia. It targets plasmid integration to the AOX1 locus. The vector was linearized with PmeI prior to transformation.

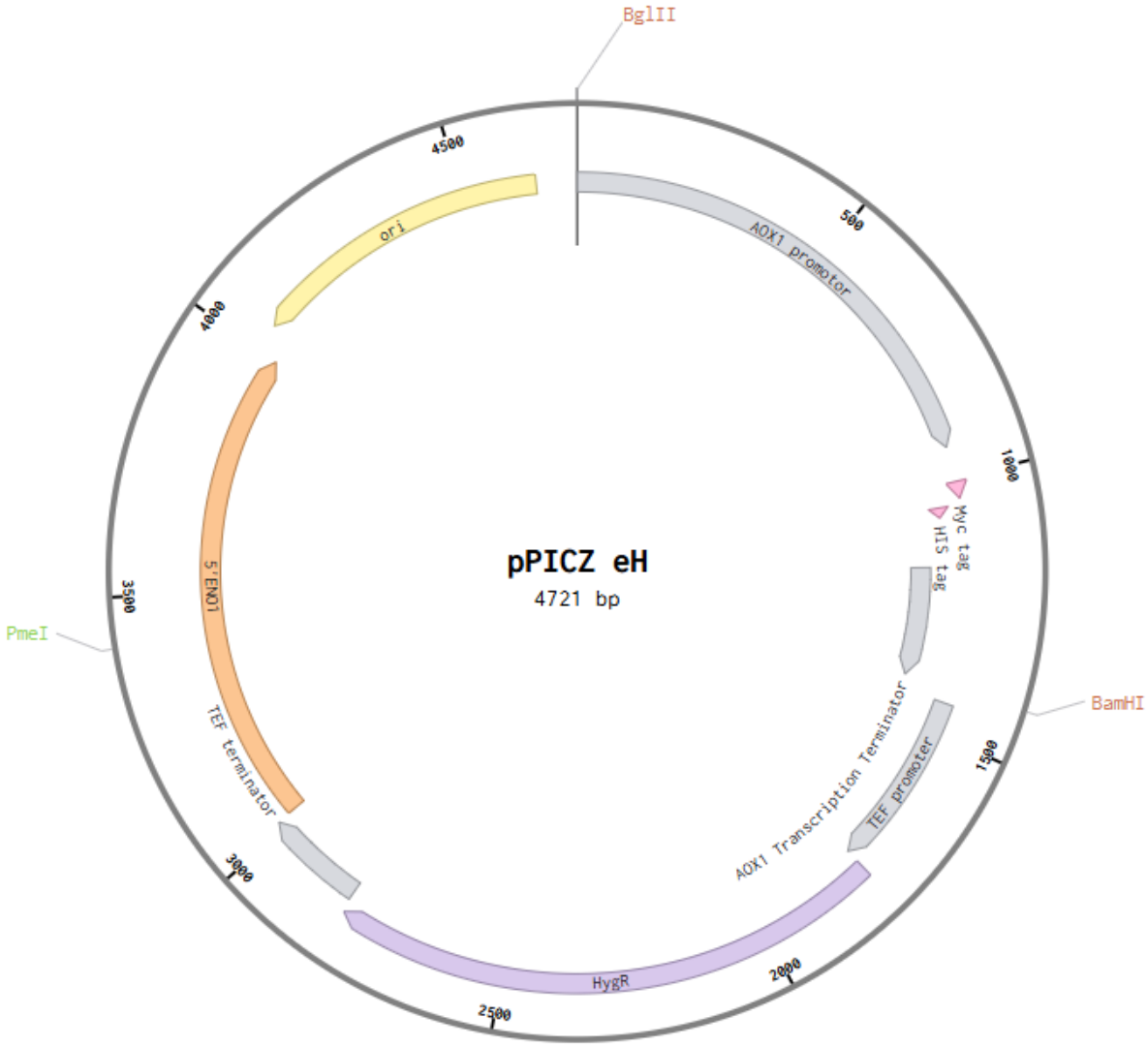

Figure 6.4: Vector map for plasmid pPICZ eH. This vector was used for expression of XyG biosynthesis related enzymes in *Pichia pastoris*. The AOX1 promoter allows methanol-inducible, high-level expression in Pichia. It targets plasmid integration to the ENO1 locus. The plasmid was created from pPICZ B & BB3_eH14* from GoldenPICS Pichia Kit. The vector was linearized with PmeI prior to transformation.

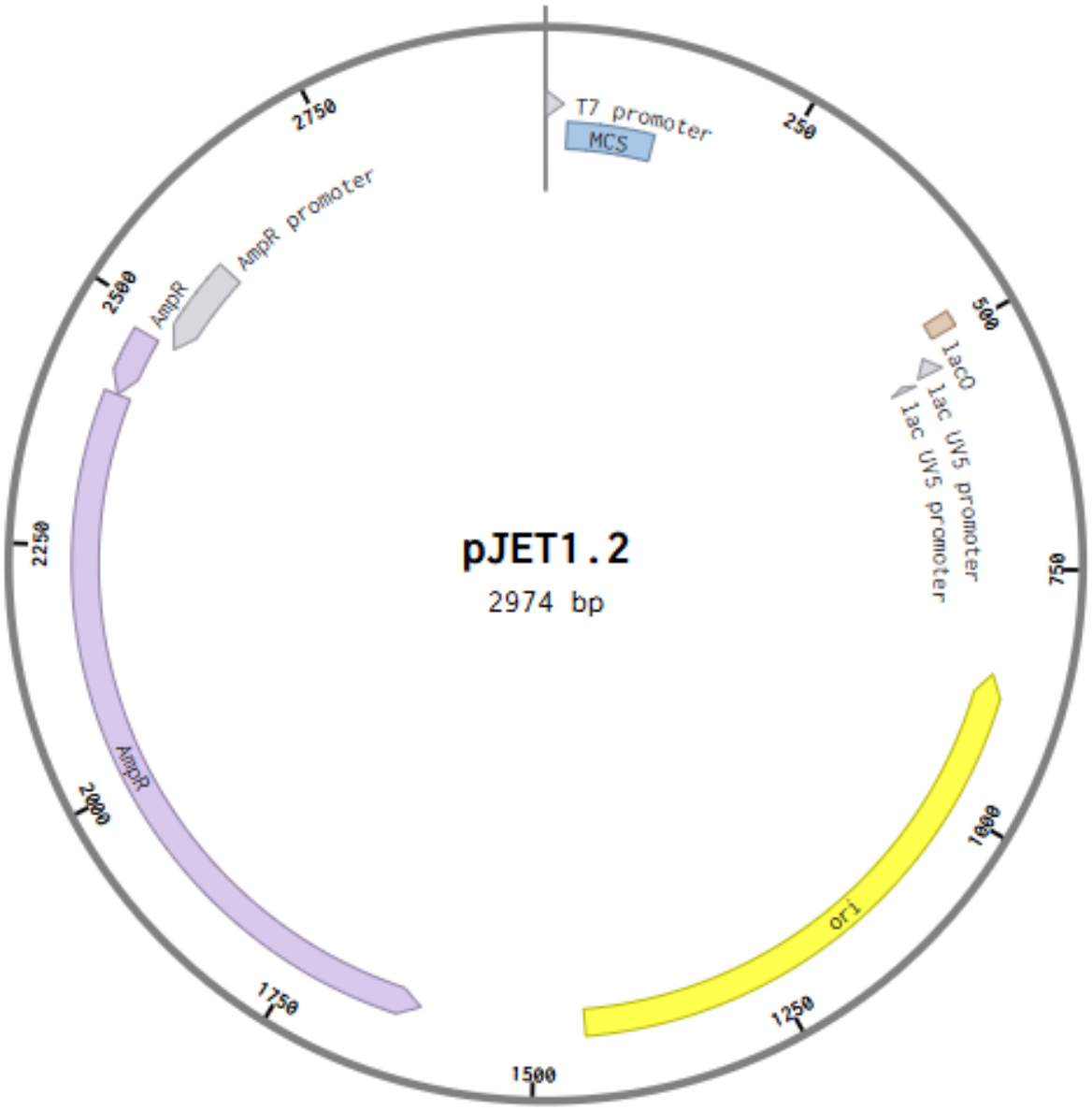

Figure 6.5: Vector map for plasmid pJET1.2. This vector was used as positive selection cloning vector with a lethal insert that allows for efficient recovery of blunt-ended PCR products according to the manual of the pJET cloning kit by Thermo Scientific.

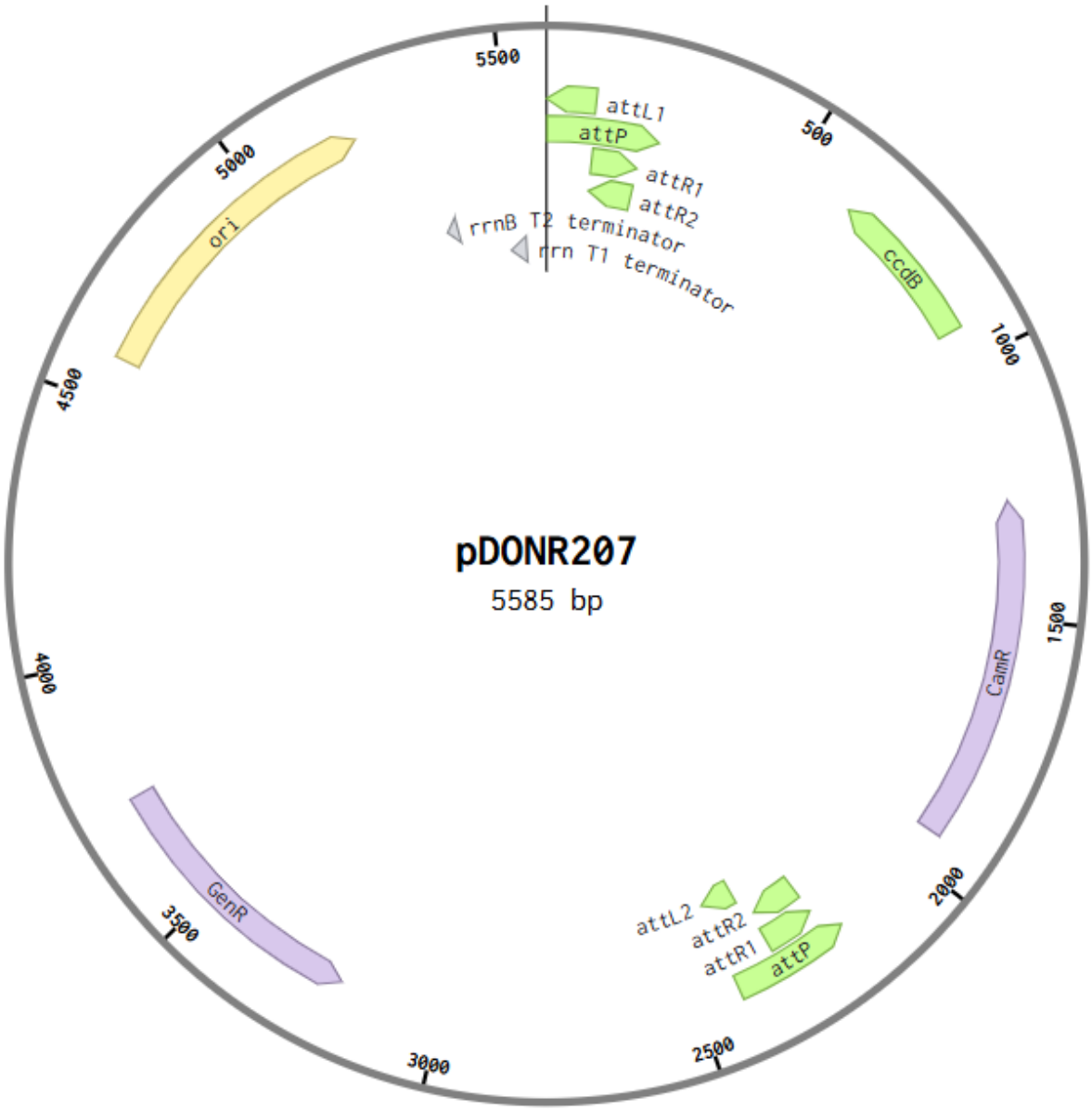

Figure 6.6: Vector map for plasmid pDONR207. This vector was used as Gateway donor vector. It contains the attP1 and attP2 sites and a gentamycin resistance marker.

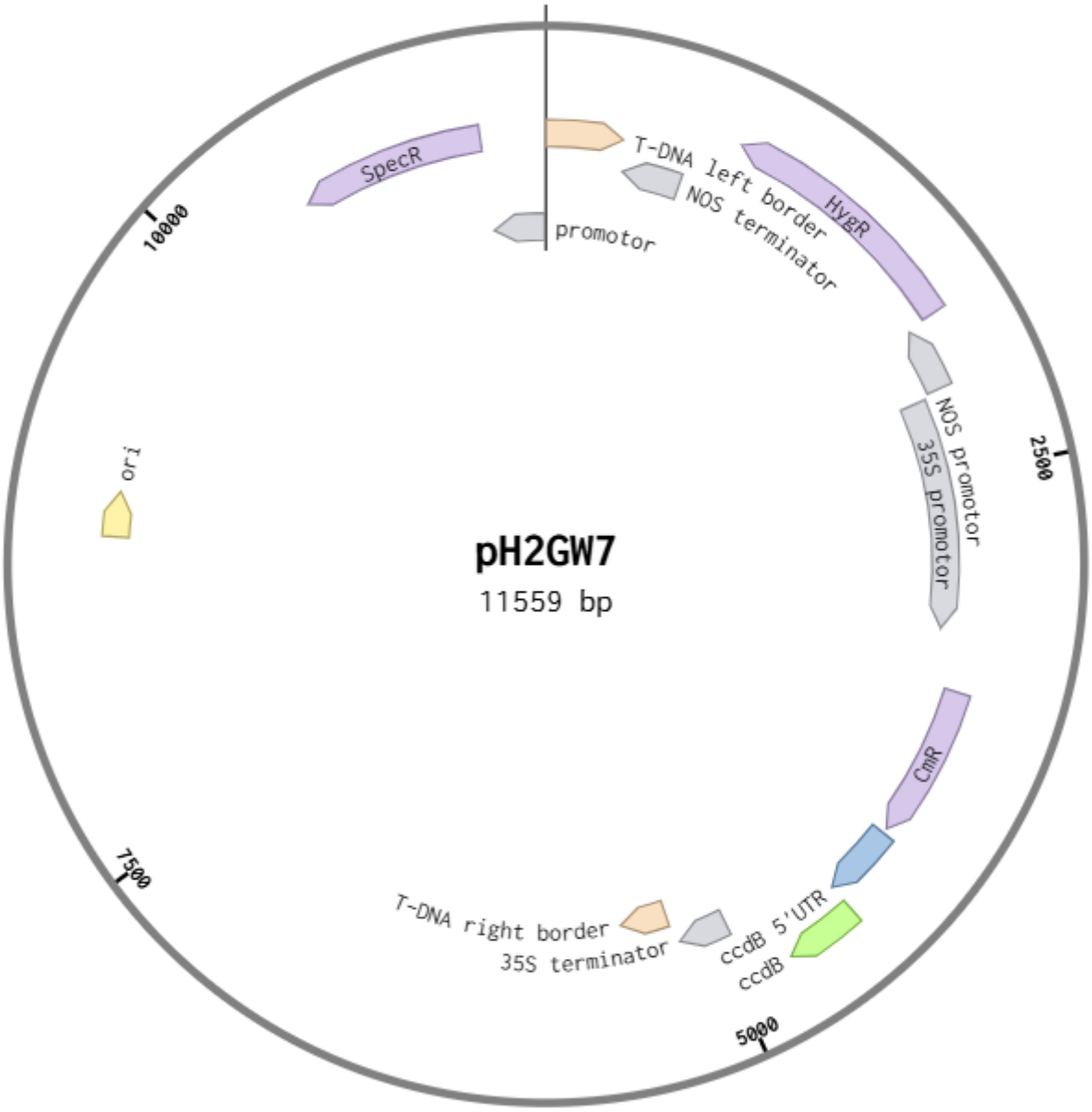

Figure 6.7: Vector map for plasmid pH2GW7. (Karimi et al., 2002). This binary plant Gateway destination vector was used for expression of Hymenaea *XXT* candidates in Arabidopsis *xxt12* and *xxt125* under the control of a 35s promotor. The vector contains a hygromycin selection marker in plants and a spectinomycin resistance in bacteria.

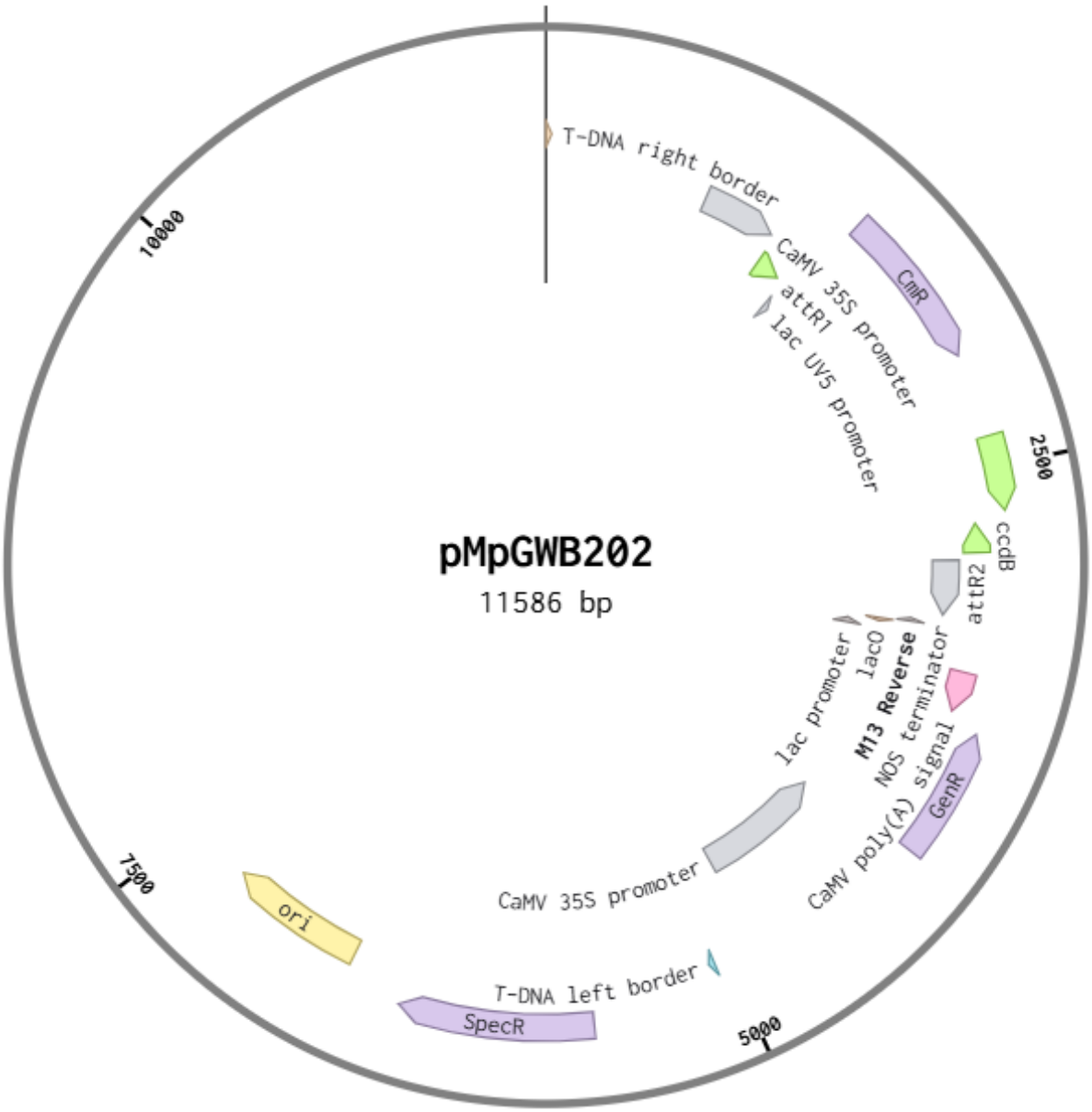

Figure 6.8: Vector map for plasmid pMpGWB202. (Ishizaki et al., 2015) This binary plant Gateway destination vector was used for expression of Hymenaea *XXT* candidates in Arabidopsis *xxt12* and *xxt125* under the control of a 35s promotor. The vector contains a gentamycin selection marker in plants and a spectinomycin resistance in bacteria.

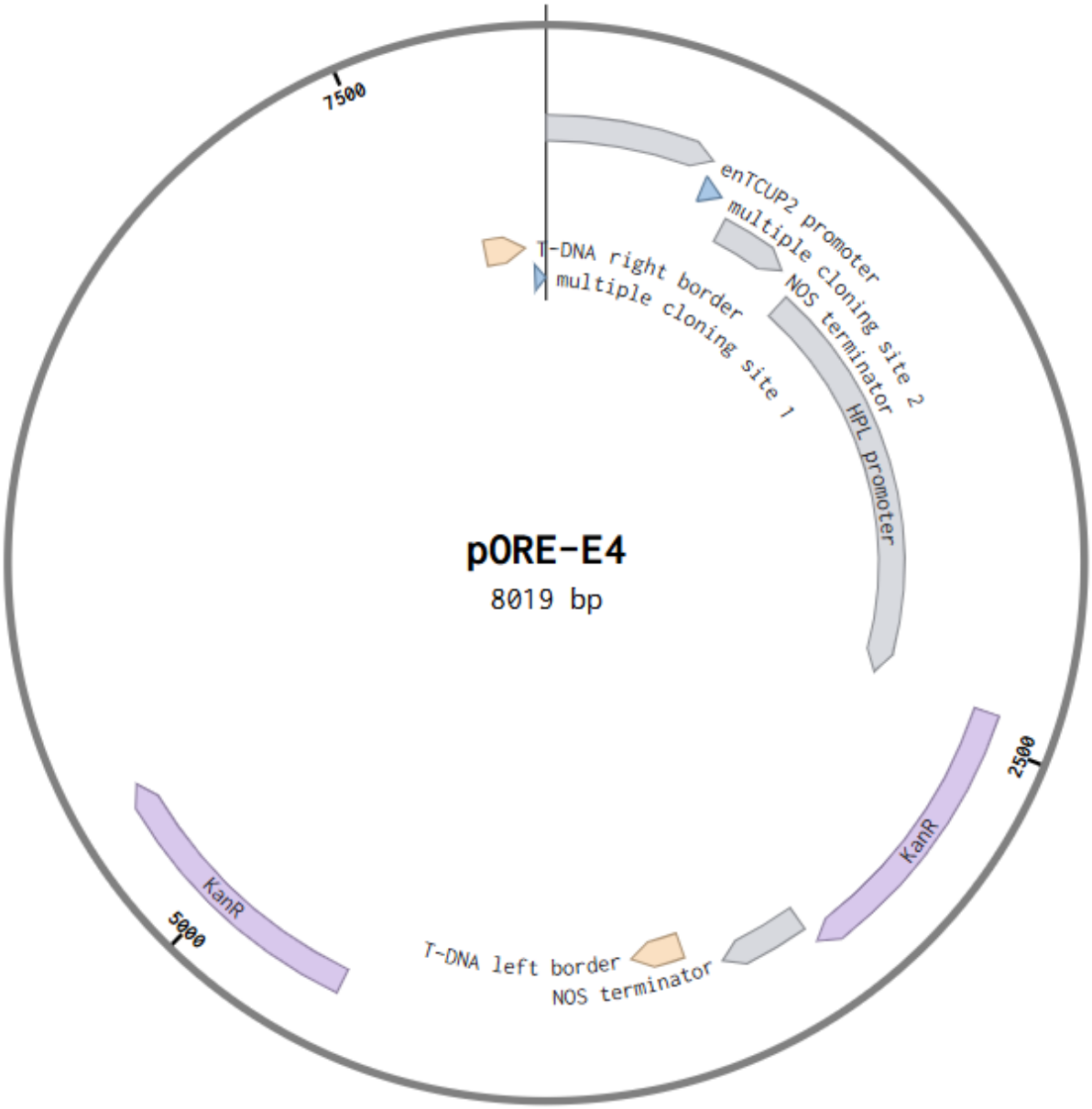

Figure 6.9: Vector map for plasmid pORE-E4. (Coutu et al., 2007) This binary plant vector was used for expression of blueberry GT 47 candidates in Arabidopsis *mur3 xlt2* under the control of the Tobacco cryptic constitutive promoter.

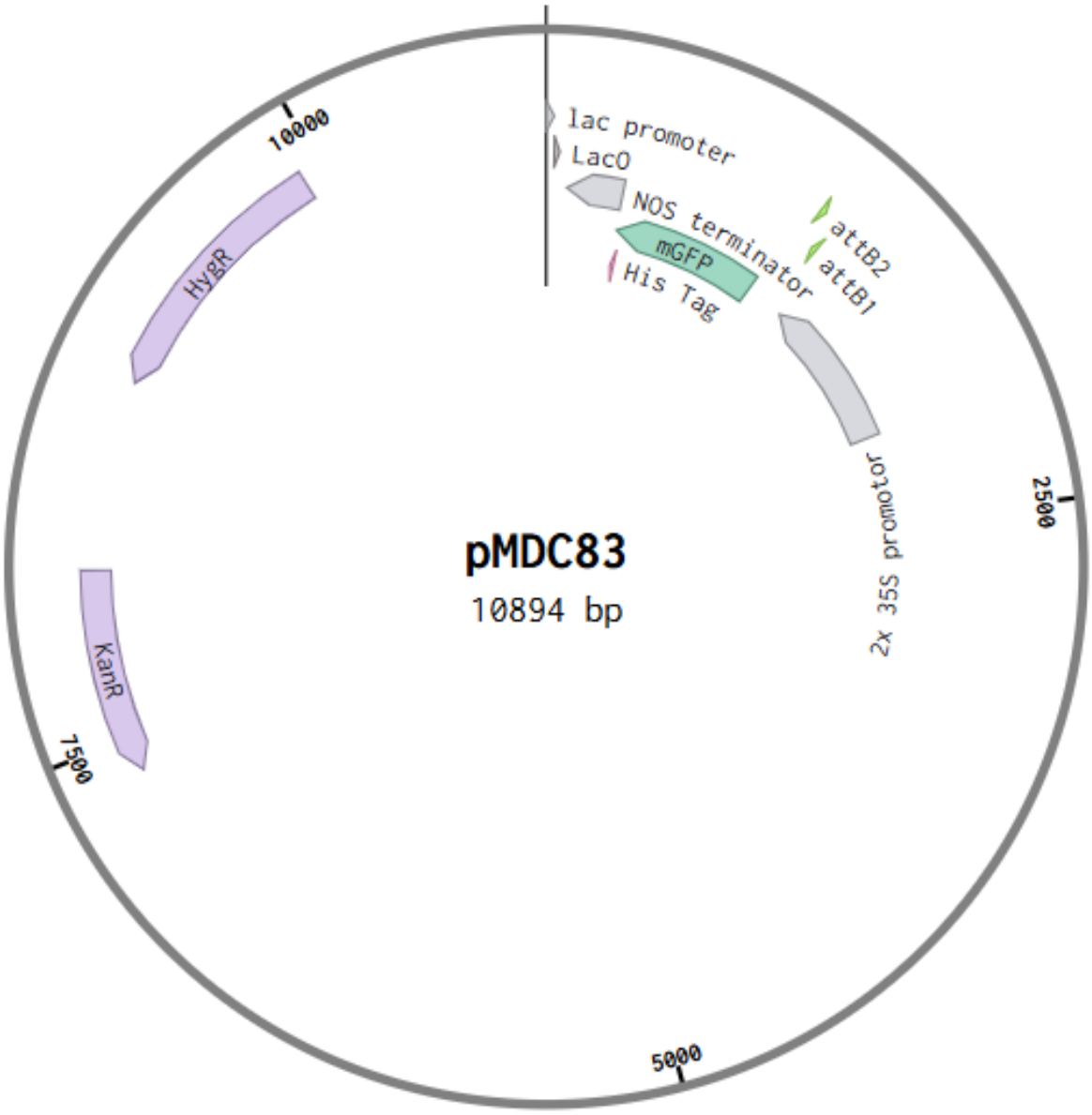

Figure 6.10: Vector map for plasmid pMDC83. (Curtis and Grossniklaus, 2003) This vector was used for transient expression of blueberry GT candidates with N-terminal GFP fusion under the control of a 35s promotor in *Nicotiana benthamiana*.

Primer Name	description	Sequence (5' to 3')
RI1F	Algal CSLC candidate *KnCSLC271* with BstBI & KpnI overhangs for introduction into pPICZ B	c**TTCGAA**ATGGGGCAAAGGAAGACTGAC
RI1R		act**GGTACC**TCAGCAGCCCAGCAGGTC
RI27F		GCGGCCCTCGGAGGGCTCCCCTGCTGCTGCG
RI27R		CGCAGCAGCAGGGGAGCCCTCCGAGGGCCGC
NG156F	Algal CSLC candidate *KnCSLC126* with overhangs EcoRI & KpnI for cloning into pPICZ B	gtc**GAATTC**ATGTTCGCCTTTATTGTCC
NG156R		cac**GGTACC**TTAGTAGCCCATCAAGTCAAG
NG159F	Algal CSLC candidate *MeCSLC* with overhangs EcoRI & KpnI for cloning into pPICZ B	ctc**GAATTC** ATGGCTCCAAACATCAGG
NG159R		act**GGTACCT**AATAGCTGCTGGTGCTCG
NG160F	Algal CSLC candidate *SmCSLC* with overhangs EcoRI & KpnI for cloning into pPICZ B	aga**GAATTCA**TGCCGCCCAACCTG
NG160R		ctc**GGTACC**TCATTTACCCATGGCGTG
RI12F	Algal XXT candidate *KnXXT* with NotI & KpnI overhangs for introduction into pPICZ eH	[illegible] **TTCGAA**ATGCGCATTCAAGCCAACAC
RI12RV2		at**GCGGCCGC**CTAGATCTCCTCTATTTC
RIPhD13F	Algal XXT candidate *MeXXT* with NotI & KpnI overhangs for introduction into pPICZ eH	c**TTCGAA**ATGGAGATAAGGAAAGCTCGG
RI13RV2		at**GCGGCCGC**TCAAAGAGGGAGG
RI14FV2	Algal XXT candidate *SmXXT* with BstBI & KpnI overhangs for introduction into pPICZ eH	c**TTCGAA**ATGCGCGGCAGCGGCGG
RI14R		ctc**GGTACC**TCAGGTGGGATCCTCTTG
VCXBT_1_F	Blueberry GT47 candidate, designed by Niklas Gawenda	ATGTTCCATCGAATTTTCG
VCXBT_1_R		TCAATCGAATTCTCTATCCTC
XBT_2_F	Blueberry GT47 candidate, designed by Niklas Gawenda	ATGTCGCTTCCAATTTCCG
XBT_2_R		TCATATTTCATTCCAATTCCCA
XBT_3_F	Blueberry GT47 candidate, with BamHI & NotI overhangs for introduction into pORE-E4	ct**GGATCC**ATGTTCAACTACGACATGC
XBT_3_R		tt**GCGGCCGC**TTAAAGATGTACATTTTGCC
XBT_4_F	Blueberry GT47 candidate, designed by Niklas Gawenda	ATGGCGACGAAGATTCGC
XBT_4_R		TTAATTACTTGCCCTCGAACG

VcXLT2_1_F	Blueberry GT47 candidate, with BamHI & NotI overhangs for introduction into pORE-E4	ct**GGATCC**ATGATTACCGTTATCGATAAAGC
VcXLT2_1_R		tt**GCGGCCGC**TTACGATGACCCTTTTCTCG
VcXLT2_2_F	Blueberry GT47 candidate, designed by Niklas Gawenda	ATGGTGCTTCCGCATCTC
VcXLT2_2_R		TCAGGAATTTGCTTTTTCCATG
VcMUR3_F	Blueberry GT47 candidate, designed by Niklas Gawenda	ATGGATAAGGGGGGTACTAAG
VcMUR3_R		TCATGAATGTCCTCTTTGCTC
VcXBTpMDCF	Blueberry GT47 candidate, with XbaI and KpnI overhangs for introduction into PMDC83	cg**TCTAGA***ACTAGTT*ATGTTCCATCGAATTTTCGG
VcXBTpMDCR		ctt**GGTACC**CCATCGAATTCTCTATCCTCCCC
RI48F	*TmUGD*, with KpnI & NotI overhangs for cloning into pPICZ eH	ctc**GGTACC**ATGGTAAAGATTTGTTG
RI48R		at**GCGGCCGC**TTAAGCGACGGCTGGCATATC
RI49F	*TmUXS2*, with KpnI & NotI overhangs for cloning into pPICZ eH	ctc**GGTACC**ATGGCTTCCGAATTGATATAC
RI49R		at**GCGGCCGC**TTATGATGAGTTTTTCG
RI68F	Gateway cloning *HcXXTA*	*GGGGACAAGTTTGTACAAAAAAGCAGGCT*TCATGTTGAAACGGTGTCTCCGTC
RI68R		*GGGGACCACTTTGTACAAGAAAGCTGGGT*TTCAAGAAGAAGCTGGCAACCTG
RI69F	Gateway cloning *HcXXTB*	*GGGGACAAGTTTGTACAAAAAAGCAGGCT*TCATGGATCAGTTTCTCGGC
RI69R		*GGGGACCACTTTGTACAAGAAAGCTGGGT*TTCAAGAAGAATTTGGTAATC
RI70F	Gateway cloning *HcXXTC*	*GGGGACAAGTTTGTACAAAAAAGCAGGCT*TCATGGGACAGGAGAATAAC
RI70R		*GGGGACCACTTTGTACAAGAAAGCTGGGT*CTAGCTTTGTGATTTACTGC

Figure 6.11: Primers for cloning. F or R denote the forward or reverse orientation. Introduced sites for restriction enzymes are marked in bold. BPs from end of DNA required for complete digestion are written in lower case. attB sites for Gateway cloning in italics. Nucleotides for reading frames are underlined.

Primer Name	description	Sequence (5' to 3')
pJET1.2F		CGACTCACTATAGGGAGAGCGGC
pJET1.2R		AAGAACATCGATTTTCCATGGCAG
PDONRF		TCGCGTTAACGCTAGCATGGATCTC
RI3F	binds pPICZ eH pAOX1 (promotor) behind SacI site	CCTGTCTATCCTGGCCC
RI3R	binds in 5'-end of *TmXXT2*	AATGTCTAAAGCACGCTGG
RI4F	binds in 3'-end of *TmXXT2*	CGAACTGGGTCTGATACACC
RI4R	binds in 5'-end of HygB resistance	CCCTCCGAGAGCTGCATC
RI5F	binds pPICZ B pAOX1 (promotor) behind PmeI site	TGACAAAAGCGTGATCTCATCC
RI5R	binds in AOX terminator	TCGAATGATTTTCCCAAACCCC
RI6F	Verification of pUC-GW-Kan-*klf00603_0080_v1.1*	GTCGCGCACCTCATGACC
RI6R		CCAGCAGCGTCACCATCG
RI7 F	Verification of Zeocin in pPICZ B	CAAGTTGACCAGTGCCGTTC
RI7 R		TCAGTCCTGCTCCTCGGC
RI8 F	Verification of pPICZ B + *KnCSLC271*	GTACTCTTGATGCTGGCACG
RI8 R		TATAAGCGGCCATCCCCATC
RI9R		CGTGCCAGCATCAAGAGTAC
RI9F		GATGGCCGCTTATATGCTGG
RI15F	Algal XXT candidate *KnXXT*	GACTGCGACGCCATCTTTAC
RI15R		GCTCCTCAAATACGGCTGTG
RI16F	Algal XXT candidate *MeXXT*	TCTGTTAGACATGTGGGCCG
RI16R		GGTCGTCCGCTTCAAAAGG
RI17F	Algal XXT candidate *SmXXT*	TTCTACAACATGGCGCACC
RI17R		GTGAACATCGCGTCAGAGTC
RI18F	Algal CSLC candidate *KnCSLC603*	GTCTTGCTGAGTTCGCTGTC
RI18R		GCAGGAACGGAAACAGGTAC
RI25F	pPICZ eH integration site ENO1	GGCTTCCGTCGCGAATATAG
RI53F	*AtUXS3*	CATCTTGCTTGTCCTGCCTC
RI53R		CGTCATAGCAACTCCGAACC
RI54F	*AtUXT3*	CCTGCACTGTTCTCTTGGAG
RI54R		GCCCAGTGACGAAAAGAGTG
RI55F	*AtUUAT1*	TTTCAATCAAGCCGTCGGTG
RI55R		CGGGAAGAAGAGCAATGACAG
NG53F	binds n-term *TmCSLC4* CDS	TCCTAATCGTGACCCTGTCC
NG53R	binds c-term *TmCSLC4* CDS	ACTTGCTCAATGGGGATTTG
NG54F	binds n-term *TmXXT2* CDS	GTCCGTTGGGTAGGGTTTTC
NG54R	binds c-term *TmXXT2* CDS	TCGCTCGGTAAAAACCATTC
NG55F	binds n-term *TmUGD* CDS	TGTTGAGAGCGGGAAGAAAC
NG55R	binds c-term *TmUGD* CDS	CCACGTGTATTGCGTGTAGG
NG56F	binds n-term *TmUXS* CDS	TTCTAACGACGGGTTTGGTC
NG56R	binds c-term *TmUXS* CDS	GAACCGGCCAACATACAATC
NG57F	binds n-term *Slc35D1* CDS	GTGTGGAGAAGCCTTTGCTC
NG57R	binds c-term *Slc35D1* CDS	CGATGTTCCATTACCCGTTC

NG106F	binds 3'-end region of enTCUP2 promoter (in pORE-E4)	CCTAACCCTAGCAGCCTCTC
NG116F	*TmCSLC4*	CCCACAAGGCTTTAACGTGC
NG116R	*TmCLSC4*	CCCACGACTCTTTGGATGCT
NG117F	*TmXXT2*	CTACCACCCTGGCTTTGGAG
NG117R	*TmXXT2*	TCACCGAACTTTCCACAGGG
NG118F	*TmUGD*	ATAGGTGCCGGTTACGTTGG
NG118R	*TmUGD*	AACCTGGCTCGTAGATTGGC
NG119F	*TmUXS*	GCATGTCCAGCTTCTCCTGT
NG119R	*TmUXS*	GGTTCCCACGACATTGGTCT
NG120F	*Slc35D1*	TTTTACGGCGTGAGCTCCTT
NG120R	*Slc35D1*	TTTCCCACCCAGAGAACTGC
NG161F	binds 5'-end region of *OsCSLC2*	GGCCTGTATCTTGCTGTTCG
NG161R	binds 3'-end region of *OsCSLC2*	CAGTCAACAGCAACAGGGAC
NG162F	binds 5'-end region of *OsXXT1*	TGACGAACCAGATCCACCTC
NG162R	binds 3'-end region of *OsXXT1*	TGAAGGCCCTTTCCATTTGC
NG163F	binds 3'-end region of *OsCSLC2*	GAAGCAGATTTCCGAGTCCG
NG164R	binds 5'-end region of *OsXXT1*	CGTTTCTGGCGAATCTCTGG
NG165F	binds 3'-end region of *TmCSLC4*	ACTTTCTGCTCAGGGTGTCC
NG166R	binds 5'-end region of *TmXXT2*	AATGTCTCAAAGCACGCTGG
NG169F	binds 5'-end region of *KnCSLC126*	CAGCATGTCGTACCACTTCG
NG169R	binds 3'-end region of *KnCSLC126*	ATGTTTTCGGTCTTGGCGTC
NG170F	binds 5'-end region of *KnCSLC271*	AGTTCTTTGGCTTCAACGGC
NG170R	binds 3'-end region of *KnCSLC271*	CCGACAGTTGCCGTTTCATC
NG171F	binds 5'-end region of *KnCSLC603*	TTTCAGGCCATCAACTTCGC
NG171R	binds 3'-end region of *KnCSLC603*	CGCACTCGTTCATGTACAGG
NG172F	binds 5'-end region of *MeCSLC*	CTGGTGCAAATCCCCATGTG
NG172R	binds 3'-end region of *MeCSLC*	GCAATGTCCATGTCCTCCAC
NG173F	binds 5'-end region of *SmCSLC*	AGGTGTTGGACGACTCTGAC
NG173R	binds 3'-end region of *SmCSLC*	GAATGTAGCACACCACCCAC
NG174F	binds 5'-end region of *TmXXT5*	AACCCTAACGAGACCTACGC
NG174R	binds 3'-end region of *TmXXT5*	GCCACCTTTCGTCACCTAATC
NG176F	*TmXXT5*	AACGAGACCTACGCACTTGG
NG176R	*TmXXT5*	GGTTTTGGAGGCGATCCAGT
inXBT3R	binds 3'-end of *VcXBT_3*	GAAATTCCCAATCCTGCCCC
inXLT2R	binds 3'-end of *VcXLT2*	CTTCCTCATTGCTCGCTCAC
RI71F	binds in 35s promotor	CCAACCACGTCTTCAAAGCA
RI72R2	Binds in *HcXXTA*	TCCAAGGAGTCCCGAACTTC
RI73R1	Binds in *HcXXTB*	CCCTGCGACTACCAAGACTG
RIP74R2	Binds in *HcXXTC*	AGGTAAGCTACCAAATGCAC
CV5F	Binds in AOX promoter	GACTGGTTCCAATTGACAAGC
CV5RV2	Binds in AOX terminator	GCAAATGGCATTCTGACATCC
PUCR2	M13/pUC in lacZ gene; flanks MCS & promoter in pORE-E4	AGCGGATAACAATTTCACACAGG
inXBT3R	Binds in 3'-end region of *VcXBT3*	GAAATTCCCAATCCTGCCCC
inXLT2R	Binds in 3'-end region of *VcXLT2*	ATCCTCCTCAACACCCCATC

Figure 6.12: Primers for genotyping and sequencing. Primers with initials NG were designed by Niklas Gawenda

Primer Name	description	Sequence (5' to 3')
AtUXT3_438_FW	To remove BamHI or BglI site in GOI	TGCAACCGTCACAGACCTTCAACTTAATATG
AtUXT3_438_RV		CATATTAAGTTGAAGGTCTGTGACGGTTGCA
AtUXT3_963_FW		AGAGAGCGAGAAGGACCCGCTAATAGCAGCT
AtUXT3_963_RV		AGCTGCTATTAGCGGGTCCTTCTCGCTCTCT
AtUXS3_30_FW	To remove BamHI or BglI site in GOI	GTACTCAGGATTGAGGTCTCTCTCTCAAGCA
AtUXS3_30_RV		TGCTTGAGAGAGAGACCTCAATCCTGAGTAC
TmUGD_306_FW	To remove BamHI or BglI site in GOI	TGGAAAAGCTGCAGACCTGACCTATTGGGAA
TmUGD_306_RV		TTCCCAATAGGTCAGGTCTGCAGCTTTTCCA
TmUGD_1125_FW		TCAGATTAGGAGAGACCTAGCTATGAAAAAG
TmUGD_1125_RV		CTTTTTCATAGCTAGGTCTCTCCTAATCTGA
TmUXS2_1197_FW	To remove BamHI or BglI site in GOI	CACCAGAGCCAAAGACCTACTTGGCTGGGAG
TmUXS2_1197_RV		CTCCCAGCCAAGTAGGTCTTTGGCTCTGGTG

Figure 6.13: Primers for site directed mutagenesis. To remove BamHI or BglI site for multimer constructs in *Pichia Pastoris* vectors.

Primer Name	XXT	description	Sequence (5' to 3')
RI33F	*XXT1/2*		CTCCGATTGGGATGAACAAC
RI33R	*XXT1/2*	Amplifies part of *HcXXTA* with RI33F, template undigested DNA	GGATGAAGCAATCCAAGTTC
RI36.2R	*XXT1/2*	Amplifies part of *HcXXTB* with RI33F, template undigested DNA	CMGGATGAAGCAABCCRAG
RI38F	*HcXXTA*	For nested pcr (pcr 2) with RI40F&R (pcr1)	GGAGGACGAACTTGGATTGC
RI38R	*HcXXTA*		CGGGTTCTCGCATGGTTTAG
RI39F	*HcXXTB*	For nested pcr (pcr 2) with RI41F&R (pcr1)	GGAATGAGAGCAGCAATCCG
RI39R	*HcXXTB*		AGGCTTATTGGGTCCGATGA
RI40F	*HcXXTA*	For nested pcr (pcr 1) with RI38F&R (pcr2), template: HcDNA digested with BspI or PflI	GAGGCAGATGGAGAGAGCTT
RI40R	*HcXXTA*		TCCCATGAAGCCTGCAGTAA
RI41F	*HcXXTB*	For nested pcr (pcr 1) with RI39F&R (pcr2), template: HcDNA digested with NdeI	ACAGTCTTGGTAGTCGCAGG
RI41R	*HcXXTB*		GATGACCCGGTAACCAGGAG
RI42.1F	*XXT3/4/5*	Amplify part of *HcXXTC*, template undigested DNA	GTGGATGGATAGTGATGC
RI42.2R	*XXT3/4/5*		CTGATCCTCTTAATCTTGGG
RI45F	*HcXXTC*	For nested pcr (pcr 1) with RI46F&R (pcr2) template: HcDNA digested with Bsp	ATTAGGTGACGAGAGGTGGC
RI45R	*HcXXTC*		AAGCTCCCTGTATTCACTGC
RI46F	*HcXXTC*	For nested pcr (pcr 2) with RI45F&R (pcr1)	ACATTTTGTGGGTTGCAAGC
RI46R	*HcXXTC*		GGATAAGGGAAGCTCAAACACC
RI64.2F	*HcXXTC*	Amplifiy part of *HcXXTC*, template undigested DNA	GGCCGBCAGATCCASAAR
RI46RV3	*HcXXTC*		GCAATTTCGCCCAATACCC
RI50FV2	*HcXXTC*	For nested pcr (pcr 1) with RI50FV3& RI65.1R (pcr2), template: HcDNA digested with EcoRI	AGGTGGAGTGGATTTGGTGG
RI65.2R	*HcXXTC*		ATGAGGTTTTGGTTCACGGC
RI50FV3	*HcXXTC*	For nested pcr (pcr 2) with RI50FV2& RI65.2R (pcr1)	GGTGTTTGAGCTTCCCTTATCC
RI65.1R	*HcXXTC*		TGAGCTTCCGAAATTAACGCC

Figure 6.14: Primers for identification of Hymenaea XXT candidates. Base/IUB Redundancy Description by Sigma-Aldrich: A (adenine) = A, C (cytosine) = C, G (guanine) = G, T (thymine) = T ; B = G+T+C, D = G+A+T, H = A+T+C, K = G+T, M = A+C, N = A+C+G+T, R = A+G, S = G+C, V = A+C+G. W = A+T, Y = C+T

Primer Name		Sequence (5' to 3')	
LBb1.3	T-DNA RB for SALK line	ATTTTGCCGATTTCGGAAC	
LB-3	T-DNA RB for SAIL line	TAGCATCTGAATTTCATAACCAATCTCGATACAC	
P745	T-DNA RB for WiscDsLox line	AACGTCCGCAATGTGTTATTAAGTTGTC	
LB	T-DNA RB for GABI line	CCCATTTGGACGTGAATGTAGACAC	
SAIL_837B10	*cslc4-3*	LP	CAGGGTAATCCAGAGCTAGGG
		RP	GATGATCTCCCGGTTTTCTTC
SAIL_187G09	*cslc5-1*	LP	AAGTTGGCTCAGCTCCAAAA
		RP	TTGACCCGTCTTCAGAACATC
SALK_088720	*cslc6-1*	LP	ACGCTCTTCTGCGTCATTCT
		RP	GTCTTTGGAATCCTCTCCGAC
wiscDsLox_497-02H	*cslc8*	LP	CACCTAGCCTGAACCAGACC
		RP	TTGAGATCCAGAGCTTGCTT
SAIL_168F02	*cslc12-2*	LP	AGCTCAGCTTCGGGTACAAA
		RP	TACGAATTCGTTGCGATTTTC
SALK_066991	*xeg113*	LP	AATCTTTCTTCTCGCTCCTGC
		RP	ACAATGCAGGAGGTTTCATTG
SALK_065083	*csla2*	LP	ACCAGTTTACAAACCCGAACC
		RP	GGTGGAAGTGGAGTGTCAAAG
SALK_071916	*csla9*	LP	CATTTTCACTAGATCCGCCAC
		RP	TCCGGTACAAGAACTGTAGCG
SAIL_785-E02	*xxt1*	LP	TAAACGTGTGTCCCCTAAACG
		RP	AGAGAAATCTCGAGACCGGAC
SALK_101308	*xxt2*	LP	TAAATTGTTTCCGCGGTACAC
		RP	AGTCACCAAAAGAACACGTGG
GABI-411G05	*xxt5*	LP	CACCGAATTCATGGGTCAAGATGGTTCGCCG
		RP	CATCACGAATTGGCCCTTTA

Figure 6.15: Primers for confirmation of Arabidopsis T-DNA lines via PCR.

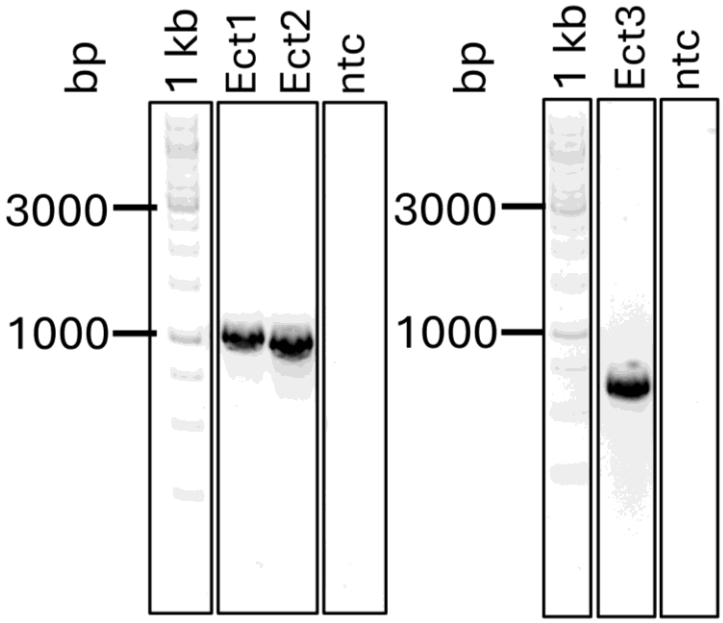

Figure 6.16: Colony PCR. pJET + parts of Hymenaea XXT candidates to confirm *E. coli* transformants (Ect). *E. coli* transformed with plasmids were verified via PCR using cell material as template with pJET1.2F & R; Ect1: pJET + part of *HcXXTA*, expected size 1,1 kbp; Ect2: pJET + part of *HcXXTB*, expected size 1,1 kbp; Ect3: pJET + part of *HcXXTC*, expected size 0,72 kbp; bp = base pairs, no template control = ntc

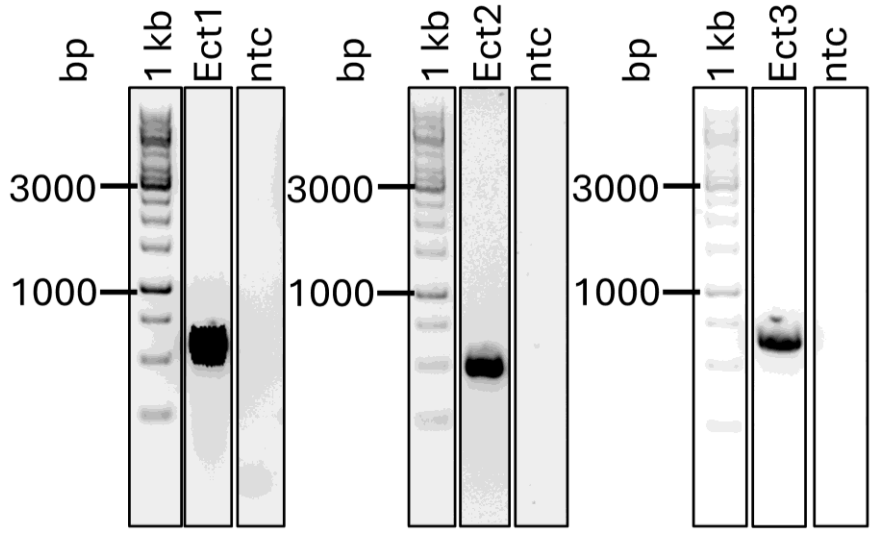

Figure 6.17: Colony PCR. To confirm *E. coli* transformants (Ect). *E. coli* transformed with pDONR + *HcXXTs* were verified via PCR using cell material as template; Ect1: pDONR + *HcXXTA*, pDONRF & RI40R; expected size 0,76 kbp; Ect2: pDONR + *HcXXTB*, pDONRF RI41R; expected size 0,59 kbp; Ect3: pDONR + *HcXXTC*, pDONRF & RI46RV3; expected size 0,75 kbp; bp = base pairs, no template control = ntc

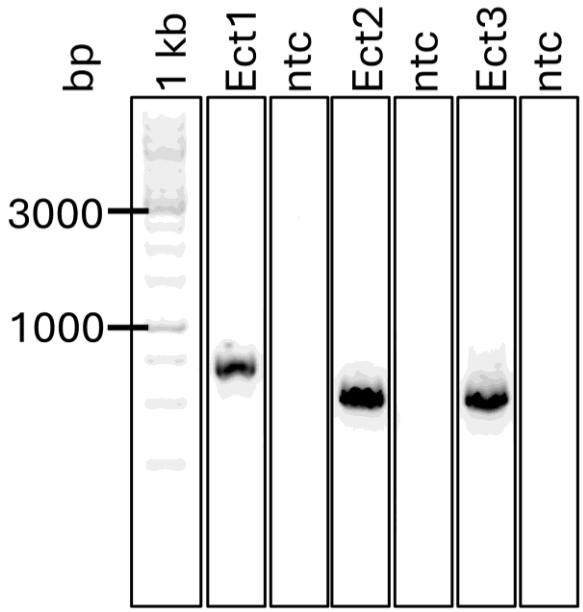

Figure 6.18: Colony PCR. To confirm *E. coli* transformants (Ect). *E. coli* transformed with pH2GW7 + *HcXXTA/B* and pMpGWB202 + *HcXXTC* were verified via PCR using cell material as template; Ect1: pH2GW7 + *HcXXTA*: RI71F & RI40R; expected size 0,8 kbp; Ect2: pH2GW7 + *HcXXTB*: RI71F & RI41R; expected size 0,7 kbp; Ect3: pMpGWB202 + *HcXXTC*: RI71F & RI46RV3; expected size 0,8 kbp; bp = base pairs, no template control = ntc

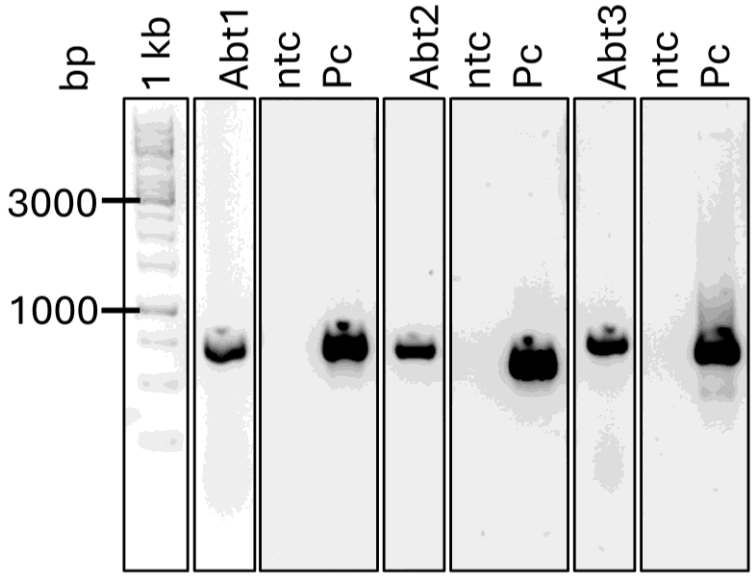

Figure 6.19: Colony PCR. To confirm Agrobacterium transformants (Abt). Agrobacterium transformed with pH2GW7 + *HcXXTA/B* and pMpGWB202 + *HcXXTC* plasmids were verified via PCR using cell material as template; Ect1: pH2GW7 + *HcXXTA*: RI71F & RI40R; expected size 0,8 kbp; Ect2: pH2GW7 + *HcXXTB*: RI71F & RI41R; expected size 0,7 kbp; Ect3: pMpGWB202 + *HcXXTC*: RI71F & RI46RV3; expected size 0,8 kbp; bp = base pairs, no template control = ntc

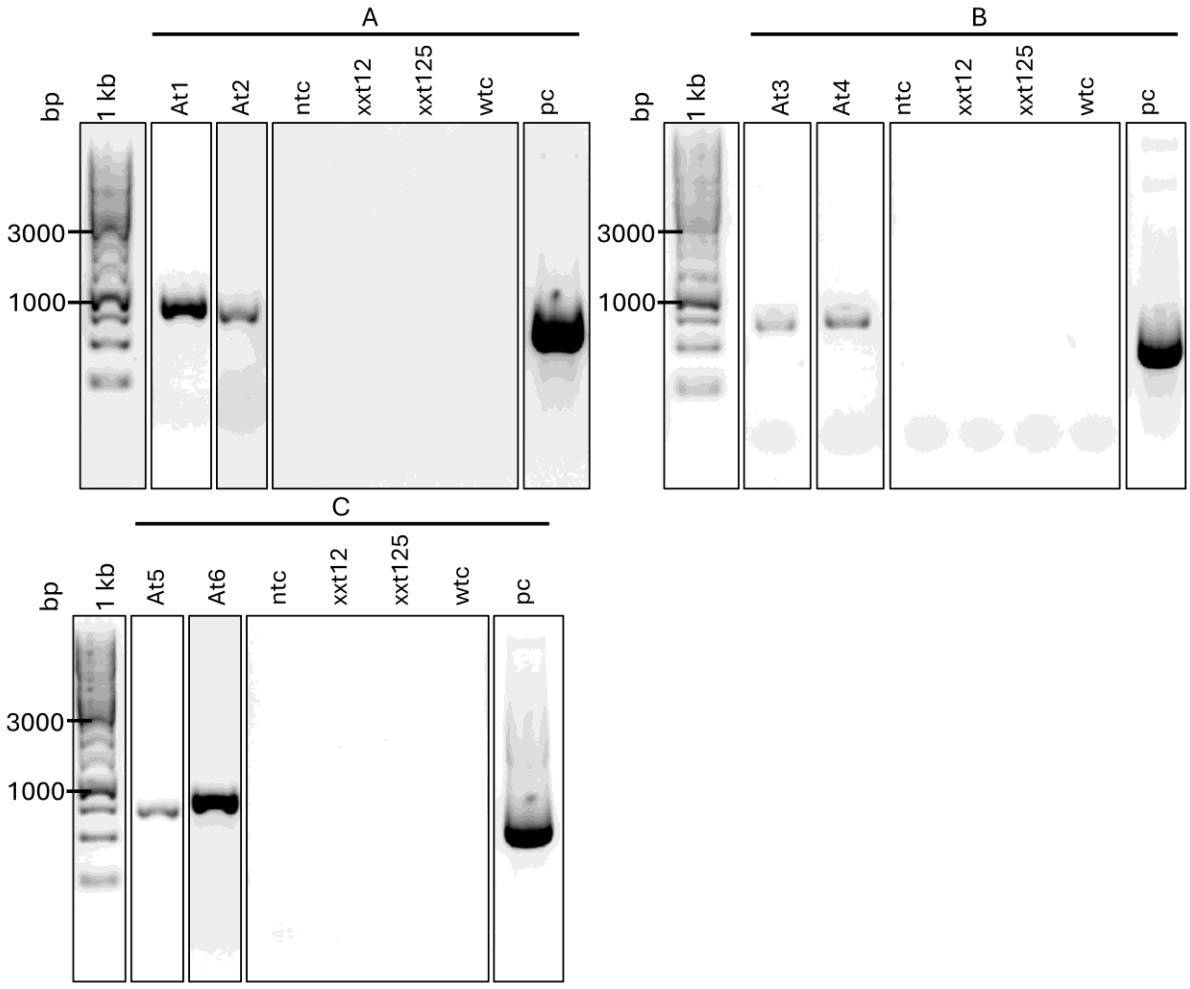

Figure 6.20: PCR to confirm T1 Arabidopsis transformants (At). Arabidopsis *xxt12* and *xxt125* transformed with pH2GW7 + *HcXXTA/B* and pMpGWB202 + *HcXXTC* were verified via PCR using gDNA as template; **A)** pH2GW7 + *HcXXTA* in *xxt12* (At1) and *xxt12*5 (At2), RI71F & RI40R; expected size 0,8 kbp; **B)** pH2GW7 + *HcXXTB* in *xxt12* (At3) and *xxt125* (At4), RI71F & RI41R; expected size 0,7 kbp; **C)** pMpGWB202 + *HcXXTC* in *xxt12* (At5) and *xxt125* (At6), RI71F & RI46RV3; expected size 0,8 kbp; bp = base pairs, no template control = ntc, wildtype control = wtc, plasmid control = pc

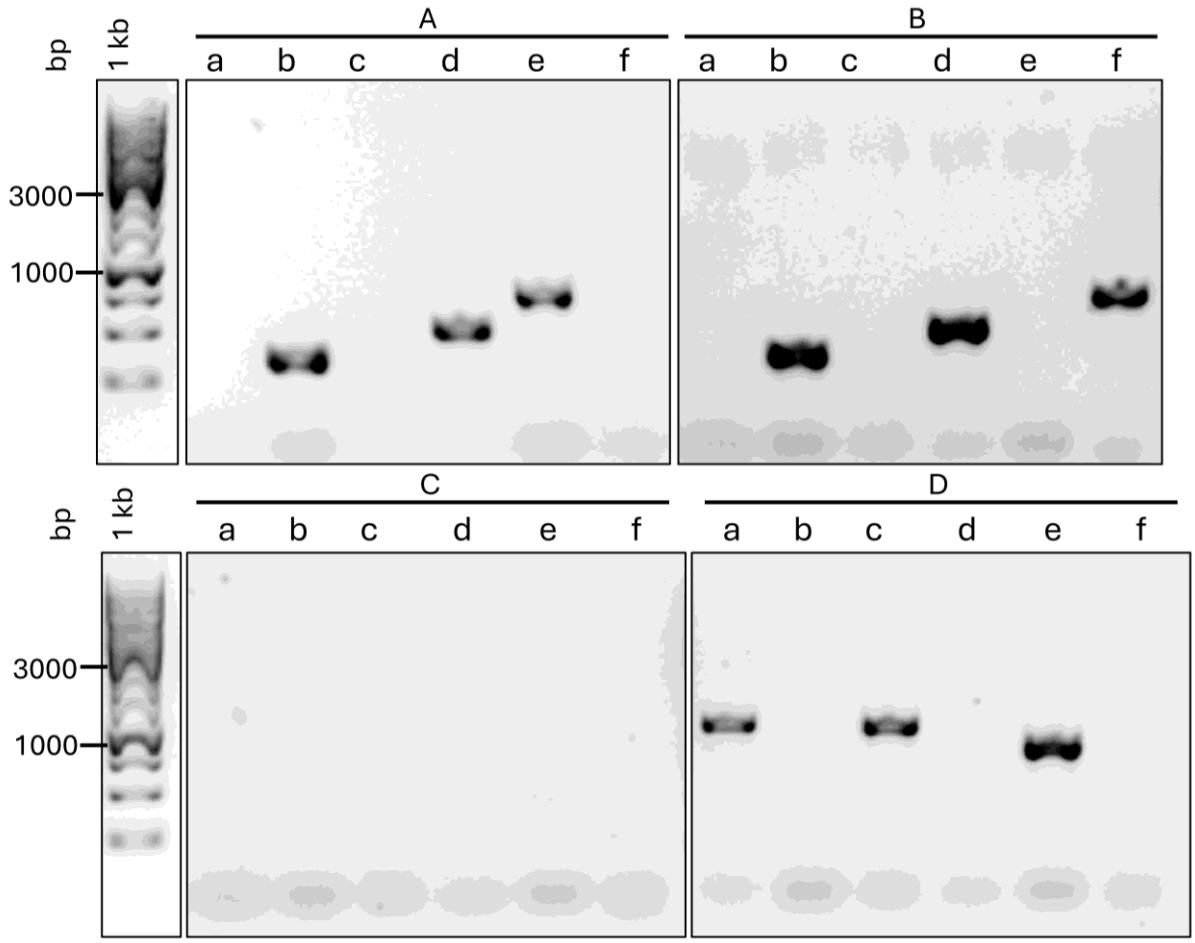

Figure 6.21: Genotyping PCR of T1 Arabidopsis *xxt12* and *xxt125*. PCR products amplifying a genomic fragment spanning the T-DNA insertion and a fragment from the T-DNA border to a genomic position to confirm presence or absence of T-DNA insertion; a: SAIL_785-E02 LP & RP, *XXT1* WT specific; b: SAIL_785-E02 RP & LB3, *xxt1* T-DNA insertion; c: SALK_101308 LP & RP, *XXT2* WT specific; d: SALK_101308 RP & LBb1.3, *xxt2* T-DNA insertion; e: P5Ef & P5r, *XXT5* WT specific; f: P5r & LB-TDNA, *xxt5* T-DNA insertion; **A)** *xxt12* double mutant, **B)** *xxt125* triple mutant, **C)** no template controls, **D)** wildtype controls, plant with no T-DNA insertion; bp = base pairs

	Hc XXTB	Hc XXTC	Os XXT1	Tm XXT2	Tm XXT5	At XXT1	A tXXT2	At XXT3	At XXT4	At XXT5
Hc XXTA	**0.396**	0.773	0.602	0.431	0.952	0.742	0.712	0.899	0.993	0.985
Hc XXTB		0.732	0.522	**0.296**	0.888	0.637	0.564	0.759	0.846	0.828
Hc XXTC			0.726	0.726	**0.509**	0.931	0.928	0.716	0.725	0.790

Figure 6.22: Root mean square deviation of HcXXT compared to known XXTs. RMSD is computed between aligned pairs of the backbone C-alpha atoms in superposed structures. Hymenaea (Hc), Arabidopsis (At), rice (Os) and nasturtium (Tm)

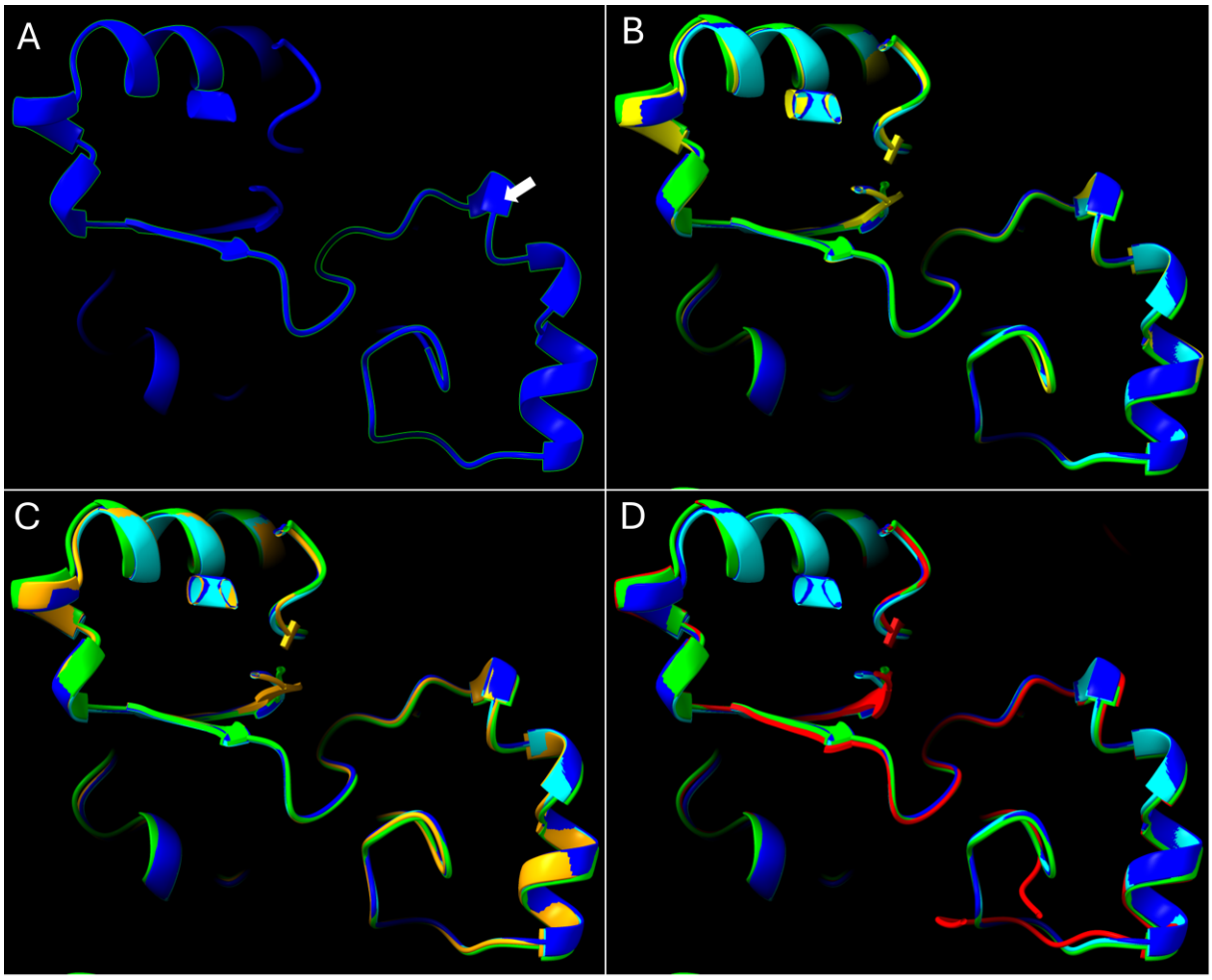

Figure 6.23: Secondary structure of essential amino acid region of Hymenaea XXTs in comparison with Arabidopsis XXT1, XXT2 and XXT5. The secondary structure of XXTs was predicted by AlphaFold and visualized using ChimeraX. The essential amino acid sequence (outlined in A) is based on (Zhang et al., 2023b) **A)** AtXXT1, arrow indicates place of isoleucin 351 which is supposed to hinder xylosylation of glucose N when the N + 2 glucosyl toward the reducing end has been xylosylated (Culbertson et al., 2018). XXT5 has a glycine residue in the corresponding location. **B)** HcXXTA (yellow) in comparison with AtXXT1 (dark blue), AtXXT2 (light blue) and AtXXT5 (green); **C)** HcXXTB (orange) in comparison with AtXXT1 (dark blue), AtXXT2 (light blue) and AtXXT5 (green); **D)** HcXXTC (red) in comparison with AtXXT1 (dark blue), AtXXT2 (light blue) and AtXXT5 (green)

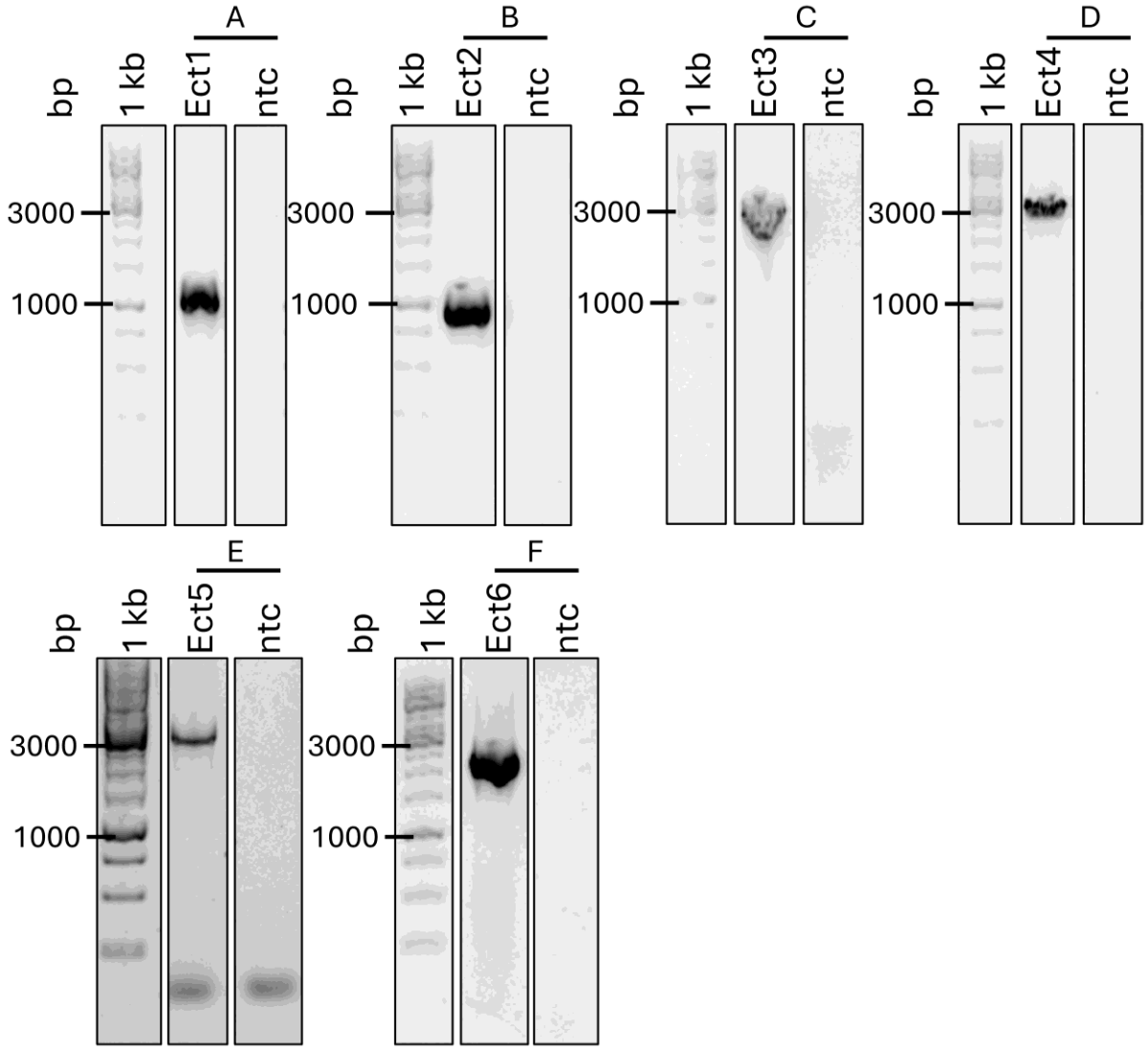

Figure 6.24: Colony PCR. To confirm *E. coli* transformants (Ect). *E. coli* transformed with plasmids were verified via PCR using cell material as template; **A)** Ect1: pPICZ eH + *TmUGD*; CV5F & NG55R (bind in AOX promotor and *TmUGD*), expected size 1,3 kbp; **B)** Ect2: pPICZ eH + *TmUXS*; NG56F & NG56R (bind in *TmUXS*), expected size 1,15 kbp; **C)** Ect3: pPICZ eH + *TmUGD* + *TmUXS2*; NG55F & NG119R (bind in *TmUGD* and *TmUX*S) expected size 3,5 kbp; **D)** Ect4: pPICZ eH + *TmUGD* + *AtUXS3*; NG55F & RI53R (bind in *TmUGD* and *AtUXS3*), expected size 3 kbp; **E)** Ect5: pPICZ eH + *TmUGD* + *TmUXS2* + *AtUUAT1*; NG119F & RIPhD55R (bind in *TmUXS* and *AtUUAT1*), expected size 2,8 kbp; **F)** Ect6: pPICZ eH + *TmUGD* + *AtUXS3* + *AtUXT3*; RIPhD53F & 54R (bind in *AtUXS3* and *AtUXT3*), expected size 2,8 kbp, bp = base pairs, no template control = ntc

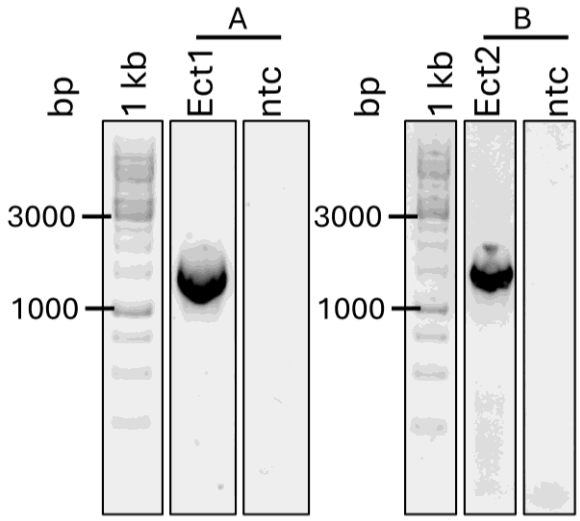

Figure 6.25: Colony PCR. To confirm *E. coli* transformants (Ect). *E. coli* transformed with plasmids were verified via PCR using cell material as template; **A)** Ect1: pPICZ + *OsCSLC2* + *TmXXT2*: NG163F + NG166R (bind in *OsCSLC2* and *TmXXT2*), expected size 1,7 kbp; **B)** Ect2: pPICZ + *OsCSLC2* + *OsXXT1*: NG163F + NG164R (bind in *OsCSLC2* and *OsXXT1*), expected size 1,7 kbp; bp = base pairs, no template control = ntc

	WT	TmCSLC4, TmXXT2, TmUGD, TmUXS & HsSLC35D1	TmCSLC4, TmXXT2, TmUGD, TmUXS, HsSLC35D1 & TXXT5
t-Xyl	0,00 [a]	0,14 [a]	0,06 [a]
		± 0,12	± 0,07
t-Man	15,13 [a]	11,88 [a]	12,34 [a]
	± 2,09	± 1,55	± 0,62
t-Glc	6,89 [a]	8,37 [a]	5,94 [a]
	± 0,52	± 2,96	± 0,73
3-Glc	11,66 [a]	10,96 [a]	13,09 [a]
	± 1,39	± 2,14	± 1,82
2-Man	20,67 [a]	16,82 [a]	17,00 [a]
	± 1,38	± 4,16	± 0,90
4-Man	0,99 [a]	0,86 [a]	0,70 [a]
	± 0,38	± 0,25	± 0,06
6-Man	**2,45 [a]**	**1,65[b]**	**2,23 [a]**
	± 0,17	± 0,11	± 0,21
6-Glc	12,69 [a]	10,03 [a]	10,47 [a]
	± 2,69	± 2,29	± 1,09
4-Glc	**1,72 [a]**	**15,87 [b]**	**12,31 [b]**
	± 0,52	± 3,99	± 5,32
2,3-Man	1,25 [a]	1,34 [a]	0,95 [a]
	± 0,09	± 0,29	± 0,11
3,4-Glc	**1,37 [a]**	**1,91 [b]**	**1,77 [b]**
	± 0,15	± 0,04	± 0,07
2,3-Glc	4,35 [a]	3,97 [a]	4,73 [a]
	± 0,34	± 0,30	± 0,68
2,4-Man	0,97 [a]	1,20 [a]	0,78 [a]
	± 0,23	± 0,37	± 0,04
3,6-Glc	5,84 [a]	5,08 [a]	5,30 [a]
	± 0,72	± 0,93	± 0,57
3,6-Man	**1,72 [ab]**	**1,40 [a]**	**1,77 [b]**
	± 0,20	± 0,17	± 0,11
2,6-Man	**11,21 [a]**	**6,58 [b]**	**9,10 [ab]**
	± 0,14	± 2,32	± 1,65
4,6-Glc	**1,11 [a]**	**1,94 [b]**	**1,47 [ab]**
	± 0,26	± 0,38	± 0,34

Figure 6.26: Glycosidic linkage analysis of Pichia pastoris strains expressing XyG biosynthesis genes - adding TmXXT5 to the five gene strain. Linkages of Pichia AIR material of WT and strains expressing XyG biosynthesis genes (TmCSLC4, TmXXT2, TmUGD, TmUXS and HsSLC35D1; TmCSLC4, TmXXT2, TmUGD, TmUXS, HsSLC35D1 and TmXXT5); WT n = 3, TmCSLC4, TmXXT2, TmUGD, TmUXS & HsSLC35D1 n = 3, TmCSLC4, TmXXT2, TmUGD, TmUXS, HsSLC35D1 & TXXT5 n = 4; results of ANOVA analysis and subsequent Tukey's test indicated ($P < 0,05$).

	WT	TmCSLC4	TmCSLC4 & TmXXT2	TmCSLC4 & TmXXT5
t-Man	12,13 [a]	8,94 [a]	8,31 [a]	13,08 [a]
	± 3,26	± 0,69	± 1,69	± 3,28
t-Glc	12,70 [a]	11,09 [a]	13,33 [a]	14,42 [a]
	± 0,99	± 0,47	± 3,83	± 1,54
3-Glc	9,07 [a]	10,82 [a]	9,49 [a]	11,09 [a]
	± 0,79	± 0,57	± 1,92	± 1,35
2-Man	**12,75 [a]**	**9,82 [ab]**	**8,30 [b]**	**12,12 [a]**
	± 1,49	± 0,75	± 0,95	± 2,73
6-Man	**4,53 [a]**	**3,40 [b]**	**3,64 [ab]**	**3,14 [b]**
	± 0,67	± 0,25	± 0,68	± 0,42
6-Glc	15,72 [a]	18,25 [a]	16,47 [a]	14,27 [a]
	± 2,53	± 1,03	± 1,41	± 2,31
4-Glc	**0,64 [a]**	**1,30 [a]**	**8,75 [b]**	**1,55 [a]**
	± 0,43	± 0,30	± 2,24	± 0,24
2,3-Man	**2,66 [a]**	**1,62 [b]**	**1,63 [b]**	**1,74 [ab]**
	± 0,82	± 0,28	± 0,29	± 0,17
3,4-Glc	1,71 [a]	2,64 [a]	2,93 [a]	1,90 [a]
	± 1,16	± 0,40	± 0,50	± 0,08
2,3-Glc	8,32 [a]	11,56 [a]	9,96 [a]	11,05 [a]
	± 1,68	± 2,11	± 3,48	± 4,14
2,4-Man	**1,90 [a]**	**1,01 [ab]**	**0,31 [b]**	**1,00 [ab]**
	± 0,92	± 0,08	± 0,62	± 0,18
3,6-Glc	**9,99 [ab]**	**11,58 [a]**	**10,14 [ab]**	**8,41 [b]**
	± 1,26	± 0,74	± 0,71	± 1,12
3,6-Man	**2,21 [a]**	**1,91 [ab]**	**1,62 [b]**	**1,72 [ab]**
	± 0,26	± 0,28	± 0,29	± 0,10
2,6-Man	5,67 [a]	6,06 [a]	4,57 [a]	4,49 [a]
	± 1,08	± 0,61	± 0,88	± 0,88
4,6-Glc	0,00 [a]	0,00 [a]	0,55 [a]	0,00 [a]
	± 0,00	± 0,00	± 0,67	± 0,00

Figure 6.27: Glycosidic linkage analysis of *Pichia pastoris* strains expressing TmCSLC4 and TmXXTs. Linkages of Pichia AIR material of WT and strains expressing XyG biosynthesis genes (TmCSLC4; TmCSLC4 and TmXXT2; TmCSLC4 and TmXXT5); n = 4 for all strains; results of ANOVA analysis and subsequent Tukey's test are indicated ($P < 0,05$).

	WT	TmCSLC4, TmXXT2, TmUGD, TmUXS & HsSLC35D1	TmCSLC4, TmXXT2, TmUGD, TmUXS, HsSLC35D1 & AtUXS3	TmCSLC4, TmXXT2, TmUGD, TmUXS, HsSLC35D1 & AtUUAT1
t-Xyl	**0,00** [a]	**0,43** [b]	**0,38** [b]	**0,55** [b]
		± 0,08	± 0,12	± 0,16
t-Man	**10,20** [a]	**7,21** [b]	**9,79** [a]	**8,48** [ab]
	± 1,34	± 0,55	± 1,35	± 1,40
t-Glc	**28,02** [a]	**25,98** [a]	**14,31** [b]	**16,68** [ab]
	± 4,55	± 6,57	± 5,64	± 3,77
3-Glc	7,05 [a]	7,20 [a]	7,78 [a]	8,36 [a]
	± 0,75	± 1,85	± 0,91	± 0,80
2-Man	**11,66** [a]	**7,18** [b]	**10,60** [a]	**8,67** [ab]
	± 0,82	± 0,92	± 1,77	± 0,96
4-Man	0,98 [a]	1,15 [a]	1,14 [a]	1,50 [a]
	± 0,46	± 0,31	± 0,20	± 0,70
6-Man	2,05 [a]	1,83 [a]	1,94 [a]	2,16 [a]
	± 0,49	± 0,25	± 0,17	± 0,10
6-Glc	13,72 [a]	11,77 [a]	13,05 [a]	13,53 [a]
	± 1,58	± 1,15	± 0,51	± 2,13
4-Glc	**2,01** [a]	**13,34** [b]	**18,08** [b]	**15,73** [b]
	± 0,29	± 2,14	± 3,69	± 3,06
2,3-Man	2,12 [a]	1,89 [a]	1,60 [a]	1,81 [a]
	± 0,06	± 0,62	± 0,44	± 0,49
3,4-Glc	1,71 [a]	2,55 [a]	1,95 [a]	2,20 [a]
	± 0,22	± 0,42	± 0,23	± 0,61
2,3-Glc	4,23 [a]	3,76 [a]	3,40 [a]	3,53 [a]
	± 0,83	± 1,43	± 0,40	± 1,03
2,4-Man	2,01 [a]	1,70 [a]	1,39 [a]	1,58 [a]
	± 0,29	± 0,64	± 0,34	± 0,57
3,6-Glc	6,64 [a]	5,78 [a]	6,52 [a]	7,05 [a]
	± 1,04	± 1,36	± 0,69	± 0,87
3,6-Man	1,76 [a]	1,90 [a]	1,62 [a]	1,79 [a]
	± 0,75	± 0,26	± 0,18	± 0,18
2,6-Man	4,41 [a]	2,79 [a]	3,63 [a]	2,89 [a]
	± 2,21	± 0,39	± 1,08	± 0,63
4,6-Glc	**1,42** [a]	**3,53** [b]	**2,80** [ab]	**3,50** [b]
	± 1,08	± 0,31	± 0,82	± 0,89

Figure 6.28: Glycosidic linkage analysis of *Pichia pastoris* strains expressing XyG biosynthesis genes - adding Arabidopsis XyG biosynthesis genes to the five gene strain. Linkages of Pichia AIR material of WT and strains expressing XyG biosynthesis genes (TmCSLC4, TmXXT2, TmUGD, TmUXS and HsSLC35D1; TmCSLC4, TmXXT2, TmUGD, TmUXS, HsSLC35D1 and AtUXS3; TmCSLC4, TmXXT2, TmUGD, TmUXS, HsSLC35D1 and AtUUAT1); n = 4 for all strains; results of ANOVA analysis and subsequent Tukey's test are indicated ($P < 0,05$).

	WT	TmCSLC4 & TmXXT2	TmCSLC4, TmXXT2, TmUXS, TmUGD & HsSLC35D1	TmCSLC4, TmXXT2, TmUXS, AtUXS3 & AtUXT3	TmCSLC4, TmXXT2, TmUXS, AtUXS3 & AtUUAT1
t-Xyl	0,00 [a]	0,00 [a]	0,10 [a]	0,15 [a]	0,12 [a]
			± 0,12	± 0,12	± 0,06
t-Man	13,19 [a]	11,37 [a]	10,40 [a]	10,31 [a]	10,50 [a]
	± 0,66	± 1,17	± 2,71	± 0,83	± 1,09
t-Glc	**5,77 [ab]**	**4,19 [a]**	**5,65 [ab]**	**6,39 [b]**	**5,65 [ab]**
	± 1,09	± 0,29	± 0,77	± 0,93	± 0,64
3-Glc	11,30	12,45	12,72	8,74	9,44
	± 0,84	± 1,80	± 3,30	± 0,64	± 1,46
2-Man	**28,93 [a]**	**28,11 [a]**	**19,55 [b]**	**17,81 [b]**	**18,63 [b]**
	± 3,57	± 2,74	± 5,84	± 1,03	± 2,61
4-Man	1,02 [a]	0,38 [a]	0,75 [a]	0,80 [a]	0,83 [a]
	± 0,66	± 0,04	± 0,35	± 0,33	± 0,66
6-Man	**2,03 [a]**	**1,40 [b]**	**1,85 [ab]**	**1,62 [ab]**	**1,75 [ab]**
	± 0,25	± 0,12	± 0,10	± 0,35	± 0,36
6-Glc	12,30 [a]	10,03 [a]	11,15 [a]	10,82 [a]	11,19 [a]
	± 2,06	± 1,26	± 1,88	± 0,85	± 0,50
4-Glc	**1,07 [a]**	**12,96 [b]**	**14,36 [b]**	**23,75 [c]**	**20,49 [bc]**
	± 0,32	± 1,55	± 8,69	± 1,80	± 1,83
2,3-Man	1,93 [a]	0,96 [a]	1,45 [a]	1,56 [a]	1,54 [a]
	± 0,74	± 0,07	± 0,50	± 0,33	± 0,46
3,4-Glc*	0,87 [a]	0,48 [a]	1,14 [a]	1,13 [a]	1,10 [a]
	± 0,30	± 0,07	± 0,76	± 0,26	± 0,63
2,3-Glc	**3,23 [ab]**	**3,24 [ab]**	**3,74 [a]**	**2,52 [b]**	**2,83 [ab]**
	± 0,55	± 0,38	± 0,81	± 0,19	± 0,46
2,4-Man	1,70 [a]	0,67 [a]	1,19 [a]	1,22 [a]	1,27 [a]
	± 0,91	± 0,07	± 0,46	± 0,32	± 0,51
4,6-Man	0,44 [a]	0,19 [a]	0,33 [a]	0,40 [a]	0,34 [a]
	± 0,16	± 0,01	± 0,19	± 0,14	± 0,18
3,6-Glc	5,71 [a]	4,29 [a]	5,32 [a]	4,83 [a]	5,22 [a]
	± 1,38	± 0,69	± 1,29	± 0,32	± 0,66
3,6-Man	**1,43 [a]**	**0,99 [b]**	**1,32 [ab]**	**1,18 [ab]**	**1,25 [ab]**
	± 0,07	± 0,22	± 0,10	± 0,18	± 0,21
2,6-Man	7,62 [a]	7,44 [a]	6,60 [a]	4,48 [a]	5,45 [a]
	± 3,17	± 1,89	± 3,51	± 0,63	± 1,70
4,6-Glc	1,45 [a]	0,85 [a]	2,36 [a]	2,30 [a]	2,40 [a]
	± 1,02	± 0,18	± 1,68	± 0,57	± 1,16

Figure 6.29: Glycosidic linkage analysis of *Pichia pastoris* strains expressing XyG biosynthesis genes - UDP-Xyl synthesis pathway with plant genes. Linkages of Pichia AIR material of WT and strains expressing XyG biosynthesis genes (TmCSLC4, TmXXT2; TmCSLC4, TmXXT2, TmUGD, TmUXS and HsSLC35D1; TmCSLC4, TmXXT2, TmUGD, AtUXT3 and AtUXS3; TmCSLC4, TmXXT2, TmUGD, TmUXS and AtUUAT1); n = 4 for all strains; results of ANOVA analysis and subsequent Tukey's test are indicated ($P < 0,05$).

	WT	TmCSLC4 & TmXXT2	OsCSLC2 &TmXXT2	OsCSLC2 & OsXXT1
t-Man	12,93 [a]	12,50 [a]	13,56 [a]	13,98 [a]
	± 0,64	± 1,03	± 0,84	± 0,43
t-Glc	4,45 [a]	4,75 [a]	4,57 [a]	4,52 [a]
	± 0,33	± 0,46	± 0,21	± 0,42
3-Glc	14,01 [a]	12,75 [a]	14,03 [a]	13,54 [a]
	± 0,93	± 0,63	± 0,31	± 1,10
2-Man	**32,86 [ab]**	**29,98 [a]**	**33,64 [b]**	**34,91 [b]**
	± 1,22	± 2,27	± 0,88	± 1,61
4-Man	**0,60 [a]**	**0,39 [b]**	**0,49 [ab]**	**0,35 [b]**
	± 0,09	± 0,09	± 0,06	± 0,06
6-Man	1,32 [a]	1,04 [a]	1,31 [a]	1,30 [a]
	± 0,13	± 0,04	± 0,10	± 0,22
6-Glc	10,17 [a]	9,13 [a]	9,90 [a]	9,33 [a]
	± 1,14	± 1,54	± 0,61	± 1,08
4-Glc	**0,65 [a]**	**9,06 [b]**	**0,77 [a]**	**0,64 [a]**
	± 0,05	± 0,94	± 0,02	± 0,12
2,3-Man	0,86 [a]	0,78 [a]	0,96 [a]	0,93 [a]
	± 0,08	± 0,12	±,10	± 0,16
3,4-Glc	0,63 [a]	0,54 [a]	0,53 [a]	0,45 [a]
	± 0,19	± 0,13	± 0,11	± 0,07
2,3-Glc	4,65 [a]	4,17 [a]	4,12 [a]	4,66 [a]
	± 0,55	± 0,36	± 0,46	± 0,62
2,4-Man	**0,63 [ab]**	**0,55 [a]**	**0,71 [b]**	**0,61 [ab]**
	± 0,04	± 0,11	± 0,03	± 0,07
4,6-Man	0,16 [a]	0,19 [a]	0,22 [a]	0,18 [a]
	± 0,02	± 0,08	± 0,07	± 0,05
3,6-Glc	4,57 [a]	4,06 [a]	4,46 [a]	4,08 [a]
	± 0,43	± 0,69	± 0,33	± 0,43
3,6-Man	1,14 [a]	1,00 [a]	1,13 [a]	1,08 [a]
	± 0,07	± 0,06	± 0,07	± 0,08
2,6-Man	9,93 [a]	8,36 [a]	9,03 [a]	9,01 [a]
	± 0,95	± 1,12	± 0,96	± 1,31
4,6-Glc	**0,43 [a]**	**0,73 [b]**	**0,57 [ab]**	**0,44 [a]**
	± 0,03	± 0,13	± 0,15	± 0,09

Figure 6.30: Glycosidic linkage analysis of Pichia strains expressing Oryza sativa CSLC and XXT. Pichia AIR material of WT and strains expressing different combinations of nasturtium and rice CSLCs and XXTs; n = 4 for all strains; results of ANOVA analysis and subsequent Tukey's test are indicated ($P < 0,05$).

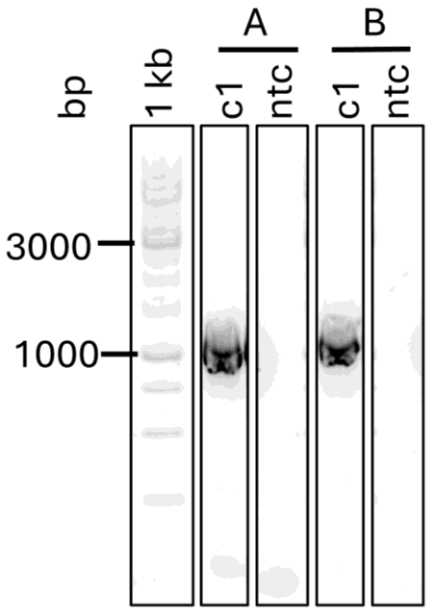

Figure 6.31: Genotyping PCR. To confirm Pichia transformants, colony (c1) transformed with the linearized plasmid pPICZ eH +*TmXXT2*; **A)** CV5F & NG54R (bind in AOX1 promoter and *TmXXT2*), expected size: 1,2 kbp; **B)** NG54F & CV5RV2 (bind in *TmXXT2* and AOX terminator), expected size: 1,25 kbp; bp = base pairs, no template control = ntc

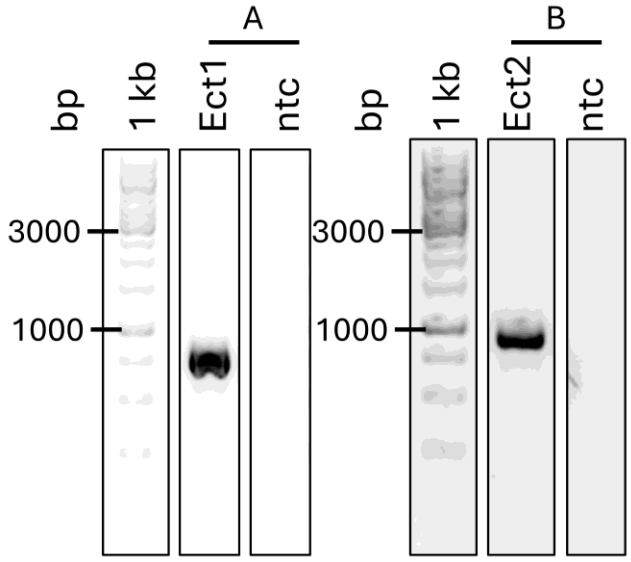

Figure 6.32: Colony PCR. To confirm *E. coli* transformants (Ect). *E. coli* transformed with plasmids were verified via PCR using cell material as template; **A)** Ect1: pPICZ B + *KnCSLC271*: NG170F&R (bind in *KnCSLC271*), expected size 0,9 kbp; **B)** Ect2: pPICZ Gateway + *KnCSLC603*: RI5F&6R (bind in AOX promotor and *KnCSLC603*), expected size 1 kbp, bp = base pairs, no template control = ntc

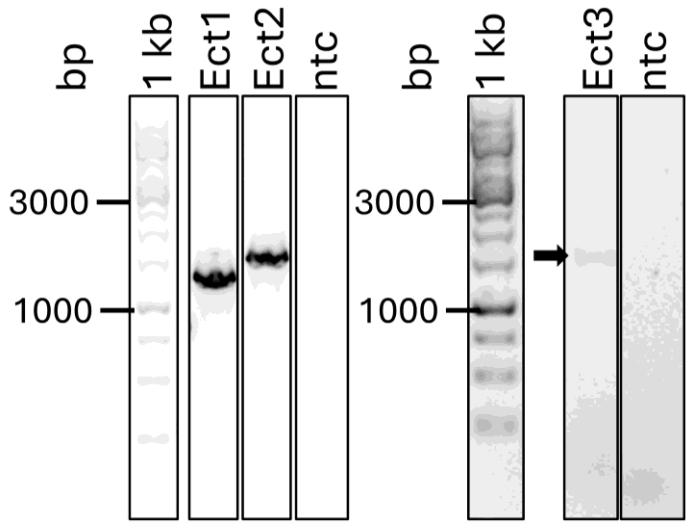

Figure 6.33: Colony PCR. To confirm *E. coli* transformants (Ect). *E. coli* transformed with plasmids were verified via PCR using cell material as template; Ect1: pPICZ eH + *KnXXT*: CV5F & CV5RV2 (bind in AOX promotor and AOX terminator), expected size 1,4 kbp; Ect2: pPICZ eH + *MeXXT*: CV5F & CV5RV2, expected size 1,7 kbp; Ect3: pPICZ eH + *SmXXT*: CV5F & CV5RV2, expected size 1,6 kbp; bp = base pairs, no template control = ntc

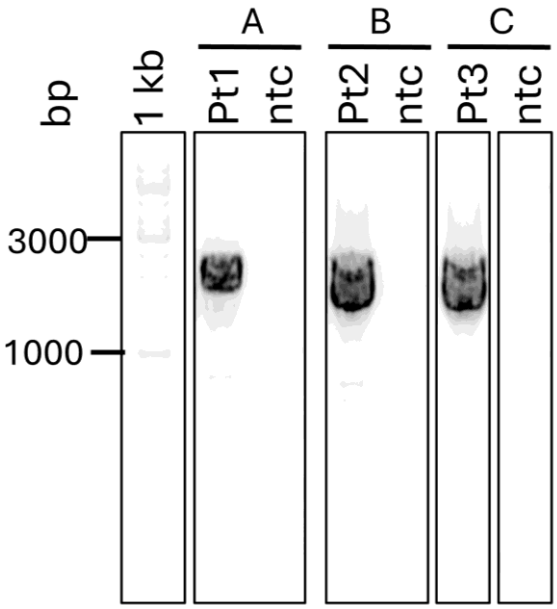

Figure 6.34: Genotyping PCR. To confirm Pichia transformants (Pt), colonies transformed with the linearized plasmids Pt1: pPICZ eH + *KnXXT*, Pt2: pPICZ eH + *MeXXT*, pPICZ eH + *SmXXT*; **A)** RI25F & RI15R (bind in ENO1 and *KnXXT*); expected size 2,3 kbp; **B)** RI25F & RI16R (bind in ENO1 and *MeXXT*); expected size 2,4 kbp; **C)** RI25F & RI17R (bind in ENO1 and *SmXXT*); expected size 2,4 kbp; bp = base pairs, no template control = ntc

KnCSLC 126	TM 5	MFAFIVQSIDKLLLITGYFYISWKQPTKEGDS GSLAVGDCGGNEEKPAFEPVVLVQIPMRNE RECYKRGIMAACRLDWPQDKLVVQVLDDSD DPDMQQLVRDEVDAWRAVGAPIRYTHRTAR TGFKAGALAHGMQDPAIQHCEYVAIFDADFV PAKDFLRRTVPKFEGQPKLALVQARWAFAN AQQNLLTRFQVISMSYHFEVEQQVQNHFNA FFGFNGTAGVWRVQALREAGGWLARTTTED MDLAVRAHMKGWNFTYLNDVTVPSELPCTY KAYCKQQQRWHAGPARLFMLTWHRSLTCP TLSAYQKFNLLVCFFWFRRFVLPVTGFLLYCI IMPLAVLLPEASLPLWFLAYMQTQAILHWLPH RGSWCLLFPYYAFENVMYRVKAQAIFSGLFN LRSAHVWVVTAKTGIDAKTENIQSGGSKCVG KEGGVANDAEPVSPVSEGSSDDAFVAHASM DPLIAYDLPELRVGLKVRTAHGRGEETSGHC TGLDSSAKRRDFGHVSSPMKRGLWSPSAG RRLSLLTPTEERAERDPSLLTSFEAGAAWRL ERTLYRLPSLREVWEKVTWANVRGFMAVRT LHVPELGWAAFVFGAMTYGISAGRYGLSVYL GMQGLGYLIAGLDLMGY	OMMMMMMMMMMMMMM MMMMMIIIIIIIIIIIIIIIIIIIIIIIIIIIIII IIIIIIIIIIIIIIIIIIIIIIIIIIIIIIIIIIIIIIIIIIIII IIIIIIIIIIIIIIIIIIIIIIIIIIIIIIIIIIIIIIIIIIIII IIIIIIIIIIIIIIIIIIIIIIIIIIIIIIIIIIIIIIIIIIIII IIIIIIIIIIIIIIIIIIIIIIIIIIIIIIIIIIIIIIIIIIIII IIIIIIIIIIIIIIIIIIIIIIIIIIIIIIIIIIIIIIIIIIIII IIIIIIIIIIIIIIIIIIIIIIIIIIIMMMMMMM MMMMMMMMMMMMMMM MMMMMMMOOOOOMMMM MMMMMMMMMMMMMIIIII IIIIIIIIIIIIIIIIIIIIIIIIIIIIIIIIIIIIIIIIIIIII IIIIIIIIIIIIIIIIIIIIIIIIIIIIIIIIIIIIIIIIIIIII IIIIIIIIIIIIIIIIIIIIIIIIIIIIIIIIIIIIIIIIIIIII IIIIIIIIIIIIIIIIIIIIIIIIIIIIIIIIIIIIIIIIIIIII IIIIIIIIIIIIIIIIIIIIIIIIIIIMMMMMM MMMMMMMMMMMMMOO OOOMMMMMMMMMMM MMMMMMMMMII
KnCSLC 271	TM 6	MGQRKTDAGLQQEEGTPKKRAHLVNFRKV QSIGLQVGFFVLLCWALSRLVYGGTLDAGTA SRGWKEFRTRWVLPLMQPVLNFLVGAFLLQ SVDKVLLVAAGVYLGLRRSGKAGAPSVAAAT TQDEGTVVGMPAYEPAVVVQIPMCNERECY RQSITAACRLDWPQDKLVIQVLDDSDQDDV QALIHEEVDAWRATGAPIFYLHRAVRAGHKA GNLAHGMQDPSAKHCEFVAILDADFVPASDF LRRTVPHFEGQPKLALVQARWAFVNPRQNL LTRFQNIHFAYHFEVEQQVQGHFNKFFGFNG TAGVWRVQALQDAGSWNDRTTVEDMDLAV RAHMLGWEFTFLNDVRVPSELPASYVAFCK QQHRWYAGPMRLCLLTAGSTLASRTLTAWH KFNLLACFFGLRRLVLPLAAYPLFCLLLPATV LVPEATVPAAVVYAMPLLLAFLHWLPHPGSW PLLLPFLVFENVLYRIKFQAIVSGVLGFKGAS DWVVTAKTGAVQEADEFDDDLDGGLEDVPE GIEVEDGALGEARDGDSVSPCSAKSVDAFV VHAGSESSDQLAAYDLPPLAAGLTVRTGREP SVMGGKKGAFRSASLPPQMKRQLSGAAER ALLSPSASRRRPGGTPRKGDAASLLTPRGR EVALKRLERTLSRLPSMQQVRQRVTWASCK RFWAARKVQGPEMGMAAYMLGAAAYGVAV GDTRYTLFLVVQGTGFLVAGLDLLGC	IIIIIIIIIIIIIIIIIIIIIIIIIIIIIMMMMMM MMMMMMMMMMMMMMM MOOOOOOOOOOOOOO OOOOOOOOOMMMMMMM MMMMMMMMMMMMMMM MMMMMMIIIIIIIIIIIIIIIIIIIIIIIIIIIII IIIIIIIIIIIIIIIIIIIIIIIIIIIIIIIIIIIIIIIIIIIII IIIIIIIIIIIIIIIIIIIIIIIIIIIIIIIIIIIIIIIIIIIII IIIIIIIIIIIIIIIIIIIIIIIIIIIIIIIIIIIIIIIIIIIII IIIIIIIIIIIIIIIIIIIIIIIIIIIIIIIIIIIIIIIIIIIII IIIIIIIIIIIIIIIIIIIIIIIIIIIIIIIIIIIIIIIIIIIII IIIIIIIIIIIIIIIIIIIIIIIIIIIMMMMM MMMMMMMMMMMMMMM MMMMOOOOOOOOOOM MMMMMMMMMMMMMMM MMIIIIIIIIIIIIIIIIIIIIIIIIIIIIIIIIII IIIIIIIIIIIIIIIIIIIIIIIIIIIIIIIIIIIIIIIIIIIII IIIIIIIIIIIIIIIIIIIIIIIIIIIIIIIIIIIIIIIIIIIII IIIIIIIIIIIIIIIIIIIIIIIIIIIIIIIIIIIIIIIIIIIII IIIIIIIIIIIIIIIIIIIIIIIIIIIIIIIIIIIIIIIIIIIIM MMMMMMMMMMMMMMM MMMMMOOOOOMMMMMM MMMMMMMMMMMMMMMI
KnCSLC 603	TM 8	MPARCRPSMPPSSLCCGCGLSCSPPRAWH RLQKFPLSRARQEAGGPSLRPAVSFCFLGLP GGAVPLAATFRCLFLPPAGPSAIVVLLSSLSL SSSHFAPAVPHRPPAAMGRPSEGSPAAAAP RSHRQQQRKGNKQPPALPTRAPFLRRGWR VPWRSAMVTLLAGGAAVGVSLVAWSVLYVS GAALAAAVAGESHPGTPLEGWRYARAKLLE	IIIIIIIIIIIIIIIIIIIIIIIIIIIIIIIIIIIIIIIIIIIII IIIIIIIIIIIIIIIIIIIIIIIIIIIIIIIIIIIIIIIIIIIII IIIIIIIIIIIIIIIIIIIIIIIIIIIIIIIIIIIIIIIIIIIII IIIIIIIIIIIIIMMMMMMMMM MMMMMMMMMMMMMMM MOOOOOOOOOOOOOO OOOOOOOOOOOOOOO

		GLPLLPAAWTRLRRRRIAPALQAAADAGVAIF LVQALDKLLQCGMAAAIFWSAAGRATRADH AAQQQQQQQARARPTPRVLVQVPMCNERE VYAQSIAAACLLEWPGEALLVQVLDDSSEKD VQHLIADEVAAWAARGAPIVYHARQAAGART VKGGYKAGNLQAGLAAAAGLGFEFVAIFDAD FMPRPDFLRIMMPHFEGRPDRALVQARWAF VNTSQNLLTRFQAINFAYHFMVEQQVGSSLC GFFGFNGTAGVWRTAAIEEAGGWDARTTVE DMDLAVRAHLCGYTFLYMNECEALCELPCT YRAYCKQQHRWNAGRARLRLFKTYQAQVS APSTSLIRLFLLSAACMFRIATMGAAHVSEPL GAVAELLACVRCAGPVVLFFLCLPAILRSRAL GVARKAYVVAVFFVLRKLILPTLAFLLFCLLLP TTIFIPEISVPVWAVFYLPTVLSLLHTAPYPRA WPYLFPFLLFENVMTRTKCGAIWDGLVGVR SAKEWVVTKKTGARAAAPPAAAASAAAFHL VSGDAVSPSARALAGAGLLQSLEDVLEAGLF PGDPTDDGADLVSTASPTARQVAHLMTGRA PLPAPGGATGEPGKAVTDGAPADVAVRGGP SRQLSWADLALGAYLVVAAGWSVLVLDGRH AFFLAFQGGAFLAAGLDLVGDPS	OOOOOOOOOOOOOOO OOOOMMMMMMMMMMM MMMMMMMMMMMMMMMII IIIIIIIIIIIIIIIIIIIIIIIIIIIIIIIIIIIIIIII IIIIIIIIIIIIIIIIIIIIIIIIIIIIIIIIIIIIIIII IIIIIIIIIIIIIIIIIIIIIIIIIIIIIIIIIIIIIIII IIIIIIIIIIIIIIIIIIIIIIIIIIIIIIIIIIIIIIII IIIIIIIIIIIIIIIIIIIIIIIIIIIIIIIIIIIIIIII IIIIIIIIIIIIIIIIIIIIIIIIIIIIIIIIIIIIIIII IIIIIIIMMMMMMMMMMMM MMMMMMMMOOOOOMMM MMMMMMMMMMMMMMM MMMMMMIIIIIIIIIIIIIIIMMMM MMMMMMMMMMMMMMM MMMMMMOOOOOOOOMM MMMMMMMMMMMMMMM MIIIIIIIIIIIIIIIIIIIIIIIIIIIIIIIIIIIIIII IIIIIIIIIIIIIIIIIIIIIIIIIIIIIIIIIIIIIIII IIIIIIIIIIIIIIIIIIIIIIIIIIIIIIIIIIIIIIII IIIIIIIIIIIIIIIIIIIIIIIMMMMMMM MMMMMMMMMMMMMMO OOMMMMMMMMMMMM MMMMMMMMIII
MeCSLC	TM 6	MAPNIRFTEWWASRDYPTRPIIVKMEKNAWS LPELKESEPLMKAEAPPAPAVEMVKSQSAK QFTWLMLLQAHKAAGCLAWVGLGVAELVKH VRKRLLTKEAIEEGVGSSEEKPRGRLLQVLR TLLLISLVMLVLEAFTHLKGWQFQSPAMSMP TRVNVQNFLHWVYLGWVHYRRAYVAPVLQ WLANSCTLLFLVQSVDRIVLCAGAAYIKLRGI KPVPKVDVFSEQDPESPYEYPMVLVQIPMC NEKECYEQSIGAVCQLEWPVDRLLIQVLDDS DDEDCQRLIRGEVERWSQKGAPIMYRHRLIR KGYKAGNLNSAMRCDYVKDYEFVAIFDADF QPKSDFLKRTVPHFAEQPDIALVQARWAFVN RDENLLTRLQLINLAFHFEVEQQVNGHFLNF FGFNGTAGVWRIKALEDSGGWLDRTTVEDM DIAVRAHLQGWKFIFLNDVEALCELPESYEAY KKQQHRWHSGPMQLFRLCLPSIIKAKISLWK KFNMVFLFFLLRKMVLPFYSFTLFCIILPCTMF VPEASLPLWVVAYVPAIMSILNIIPAPKSFPFIV PYLLFENTMSVTKFNAMVAGLFQLGSAYEW VVTKKTGRASEADLLAMVHPDPAAETLPALH ARSVSESGIDALADKMVTELVVAPTTPVATT PPPAKPAPKQKKIQKMYRKELSLALLLLVAAS RSLLTEHGMHFYFLAFQGLTFLVVGLDLIGEH QQL	IIIIIIIIIIIIIIIIIIIIIIIIIIIIIIIIIIIIIIII IIIIIIIIIIIIIIIIIIIIIIIIIIIIIIIIIIIIIIII IIIIIIIIIIIIIIIIIIIIIMMMMMMMM MMMMMMMMMMMMMMO OOOOOOOOOOOOOOO OOOOOOOOOOOOOOO OOOOOOOOOOMMMMMM MMMMMMMMMMMMMMM MMMMMIIIIIIIIIIIIIIIIIIIIIIIIIII IIIIIIIIIIIIIIIIIIIIIIIIIIIIIIIIIIIIIIII IIIIIIIIIIIIIIIIIIIIIIIIIIIIIIIIIIIIIIII IIIIIIIIIIIIIIIIIIIIIIIIIIIIIIIIIIIIIIII IIIIIIIIIIIIIIIIIIIIIIIIIIIIIIIIIIIIIIII IIIIIIIIIIIIIIIIIIIIIIIIIIIIIIIIIIIIIIII IIIIIIIIIIIIIIIIIIIMMMMMMMM MMMMMMMMMMMMMMO OOOOOOOOOOMMMMM MMMMMMMMMIIIIIIIIIIIIIIIIII IIIIIIIIIIIIIIIIIIIIIIIIIIIIIIIIIIIIIIII IIIIIIIIIIIIIIIIIIIIIIIIIIIIIIIIIIIIIIII IIIIIIIIMMMMMMMMMMM MMMMMMOOOOOOMMMM MMMMMMMMMMMMMMMII IIII
SmCSLC	TM 6	MPPNLDFQDWCAAAAATKEALPPRPIMVKV DKAAYAMPELDTSLIPALPEIGERKRNAKQLT WVLLLKAHKAAGCIAWLGVGLVTFLTAVRHR LLTKQGLGKTVGGGDSKPRSRLLRVLRIFLLV VLGFFVFEAVAHAFGWQHHVPQFHRLSTVG	IIIIIIIIIIIIIIIIIIIIIIIIIIIIIIIIIIIIIIII IIIIIIIIIIIIIIIIIIIIIIIIIIIIIIIIIIIIIIII IIIIIIIIIIIIIIIIIIIIMMMMMMMM MMMMMMMMMMMMMMO OOOOOOOOOOOOOOO

		FYNLLHWSYLSWVSFRKKYIAPPLQFFANTC TYLFIFQSIDRVVLSLGCFWIRLRGLRPQPKV ELEEAGADLERAVDHYPMVLIQVPMCNERE CYEQAITAACQMDWPKTRMLVQVLDDSDDV TIQKLIRGEVQRWLQKGSPITYRHRLLRRGY KAGNLQSAMSCDYVKDYEFVAIFDADFQPKP DFLKKTVLHFEEQPDLALVQARWSFINKDEN LLTRLQNINLSFHFEVEQQVNGTFINFFGFNG TAGVWRIAALEDSGGWLDRTTVEDMDIAVR AHLKGWKFIFLNDVEALCELPESYEAYRKQQ HRWHSGPMQLFRLCLPDIITAKVALWKKFNM IFLFFLLRKMILPFYSFTLFCIILPLTMFVPEASL PLWVVCYIPGAMSILNVIPSPRSFPFLVPYLLF ENTMSVTKFQAMISGLFQLNSASEWVVTKKT GRSSEADLLAAVREVKAENGPPLPSHARAA SETCLDSLKEQQSALQVAAESPKLKLKPKRT VQRMYRKELALALLLLVAAARSLMSERGMHF YFLLFQGLAFLVVGLDLIGEPQKPDSFFALLA GHAMGK	OOOOOOOOOOOOOOO OOOOOOOOMMMMMMMM MMMMMMMMMMMMMMMII IIIIIIIIIIIIIIIIIIIIIIIIIIIIIIIIIIIIIIII IIIIIIIIIIIIIIIIIIIIIIIIIIIIIIIIIIIIIIII IIIIIIIIIIIIIIIIIIIIIIIIIIIIIIIIIIIIIIII IIIIIIIIIIIIIIIIIIIIIIIIIIIIIIIIIIIIIIII IIIIIIIIIIIIIIIIIIIIIIIIIIIIIIIIIIIIIIII IIIIIIIIIIIIIIIIIIIIIIIIIIIIIIIIIIIIIIII IIIIIIIMMMMMMMMMMMMM MMMMMMMMMMMMMOO OOOOOOOOMMMMMMMM MMMMMMMMMIIIIIIIIIIIIIIIII IIIIIIIIIIIIIIIIIIIIIIIIIIIIIIIIIIIIIIII IIIIIIIIIIIIIIIIIIIIIIIIIIIIIIIIIIIIIIII MMMMMMMMMMMMMMM MMMOOOOMMMMMMMM MMMMMMMMMMMMMIIIIIIIII IIIIIIIIIII
AtCSLC4 AT3G281 80	TM 6	MAPNSVAVTMEKPDNFSLLEINGSDPSSFPD KRKSISPKQFSWFLLLKAHRLISCLSWLVSSV KKRIAFSAKNINEEEDPKSRGKQMYRFIKACL VISIIALSIEIVAHFKKWNLDLINRPSWEVYGLV EWSYMAWLSFRSDYIAPLVISLSRFCTVLFLI QSLDRLVLCLGCFWIKFKKIEPKLTEESIDLED PSSFPMVLIQIPMCNEREVYEQSIGAASQLD WPKDRILIQVLDDSDDPNLQLLIKEEVSVWAE KGVNIIYRHRLIRTGYKAGNLKSAMTCDYVKD YEFVTIFDADFTPNPDFLKKTVPHFKGNPELG LVQARWSFVNKDENLLTRLQNINLCFHFEVE QQVNGVFLNFFGFNGTAGVWRIKALEESGG WLERTTVEDMDIAVRAHLNGWKFIYLNDVEV TCELPESYEAYKKQQHRWHSGPMQLFRLCL PSIIKSKISVWKKANLIFLFFLLRKLILPFYSFTL FCIILPLTMFIPEAELPLWIICYVPIFISLLNILPS PKSFPFLVPYLLFENTMSITKFNAMISGLFQF GSAYEWVVTKKTGRSSESDLLAFAEKEEKLH RRNSESGLELLSKLKEQETNLVGQETVKKSL GGLMRPKNKKKTNMVFKKELGLAFLLLTAAA RSFLSAHGLHFYFLLFQGLSFLVVGLDLIGEQ IS	IIIIIIIIIIIIIIIIIIIIIIIIIIIIIIIIIIIIIIII IIIIIIIIIIIIIIIIIIIIIIIIIIIIIIIIIIIIIIIM MMMMMMMMMMMMMMM MMMMMOOOOOOOOOOO OOOOOOOOOOOOOOO OOOOOOMMMMMMMMM MMMMMMMMMMMMMMM MMMMIIIIIIIIIIIIIIIIIIIIIIIIIIIIIIII IIIIIIIIIIIIIIIIIIIIIIIIIIIIIIIIIIIIIIII IIIIIIIIIIIIIIIIIIIIIIIIIIIIIIIIIIIIIIII IIIIIIIIIIIIIIIIIIIIIIIIIIIIIIIIIIIIIIII IIIIIIIIIIIIIIIIIIIIIIIIIIIIIIIIIIIIIIII IIIIIIIIIIIIIIIIIIIIIIIIIIIIIIIIIIIIIIII IIIIIIIIIIIIIIIIMMMMMMMMM MMMMMMMMMMMMMMM MOOOOOOOOOMMMMM MMMMMMMMMMMMIIIIIIIIII IIIIIIIIIIIIIIIIIIIIIIIIIIIIIIIIIIIIIIII IIIIIIIIIIIIIIIIIIIIIIIIIIIIIIIIIIIIIIII IIIIMMMMMMMMMMMMM MMMMMMMOOOOMMMM MMMMMMMMMMMMMMM MMIIIII
AtCSLC5 AT4G315 90	TM 6	MAPRLDFSDWWAKDTRKGTPVVVKMENPN YSVVEIDGPDSAFRPVEKSRGKNAKQVTWV LLLKAHRAVGCLTWLATVFWSLLGAIKKRLSF THPLGSEKLGRDRWLFTAIKLFLAVSLVILGF EIVAYFRGWHYFQSPSLHIPTSTLEIQSLFHL VYVGWLTLRADYIAPPIKALSKFCIVLFLIQSV DRLVLCLGCFWIKYKKIKPRFDEEPFRNDDA EGSGSEYPMVLVQIPMCNEREVYEQSISAVC QLDWPKDRILVQVLDDSNDESIQQLIKAEVAK WSQKGVNIIYRHRLVRTGYKAGNLKSAMSC	IIIIIIIIIIIIIIIIIIIIIIIIIIIIIIIIIIIIIIII IIIIIIIIIIIIIIIIIIIIIIIIIIIIIIIIIIIIIIII IIIIIIIIIIIIIMMMMMMMMMM MMMMMMMMMMOOOOOO OOOOOOOOOOOOOOO OOOOOOOOOOOOOOO OOOMMMMMMMMMM MMMMMMMMMMMMIIIII IIIIIIIIIIIIIIIIIIIIIIIIIIIIIIIIIIIIIIII IIIIIIIIIIIIIIIIIIIIIIIIIIIIIIIIIIIIIIII

		DYVEAYEYVAIFDADFQPTPDFLKLTVPHFKD NPELGLVQARWTFVNKDENLLTRLQNINLCF HFEVEQQVNGVFLNFFGFNGTAGVWRIKAL EESGGWLERTTVEDMDIAVRAHLHGWKFIYL NDVKVLCEVPESYEAYKKQQHRWHSGPMQ LFRLCLGSILTSKIAIWKKANLILLFFLLRKLILP FYSFTLFCIILPLTMFVPEAELPVWVICYIPVF MSFLNLLPSPKSFPFIVPYLLFENTMSVTKFN AMVSGLFQLGSSYEWIVTKKAGRSSESDLLS ITEKETPTKKSQLLRGVSDSELLELSQLEEQK QAVSKKPVKKTNKIYHKELALAFLLLTAALRS LLAAQGVHFYFLLFQGVTFLLVGLDLIGEQMS	IIIIIIIIIIIIIIIIIIIIIIIIIIIIIIIIIIIIIIIIIIIIIII IIIIIIIIIIIIIIIIIIIIIIIIIIIIIIIIIIIIIIIIIIIIIII IIIIIIIIIIIIIIIIIIIIIIIIIIIIIIIIIIIIIIIIIIIIIII IIIIIIIIIIIIIIIIIIIIIIIIIIIIIIIIIIIIIIIIIIIIIII IIIIMMMMMMMMMMMMMM MMMMMMMMMMMMOOO OOOOOOOMMMMMMMMM MMMMMMMMIIIIIIIIIIIIIIIIIIIIIII IIIIIIIIIIIIIIIIIIIIIIIIIIIIIIIIIIIIIIIIIIIIIII IIIIIIIIIIIIIIIIIIIIIIIIIIIIIIIIIIIMMMM MMMMMMMMMMMMMMO OOMMMMMMMMMMMMM MMMMMMMMMIIII
AtCSLC6 AT3G073 30	TM 6	MSRSQNEEFQQWWNKQRDRNNHDVLYAG DDEAFLTVEIRTPATVDPDKDRIRTRTVRQLS RLYLLKFKQLASSFLWIGNSFLYLVRTANRRI ANDNPPSVSSSARLYRLIKGFLVVVVLLLCFE LAAYFKGWHFTPPSVASAEVAVEVVYAWWL EIRASYLAPPLQSLTNVCIVLFLIQSVDRLVLV LGCFWIKLRRIKPVASMEYPTKLVGEGVRLE DYPMVIVQIPMCNEKEVYQQSIGAVCMLDW PRERMLVQVLDDSSELDVQQLIKAEVQKWQ QRGVRIVYRHRLIRTGYKAGNLKAAMNCEYV KDYEFVAIFDADFQPPADFLKKTVPHFKGNE ELALVQTRWAFVNKDENLLTRLQNINLSFHF EVEQQVNGVFINFFGFNGTAGVWRIKALEDC GGWLERTTVEDMDIAVRAHLCGWKFIYLND VKCLCELPESYEAYKKQQYRWHSGPMQLFR LCFFDILRSKVSAAKKANMIFLFFLLRKLILPFY SFTLFCVILPLTMFFPEANLPSWVVCYIPGIM SILNIIPAPRSFPFIVPYLLFENTMSVTKFGAMI SGLFKFDSSYEWVVTKKLGRSSEADLVAYAE SGSLVESTTIQRSSSDSGLTELSKLGAAKKA GKTKRNRLYRTEIALAFILLAASVRSLLSAQGI HFYFLLFQGITFVIVGLDLIGEQVS	IIIIIIIIIIIIIIIIIIIIIIIIIIIIIIIIIIIIIIIIIIIIIII IIIIIIIIIIIIIIIIIIIIIIIIIIIIIIIIIIIIIIIIIIIIIII IIIIIIIIIIIIIIMMMMMMMMMMM MMMMMMMMMMOOOOOO OOOOOOOOOOOOOOOO OOOOOOOOOOOOMMMM MMMMMMMMMMMMMMM MMMMMMMMMMIIIIIIIIIIIIIIIII IIIIIIIIIIIIIIIIIIIIIIIIIIIIIIIIIIIIIIIIIIIIIII IIIIIIIIIIIIIIIIIIIIIIIIIIIIIIIIIIIIIIIIIIIIIII IIIIIIIIIIIIIIIIIIIIIIIIIIIIIIIIIIIIIIIIIIIIIII IIIIIIIIIIIIIIIIIIIIIIIIIIIIIIIIIIIIIIIIIIIIIII IIIIIIIIIIIIIIIIIIIIIIIIIIIIIIIIIIIIIIIIIIIIIII IIIIIIIIIIIIIIIIIIIIIIIIIIIIIIIIIIIIIMMM MMMMMMMMMMMMMMM MMMMMMMMOOOOOOOO OOOMMMMMMMMMMMM MMMMIIIIIIIIIIIIIIIIIIIIIIIIIIIIIIIIIII IIIIIIIIIIIIIIIIIIIIIIIIIIIIIIIIIIIIIIIIIIIIIII IIIIIIIIIIIIIIIIIIMMMMMMMMM MMMMMMMMMOOOOMM MMMMMMMMMMMMMMM MMMMMIIII
AtCSLC8 AT2G246 30	Tm 6	MAPRFDFSDLWAKETRRGTPVVVKMENPNY SIVEVEEPDSAFQPMEKSRGKNAKQVTWVL LLKAHKAVGCLTWVATVFWSLLGSVKRRLSF THPLGSERLGRDGWLFSAIKLFLVASLAILAF ELVAYYRGWHYFKNPNLHIPTSKLEIQSLLHL FYVGWLSLRADYIAPPIKALSKFCIVLFLVQSV DRLILCLGCLWIKFKKIKPRIDEEHFRNDDFE GSGSEYPMVLVQIPMCNEREVYEQSISAVC QLDWPKDRLLVQVLDDSDDESIQELIRDEVT KWSQKGVNIIYRHRLVRTGYKAGNLKSAMS CDYVEAYEFVAIFDADFQPNSDFLKLTVPHF KEKPELGLVQARWAFVNKDENLLTRLQNINL CFHFEVEQQVNGVFLNFFGFNGTAGVWRIK ALEESGGWLERTTVEDMDIAVRAHLHGWKFI YLNDVKVLCEVPESYEAYKKQQHRWHSGP	IIIIIIIIIIIIIIIIIIIIIIIIIIIIIIIIIIIIIIIIIIIIIII IIIIIIIIIIIIIIIIIIIIIIIIIIIIIIIIIIIIIIIIIIIIIII IIIIIIIIIIIIIIMMMMMMMMMMM MMMMMMMMMMOOOOOO OOOOOOOOOOOOOOOO OOOOOOOOOOOOOOOO OOOMMMMMMMMMMMM MMMMMMMMMMMMMMIIIII IIIIIIIIIIIIIIIIIIIIIIIIIIIIIIIIIIIIIIIIIIIIIII IIIIIIIIIIIIIIIIIIIIIIIIIIIIIIIIIIIIIIIIIIIIIII IIIIIIIIIIIIIIIIIIIIIIIIIIIIIIIIIIIIIIIIIIIIIII IIIIIIIIIIIIIIIIIIIIIIIIIIIIIIIIIIIIIIIIIIIIIII IIIIIIIIIIIIIIIIIIIIIIIIIIIIIIIIIIIIIIIIIIIIIII IIIIIIIIIIIIIIIIIIIIIIIIIIIIIIIIIIIIIIIIIIIIIII IIIIMMMMMMMMMMMMMM

		MQLFRLCLRSILTSKIAMWKKANLILLFFLLRK LILPFYSFTLFCVILPITMFVPEAELPIWVICYV PIFMSLLNILPAPKSFPFIVPYLLFENTMSVTK FNAMVSGLFQLGSSYEWIVTKKAGRSSESDL LALTDKESEKMPNQILRGVSDSELLEISQVEE QKKQPVSVKKTNKIFHKELALAFLLLTAAVRS LLASQGVHFYFLLFQGLTFLLVGLDLIGEQMS	MMMMMMMMMMMMOOO OOOOOOOMMMMMMMMM MMMMMMMMIIIIIIIIIIIIIIIIIIII IIIIIIIIIIIIIIIIIIIIIIIIIIIIIIIIIIIIII IIIIIIIIIIIIIIIIIIIIIIIIIMMMMMM MMMMMMMMMMMMMMM OOOOMMMMMMMMMM MMMMMMMMMMIIII
AtCSLC12 AT4G079 60	Tm 6	MAPKFEWWAKGNNNNTRKGTPVVVKMENP NNWSMVELESPSHDDFLVRTHEKSRNKNAR QLTWVLLLKAHRAAGCLTSLGSALFALGTAV RRRIAAGRTDIEISSSGVGSLQKQNHTKKSKL FYSCLKVFLWLSLILLGFEIAAYFKGWSFGTS KLQLQFIFNKGFFDWVYTRWVLLRVEYLAPP LQFLANGCIVLFLVQSLDRLILCLGCFWIRFKK IKPVPKPDSISDLESGDNGAFLPMVLVQIPMC NEKEVYQQSIAAVCNLDWPKGKILIQILDDSD DPITQSLIKEEVHKWQKLGARIVYRHRVNRE GYKAGNLKSAMNCSYVKDYEFVAIFDADFQP LPDFLKKTIPHFKDNEEIGLVQARWSFVNKEE NLLTRLQNINLAFHFEVEQQVNSVFLNFFGF NGTAGVWRIKALEDSGGWLERTTVEDMDIA VRAHLHGWKFVFLNDVECQCELPESYEAYR KQQHRWHSGPMQLFRLCLPAVIKSKISIGKK FNLIFLFFLLRKLILPFYSFTLFCIILPMTMFVPE AELPAWVVCYIPATMSFLNILPAPKSFPFIVPY LLFENTMSVTKFNAMVSGLFQLGSAYEWVV TKKSGRSSEGDLAALVEKDEKTTKHQRGVS APETEAEKKAEKTKRKKKKHNRIYMKELSLA FLLLTAATRSLLSAQGIHFYFLLFQGISFLLVG LDLIGEQVE	IIIIIIIIIIIIIIIIIIIIIIIIIIIIIIIIIIIIIIIIIIII IIIIIIIIIIIIIIIIIIIIIIIIIIIIIIIIIIIIIIIIIIII IIIIIIIIIIIIIIIIIIIIIIIIIIIIIIIMMMMM MMMMMMMMMMMMMMM MOOOOOOOOOOOOOO OOOOOOOOOOOOOOO OOOOOOOMMMMMMMMM MMMMMMMMMMMMMMM MMIIIIIIIIIIIIIIIIIIIIIIIIIIIIIIIIIIII IIIIIIIIIIIIIIIIIIIIIIIIIIIIIIIIIIIIII IIIIIIIIIIIIIIIIIIIIIIIIIIIIIIIIIIIIII IIIIIIIIIIIIIIIIIIIIIIIIIIIIIIIIIIIIII IIIIIIIIIIIIIIIIIIIIIIIIIIIIIIIIIIIIII IIIIIIIIIIIIIIIIIIIIIIIIIIIIIIIIIIIIII IIIIIIIIIIIIIMMMMMMMMM MMMMMMMMMMMMMMM OOOOOOOOOOOOMMMM MMMMMMMMMMMMIIIIIIIIII IIIIIIIIIIIIIIIIIIIIIIIIIIIIIIIIIIIIII IIIIIIIIIIIIIIIIIIIIIIIIIIIIIMMM MMMMMMMMMMMMMMM MMMOOOOMMMMMMMM MMMMMMMMMMMMIIIII
TmCSLC4	TM 6	MAPNSVVVTIENPTSISVKEMMKKSDSESLF PDKQKKSVSSKQFTWFLLLKAHKALTCLSWL AMASKSLCSSVKKRVSSSDISEEEEEHPKSR GKLYRFIKVFLSISVLALIVEIIAYYMKWNLGS MIQPWGIQGFLHWSYMAWLSFRLDYIAPLVG LLSQFCIVLFMIQSLDRLILCIGCFWIKYKNLK PKIDENAYDIEDNSSFPMVLVQIPMCNEREV YEQSIGAVCQLDWPKDRILIQVLDDSDDSSL QLLIKEEVSSWRQKGVNIIYRHRLIRTGYKAG NMKSAMGCDYVKDYEFVAIFDADFQPNPDF LKLTMPHFKGDPEVGLVQARWSFVNKDENL LTRLQNINLCFHFEVEQQVNGVFLNFFGFNG TAGVWRIKALEESGGWLERTTVEDMDIAVRA HLNGWKFVFLNDVKVLCELPESYEAYKKQQ HRWHSGPMQLFRLCLPSVLSSKISAWKKAN LIFLFFLLRKLILPFYSFTLFCIILPLTMFIPETEL PLWVICYIPIFMSFLNILPSPKSFPFLVPYLLFE NTMSVTKFNAMISGLFQLGSAYEWVVTKKT GRSSESDLLALAEKEEKILRRNSESGLEMLS KLKEQEEIAPLKKVTKKKKNKIFRKELALAFLL	IIIIIIIIIIIIIIIIIIIIIIIIIIIIIIIIIIIIIIIIIIII IIIIIIIIIIIIIIIIIIIIIIIIIIIIIIIIIIIIIIIIIIII IIIIMMMMMMMMMMMMMM MMMMMMMOOOOOOOOO OOOOOOOOOOOOOOO OOOOOOOOOMMMMMM MMMMMMMMMMMMMMM MMMMMIIIIIIIIIIIIIIIIIIIIIIIIIIIII IIIIIIIIIIIIIIIIIIIIIIIIIIIIIIIIIIIIII IIIIIIIIIIIIIIIIIIIIIIIIIIIIIIIIIIIIII IIIIIIIIIIIIIIIIIIIIIIIIIIIIIIIIIIIIII IIIIIIIIIIIIIIIIIIIIIIIIIIIIIIIIIIIIII IIIIIIIIIIIIIIIIIIIIIIIIIIIIIIIIIIIIII IIIIIIIIIIIIIIIIIMMMMMMMMM MMMMMMMMMMMMMMM MMOOOOOOOOOOMMMM MMMMMMMMMMMMMIIIIIIII IIIIIIIIIIIIIIIIIIIIIIIIIIIIIIIIIIIIII IIIIIIIIIIIIIIIIIIIIIIIIIIIIIIIIIIIII MMMMMMMMMMMMMMM

		LTAAGRSLLSAQGVHFYFLLFQGLSFLVVGL DLIGEQMS	MMMOOOOMMMMMMMM MMMMMMMMMMMMMIIIII

Figure 6.35: Predicted topologies of CSLCs. Amino acid sequences and predicted Topologies of various CSLCs, TM = transmembrane protein, O = outside - the corresponding amino acid is outside of the membrane surrounding cell compartment, I = inside - the corresponding amino acid is inside of the membrane surrounding cell compartment, M = the corresponding amino acid is inside of the membrane

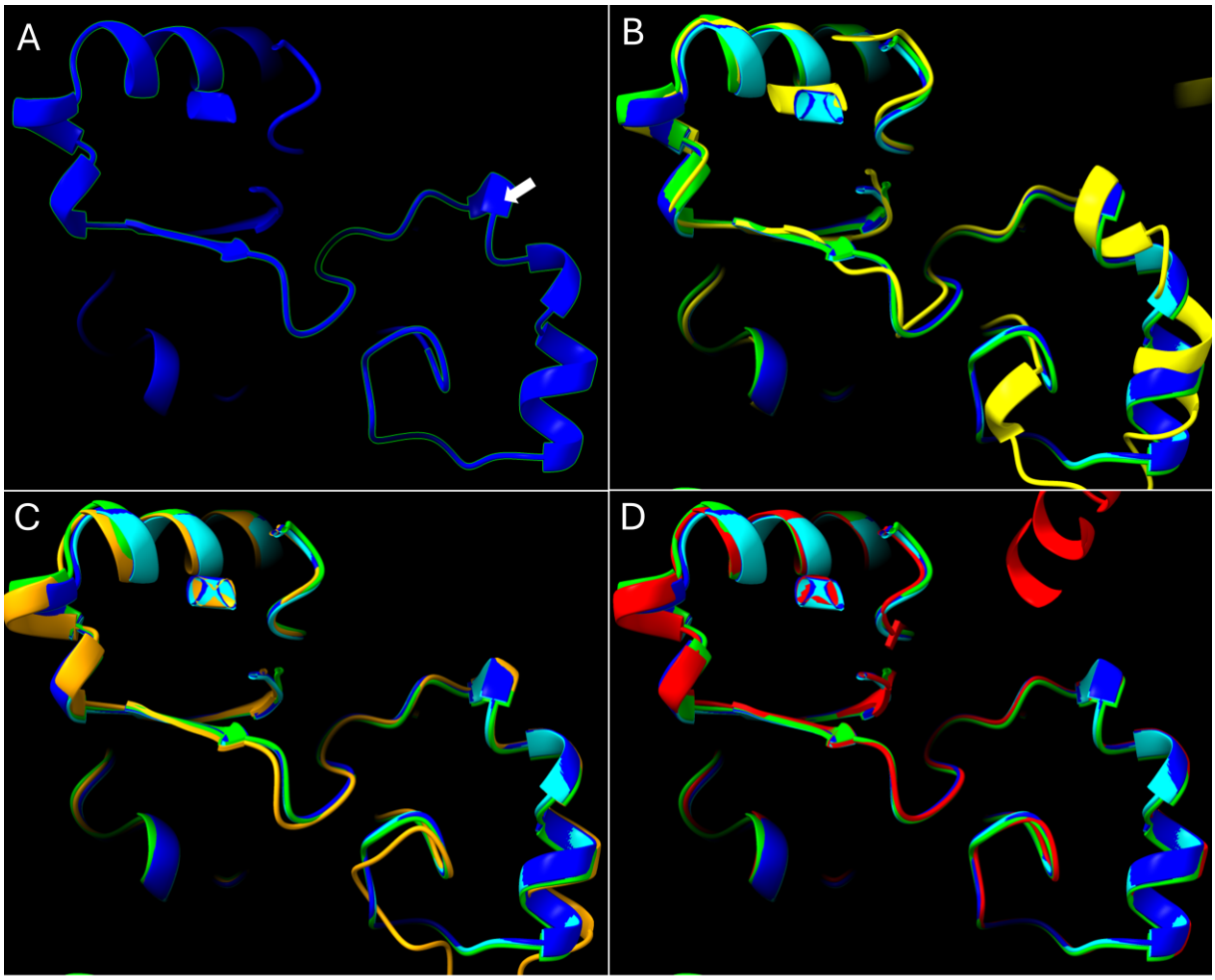

Figure 6.36: Secondary structure of essential amino acid region of algae XXTs in comparison with Arabidopsis XXT1, XXT2 and XXT5. The secondary structure of XXTs was predicted by AlphaFold and visualized using ChimeraX. The essential amino acid sequence (outlined in A) is based on (Zhang et al., 2023b) **A)** AtXXT1, arrow indicates place of Isoleucin 351 which is supposed to hinder xylosylation of glucose N when the N + 2 glucosyl toward the reducing end has been xylosylated (Culbertson et al., 2018). XXT5 has a glycine residue in the corresponding location. **B)** KnXXT (yellow) in comparison with AtXXT1 (dark blue), AtXXT2 (light blue) and AtXXT5 (green); **C)** MeXXT (orange) in comparison with AtXXT1 (dark blue), AtXXT2 (light blue) and AtXXT5 (green); **D)** SmXXT (red) in comparison with AtXXT1 (dark blue), AtXXT2 (light blue) and AtXXT5 (green)

KnXXT kfl0010 1_0170 _v1.1	TM 1	MAFKPTLFTKEKKMQRPFFHFCMF LVICVGAITLANYRRSKLPALIGAKL PPAIGTVDQGGTDNAADGVRLMLV TGTDGRPCSSARGAEILIRSLKNKV DYARLHDIPLYYAMETFDDAYDIYW VKLPLLKKLMHTHPTIEWFMWV**DC** **D**AIFTDMTRGIPLDEYTDYNLVLSG NATAVFEEPDWLGLNTGAFLIRNC QWSVDLLDATMALGNRYTTRRDTG LLLNKVLRGRAEASHGKEWPADDQ TTLIYLMATQPHLWKEKTLLDTTSM YHNWWVLVSQPLDQLLEDADASM PATWRPFISHFTGCKFCHVQHADE GQKEACMDTFDRLYRFADNQVLER FQLRHKSVDTEEIQEI	IIIIIIIIIIIIIIIIIMMMMMMMMMMMMMMMM MMOOOOOOOOOOOOOOOOOOOOOO OOOOOOOOOOOOOOOOOOOOOOOO OOOOOOOOOOOOOOOOOOOOOOOO OOOOOOOOOOOOOOOOOOOOOOOO OOOOOOOOOOOOOOOOOOOOOOOO OOOOOOOOOOOOOOOOOOOOOOOO OOOOOOOOOOOOOOOOOOOOOOOO OOOOOOOOOOOOOOOOOOOOOOOO OOOOOOOOOOOOOOOOOOOOOOOO OOOOOOOOOOOOOOOOOOOOOOOO OOOOOOOOOOOOOOOOOOOOOOOO OOOOOOOOOOOOOOOOOOOOOOOO OOOOOOOOOOOOOOOOOOOOOOOO OOOOOOOOOOOO
MeXXT ME000 051S08 080	GL OB	MEIRKARHPRERYGTIKATTFNITSE DGCKKIDWDKQREAYKARHPGCN VSRTTEQPSIMMLTGSSPKVCETS MGDRLLLQALKNKIDYCRPRGIEIFY NMASFDAELTNFWAKLPVLRMAML KHPHVEWFWWV**DAD**VYFTDMLFD MPMASYEKYEMVVPGYYDHVYKH KDWVGLNTGVFLTRNNQWTLDLLD MWAVFGPVGKVRDEAGLFFERELP GRPPFEADDQSALVYLLNKHNDTL RERVFLETSYILHGYWHVLVDKYED MMAHNSPGVIPHGNDKCPFTTHFV GCKPCGNYGEDRQRCFRQMIRAF NFADNQIIRRIGLQHVNLASWQVKP LPAVREEAVKKTKTAWTLKEEGLG PGQAGLPPCYHQREDEVAARRTQL HQDRVMFRGHTPSNNFVLVGGYR TGPRSFTAIGLARLAWRSQRKVER CTWTSLDGDQEDGTMESELSLFLC LPL	OOOOOOOOOOOOOOOOOOOOOOOO OOOOOOOOOOOOOOOOOOOOOOOO OOOOOOOOOOOOOOOOOOOOOOOO OOOOOOOOOOOOOOOOOOOOOOOO OOOOOOOOOOOOOOOOOOOOOOOO OOOOOOOOOOOOOOOOOOOOOOOO OOOOOOOOOOOOOOOOOOOOOOOO OOOOOOOOOOOOOOOOOOOOOOOO OOOOOOOOOOOOOOOOOOOOOOOO OOOOOOOOOOOOOOOOOOOOOOOO OOOOOOOOOOOOOOOOOOOOOOOO OOOOOOOOOOOOOOOOOOOOOOOO OOOOOOOOOOOOOOOOOOOOOOOO OOOOOOOOOOOOOOOOOOOOOOOO OOOOOOOOOOOOOOOOOOOOOOOO OOOOOOOOOOOOOOOOOOOOOOOO OOOOOOOOOOOOOOOOOOOOOOOO OOOOOOOOOOOOOOOOOOOOOOOO OOOOOOOOOOOOOOOOOOOOOOOO OOOO
SmXXT M0000 81S226 76	TM 1	MRGSGGGMWPPTAGGWGRQLAR AANNVKITLVCSLVTFLVLRGTLGA GRFGTPSHDAQRLVGAASLRPHRR ALKWHVLGSDKPPEAEEEFLYDPR RPYSLGPKISDWNERREMAIAHKP GCNVSASGRPRMMLVTGSQPKEC ENPLGDHLLLMAFKNKMDYCRLHD VEVFYNMAHLDRVMSGFWAKLPLL RHLMLSHPEIEWFWWM**DSD**AMFT DMVFELPMEKYEPYDMVLHGWER DVYELERWVGLNTGSFLIRNNQWIL DMLDVWAQMGPKGRVRTEAGKLL TAALKDRPAFEADDQSALVYLLIKN QAEWRPHVYLEQTYFLHGYWGIIV DKYEELMAKHHPGYGDERWPFVT HFVGCKPCSLADNYDAERCVVQM	IIIIIIIIIIIIIIIIIIIIIIIIIIIIMMMMMMMMMMMMM OOOOOOOOOOOOOOOOOOOOOOOO OOOOOOOOOOOOOOOOOOOOOOOO OOOOOOOOOOOOOOOOOOOOOOOO OOOOOOOOOOOOOOOOOOOOOOOO OOOOOOOOOOOOOOOOOOOOOOOO OOOOOOOOOOOOOOOOOOOOOOOO OOOOOOOOOOOOOOOOOOOOOOOO OOOOOOOOOOOOOOOOOOOOOOOO OOOOOOOOOOOOOOOOOOOOOOOO OOOOOOOOOOOOOOOOOOOOOOOO OOOOOOOOOOOOOOOOOOOOOOOO OOOOOOOOOOOOOOOOOOOOOOOO OOOOOOOOOOOOOOOOOOOOOOOO OOOOOOOOOOOOOOOOOOOOOOOO OOOOOOOOOOOOOOOOOOOOOOOO

		NRAFNFADNQVLQHYGYSHKHLNT TAIEAVNTTALEASRHPEQEDPT	OOOOOOOOOOOOOOOOOOOOOOOO O
AtXXT1 At3g62 720	TM 1	MIEKCIGAHRFRRLQRFMRQGKVTI LCLVLTVIVLRGTIGAGKFGTPEKDI EEIREHFFYTRKRGEPHRVLVEVSS KTTSSEDGGNGGNSYETFDINKLFV DEGDEEKSRDRTNKPYSLGPKISD WDEQRRDWLKQNPSFPNFVAPNK PRVLLVTGSAPKPCENPVGDHYLL KSIKNKIDYCRIHGIEIFYNMALLDAE MAGFWAKLPLIRKLLLSHPEIEFLW WM**DSD**AMFTDMVFELPWERYKDY NLVMHGWNEMVYDQKNWIGLNTG SFLLRNSQWSLDLLDAWAPMGPK GKIREEAGKVLTRELKDRPAFEADD QSAMVYLLATEREKWGGKVYLESG YYLHGYWGILVDRYEEMIENHKPG FGDHRWPLVTHFVGCKPCGKFGD YPVERCLRQMDRAFNFGDNQILQM YGFTHKSLGSRRVKPTRNQTDRPL DAKDEFGLLHPPFKAAKLSTTTT	IIIIIIIIIIIIIIIIIIIIIIIIMMMMMMMMMMMOOO OOOOOOOOOOOOOOOOOOOOOOOO OOOOOOOOOOOOOOOOOOOOOOOO OOOOOOOOOOOOOOOOOOOOOOOO OOOOOOOOOOOOOOOOOOOOOOOO OOOOOOOOOOOOOOOOOOOOOOOO OOOOOOOOOOOOOOOOOOOOOOOO OOOOOOOOOOOOOOOOOOOOOOOO OOOOOOOOOOOOOOOOOOOOOOOO OOOOOOOOOOOOOOOOOOOOOOOO OOOOOOOOOOOOOOOOOOOOOOOO OOOOOOOOOOOOOOOOOOOOOOOO OOOOOOOOOOOOOOOOOOOOOOOO OOOOOOOOOOOOOOOOOOOOOOOO OOOOOOOOOOOOOOOOOOOOOOOO OOOOOOOOOOOOOOOOOOOOOOOO OOOOOOOOOOOOOOOOOOOOOOOO OOOOOOOOOOOOOOOOOOOOOOOO OOOOOOOOOOOOOO
AtXXT2 At4g02 500	TM 1	MIERCLGAYRCRRIQRALRQLKVTIL CLLLTVVVLRSTIGAGKFGTPEQDL DEIRQHFHARKRGEPHRVLEEIQTG GDSSSGDGGGNSGGSNNYETFDI NKIFVDEGEEEKPDPNKPYTLGPKI SDWDEQRSDWLAKNPSFPNFIGPN KPRVLLVTGSAPKPCENPVGDHYL LKSIKNKIDYCRLHGIEIFYNMALLDA EMAGFWAKLPLIRKLLLSHPEIEFL WWM**DSD**AMFTDMAFELPWERYK DYNLVMHGWNEMVYDQKNWIGLN TGSFLLRNNQWALDLLDTWAPMGP KGKIREEAGKVLTRELKDRPVFEAD DQSAMVYLLATQRDAWGNKVYLES GYYLHGYWGILVDRYEEMIENYHP GLGDHRWPLVTHFVGCKPCGKFG DYPVERCLKQMDRAFNFGDNQILQI YGFTHKSLASRKVKRVRNETSNPL EMKDELGLLHPAFKAVKVQTNQV	IIIIIIIIIIIIIIIIIIIIIIIIMMMMMMMMMMMOOO OOOOOOOOOOOOOOOOOOOOOOOO OOOOOOOOOOOOOOOOOOOOOOOO OOOOOOOOOOOOOOOOOOOOOOOO OOOOOOOOOOOOOOOOOOOOOOOO OOOOOOOOOOOOOOOOOOOOOOOO OOOOOOOOOOOOOOOOOOOOOOOO OOOOOOOOOOOOOOOOOOOOOOOO OOOOOOOOOOOOOOOOOOOOOOOO OOOOOOOOOOOOOOOOOOOOOOOO OOOOOOOOOOOOOOOOOOOOOOOO OOOOOOOOOOOOOOOOOOOOOOOO OOOOOOOOOOOOOOOOOOOOOOOO OOOOOOOOOOOOOOOOOOOOOOOO OOOOOOOOOOOOOOOOOOOOOOOO OOOOOOOOOOOOOOOOOOOOOOOO OOOOOOOOOOOOOOOOOOOOOOOO OOOOOOOOOOOOOOOOOOOOOOOO OOOOOOOOOOOOOOO
AtXXT3 At5g07 720	TM 1	MGKEDGFRTQKRVSTASSAAAGVL PTTMASGGVRRPPPRGRQIQKTFN NVKMTILCGFVTILVLRGTIGINFGTS DADVVNQNIIEETNRLLAEIRSDSDP TDSNEPPDSDLDLNMTYTLGPKITN WDQKRKLWLTQNPDFPSFINGKAK VLLLTGSPPKPCDNPIGDHYLLKSV KNKIDYCRIHGIEIVYNMAHLDKELA GYWAKLPMIRRLMLSHPEIEWIWW M**DSD**ALFTDMVFEIPLSRYENHNLV	IIIIIIIIIIIIIIIIIIIIIIIIIIIIIIIIIIIIIIIIIIIIIIIIIIIIIMMMM MMMMMMMOOOOOOOOOOOOOOOO OOOOOOOOOOOOOOOOOOOOOOOO OOOOOOOOOOOOOOOOOOOOOOOO OOOOOOOOOOOOOOOOOOOOOOOO OOOOOOOOOOOOOOOOOOOOOOOO OOOOOOOOOOOOOOOOOOOOOOOO OOOOOOOOOOOOOOOOOOOOOOOO OOOOOOOOOOOOOOOOOOOOOOOO OOOOOOOOOOOOOOOOOOOOOOOO

		IHGYPDLLFDQKSWIALNTGSFLFR NCQWSLDLLDAWAPMGPKGPIREE AGKILTANLKGRPAFEADDQSALIYL LLSQKETWMEKVFVENQYYLHGF WEGLVDKYEEMMEKYHPGLGDER WPFITHFVGCKPCGSYADYAVERC LKSMERAFNFADNQVLKLYGFGHR GLLSPKIKRIRNETTFPLKFVDRFDI RRTTPLKIEARS	OOOOOOOOOOOOOOOOOOOOOOOO OOOOOOOOOOOOOOOOOOOOOOOO OOOOOOOOOOOOOOOOOOOOOOOO OOOOOOOOOOOOOOOOOOOOOOOO OOOOOOOOOOOOOOOOOOOOOOOO OOOOOOOOOOOOOOOOOOOOOOOO OOOOOOOOOOOOOOOOOOOOOOOO OOOOOOOOOOOOOOOOO
AtXXT4 At1g18 690	TM 1	MFQDGSRSSGSGRGLSTTAVSNG GWRTRGFLRGWQIQNTLFNNIKFMI LCCFVTILILLGTIRVGNLGSSNADS VNQSFIKETIPILAEIPSDSHSTDLAE PPKADVSPNATYTLEPRIAEIPSDVH STDLVELPKADISPNATYTLGPRIAE IPSDSHLTDLLEPPKADISPNATYTL GPKITNWDSQRKVWLNQNPEFPNI VNGKARILLLTGSSPGPCDKPIGNY YLLKAVKNKIDYCRLHGIEIVYNMAN LDEELSGYWTKLPMIRTLMLSHPEV EWIWWM**DSD**ALFTDILFEIPLPRYE NHNLVIHGYPDLLFNQKSWVALNT GIFLLRNCQWSLDLLDAWAPMGPK GKIRDETGKILTAYLKGRPAFEADD QSALIYLLLSQKEKWIEKVYVENQY YLHGFWEGLVDRYEEMIEKYHPGL GDERWPFVTHFVGCKPCGSYADY AVDRCFKSMERAFNFADNQVLKLY GFSHRGLLSPKIKRIRNETVSPLESV DKFDIRRMHMETKP	IIIIIIIIIIIIIIIIIIIIIIIIIIIIIIIIIIIIIIIIIIIIIMMMMMMM MMMMMMMMMMOOOOOOOOOOOOO OOOOOOOOOOOOOOOOOOOOOOOO OOOOOOOOOOOOOOOOOOOOOOOO OOOOOOOOOOOOOOOOOOOOOOOO OOOOOOOOOOOOOOOOOOOOOOOO OOOOOOOOOOOOOOOOOOOOOOOO OOOOOOOOOOOOOOOOOOOOOOOO OOOOOOOOOOOOOOOOOOOOOOOO OOOOOOOOOOOOOOOOOOOOOOOO OOOOOOOOOOOOOOOOOOOOOOOO OOOOOOOOOOOOOOOOOOOOOOOO OOOOOOOOOOOOOOOOOOOOOOOO OOOOOOOOOOOOOOOOOOOOOOOO OOOOOOOOOOOOOOOOOOOOOOOO OOOOOOOOOOOOOOOOOOOOOOOO OOOOOOOOOOOOOOOOOOOOOOOO OOOOOOOOOOOOOOOOOOOOOOOO OOOOOOOOOOOOOOOOOOOOOOOO OOOOOOOOOOOOOOOOOOOOOOOO OOOOOO
AtXXT5 At1g74 380	TM 1	MGQDGSPAHKRPSGSGGGLPTTT LTNGGGRGGRGGLLPRGRQMQKT FNNIKITILCGFVTILVLRGTIGVGNL GSSSADAVNQNIIEETNRILAEIRSD SDPTDLDEPQEGDMNPNATYVLGP KITDWDSQRKVWLNQNPEFPSTVN GKARILLLTGSPPKPCDNPIGDHYLL KSVKNKIDYCRLHGIEIVYNMAHLD KELAGYWAKLPMIRRLMLSHPEVE WIWWM**DSD**ALFTDILFQIPLARYQK HNLVIHGYPDLLFDQKSWIALNTGS FLLRNCQWSLDLLDAWAPMGPKG PIRDEAGKVLTAYLKGRPAFEADDQ SALIYLLLSQKDTWMEKVFVENQYY LHGFWEGLVDRYEEMIEKYHPGLG DERWPFVTHFVGCKPCGSYADYA VERCLKSMERAFNFADNQVLKLYG FSHRGLLSPKIKRIRNETVSPLEFVD KFDIRRTPVETKPQN	IIIIIIIIIIIIIIIIIIIIIIIIIIIIIIIIIIIIIIIIIIIIIIIIIMMMMMM MMMMMMMMMOOOOOOOOOOOOOO OOOOOOOOOOOOOOOOOOOOOOOO OOOOOOOOOOOOOOOOOOOOOOOO OOOOOOOOOOOOOOOOOOOOOOOO OOOOOOOOOOOOOOOOOOOOOOOO OOOOOOOOOOOOOOOOOOOOOOOO OOOOOOOOOOOOOOOOOOOOOOOO OOOOOOOOOOOOOOOOOOOOOOOO OOOOOOOOOOOOOOOOOOOOOOOO OOOOOOOOOOOOOOOOOOOOOOOO OOOOOOOOOOOOOOOOOOOOOOOO OOOOOOOOOOOOOOOOOOOOOOOO OOOOOOOOOOOOOOOOOOOOOOOO OOOOOOOOOOOOOOOOOOOOOOOO OOOOOOOOOOOOOOOOOOOOOOOO OOOOOOOOOOOOOOOOOOO

TmXXT 2	TM 1	MIERCLGAQRSRKIQRALRHCKVTA LCLVLTVVVLRGTIGAGKFGTPEQD FVDIRDHFYSRKRSEPHRVLEEVQT TTSSSSSSDSSKSSGNNNNYEQFD VNSIFVHEGEDDKPDPSKPYSLGPK ISDWDEQRSQWLKQNPDFPNFVQ PSKPRVLLVTGSSPKPCENPVGDH YLLKSIKNKIDYCRVHGIEIFYNMALL DAEMAGFWAKLPLIRKLLLSHPEVE FLWWM**DSD**AMFTDMAFELPWERY KDVNLVMHGWNEMVYDEKNWIGL NTGSFLLRNTQWALDLLDVWAPMG PKGKVRDDAGKILTRELKNRPVFEA DDQSAMVYLLATQREQWGNKVYL ENAYYLHGYWGILVDRYEEMIENY HPGFGDHRWPLVTHFVGCKPCGK FGDYPVERCLRQMDRAFNFGDNQI LQIYGFTHKTLASKRVKRVRNETSM PLEVKDELGLIHPPFKAVKVASG	IIIIIIIIIIIIIIIIIIIIIIIIIMMMMMMMMMMOOOO OOOOOOOOOOOOOOOOOOOOOOOO OOOOOOOOOOOOOOOOOOOOOOOO OOOOOOOOOOOOOOOOOOOOOOOO OOOOOOOOOOOOOOOOOOOOOOOO OOOOOOOOOOOOOOOOOOOOOOOO OOOOOOOOOOOOOOOOOOOOOOOO OOOOOOOOOOOOOOOOOOOOOOOO OOOOOOOOOOOOOOOOOOOOOOOO OOOOOOOOOOOOOOOOOOOOOOOO OOOOOOOOOOOOOOOOOOOOOOOO OOOOOOOOOOOOOOOOOOOOOOOO OOOOOOOOOOOOOOOOOOOOOOOO OOOOOOOOOOOOOOOOOOOOOOOO OOOOOOOOOOOOOOOOOOOOOOOO OOOOOOOOOOOOOOOOOOOOOOOO OOOOOOOOOOOOOOOOOOOOOOOO OOOOOOOOOOOOOOOOOOOOOOOO OOOOOOOOOOOOO
TmXXT 5	TM 1	MGQEIFTPQKRASGGGGGLPTTTA NVNRGRAAPRGRQIHKTFNNIKITLL CGFVTILVLRGTIGVGNLGGSDDTV NQNIIEETNRILAEIRSDSEPGDPEG NAEVFMNPNETYALGPKITNWDDE RKVWLTQNPEFPSLVHGKARILLVT GSPPKPCDNAIGDHYLLKAIKNKIDY CRLHGIEIVYNLAHLDKELAGYWAK LPLIRKLMLSHPEVEWIWWM**DSD**A LFTDMVFEIPLSKYEKSNLVIHGYPD LLYDQKSWIALNTGSFLFRNCQWS LDLLDVWAPMGPKGPIREEAGKVL TGFLKGRPAFEADDQSALIYLLLSQ KDKWMDKVYVENQYYLHGFWEGL VDRYEEMMEKYHPGLGDERWPFV THFVGCKPCGSYADYAVERCLKSM ERAFNFADNQVLKLYGFGHRGLLS PKIKRIRNETSTPLEFVERFDIRRSA GHVGKVGS	IIIIIIIIIIIIIIIIIIIIIIIIIIIIIIIIIIIIIIIIIIIIIIIIMMMMMM MMMMMOOOOOOOOOOOOOOOOOO OOOOOOOOOOOOOOOOOOOOOOOO OOOOOOOOOOOOOOOOOOOOOOOO OOOOOOOOOOOOOOOOOOOOOOOO OOOOOOOOOOOOOOOOOOOOOOOO OOOOOOOOOOOOOOOOOOOOOOOO OOOOOOOOOOOOOOOOOOOOOOOO OOOOOOOOOOOOOOOOOOOOOOOO OOOOOOOOOOOOOOOOOOOOOOOO OOOOOOOOOOOOOOOOOOOOOOOO OOOOOOOOOOOOOOOOOOOOOOOO OOOOOOOOOOOOOOOOOOOOOOOO OOOOOOOOOOOOOOOOOOOOOOOO OOOOOOOOOOOOOOOOOOOOOOOO OOOOOOOOOOOOOOOOOOOOOOOO OOOOOOOOOOOOOOOOOOOOOOOO OOOOOOOOOOOOOOO
OsXXT 1 LOC_O s03g18 820	TM 1	MWVAERVVGERRMREIQRFARNA KLTVVCLLLTVVVLRGTVGAGKFGT PQQDLIELRHRFISHPHRALAEHHD ALSRGGGSSSSSGRAAQRDDEPD PPPRTLRDPPYTLGPKISDWDEQR AAWHRRHPETPPFVNDVKPRVLLV TGSSPKPCENPVGDHYLLKSIKNK MDYCRVHGLEIFYNMALLDAEMAG FWAKLPLLRALLLAHPEIEFLWWM**D** **SD**AMFSDMAFELPWERYGPYNLIM HGWDEMVYDDKNWIGLNTGSFLLR NCQWSLDFLDTWAPMGPKGPVRIE AGKVLTKYLKDRPVFEADDQSAMV YILATEREKWGDKVYLENGYYLHG	IIIIIIIIIIIIIIIIIIIIIIIIIIMMMMMMMMMMMOOO OOOOOOOOOOOOOOOOOOOOOOOO OOOOOOOOOOOOOOOOOOOOOOOO OOOOOOOOOOOOOOOOOOOOOOOO OOOOOOOOOOOOOOOOOOOOOOOO OOOOOOOOOOOOOOOOOOOOOOOO OOOOOOOOOOOOOOOOOOOOOOOO OOOOOOOOOOOOOOOOOOOOOOOO OOOOOOOOOOOOOOOOOOOOOOOO OOOOOOOOOOOOOOOOOOOOOOOO OOOOOOOOOOOOOOOOOOOOOOOO OOOOOOOOOOOOOOOOOOOOOOOO OOOOOOOOOOOOOOOOOOOOOOOO OOOOOOOOOOOOOOOOOOOOOOOO

		YWGILVDRYEEMLENYHPGLGDHR WPLVTHFVGCKPCGKFGDYPVER CLKQMERAFNFGDNQILQMYGFTH KSLGSRKVKRIRNETSNPLDVKDEL GLLHPAFKAMKTTST	OOOOOOOOOOOOOOOOOOOOOOO OOOOOOOOOOOOOOOOOOOOOOO OOOOOOOOOOOOOOOOOOOOOOO OOOOOOOOOOOOOOOOOOOOOOO

Figure 6.37: Predicted topologies of XXTs. Amino acid sequences and predicted Topologies of various XXTs, TM = transmembrane protein, GLOB = globular protein, O = outside - the corresponding amino acid is outside of the membrane surrounding cell compartment, I = inside - the corresponding amino acid is inside of the membrane surrounding cell compartment, M = the corresponding amino acid is inside of the membrane, DxD motif which coordinates metal cofactors of GTs is underlined

	WT	TmXXT2 & Kn126CSLC	TmXXT2 & Kn271CSLC	TmXXT2 & Kn603CSLC	TmXXT2 & MeCSLC	TmXXT2 & SmCSLC
t-Man	13,18 [a]	12,00 [a]	13,02 [a]	13,25 [a]	11,27 [a]	13,21 [a]
	± 1,61	± 1,25	± 0,74	± 1,76	± 0,95	± 1,32
t-Glc	4,91 [a]	5,19 [a]	5,68 [a]	5,16 [a]	4,96 [a]	4,64 [a]
	± 0,38	± 1,27	± 0,58	± 0,71	± 0,59	± 0,09
3-Glc	13,00 [a]	12,16 [a]	12,73 [a]	13,51 [a]	13,15 [a]	11,51 [a]
	± 2,25	± 0,61	± 3,81	± 1,45	± 1,02	± 1,39
2-Man	23,98 [a]	22,70 [a]	22,79 [a]	25,61 [a]	20,89 [a]	24,04 [a]
	± 1,99	± 2,95	± 2,05	± 4,04	± 1,54	± 2,65
4-Man	0,84 [a]	0,95 [a]	0,95 [a]	0,89 [a]	0,98 [a]	0,90 [a]
	± 0,13	± 0,22	± 0,54	± 0,27	± 0,32	± 0,21
6-Man	2,15 [a]	2,47 [a]	2,11 [a]	2,08 [a]	2,14 [a]	2,34 [a]
	± 0,40	± 0,22	± 0,27	± 0,42	± 0,14	± 0,22
6-Glc	12,62 [a]	13,30 [a]	13,60 [a]	12,89 [a]	14,31 [a]	12,49 [a]
	± 1,71	± 1,05	± 1,66	± 2,72	± 2,14	± 0,57
4-Glc	**1,11 [a]**	**0,80 [a]**	**1,21 [ab]**	**0,90 [a]**	**3,69 [c]**	**1,94 [b]**
	± 0,30	± 0,14	± 0,33	± 0,14	± 0,72	± 0,26
2,3-Man	1,25 [a]	1,16 [a]	1,23 [a]	1,17 [a]	1,29 [a]	1,32 [a]
	± 0,10	± 0,21	± 0,22	± 0,24	± 0,32	± 0,17
3,4-Glc	1,68 [a]	1,41 [a]	1,88 [a]	1,35 [a]	1,51 [a]	1,38 [a]
	± 0,56	± 0,36	± 0,84	± 0,28	± 0,49	± 0,23
2,3-Glc	7,96 [a]	5,51 [a]	7,13 [a]	5,51 [a]	6,52 [a]	5,61 [a]
	± 1,60	± 1,66	± 3,02	± 0,90	± 1,03	± 3,08
2,4-Man	1,20 [a]	1,04 [a]	1,18 [a]	1,08 [a]	1,11 [a]	1,09 [a]
	± 0,27	± 0,23	± 0,67	± 0,32	± 0,37	± 0,23
3,6-Glc	5,67 [a]	6,75 [a]	5,93 [a]	5,92 [a]	6,47 [a]	5,88 [a]
	± 0,67	± 0,98	± 0,50	± 1,02	± 0,96	± 0,14
3,6-Man	1,28 [a]	1,73 [a]	1,43 [a]	1,31 [a]	1,38 [a]	1,57 [a]
	± 0,21	± 0,15	± 0,40	± 0,27	± 0,12	± 0,12
2,6-Man	8,24 [a]	11,18 [a]	8,06 [a]	8,50 [a]	9,21 [a]	11,09 [a]
	± 2,24	± 2,07	± 1,89	± 3,72	± 1,93	± 0,66
4,6-Glc	0,92 [a]	1,65 [a]	1,07 [a]	0,87 [a]	1,14 [a]	0,99 [a]
	± 0,19	± 1,54	± 0,32	± 0,20	± 0,22	± 0,13

Figure 6.38: Glycosidic linkage analysis of *Pichia pastoris* strains expressing a CGA CSLC and TmXXT2. Pichia AIR material of WT and strains expressing TmXXT2 and an algae CSLC each, n = 4 for all strains; results of ANOVA analysis and subsequent Tukey's test indicated ($P < 0,05$).

	WT	MeCSLC	SmCSLC
t-Man	12,43 [a]	11,24 [a]	10,09 [a]
	± 2,74	± 1,13	± 0,41
t-Glc	14,43 [a]	14,70 [a]	13,44 [a]
	± 0,77	± 0,73	± 0,45
3-Glc	**7,97 [a]**	**10,94 [b]**	**11,88 [b]**
	± 1,22	± 0,82	± 0,71
2-Man	**13,55 [a]**	**11,35 [b]**	**11,17 [b]**
	± 1,18	± 1,05	± 0,65
6-Man	4,73 [a]	3,59 [a]	3,11 [a]
	± 1,36	± 0,54	± 0,23
6-Glc	14,65 [a]	14,72 [a]	16,01 [a]
	± 1,87	± 0,77	± 0,90
4-Glc	**0,73 [a]**	**1,20 [b]**	**0,83 [a]**
	± 0,14	± 0,18	± 0,06
2,3-Man	2,06 [a]	2,10 [a]	1,82 [a]
	± 0,13	± 0,28	± 0,32
3,4-Glc	1,71 [a]	2,62 [a]	2,50 [a]
	± 1,33	± 0,72	± 0,80
2,3-Glc	7,79 [a]	10,39 [a]	11,12 [a]
	± 2,68	± 1,51	± 1,78
2,4-Man	0,86 [a]	0,99 [a]	0,95 [a]
	± 0,60	± 0,33	± 0,27
3,6-Glc	**9,64 [ab]**	**9,20 [a]**	**10,28 [b]**
	± 0,15	± 0,73	± 0,50
3,6-Man	2,55 [a]	1,87 [a]	1,77 [a]
	± 0,80	± 0,10	± 0,06
2,6-Man	**6,89 [a]**	**5,10 [b]**	**5,02 [b]**
	± 0,93	± 1,06	± 0,59

Figure 6.39: Glycosidic linkage analysis of *Pichia pastoris* strains expressing a CGA CSLC. Linkages of Pichia AIR material of WT and strains expressing an algae CSLC only, n = 4 for all strains; results of ANOVA analysis and subsequent Tukey's test indicated ($P < 0,05$).

	WT	KnXXT & Kn126CSLC	KnXXT & Kn271CSLC	KnXXT & Kn603CSLC	KnXXT & MeCSLC	KnXXT & SmCSLC
t-Man	14,90 [a]	15,37 [a]	17,16 [a]	16,85 [a]	14,64 [a]	14,62 [a]
	± 1,00	± 0,40	± 1,39	± 2,76	± 1,29	± 1,11
t-Glc	5,48 [a]	6,77 [a]	6,99 [a]	6,47 [a]	5,90 [a]	5,81 [a]
	± 0,53	± 0,31	± 0,87	± 0,68	± 0,34	± 1,28
3-Glc	11,67 [a]	10,92 [a]	10,88 [a]	11,62 [a]	11,17 [a]	9,96 [a]
	± 0,96	± 3,14	± 1,22	± 2,29	± 3,25	± 0,16
2-Man	25,60 [a]	22,76 [a]	22,59 [a]	22,67 [a]	22,87 [a]	21,70 [a]
	± 2,22	± 0,53	± 2,25	± 1,16	± 1,77	± 2,31
4-Man	0,96 [a]	1,33 [a]	1,06 [a]	1,32 [a]	1,17 [a]	1,46 [a]
	± 0,20	± 0,42	± 0,15	± 0,13	± 0,41	± 0,08
6-Man	**2,17 [a]**	**2,61 [ab]**	**2,66 [ab]**	**2,33 [ab]**	**2,85 [ab]**	**3,35 [b]**
	± 0,31	± 0,82	± 0,29	± 0,32	± 0,47	± 0,13
6-Glc	12,80 [a]	13,62 [a]	13,86 [a]	13,19 [a]	12,26 [a]	12,69 [a]
	± 2,20	± 0,48	± 1,47	± 2,02	± 1,26	± 1,00
4-Glc	**0,89 [a]**	**1,30 [ab]**	**1,13 [ab]**	**1,24 [ab]**	**1,55 [b]**	**1,25 [ab]**
	± 0,14	± 0,21	± 0,04	± 0,15	± 0,30	± 0,42
2,3-Man	0,89 [a]	1,28 [a]	1,03 [a]	1,21 [a]	1,31 [a]	1,25 [a]
	± 0,07	± 0,02	± 0,11	± 0,19	± 0,24	± 0,36
3,4-Glc	**1,15[a]**	**1,73[ab]**	**1,54[ab]**	**1,78[b]**	**1,77[b]**	**1,92[b]**
	± 0,10	0,06	± 0,23	± 0,38	± 0,26	± 0,05
2,3-Glc	4,88 [a]	4,71 [a]	3,58 [a]	4,13 [a]	4,52 [a]	3,05 [a]
	± 0,61	2,04	± 0,57	± 1,10	± 1,31	± 0,68
2,4-Man	**0,76 [a]**	**1,00 [ab]**	**0,78 [ab]**	**0,94 [ab]**	**1,08 [ab]**	**1,19 [b]**
	± 0,08	0,11	± 0,11	± 0,09	± 0,23	± 0,13
3,6-Glc	5,62 [a]	5,62 [a]	6,20 [a]	6,23 [a]	5,63 [a]	7,41 [a]
	± 0,70	0,27	± 0,28	± 1,36	± 0,70	± 1,93
3,6-Man	1,34 [a]	1,47 [a]	1,54 [a]	1,64 [a]	1,61 [a]	2,48 [a]
	± 0,17	0,49	± 0,23	± 0,96	± 0,23	± 0,19
2,6-Man	10,28 [a]	8,57 [a]	8,21 [a]	7,46 [a]	10,80 [a]	10,56 [a]
	± 1,83	± 3,46	± 2,76	± 3,20	± 0,64	± 2,89
4,6-Glc	**0,61 [a]**	**0,93 [ab]**	**0,80 [a]**	**0,90 [ab]**	**0,88 [ab]**	**1,30 [b]**
	± 0,11	± 0,12	± 0,02	± 0,05	± 0,16	± 0,39

Figure 6.40: Glycosidic linkage analysis of *Pichia pastoris* strains expressing a CGA CSLC and an algae XXT. Linkages of Pichia AIR material of WT and strains expressing an algae CSLC and an algae XXT; WT n= 4, KnXXT & Kn126CSLC n = 2, KnXXT & Kn271CSLC n = 3, KnXXT & Kn603CSLC n = 4, KnXXT & MeCSLC n = 4, KnXXT & SmCSLC n = 2; results of ANOVA analysis and subsequent Tukey's test are indicated ($P < 0,05$).

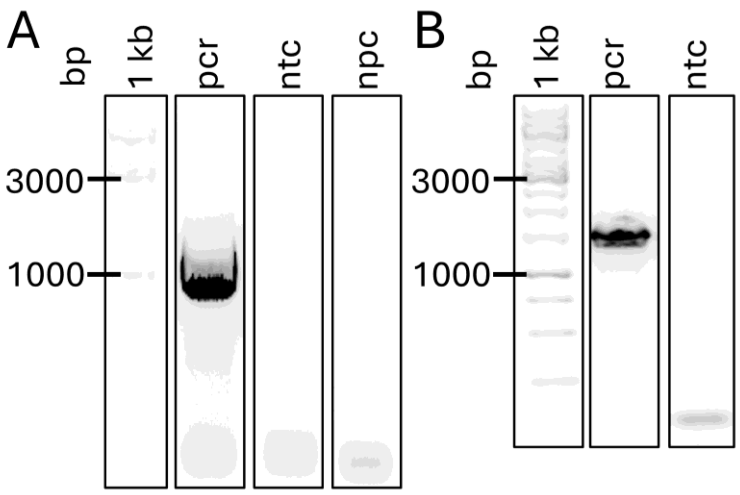

Figure 6.41: PCR to subclone and confirm *VcXBT* in pMDC83. A) Amplification of *VcXBT* from plasmid introducing XbaI/KpnI overhangs for cloning into pMDC83, VcXBTpMDCF&R, expected size 1,5 kbp; **B)** Colony PCR of pMDC83 + *VcXBT* or to confirm *E. coli* transformants. *E. coli* transformed with plasmids were verified via PCR using cell material as template with primers, VcXBTpMDCF&R, expected size 1,5 kbp; bp = base pairs, no template control = ntc, npc = no polymerase control


Tree Scale: 1
PpXDT Pp201625
SlXST2 Sl07g049610
SlXST1 Sl07g044960
VaccDscaff16 processed gene 153 5
VaccDscaff18 processed gene 250 3
VaccDscaff7 processed gene 279 7
VaccDscaff31 processed gene 65 6
VcXBT 1 bluecrop (VcXBT)
VaccDscaff16 processed gene 173 7
VaccDscaff7 processed gene 259 5
VcXBT 2 bluecrop
VaccDscaff18 processed gene 229 3
VaccDscaff31 processed gene 85 3
VaccDscaff16 processed gene 154 8
VaccDscaff18 processed gene 249 0
VaccDscaff7 processed gene 279 0
VcXBT 3 bluecrop
VaccDscaff31 processed gene 66 9
VaccDscaff7 processed gene 279 12
VaccDscaff31 processed gene 66 6
VaccDscaff7 processed gene 278 17
VaccDscaff31 processed gene 66 10
VaccDscaff16 processed gene 154 9
VaccDscaff18 processed gene 248 5
VaccDscaff16 processed gene 138 3
VaccDscaff31 processed gene 50 2
VaccDscaff7 processed gene 302 0
VaccDscaff7 processed gene 279 2
VaccDscaff18 processed gene 249 17
VaccDscaff31 processed gene 66 5
VaccDscaff18 processed gene 249 21
VaccDscaff18 processed gene 249 32
VaccDscaff16 processed gene 154 1
VcXBT 4 bluecrop
VaccDscaff16 processed gene 153 3
VaccDscaff18 processed gene 250 15
VaccDscaff7 processed gene 280 0
VaccDscaff31 processed gene 65 5
XLT2 clade
VaccDscaff16 processed gene 154 5
VaccDscaff7 processed gene 278 7
VcXLT2 2 bluecrop
VaccDscaff18 processed gene 247 18
VaccDscaff31 processed gene 67 11
AtXLT2 AT5G62220 1
TmXLT2
VcXLT2 1 bluecrop (VcXLT2)
VaccDscaff21 processed gene 77 6
VaccDscaff26 processed gene 75 17
VaccDscaff29 processed gene 77 6
VaccDscaff33 processed gene 260 14
OsXLT2 Os04g48480
AtGT20 AT5G41250 1
AtXUT AT1G63450
VaccDscaff20 processed gene 322 14
VaccDscaff49 processed gene 45 12
VaccDscaff28 processed gene 51 23
VaccDscaff44 processed gene 42 16
AtGT17 AT1G68470 1
AtGT19 AT4G22580 1
VaccDscaff46 processed gene 22 40
VaccDscaff22 processed gene 143 14
VaccDscaff43 processed gene 225 23
VaccDscaff3 processed gene 336 1
VaccDscaff25 processed gene 96 2
VaccDscaff14 processed gene 99 2
VaccDscaff2 processed gene 69 1
AtGT14 AT4G13990 1
AtGT15 AT2G31990 1
AtGT13 AT2G32740 1
AtGT12 AT2G32750
AtGT11 AT2G29040 1
VaccDscaff15 processed gene 323 43
VaccDscaff24 processed gene 81 41
VaccDscaff19 processed gene 352 0
VaccDscaff11 processed gene 333 45
VaccDscaff19 processed gene 351 7
MUR3 clade
OsMUR3 Os03g05110
SlMUR3 Sl09g064470
EgMUR3 NP 001306902 1
AtMUR3 AT2G20370 1
TmMUR3
VaccDscaff47 processed gene 154 3
VaccDscaff43 processed gene 46 2
VaccDscaff22 processed gene 328 0
VcMUR3 bluecrop (VcMUR3)
VaccDscaff46 processed gene 162 7

Figure 6.42: Phylogeny of XyG-related GT47 proteins. Blueberry proteins with similarity to XyG GT47 glycosyltransferase proteins obtained from a blastP search against Genome Database for Vaccinium (GDV; VaccDscaff-Genes, names consistent with results of blastP search), cloned candidate genes from blueberry (*Vaccinium corymbosum* bluecrop cultivar) and functionally described GT47 XyG glycosyltransferases from various species in a phylogenetic tree. The scale bar indicates the number of substitutions per site, branch lengths are directly related to the amount of genetic change between shown genes. XLT2 and MUR3 clades are indicated in green and purple, respectively; At, *Arabidopsis thaliana*; Os, *Oryza sativa* (rice); Tm, *Tropaeolum majus* (nasturtium); Sl, *Solanum lycopersicum* (tomato); Eg, *Eucalyptus grandis* (Eucalyptus).

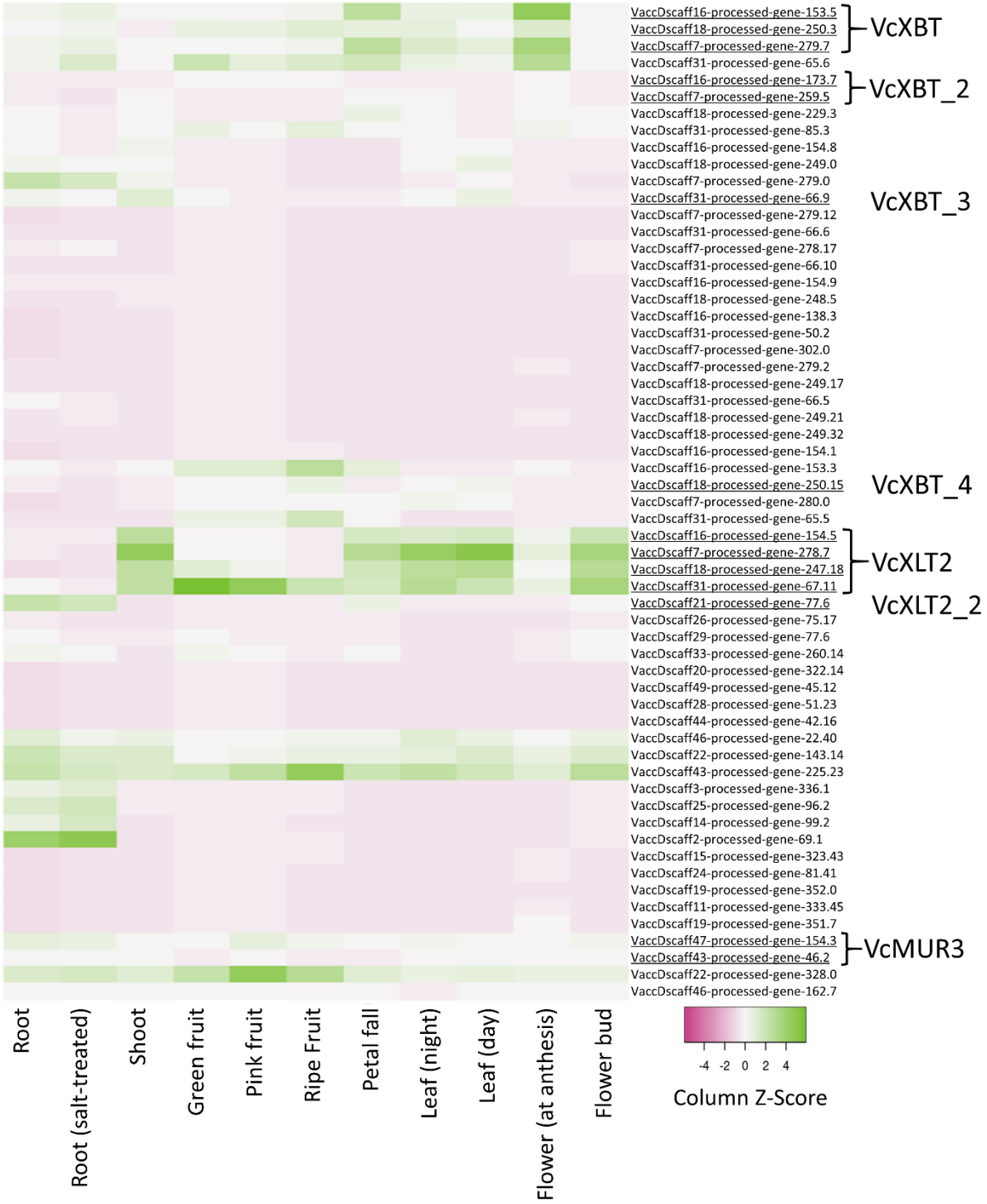

Figure 6.43: Expression heatmap of blueberry GT47 glycosyltransferase candidates. Expression in different tissues based on "V. corymbosum cv. Draper Expression in Tissue during Fruit Development, FPKM" from GDV; FPKM = fragments per kilobase of transcript per million fragments mapped) using heatmapper.ca/expression. The order of the genes in the heatmap corresponds to the order presented in the phylogenetic tree in Fig. 6.42. The Row Z-Score is a scaling method for visualization in heat maps. Underlined genes: sequence was used to design primers for cloning the corresponding genes from fruits of the *V. corymbosum* bluecrop.

[Extern] RE: Request for Permission to Reuse Published Data in PhD Thesis

Von Ingram, Jonathan <jingram@wiley.com>
An Ronja.Immelmann@hhu.de <Ronja.Immelmann@hhu.de>
Kopie Lewis, Andrea <alewis@wiley.com>, Plant Direct <PlantDirect@wiley.com>
Datum 2025-05-28 11:21

Dear Ronja

My apologies for the delay. I am pleased to confirm this permission on behalf of Plant Direct.

Regards, Jonathan

Dr Jonathan Ingram | Supervising Editor, Plant Direct
T +44 (0) 1865 476304 | M +44 (0) 7827 234382
Wiley | Research | Publishing Development

-----Original Message-----
From: Ronja Catharina Immelmann <Ronja.Immelmann@hhu.de>
Sent: Friday, May 2, 2025 2:29 PM
To: Plant Direct <plantdirect@wiley.com>
Subject: Request for Permission to Reuse Published Data in PhD Thesis

⛔ This is an external email.

Dear Editorial Office,

I hope this message finds you well.

I am writing to formally request permission to reuse data and figures from my article published in Plant Direct, titled “Identification of a xyloglucan beta-xylopyranosyltransferase from Vaccinium corymbosum,”
https://urldefense.com/v3/__https://doi.org/10.1002/pld3.514__;!!N11eV2iwtfs!umBlgnWd5RNts0TXDvvl4dMIYQ7upirzMGNcFY7FIQU17VxqEmKEjCv5zY2KiGmWuj17RvNhGusL_eVCWh42TX7APAym$
, in my upcoming PhD thesis.

I understand that Plant Direct articles are published under the terms of the Creative Commons Attribution License (CC BY), which permits reuse of content provided that proper attribution is given. While this license allows for such use, I would like to obtain formal approval from the journal as a courtesy and to comply with academic best practices, particularly as my institution advises obtaining explicit permission when reusing previously published material in a doctoral thesis.

The thesis will be submitted to Heinrich-Heine-Universität Düsseldorf and may be made publicly available through the university's institutional repository.

Please let me know if any further information is required, or if there are specific conditions I should observe when reusing this material.

Thank you very much for your time and consideration.

Kind regards,
Ronja Immelmann
Institute for Plant Cell Biology and Biotechnology Heinrich-Heine-Universität Düsseldorf

Figure 6.44: Permission to reuse published data and figures. Reproduction of content published in *Plant Direct* under the title *"*Identification of a xyloglucan beta-xylopyranosyltransferase from Vaccinium corymbosum" (Plant Direct, 2023 Jul 25; 7(7)). Reuse of this material in this thesis was authorized by Dr. Jonathan Ingram, Supervising Editor at Plant Direct, on May 28, 2025.

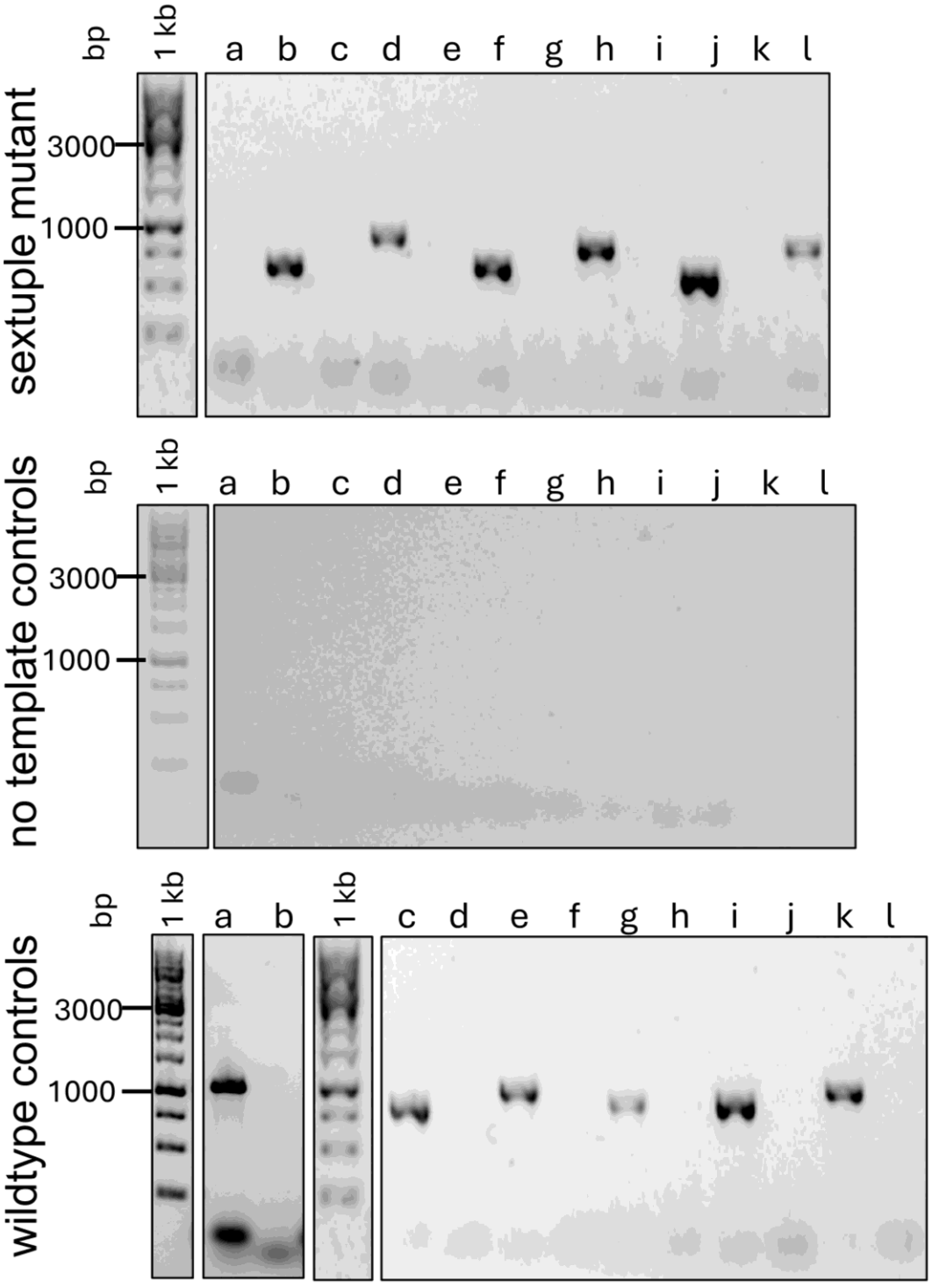

Figure 6.45: Genotyping PCR of sextuple mutant *xeg113cslc456812* and controls. PCR products amplifying a genomic fragment spanning the T-DNA insertion and a fragment from the T-DNA border to a genomic position to confirm presence or absence of T-DNA insertion; a: SALK_06691-LP & RP, *XEG113* WT specific; b: SALK_06691-RP & LBb1.3, *xeg113* T-DNA insertion; c: SAIL_837B10-LP & RP, *CSLC4* WT specific; d: SAIL_837B10-RP & LB-3, *cslc4* T-DNA insertion; e: SAIL_187G09-LP & RP, *CSLC5* WT specific; f: SAIL_187G09-RP & LB-3, *cslc5* T-DNA insertion; g: SALK_088270-LP & RP, *CSLC6* WT specific; h: SALK_088270-RP & LBb1.3, *cslc6* T-DNA insertion; i: WiscDsLox_497-02H-LP & RP, *CSLC8* WT specific; j: WiscDsLox_497-02H-RP & P745, *cslc8* T-DNA insertion; k: SAIL_168F02-LP & RP, *CSLC12* WT specific; l: SAIL_168F02-RP & LB-3, *cslc12* T-DNA insertion; **A)** *xeg113cslc456812* sextuple mutant **B)** no template controls **C)** wildtype controls, plant with no T-DNA insertion; bp = base pairs

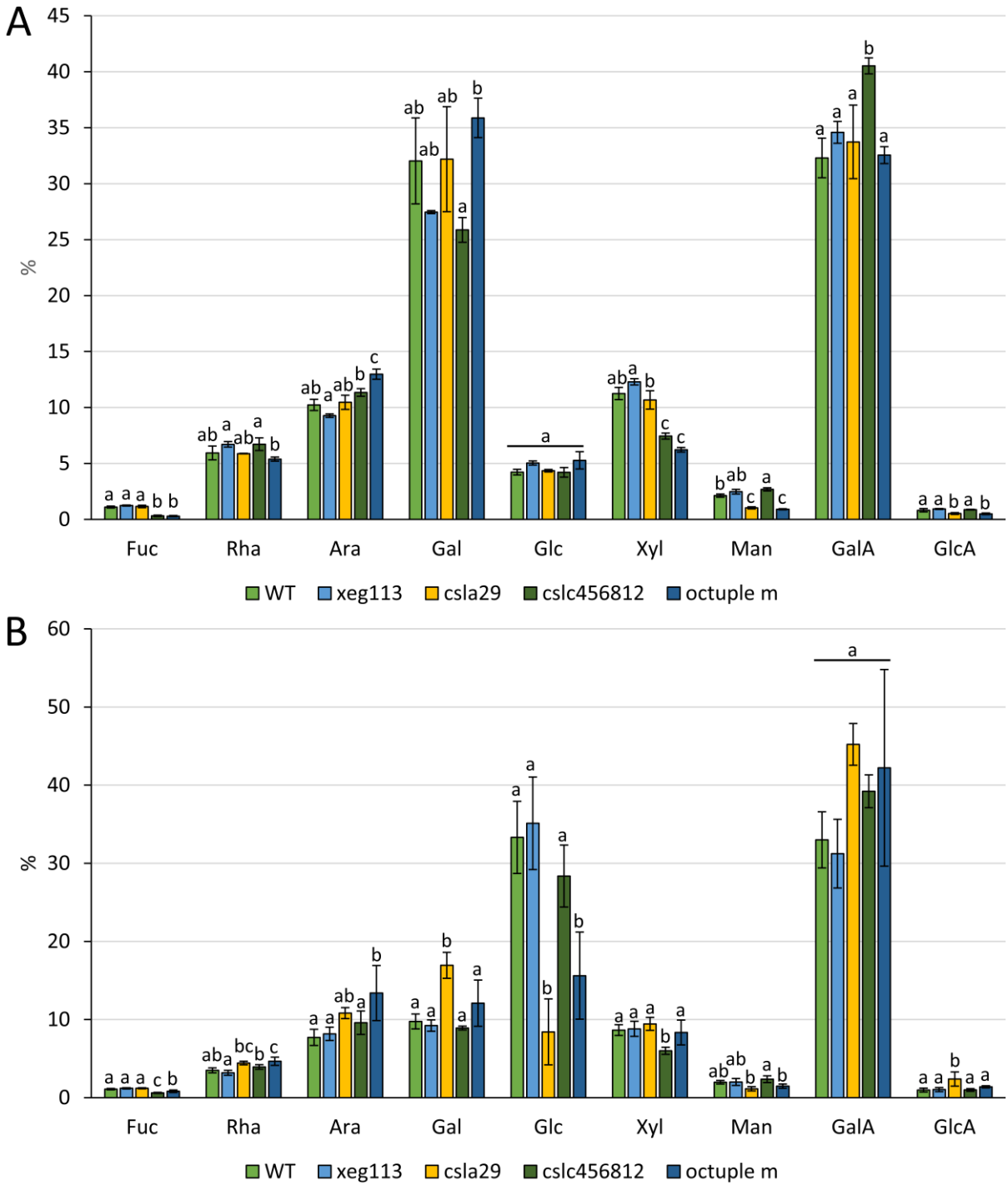

Figure 6.46: Monosaccharide composition of Arabidopsis etiolated hypocotyls and leaf material of octuple mutant and controls (relative). A) Relative abundance of the molecular abundance of monosaccharides in 1 mg AIR (in %) of 5 days-old etiolated seedlings, WT n = 4, *xeg113* n=2, *csla29* n =3, *cslc456812* n= 3, octuple mutant n = 3; **B)** Relative abundance of the molecular abundance of monosaccharides in 1 mg AIR (in %) of 4 weeks old leaf material, WT n = 6, *xeg113* n=6, *csla29* n =3, *cslc456812* n= 5, octuple mutant n = 5; Fuc = fucose, Rha = rhamnose, Ara = arabinose, Gal = galactose, Glc = glucose, Xyl = xylose, Man = mannose, GalA = galacturonic acid, GlcA = glucuronic acid

7. Acknowledgment

First and foremost, I would like to express my sincere gratitude to Prof. Dr. Markus Pauly for giving me the opportunity to pursue my PhD in his institute and for his continuous scientific support. I am particularly thankful for the well-organized work environment he fostered, as well as his constructive feedback, especially during the writing phase of both my paper and thesis.

I would also like to thank Prof. Dr. Ilka Axmann for kindly agreeing to be my mentor.

My heartfelt thanks go to my co-supervisor, Dr. Vicente Ramirez Garcia, for his valuable scientific guidance and hands-on support in the lab, particularly for the crossing of my Arabidopsis lines and for providing the Hymenaea XXT RMSD values. I am grateful for his insightful advice and mentorship in navigating the academic world.

My special thanks go to Niklas Gawenda, whose foundational work on the xyloglucan projects I had the privilege of building upon.

I am deeply grateful to Katharina Grosche for her generous assistance with analytical instruments, her patience during the data analysis process and her company in the analytical lab, especially during the long hours of linkage analysis. Her support contributed greatly to staying focused and balanced throughout this project.

Many thanks to Barbara Schulten, Felix Roth, and Konstantin Shek for ensuring the smooth operation of the institute and for their help with genotyping and plant care.

I am grateful to all current and former members of the Institute for Plant Cell Biology and Biotechnology at HHU for their continued support and for cultivating a collegial, welcoming work atmosphere. A special shoutout to the beloved Mensa-Crew for the fun we shared during our lunch breaks.

I am also grateful to the members and former members of the Synthetic Microbiology Institute and of the Metabolomics and Metabolism Institute.

I would like to acknowledge my collaborators, Luiz-Eduardo Del-Bem and Sang-Jin Kim, for providing the opportunity to work on the algal xyloglucan project, as well as for sharing sequence data, plasmids, and AIR material essential to the analysis.

Special thanks to the Center for Advanced Imaging (CAi) at Heinrich Heine University Düsseldorf for access to the Olympus FV3000 Confocal Laser Scanning Microscope (DFG-INST 1358/44-1 FUGB) and in particular to Dr. Sebastian Hänsch for his assistance during image acquisition.

I also acknowledge CeMSA@HHU (Center for Molecular and Structural Analytics at Heinrich Heine University Düsseldorf) for recording NMR-spectroscopic data and for granting us access to the MALDI-TOF/TOF UltrafleXtreme (Bruker Daltonik) when our own instrumentation was unavailable.

I thank Hof Vinnemann in Olfen for supplying blueberry material and Palmengarten Frankfurt for providing Hymenaea material.

Darüber hinaus möchte ich mich bei meiner Familie und meinen Freunden bedanken.

Ein besonderer Dank gilt meinem Freund Uwe, der mich in den vergangenen Monaten mit großer Geduld und viel Verständnis begleitet hat, selbst in Zeiten, in denen meine Nerven am Ende waren. Meiner Mami danke ich für ihre ständige Bereitschaft, Taschentücher zum Ausheulen oder ein Glas Wein zur Beruhigung bereitzuhalten. Danke an meine Schwestern Stella und Ylva, mit denen man sich immer gut unterhalten, ausgelassen feiern oder die Pisten unsicher machen konnte. Ein großes Dankeschön auch an meine Großeltern Karin und Ulrich, die mich stets mit gutem Essen oder einer Partie Skat unterhalten haben.
Diese Arbeit widme ich meinem Bruder Ole, der nicht mehr die Gelegenheit hatte, eine eigene Abschlussarbeit zu verfassen. Ole und Karin, die die Abgabe und Verteidigung meiner Doktorarbeit leider nicht mehr miterleben konnten, waren in Gedanken und im Herzen stets bei mir.